

**MODELING PHASE SYNCHRONIZATION  
OF INTERACTING NEURONAL POPULATIONS**

FROM PHASE REDUCTIONS TO COLLECTIVE BEHAVIOR  
OF OSCILLATORY NEURAL NETWORKS

Bastian Pietras, MSc

THESIS SUBMITTED FOR A  
DOUBLE PhD DEGREE  
UNDERTAKEN AT



DEPARTMENT OF  
HUMAN MOVEMENT SCIENCES  
VRIJE UNIVERSITEIT AMSTERDAM  
AMSTERDAM, NL

DEPARTMENT OF PHYSICS  
LANCASTER UNIVERSITY  
LANCASTER, UK

December 2018

VRIJE UNIVERSITEIT

**Modeling phase synchronization  
of interacting neuronal populations**

From phase reductions to collective behavior  
of oscillatory neural networks

ACADEMISCH PROEFSCHRIFT

ter verkrijging van de graad Doctor  
aan de Vrije Universiteit Amsterdam  
en The University of Lancaster,  
op gezag van de rector magnifici  
prof.dr. V. Subramaniam  
en prof.dr. M.E. Smith,  
in het openbaar te verdedigen  
ten overstaan van de promotiecommissie  
van de Faculteit der Gedrags- en Bewegingswetenschappen  
op donderdag 20 december 2018 om 9.45 uur  
in de aula van de universiteit,  
De Boelelaan 1105

door

Bastian Pietras

geboren te Herford, Duitsland

promotoren: prof.dr. A. Daffertshofer

prof.dr. A. Stefanovska

copromotor: prof.dr. P.V.E. McClintock

# DECLARATION

This thesis is my original work. I have written this thesis as part of a double PhD degree undertaken at Vrije Universiteit Amsterdam and at Lancaster University. The thesis is submitted to both universities. There exist two versions that are identical in title and content, but they are different in form (format and pagination) as the respective regulations of the two universities and their requirements with respect to form are different.

Chapter 6 of this thesis contains parts of my joint research with Robert Ton. Robert included an earlier version as Chapter 5 of his PhD thesis “The Power of Synchronous Rhythms – Self-Similarity in Phase Dynamics, Neural Masses, and the Brain”. Robert was granted the degree of doctor and his thesis was published in June 2016. With the exception of Chapter 6, my thesis has not been submitted, in whole or in part, for a degree at either of the two universities named above or at any other university. Nor does it contain, to the best of my knowledge and belief, any material published or written by another person, except acknowledged in the text.



This dissertation has been accomplished within the COSMOS project. That project has received funding from the European Union’s Horizon 2020 research and innovation programme under the Marie Skłodowska-Curie grant agreement No. 642563.

---

# LIST OF PUBLICATIONS

Parts of the work presented in this thesis have been published in the following papers:

- A. Daffertshofer, R. Ton, B. Pietras, M. Kringelbach & G. Deco. Scale-freeness or partial synchronization in neural mass phase oscillator networks: Pick one of two?, *NeuroImage* **180** 428–441, 2018. (Work from Chapter 6.)
- B. Pietras, N. Deschle & A. Daffertshofer. Equivalence of coupled networks and networks with multimodal frequency distributions: Conditions for the bimodal and trimodal case, *Phys. Rev. E* **94**, 052211, 2016. (Work from Chapter 4.)
- B. Pietras & A. Daffertshofer. Ott-Antonsen attractiveness for parameter-dependent oscillatory systems, *Chaos* **26**, 103101, 2016. (Work from Chapter 5.)

The following manuscript is currently under review:

- B. Pietras & A. Daffertshofer. Networks of coupled oscillators and phase reduction techniques, *submitted for publication*, 2018. (Work from Chapters 2 and 3.)

Parts of the work have also been presented at the following scientific meetings and workshops:

- B. Pietras & A. Daffertshofer. Phase dynamics of coupled neural oscillators: general principles of and differences between reduction techniques. *4th ICMNS Conference. 10-14 June 2018. Juan-Les-Pins, France.* Oral presentation.
- B. Pietras & A. Daffertshofer. Reduced phase models of networks of neural oscillators and their limitations. *AMCOS Conference. 19-23 March 2018. Barcelona, Spain.* Poster presentation.
- B. Pietras & A. Daffertshofer. Exact low-dimensional mean-field dynamics of neuronal networks – networks of spiking neurons. *SIAM Conference on Applications of Dynamical Systems. 21-25 May 2017. Snowbird, Utah.* Oral presentation.

---

- B. Pietras. The Ott-Antonsen ansatz – theory and applications. *COSMOS Retreat. 26-31 March 2017. Wittenberg, Germany.* Oral presentation.
- B. Pietras, N. Deschle & A. Daffertshofer. Multimodal or coupled networks: just a matter of taste?, and: Ott-Antonsen attractiveness for parameter-dependent systems. *Multistability and Tipping: From Mathematics and Physics to Climate and Brain. International Seminar & Workshop. 19 September - 14 October 2016. Dresden, Germany.* Oral and poster presentation.
- B. Pietras & A. Daffertshofer. Ott-Antonsen attractiveness for parameter-dependent systems. *Patterns of Dynamics. 25-29 July 2016. Berlin, Germany.* Oral presentation.
- B. Pietras, N. Deschle & A. Daffertshofer. Multimodal or coupled networks: just a matter of taste? *XXXVI Dynamics Days Europe. 06-10 June 2016. Corfu, Greece.* Oral presentation.
- B. Pietras, N. Deschle & A. Daffertshofer. Coupled networks and networks with bimodal frequency distributions are equivalent. *2nd ICMNS Conference. 29-01 May 2016. Juan-Les-Pins, France.* Poster presentation.
- B. Pietras. Phase-reduction techniques near and away from bifurcation points. *Problems and challenges: multiple scales and coherent structures. 20 April 2016. Münster, Germany.* Oral presentation.
- B. Pietras, N. Deschle & A. Daffertshofer. Coupled networks and networks with bimodal frequency distributions are equivalent. *8th ESCGO Conference. 10-14 April 2016. Lancaster, UK.* Poster presentation.

---

Bastian Pietras, MSc

*Modeling phase synchronization of interacting neuronal populations –  
From phase reductions to collective behavior of oscillatory neural networks.*

Thesis submitted for a double PhD degree in December 2018.

## ABSTRACT

Synchronous, coherent interaction is key for the functioning of our brain. The co-ordinated interplay between neurons and neural circuits allows to perceive, process and transmit information in the brain. As such, synchronization phenomena occur across all scales. The coordination of oscillatory activity between cortical regions is hypothesized to underlie the concept of phase synchronization. Accordingly, phase models have found their way into neuroscience.

The concepts of neural synchrony and oscillations are introduced in *Chapter 1* and linked to phase synchronization phenomena in oscillatory neural networks.

*Chapter 2* provides the necessary mathematical theory upon which a sound phase description builds. I outline phase reduction techniques to distill the phase dynamics from complex oscillatory networks. In *Chapter 3* I apply them to networks of weakly coupled Brusselators and of Wilson-Cowan neural masses. Numerical and analytical approaches are compared against each other and their sensitivity to parameter regions and nonlinear coupling schemes is analyzed.

In *Chapters 4* and *5* I investigate synchronization phenomena of complex phase oscillator networks. First, I study the effects of network-network interactions on the macroscopic dynamics when coupling two symmetric populations of phase oscillators. This setup is compared against a single network of oscillators whose frequencies are distributed according to a symmetric bimodal Lorentzian. Subsequently, I extend the applicability of the Ott-Antonsen ansatz to parameter-dependent oscillatory systems. This allows for capturing the collective dynamics of coupled oscillators when additional parameters influence the individual dynamics.

*Chapter 6* draws the line to experimental data. The phase time series of resting state MEG data display large-scale brain activity at the edge of criticality. After reducing neurophysiological phase models from the underlying dynamics of Wilson-Cowan and Freeman neural masses, they are analyzed with respect to two complementary notions of critical dynamics.

A general discussion and an outlook of future work are provided in the final *Chapter 7*.

»Gut, daß du fragst!« sagte er lachend. »Man muß immer fragen, man muß immer zweifeln.«

Herrmann Hesse – *Demian* (1919)

# CONTENTS

<b>1</b>	<b>Introduction</b>	<b>1</b>
1.1	Neural synchronization and oscillations . . . . .	3
1.1.1	From correlated behavior to phase synchrony . . . . .	5
1.1.2	Phase synchronization of large-scale brain networks . . . . .	6
1.2	Towards modeling . . . . .	7
1.2.1	Modeling large-scale oscillatory brain networks . . . . .	8
1.2.2	Modeling neural oscillators . . . . .	8
1.2.3	Phase and amplitude description of neural oscillators . . . . .	10
1.2.4	Collective dynamics of coupled phase oscillators . . . . .	10
1.3	Contributions of the dissertation & research questions . . . . .	12
1.4	Outline of the dissertation . . . . .	13
<b>2</b>	<b>Phase reduction techniques for oscillator networks</b>	<b>15</b>
2.1	Phase dynamics of oscillator networks . . . . .	16
2.1.1	Phase definition . . . . .	20
2.1.2	Phase response . . . . .	22
2.1.3	Phase dynamics of a single oscillator . . . . .	24
2.1.4	Phase dynamics of oscillator networks . . . . .	25
2.1.5	Collective behavior . . . . .	26
2.1.5.1	Synchronization . . . . .	27
2.1.5.2	Between incoherence and full synchrony . . . . .	29
2.2	Analytic phase reduction techniques . . . . .	31
2.2.1	Center manifold and normal form . . . . .	34
2.2.1.1	Hopf normal form . . . . .	38
2.2.1.2	Nonlinear coupling terms in Hopf normal forms* . .	41
2.2.2	Identifying the Hopf normal form . . . . .	43
2.2.2.1	Kuramoto's reductive perturbation . . . . .	44
2.2.2.2	Poincaré's reduction via nonlinear transforms . . .	47
2.2.2.3	Takens' reduction via Lie brackets . . . . .	49
2.2.3	Interlude . . . . .	51
2.2.4	Winfree's reduction via isochrons . . . . .	52
2.2.5	Kuramoto's reduction via Floquet eigenvectors . . . . .	54

---

2.2.6	Ashwin & Rodrigues' reduction via $S_N \times S^1$ -symmetry . . . . .	56
2.2.7	Haken's reduction via averaging . . . . .	59
2.3	Numerical phase reduction techniques . . . . .	62
2.3.1	Adjoint method . . . . .	64
2.3.1.1	Malkin's theorem . . . . .	64
2.3.1.2	Ermentrout & Kopell's reduction . . . . .	66
2.3.2	Direct method . . . . .	68
<b>3</b>	<b>Collective behavior of coupled oscillators and their reduced phase models</b>	<b>70</b>
3.1	Networks of identical Brusselators . . . . .	71
3.1.1	Single node dynamics . . . . .	72
3.1.2	Coupled Brusselators . . . . .	72
3.1.3	Identifying the Hopf normal form . . . . .	74
3.1.4	Comparing analytic and numerical phase reductions . . . . .	75
3.1.4.1	Linear coupling . . . . .	75
3.1.4.2	Nonlinear coupling . . . . .	79
3.1.5	Other analytic phase reduction techniques . . . . .	82
3.1.5.1	Isochrons, Floquet eigenvectors, $S_N \times S^1$ -symmetry	82
3.1.5.2	Haken's reduction via averaging . . . . .	82
3.1.6	Summary & remarks . . . . .	83
3.2	Networks of identical Wilson-Cowan neural masses . . . . .	86
3.2.1	Single node dynamics . . . . .	87
3.2.2	Coupled Wilson-Cowan neural masses . . . . .	88
3.2.3	Identifying the Hopf normal form . . . . .	89
3.2.4	Haken's reduction via averaging . . . . .	93
3.2.5	Comparing analytic and numerical phase reductions . . . . .	95
3.2.6	Numerical methods identify collective dynamics . . . . .	98
3.2.7	Summary & remarks . . . . .	100
3.3	Discussion . . . . .	101
3.3.1	Low-dimensional description of network behavior . . . . .	102
3.3.2	Cluster states . . . . .	102
3.3.3	Identical versus heterogeneous oscillators . . . . .	103
3.3.4	Extended analytic phase reduction techniques . . . . .	104
3.3.4.1	Stochastic and time-varying systems . . . . .	104
3.3.4.2	Systems with delay . . . . .	108
3.3.5	Coupling functions . . . . .	110
3.3.5.1	Coupling-induced behavior . . . . .	111
3.3.5.2	Effects of structural connectivity . . . . .	116

---

3.3.6	Phase versus other oscillators	119
3.3.6.1	Nonlinear oscillators	119
3.3.6.2	Non-smooth oscillators	120
3.3.7	Phase-amplitude models	121
3.3.8	Analytic approaches versus numerics – a final word	122
<b>4</b>	<b>Interactions between networks of heterogeneous phase oscillators</b>	<b>123</b>
4.1	‘Multimodal networks’ or ‘networks of networks’?	124
4.2	Revisiting the existing theory on interacting populations of Kuramoto phase oscillators	125
4.3	Two-population dynamics along the Ott-Antonsen ansatz	128
4.4	Extension to three interacting populations	135
4.4.1	Symmetric trimodal network	137
4.4.2	Three coupled symmetric networks	140
4.5	Discussion and conclusion	142
<b>5</b>	<b>Parameter-dependent oscillatory systems</b>	<b>144</b>
5.1	Collective dynamics and parameter dependence	145
5.2	Extending the Ott-Antonsen ansatz for parameter-dependent systems	146
5.2.1	Parameter-dependent systems	147
5.2.2	General parameter distributions	151
5.3	Networks of quadratic integrate-and-fire neurons	153
5.4	Further applications	155
5.4.1	Winfree model	157
5.4.2	Limit-cycle oscillations with shear	158
5.4.3	Heterogeneous mean field models	163
5.4.4	Non-local coupling	165
5.4.5	External forcing and time delay	166
5.5	Relaxation dynamics towards the Ott-Antonsen manifold	168
5.6	Discussion and conclusion	170
<b>6</b>	<b>Criticality in neural mass phase oscillator models</b>	<b>173</b>
6.1	Scale-freeness and partial synchronization	174
6.2	Phase description of neural mass models	175
6.2.1	Wilson-Cowan model	175
6.2.2	Freeman model	177
6.3	Comparing model behavior with experimental MEG data	180
6.3.1	Power-law behavior	180
6.3.2	Functional connectivity	181
6.3.3	Synchronization	182

---

6.4	Results . . . . .	183
6.4.1	Power-law behavior . . . . .	183
6.4.2	Functional connectivity & synchronization . . . . .	183
6.5	Discussion . . . . .	187
6.6	Conclusion . . . . .	190
6.7	Appendix . . . . .	191
6.7.1	Detrended fluctuation analysis with model comparison . . .	191
6.7.2	Correlating functional and structural connectivity . . . . .	193
<b>7</b>	<b>Epilogue</b>	<b>195</b>
7.1	Revisiting the research questions . . . . .	197
7.2	Networks of complex neural oscillators and phase reductions . . . .	199
7.3	The predictive power and limitations of (reduced) phase models . .	201
7.3.1	Observables . . . . .	204
7.3.2	Modeling experimental data . . . . .	205
7.4	Coupled neural masses and other neural oscillator models . . . . .	207
7.4.1	Emergence of higher harmonics in the phase interaction function . . . . .	207
7.4.2	A note on integrate-and-fire neurons . . . . .	210
7.5	Concluding remarks and outlook . . . . .	212
<b>Supplementary material</b>		<b>215</b>
S.1	Kuramoto's reductive perturbation . . . . .	216
S.2	Higher-order corrections and nonlinear coupling . . . . .	221
S.3	Poincaré's reduction via nonlinear transforms . . . . .	226
S.4	Takens' reduction via Lie brackets . . . . .	237
S.5	Ashwin & Rodrigues' reduction via $S_N \times S^1$ -symmetry . . . . .	242
S.6	Malkin's adjoint method . . . . .	248
S.7	Limit of infinite attraction method . . . . .	249
<b>Bibliography</b>		<b>252</b>
<b>Main contributions</b>		<b>272</b>
<b>Acknowledgements</b>		<b>273</b>

# LIST OF FIGURES

2.1	A network of coupled oscillators . . . . .	17
2.2	An uncoupled planar oscillator . . . . .	18
2.3	Amplitude and phase description . . . . .	19
2.4	Phase map and isochrons . . . . .	22
2.5	Phase response of limit-cycle oscillators . . . . .	24
2.6	Non-trivial collective dynamics . . . . .	30
3.1	Stable synchrony of linearly coupled Brusselators . . . . .	78
3.2	Cluster states of linearly coupled Brusselators . . . . .	79
3.3	Stable synchrony of nonlinearly coupled Brusselators . . . . .	81
3.4	Cluster states of nonlinearly coupled Brusselators . . . . .	81
3.5	Network of two coupled Wilson-Cowan neural masses . . . . .	87
3.6	Bifurcation diagram of the uncoupled Wilson-Cowan model . . . . .	88
3.7	Phase interaction function of the Wilson-Cowan model . . . . .	97
3.8	Oscillatory regime of the Wilson-Cowan model . . . . .	99
3.9	Non-trivial network dynamics of coupled Wilson-Cowan oscillators .	100
3.10	Oscillation birth bifurcation diagram . . . . .	113
3.11	Oscillation birth network dynamics . . . . .	114
3.12	Oscillation death bifurcation diagram . . . . .	115
3.13	Oscillation death network dynamics . . . . .	115
3.14	Hagmann and small-world connectivity matrices . . . . .	117
3.15	Network dynamics with non-trivial connectivity . . . . .	118
3.16	Phase dynamics with non-trivial connectivity . . . . .	119
4.1	Two coupled networks vs. one bimodal network . . . . .	125
4.2	Bifurcation boundaries of two-population network . . . . .	130
4.3	Partial derivatives of $\partial_\kappa G$ . . . . .	132
4.4	Bifurcation boundaries (cross-section) of two-population network .	132
4.5	Bifurcation boundaries (back view) of two-population network .	134
4.6	Bistability region of two-population network . . . . .	134
4.7	Three coupled networks vs. one trimodal network . . . . .	136
4.8	Bifurcation boundaries of trimodal network . . . . .	138
4.9	Bifurcation boundaries of three-population network . . . . .	141

---

6.1	Coupling structure of both neural mass networks . . . . .	177
6.2	DTI-derived structural connectivity matrices . . . . .	178
6.3	DFA results for the $R(t)$ autocorrelations . . . . .	184
6.4	Pearson correlation values between the $P^S$ and $P^{(\text{MEG})}$ matrices . .	185
6.5	Mean values $\langle R(t) \rangle$ as function of delay and coupling strength . . .	185
6.6	Mean values $\langle R(t) \rangle$ for large coupling strengths . . . . .	186
6.7	Pearson correlation values between the $P^S$ and $S_{kl}$ matrices . . . .	194
7.1	Higher harmonics in the Wilson-Cowan phase sensitivity function .	209
7.2	Phase sensitivity functions of generic neural oscillator models . . .	210

## LIST OF TABLES

3.1	Brusselator phase models for linear coupling close to the Hopf bifurcation . . . . .	84
3.2	Brusselator phase models for linear coupling away from the Hopf bifurcation . . . . .	84
3.3	Brusselator phase models for nonlinear coupling close to the Hopf bifurcation . . . . .	85
3.4	Brusselator phase models for nonlinear coupling away from the Hopf bifurcation . . . . .	85
3.5	Wilson-Cowan phase models very close to the Hopf bifurcation . . .	96
3.6	Wilson-Cowan phase models away from the Hopf bifurcation . . . .	97

# CHAPTER 1

## Introduction

*Interaction is key –*

Life builds upon interactions in every possible way, be they imaginable or not. Interaction often bears communication, which can be regarded as a form of interaction that involves information transfer between the participating entities. Analogously to the saying “one cannot not communicate” by the communication theorist Paul Watzlawick, interaction arises naturally whenever two or more people, objects, entities belong to the same, or form a, bigger entity. A clear definition of interaction between entities implies that they act in such a manner so as to affect one another. This interplay of an ensemble of discrete units is commonly framed in the notion of a network, where it gives rise to emergent collective behavior.

One of the most fascinating examples of a complex network is the human brain. Without interaction the brain is not able to function. Coordinated and synchronized interaction facilitates communication. In this way information can be perceived, processed, and exchanged across the brain. Despite a tremendous history of brain research, however, the mechanisms behind the functioning of our brain remain a mystery. Interaction occurs on a multitude of spatial and temporal scales. But how do different neural processes interact along anatomical structures and generate recognizable patterns of functional brain activity? And, how do these patterns lead to coherent behavior and cognition? Answers to these questions have continued to elude researchers for ages.

Over the past two decades, a hypothesis has become manifest that the exchange of information and the communication in the brain occur via phase synchronization<sup>1</sup>. Synchronous firing activity within a neural population gives rise to oscillatory brain signals that are believed to encode information. Their transmission across different brain areas relies on a careful coordination of these neural oscillations. Presumably, it is the respective phase relationship between the neural dynamics that plays a key role in neuronal communication. Oscillatory behavior abounds on all different scales of the human brain. On mesoscopic and macroscopic levels one often refers to these oscillations as brain rhythms<sup>2–4</sup>. Different frequency bands have been associated with distinct cortical functions. A disruption of the regular interplay of this oscillatory activity, such as the suppression of certain frequencies, is often deemed a signature for pathologies<sup>5,6</sup>. All the more it is important to understand the underlying mechanisms how these oscillations emerge, evolve, and dissolve under a changing environment, and how cortical oscillations interact and influence each other in order to generate large-scale synchronization patterns. Understanding the neuronal and cortical mechanisms that are linked to perception, to cognitive and motor functions, but also to diseases, is among the most important and yet unresolved problems of this century<sup>1,7–10</sup>. Oscillatory network activity is central to this dissertation.

There are numerous approaches to unravel the mysterious orchestration of in-

tertwined neural processes, both experimental and theoretical. Bridging the gap between experiments and theory, however, has only been achieved in very restrictive cases and mainly on very small scales. An overall and generic picture linking these two sides of the same coin is still being sought for. To detect brain rhythms experimentally, neuroimaging techniques such as electro- or magnetoencephalography (EEG/MEG) or functional magnetic resonance imaging (fMRI) are commonly resorted to. EEG and MEG measure voltage fluctuations resulting from ionic currents within the neurons, i.e. they record electrical activity of the brain. On the other hand, fMRI detects changes of the cerebral blood flow via the so-called BOLD contrast, which is an indirect marker of brain activity. Given the non-invasive nature of these techniques, the recorded data display synchronous activity of several thousands of interacting neurons rather than the dynamics of a single neuron. This population dynamics, or mean field behavior, has often very little in common with what happens on the microscopic scale. An urgent challenge in theoretical neuroscience is to deduce macroscopic dynamics from activity on these much smaller scales<sup>11–15</sup>.

## 1.1 Neural synchronization and oscillations

The functioning of the human brain dwells on coordinated and coherent co-activity of a multitude of neurons. Perceptual, cognitive and motor functions are believed to require an orchestration of distributed neuronal processes. If spike discharges of a large number of neurons exhibit correlated behavior in different areas of the brain, their (large-scale) integration leads to, e.g., cognition or limb movements. Unraveling this integration process poses an intriguing question in itself, and is often referred to as the *binding problem*<sup>16</sup>. The mechanisms to bind distributed neuronal activity can broadly be classified in two different but complementary strategies. On the one hand, *binding by convergence* results in the grouping of specialized neurons that encode a particular fixed constellation of contextual features. On the other hand, *dynamic binding* assembles individual neurons dynamically to generate and represent a particular pattern at a particular point in time<sup>17</sup>. One neuron can participate in the representation of one pattern in one moment, but an instant later it is involved in encoding a different pattern. This dynamic and flexible recruiting of neurons and/or neuronal populations is called assembly coding<sup>18–20</sup>. The high temporal precision of synchronizing neuronal discharges in the millisecond range allows for generating a sequence of subsequently active assemblies, which can effectively encode complex information to be exchanged among cortical networks. Time is thus an important coding dimension to process and exchange information.

As hypothesized, e.g., by Buszaki and co-workers<sup>21</sup>, the temporal organization of neuronal activity capitalizes on self-organized information retention and local-global integration. The ability to preserve and store information is just as important as integrating distributed local processes into globally ordered states and controlling local computations through global brain activity. Moreover, these two features can be maintained by a hierarchical system of brain rhythms<sup>3,4</sup>. Hence, synchronization of cortical activity and neural oscillations can be considered hallmarks of the temporal coordination of distributed brain activity.

Brain oscillations as characterized by rhythmic changes in, e.g., local field potentials, set a recurrent temporal reference frame and thereby allow for temporal coding within oscillatory cycles. The ups and downs in fluctuating local field potentials reflect high and low degrees, respectively, of the synchronization of neuronal currents within a certain brain area. That is why synchronization and neural oscillations are often used interchangeably to express coherent activity of a population of neurons. However, there is a subtle difference between the two phenomena<sup>18</sup>. Oscillatory activity, on the one hand, can be induced on a population level through single oscillatory neurons, so-called pacemaker cells. It may also manifest as an emergent property of the underlying network architecture when a particular dynamic circuit motif is activated. Such a motif comprises the physical circuit structure, its electrophysiological signature, and the corresponding computational function<sup>22</sup>. Upon activation it leads to characteristic rhythmic neuronal activity. Synchronization, on the other hand, can occur in the absence of oscillations. Two cells may always discharge simultaneously but at irregular intervals when driven by common noise. Or, a presented stimulus induces simultaneous bursting of neural populations. This is a typical signature of response synchronization, which can be non-repetitive, but also recurrent. In this way, synchronization can lead to oscillations. Similarly, oscillations may facilitate synchronization. For instance, shared oscillatory input can drive a neural population close to the firing threshold where it becomes prone to particular stimuli that induce response synchronization. Oscillatory activity can thus be seen as an indicator for synchrony.

While oscillatory population activity can be related to synchronous interaction of single cells, one should be careful when relating single cell responses to synchronous network activity. There is a certain microscopic-macroscopic dichotomy with respect to the transition from individual neuronal dynamics to the collective behavior of a neural population. It may happen that individual discharges of a neuron are precisely time-locked with the oscillating field potential, but the auto-correlation function does not show any sign of oscillatory activity on the neuron level. The seminal work by Brunel and Hakim offered a theoretical account of a collection of experimental studies hinting at so-called sparse synchronization of

neuronal networks<sup>23</sup>. By contrast, regular spiking activity of single neurons does not necessarily result in (regular) oscillations on the population level, but can also lead to collective chaos, see, e.g., the recent modeling study<sup>24</sup>. Likewise, asynchronous network states can emerge in spite of a considerable amount of shared input<sup>25</sup>. Discernible neural network activity depends on correlated activity of a large number of neurons. Such neural correlation, or synchronization, occurs on some (smaller or larger) time scale, and with or without oscillations. Moreover, synchronous oscillations produce and enhance temporal correlations between neurons, thus providing a temporal reference frame for encoding and decoding information. A temporal structure of neural responses is crucial for distinguishing synchronous from asynchronous states, and for establishing synchronization over large distances<sup>18</sup>. For this reason, it is widely accepted that brain rhythms and cortical oscillations play an important part in neural communication, which is underlined by the abundant literature on rhythmic, synchronous brain activity. In the remainder of this dissertation the cellular and circuit basis of emergent collective dynamics will not be addressed further; the interested reader is referred to the extensive review by Wang<sup>26</sup> for more details.

Different brain rhythms may indicate different states and functions, which require integration of neural processes at different temporal and different spatial scales. Brain rhythms cover a broad range of different frequency bands spanning more than four orders of magnitude<sup>3</sup>. The higher the frequency, the higher the temporal precision. By contrast, the amplitude of oscillations increases for lower frequencies, which hints at a bigger size of a synchronously active cell assembly. By this, binding by synchrony can be achieved over large distances. The focus of this dissertation lies on synchronization effects of large-scale brain networks, hence on rather slow-frequency but robust oscillations of cortical activity. Here, a particular kind of synchronization becomes attractive for identifying the network dynamics, which builds on the concept of phase synchronization.

### 1.1.1 From correlated behavior to phase synchrony

In general, synchronization indicates (time-)coordinated interaction. When considering time series of experimental or synthetic data, synchrony manifests in some correlation structure of the respective time series. There exists a variety of synchrony measures that help to classify the kind and quantify the degree of synchronized activity. Synchrony measures range from correlation coefficients to magnitude-squared coherence, from phase coherence to Granger causality, from phase synchrony indices to information-theoretic divergence measures, and from state space based measures to stochastic event synchrony measures<sup>27</sup>. Some of these measures show a strong correlation among one another, whereas others are

independent from the rest. When studying a population of neurons, neuronal synchrony measures<sup>28</sup> can be used to quantify the degree to which firing rates of individual neurons are related. Typically, a synchrony measure is normalized between 0 and 1, with 0 denoting an asynchronous, or incoherent, state, whereas 1 refers to full synchronization when the individual firing times are all identical. In the following, I will usually assume that the mean firing rate of a neuronal population fluctuates rhythmically around some mean value. If two or more of such populations interact, it is convenient to describe the degree of synchronization between them in terms of the characteristics of their oscillatory dynamics.

Oscillations, generally speaking, are characterized through their *frequency* and *amplitude*. For a given frequency, one can define the *period* as the duration of time of one cycle of oscillation. The period is the time needed between successive occurrences of, e.g., the same level of activity. In between those periods, one can further determine the *phase* of oscillation, which continuously increases between 0 and  $2\pi$  during one period and thereby indicates the fraction of period already covered. Phase and amplitude thus become the main (time-resolved) determinants of the state of oscillation. Consequently, oscillatory neural activity is commonly analyzed with respect to their phase and amplitude dynamics.

For interacting neuronal populations it appears natural to use synchrony measures that refer to the corresponding phases and amplitudes. Instantaneous phases and amplitudes can be extracted from the signals by the Hilbert transform or by time-frequency transforms. Phase synchrony measures<sup>29</sup> aim at quantifying the closeness of the phases when mapped on the unit circle. Alternative measures often dwell on mutual information such as the frequency coherence in the time-frequency domain. They are strongly correlated with phase synchrony measures, but, strictly speaking, not directly linked<sup>27</sup>. And, there are also measures that analyze the amplitude synchronization of oscillatory dynamics. When considering only weak coupling regimes, however, amplitude modulations can be widely discarded. In consequence, the relevant information about the network state can be inferred exclusively from phase synchrony measures.

### 1.1.2 Phase synchronization of large-scale brain networks

Brain rhythms and neuronal oscillations become predominant for describing brain dynamics when considering meso- or macroscopic spatial scales. This is underlined by a plethora of experimental studies relying on both invasive and non-invasive neuroimaging techniques. There is reason to believe that information processing in the brain is intrinsically linked to synchronization phenomena of oscillatory dynamics<sup>30,31</sup>. Non-invasive EEG and MEG studies typically depict distributed

cortical activity as of large-scale brain networks. Although M/EEG recordings have high temporal resolution, they reflect activity on rather coarse spatial scales given that signals to be perceivable require synchronous neuronal currents of a large number of neurons, commonly of the order of  $10^4$  to  $10^5$  cells. The resulting time series of the recordings are duly and extensively analyzed for their extracted phase and amplitude dynamics. Emerging synchronization patterns in the data are then assigned to particular brain functions corresponding to the underlying hypothesis or the behavioral observations. The research on the phase dynamics of cortical oscillatory activity is rather recent compared to amplitude modulations in the M/EEG. However, there are several reports indicating that the phase dynamics play a crucial role for information processing and inter-cortical communication<sup>1,32–35</sup>. Phase synchronization plays also an integral part in defining functional connectivity structures of the brain. The technological advance of modern brain imaging methods has led to elucidate the interplay of structural and functional brain connectivity. The structure of anatomical connections between brain areas is widely believed to facilitate temporal synchronization of neural activity, and thus leads to spatial patterns of functional connectivity, even in spatially remote areas. Yet, the extent to which structure shapes function is still unclear<sup>36,37</sup>. In order to unveil functional brain connectivity, it is crucial to identify functional modules consisting of remote but synchronized neuronal populations. This can be achieved by analyzing the phase dynamics of the different brain areas.

## 1.2 Towards modeling

Mathematical theory and computational modeling have gone along with experimental neuroscientific research ever since. The theoretical underpinning of experimentally observed behavior does not only support research paradigms, but, importantly, adds to the general scientific knowledge. Modeling helps to understand the mechanisms behind complex behavior. At the same time, it can provide crucial information about future study design and save time and money otherwise spent for long and expensive, yet foredoomed experiments. That does not mean that models downgrade or diminish the importance of experiments. On the contrary, experiments are invaluable for scientific progress. Modeling can aid to explain and even predict particular phenomena, and thereby shape experimental observations. In this regard, a careful conception of underlying assumptions is vital to build relevant and verifiable models, which are fundamental for a comprehensive theory where models and experiments go hand in hand.

### 1.2.1 Modeling large-scale oscillatory brain networks

Much progress has been made in the direction of theoretical, mathematical and computational neuroscience. There exists a plethora of physiologically motivated and highly accurate neuronal models to investigate synchronization properties. Given their inherent complexity, a thorough analysis can be challenging even despite ever increasing computational capacities. In some cases, models of cortical oscillations can be simplified to coupled phase oscillators, which often take a modified form of the seminal Kuramoto model<sup>38–40</sup>. In recent years, the use of phase oscillator models has been popularized in order to describe synchronization phenomena of oscillatory neural networks<sup>see, e.g., 41–49</sup>. Phase models have been widely used to explain anatomical effects on synchronization in terms of functional connectivity<sup>50–55</sup> as well as on the route of synchronization<sup>56,57</sup>. The emergence of functional modules can exemplarily be explained through remote synchronization of phase oscillators<sup>58,59</sup>. And also spatial patterns in the visual cortex have been modeled in a similar way<sup>60</sup>. Moreover, local population dynamics may play a significant role in shaping functional connectivity patterns, and neural phase oscillator models have been successfully used to explain how changes in the local dynamics affect functional connectivity<sup>61</sup>. Phase models have also been applied to investigate the effect of cortical lesions on overall dynamics by introducing random perturbations to a synchronized state<sup>62</sup> or by removing network nodes<sup>63</sup>. Similarly, the concept of the brain as a dynamical system close to a critical regime has been manifested through the analysis of phase models <sup>see, e.g., 64–68</sup>.

The wide use of phase oscillator models in neuroscience, however, comes at a price. Despite the simplicity of phase oscillator dynamics, the reduction to phase models requires great care. Any (heuristic) approximation of an oscillatory neural network with a phase model has to withstand the confrontation with the extracted or, alternatively, rigorously reduced phase dynamics of the original dynamics of interacting neural oscillators. By avoiding this intermediate step of phase reduction the phase description of the oscillatory model is bereft of its fundamental justification. The link from the actual dynamics to the phase model may become spurious and its validity questionable. Certainly, a rigorous derivation from the underlying dynamics to the phase dynamics can be laborious. But doing so will clearly add to the significance of the network analysis and, more importantly, to its impact in the scientific world.

### 1.2.2 Modeling neural oscillators

In view of large-scale oscillatory brain networks, the elementary network components can be assumed to be neural populations consisting of a large number of

neurons. Modeling the collective dynamics of a population of neurons experienced a literal boost in the 1970s, when various phenomenological neural mass models emerged as mean field models of neural population activity<sup>69–76</sup>. Phenomenological models are advantageous in that they pass over the cellular and circuit properties of the neural populations and thereby avoid to resolve an often recurring dichotomy between seemingly stochastic dynamics of single neurons and synchronous collective dynamics<sup>26</sup>. Rather, they aim at integrating a handful of general assumptions on the collective of neurons, which results in coarse-grained macroscopic variables that describe the neural mass behavior. Traditionally, the notion of a neural mass model has been introduced as a form of an ensemble density model<sup>75</sup>. The full ensemble density is replaced with a mass at a particular point, i.e., a delta function, and the density dynamics is summarized by the location of that mass. The resulting neural mass model then comprises a set of differential equations that describe the evolution of the (expectation of a) probabilistic mode of the system<sup>11</sup>. Ignoring all higher moments, neural mass models are comparably simple mean field models. The simplicity in terms of only a few coupled differential equations is however undermined by their nonlinear character, typically involving a variant of a sigmoid function.

A seminal neural mass model has been proposed by Wilson and Cowan<sup>69,70</sup>. It describes the (mean) activity of excitatory and inhibitory neurons within a population of synaptically coupled neurons. Among the plethora of different approaches to model collective neural activity, it stands out for the fact that it can be readily derived from microscopic single-neuron descriptions and it provides at the same time a comprehensive link toward macroscopic descriptions of cell assemblies<sup>77</sup>. It can be viewed as an intermediate but in some sense generic description of a densely connected neural population as in a particular cortical region<sup>42</sup>. When assuming strong coherence within a certain area, the ensemble activity can be approximated by the population mean and the effect of the variance is negligible, which motivates the mean field approach over a Fokker-Planck approach to describe the collective dynamics<sup>15</sup>. Accordingly, the Wilson-Cowan neural mass model represents the interdependent collective neuronal dynamics in terms of the mean firing rates of the excitatory and inhibitory parts of the population. It exhibits rich dynamic behavior as well as different transitions to oscillatory dynamics<sup>78,79</sup>. This makes it also exemplary for a neural oscillator model. For a particular choice of parameters, the model features stable limit-cycle oscillations between the firing rates of the excitatory and inhibitory neurons, respectively. These oscillations reflect a waxing and waning of locally synchronized (firing) activity. Hence, synchronization within a neural population is crucial for generating (local) cortical oscillations of a neural mass.

### 1.2.3 Phase and amplitude description of neural oscillators

Rhythmic behavior of neural mass models is manifested in the oscillatory dynamics of the macroscopic variables. If these dynamics are periodic, then the phase space spanned by the macroscopic variables exhibits a limit cycle. This limit cycle can be conveniently parametrized by a scalar phase variable, so that the state of the neural oscillator is identified by a unique value between 0 and  $2\pi$  during one period of oscillation. If this limit cycle is stable, then the dynamics in a close vicinity will be attracted towards the limit cycle. In this case, the distance to the limit cycle can be captured by so-called amplitude variables. Taken together, the dynamics of a neural oscillator can be rewritten in terms of phase and amplitude variables. In general, this reformulation does not lead to a reduction of dimensionality and the dynamics of the phase-amplitude model are as complex as the original dynamics. However, if the attraction to the limit cycle is sufficiently fast, then the dynamics away from the limit cycle can be approximated by the dynamics on the limit cycle. Thus, the possibly high-dimensional dynamics of the neural oscillator can be uniquely identified by a one-dimensional phase variable.

This phase reduction becomes especially useful when studying a network of interacting neural oscillators. The analysis of the full system is daunting and a simplification desirable. The phase reduction approach retains its justification as long as interactions are weak, that is, the coupling strength between oscillators is sufficiently small. To be precise, the coupling is weak enough to invoke only small perturbations off the respective limit cycles so that amplitude effects are negligible. The reduced phase model can be analyzed along the well-established techniques for networks of coupled phase oscillators. Eventually, the resulting findings on the synchronization properties of the network are equally valid for the full system under the assumptions inherent to the preceding phase reduction.

### 1.2.4 Collective dynamics of coupled phase oscillators

The analytical and computational advantage of phase dynamics is striking when compared to high-dimensional and typically nonlinear dynamics of oscillatory neural networks. As mentioned earlier, phase synchrony measures provide a convenient means to quantify the correlation between phase time series. In fact, such a measure introduces a powerful macroscopic observable that allows to describe the qualitative collective dynamics of an oscillatory network. When considering a network of globally coupled phase oscillators, as is, e.g., the Kuramoto model, there exists a rigorous theory to describe the state of the network with a few macroscopic variables. Following either the Watanabe-Strogatz<sup>80</sup> or the Ott-Antonsen theory<sup>81–83</sup>, the time evolution of these macroscopic variables can be exactly de-

rived if the network satisfies some generic conditions, which will be addressed in more detail later. It thus becomes possible to characterize low-dimensional behavior of the collective dynamics in a straightforward way.

Given that we deal with phase time series, we have to assess their correlation in terms of circular, or directional, statistics<sup>84</sup>. Identifying each phase  $\phi \in [0, 2\pi)$  as a point  $z \in \mathbb{C}$  on the complex unit circle  $\{z \in \mathbb{C}: |z| = 1\}$  through  $z = e^{i\phi}$ , the  $n$ th moment  $m_n$  of the (circular) distribution of phases is given by

$$m_n = \int_0^{2\pi} P(\phi) z^n d\phi ,$$

where  $P(\phi)$  is the probability density function of the circular distribution. For a finite set of phases,  $\phi_k$ ,  $k = 1, \dots, N < \infty$ , these moments are analogously defined as

$$m_n = \frac{1}{N} \sum_{j=1}^N z_j^n , \quad \text{with} \quad z_j = e^{i\phi_j} .$$

In the physics literature, the first moment  $m_1$  is usually referred to as the complex-valued *Kuramoto order parameter*<sup>38</sup>  $Z \in \mathbb{C}$ ,

$$m_1 = Z = R e^{i\Psi} \quad \text{where} \quad R = |m_1| \quad \text{and} \quad \Psi = \arg(m_1) .$$

The Kuramoto order parameter is the main observable within the Watanabe-Strogatz and Ott-Antonsen theories, and its time evolution is found to follow a low-dimensional system of ordinary differential equations. The absolute value  $R = |Z|$  is sometimes called the real-valued Kuramoto order parameter<sup>[1]</sup>. It takes values between 0 and 1. If  $R = 0$ , then all phases are equally distributed along the complex unit circle and the corresponding macroscopic state is said to be asynchronous. By contrast, if the network is fully synchronized and all phases are identical, then  $R = 1$ . When analyzing experimentally recorded data and the extracted phase time series, one also resorts to the circular variance  $CV = 1 - R$ , which is 0 for full synchrony, and increases up to  $CV = 1$  the more asynchronous the network dynamics become.

Throughout the dissertation, the Kuramoto order parameter will serve as the main macroscopic observable to quantify the collective dynamics of oscillatory networks. It can also be applied to only a subset of oscillators. In this way, it is possible to quantify the coherence within substructures of the network, which have previously been identified, e.g., by means of phase clustering. Likewise, one can determine population-specific degrees of synchronization when a network consists

---

<sup>[1]</sup> Alternatively, we can compute  $R = |Z| = \sqrt{C^2 + S^2}$  with  $C = \frac{1}{N} \sum_j \cos \phi_j$  and  $S = \frac{1}{N} \sum_j \sin \phi_j$ .

of multiple populations of phase oscillators. The interplay between these *local* Kuramoto order parameters then allows to draw conclusions about such network-network interactions in terms of their respective collective dynamics.

## 1.3 Contributions of the dissertation & research questions

The modeling of phase synchronization phenomena in oscillatory neural networks is the recurrent theme of this dissertation. In the preceding sections, the fundamental ideas of synchronizing neural oscillations and their putative key role for cortical communication have been addressed. As mentioned above, a comprehensive theory of the functioning of the brain builds upon both experiments and theoretical models. I focus on the modeling of neural dynamics and the interaction of oscillatory activity across different brain regions. Aiming for a mathematically rigorous model description, the immediate link to experimental data may appear spurious in some of the following chapters. Nevertheless, this rigor is important to rule out model-inherent inconsistencies when explaining experimental observations. In the end, a unifying theory of the brain will not be complete unless exact models can explain the mechanisms leading to experimentally observed behavior and withstand scrutiny from both a theoretical and experimental perspective. In this regard my dissertation scrutinizes existing approaches to explain phase synchronization phenomena in oscillatory neural networks.

The main contributions are twofold. The first part provides an extensive introduction to phase reductions of general oscillatory networks. As an inventory of different phase reduction techniques, its contribution is mainly methodological. In due course, the examination of existing techniques, their comparison and juxtaposition, as well as extensions of the techniques have been guided along the question

- *What is the best way to distill the phase dynamics of a complex oscillatory network?*

The second part addresses more specific applications of phase models in the realm of computational neuroscience. The aim is to explore the scope of phase oscillator networks for describing neuronal synchronization phenomena. Accordingly, a rigorous reduction of oscillatory neural networks into appropriate phase models is here of less concern than identifying which synchronization patterns can be realized when focusing on phase dynamics alone. The key advantage of phase models is that a particular class of them can be rigorously analyzed within the

Ott-Antonsen theory. Describing the network synchronization in terms of the Kuramoto order parameter introduced above, the theory allows to derive an exact low-dimensional system of differential equations that governs the time evolution of the Kuramoto order parameter. An immediate question is whether the restrictions on the class of phase models applicable for the Ott-Antonsen theory can be loosened. The corresponding research question thus reads:

- *Under which circumstances can a low-dimensional description capture the collective dynamics of complex phase oscillator networks?*

Even if phase models do not fall in the applicable class, the concept of phase synchronization remains very appealing for its direct expression in the easy-to-interpret Kuramoto order parameter. This suggests to reduce biophysically realistic neural oscillator models into phase models. While the former establish an immediate link to neural recordings, the latter conveniently capture the phase dynamics of interest. But, and this becomes the third research question:

- *Do phase oscillator networks cover seminal characteristics of experimental data from the cortex?*

This dissertation strives for shedding light on these three research questions. They are, understandably, intricately linked with one another. Yet, answers to them have to be found in different fields such as nonlinear dynamics, complex systems, and bifurcation theory. Combining insights from mathematical analyses, numerical simulations and experimental data analysis will aid to explore and to model phase synchronization phenomena of oscillatory neural networks.

## 1.4 Outline of the dissertation

In *Chapter 2* I provide the mathematical backbone of phase reduction techniques. After a more general introduction to the phase description of oscillator networks, I explicate different analytic and numeric phase reduction techniques including an outline of the mathematical theory that is necessary to distill the phase dynamics from network models of coupled oscillators.

The different reduction techniques will be applied subsequently to two classic examples in *Chapter 3*. Performing the phase reductions point-by-point allows for a thorough comparison between analytic and numeric techniques as well as between model predictions and the actual collective network behavior.

*Chapter 4* is devoted to network-network interactions between populations of heterogeneous phase oscillators. Dwelling on the Ott-Antonsen ansatz, I derive the

governing equations of the collective dynamics of two coupled networks and investigate their possible synchronization patterns. Moreover, I compare the macroscopic dynamics to those of a single network with a bimodal frequency distribution.

In *Chapter 5* I extend the applicability of the Ott-Antonsen ansatz to parameter-dependent oscillatory systems. This is illustrated for a network of quadratic integrate-and-fire neurons, for which I derive the exact dynamics of the macroscopic observables. Moreover, I briefly revise a variety of further complex network examples that fall within the class of parameter-dependent systems that is applicable for the Ott-Antonsen ansatz and thus entails a low-dimensional description of the network dynamics.

The model performance of neurophysiological phase oscillator networks is tested against experimental data from the human cortex in *Chapter 6*. The resting state MEG data feature two distinct notions of criticality, namely partial phase synchronization and scale-free temporal dynamics. Given two seminal neural mass models, their respective phase dynamics is derived and analyzed with respect to these two dynamical features of criticality.

Finally, *Chapter 7* provides a general discussion of the results of this dissertation and their implications. The use of phase models in computational neuroscience thrives on the straightforward link to identify (phase) synchronization phenomena in networks of coupled neural oscillators. In view of the main research questions I will reflect on the reduction of phase models from complex oscillator networks, on the power of such phase models and on the involved macroscopic observables. I also address the modeling of complex dynamic spectra of experimental data, the representativeness of neural mass models as neural oscillators and possible extensions of the presented work.

# CHAPTER 2

## Phase reduction techniques for oscillator networks

*Investigating the dynamics of a network of oscillatory units is a timely and urgent topic at the frontiers of science. Often, the focus is on phase synchronization properties that are believed to play an important role in information transfer within a network. Defining the phase dynamics, however, is not a trivial task per se. The literature provides an arsenal of solutions, in particular for the case of so-called weakly coupled oscillators. Here, we provide a catalogue of popular techniques for deriving such phase dynamics. They fall into three classes. (i) Many phase reduction techniques starting off with a Hopf normal form description provide mathematical rigor. Unfortunately, they come with a caveat in that the proper normal form has to be derived first. We explicate several ways to do that, both analytically and numerically. (ii) Other analytic techniques capitalize on time scale separation and/or averaging over cyclic variables. While appealing for their more intuitive implementation, they often lack accuracy. (iii) Direct numerical approaches help to identify non-trivial network behavior but come at the cost of exhaustive and laborious parameter scans. We here review the necessary mathematical details that underlie the different phase reduction techniques and prepare them for further application.*

Adapted from: Pietras B., Daffertshofer A. (2018). *Network dynamics of coupled oscillators and phase reduction techniques, (Sections 2 – 4)*. Under review.

## 2.1 Phase dynamics of oscillator networks

Recorded signals from oscillator networks often stand out for their dynamical richness, which is typically manifested in non-trivial or complex macroscopic dynamics. In a network, macroscopic complexity emerges through an interplay of the activity of individual nodes. The interaction between the nodes can hence be considered crucial for the complexity of the network as a whole. To provide a dynamical account of this macroscopic behavior, one typically introduces phases and amplitudes at every node, even if the precise oscillator dynamics are unknown. In fact, this dynamics might already be very complicated. However, if phase-amplitude interactions can be neglected at the nodal level, the respective phase and amplitude dynamics decouple from one another. In this case it suffices to focus on the first. Eventually, the macroscopic network dynamics can be expressed in terms of nodal phases only. The separation of phase and amplitude dynamics at the nodal level is a typical characteristic of weakly connected networks, or, more specific, *weakly coupled oscillators*. The attribute ‘weak’ implies that at every node, perturbations through external forcing or internal coupling are sufficiently small when compared to the size of the state variable of the unperturbed, single-node dynamics. Large perturbations may induce a qualitative change in the network dynamics rather than mere quantitative adjustments that, in the case of isolated perturbations, will lead to an asymptotic return to the state prior to the perturbation. Put differently, there is a critical strength of perturbation at which the network undergoes a transition from one macroscopic behavior to a qualitatively distinct macroscopic behavior. This critical value is arguably reached whenever a bifurcation in the dynamics occurs in at least one of the nodes. Then, dynamical systems theory no longer allows for describing the node evolution by its linear approximation. We will hence assume that this critical perturbation strength will not be exceeded, implying that the nodes of the network are weakly coupled.

To illustrate a weakly coupled network, we sketch five nonlinear oscillators in Fig. 2.1. Every node shows oscillatory behavior in the two-dimensional state variables  $\mathbf{x}_k = (x_k, y_k) \in \mathbb{R}^2$ ,  $k = 1, \dots, 5$ . In the absence of coupling, the nodal dynamics will converge towards stable limit cycles in the  $x - y$  planes shown in Fig. 2.2. There is a closed orbit in the coordinate plane<sup>[1]</sup> spanned by the two state variables  $x_k$  and  $y_k$ . Each of the state variables is periodic in time,  $x_k(t) = x_k(t+T)$

---

<sup>[1]</sup> Usually, this coordinate space is called the phase space. In two dimensions, it is also referred to as the phase plane of  $x_k$  and  $y_k$ . However, to avoid confusion between the ‘phase as a state’ and the ‘phase as function of time’, we stick to the notion of ‘coordinate plane’. For the same reason we do not adopt the notion of ‘phase transitions’ but rather refer to ‘qualitative changes in macroscopic behavior’ to describe the transition from one dynamical regime of the collective dynamics to another.

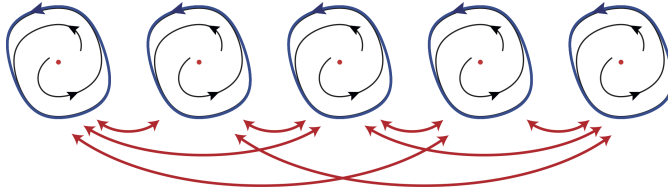


**Figure 2.1:** A network of weakly coupled planar limit cycle oscillators. Each oscillator  $k = 1, \dots, N = 5$ , is described in the two-dimensional state variables  $\mathbf{x}_k = (x_k, y_k)$ . The coupling between oscillators is depicted as red arrows. Without coupling, each oscillator follows the blue limit-cycle trajectory. Upon perturbation, the oscillator will be kicked away from the limit cycle and follows a trajectory that leads exponentially fast towards the globally attracting limit cycle. Globally attracting implies that the basin of attraction spans the whole  $x - y$  plane except for the unstable origin (red). Two trajectories from within the basin of attraction are shown in black.

and  $y_k(t) = y_k(t+T)$  for some period  $T > 0$ . On the limit cycle, one can introduce a phase  $\theta^c = \theta^c(t)$  that increases monotonically from 0 to  $2\pi$  during one period  $T$  after which it is reset to zero – throughout this *Chapter*, the superscript  $\mathcal{C}$  indicates that the variables are evaluated exactly on the limit cycle. A perturbation, e.g., via the coupling to another oscillator  $\mathbf{x}_{j \neq k}$ , can kick the oscillator away from its limit cycle. If the perturbation is weak enough and the oscillator remains in the so-called basin of attraction of the limit cycle, the oscillator’s trajectory will spiral back into the limit cycle; see Fig. 2.3 (panel a). As will be shown below, also in this case a monotonically increasing  $2\pi$ -periodic phase can be defined that we will denote as  $\theta = \theta(t)$ .

Next to the phase, one can define an amplitude variable  $r_k$  that describes the distance to the limit cycle. This amplitude variable is different from the actual amplitude  $R_k$  of oscillator  $k$ , which is given as the (Euclidean) distance to the center of oscillation, which we set to the origin, such that  $R_k^2 = x_k^2 + y_k^2$ ; Fig. 2.3 (panel b). While the amplitude of the limit cycle oscillation  $R_k^c$  wobbles steadily around a constant, non-zero value, the amplitude  $R_k$  approaches  $R_k^c$  after a short transient. By contrast, the amplitude variable  $r_k$  is the distance to the limit cycle:  $r_k = R_k^c - R_k$ . It converges to zero as the oscillator reaches the stable limit cycle. In general, one can convert the amplitude variable  $r_k$  to the actual amplitude of oscillation  $R_k$  and vice versa. In the following, we will refer to the distance to the limit cycle  $r_k$  as the amplitude dynamics unless stated otherwise.

Phase and amplitude descriptions can readily be extended to oscillatory dynamics in more than two dimensions. And, if oscillators approach their respective limit cycles exponentially fast, one can focus solely on the phase dynamics. The different time scales at which fast amplitudes and rather slow phases evolve allows for time scale separation. If additionally the perturbations are sufficiently weak so that the oscillators are not kicked too far off the limit cycle trajectory, the ampli-

tude values will converge to their asymptotic value in a fraction of a period; see Figure 2.3. Hence, it appears reasonable to consider the amplitudes constant and approximate them with their asymptotic values. In consequence, one can represent a high-dimensional dynamics at every node by its one-dimensional phase dynamics only. This greatly facilitates the study of synchronization and other complex collective phenomena in oscillator networks.

In the following, we will provide a rigorous account of how the network dynamics of weakly coupled oscillators can be reduced to a phase model. To do so, we presume that the network consists of  $N \gg 1$  nodes, whose dynamical state is given by the vector  $\mathbf{x}_k = \mathbf{x}_k(t) \in \mathcal{X}$ ,  $k = 1, \dots, N$ , where  $\mathcal{X} \subset \mathbb{R}^n$  is an  $n$ -dimensional state space. The evolution of the state vector is governed by the dynamical system  $\dot{\mathbf{x}}_k = \mathcal{F}_k(\mathbf{x}_1, \dots, \mathbf{x}_N; \mu_k)$ , which shall be of the form<sup>[2]</sup>

$$\dot{\mathbf{x}}_k = \mathbf{f}_k(\mathbf{x}_k; \mu_k) + \kappa \mathbf{g}_k(\mathbf{x}_1, \mathbf{x}_2, \dots, \mathbf{x}_N) . \quad (2.1)$$

The function  $\mathbf{f}_k: \mathbb{R}^n \rightarrow \mathbb{R}^n$  determines the node-specific dynamics without coupling, while  $\mathbf{g}_k: \mathbb{R}^{N \times n} \rightarrow \mathbb{R}^n$  comprises all coupling effects on oscillator  $\mathbf{x}_k$  through other nodes  $\mathbf{x}_{j \neq k}$ . The overall coupling strength is denoted by  $\kappa \in \mathbb{R}$  and  $\mu_k$  are bifurcation parameters. We will further impose three main assumptions:

- (1) The network is weakly coupled. In particular, we assume that the coupling strength  $\kappa \ll 1$  is sufficiently small that it cannot induce bifurcations, that

<sup>[2]</sup> In general, the vector field  $\mathcal{F}_k = \mathcal{F}_k(\mathbf{x}_1, \dots, \mathbf{x}_N, t)$ , and hence also  $\mathbf{f}_k = \mathbf{f}_k(\mathbf{x}_K, t)$  and  $\mathbf{g}_k = \mathbf{g}_k(\mathbf{x}_1, \dots, \mathbf{x}_N, t)$ , can explicitly depend on time  $t$ . The theory developed below also holds in this non-autonomous case. For the sake of conciseness, however, we consider here only autonomous individual dynamics  $\mathbf{f}_k$  and state-dependent coupling  $\mathbf{g}_k$  without further time variations and refer to *Section 3.3* for a corresponding discussion.

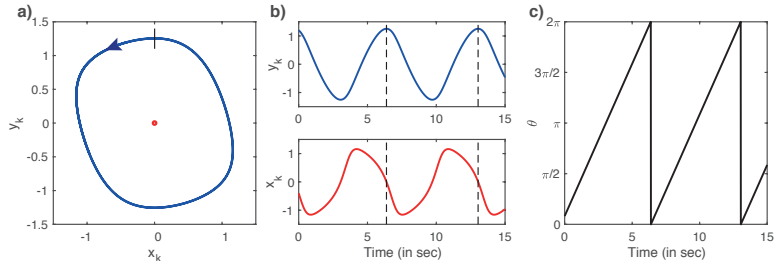


**Figure 2.2:** An uncoupled planar limit cycle oscillator. (a) The two-dimensional state variable  $\mathbf{x}_k = (x_k, y_k)$  follows a closed periodic orbit in the  $x - y$  plane, the oscillator's limit cycle. (b) The state variables  $x_k(t) = x_k(t + T)$  and  $y_k(t) = y_k(t + T)$  are periodic in time. (c) The corresponding phase  $\theta$  of the oscillator increases monotonically between 0 and  $2\pi$  during one period  $T$ . We choose a reference point on the limit cycle where the value of  $y_k$  is maximal, see the dashed lines in (a) and (b). Whenever the oscillatory crosses this point, the phase is reset to  $\theta = 0$ .

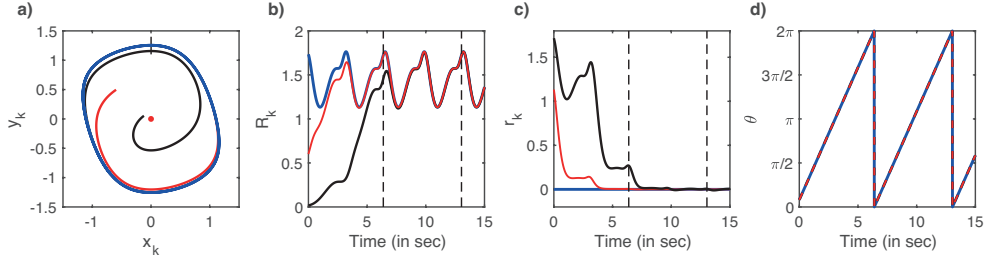


**Figure 2.3:** Amplitude and phase description. (a) Two trajectories (black, red) converge to the oscillator's limit cycle (blue). (b) The amplitudes in oscillation  $R_k^2 = x_k^2 + y_k^2$  as the distance from the origin. (c) The amplitudes  $r_k = R_k^c - R_k$  denote the distance from the limit cycle  $\mathcal{C}$ . (d) The respective phases  $\theta$  coincide for all times  $t \geq 0$ .

is,

$$0 < |\kappa| \ll |\mu_k| \ll 1.$$

- (2) The oscillators are nearly identical, i.e. the node-specific dynamics can be written as  $\dot{\mathbf{f}}_k = \mathbf{f} + \varepsilon \tilde{\mathbf{f}}_k$  for some small fluctuations  $\tilde{\mathbf{f}}_k$  with  $|\varepsilon| \ll 1$ ; these fluctuations will be subsumed into the term  $\kappa \mathbf{g}_k$ .
- (3) The coupling structure is pairwise, i.e. the coupling function can be decomposed into the sum of pairwise interactions, unless stated otherwise.

By virtue of these assumptions, one can rewrite the dynamical system as

$$\dot{\mathbf{x}}_k = \mathbf{f}(\mathbf{x}_k; \mu) + \kappa \sum_{j=1}^N \mathbf{g}_{kj}(\mathbf{x}_k, \mathbf{x}_j) \quad (2.2)$$

with  $\mu$  being a general *bifurcation parameter*. In the remainder of this section we will introduce the mathematical ingredients that enable us to transform (2.2) into the phase model

$$\dot{\theta}_k = \omega + \kappa \sum_{j=1}^N H_{kj}(\theta_k - \theta_j) . \quad (2.3)$$

In particular, we will characterize the state  $\mathbf{x}_k$  of every oscillatory node by a phase variable  $\theta_k$ ,  $k = 1, \dots, N$ . The corresponding phase dynamics comprises a *natural frequency* term  $\omega$  and contributions from the other oscillators. These contributions sum up by means of the so-called *phase interaction functions*  $H_{kj}$  that depend on the pairwise phase differences  $\theta_k - \theta_j$  between oscillators  $k$  and  $j$ .

### 2.1.1 Phase definition

The detailed form of oscillators may vary substantially within and between networks under study. To define phase variables, the oscillatory dynamics are required to exhibit self-sustaining limit cycle oscillations. We illustrate this for the case of a single oscillator that we write as

$$\begin{aligned}\dot{\mathbf{x}} &= \mathcal{F}_x(\mathbf{x}, \mathbf{p}; \mu) , \\ \dot{\mathbf{p}} &= \mathcal{F}_p(\mathbf{x}, \mathbf{p}; \mu) .\end{aligned}\tag{2.4}$$

The vector  $\mathbf{x} = \mathbf{x}(t) \in \mathcal{X} \subset \mathbb{R}^n$  represents the state variables  $x_1, x_2, \dots, x_n \in \mathbb{R}$  that evolve according to a vector field  $\mathcal{F}_x$ . This dynamics is subject to perturbations  $\mathbf{p} = \mathbf{p}(t) \in \mathbb{R}^n$ , whose evolution is governed by a vector field  $\mathcal{F}_p$ . As said,  $\mu$  is a general bifurcation parameter that we will drop in this section whenever possible to ease legibility. If we consider merely additive perturbations, the first equation in (2.4) becomes

$$\dot{\mathbf{x}} = \mathbf{f}(\mathbf{x}) + \kappa \mathbf{p}(t) ,\tag{2.5}$$

where the perturbations are scaled by the parameter  $\kappa$ , which is typically considered small. In light of the network cases (2.1) and (2.2), the intrinsic network coupling is simply replaced by the external perturbations  $\mathbf{p}$ .

**Oscillators** If a solution  $\mathbf{x}(t)$  of (2.4) is periodic in time,  $\mathbf{x}(t) = \mathbf{x}(t + T)$  for some constant  $T > 0$ , then (2.4) describes oscillatory dynamics. For a given vector field  $\mathcal{F} = (\mathcal{F}_x, \mathcal{F}_p)$  one can associate the flow  $\phi(t)$  with  $\mathcal{F}$  starting at some initial state  $\mathbf{x}_0 \in \mathcal{X}$  as  $\mathbf{x}(t) = \phi(t; \mathbf{x}_0, \mathbf{p})$ . If (2.4) exhibits a stable time-periodic dynamics without external perturbations,  $\mathbf{p} \equiv \mathbf{0}$ , then the dynamical system  $\dot{\mathbf{x}} = \mathcal{F}_x(\mathbf{x}, \mathbf{0}) = \mathbf{f}(\mathbf{x})$  describes an oscillator and the corresponding flow will be denoted by  $\mathbf{x}(t) = \phi(t; \mathbf{x}_0)$ .

**Limit cycles & basin of attraction** The stable, non-constant, time-periodic solution  $\mathbf{x}^c(t) = \mathbf{x}^c(t + T)$  of an oscillator  $\dot{\mathbf{x}} = \mathbf{f}(\mathbf{x})$  follows a trajectory along a closed periodic orbit  $\mathcal{C} \subset \mathcal{X}$ . This stable periodic orbit is referred to as the oscillator's limit cycle. If we choose an initial condition  $\mathbf{x}(t_0) = \mathbf{x}_0^c \in \mathcal{C}$  on the limit cycle, then the unperturbed flow  $\phi(t; \mathbf{x}_0^c)$  will stay on  $\mathcal{C}$  for all times  $t \geq t_0$ . One can parametrize the limit cycle as the set

$$\mathcal{C} := \{\mathbf{x}^c \in \mathcal{X} \mid \mathbf{x}^c = \phi(t; \mathbf{x}_0^c), t \in [0, T)\} .\tag{2.6}$$

The smallest positive constant  $T > 0$  such that  $\mathcal{C}$  in (2.6) is a closed orbit is called the *period*. The corresponding angular *frequency*  $\omega$  of the oscillator  $\mathbf{x}^c$  will be  $\omega = 2\pi/T$ . We always consider the limit cycle  $\mathcal{C}$  to be hyperbolically stable and without self-crossings.

A *hyperbolically stable limit cycle*  $\mathcal{C}$  attracts all solutions with initial conditions  $\mathbf{x}_0 \in \mathcal{B}$  in a close vicinity  $\mathcal{B} = \mathcal{B}(\mathcal{C})$  of  $\mathcal{C}$ . The maximal open set of these initial points is the basin of attraction. Formally, it can be given by  $\mathcal{B}(\mathcal{C}) := \{\mathbf{x}_0 \in \mathcal{X} \mid \lim_{t \rightarrow \infty} \text{dist}(\phi(t; \mathbf{x}_0), \mathcal{C}) = 0\}$ , where  $\text{dist}(\mathbf{x}, \mathcal{C}) := \inf_{\mathbf{x}^c \in \mathcal{C}} \|\mathbf{x} - \mathbf{x}^c\|_2$  is the distance from  $\mathbf{x} \in \mathcal{X}$  to the set  $\mathcal{C} \subset \mathcal{X}$  in the Euclidean norm  $\|\cdot\|_2$  on  $\mathbb{R}^n$ .

**Phase** The limit cycle  $\mathcal{C}$  is a one-dimensional manifold in  $\mathbb{R}^n$ . Every one-dimensional manifold can be parametrized by a scalar variable. In the case of limit cycle oscillations, the most appropriate variable is the phase  $\theta$  that results from a smooth bijective phase map  $\Theta: \mathcal{C} \rightarrow \mathbb{S}^1$ , where  $\Theta(\mathbf{x}^c) = \theta^c$ . Naturally, a phase-reparametrization of the limit cycle (2.6) can be achieved by introducing  $\theta = \omega t$ .

The notion of phase can be extended to the limit cycle's basin of attraction  $\mathcal{B}(\mathcal{C})$ . This is an important statement because it underlies all of the to-be-discussed mathematical descriptions of phase dynamics<sup>[3]</sup>. We briefly show that this is true: Without loss of generality, we consider a reference point  $\mathbf{x}_0^c$  of zero phase by putting  $\Theta(\mathbf{x}_0^c) = 0$ . In the absence of external perturbation, the phase  $\theta^c$  increases constantly on the limit cycle  $\mathcal{C}$ . In particular, we have  $\theta^c = \Theta(\phi(t; \mathbf{x}_0^c)) = \omega t + \Theta(\mathbf{x}_0^c) = \omega t$  and  $\dot{\theta}^c = \omega$ . Within the basin of attraction, one can define the unique asymptotic phase  $\theta$  of the oscillator  $\mathbf{x} \in \mathcal{B}(\mathcal{C})$  as

$$\theta := \Theta(\mathbf{x}) \in [0, 2\pi) \quad (2.7)$$

such that  $\lim_{t \rightarrow \infty} \|\phi(t; \mathbf{x}) - \phi(t; \phi(\theta/\omega; \mathbf{x}_0^c))\|_2 = 0$  holds. The asymptotic phase  $\theta$  increases along all unperturbed trajectories by means of  $\theta = \omega t + \Theta(\mathbf{x})$  at the same constant rate  $\omega$ . This enables us to use  $\mathbf{x}^c(t)$  and  $\mathbf{x}^c(\theta)$  interchangeably when parametrizing the time  $t = \theta/\omega$  along the limit cycle. We can therefore rephrase

---

<sup>[3]</sup> While arguably abstract, our notion of phase enables us to define a phase even for non-smooth oscillators. An example for this is a so-called integrate-and-fire dynamics, in which a scalar state variable  $x$  monotonically increases according to  $\dot{x} = f(x)$  between two thresholds  $\nu_r < \nu_f$  with  $f(x) > 0$  for  $x \in [\nu_r, \nu_f]$ . When reaching the upper (firing) threshold  $\nu_f$ , the state will be instantaneously reset to the lower (reset) threshold  $\nu_r$  and start integrating again. In that case one can define the asymptotic phase map  $\Theta$  as the bijective change of variables

$$\Theta(x): x \mapsto \omega \int_{\nu_r}^x \frac{1}{f(y)} dy ,$$

with the threshold values  $\nu_r$  and  $\nu_f$  mapped to  $\theta = 0$  and  $\theta = 2\pi$ , respectively.

the condition above that defines the asymptotic phase more intuitively as

$$\lim_{t \rightarrow \infty} |\mathbf{x}(t) - \mathbf{x}^c(\theta(t))| = 0. \quad (2.8)$$

**Isochrons** Sets of points  $\mathbf{x} \in \mathcal{B}(\mathcal{C})$  with the same asymptotic phase  $\Theta(\mathbf{x}) = \theta$  are called isochrons. Accordingly, (2.8) can be regarded as the *isochron condition*. As to a rigorous definition, the isochron  $\mathcal{I}(\theta)$  associated with the phase  $\theta$  is the set  $\mathcal{I}(\theta) := \{\mathbf{x} \in \mathcal{B}(\mathcal{C}) \mid \Theta(\mathbf{x}) = \theta\}$ , which is a co-dimension one sub-manifold in  $\mathcal{B}(\mathcal{C})$  that transversally crosses the periodic orbit  $\mathcal{C}$ .

We illustrate the concept of isochrons and the asymptotic phase map in Fig. 2.4. The isochrons are perpendicular to the limit cycle. In general, isochrons cover the whole basin of attraction  $\mathcal{B}(\mathcal{C})$ . In mathematical terms, they define a so-called fibration of  $\mathcal{B}(\mathcal{C})$ .

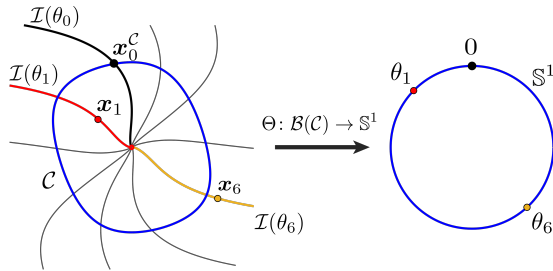


**Figure 2.4:** Phase map  $\Theta: \mathcal{B}(\mathcal{C}) \rightarrow \mathbb{S}^1$  associates to each point  $x_j$  in the neighborhood  $\mathcal{B}(\mathcal{C})$  of the limit cycle  $\mathcal{C}$  an asymptotic phase  $\theta_j \in \mathbb{S}^1$ . The set of all points in  $\mathcal{B}(\mathcal{C})$  that are mapped onto the same phase  $\theta$  forms the isochron  $\mathcal{I}(\theta)$  associated with phase  $\theta$ . Shown are ten isochrons associated to the phases  $\theta_n = nT/10$ ,  $n = 0, \dots, 9$ . An arbitrarily chosen reference point  $\mathbf{x}_0^c \in \mathcal{C}$  serves as the initial phase  $\theta = 0$ .

## 2.1.2 Phase response

**Phase response curve** The phase response curve or phase resetting curve is a crucial determinant for the interaction between oscillators. It measures to what extent an external perturbation  $\mathbf{p}(t)$  advances or pushes back the asymptotic phase of an oscillator. A perturbation thus leads to a phase advance or phase delay, respectively. More formally, given a trajectory  $\mathbf{x}^c(t)$  along the limit cycle subject to a pulse-like perturbation  $\mathbf{p}(t)$  during an infinitesimal time interval  $\mathcal{T} = \lim_{\delta \rightarrow 0} (t_0 - \delta, t_0 + \delta)$ , i.e.  $\mathbf{p}(t \in \mathcal{T}) \neq 0$ , an immediate strategy to identify the corresponding phase response  $G(\theta, \mathbf{p})$  at phase  $\theta_0 = \Theta(\mathbf{x}^c(t_0))$  reads:

- (i) determine the perturbed point  $\lim_{\delta \rightarrow 0} \tilde{\mathbf{x}}(t_0 + \delta) \in \mathcal{B}(\mathcal{C})$  and its corresponding asymptotic phase  $\Theta(\tilde{\mathbf{x}})$ ;

- (ii) take the difference between the perturbed asymptotic phase and the unperturbed phase  $\Theta(\mathbf{x}^c) = \theta_0$ ;
- (iii) repeat (i) and (ii) for all phases  $\theta_0 = \theta \in \mathbb{S}^1$  in order to determine the *phase response curve*

$$G(\theta; \mathbf{p}) = \Theta(\tilde{\mathbf{x}}) - \Theta(\mathbf{x}^c) = \Theta(\mathbf{x}^c + \mathbf{p}) - \theta . \quad (2.9)$$

One can determine the phase response curve also for arbitrary perturbations during finite time intervals  $\mathcal{T} = (t_0, t_1)$  with  $t_1 > t_0$ . For this, the first step above has to be modified slightly:

- (i<sub>a</sub>) determine the perturbed point  $\tilde{\mathbf{x}}(t_1) = \phi(t_1; \tilde{\mathbf{x}}(t_0), \mathbf{p}) = \phi(t_1; \mathbf{x}^c(t_0), \mathbf{p})$  and the unperturbed one  $\mathbf{x}^c(t_1) = \phi(t; \mathbf{x}^c(t_0))$ , as well as the corresponding (asymptotic) phases  $\Theta(\tilde{\mathbf{x}}(t_1))$  and  $\Theta(\mathbf{x}^c(t_1))$ .

The dynamics has to be integrated to determine both the perturbed and unperturbed state at time  $t = t_1$ . One can continue integrating for longer times, ideally for  $t \rightarrow \infty$  and, subsequently, estimate the asymptotic phase difference according to

$$G(\theta; \mathbf{p}) = \Theta\left(\lim_{t \rightarrow \infty} \phi(t; \mathbf{x}^c(t_0), \mathbf{p})\right) - \Theta\left(\lim_{t \rightarrow \infty} \phi(t; \mathbf{x}^c(t_0))\right) .$$

Note that this definition coincides with

$$G(\theta; \mathbf{p}) = \Theta(\phi(t_1; \mathbf{x}^c(t_0), \mathbf{p})) - \Theta(\phi(t_1; \mathbf{x}^c(t_0))) .$$

In the following we will only consider pulse-like perturbations  $\mathbf{p}(t)$  that are non-zero at the time instant  $t_0$  of the pulse, and therefore omit the explicit time-dependence of  $\mathbf{p}$ .

**Infinitesimal phase response curve** If the perturbation is pulse-like, i.e.  $\mathcal{T} \rightarrow \delta(t_0)$ , and sufficiently weak,  $|\mathbf{p}| \ll 1$ , then it is convenient to express the phase response in terms of the infinitesimal phase response curve<sup>[4]</sup>. Using the directional derivative  $D\Theta(\mathbf{x})[\mathbf{y}] := \lim_{h \rightarrow 0} [\Theta(\mathbf{x} + h\mathbf{y}) - \Theta(\mathbf{x})]/h$ , we can define the *infinitesimal phase response curve* as a map  $Q : \mathbb{S}^1 \rightarrow \mathbb{R}$  with

$$Q(\theta) := D\Theta(\mathbf{x}^c)[\partial_{\mathbf{p}} \mathcal{F}(\mathbf{x}^c, \mathbf{0})] = \nabla_x \Theta(\mathbf{x}^c) \cdot \partial_{\mathbf{p}} \mathcal{F}(\mathbf{x}^c, \mathbf{0}) .$$

Here, we expressed the directional derivative as the inner product in  $\mathbb{R}^n$ .  $\nabla_x \Theta(\mathbf{x}^c)$  denotes the gradient of the asymptotic phase map  $\Theta$  evaluated on the limit cycle  $\mathcal{C}$ ,

<sup>[4]</sup> Several papers refer to this as *infinitesimal phase resetting curve* or *phase response function*.

and  $\partial_p \mathcal{F}(\mathbf{x}^c, \mathbf{0})$  corresponds to an infinitesimal perturbation from the limit cycle trajectory  $\mathbf{x}^c$  at phase  $\theta$ .

**Phase sensitivity function** The afore-introduced gradient now written as

$$\mathbf{Z}(\theta) = \nabla_x \Theta(\mathbf{x}^c(\theta)) = \nabla \Theta(\mathbf{x})|_{\mathbf{x}=\mathbf{x}^c(\theta)}, \quad (2.10)$$

can serve to determine the phase response.  $\mathbf{Z}: \mathbb{S}^1 \rightarrow \mathbb{R}^n$  is commonly referred to as *phase sensitivity function* or linear response function<sup>85</sup>. It is closely related to the infinitesimal phase response curve  $Q$ : If  $\partial_p \mathcal{F}(\mathbf{x}^c, \mathbf{0})$  is a unit vector  $\mathbf{e}_j$  along the  $j$ -th direction, then we have  $Q(\theta) = Z_j(\theta)$ . In fact, this follows immediately from the dynamics (2.5) with uni-directional additive perturbation  $\kappa \mathbf{p} = \kappa \mathbf{e}_j$ . The phase response curve (2.9) can always be computed using  $Q(\theta)$  since the definitions (2.10) and (2.9) imply

$$Z_j(\theta) = \lim_{p \rightarrow 0} \frac{G(\theta, p \mathbf{e}_j)}{p}. \quad (2.11)$$

In Fig. 2.5, we depict the phase sensitivity functions of two classic examples, the Stuart-Landau and the Rayleigh oscillator. The components of  $\mathbf{Z} = (Z_x, Z_y)$  describe the effect of infinitesimal perturbations in the  $x$ - and  $y$ -direction, respectively. While the phase sensitivity function of the Stuart-Landau oscillator is sinusoidal in both components, the slightly angular limit cycle dynamics of the Rayleigh oscillator results in more complicated phase responses as indicated by the phase sensitivity function.

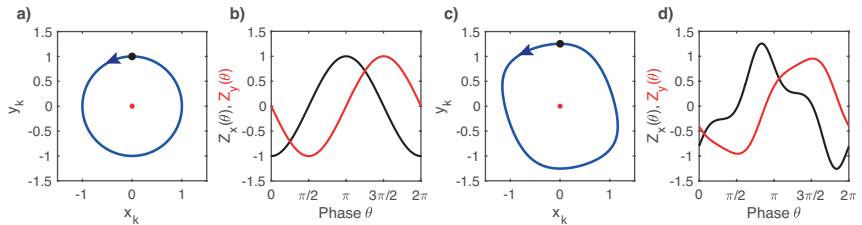


**Figure 2.5:** Phase response of limit-cycle oscillators. (a) Circular limit cycle of the Stuart-Landau oscillator  $\dot{z} = z - (1 + i)|z|^2 z$  with  $z = x + iy$  and (b) the two sinusoidal components of the phase sensitivity function  $\mathbf{Z} = (Z_x, Z_y)$ , characterizing the response to infinitesimal perturbations in the  $x$ - and  $y$ -direction, respectively. (c) The Rayleigh oscillator  $\dot{x} = y, \dot{y} = -\omega + (1 - x^2)y$  and (c) its phase sensitivity function.

### 2.1.3 Phase dynamics of a single oscillator

For infinitesimal perturbations  $|\mathbf{p}| \ll 1$ , the phase response curve (2.9) can be linearly approximated by the aforementioned phase sensitivity function (2.10) in

terms of

$$G(\theta; \mathbf{p}) \cong \mathbf{Z}(\theta) \cdot \mathbf{p} . \quad (2.12)$$

Whenever the dynamics stays close to the limit cycle  $\mathcal{C}$ , one may further approximate each  $\mathbf{x}$  by its corresponding value  $\mathbf{x}^c$  on  $\mathcal{C}$  such that the reduced phase dynamics can be given by

$$\dot{\theta} = \omega + G(\theta; \mathbf{p}) = \omega + \varepsilon \mathbf{Z}(\theta) \cdot \mathbf{p} . \quad (2.13)$$

In (2.13) we used the parameter  $\kappa = \varepsilon \ll 1$  to indicate that the perturbation is very small. In other words, the phase response to a weak, pulse-like perturbation  $\mathbf{p}$  at phase  $\theta^c$  can be approximated by the product  $\mathbf{Z}(\theta^c) \cdot \mathbf{p}$ .

More rigorously, small perturbations  $|\mathbf{p}| \ll 1$  do not kick the oscillator too far away from the limit cycle  $\mathcal{C}$  and the dynamics  $\mathbf{x}$  can be approximated sufficiently well by the value on the periodic orbit,  $\mathbf{x}(t) \approx \mathbf{x}^c(t)$ , see Fig. 2.3. Moreover, one can formally expand the dynamics  $\dot{\mathbf{x}} = \mathcal{F}(\mathbf{x}, \mathbf{p})$  for small  $\mathbf{p}$  around the unperturbed dynamics  $\mathbf{f}(\mathbf{x})$ , i.e.,  $\mathcal{F}(\mathbf{x}, \mathbf{p}) = \mathbf{f}(\mathbf{x}) + \partial_{\mathbf{p}} \mathcal{F}(\mathbf{x}, \mathbf{0}) \mathbf{p} + \mathcal{O}^2(\mathbf{p})$ . Taken together, we obtain the asymptotic phase dynamics

$$\dot{\theta} = \frac{d}{dt} \Theta(\mathbf{x}) = \nabla_{\mathbf{x}} \Theta(\mathbf{x}) \cdot \dot{\mathbf{x}} \approx \nabla_{\mathbf{x}} \Theta(\mathbf{x}^c) \cdot \dot{\mathbf{x}}^c \approx \nabla_{\mathbf{x}} \Theta(\mathbf{x}^c) \cdot [\mathbf{f}(\mathbf{x}^c) + \partial_{\mathbf{p}} \mathcal{F}(\mathbf{x}^c, \mathbf{0}) \mathbf{p}]$$

and because  $\dot{\theta}^c = \nabla_{\mathbf{x}} \Theta(\mathbf{x}^c) \cdot \mathbf{f}(\mathbf{x}^c) = \omega$  holds, this form reduces at first order to (2.13).

## 2.1.4 Phase dynamics of oscillator networks

The phase model (2.13) can be extended to a network of oscillators  $\mathbf{x}_1, \dots, \mathbf{x}_N$  with dynamics (2.2). In the uncoupled case, i.e. for  $\kappa = 0$ , the systems  $\dot{\mathbf{x}}_k = \mathbf{f}(\mathbf{x}_k)$  have the same hyperbolically stable limit cycle  $\mathcal{C}$  with period  $T > 0$  and frequency  $\omega = 2\pi/T$ . Starting again with defining phase variables  $\theta_k$  according to the isochron condition (2.8) and following the same reasoning as in the single oscillator case, we end up with

$$\dot{\theta}_k = \omega + \kappa \mathbf{Z}(\theta_k) \cdot \sum_{j=1}^N \mathbf{g}_{kj}(\theta_k, \theta_j) ;$$

here, we abbreviated  $\mathbf{g}_{kj}(\theta_k, \theta_j) = \mathbf{g}_{kj}(\mathbf{x}^c(\theta_k), \mathbf{x}^c(\theta_j))$ . If the coupling is again sufficiently weak, one can make use of *averaging*. For this, we introduce *relative*

phase variables  $\theta_k = \phi_k + \omega t$  and find

$$\dot{\phi}_k = \kappa \mathbf{Z}(\phi_k + \omega t) \cdot \sum_{j=1}^N \mathbf{g}_{kj}(\phi_k + \omega t, \phi_j + \omega t)$$

with  $0 < \kappa \ll 1$ . In order to apply averaging appropriately, the (relative) phases  $\phi_k$  have to be slow variables. To be precise, they have to be so slow that they do not vary within a period. Then, one can average the right-hand side over one period, which yields the sought-for phase dynamics (2.3),

$$\dot{\theta}_k = \omega + \kappa \sum_{j=1}^N H_{kj}(\theta_k - \theta_j) ,$$

with the *phase interaction function*

$$H_{kj}(\psi) = \frac{1}{2\pi} \int_0^{2\pi} \mathbf{Z}(\varphi + \psi) \cdot \mathbf{g}_{kj}(\varphi + \psi, \varphi) d\varphi . \quad (2.14)$$

More detailed derivations can be found in, e.g., Kuramoto's seminal book<sup>38</sup> (Chapter 5) or Ermentrout and Terman's textbook<sup>86</sup> (Chapter 8.3); see also the recent review<sup>87</sup> by Nakao.

In what follows, the network (2.2) and its phase dynamics (2.3) will be our central equations. We will present different ways how to determine the phase interaction function (2.14). Obtaining analytical expressions of  $H_{kj}$  can be an arduous endeavor. The exact determination of the natural frequency  $\omega$  as well as of  $H_{kj}$  depends on an accurate description of the limit cycle and related quantities, e.g., the phase map  $\Theta$  of every oscillator  $\mathbf{x}_k$ . Accordingly, one would determine the phase sensitivity function  $\mathbf{Z}$  first and subsequently  $H_{kj}$ . How this can be done numerically will be sketched in *Section 2.3*. Numerics, however, may fail to unravel the details about the link between the original oscillator dynamics and the reduced phase model. Therefore, we start with an overview of analytic approaches in *Section 2.2*.

## 2.1.5 Collective behavior

Before going into the details of phase reductions of complex oscillator networks, we briefly recapitulate how macroscopic behavior may look like and how it is typically evaluated and categorized. The by now conventional outcome measures will be included in our quality assessment of the to-be-explained techniques. For the sake of simplicity and in line with our main assumptions above, we consider a pairwise coupling structure where the existence of a link between two oscillators  $k \neq j$  is

prescribed by adjacency values  $C_{kj}$ . Moreover, we consider the pairwise coupling functions  $\mathbf{g}_{kj}(\mathbf{x}_k, \mathbf{x}_j) = C_{kj}\mathbf{g}(\mathbf{x}_k, \mathbf{x}_j)$  to differ only by this factor. This leads to a slight simplification of the oscillator network dynamics and the corresponding phase dynamics, but suffices to prepare various examples to come.

Considering pairwise coupling, the general dynamical form of (2.2) reduces to

$$\dot{\mathbf{x}}_k = \mathbf{f}(\mathbf{x}_k; \mu) + \frac{\kappa}{N} \sum_{j=1}^N C_{kj} \mathbf{g}(\mathbf{x}_k, \mathbf{x}_j) \quad (2.15)$$

When the coupling matrix  $C = \{C_{kj}\}_{k,j}$  has only binary entries, it is also referred to as adjacency matrix. The pairwise coupling structure in (2.15) leads to the phase dynamics

$$\dot{\theta}_k = \omega + \frac{\kappa}{N} \sum_{j=1}^N C_{kj} H(\theta_k - \theta_j) , \quad (2.16)$$

where  $H$  is the sole phase interaction function. Comparing this with (2.3) and (2.14), we have replaced  $H_{kj}$  with  $C_{kj}H$  so that we have to determine the phase interaction function only once instead for each pair of oscillators individually. Moreover, the function  $H$  is periodic with period  $T = 2\pi/\omega$ . It can hence be expressed as a Fourier series

$$H(\psi) = \sum_{n \geq 0} a_n \cos(n\psi) + b_n \sin(n\psi) . \quad (2.17)$$

The (number of) Fourier components  $a_n$  and  $b_n$  insinuate the ‘degree of complexity’ in the phase dynamics. In fact, including higher harmonics ( $n > 1$ ) may give rise to modularity and clustering of phases, or even to switching behavior between clusters.

### 2.1.5.1 Synchronization

Synchronization and de-synchronization are arguably the most discussed phenomena in oscillator networks. In case of two coupled oscillators 1 and 2 with  $C_{12} = C_{21} = 1$ , conditions for their synchronization can be summarized as follows. If the oscillators have identical natural frequencies,  $\omega_1 = \omega_2$ , and the frequency mismatch  $\Delta = \omega_1 - \omega_2$  vanishes, then the oscillators will synchronize in-phase with  $\theta_1(t) = \theta_2(t)$  for large enough  $t$  or out-of-phase with  $|\theta_1(t) - \theta_2(t)| = \pi$ . In fact, when defining  $\Gamma(\psi) = H(\psi) - H(-\psi)$  one can write  $\dot{\theta}_k - \dot{\theta}_j := \dot{\psi} = \Delta + \kappa\Gamma(\psi)$ . The resulting in-phase synchronized solution  $\psi = 0$  is stable for  $\kappa\Gamma'(0) = 2\kappa H'(0) > 0$ . In this case, the phase model exhibits *attractive coupling*. On the other hand, the anti-phase solution,  $\psi = \pm\pi$ , is stable if  $\kappa H'(\pm\pi) > 0$ . Then one speaks of *repulsive coupling*. For non-identical oscillators,  $\omega_k \neq \omega_j$ , *phase locking* or *mutual*

*synchronization*, can be observed as long as  $\kappa \min \Gamma(\psi) < \Delta < \kappa \max \Gamma(\psi)$  holds.

All these properties can be extended to networks of more than two coupled oscillators. To illustrate this, we consider positive coupling strengths  $\kappa > 0$  from now on, unless stated otherwise. If  $H(\psi)$  consists only of first harmonics, i.e.  $a_1, b_1 \neq 0$  but  $a_n = b_n = 0$  for all  $n > 1$ , we retrieve the seminal Kuramoto-Sakaguchi model

$$\dot{\theta}_k = \omega_k - \kappa \sum_{j=1}^N \sin(\theta_k - \theta_j + \alpha)$$

with phase lag parameter  $\alpha$ . In our previous notation, we have  $C_{kj} = -1$  for all  $k, j$ . The special case  $\alpha = 0$  yields the classic Kuramoto model, for which  $a_1 = 0$  and  $b_1 > 0$ . By construction, the Kuramoto model ‘only’ features attractive coupling. The more general Kuramoto-Sakaguchi model, whose phase interaction function is commonly written as  $H(\psi) = A \sin(\psi + \alpha)$ , exhibits also attractive coupling<sup>[5]</sup> for  $|\alpha| \leq \pi/2$ . In networks of identical and globally coupled oscillators, the strength of (attractive) coupling can be arbitrarily small such that the network synchronizes. For non-identical oscillators, by contrast, the heterogeneity in the natural frequency terms tends to suppress synchronization. Yet, when the coupling exceeds a critical value, a transition to collective synchronization can be observed<sup>38,85</sup>.

Commonly, the degree of network synchronization is measured in terms of the *complex Kuramoto order parameter* defined as

$$Re^{i\Psi} = \frac{1}{N} \sum_{k=1}^N e^{i\theta_k}. \quad (2.18)$$

The modulus  $R$  and the complex argument  $\Psi$  represent the amplitude and phase, respectively, of collective oscillations, that is, of the mean field behavior.  $R$  takes values between  $R = 0$ , corresponding to a fully incoherent state, and  $R = 1$ , corresponding to complete synchronization of all oscillators. The Kuramoto model provides a seminal example of a synchronizable phase oscillator network. In the continuum limit,  $N \rightarrow \infty$ , and for an appropriately chosen distribution  $g(\omega)$  of natural frequencies, it can be solved analytically. When increasing the coupling strength, the real-valued Kuramoto order parameter  $R$  undergoes a pitchfork-

<sup>[5]</sup> We can use trigonometric identities to write  $a_1 \cos(\psi) + b_1 \sin(\psi) = A \sin(\psi + \alpha)$  with  $A^2 = a_1^2 + b_1^2$  and  $\alpha = \arctan(a_1/b_1)$ ; the latter is the quadrant corrected inverse tangent. If we fix the sign of  $A$  by imposing  $A = \text{sgn}(b_1)[a_1^2 + b_1^2]^{1/2}$ , we find  $\alpha = \arctan(a_1/b_1) \in (-\pi/2, \pi/2)$  for  $b_1 > 0$ , and  $|\alpha| > \pi/2$  for  $b_1 < 0$ . Hence, the coupling is attractive whenever  $b_1 > 0$ . When  $b_1 < 0$ , the repulsive character of the coupling can be revoked through negative coupling strengths  $\kappa < 0$ , in which case  $\kappa A > 0$ . On the other hand, using the convention  $\text{sgn}(A) = \text{sgn}(a_1)$ , synchronization may not occur when  $\kappa A > 0$  is fulfilled.

bifurcation at a critical value (which depends on the properties of  $g$ ) and the state of the network switches from incoherence to (partial) synchronization <sup>see 38,81,87</sup>.

### Stability of the synchronized solution

A different approach to assess the network behavior of identical, coupled systems, not necessarily phase oscillators, is based on the master stability function (MSF) formalism<sup>88</sup>. The MSF approach is used to determine the stability of the fully synchronized state, corresponding to a vanishing order parameter  $R = 0$ , in terms of the eigenstructure of the connectivity matrix <sup>see also 89</sup>. For our phase model  $\dot{\theta}_k = \omega + \kappa \sum_j C_{kj} H(\theta_k - \theta_j)$ , we are interested in the stability of the synchronous state  $\theta_k = \theta$  for all  $k$ , that is,  $\theta_k - \theta_j = 0$  for all  $j \neq k$ . Given that close to full synchrony the phase differences tend to be small, we can expand  $H$  around the origin and find at first order  $H(\theta_k - \theta_j) \approx H'(0)[\theta_k - \theta_j]$ . Writing the phase model in vector form, one can find the Jacobian  $\hat{H}$  at the synchronous state  $\Theta_0 = (\theta, \dots, \theta)$  with entries  $\hat{H}_{kj}$  having graph-Laplacian structure  $\hat{H}_{kj} = \kappa H'(0)(C_{kj} - \delta_{kj} \sum_l C_{kl})$ . The (linear) stability of the synchronous state here depends on the eigenvalues of  $\hat{H}$ . We note that one eigenvalue is always zero. If the network is globally coupled, i.e.,  $C_{kj} = 1$  for all  $j, k$ , the synchronized state is stable if  $\kappa H'(0) > 0$  and unstable if  $\kappa H'(0) < 0$  <sup>cf. 61</sup>. Nicosia and co-workers recently used a similar approach to investigate the mechanisms behind remote synchronization behavior<sup>58</sup>. When full synchronization cannot be achieved, network symmetries play a crucial role in establishing functional modules, which do not even require structural connectivity as represented in the adjacency matrix  $C_{kj}$ .

#### 2.1.5.2 Between incoherence and full synchrony

Observed macroscopic behavior emerges from the dynamics of the network's nodes. However, collective dynamics also influence the individual oscillators in turn. It is therefore often convenient to rewrite the phase model (2.16) & (2.17) in the form of a single oscillator that is driven by the mean field variables  $R(t)$  and  $\Psi(t)$ :

$$\dot{\theta}_k = \omega_k + \kappa \sum_{n \geq 0} a_n(R) \cos(\Psi - \theta_k) + b_n(R) \sin(\Psi - \theta_k) . \quad (2.19)$$

The Fourier amplitudes  $a_n, b_n$  now depend on  $R$ , possibly in a nonlinear way. Rosenblum and Pikovsky investigated a form of the Kuramoto-Sakaguchi model<sup>90–92</sup> where  $a_1$  and  $b_1$  depended on both  $R$  and  $R^3$ . Due to this nonlinear coupling, a self-consistent partial synchrony solution can arise with  $0 < R < 1$  at the border between stability and instability domains for the synchronous state. Moreover, Rosenblum and Pikovsky found a mismatch between the time-averaged fre-

quencies of the oscillators and the frequency of the mean field, which they called self-organized quasiperiodic solutions. Detecting these non-trivial states requires a more careful inspection of the network behavior than merely considering the (averaged) evolution of the order parameter. Poincaré sections can hint at the quasiperiodic character of the mean-field solution. Furthermore, the evolution of the (instantaneous) phases, or of their distribution, sheds light on the actual collective dynamics.

Higher harmonics in the phase model increase the variety of non-trivial network behavior. For instance, for a biharmonic phase interaction function  $H$ , i.e. where in addition  $a_2, b_2 \neq 0$ , the occurrence of balanced two-phase-cluster states is expected, and has frequently been reported<sup>93–95</sup>. In particular, one can indicate stability boundaries for cluster states according to the eigenvalues associated with intracluster and intercluster perturbations, respectively. The eigenvalues for intracluster perturbations can be computed as  $\lambda_n^{\text{intra}} = \sum_{k=1}^{\infty} b_{kn}$ , with  $b_m, m = kn$ , the (odd) Fourier amplitudes of  $H$ . Combining them with those for intercluster perturbations, we can determine the stability of synchronized (one-cluster,  $\lambda_1^{\text{intra}}$ ) and anti-phase cluster solutions (balanced two-cluster,  $\lambda_2^{\text{intra}}, \lambda_2^{\text{inter}}$ ) using  $\lambda_1^{\text{intra}} = H'(0)$ ,  $\lambda_2^{\text{intra}} = \frac{1}{2}(H'(0) + H'(\pi))$ , and  $\lambda_2^{\text{inter}} = H'(\pi)$ . The biharmonic phase model will feature global synchrony for  $\kappa b_1 > 0$ , and a balanced two-cluster state will be realized if  $\kappa b_1 < 0$  and  $\kappa b_2 > 0$ . Moreover, heteroclinic cycles may occur when  $\kappa b_1 < 0, \kappa b_2 < 0$  and  $b_1$  is comparable to  $b_2$ . Heteroclinic cycles define a slow switching behavior of individual oscillators between two clusters. As illustrated in Fig. 2.6 (panel a), slow switching is characterized by spontaneous decreases of the real-valued Kuramoto order parameter (top panel). During these

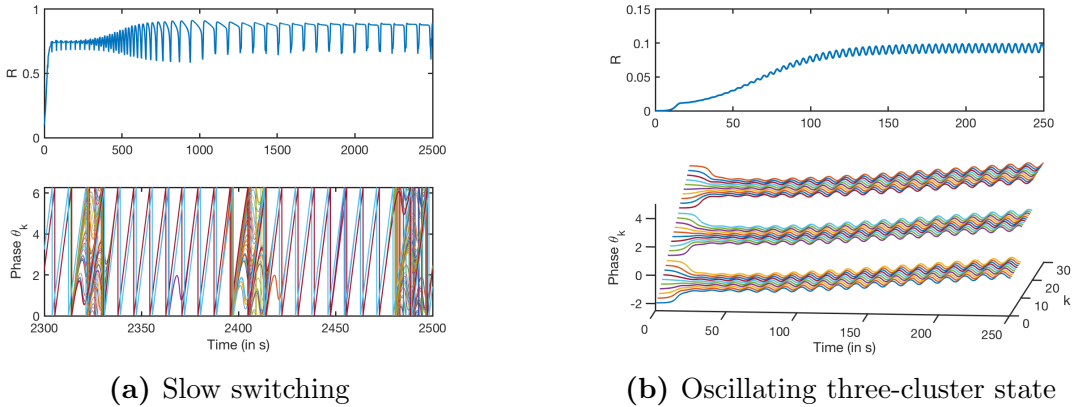


**Figure 2.6:** (a) Slow switching between two clusters in a network of  $N = 1000$  biharmonically coupled phase oscillators. (b) Oscillating three-cluster state for  $N = 30$  identical phase oscillators with phase interaction function  $H(\psi) = \sqrt{2}\sin(\psi + \pi/4) - 0.09\sin(2\psi) + 0.16\sin(3\psi) - 0.09\sin(4\psi) - 0.03\sin(5\psi) - 0.06\sin(6\psi)$ . Top panels: time evolution of the real-valued Kuramoto order parameter. Bottom: time evolution of the individual phases.

rapid drops of synchrony some oscillators switch from one cluster to the other as can be seen in the corresponding phase evolution (lower panel). Kori and Kuramoto<sup>96,97</sup> argued that slow-switching may be explained as an effective convergence to an unstable unbalanced two-cluster solution, and explored the effect of delay on the robustness of the mechanism.

Clusella and co-workers summarize the possible macroscopic dynamics for identical biharmonically coupled phase oscillators in<sup>98</sup>. They also reported self-consistent partial synchrony solutions; see also the work by Komarov and Pikovsky for an analytic account of the network behavior for a biharmonic coupling function<sup>99,100</sup>.

When further increasing the number of harmonics in the phase interaction function, even small networks of identical phase oscillators can display very rich collective behavior up to macroscopic chaos, as has been shown for fourth harmonics in<sup>101</sup>. Numerical simulations can give insight into the variety of clustering behavior when more than two harmonics are present; e.g., Okuda reported an oscillating three-cluster state in<sup>93</sup>. While the order parameter dynamics may hint at such non-trivial network behavior, it typically fails to provide a clear picture of the actual phase dynamics. The oscillating order parameter in Fig. 2.6 (panel b, top) does not provide any sign that there are actually three oscillating cluster states as revealed by the phase time series (bottom). For that reason, it is important to identify the characteristics of the collective behavior first and subsequently choose an appropriate macroscopic observable that is able to capture the actual dynamics.

## 2.2 Analytic phase reduction techniques

The literature comes with a variety of analytic phase reduction techniques. Primary disciplines providing these techniques are the physics of complex systems and applied mathematics while engineering adds more to the numerical approaches. As such the techniques are often tailored to more or less specific settings. While this, in principle, should not be a problem, there are important differences in the resulting phase models. These differences are not ‘only’ quantitative ones but can be qualitative in nature, as will be illustrated in *Chapter 3*.

The goal of analytic phase reduction is not only to reduce an oscillator network into a phase model of the form (2.3) but to derive explicit expressions of the natural frequency  $\omega$  and of the phase interaction function  $H_{kj}$  in terms of the parameters of the underlying oscillator model. As outlined in *Section 2.1*, the phase interaction function  $H_{kj}$  can be determined through the phase sensitivity function  $\mathbf{Z}(\theta)$  and through the coupling function  $\mathbf{g}_{kj}$ , cf. (2.14). Both of them depend on the limit cycle properties of the underlying dynamics. To extract these

properties we make use of an important observation: Oscillator dynamics on the limit cycle are similar across models if these oscillations emerge through the same particular type of bifurcation. This similarity gives rise to *canonical models* for every type of bifurcation, which capture the essence of the dynamics near the bifurcation point. All dynamical systems with similar dynamical behavior can be transformed into a canonical model.

The insights from a canonical model can be very fruitful for identifying the phase dynamics of the oscillator network. To derive the phase dynamics for systems close to the same bifurcation, it suffices to consider canonical models of the corresponding dynamical systems<sup>78</sup>. Even without knowing the exact equations of the canonical model, the phase sensitivity function can often be anticipated to have a particular form that is characteristic for the type of bifurcation see, e.g., 102,103. However, in order to determine the exact form of the other indispensable ingredient necessary for deriving the phase dynamics, that is, the coupling function  $\mathbf{g}_{kj}$  evaluated at the limit cycle, we crucially depend on the equations of the canonical model. Unfortunately, there is a caveat. As Hoppensteadt and Izhikevich properly remarked in their textbook<sup>78</sup>, there does not exist a general algorithm for deriving canonical models. Normal form and center manifold theories have proven successful candidates to obtain simplified equations and to reduce their dimension, respectively. We will clarify the intricate link between these theories in *Section 2.2.1*, and illustrate how to apply them in the subsequent sections. In some cases, however, the derivation of canonical models cannot avoid heuristic arguments and restrictive approximations. This is in particular true if bifurcations are global<sup>[6]</sup>. When an oscillatory dynamics is close to a Hopf bifurcation, which is a local bifurcation, one can utilize sound mathematical approaches to explicitly derive a canonical model. As we base the derivations on normal form theory, we will refer to it as a normal form. In fact, we will specify it as a Hopf normal form due to the particular type of bifurcation that will be considered here. Once a Hopf normal form is obtained, it can be further reduced to the phase dynamics. A rigorous analytic phase reduction is thus a two-step approach: it consists of a normal form reduction and a subsequent phase reduction of the normal form. Note that the resulting phase dynamics is described in terms of the original parameters. Indeed, the normal form/canonical model is achieved through an exact transformation of the underlying system. Likewise, the phase reduction of the

---

<sup>[6]</sup> A local bifurcation is characterized through the loss of stability or the disappearance of an equilibrium. Qualitative changes of the system's dynamical behavior are localized in a small neighborhood. Outside this neighborhood the dynamics remains qualitatively identical unless other bifurcations occur there simultaneously. If one cannot confine the qualitative changes through a bifurcation to a (small) neighborhood, one speaks of a global bifurcation. Examples for local bifurcations are saddle-node, pitchfork, transcritical or Hopf bifurcations, while homoclinic and saddle-node on a limit cycle (SNIC) bifurcation are of global character.

Hopf normal form is an exact transformation into the phase model.

Reduced phase models are not unique. This is also true for coupled dynamical systems near Hopf bifurcations. Both for normal form reductions as well as for subsequent phase reductions one can pick and choose one out of various alternatives. We will present three of the Hopf normal form reductions in *Sections 2.2.2.1–2.2.2.3*. They are representative for the most commonly used normal form reduction techniques, and dwell on time-scale separation and perturbation arguments (dating back to Kuramoto), subsequent near-identity coordinate transformations (Poincaré), and a Lie bracket formalism (Takens), respectively. In *Sections 2.2.4–2.2.7* four different phase reduction techniques will be outlined. In principle, they are applicable to any network of coupled dynamical systems that exhibit stable oscillations. However, three of them, namely Winfree’s reduction via isochrons, Kuramoto’s reduction via Floquet eigenvectors, and Ashwin & Rodrigues’ reduction via symmetries, capitalize to some degree on the aforementioned Hopf normal form and there they can be solved to all extent. The fourth one that falls into the category of averaging and/or time-scale separation approaches has been extensively used in the context of nonlinear optics dating back to Haken. Strictly speaking it does not require a normal form description. Our juxtaposition of these techniques will point at how they differ in their conceptual background and methodological implementation, the general applicability, as well as their accuracy. For the latter we will particularly focus on the correct determination of the coupling function, where we even extend the existing theory by incorporating nonlinear coupling terms. After all, the coupling defines the interaction between oscillators and is thus crucial for the collective dynamics.

Before going into *medias res* along exemplary applications in *Chapter 3*, we will first provide a very concise inventory of generic analytic techniques to treat oscillator networks and their phase dynamics. All of them apply to general dynamics with the only assumption that they exhibit stable oscillatory behavior. However, we will concentrate on oscillators that are close to a so-called Hopf bifurcation, i.e. around the transition at which oscillations with a finite frequency emerge or vanish. The Hopf bifurcation allows to rigorously derive a canonical model<sup>[7]</sup>. We

---

[7] The Hopf bifurcation is the only type of bifurcation that allows a step-for-step reduction of the phase dynamics without rough heuristics. In fact, the seminal work by Eric Shea-Brown and co-workers<sup>102</sup> provides a welcoming account of phase reductions of the four co-dimension one bifurcations that lead to oscillatory dynamics: *Hopf*, *Bautin*, *SNIC* and *homoclinic*. The global character of the SNIC and homoclinic bifurcations, however, requires an educated guess about the limit cycle trajectories away from the respective fixed points undergoing the particular bifurcation, so that the corresponding phase sensitivity function cannot be parametrized in terms of the original oscillator dynamics. Moreover, the Bautin bifurcation (or generalized Hopf bifurcation) has the normal form that agrees with that of the Hopf bifurcation except for the sign of the parameter of the cubic term is different. This leads to a subcritical Hopf bifurcation, whose branch of unstable periodic orbits becomes stable at a saddle-node

will present three different reduction techniques in *Section 2.2.2*. Central to these reductions are center manifolds and normal forms. Due to their importance, we will revisit the corresponding theories briefly.

### 2.2.1 Center manifold and normal form

The concepts of center manifolds and of normal forms are so closely related that many textbooks do not bother to distinguish between them. Often, the *center manifold reduction* of a dynamical system is computed first in order to reduce the dimension of the system. Afterwards, this simplified, lower-dimensional system is brought into normal form. However, there is a subtle conceptual difference to the actual *normal form reduction*. A normal form reduction is characterized through smooth, consecutive transformations or changes of coordinates, which preserve the essential characteristics of the underlying dynamical system and which do not reduce its dimension. Via the coordinate transformations a normal form reduction leads to a thorough picture of the dynamics in terms of the system's stable, unstable and center manifolds. Normal form reductions even provide the stable and unstable fibrations over the center manifold<sup>104</sup>. In this sense, normal forms can be considered more general because the reduced analytic expressions accurately describe the dynamics also away from bifurcation points. We will briefly summarize center manifolds and normal forms in the following.

**Center manifold** Whenever a dynamical system passes through a bifurcation, there is a sudden qualitative change in the system's behavior. For instance, a fixed point solution of the dynamical system switches its stability. This change in stability is represented in the spectrum of the linearized dynamics about the fixed point: the real part of at least one eigenvalue changes signs and becomes zero at the critical bifurcation point. The *center manifold* is an invariant manifold corresponding to the eigenvectors associated with the eigenvalues with zero real part<sup>[8]</sup>. The dynamics on the center manifold is slower than that on the stable and unstable manifolds, corresponding to the eigenvalues with negative and positive non-vanishing real parts, respectively. The attraction towards the stable manifold as well as the repulsion from the unstable manifold are exponentially fast. Hence, it is possible to determine the entire dynamics via the center, or critical, modes, i.e. through the variables  $\mathbf{x}_{\text{slow}}$  corresponding to the slow flow along the center

---

bifurcation of periodic orbits. Given the similarity of their normal forms, it appears reasonable to restrict our considerations on the phase reduction of oscillatory dynamics that emerge through a Hopf bifurcation.

<sup>[8]</sup> The eigenvectors associated with the eigenvalues with vanishing real part span the center eigenspace of the respective fixed point. The center manifold has the same dimension as the center eigenspace and is tangential to it at the fixed point.

manifold. More formally, the local behavior of the fast variables  $\mathbf{x}_{\text{fast}}$  around the fixed point can be expressed as

$$\mathbf{x}_{\text{fast}} = \mathbf{C}(\mathbf{x}_{\text{slow}}) . \quad (2.20)$$

Importantly, the function  $\mathbf{C}$ , albeit arbitrary, only contains terms of second and higher order. In fact, the expression (2.20) characterizes the center manifold locally with the corresponding dynamics given by

$$\dot{\mathbf{x}}_{\text{slow}} = \mathbf{L}\mathbf{x}_{\text{slow}} + \mathbf{N}(\mathbf{x}_{\text{slow}}, \mathbf{C}(\mathbf{x}_{\text{slow}})) . \quad (2.21)$$

The real parts of all the eigenvalues of the matrix  $\mathbf{L}$  vanish and  $\mathbf{N}$  contains all the nonlinear terms. This *center manifold reduction* effectively reduces the dimensionality of the system to the number of eigenvalues with vanishing real part. One may interpret this dimensionality reduction in that the fast variables  $\mathbf{x}_{\text{fast}}$  are prescribed by the slow ones  $\mathbf{x}_{\text{slow}}$ , which in the physics literature is often referred to as Haken's *slaving principle*<sup>105,106</sup>.

In the case of a supercritical Hopf bifurcation, a stable fixed point loses stability as a pair of complex conjugate eigenvalues crosses the imaginary axes and stable limit-cycle oscillations emerge. Hence, we have two eigenvalues with zero real part, and the corresponding center manifold is two-dimensional.

**Normal form** The normal form of a bifurcation is the ‘simplest’, reduced equation (2.21) that exhibits the qualitative features of the bifurcation type. The dimension of the normal form coincides with the number of critical modes, and hence with the dimension of the center manifold. The normal form can be achieved, e.g., by removing all non-resonant terms in the nonlinear function  $\mathbf{C}$ .<sup>[9]</sup>

Although the nomenclature appears somewhat misleading, normal form reductions do not necessarily result in the normal form of a bifurcation as defined above. This is only true close to bifurcations of dynamical systems where all eigenvalues have zero real part, e.g., as in the case of a Hopf bifurcation in a two-dimensional dynamical system. The reason for this is that normal form reductions yield a simplified equation – a ‘normal form’ in the strict sense – of the same dimension as

---

<sup>[9]</sup> In consequence, the normal form will contain only *resonant monomials*  $w_1^{m_1} \cdot \dots \cdot w_n^{m_n}$  with  $m_j \in \mathbb{N}, j = 1, \dots, n$ , satisfying

$$m_1 + \dots + m_n = k \quad \text{and} \quad m_1\lambda_1 + \dots + m_n\lambda_n - \lambda_k = 0, \quad \text{for each } k \geq 2. \quad (2.22)$$

For pure imaginary eigenvalues  $\lambda_j$  of the dynamic's Jacobian, the second equation of (2.22) becomes indeed a resonance among frequencies in the usual sense. This resonance property can be proven in a straightforward way for the semi-simple normal form style <sup>cf. Theorem §2.1.5, 107</sup>, see also below.

that of the underlying dynamical system. As such, a normal form reduction is a rigorous transformation of a dynamical system into a simplified equation without reducing its dimension, whereas a center manifold reduction reduces the dimension without simplifying the equation<sup>[10]</sup>. Interestingly, given the normal form through a normal form reduction, the critical center modes will ‘miraculously’ decouple from the fast variables and the normal form of the bifurcation on the center manifold is retained<sup>104,108</sup>. In the following we will refer to the ‘normal form of a bifurcation’ simply as *normal form* unless stated otherwise.

**A bit of history** Normal form theory goes back to Poincaré’s work<sup>109</sup> and has ever since attracted attention as a technique of transforming nonlinear differential equations to generic and simpler standard forms near a (local) bifurcation point. The precise normal form can be determined in different ways. While coordinate transformations have been frequently used, addressing normal form calculations more categorically involves a matrix representation method, an adjoint method and a method based on the representation theory of the Lie algebra  $sl(2, \mathbb{R})$ . All these methods are strongly connected and, as mentioned earlier, based on the ideas of Takens<sup>110,111</sup>. The resulting normal form can be expressed as lying in the kernel of an adjoint linear operator on the space of homogeneous polynomials<sup>104,107,112</sup>. Alternatively, a perturbation technique has been proposed by Nayfeh<sup>113</sup> and Yu<sup>114</sup>, which dwells on the methods of multiple time scales<sup>115</sup> and of intrinsic harmonic balancing<sup>116</sup>. The reductive perturbation approach of Kuramoto in *Section 2.2.2.1* below also uses a two time-scale separation.

**More recent developments** Other approaches to derive normal forms can be subsumed into time averaging<sup>112,117</sup>, a Lyapunov-Schmidt reduction method<sup>118</sup>, and a singular point value method<sup>119,120</sup>. The latter were originally meant to determine focus, or focal, values of a (degenerated Hopf) critical point to prove the existence (and the maximal amount of multiple) limit cycle(s), but this requires to computation of higher-order normal forms<sup>121</sup>. The idea behind the singular point value method is to introduce formal power series and recursive forms to calculate singular point quantities. The Lyapunov-Schmidt reduction approach, on the other hand, elegantly reformulates the problem of proving the existence of periodic solutions emerging from Hopf bifurcations as that of finding a family of solutions of an abstract equation in a functional space of periodic functions. Its reformulation in terms of functional analysis allows for a generalization of the problem in infinite-dimensional space *cf.*<sup>122</sup>. Essentially, one projects the entire system un-

---

<sup>[10]</sup> A center manifold reduction may even lead to the loss of some important nonlinear properties of the system under study that are linked to the dynamics on the stable and unstable manifolds.

der study into the subspace that is spanned by the eigenvectors associated with the pair of purely imaginary eigenvalues at the Hopf point. In contrast to the other approaches, this results into a set of algebraic equations while the others yield differential equations<sup>121</sup>. From the point of view of projecting the system into a specific subspace, also the methods of time averaging and of multiple time scales fall in the same category. For time averaging one transforms the original autonomous system  $\dot{\mathbf{x}} = \mathbf{f}(\mathbf{x}; \mu)$  into a non-autonomous one via  $\mathbf{y} = \exp(t\mathbf{J})\mathbf{x}$ . Here,  $\mathbf{J}$  is the Jacobian of the vector field  $\mathbf{f}(\mathbf{x}; \mu)$  at  $\mathbf{x} = 0$ . Moreover, the domain  $\Omega \subset \mathbb{R}^n$  of  $\mathbf{x} \in \Omega$  is invariant under the Lie group  $\Gamma = \{\exp(t\mathbf{J}) \mid t \in \mathbb{R}\}$ . The time-dependent system is subsequently solved using the conventional averaging method<sup>117,123,124</sup>. It is important to realize that most of these methods rely on a ‘preprocessing’ and a dimensionality reduction following center manifold theory, which assures the existence of an *amplitude equation* and also indicates its order. For instance, the singular point value method first applies a center manifold reduction to the original dynamics, which yields a two-dimensional center manifold associated with the Hopf bifurcation. The perturbation method, by contrast, does not necessarily require such a center manifold reduction<sup>121,125,126</sup>.

**Uniqueness of normal forms** Given the plethora of derivation schemes, it appears obvious to ask whether they all result into the same, unique normal form. Needless to say, uniqueness of normal forms can, in general, not be guaranteed, at least not for ‘classic’ normal forms. Yet, classic normal forms are usually simple enough to become solvable and can be truncated at a given degree. This leaves the question of asymptotic validity. That is, is a normal form in terms of a (formal) series, or a truncated normal form, a reasonably good approximation of the original dynamics? In fact, quite detailed error analyses can be found in the literature<sup>104,127,128</sup>. Murdock presents several error estimates in Chapter 5<sup>104</sup>, among which there is a basic theorem that allows to estimate an asymptotic error (depending on the order of truncation and on the initial distance) if (a) the matrix of the linear term is *semi-simple* and has all its eigenvalues on the imaginary axis, and (b) if the semi-simple normal form style is used, see Lemma 5.3.6<sup>104[11]</sup>. Fixing a normal form style, however, does not necessarily determine a unique normal

---

<sup>[11]</sup> An  $M \times M$  matrix  $\mathbf{A}$  is called semi-simple if it is diagonalizable with diagonal entries  $\lambda_1, \dots, \lambda_M \in \mathbb{C}$ , otherwise  $\mathbf{A}$  is non-semi-simple. A *normal form style* is connected with the choice of a complementary subspace  $\mathcal{H}_k$  of the image of a homological operator applied to a particular vector space  $\mathcal{P}_k$ , as will be shown below. The operator is associated with the Jacobian, that is, with the linear term of the dynamics. In the case that the Jacobian is semi-simple, e.g., in the case of a Hopf bifurcation, there is only one useful choice of  $\mathcal{H}_k$  as the kernel of the operator applied to  $\mathcal{P}_k$ , which is the *semi-simple normal form style*. For non-semi-simple Jacobians, the mainly used styles are the adjoint operator or inner product normal form popularized by Elphick and co-workers<sup>129</sup>, and the  $\text{sl}(2, \mathbb{R})$  normal form due to Cushman and Sanders<sup>130</sup>.

form<sup>104</sup>. The main reason being is that all higher order terms in the normal form are normalized with respect to the linear term only, i.e. the normal form satisfies a condition which is defined through the Jacobian. A more complete normalization, by contrast, builds on a series of normalizations: first the quadratic term is normalized with respect to the linear one, then the cubic term is normalized with respect to the sum of the linear and quadratic terms, etc.<sup>[12]</sup>.

### 2.2.1.1 Hopf normal form

In view of illustrating the pure theory above, we consider different reduction techniques that lead to networks of oscillators in Hopf normal form. We will duly introduce Hopf normal forms in this section both for an uncoupled oscillator, as well as for coupled oscillators in a network. In *Section 2.2.2.1* we will present a physically motivated, reductive perturbation approach promoted by Kuramoto<sup>38</sup>. Its inherent separation of time-scales lets this approach resemble a center manifold reduction. A mathematical approach of a Hopf normal form reduction using nonlinear, so-called Poincaré transformations will be subject in *Section 2.2.2.2*. For simplicity, we will consider a two-dimensional system so that the dimension of the phase space already coincides with the one of the expected center manifold. While this approach is hence kept as mathematically exact as possible, the concept extends naturally to general  $n$ -dimensional systems, where the governing equations restricted to the center manifold can be computed with a projection method as outlined in Chapter 5.4<sup>122</sup>. Ultimately, we will provide a rather general normal form reduction approach in *Section 2.2.2.3* that goes back to early ideas of Takens<sup>111</sup> and utilizes an adjoint linear operator expressed in a Lie bracket formalism. To compare it against the two other methods, we have applied it exemplarily to a two-dimensional system in *Section S.4* of the *Supplementary Material*, where we also showed the computations of Hopf normal forms of higher order.

**Hopf normal form of a single oscillator** The Hopf normal form of a single oscillator in the vicinity of a (supercritical) Hopf bifurcation generally reads

$$\dot{w} = f(w; \mu) = \sum_{m=0}^{M-1} (-1)^m \sigma_m |w|^{2m} w + \mathcal{O}^{2M}(w) , \quad w \in \mathbb{C} , \quad (2.23)$$

---

<sup>[12]</sup> The resulting *higher-level normal forms* require more advanced calculations see, e.g.,<sup>117,131</sup>. The actual ideas of these fully normalized normal forms go back to Belitskii<sup>132</sup> and the work by Baider and co-workers<sup>133,134</sup>. One can find alternative notions for higher-level normal forms in the literature like *hypernormal forms*, *simplest normal forms*, or *unique normal forms*. Higher-level normal forms can differ for distinct normal form styles applied, but uniqueness may be established within a fixed normal form style.

with complex-valued coefficients  $\sigma_m = \sigma_m(\mu) \in \mathbb{C}$ . The parameter  $\mu \in \mathbb{R}$  denotes the bifurcation parameter and can be viewed as the distance to the Hopf bifurcation at  $\mu = 0$ . The integer  $M \in \mathbb{N}$  defines the order of the Hopf normal form. For second order, i.e. for  $M = 2$ , equation (2.23) takes on the form of a complex *Stuart-Landau oscillator*.

The complex-valued  $w \in \mathbb{C}$  can be written in polar coordinates  $(R, \theta)$  as  $w = R e^{i\theta}$ , or in planar coordinates  $\mathbf{x} = (x, y) \in \mathbb{R}^2$  as  $w = x + iy$ . Then the radius  $R \geq 0$  and angle  $\theta \in \mathbb{S}^1$  satisfy  $R = \sqrt{x^2 + y^2}$  and  $\theta = \text{atan2}(y, x)$ . The Hopf normal form (2.23) reads in polar coordinates

$$\dot{R} = \sum_{m=0}^{M-1} (-1)^m u_m R^{2m+1} = R \cdot \Re, \quad \dot{\theta} = \sum_{m=0}^M (-1)^m v_m R^{2m} = \Im, \quad (2.24)$$

with  $\sigma_m = u_m + iv_m$  and real-valued  $u_m, v_m \in \mathbb{R}$ , we abbreviated

$$\Re = \sum_{m=0}^{M-1} (-1)^m u_m R^{2m}, \quad \Im = \sum_{m=0}^M (-1)^m v_m R^{2m}.$$

The corresponding planar dynamics of (2.23) is

$$\dot{\mathbf{x}} = \begin{pmatrix} \Im & -\Re \\ \Re & \Im \end{pmatrix} \mathbf{x}. \quad (2.25)$$

Note that in (2.24) the radial dynamics  $\dot{R}$  decouples from the angular dynamics  $\dot{\theta}$ . If the parameters  $\sigma_m = u_m + iv_m$  are such that  $\dot{R}$  has a stable non-trivial solution  $R^c$ , then there exists a  $T$ -periodic circular limit-cycle solution of (2.23),

$$w^c(t) = x^c(t) + iy^c(t) = R^c e^{i\theta^c}, \quad \text{or} \quad \mathbf{x}^c(t) = \begin{pmatrix} x^c(t) \\ y^c(t) \end{pmatrix} = R^c \begin{pmatrix} \cos \theta^c \\ \sin \theta^c \end{pmatrix}$$

with constant radius  $R^c$  and constantly increasing phase  $\theta^c(t) = \omega t + \theta_0$ . The period  $T = 2\pi/\omega$  is defined through the frequency  $\omega$ . Note that both  $R^c$  and  $\omega$  depend on the normal form coefficients  $\sigma_m$  or  $(u_m, v_m)$ , respectively, with  $m = 0, \dots, M-1$ .<sup>[13]</sup> Without loss of generality we set  $\theta_0 = 0$  so that  $\theta^c$  is uniquely defined through the frequency  $\omega$ .

---

<sup>[13]</sup> For second order Hopf normal forms, i.e.  $M = 2$ ,  $R^c = \sqrt{u_0/u_1}$  and  $\omega = v_0 - u_0 v_1/u_1$  if  $u_0, u_1 > 0$ . For third order,  $M = 3$ ,  $R^c > 0$  solves  $u_0 - u_1 R^2 + u_2 R^4 = 0$  if  $u_0, u_1, u_2 > 0$  and  $u_1^2 - 4u_0 u_2 \geq 0$ . The frequency  $\omega$  then depends on  $u_0, u_1, u_2, v_0, v_1, v_2$ .

**Hopf normal form with coupling** If we consider an oscillator in Hopf normal form as one node in a network of oscillators, the governing dynamics read

$$\dot{w}_k = f(w_k; \mu) + \kappa g_k(w_1, \dots, w_N) \stackrel{(2.23)}{=} \sum_{m=0}^{M-1} (-1)^m \sigma_m |w_k|^{2m} w_k + \kappa g_k(w_1, \dots, w_N) , \quad (2.26)$$

with coupling function  $g_k : \mathbb{C}^N \rightarrow \mathbb{C}$  that depends on all other oscillators  $w_{j \neq k} \in \mathbb{C}$ . The coupling strength  $\kappa$  is usually assumed to be small,  $|\kappa| \ll 1$ .<sup>[14]</sup>

Capitalizing on the assumption of exclusively pairwise interactions as in (2.2), then normal form reductions preserve this pairwise coupling structure; the proper derivation can be found in *Section S.3* of the *Supplementary Material*. For simplicity, we further assume that the pairwise coupling functions  $g_{kj}$  between oscillators coincide up to an adjacency value  $C_{kj} \in \{0, 1\}$  that denotes structural connectivity between nodes. Hence, the coupling simplifies to

$$g_k(w_1, \dots, w_N) = \frac{1}{N} \sum_{j=1}^N g_{kj}(w_k, w_j) = \frac{1}{N} \sum_{j=1}^N C_{kj} g(w_k, w_j) . \quad (2.27)$$

In summary, we consider the network dynamics

$$\dot{w}_k = \sum_{m=0}^{M-1} (-1)^m \sigma_m |w_k|^{2m} w_k + \frac{\kappa}{N} \sum_{j=1}^N C_{kj} g(w_k, w_j) . \quad (2.28)$$

Two remarks are due at this point: First, thanks to the pairwise coupling structure it suffices to consider only two coupled oscillators  $w, w'$  with dynamics

$$\dot{w} = f(w; \mu) + \kappa g(w, w') , \quad (2.29)$$

and a similar equation holds for  $w'$ . The analytic results of (2.29) can be readily extended to the whole network in an analogous way. Second, the coupling function  $g(w, w')$  in (2.29) depends in general also on the complex conjugates of  $w$  and  $w'$ . We can formally expand  $g(w, w')$  as a power series

$$g(w, \bar{w}, w', \bar{w}') = \sum_{k+l+m+n \geq 0} g_{klmn} w^k \bar{w}^l w'^m \bar{w}'^n \quad (2.30)$$

with complex-valued coefficients  $g_{klmn} \in \mathbb{C}$ . Importantly, not all of these coefficients contribute to the reduced phase dynamics. Indeed, only linear and cubic terms provide substantial contributions to the first and second harmonics of the resulting phase model; see the subsequent *sub-section 2.2.1.2\** that builds on<sup>95</sup>.

---

<sup>[14]</sup> In line with the foregoing sections we refrain from an explicit time-dependence of the coupling function  $g_k$ , but note that the theory also holds for time-varying functions.

**Hopf normal form of an oscillator network** Considering a network of coupled oscillators close to a supercritical Hopf bifurcation, the Hopf normal form of the full network reads<sup>[15]</sup>

$$\dot{w}_k = \alpha w_k - \beta |w_k|^2 w_k + \frac{\kappa}{N} \sum_{j=1}^N C_{kj} [\gamma w_j + \delta \bar{w}_k w_j^2] . \quad (2.31)$$

For the sake of legibility we renamed  $\sigma_1 = \alpha$  and  $\sigma_2 = \beta$ , and introduced the complex-valued coupling parameters  $\gamma = \gamma_R + i\gamma_I$  and  $\delta = \delta_R + i\delta_I$ . With the definitions in *Section 2.2.1*, (2.31) defines the Hopf normal form of the entire network  $w_1, \dots, w_N$  as the monomials

$$\sum_{j=1}^N w_j \quad \text{and} \quad \bar{w}_k \sum_{j=1}^N w_j^2$$

are the only resonant monomials of the pairwise coupling function (2.27).

### 2.2.1.2 Nonlinear coupling terms in Hopf normal forms\*

Allowing for nonlinear coupling terms (2.30) in the network dynamics (2.28), the corresponding phase interaction function  $H$  of the reduced phase model includes also higher harmonics, which may hint at richer collective behavior, see *Section 2.1.5*. However, only a few nonlinear terms  $g_{klmn}$  contribute to the (averaged) phase interaction function  $H$ . To be more precise, only two terms,  $g_{0010}$  and  $g_{0120}$ , are the dominant contributors to the first and second harmonics of  $H$  at leading order.

To demonstrate this result, we consider the dynamics (2.29) of two coupled oscillators in Hopf normal form of arbitrary order  $M \geq 1$ . As mentioned in the previous sub-section, without coupling,  $\kappa = 0$ , we find a stable limit-cycle solution  $w^c(t) = R^c e^{i\theta^c(t)}$  for the two oscillators; for the sake of legibility we will drop the  $^c$  and refer to them as  $w, w'$ . The resulting phase model takes then the form  $\dot{\theta} = \omega + \kappa H(\theta - \theta')$ , where the phase interaction function  $H$  can be expanded in Fourier space as in (2.17). In the complex plane, we can compute  $H$  as

$$H(\theta - \theta') = \langle Z(\theta) \cdot g(w, \bar{w}, w', \bar{w}') \rangle , \quad (2.32)$$

where  $a \cdot b = (\bar{a}b + a\bar{b})/2$  with  $a, b \in \mathbb{C}$  is the complex dot product, the averaging can be expressed in compressed form as  $\langle f(\theta, \theta') \rangle = \frac{1}{2\pi} \int_0^{2\pi} f(\theta + \vartheta, \theta' + \vartheta) d\vartheta$  and

---

<sup>[15]</sup> To be precise, (2.31) is the Hopf normal form of the full network (2.28) with  $S_N \times S^1$ -equivariance and for exclusively pairwise interactions and large network size  $N \gg 1$ , see *Section S.5*.

the (complex-valued) phase sensitivity function is given by  $Z(\theta) = \frac{-c_2+i}{R}e^{i\theta}$ ; see also *Section 2.2.4*.

The assumption of the Hopf normal form implies that  $f(w, \bar{w})$  consists only of the resonant terms  $|w|^n w$  with  $n = 0, 1, 2, \dots$ , and that the dynamics  $\dot{w} = f(w, \bar{w})$  is rotation invariant. Consequently, both  $w(\theta)$  and the phase sensitivity function  $Z(\theta)$  are of the form  $w = w(0)e^{i\theta}$  and  $Z(\theta) = Z(0)e^{i\theta}$ . For direct linear coupling  $g(w, \bar{w}, w', \bar{w}') = g_{0010}w'$  the interaction function  $H(\theta - \theta') = \langle Z(\theta) \cdot g_{0010}w'(\theta') \rangle$  thus contains only first harmonics.

Being near a supercritical Hopf bifurcation, the amplitude of the oscillations is  $R = |w| = \mathcal{O}(\sqrt{\mu})$ , where  $\mu$  denotes the distance to the Hopf bifurcation in parameter space. Introducing  $\varepsilon^2 = \mu$ , we have  $R = \mathcal{O}(\varepsilon)$  and  $Z(\theta) = \mathcal{O}^{-1}(\varepsilon)$ . Any higher order term  $|w|^n w$  in  $f(w, \bar{w})$  presents then corrections of order  $\mathcal{O}^3(\varepsilon)$  and  $\mathcal{O}^1(\varepsilon)$  to  $w(\theta)$  and  $Z(\theta)$ , respectively. In view of the expansion in Fourier space (2.17), these terms lead to corrections of order  $\mathcal{O}^2(\varepsilon)$  in  $a_1$  and  $b_1$ , but they do not contribute to higher harmonics  $a_n, b_n \neq 0$  for  $n \geq 2$ .

If we want the phase interaction function  $H$  to contain higher harmonics, we thus have to take higher-order terms  $g_{klmn}$  in the coupling function  $g(w, \bar{w}, w', \bar{w}')$  into account. For simplicity, we consider  $g(w, \bar{w}, w', \bar{w}') = w^k \bar{w}^l w'^m \bar{w}'^n$  a single monomial with  $k, l, m, n \geq 0$  and  $g_{klmn} = \delta_{klmn}$ . Then we have  $Z \cdot g = \mathcal{O}^{k+m+n+l-1}(\varepsilon)$ . On the other hand, it is

$$Z \cdot g(w, w') \propto e^{-i\theta} \cdot (e^{i\theta})^k (e^{-i\theta})^l (e^{i\theta'})^m (e^{-i\theta'})^n = e^{i(k-l-1)\theta} e^{i(m-n)\theta'}.$$

The latter term contributes to the amplitudes  $a_j$  and  $b_j$  of the  $j$ -th harmonic ( $j > 0$ ) when it is a function of only  $\pm j(\theta - \theta')$ . This means that the set  $(k, l, m, n)$  has to fulfill  $k - l - 1 = \pm j$  and  $m - n = \mp j$ . In particular, the term  $\bar{w}^{j-1} w'^j = \mathcal{O}^{2j-1}(\varepsilon)$  contributes significantly to  $a_j$  and  $b_j$ . Therefore, the amplitudes of the  $j$ -th harmonic are of order  $\mathcal{O}(Z \cdot g(w, w')) = \mathcal{O}^{(2j-1)-1}(\varepsilon)$ , that is,

$$a_j, b_j = \mathcal{O}^{2(j-1)}(\varepsilon). \quad (2.33)$$

Note that the reasoning above is in line with the coefficient  $a_0$  of the zeroth harmonic,  $j = 0$ , whose major contributions come from the monomial  $g(w, \bar{w}, w', \bar{w}') = w$  and result into a constant increase or decrease of the natural frequency depending on the sign of  $a_0$ . For  $j > 0$ , the term  $w^{j+1} \bar{w}'^j = \mathcal{O}^{2j+1}(\varepsilon)$  gives contributions of order  $\mathcal{O}^{2j}(\varepsilon)$  to the  $j$ -th harmonic. However, these contributions present only minor corrections as they are smaller than  $a_j, b_j$  of two orders of magnitude, and can therefore be neglected. Following this argumentation, we consider coupling terms of order 3, which yield contributions of order  $\mathcal{O}^2(\varepsilon)$  to the phase dynamics. The terms  $w^2 \bar{w}', |w|^2 w'$ , and  $|w'|^2 w'$  contribute to the first harmonics  $a_1, b_1$ .

However, their values differ at one order of magnitude from  $a_1, b_1$ , so that their contributions can be neglected. Likewise,  $|w|^2 w$  and  $w|w'|^2$  contribute negligibly to the zeroth harmonic, namely by less than two orders of magnitude. The only cubic resonant term that affects the phase dynamics is  $\bar{w}w'^2$ , which contributes to the second harmonics  $a_2, b_2$  at the same order of magnitude  $\mathcal{O}^2(\varepsilon)$ .

Moreover, we can show that no monomial in  $g(w, \bar{w}, w', \bar{w}')$  of even order will contribute to  $H$ . Indeed, employing the inner product in complex form (2.32) for  $g(w, w') \propto \exp(i(k-l)\theta + i(m-n)\theta')$ , we have

$$\begin{aligned} H(\theta - \theta') &\propto \frac{1}{2\pi} \int_0^{2\pi} \alpha_{klmn} e^{-i(\theta+\vartheta)} e^{i((k-l)\theta + (m-n)\theta' + (k-l+m-n)\vartheta)} \\ &\quad + \beta_{klmn} e^{i(\theta+\vartheta)} e^{-i((k-l)\theta + (m-n)\theta' + (k-l+m-n)\vartheta)} d\vartheta \\ &\propto \frac{1}{2\pi} \int_0^{2\pi} \alpha_{klmn} e^{i((k-l+m-n-1)\vartheta)} + \beta_{klmn} e^{-i((k-l+m-n-1)\vartheta)} d\vartheta , \end{aligned} \quad (2.34)$$

where  $\alpha_{klmn}, \beta_{klmn} \in \mathbb{C}$  are constants. Due to the inherent averaging in (2.34) and as  $\exp(in\vartheta)$  is  $2\pi$ -periodic,  $H(\theta - \theta')$  will vanish if  $(k - l + m - n)$  is even. This means that only monomials of odd order will contribute to the phase interaction function  $H$ .

## 2.2.2 Identifying the Hopf normal form

The starting point for all the Hopf normal form reductions is the oscillator network (2.1), where each node  $\mathbf{x}_k \in \mathbb{R}^n$  is close to a supercritical Hopf bifurcation. More specifically and given the main assumptions on weak coupling, (nearly) identical oscillators and the pairwise coupling structure, we reconsider (2.15),

$$\dot{\mathbf{x}}_k = \mathbf{f}(\mathbf{x}_k; \mu) + \frac{\kappa}{N} \sum_{j=1}^N C_{kj} \mathbf{g}(\mathbf{x}_k, \mathbf{x}_j)$$

with vector functions  $\mathbf{f} = (f_1, \dots, f_n) : \mathbb{R}^n \rightarrow \mathbb{R}^n$  and  $\mathbf{g} = (g_1, \dots, g_n) : \mathbb{R}^{N \times n} \rightarrow \mathbb{R}^n$  and small coupling strength  $|\kappa| \ll 1$ . Without coupling,  $\kappa = 0$ , each node has a stable fixed point solution  $\tilde{\mathbf{x}}_k$ . Then  $\mathbf{f}(\mathbf{x} = \tilde{\mathbf{x}}_k; \mu) = \mathbf{0}$  for all  $k = 1, \dots, N$  and small values of the bifurcation parameter  $\mu \in \mathbb{R}$ .

The essential assumption for the supercritical Hopf bifurcation is that there is a parameter value  $\mu = \mu_k$  such that each fixed point  $\tilde{\mathbf{x}}_k$  undergoes a supercritical Hopf bifurcation in the absence of coupling: For  $\mu < \mu_k$ , the dynamics (2.15) has a stable fixed point, which loses stability at  $\mu = \mu_k$ , and stable oscillations emerge for  $\mu > \mu_k$ . Without loss of generality we translate the fixed point to the origin, i.e.  $\tilde{\mathbf{x}}_k = \mathbf{0}$  for all  $k$ , and assume that  $\mu_k = 0$ . Then for  $\mu > 0$ , each node exhibits stable limit cycle oscillations with natural frequency  $\omega_k \neq 0$  and

amplitude  $R_k = \mathcal{O}(\varepsilon)$  where  $\varepsilon = \sqrt{\mu}$ .

In the following sub-sections we will illustrate three different ways how to reduce (2.15) to the Hopf normal form network (2.31),

$$\dot{w}_k = \alpha w_k - \beta |w_k|^2 w_k + \frac{\kappa}{N} \sum_{j=1}^N C_{kj} [\gamma w_j + \delta \bar{w}_k w_j^2] .$$

Note that all four parameters  $\alpha, \beta, \gamma, \delta \in \mathbb{C}$  will depend on the functions  $\mathbf{f}$  and  $\mathbf{g}$  as well as on the bifurcation parameter  $\mu$ . The different Hopf normal form reductions to be presented below vary not only in their methodical approach, but also in their accuracy. To be precise, while, e.g., the reductive perturbation approach in *Section 2.2.2.1* discards any higher order dependence on  $\mu$ , the nonlinear transforms approach, *Section 2.2.2.2*, respects this  $\mu$ -dependence at all times. The differences between the reduction techniques<sup>[16]</sup> may be negligible for small-amplitude oscillations, that is, close to the Hopf bifurcation point with  $0 < \mu \ll \mu_0 \ll 1$ . But the resulting normal form techniques will diverge drastically when the amplitudes of oscillation become larger. These differences eventually become evident in the reduced phase dynamics and may cause qualitatively different collective dynamics.

In anticipation of *Section 2.2.3*, the subsequent phase reductions of the reduced Hopf normal form dynamics (2.31) are all identical within the theory of weakly coupled oscillators. Hence, possible inconsistencies between the resulting phase models are solely due to the different levels of accuracy of the normal form reductions. For this reason, we will refer to the analytic phase reduction techniques as their underlying normal form reductions, *reductive perturbation reduction* and the *nonlinear transform reduction*, respectively.

### 2.2.2.1 Kuramoto's reductive perturbation

To outline Kuramoto's early approach to derive the Hopf normal form we adopt the reasoning of Chapter 2 in his seminal book "Chemical Oscillations, Turbulence, and Waves"<sup>38</sup>. The approach belongs to the general group of *reductive perturbation methods*, which include all related techniques using stretched space-time coordinates. It builds on the method of multiple scales by dwelling on a small parameter expansion, much related to bifurcation theory<sup>135</sup>. Although the

<sup>[16]</sup> The accuracy of the reductive perturbation method is at first order in  $\mu$ . The accuracy of the nonlinear transform approach is at the same order in  $\mu$  as the order  $M$  of the normal form. As to the third approach based on Takens, it is possible to achieve the same accuracy as with the nonlinear transform approach. To do so, one assumes the parameter  $\mu$  to be an additional variable and consider the  $n + 1$ -dimensional, so-called extended system. The subsequent transformations then become parameter-dependent and can be implemented in the corresponding algorithm, see *Section 2.2.2.3* and<sup>108</sup>. For the sake of simplicity, however, we present only the non-extended system, thereby providing another normal form with the same accuracy as the reductive perturbation approach.

mathematical theory in the presented reductive perturbation approach lacks some precision, as has already been noted by Haken and Kuramoto<sup>136,137</sup>, the method has proven to be of indisputable utility in practice.

The ultimate goal of the reductive perturbation approach is to derive a so-called amplitude equation, which coincides with the canonical model of the the network of oscillators close to a supercritical Hopf bifurcation. Given the system (2.15), we recall that we can actually focus on two coupled oscillators  $\mathbf{x}, \mathbf{x}' \in \mathbb{R}^n$  with dynamics

$$\dot{\mathbf{x}} = \mathbf{f}(\mathbf{x}; \mu) + \kappa \mathbf{g}(\mathbf{x}, \mathbf{x}') \quad (2.35)$$

and an analogous expression for  $\mathbf{x}'$ ,  $\dot{\mathbf{x}'} = \mathbf{f}(\mathbf{x}'; \mu) + \kappa \mathbf{g}(\mathbf{x}', \mathbf{x})$ . Due to the symmetry it suffices to consider only the dynamics of  $\mathbf{x}$  in the following. The stable fixed point solution  $\mathbf{x} = \mathbf{0}$  undergoes a Hopf bifurcation at  $\mu = 0$ , giving rise to stable limit-cycle oscillations with amplitude  $R = \mathcal{O}(\varepsilon)$  where  $\varepsilon = \sqrt{\mu}$ . In the following we will only consider  $\mu > 0$  and small coupling strengths  $0 \leq |\kappa| \ll \mu \ll 1$ . We further substitute  $\kappa \mapsto \varepsilon^2 \kappa$ , which indicates the smallness of  $\kappa$  compared to  $\mu$ . The dynamics (2.35) thus becomes

$$\dot{\mathbf{x}} = \mathbf{f}(\mathbf{x}; \varepsilon^2) + \varepsilon^2 \kappa \mathbf{g}(\mathbf{x}, \mathbf{x}') .$$

Next, we expand  $\mathbf{f}(\mathbf{x}; \varepsilon^2)$  around  $\mathbf{x} = 0$  in terms of

$$\mathbf{f}(\mathbf{x}; \varepsilon^2) = \mathbf{n}_1(\mathbf{x}; \varepsilon^2) + \mathbf{n}_2(\mathbf{x}, \mathbf{x}; \varepsilon^2) + \mathbf{n}_3(\mathbf{x}, \mathbf{x}, \mathbf{x}; \varepsilon^2) + \mathcal{O}^4(\mathbf{x}) , \quad (2.36)$$

where the functions  $\mathbf{n}_k$  are given by

$$\mathbf{n}_k(\mathbf{u}^{(1)}, \mathbf{u}^{(2)}, \dots, \mathbf{u}^{(k)}; \varepsilon^2) = \sum_{i_1, \dots, i_k=1}^n \frac{1}{k!} \left( \frac{\partial^k \mathbf{f}(\mathbf{x}; \varepsilon^2)}{\partial x_{i_1} \partial x_{i_2} \dots \partial x_{i_k}} \right)_{\mathbf{x}=0} u_{i_1}^{(1)} u_{i_2}^{(2)} \dots u_{i_k}^{(k)} \quad (2.37)$$

with  $\mathbf{u}^{(j)} = (u_1^{(j)}, \dots, u_n^{(j)})^\top \in \mathbb{R}^n$ . We further expand  $\mathbf{n}_k$  with respect to  $\varepsilon^2$  and immediately obtain

$$\mathbf{f}(\mathbf{x}; \varepsilon^2) = \hat{\mathbf{L}}_0 \mathbf{x} + \varepsilon^2 \hat{\mathbf{L}}_1 \mathbf{x} + \mathbf{n}_2(\mathbf{x}, \mathbf{x}) + \mathbf{n}_3(\mathbf{x}, \mathbf{x}, \mathbf{x}) + \mathcal{O}^4(\mathbf{x}) , \quad (2.38)$$

where  $\mathbf{n}_2(\mathbf{x}, \mathbf{x}) = \mathbf{n}_2(\mathbf{x}, \mathbf{x}; \varepsilon^2 = 0)$  and a similar expression for  $\mathbf{n}_3$ ; see also *Section S.1* in the *Supplementary Material*. In (2.38) we omitted all  $\mathcal{O}(\varepsilon^2)$  terms in  $\mathbf{n}_2$  and  $\mathbf{n}_3$ . Since we assumed  $\mathbf{x}$  to undergo a Hopf bifurcation, the operator  $\hat{\mathbf{L}}_0$  has a pair of purely imaginary eigenvalues  $\pm i\omega_0$ , while the other  $n - 2$  eigenvalues have non-vanishing real part. Let  $\mathbf{u}$  and  $\mathbf{v}$  denote the right and left eigenvectors of  $\hat{\mathbf{L}}_0$ , respectively, corresponding to the eigenvalue  $+i\omega_0$ . That is,  $\hat{\mathbf{L}}_0 \mathbf{u} = i\omega_0 \mathbf{u}$  and  $\mathbf{v} \hat{\mathbf{L}}_0 = i\omega_0 \mathbf{v}$ . They are normalized as  $\mathbf{v} \mathbf{u} = v_1 u_1 + \dots + v_n u_n = 1$

and fulfill  $\mathbf{v}\bar{\mathbf{u}} = \bar{\mathbf{v}}\mathbf{u} = 0$ . Furthermore, let  $\mathbf{x}_0$  denote the solution to the linearized unperturbed system,  $\dot{\mathbf{x}} = \hat{\mathbf{L}}_0\mathbf{x}$ , which can be given as

$$\mathbf{x}_0(t) = w e^{i\phi(t)} \mathbf{u} + \bar{w} e^{-i\phi(t)} \bar{\mathbf{u}} . \quad (2.39)$$

$w$  is an arbitrary complex number (the ‘‘complex amplitude’’), and  $\phi(t) = \omega_0 t$ . In general, however, a solution  $\mathbf{x}(t)$  that satisfies the full dynamics (2.35) will deviate from  $\mathbf{x}_0(t)$ . When introducing a rescaled time,  $\tau = \varepsilon^2 t$ , and considering  $w = w(\tau)$  to be time-dependent (on the slower time scale), we can describe the time-asymptotic behavior of  $\mathbf{x}(t)$  in the form

$$\begin{aligned} \mathbf{x} &= \mathbf{x}_0(w, \bar{w}, \phi) + \boldsymbol{\rho}(w, \bar{w}, w', \bar{w}', \phi) , \\ \dot{w} &= f(w, \bar{w}) + \kappa g(w, \bar{w}, w', \bar{w}') . \end{aligned} \quad (2.40)$$

The functions  $\boldsymbol{\rho}, f, g$  are to be determined through perturbations, i.e., by considering a ‘small’ deviation from the exact solution  $\mathbf{x} = \mathbf{x}_0$  and expanding  $\boldsymbol{\rho}, f, g$  around it. Equation (2.40) is referred to as *amplitude equation*. The explicit form of  $f(w, w')$  in lowest order is

$$f(w, \bar{w}) = \alpha w - \beta |w|^2 w . \quad (2.41)$$

Here,  $\alpha$  and  $\beta$  satisfy

$$\begin{aligned} \alpha &= \mathbf{v} \hat{\mathbf{L}}_1 \mathbf{u} , \\ \beta &= -3\mathbf{v} \mathbf{n}_3(\mathbf{u}, \mathbf{u}, \bar{\mathbf{u}}) + 4\mathbf{v} \mathbf{n}_2 \left( \mathbf{u}, \hat{\mathbf{L}}_0^{-1} \mathbf{n}_2(\mathbf{u}, \bar{\mathbf{u}}) \right) \\ &\quad + 2\mathbf{v} \mathbf{n}_2 \left( \bar{\mathbf{u}}, (\hat{\mathbf{L}}_0 - 2i\omega_0 \mathbf{I})^{-1} \mathbf{n}_2(\mathbf{u}, \mathbf{u}) \right) , \end{aligned} \quad (2.42)$$

where  $\mathbf{I}$  denotes an  $n$ -dimensional identity matrix; cf. Eqs. (2.2.17–20) in<sup>38</sup>. The exact derivation with all mathematical details as well as a general form of the coupling function  $g(w, \bar{w}, w', \bar{w}')$  can be found in *Section S.1* in the *Supplementary Material*.

Linear coupling can be either diffusive or direct (non-diffusive), i.e  $\mathbf{g} = \mathbf{g}_{\text{diff}}$  or  $\mathbf{g} = \mathbf{g}_{\text{dir}}$ , respectively, yielding

$$\left. \begin{aligned} \mathbf{g}_{\text{diff}}(\mathbf{x}, \mathbf{x}') &= \hat{\mathbf{D}}(\mathbf{x}' - \mathbf{x}) \\ \mathbf{g}_{\text{dir}}(\mathbf{x}, \mathbf{x}') &= \hat{\mathbf{D}}\mathbf{x}' \end{aligned} \right\} \implies \left\{ \begin{aligned} g_{\text{diff}}(w, w') &= \gamma(w' - w) \\ g_{\text{dir}}(w, w') &= \gamma w' \end{aligned} \right. , \quad (2.43)$$

with  $\gamma = \mathbf{v} \hat{\mathbf{D}} \mathbf{u}$  and  $\hat{\mathbf{D}} \in \mathbb{R}^{n \times n}$ , see also<sup>95</sup>.

According to (2.31), a second-order amplitude equation for weakly coupled oscillators near a supercritical Hopf bifurcation point with linear coupling  $\kappa\gamma w'$  obeys

the form

$$\dot{w} = \alpha w - \beta |w|^2 w + \kappa(\gamma w' + \delta \bar{w} w'^2) , \quad (2.44)$$

where the complex constants  $\alpha, \beta$ , and  $\gamma$  are given in (2.42) and (2.43), and  $\delta \in \mathbb{C}$  reads

$$\delta = 2\mathbf{v}\mathbf{n}_2 \left( \bar{\mathbf{u}}, (\hat{\mathbf{L}}_0 - 2i\omega_0 \mathbf{I})^{-1} \hat{\mathbf{D}} (\hat{\mathbf{L}}_0 - 2i\omega_0 \mathbf{I})^{-1} \mathbf{n}_2(\mathbf{u}, \mathbf{u}) \right) . \quad (2.45)$$

For more general, nonlinear couplings  $\mathbf{g}(\mathbf{x}, \mathbf{x}') = \sum_{j,k \geq 0} \mathbf{G}_{jk}(\mathbf{x}, \mathbf{x}')$ , only the parameter  $\delta$  in (2.44) changes to

$$\begin{aligned} \delta = 2\mathbf{v}\mathbf{n}_2 & \left( \bar{\mathbf{u}}, (\hat{\mathbf{L}}_0 - 2i\omega_0 \mathbf{I})^{-1} \left[ \mathbf{G}_{01} (\hat{\mathbf{L}}_0 - 2i\omega_0 \mathbf{I})^{-1} \cdot \mathbf{n}_2(\mathbf{u}, \mathbf{u}) - \mathbf{G}_{02}(\mathbf{u}, \mathbf{u}) \right] \right) \\ & - \mathbf{v}\mathbf{G}_{11}(\bar{\mathbf{u}}, (\hat{\mathbf{L}}_0 - 2i\omega_0 \mathbf{I})^{-1} \mathbf{n}_2(\mathbf{u}, \mathbf{u})) + \mathbf{v}\mathbf{G}_{12}(\bar{\mathbf{u}}, \mathbf{u}, \mathbf{u}) , \end{aligned} \quad (2.46)$$

where  $\mathbf{G}_{01}$  is the matrix corresponding to direct linear coupling, that is,  $\mathbf{G}_{01} = \hat{\mathbf{D}}$ , see (2.43), and  $\mathbf{G}_{jk}$  are nonlinear coupling terms of order  $j + k$  as defined in *Section S.2 in the Supplementary Material*. For linear coupling all  $\mathbf{G}_{jk}$  vanish except for  $\mathbf{G}_{01}$ , in which case we retrieve (2.45).

### 2.2.2.2 Poincaré's reduction via nonlinear transforms

Instead of employing perturbation theory one can alternatively derive the Hopf normal form via nonlinear transforms, as already used by Poincaré. To introduce this, we follow closely the line of argument in Kuznetsov's textbook<sup>122</sup> (Chapter 3). We consider again the dynamics (2.35) for two weakly coupled oscillators as in the previous sub-section. To simplify notation, we restrict our case to only two dimensions  $\mathbf{x} = (x, y), \mathbf{x}' = (x', y') \in \mathbb{R}^2$ . The straightforward extension to  $n$ -dimensional dynamical systems can be found in Chapter 5<sup>122</sup>. As usual, for  $\mu = 0$  both uncoupled units undergo a supercritical Hopf bifurcation. We can decompose  $\mathbf{f}$  into a linear and nonlinear part,

$$\mathbf{f}(\mathbf{x}) = \mathbf{L}(\mu)\mathbf{x} + \mathbf{F}(\mathbf{x}; \mu) ,$$

where  $\mathbf{L}(\mu)$  has eigenvalues  $\lambda(\mu) = \varrho(\mu) \pm i\omega(\mu)$  that satisfy  $\varrho(0) = 0$  and  $\omega(0) = \omega_0 > 0$ . The goal of the nonlinear transform approach is to rewrite the dynamics in a generic form (2.26) and to provide an instruction how to determine the corresponding complex parameters with a sequence of near-identity transformations. For this, the two main steps are as follows: (i) transform the uncoupled part  $\mathbf{f}(\mathbf{x}; \mu)$  into the desired Hopf normal form  $\alpha(\mu)w - \beta(\mu)|w|^2 w$ , and (ii) apply the transformation to the coupling term  $\mathbf{g}(\mathbf{x}, \mathbf{x}')$  and derive the respective parameters of the coupling function  $g(w, w')$ . The nonlinear coupling terms in  $\mathbf{g}(\mathbf{x}, \mathbf{x}')$

can pose a challenge, indeed. That is why often all nonlinear coupling terms are disregarded in order to derive the reduced coupling function  $g(w, w')$ . We here show, however, how nonlinear coupling terms can be treated within the nonlinear transforms approach. In the following, we briefly sketch the strategy and refer to *Section S.3* in the *Supplementary Material* for all mathematical details.

(i) We write the dynamics (2.35) in complex form

$$\dot{z} = \lambda z + \tilde{f}(z, \bar{z}; \mu) + \kappa \tilde{g}(z, \bar{z}, z', \bar{z}'; \mu) , \quad (2.47)$$

where the transformation  $\mathbf{x} \in \mathbb{R}^2 \mapsto z \in \mathbb{C}$  in the complex plane is determined by the eigenvectors of the Jacobian  $\mathbf{L}$ . Provided that the uncoupled part of (2.47) can be approximated in polynomial from up to third order, that is,

$$\dot{z} = \lambda z + \sum_{2 \leq k+l \leq 3} f_{kl} z^k \bar{z}^l + \mathcal{O}^4(z) , \quad (2.48)$$

we can achieve the Hopf normal form for an uncoupled oscillator  $\dot{w} = \lambda w - \beta|w|^2 w + \mathcal{O}^4(w)$  via a *Poincaré transformation*, i.e. a nonlinear near-identity coordinate transform

$$z = \psi(w) = w + \sum_{2 \leq k+l \leq 3} h_{kl} w^k \bar{w}^l . \quad (2.49)$$

The coefficients  $h_{jk}$  depend on  $\lambda$  and the  $f_{kl}$  and can be identified through introducing a local inverse transform and a subsequent comparison of coefficients, see *Section S.3*.

(ii) The more cumbersome part is to reduce the coupling function  $g(w, w') = g(w, \bar{w}, w', \bar{w}')$  explicitly. This yields a formal power series

$$g(w, \bar{w}, w', \bar{w}') = \sum_{k+l+m+n \geq 0} g_{klmn} w^k \bar{w}^l w'^m \bar{w}'^n , \quad (2.50)$$

from  $\tilde{g}(z, z') = \tilde{g}(z, \bar{z}, z', \bar{z}')$  using the transform (2.49). Note that the near-identity character of the transforms leaves the linear terms of  $\tilde{g}(z, z')$  unchanged. This means, in case of direct linear coupling  $\tilde{g}(z, z') = \gamma z'$  we can directly infer the coefficients  $g_{0010}$ . However, due to the higher order terms in (2.49), we readily find coefficients  $g_{klmn}$  with  $k+l+m+n > 1$ . As mentioned above, we do not need to calculate all of them. The coefficients of third order are  $g_{2100}, g_{2001}, g_{0120}, g_{0021}, g_{1110}, g_{1011}$  and those contributing dominantly

to the first and second harmonics of the phase model can be given by

$$g_{0010} = \tilde{g}_{0010}$$

$$g_{0120} = \frac{1}{2} \left( \tilde{g}_{0120} - h_{11}\tilde{g}_{0020} - h_{01}\overline{\tilde{g}_{0002}} + h_{20}\tilde{g}_{0110} + \overline{h_{02}}\tilde{g}_{0101} \right. \\ \left. - h_{11}h_{20}\tilde{g}_{0010} - h_{11}\overline{h_{02}}\tilde{g}_{0001} - |h_{02}|^2\overline{\tilde{g}_{0010}} - h_{20}h_{02}\overline{\tilde{g}_{0001}} \right) ,$$

where  $\tilde{g}_{klmn}$  are the coefficients of the respective power series of  $\tilde{g}(z, \bar{z}, z', \bar{z}')$  in (2.47). These coefficients again depend on the foregoing transformation into complex coordinates and can be expressed in terms of the eigenvectors of  $\mathbf{L}$  and of the original coupling term  $\mathbf{g}(\mathbf{x}, \mathbf{x}')$ . The resulting expression become rather lengthy and we refrain from computing them explicitly but note that the method can be implemented in algorithmic form<sup>[17]</sup>.

### 2.2.2.3 Takens' reduction via Lie brackets

This admittedly more abstract, yet frequently used technique to compute the Hopf normal form has been introduced by Leung and co-workers<sup>138,139</sup> but is coined according to Takens' corresponding work<sup>111</sup>. The approach belongs to the class of the so-called matrix representation methods. It allows for determining arbitrary higher-order Hopf normal forms, though the resulting normal form is of the same order of accuracy as the reductive perturbation technique in *Section 2.2.2.1*<sup>[18]</sup>. We again start off with dynamics (2.35) in the vicinity of the fixed point  $\mathbf{x} = 0$  with  $|\mu| \ll 1$  sufficiently small. After diagonalizing the Jacobian  $\mathbf{L}(\mu) = \mathbf{D}\mathbf{f}(\mathbf{x}; \mu)$  evaluated at  $(\mathbf{x}; \mu) = (0, 0)$ , we find the dynamics in Jordan normal form

$$\dot{\mathbf{z}} = \mathbf{J}\mathbf{z} + \mathbf{F}(\mathbf{z}) + \kappa\mathbf{G}(\mathbf{z}, \mathbf{z}') , \quad (2.51)$$

with  $\mathbf{J} = \text{diag}(\lambda_1, \dots, \lambda_n)$ , where  $\lambda_j \in \mathbb{C}$ ,  $j = 1, \dots, n$ , are the complex eigenvalues of  $\mathbf{L}(0)$ , and  $\mathbf{F}$  comprises all nonlinear terms in  $\mathbf{z}$ . As usual, we first consider (2.51) with  $\kappa = 0$  and neglect the coupling function  $\mathbf{G}(\mathbf{z}, \mathbf{z}')$  for the time being. Once

---

<sup>[17]</sup> There is a prevailing and inherent dependence of all coefficients on the bifurcation parameter  $\mu$ . Evaluating the resulting formulas at the bifurcation point,  $\mu = 0$ , reveals the similarity to the *reductive perturbation approach*, cf. *Section 2.2.2.1*. For instance, we can determine the parameter  $\beta(0) = \beta(\mu = 0)$  that relates to the cubic term in the normal form as

$$\beta(0) = -\frac{i}{2\omega_0} (f_{20}f_{11} - 2|f_{11}|^2 - \frac{1}{3}|f_{02}|^2) - \frac{1}{2}f_{21} .$$

This closely resembles equation (2.42) in the previous sub-section.

<sup>[18]</sup> The technique presented here applies only to vector fields that have a single zero eigenvalue or a single pair of purely imaginary eigenvalues<sup>112</sup>. Moreover, we restrict the theory to the semi-simple case only, that is, the dynamics have a diagonalizable linear part.

we have established a transformation

$$\mathbf{z} = \mathbf{P}(\mathbf{w}) = \mathbf{w} + \mathbf{p}(\mathbf{w}) , \quad (2.52)$$

which removes all irrelevant terms (up to a given order) from the Taylor series of

$$\dot{\mathbf{w}} = (\mathbf{D}\mathbf{P}(\mathbf{w}))^{-1} [\mathbf{J}\mathbf{P}(\mathbf{w}) + \mathbf{F}(\mathbf{P}(\mathbf{w}))] , \quad (2.53)$$

we can apply the same change of coordinates also to the coupling terms. The transformation (2.52) is nearly-identical due to its linear part, such that  $\mathbf{G}(\mathbf{z}, \mathbf{z}')$  and the transformed coupling function  $\tilde{\mathbf{G}}(\mathbf{w}, \mathbf{w}')$  coincide up to first order. We expand the nonlinear function  $\mathbf{F}(\mathbf{z})$  as a series of homogeneous polynomials

$$\mathbf{F}(\mathbf{z}) = \mathbf{F}_2(\mathbf{z}) + \mathbf{F}_3(\mathbf{z}) + \cdots + \mathbf{F}_r(\mathbf{z}) + \mathcal{O}^{r+1}(\mathbf{z}) , \quad \mathbf{F}_k \in \mathcal{P}_k , \quad (2.54)$$

where  $\mathcal{P}_k$  is the set of homogeneous polynomials of order  $k$ , and  $r \in \mathbb{N}$ . Next, we introduce an adjoint operator  $L_J: \mathcal{P}_k \rightarrow \mathcal{P}_k$  via

$$L_J(\mathbf{Y})(\mathbf{z}) = [\mathbf{Y}, \mathbf{J}\mathbf{z}] (\mathbf{z}) = \mathbf{J}\mathbf{Y}(\mathbf{z}) - (\mathbf{D}\mathbf{Y}(\mathbf{z}))\mathbf{J}\mathbf{z} , \quad (2.55)$$

where  $[\cdot, \cdot]$  denotes the Lie bracket. With this definition we can immediately use the Takens' normal form theorem<sup>111,112,138</sup>: Given a system  $\dot{\mathbf{z}} = \mathbf{J}\mathbf{z} + \mathbf{F}(\mathbf{z})$  of differential equations, with  $\mathbf{F} = \mathbf{F}_2 + \mathbf{F}_3 + \dots$  as in (2.54) truncated at order  $r$ ,  $\mathbf{F}(\mathbf{0}) = \mathbf{0}$ , choose a complement  $\mathcal{H}_k$  of  $L_J(\mathcal{P}_k)$ , such that  $\mathcal{P}_k = L_J(\mathcal{P}_k) \oplus \mathcal{H}_k$ . Then, there is an analytic change of coordinates in a neighborhood of the origin which transforms the system above to  $\dot{\mathbf{w}} = \mathbf{h}(\mathbf{w}) = \mathbf{h}_1(\mathbf{w}) + \mathbf{h}_2(\mathbf{w}) + \cdots + \mathbf{h}_r(\mathbf{w}) + R_r$  with  $\mathbf{h}_1(\mathbf{w})$  being the linear term and  $\mathbf{h}_k \in \mathcal{H}_k$  for  $k = 2, \dots, r$ , and residual  $R_r = \mathcal{O}^{r+1}(\mathbf{w})$ . The proof of this theorem is constructive and by induction, using a series of coordinate transforms  $\mathbf{z} = \mathbf{w} + \mathbf{p}_k(\mathbf{w})$  with  $\mathbf{p}_k$  homogeneous polynomials of degree  $k$  with  $k = 1, \dots, r$ . The coefficients of  $\mathbf{p}_k$  are to be determined in each step such that

$$\mathbf{F}_k(\mathbf{w}) + L_J(\mathbf{p}_k)(\mathbf{w}) \in \mathcal{H}_k . \quad (2.56)$$

Details of the proof and further examples can be found in<sup>104,111–113,138,139</sup>[19]. Since we address classical, first-level normal forms only, the entire transformation procedure is based on the Jacobian, that is, on the linearized dynamics near the bifurcation point. If the bifurcation possesses a certain symmetry, these symmetry properties become apparent in the Jacobian and are thus induced on the nonlinear

---

<sup>[19]</sup>  $\mathbf{J}$  is semi-simple, so the complement  $\mathcal{H}_k$  will be chosen as  $\mathcal{H}_k = \ker(L_J(\mathcal{P}_k))$  as mentioned above. In this case, a direct calculation shows that  $\mathcal{H}_k$  is spanned by all resonant monomials of order  $k$  for each  $k \geq 2$ , from which (2.22) follows.

part of the computed normal form. In particular, systems near a Hopf bifurcation are mapped by a polynomial transformation to a normal form that has circular symmetry.

A practical application of this computational approach to a two-dimensional system  $\mathbf{z} = (z_1, z_2)$  near the Hopf bifurcation can be found in *Section S.5* of the *Supplementary Material* including further mathematical details. Unfortunately, the complexity of computing the coefficients for higher order normal forms increases rapidly as the determination of parameters builds recursively upon each other and on the lower order near-identity transformations  $\mathbf{p}_k, k \leq 4$ . It hence becomes necessary to implement efficient algorithms in symbolic computation software without running in danger of overflow errors due to memory storage. An arithmetic algorithm including the computation of normal forms up to order 11 has been presented in<sup>139</sup>. In fact, once higher-order normal forms and their corresponding series of transformations  $\mathbf{p}_k$  have been established, the latter can be applied to the coupling term  $\kappa \mathbf{G}(\mathbf{z}, \mathbf{z}')$  of (2.51). For our purposes, however, it is sufficient to consider the transformed coupling up to third order. Since we already illustrated the derivation of the coupling term using nonlinear transforms in great detail in *sub-section 2.2.2.2*, we here refrain from further heavy mathematics.

### 2.2.3 Interlude

Against the background of normal form reductions from the previous *Section 2.2.2*, we will now introduce four commonly used techniques to reduce oscillator networks to phase models. *Section 2.2.4* will be devoted to the explicit computation of the asymptotic phase map  $\Theta(w)$ , whose gradient evaluated at the limit cycle readily provides the phase sensitivity function  $\mathbf{Z}$ . This method has already been promoted by Winfree<sup>85</sup> but reaches its limits when considering Hopf normal forms of order higher than  $M = 2$ . In this case, Kuramoto's method using Floquet eigenvectors can be applied, which will be presented in *Section 2.2.5*. In *Section 2.2.6* we revise an elegant phase reduction approach dwelling on equivariant theory and symmetry properties of the network. This approach requires the network to be in Hopf normal form. While the previous two methods can, in principle, be applied to any dynamical systems that exhibit stable limit cycle oscillations, the Hopf normal form presents one of the few examples where they can be explicitly exerted to all extent. In *Section 2.2.7* we will reconsider averaging theory. The *rotating wave approximation* and *slowly varying amplitude approximation* introduced there are widely applicable and also hold for oscillatory networks beyond the weak coupling assumption. However, for oscillator networks in Hopf normal form within the theory of weakly coupled oscillators, all four presented phase reduction techniques

(Winfree, Kuramoto, Ashwin & Rodrigues, and Haken) will result in the same reduced phase model despite the different methodical approaches. To demonstrate this, we use, as usual, a network of weakly coupled oscillators. They are close to a supercritical Hopf bifurcation such that we can use the Hopf normal form description (2.31) of the network,

$$\dot{w}_k = \alpha w_k - \beta |w_k|^2 w_k + \frac{\kappa}{N} \sum_{j=1}^N C_{kj} [\gamma w_j + \delta \bar{w}_k w_j^2] , \quad (2.57)$$

with sufficiently small coupling  $|\kappa| \ll 1$ . Then, all the analytic phase reduction techniques will result in the phase model (2.16),

$$\dot{\theta}_k = \omega + \kappa \sum_{j=1}^N C_{kj} H(\theta_k - \theta_j) , \quad (2.58)$$

where the phase interaction function  $H$  can be expanded as a Fourier series (2.17),

$$H(\psi) = \sum_{n \geq 0} a_n \cos(n\psi) + b_n \sin(n\psi) . \quad (2.59)$$

The analytic phase reduction techniques present mathematical recipes along which we can determine the frequency  $\omega$  and the amplitudes  $a_n, b_n$  of the Fourier modes in terms of the normal form coefficients  $\alpha = u_0 + iv_0, \beta = u_1 + iv_1$  as well as  $\gamma = \gamma_R + i\gamma_I$  and  $\delta = \delta_R + i\delta_I$ . The frequency and the Fourier coefficients of first and second harmonics of the reduced phase models will coincide across all analytic phase reduction techniques. The frequency reads  $\omega = u_0(c_0 - c_2)$  and the Fourier coefficients are

$$\begin{aligned} a_1 &= \gamma_R(c_1 - c_2) , & b_1 &= -\gamma_R(1 + c_1 c_2) , \\ a_2 &= R^2 \delta_R(c_3 - c_2) , & b_2 &= -R^2 \delta_R(1 + c_2 c_3) , \end{aligned} \quad (2.60)$$

where we abbreviated  $c_0 = v_0/u_0, c_2 = v_1/u_1, c_1 = \gamma_I/\gamma_R$ , and  $c_3 = \delta_I/\delta_R$ , and  $R$  denotes the amplitude of oscillation.

## 2.2.4 Winfree's reduction via isochrons

The idea behind the reduction via isochrons dwells on explicit expressions of the asymptotic phase map  $\Theta(\mathbf{x})$  along the isochrons  $\mathcal{I}(\theta)$  and of the limit cycle  $\mathcal{C}$ . Once these expressions have been obtained, the phase sensitivity function can be determined as the gradient of the asymptotic phase map and the coupling function can be evaluated at the limit cycle as has been outlined in Section 2.1.4. Their product eventually determines the phase sensitivity function  $H$ , which is the

backbone of the phase model (2.16). In principle, this approach can be applied to every dynamical system that exhibits stable limit cycle oscillations. However, it is essential to include explicit expressions of  $\Theta$  and  $\mathcal{C}$ , which, unfortunately, cannot be obtained analytically in the majority of cases.

Here, we illustrate the procedure along a network of oscillators in Hopf normal form (2.31) of second order,  $M = 2$ . The uncoupled oscillator in polar coordinate form (2.24) has a globally attracting limit cycle

$$w^c(t) = R^c e^{i\omega t}$$

with radius  $R^c = \sqrt{c_2}$  and frequency  $\omega = v_0 - v_1 c_2$  with  $c_2 = u_0/u_1$ . The asymptotic phase map  $\theta = \Theta(w)$  defined in *Section 2.1.1* for  $\mathbf{x} = (\text{Re}(w), \text{Im}(w))$  in  $\mathbb{R}^2 \setminus \{\mathbf{0}\}$  fulfills  $\dot{\theta} = \omega$ . Its explicit form reads

$$\Theta(w = R^c e^{i\phi}) = \arg w - \frac{v_1}{u_1} \ln \left| \frac{w}{w^c} \right| = \phi - \frac{\beta_I}{\beta_R} \ln \left| \frac{R}{R^c} \right| .$$

The phase sensitivity function  $\mathbf{Z}(\theta) = (Z_x(\theta), Z_y(\theta)) = \nabla \Theta(w)|_{w=w^c}$  is the gradient of the phase map  $\Theta$  evaluated at the limit cycle  $w^c$ . For infinitesimally small and pulse-like perturbations  $\mathbf{p} = x_p + iy_p$ , we can compute  $\mathbf{Z}$  also via the phase response function  $G(\theta, \mathbf{p} = x_p + iy_p) = \Theta(w^c(\theta) + \mathbf{p}) - \theta$  according to (2.11) as

$$\mathbf{Z}(\theta) = \begin{pmatrix} Z_x(\theta) \\ Z_y(\theta) \end{pmatrix} = \begin{pmatrix} \partial_x G(\theta, \mathbf{p}) \\ \partial_y G(\theta, \mathbf{p}) \end{pmatrix}_{x_p=y_p=0}$$

The explicit forms of  $\mathbf{Z}(\theta) \in \mathbb{R}^2$  as well as of the corresponding complex-valued form  $Z(\theta) = Z_x(\theta) + iZ_y(\theta)$  are

$$\mathbf{Z}(\theta) = \frac{1}{R^c} \begin{pmatrix} -\sin \theta - c_2 \cos \theta \\ -c_2 \sin \theta + \cos \theta \end{pmatrix} \quad \text{and} \quad Z(\theta) = \frac{-c_2 + i}{R^c} e^{i\theta} . \quad (2.61)$$

When considering the network dynamics (2.31), we strive for the phase model (2.16) with interaction function  $H$ , which was defined as the scalar product of the (real-valued vector function)  $\mathbf{Z}$  and the corresponding (real-valued) coupling function  $\mathbf{g}$  in vector form<sup>[20]</sup> averaged over one period  $T = 2\pi/\omega$ . In the complex plane, the scalar product becomes the complex dot product<sup>[21]</sup> and the phase interaction

<sup>[20]</sup> The coupling function  $\mathbf{g} = (g_x, g_y)$  as required for the computation of  $H$  has components  $g_x = g_x(\theta_k, \theta_j), g_y = g_y(\theta_k, \theta_j)$ , which are the real and imaginary parts, respectively, of  $g(w_k^c(\theta_k), w_j^c(\theta_j))$ .

<sup>[21]</sup> The complex dot product for  $a, b \in \mathbb{C}$  is defined as  $a \cdot b = (\bar{a}b + a\bar{b})/2$ .

function can be computed as

$$H(\psi) = \frac{1}{2\pi} \int_0^{2\pi} (-c_2 + i)e^{i(\psi+\varphi)} \cdot (\gamma e^{i(\psi+\varphi)} + \delta(R^c)^2 e^{-i(\psi-\varphi)}) d\varphi .$$

Evaluating the integral results exactly in (2.17) & (2.60).

### 2.2.5 Kuramoto's reduction via Floquet eigenvectors

When allowing for general oscillatory dynamics, deriving explicit formulas for the asymptotic phase map  $\Theta(\mathbf{x})$  and for the isochrons of an oscillator  $\dot{\mathbf{x}} = \mathbf{f}(\mathbf{x}) \in \mathbb{R}^n$  becomes too complicated to follow the theory of the previous *Section 2.2.4*. This is already true when considering the Hopf normal form of order  $M = 3$ . Yet, we can overcome this problem by exploiting the relationship between the asymptotic phase and the eigenvectors associated with the linearized part of  $\mathbf{f}(\mathbf{x})$  about its periodic limit cycle solution  $\mathbf{x}^c$ . The underlying theory of first-order linear systems with periodic coefficients is called Floquet theory<sup>140</sup> and has been promoted by Kuramoto to being applied for phase reductions<sup>38</sup>. Also this technique can be applied, in principle, to any dynamical system with stable limit cycle oscillations. While it does no longer rely on the explicit form of the phase map  $\Theta$ , it still requires an explicit expression of the limit cycle  $\mathcal{C}$ .

Before we illustrate Kuramoto's reduction for a network of oscillators in Hopf normal form of order  $M = 2$  and  $3$ , we will briefly revise the idea of Floquet eigenvectors. These will be used to derive the phase sensitivity function  $\mathbf{Z}$ . Note that once  $\mathbf{Z}$  is obtained, the computation of the phase interaction function  $H$  will follow the same procedure as in the previous section. To start with we consider an oscillator  $\dot{\mathbf{x}} = \mathbf{f}(\mathbf{x})$  with a stable  $T$ -periodic limit cycle solution  $\mathbf{x}^c$ . For small deviations  $\mathbf{u}(t)$  off  $\mathbf{x}^c(t)$ , we find for  $\mathbf{x}(t) = \mathbf{x}^c(t) + \mathbf{u}(t)$  the linear system

$$\dot{\mathbf{u}} = \mathbf{L}(t)\mathbf{u} , \quad \text{with} \quad \mathbf{L}(t) = \nabla \mathbf{f}(\mathbf{x}) \Big|_{\mathbf{x}=\mathbf{x}^c(t)} \quad (2.62)$$

and  $\mathbf{L}(t)$  is a  $T$ -periodic  $n \times n$ -matrix. A general solution of (2.62) takes the form  $\mathbf{u}(t) = \mathbf{S}(t)e^{\Lambda t}\mathbf{u}(0)$ , where  $\mathbf{S}(t)$  is a  $T$ -periodic matrix with initial condition  $\mathbf{S}(0) = \mathbf{I}$  and  $\Lambda$  is a time-independent matrix. The matrix exponential  $\exp(\Lambda t)$  is defined in the usual way.<sup>[22]</sup> The normalized left and right eigenvectors of  $\Lambda$  associated with eigenvalue  $\lambda_j$  will be denoted by  $\mathbf{v}_j$  and  $\mathbf{u}_j$ . The limit cycle solution  $\mathbf{x}^c$  being stable implies  $\text{Re}(\lambda_j) \leq 0$ . While one eigenvalue  $\lambda_0 \equiv 0$  vanishes, which corresponds to (phase) disturbances along the periodic orbit  $\mathcal{C} = \{\mathbf{x}^c(t) \mid t \in \mathbb{R}\}$ , the other eigenvalues  $\lambda_1, \dots, \lambda_{n-1}$  are assumed to have negative real parts. Fur-

<sup>[22]</sup>  $e^{\Lambda t} = \sum_{k=0}^{\infty} \frac{1}{k!} \Lambda^k t^k = \mathbf{I}_n + \Lambda t + \frac{\Lambda^2 t^2}{2!} + \dots$

thermore, we set  $\mathbf{u}_0 = \dot{\mathbf{x}}^c(0)$ .  $\mathbf{u}_0$  is thus a tangent vector of  $\mathcal{C}$  at point  $\mathbf{x}^c(0)$  and has the same direction as that of the infinitesimal phase disturbances. Moreover,  $\mathbf{u}_0$  satisfies  $\mathbf{S}(t)\mathbf{u}_0 = \dot{\mathbf{x}}^c(t)$ .<sup>[23]</sup> Next we use the facts that the phase sensitivity function  $\mathbf{Z}(\theta)$  is normal to the tangent space  $T(\theta)$  of the isochron  $\mathcal{I}(\theta)$  at point  $\theta(t) = \mathbf{x}^c(\theta(t))$ , and that  $T(0)$  is free from the zero-eigenvector component, cf. *Section 2.2.4* and *Chapter 3.4*<sup>38</sup>. This means that  $\mathbf{Z}(0)\mathbf{u}_j = 0$  for all  $j > 0$ , hence  $\mathbf{Z}(0)$  must be proportional to the left zero-eigenvector  $\mathbf{v}_0$ . As  $\mathbf{Z}(\theta)$  has been introduced as the gradient of the asymptotic phase map  $\Theta(\mathbf{x})$  evaluated on the limit cycle, we can differentiate  $\Theta(\mathbf{x}^c) = \theta^c(t)$  on the limit cycle and find  $\mathbf{Z}(\theta) \cdot \dot{\mathbf{x}}^c(t) = \omega$ , where we used that  $\dot{\theta}^c = \omega = 2\pi/T$ . Identifying  $\mathbf{Z}(t)$  with  $\mathbf{Z}(\theta)$  via  $\theta \mapsto t/\omega$ , we can combine our findings above and arrive at

$$\mathbf{Z}(t) = \omega \mathbf{v}_0 \mathbf{S}(t)^{-1}. \quad (2.63)$$

Now, we can apply the result to  $M$ th order Hopf normal forms (2.23). In fact, we have to determine  $\mathbf{v}_0$  and  $\mathbf{S}(t)$  to derive the phase sensitivity function  $\mathbf{Z}$ . To do so, we consider a stable limit cycle solution  $w^c(t) = R^c e^{i\omega t}$  in the polar coordinate dynamics (2.24). A small deviation  $z(t)$  off the limit-cycle trajectory  $w^c(t)$  as  $w(t) = w^c(t) [1 + z(t)]$  has the linearized dynamics

$$\dot{z} = \left( \sum_{m=0}^{M-1} (-1)^m (u_m + iv_m) (R^c)^{2m} m \right) (z + \bar{z}) + \mathcal{O}^2(z) =: (\varsigma_R + i\varsigma_I)(z + \bar{z}) + \mathcal{O}^2(z). \quad (2.64)$$

Separating real and imaginary parts in terms of  $z = \xi + i\eta$ , we can simplify (2.64) in matrix form as

$$\frac{d}{dt} \begin{pmatrix} \xi \\ \eta \end{pmatrix} = \mathbf{\Lambda} \begin{pmatrix} \xi \\ \eta \end{pmatrix} \quad \text{where} \quad \mathbf{\Lambda} = -2\varsigma_R \begin{pmatrix} 1 & 0 \\ c_2 & 0 \end{pmatrix} \quad (2.65)$$

with  $c_2 = \varsigma_I/\varsigma_R$ . Usually,  $c_2 = c_2^M$  depends on the order of the Hopf normal form<sup>[24]</sup>. The eigenvalues of  $\mathbf{\Lambda}$  are  $\lambda_0 = 0$  and  $\lambda_1 = -2\varsigma_R$  with corresponding left

---

<sup>[23]</sup> Indeed, differentiating  $\dot{\mathbf{x}}_0(t) = \mathbf{f}(\mathbf{x}_0(t))$  on both sides results in

$$\frac{d}{dt} \dot{\mathbf{x}}^c(t) = \frac{d}{dt} \mathbf{f}(\mathbf{x}^c(t)) = \nabla \mathbf{f}(\mathbf{x})|_{\mathbf{x}=\mathbf{x}^c(t)} \cdot \dot{\mathbf{x}}^c(t) = \mathbf{L}(t) \dot{\mathbf{x}}^c(t).$$

So  $\dot{\mathbf{x}}^c(t)$  is a particular solution of  $\dot{\mathbf{u}} = \mathbf{L}(t)\mathbf{u}$ . Thus we can write  $\dot{\mathbf{x}}^c(t) = \mathbf{S}(t) e^{\mathbf{\Lambda} t} \dot{\mathbf{x}}^c(0)$ . Using the definition of the matrix exponential together with  $\mathbf{\Lambda} \mathbf{u}_0 = \lambda_0 \mathbf{u}_0 = 0$ , the right-hand side reduces to  $\mathbf{S}(t) \mathbf{u}_0$  as wanted.

<sup>[24]</sup> For second ( $M = 2$ ) and third order ( $M = 3$ ) Hopf normal forms

$$\dot{\omega} = \sum_{m=0}^{M-1} (-1)^m \sigma_m |\omega|^{2m} \omega, \quad \text{with} \quad \sigma_m = u_m + iv_m,$$

and right eigenvectors

$$\begin{aligned}\mathbf{u}_0 &= R^c \omega \begin{pmatrix} 0 \\ 1 \end{pmatrix}, & \mathbf{u}_1 &= \begin{pmatrix} 1 \\ c_2 \end{pmatrix}, \\ \mathbf{v}_0 &= \frac{1}{R^c \omega} (-c_2, 1), & \mathbf{v}_2 &= (1, 0);\end{aligned}\quad (2.66)$$

the factor  $R^c \omega$  is for consistency with  $\mathbf{u}_0 = \dot{\mathbf{x}}^c(0)$ . Moreover, we find the matrix  $\mathbf{S}(t)$  by linking the deviations  $\xi, \eta$  from  $w^c$  in the complex plane with deviations  $\mathbf{u} \in \mathbb{R}^2$  of the corresponding planar limit cycle solution  $\mathbf{x}^c$  via

$$\mathbf{u}(t) = R^c \mathbf{S}(t) \begin{pmatrix} \xi(t) \\ \eta(t) \end{pmatrix} \quad \text{where } \mathbf{S}(t) = \begin{pmatrix} \cos(\omega t) & -\sin(\omega t) \\ \sin(\omega t) & \cos(\omega t) \end{pmatrix}. \quad (2.67)$$

According to (2.63), the phase sensitivity function is given by

$$\mathbf{Z}(t) = \omega \mathbf{v}_0 \mathbf{S}(t)^{-1} = \frac{1}{R^c} \begin{pmatrix} -\sin(\omega t) - c_2 \cos(\omega t) \\ -c_2 \sin(\omega t) + \cos(\omega t) \end{pmatrix} \quad (2.68)$$

By the change of variables  $t \mapsto \theta/\omega$ , we arrive at the same form (2.61) as in the previous section.

The shape of the phase sensitivity function  $\mathbf{Z}(\theta)$  does not change when incorporating higher order terms in the Hopf normal form (2.23). In fact, the preceding normal form reduction imposes circular symmetry on the dynamics, so that the oscillations with constant radius of the Hopf normal form are to be expected. Incorporating higher order terms in the Hopf normal form increases the accuracy further away from the bifurcation point. These terms will lead at most to a horizontal translation of the phase sensitivity function. Still, this can have important consequences for the synchronization properties of the network.  $\mathbf{Z}$  is an integral part of the phase interaction function  $H$  and shifting  $\mathbf{Z}$  might change the slope of  $H$  at the origin,  $H'(0)$ , which determines the stability of the fully synchronized network state, see also *Section 2.1.5*.

## 2.2.6 Ashwin & Rodrigues' reduction via $S_N \times S^1$ -symmetry

In their recent work, Ashwin and Rodrigues proposed an elegant phase reduction technique by exploiting the symmetry properties of a network of weakly coupled oscillators<sup>141</sup>, see also<sup>142</sup>. In this way it is possible to derive a phase model that respects interaction terms beyond mere pairwise coupling. In fact, Ashwin and

---

we have

$$c_2^2 = \frac{v_1}{u_1}, \quad \text{and} \quad c_2^3 = \frac{v_2}{u_2} \left( 1 - u_1 [u_1^2 - 4v_0 u_2]^{-1/2} \right) + v_1 [u_1^2 - 4u_0 u_2]^{-1/2}.$$

Rodrigues derived terms that represent pairwise, triplet and quadruplet phase interactions. As such, this symmetry approach presents an important extension to previous reported reduction techniques, especially when dealing with networks featuring complex coupling functions of multiple interacting oscillators. Note, however, that in its rigorous mathematical form, this symmetry approach requires each oscillator to undergo a generic supercritical Hopf bifurcation and, in addition, to meet strong symmetry assumptions, which will be specified below. Although this setting appears restrictive at first, we sketch an idea how to loosen some of the assumptions. As any dynamical system close to a Hopf bifurcation can be reduced in Hopf normal form, this will again be our starting point for the following brief revision of the reduction technique. Moreover, we demonstrate that for pairwise coupling, it will lead to the same phase model as the other previously presented methods.

Given a network of  $N \geq 4$  all-to-all coupled oscillators, where each can be described in Hopf normal form given by  $\dot{w}_k = f(w_k; \mu) + \kappa g(w_k, w_1, \dots, w_{k-1}, w_{k+1}, \dots, w_N)$  as in (2.23), the symmetry assumptions by Ashwin and Rodrigues manifest in the network dynamics

$$\dot{w}_k = f(w_k; \mu) + \kappa g(w_k, w_1, \dots, w_{k-1}, w_{k+1}, \dots, w_N) \quad (2.69)$$

through a full permutation symmetry  $S_N$  and through the rotational invariance  $S^1$ . Intuitively, full permutation is given if the dynamics (2.69) can be interchangeably used for any two oscillators  $k \neq j$ . That is, the network dynamics remains the same for any permutation  $\sigma \in S_N$  with

$$\sigma(w_1, \dots, w_N) = (w_{\sigma^{-1}(1)}, \dots, w_{\sigma^{-1}(N)}) .$$

As  $f$  is the same for all oscillators, this means that

$$g(w_k, w_1, \dots, w_N) = g(w_1, w_2, \dots, w_N)$$

is symmetric under all permutations of the last  $N - 1$  arguments that fix the first. In particular, we need the network to be globally (all-to-all) coupled with  $C_{kj} = 1$  for all  $k \neq j$  with the same coupling function for all nodes.

Rotational invariance is fulfilled if both the uncoupled term  $f$  and the coupling  $g$  are in Hopf normal form. To be more precise, (2.69) is rotational invariant if the rotation of all variables  $w_1, \dots, w_N$  by the same phase  $\theta \in \mathbb{S}^1$  does not change the network dynamics. Formally, the action of the group  $S^1$  on  $\mathbb{C}^N$  is defined by

$$\theta(w_1, \dots, w_N) := e^{i\theta}(w_1, \dots, w_N)$$

for any (phase)  $\theta \in \mathbb{S}^1$ . Indeed, the non-vanishing, resonant polynomial components (monomials) appearing in the Hopf normal form are exactly those that satisfy the circular  $S^1$  symmetry. While we previously assumed  $g$  to be an arbitrary power series in its variables, this power series is restricted to consist of only resonant monomials. For  $g$  with monomials of degree lower or equal to three, we have at most 11 non-vanishing terms that fulfill the symmetry assumptions<sup>141</sup>. For weak coupling  $|\kappa| \ll 1$  and using equivariant theory, Ashwin and Rodrigues derived a phase model

$$\dot{\theta}_k = \tilde{\omega}(\theta, \kappa) + \kappa \left( H_k^{(2)}(\theta) + H_k^{(3)}(\theta) + H_k^{(4)}(\theta) \right) , \quad (2.70)$$

which allows interactions of up to four phases: The functions  $H_k^{(j)}$  denote the sums over pairwise, triplet and quadruplet interactions of the phases for  $j = 2, 3, 4$ , respectively, and  $\theta = (\theta_1, \dots, \theta_N)$  is the phase vector. In *Section S.5* of the *Supplementary Material*, we provide the explicit expressions of the particular terms in (2.70).

If we consider only pairwise interactions in the coupling function  $g$  as in (2.15) and (2.16), then the dynamics (2.70) reduces to

$$\begin{aligned} \dot{\theta}_k = & \omega - \kappa \mu \frac{\vartheta_4}{u_1} \cos(\psi_4) + \frac{\kappa}{N} \sum_{j=1}^N \left[ \xi_1^0 \cos(\theta_j - \theta_k + \chi_1^0) \right. \\ & \left. + \mu \left( \xi_1^1 \cos(\theta_j - \theta_k + \chi_1^1) + \xi_2^1 \cos(2(\theta_j - \theta_k) + \chi_2^1) \right) \right] \end{aligned} \quad (2.71)$$

with parameters defined in *Section S.5*. Note that (2.71) consists of the first two harmonics only. Indeed, the terms  $\xi_1^0 \cos(\varphi + \chi_1^0) + \varepsilon \xi_1^1 \cos(\varphi + \chi_1^1)$  can be comprised by trigonometric identities. Furthermore, the constant term  $-\vartheta_4/u_1 \cos(\psi_4)$  presents only minor corrections to the natural frequency  $\omega = v_0 - u_0 v_1/v_2$ . Likewise, the term  $\xi_1^1 \cos(\theta_j - \theta_k + \chi_1^1)$  can be discarded as it contributes only negligibly to the first harmonics. By neglecting all non-dominant terms, we retrieve a phase model of the form

$$\dot{\theta}_k = \omega + \frac{\kappa}{N} \sum_{j=1}^N \left[ \xi_1^0 \cos(\theta_j - \theta_k + \chi_1^0) + \mu \xi_2^1 \cos(2(\theta_j - \theta_k) + \chi_2^1) \right] . \quad (2.72)$$

The parameters  $\xi_1^0, \chi_1^0$  and  $\xi_2^1, \chi_2^1$  for first and second harmonic correspond exactly to the coupling coefficients  $\gamma$  and  $\delta$  of the coupling function as considered in (2.16). Moreover, the amplitude of the second harmonics scale with  $\mu = (R^c)^2$  close to the Hopf bifurcation.

In view of a practical application of the theory outlined above, we are confronted with two major concerns. First, the normal form transformation, as introduced

in *Section 2.2.1*, recasts only the uncoupled part in Hopf normal form, which satisfies the required symmetry conditions. The transformed coupling function, however, exhibits in general terms of all powers and is a priori not shaped to comply with the  $S^1 \times S_N$ -symmetry as assumed in (2.69). Nonetheless, the averaging inherent to determine the phase interaction function  $H$  has shown that only a specific selection of coupling terms contributes to the phase dynamics (at leading order), see *Section 2.2.1.2\**. Hence, averaging – which is intrinsically tied to the assumption of weak coupling and slowly varying phase deviations<sup>38,78</sup> – imposes the symmetry constraints on the coupling function  $g(w_k, w_1, \dots, w_N)$  after the normal form reduction.

The second concern refers to the the underlying connectivity structure of the network. Indeed, for any particular choice of coupling topology other than global, all-to-all coupling, the permutation symmetry  $S_N$  cannot be upheld. However, for a coupling function  $\mathbf{h} = (h_1, \dots, h_N)$  we can heuristically define a substitution operator  $\mathcal{K}$  via the formal convolution

$$(\mathcal{K} \star h)_j(w_1, \dots, w_N) = h_j(C_{j1}w_1, \dots, C_{jN}w_N) .$$

Then, we can first follow the theory presented in this section to derive (2.72), and subsequently apply the convolution  $\mathcal{K} \star g$ , which reveals the phase model

$$\dot{\theta}_k = \omega + \frac{\kappa}{N} \sum_{j=1}^N C_{kj} [\xi_1^0 \cos(\theta_j - \theta_k + \chi_1) + R^{c2} \xi_2^1 \cos(2(\theta_j - \theta_k) + \chi_2)] .$$

Using trigonometric identities, we eventually arrive at the Fourier coefficients of the desired form as in (2.17) & (2.60).

## 2.2.7 Haken's reduction via averaging

Although the previous phase reduction techniques are formulated for rather general oscillatory dynamical systems, their practical application is limited to a few exceptional cases in which either explicit formulas for the limit cycle and the asymptotic phase maps are available, or the dynamics has already been reduced to normal form. An alternative and more direct approach to reduce an oscillatory network to its phase dynamics, has been promoted by Haken and applies averaging.

The idea is to average each oscillator over one cycle when assuming that its amplitude and phase change slowly as compared to the oscillator's frequency. Following a three-step approach, first the time-dependent amplitude and phase are fixed. The system is then integrated over one period to remove all harmonic oscillations; see also<sup>143,144</sup> for a more rigorous reasoning. Last, amplitude and phase are

considered again to be time-dependent <sup>see<sup>42,112</sup></sup>. Haken popularized this procedure as a combination of rotating wave and slowly varying amplitude approximations<sup>105</sup>. While this technique is usually applied to weakly nonlinear oscillations described by second-order differential equations, see for an overview <sup>e.g.,<sup>115,145</sup></sup>, it can also be applied to systems of first-order differential equations, as will be illustrated below. Moreover, this phase reduction technique can also be applied for oscillatory networks beyond the limit of weak coupling.<sup>[25]</sup> In fact, it allows to (analytically) reduce oscillatory network dynamics that are induced through (strong) coupling between the (excitable) elements, see <sup>e.g.,<sup>42</sup></sup> and *Section 3.3.5.1*. As averaging is applied to the linearized dynamics around an unstable fixed point within a stable limit cycle solution  $\mathbf{x}^c$  (in contrast to the linearized dynamics around  $\mathbf{x}^c$  as in *Section 2.2.5*), this technique loses accuracy for large-amplitude oscillations, see also *Section 3.1*. Still, it provides a straightforward phase model whose parameters are directly linked to those of the underlying oscillatory model, and presents a valuable addition to the variety of phase reduction techniques. Above all, when applied in the framework of weakly coupled oscillators, the reduction results in the same phase model as obtained with the other reduction techniques, which will be illustrated below for coupled oscillators in second order Hopf normal form.

Applying Haken's reduction technique to an oscillatory network requires that every node in the network exhibits stable limit cycle oscillations that can be transformed by an appropriate change of variables into (nearly) circular shape.<sup>[26]</sup> Note that these oscillations may also be coupling induced. In the following we will assume that each node describes stable circular oscillations. In case of planar oscillatory systems  $\dot{\mathbf{x}}_k = \mathbf{f}(\mathbf{x}; \mu) + \kappa \mathbf{g}_k(\mathbf{x}_1, \dots, \mathbf{x}_N)$  with state vector  $\mathbf{x}_k = (x_k, y_k) \in \mathbb{R}^2$ , we can perform a polar coordinate transformation  $x_k = R_k \cos(\theta_k)$ ,  $y_k = R_k \sin(\theta_k)$  with  $\theta_k = \omega t + \phi_k$ . Note that while  $R_k^2 = x_k^2 + y_k^2$  and  $\theta_k = \text{atan}(y_k, x_k)$ , the (central) frequency  $\omega$  has to be determined, e.g., as the mean of individual frequencies  $\omega = (1/N) \sum_j \omega_j$ , or alternatively, as the (absolute value of the) imaginary part of the complex conjugate pair of eigenvalues of the Jacobian of  $\mathbf{f}$ , that is,  $\omega = \text{Im}(\lambda_+)$  with  $\lambda_{\pm} \in \mathbb{C}$  the pair of complex eigenvalues.  $\phi_k$  denotes a slowly varying phase deviation of unit  $k$  from the mean. Assuming that  $R_k, \phi_k$  hardly change over one period of oscillation,  $T = 2\pi/\omega$ , i.e.

$$\left| \dot{R}_k / R_k \right| \ll \omega \quad \text{and} \quad \left| \dot{\phi}_k / \phi_k \right| \ll \omega , \quad (2.73)$$

---

<sup>[25]</sup> Note the change from “oscillator network” to “oscillatory network” as we have introduced “oscillators” in *Section 2.1.1* such that they exhibit stable limit cycle oscillations without external coupling.

<sup>[26]</sup> Such a coordinate change is always possible for, e.g., oscillations that emerge through a Hopf bifurcation. Away from that point, higher order corrections might be in place; for a corresponding approximation scheme <sup>see<sup>143</sup></sup>.

one can average the dynamics over the interval  $[0, T)$  by means of  $\langle f(s) \rangle := \frac{1}{T} \int_0^T f(s) ds$ . Exploiting trigonometric identities, the (averaged) dynamics  $\dot{\phi}_k$  and  $\dot{R}_k$  can be expressed in the state variables  $x_k, y_k$  as<sup>[27]</sup>

$$\dot{\phi}_k = -\omega_k + \left\langle \frac{1}{R_k^2} (x_k \dot{y}_k - y_k \dot{x}_k) \right\rangle \quad (2.74a)$$

$$\dot{R}_k = \left\langle \frac{x_k \dot{x}_k + y_k \dot{y}_k}{R_k} \right\rangle. \quad (2.74b)$$

We retrieve the full phase dynamics by inserting (2.74a) into  $\dot{\theta}_k = \omega + \dot{\phi}_k$ . Note that the system (2.74) describes both phase and amplitude dynamics, which can be reduced further if we assume that the (non-trivial) fixed point solution of (2.74b) approximates the (time-varying) amplitude  $R_k$  sufficiently well. Upon inserting the (stationary) solution  $R_k$  into (2.74a), we eventually find the reduced phase dynamics  $\dot{\phi}_k$ , which will split into a natural frequency part of order  $\mathcal{O}(1)$  and a coupling part of order  $\mathcal{O}(\kappa)$ .

A mathematical rigorous application of the Haken approach, as noted above, respects the basic assumption of weakly coupled oscillators in that we find stable limit cycle oscillations already in the uncoupled case. For two coupled oscillators  $w, w' \in \mathbb{C}$  in second order Hopf normal form with nonlinear coupling as in (2.31),

$$\dot{w} = \alpha w - \beta |w|^2 w + \kappa (\gamma w' + \delta \bar{w} w'^2),$$

where  $\gamma = \gamma_R + i\gamma_I$  and  $\delta = \delta_R + \delta_I$ , we consider the dynamics (2.25) in two-dimensional real-valued coordinates  $w = x_1 + iy_1$  and  $w' = x_2 + iy_2$ . We first transform the nonlinear coupling terms in real coordinates and use polar coordinates  $w = R e^{i(\omega+\phi)}$ ,  $w' = R' e^{i(\omega+\phi')}$  as above. In particular, we can use the following identities

$$\langle x_k y_k \rangle = 0 \quad \text{and} \quad \langle x_k^2 \rangle = \langle y_k^2 \rangle = \frac{1}{2} R_k^2. \quad (2.75)$$

Inserting them and the corresponding  $(x_k, y_k)$ -dynamics in (2.74), we define  $\psi =$

---

<sup>[27]</sup> The averaging in (2.74) is sound also from a time-scale separation argument. The assumption (2.73) implies that  $\phi_k = \phi_k(\tau)$  and  $R_k = R_k(\tau)$  depend on a slower time  $\tau = \varepsilon t$ . As a result, we obtain the dynamics of the phase deviation  $\phi_k$  and of the slowly varying amplitude  $R_k$  by averaging over the period  $T_k = 2\pi/\omega_k$ . Indeed, using polar coordinates in the angular brackets of (2.74) one can see that all terms at least of order  $\mathcal{O}(R_k)$ . Close to the supercritical Hopf bifurcation,  $0 < R_k \ll 1$  is small so that this averaging is appropriate.

$\phi - \phi'$  and arrive at

$$\begin{aligned} \dot{\phi} &= -\omega + v_0 - v_1 R^2 \\ &+ \kappa \left[ \frac{R'}{R} \left( \gamma_I \cos \psi - \gamma_R \sin \psi \right) + R'^2 \left( \delta_I \cos(2\psi) - \delta_R \sin(2\psi) \right) \right] \end{aligned} \quad (2.76a)$$

$$\begin{aligned} \dot{R} &= u_0 R - u_1 R^3 \\ &+ \kappa \left[ R' \left( \gamma_R \cos \psi + \gamma_I \sin \psi \right) + R R'^2 \left( \delta_R \cos(2\psi) + \delta_I \sin(2\psi) \right) \right]. \end{aligned} \quad (2.76b)$$

In the case of weak coupling  $\kappa \ll 1$  and close to the Hopf bifurcation  $R \ll 1$ , the  $R$ -dynamics (2.76b) evolves very slowly compared to  $\phi$ . Therefore, one can assume that  $R$  and  $R'$  are constant and do not vanish. We can solve (2.76b) for  $R^2$  by setting  $\dot{R} = 0$  as

$$R^2 = \frac{u_0}{u_1} + \frac{\kappa}{u_1} \left[ \frac{R'}{R} \left( \gamma_R \cos \psi + \gamma_I \sin \psi \right) + R'^2 \left( \delta_R \cos(2\psi) + \delta_I \sin(2\psi) \right) \right],$$

which is close to the uncoupled limit cycle radius  $R^c = \sqrt{u_0/u_1}$ . Substituting  $R^c$  into (2.76a) and using  $\dot{\theta} = \omega + \dot{\phi}$ , we find that

$$\begin{aligned} \dot{\theta} &= v_0 - u_0 \frac{v_1}{u_1} + \kappa \left\{ \left[ \left( \gamma_I - \gamma_R \frac{v_1}{u_1} \right) \cos(\theta - \theta') - \left( \gamma_R + \gamma_I \frac{v_1}{u_1} \right) \sin(\theta - \theta') \right] + \right. \\ &\left. + R^{c2} \left[ \left( \delta_I - \delta_R \frac{v_1}{u_1} \right) \cos(2(\theta - \theta')) - \left( \delta_R + \delta_I \frac{v_1}{u_1} \right) \sin(2(\theta - \theta')) \right] \right\}. \end{aligned} \quad (2.77)$$

This result can immediately be extended to a network of coupled oscillators yielding the phase model (2.17) with Fourier coefficients (2.60).

## 2.3 Numerical phase reduction techniques

As repeatedly said, analytic techniques can provide useful information about the properties of the limit cycle behavior of the coupled oscillators, which can be used to determine the corresponding phase model explicitly in terms of the underlying model equations. Analytic expressions thus explicitly link the parameters of the original dynamics to those of the phase model. This allows to predict reliably how specific model parameters shape the phase dynamics of the system. However, as we have seen in the previous sections, only few examples are mathematically tractable and often an intricate normal form reduction has to precede the actual phase reduction. Furthermore, the accuracy of such analytic approaches scales with the distance to the bifurcation point. And, as appealing as the analytic reduction techniques are, as bulky can be the accompanying algebraic computations. Thus, one may look for a compromise between the qualitative insights mentioned above

and quantitative accuracy of the phase reduction.

More accurate reduction techniques heavily rely on a careful assessment of the limit cycle's properties, such as its shape and its dynamics. This assessment can be automatized numerically, giving rise to the notion of *numerical phase reduction techniques*. In contrast to analytic reduction techniques, the numerical approaches do not necessarily aim at explicit equations that describe the limit cycle, but store all numeric values that are needed in the subsequent reduction steps. In this way the phase dynamics can be obtained with high accuracy, both near and far from bifurcation points; see also *Sections 3.1 and 3.2* for illustration.

Conceptually, numerical approaches can be distinguished between *adjoint* and *direct methods*, which will be presented in the following sub-sections 2.3.1 and 2.3.2, respectively. In a nutshell, direct methods numerically evaluate the phase response to perturbations  $\mathbf{p}$  via the phase response function  $G(\theta, \mathbf{p})$ , whereas adjoint methods numerically compute the phase sensitivity function  $\mathbf{Z}(\theta)$ , which has been defined in Section 2.1.2. In a strict sense, both of them build on a thorough analytic basis. Yet, determining the phase response properties of an oscillator is not enough to constitute a phase model of the form (2.3). One also needs to incorporate the coupling function  $\mathbf{g}_{kj}$  to estimate the phase interaction function  $H_{kj}$  introduced already in (2.14) as

$$H_{kj}(\psi) = \frac{1}{2\pi} \int_0^{2\pi} \mathbf{Z}(\varphi + \psi) \cdot \mathbf{g}_{kj}(\varphi + \psi, \varphi) d\varphi. \quad (2.78)$$

Recall that the coupling function  $\mathbf{g}$  in (2.14) is evaluated on the limit cycle  $\mathcal{C}$ . Even if  $\mathcal{C}$  cannot be determined analytically, this can be achieved numerically. Deriving numerically the phase model thus combines the numerical computation of the phase response, which becomes the phase sensitivity function  $\mathbf{Z}(\theta)$  in the limit of infinitesimal perturbations, and the evaluation of the coupling function  $\mathbf{g}(\theta_k, \theta_j)$  at the numerically estimated limit cycle. We will refer to this algorithmic procedure as a numerical phase reduction technique. The particular type of numerical phase reduction technique eventually depends on whether  $\mathbf{Z}(\theta)$  is determined with an adjoint or a direct method. In the following sub-sections we will revise the main ideas behind the different methods, where we focus mainly on the computation of  $\mathbf{Z}(\theta)$ , and refer to several numerical toolboxes for more details about their implementation.

To anticipate, both adjoint and direct techniques provide very similar results. In our applications in *Sections 3.1 and 3.2* we will hence use them interchangeably as “the” numerical phase reduction technique.

### 2.3.1 Adjoint method

The adjoint method presents an accurate way to derive the phase dynamics of coupled oscillators<sup>78,86,146,147</sup>. It is closely related to the direct method in the limit of infinitesimal perturbations due to the link between the phase sensitivity function and the phase response function, see Section 2.2.4 and<sup>102</sup>. From a mathematical point of view they are even equivalent, together with the method based on Floquet eigenvectors in Section 2.2.5, since all of them evaluate the linearized dynamics around the oscillator's stable limit cycle. Due to the practical advantage of numerical algorithms, the adjoint and direct methods present powerful alternatives to analytic reduction techniques.

#### 2.3.1.1 Malkin's theorem

The adjoint method has been summarized in Theorem 9.2<sup>78</sup> by Hoppensteadt and Izhikevich. It follows earlier work by Malkin<sup>148</sup> and is often referred to as *Malkin's method*. Malkin's theorem states that for a network of weakly coupled oscillators  $\dot{\mathbf{x}}_k = \mathbf{f}_k(\mathbf{x}_k) + \kappa \mathbf{g}_k(\mathbf{x}_1, \dots, \mathbf{x}_N) \in \mathbb{R}^n$ , where each uncoupled oscillator has an exponentially orbitally stable  $T$ -periodic solution  $\mathbf{x}_k^c$ , the reduced phase dynamics is given by  $\dot{\theta}_k = \omega + \kappa H_k(\theta - \theta_k)$  with  $\omega = 2\pi/T$ , phase vector  $\Psi := (\theta_1 - \theta_k, \dots, \theta_N - \theta_k)$ , and the phase interaction function  $H_k$  at first order

$$H_k(\Psi) = \frac{1}{2} \int_0^{2\pi} \mathbf{Z}_k(\varphi) \cdot \mathbf{g}_k(\mathbf{x}_1^c(\varphi + \theta_1 - \theta_k), \dots, \mathbf{x}_N^c(\varphi + \theta_N - \theta_k)) d\varphi ,$$

The oscillators' phase sensitivity function  $\mathbf{Z}_k(\theta) \in \mathbb{R}^n$  is the unique non-trivial  $T$ -periodic solution to the linear system<sup>[28]</sup>

$$\dot{\mathbf{y}} = - \left( \nabla \mathbf{f}_k(\mathbf{x}) \big|_{\mathbf{x}=\mathbf{x}_k^c(t)} \right)^\top \mathbf{y}(t) \quad (2.79)$$

satisfying the normalization condition

$$\mathbf{y}(0) \cdot \mathbf{f}_k(\mathbf{x}_k^c(0)) = \omega . \quad (2.80)$$

This theorem is fairly general and can also be extended for weakly coupled oscillators whose stable limit cycle oscillations have slightly different periods  $T_k$ , see<sup>78</sup>. Moreover, the theorem does not rely on assumptions of the kind that any oscillator is required to be close to some bifurcation point.

In the case of a network of (nearly) identical oscillators,  $\mathbf{f}_k = \mathbf{f}$ , equations (2.79) & (2.80) must only be solved once to retrieve the phase sensitivity function

<sup>[28]</sup> We again identify  $\mathbf{Z}_k(\theta)$  and  $\mathbf{Z}_k(t)$  via the constantly increasing phase  $\dot{\theta} = \omega$  on the limit cycle and by fixing a reference phase  $\theta_0 = 0$  at  $t = 0$ .

$\mathbf{Z}$ . An alternative but illustrative proof that  $\mathbf{Z}$  solves (2.79) & (2.80) has been provided by<sup>102</sup>, see also *Section S.6* in the *Supplementary Material*. In a nutshell, when considering an infinitesimal perturbations  $\mathbf{p}$  to the stable limit cycle solution  $\mathbf{x}^c(t)$  at time  $t = 0$ , then  $\mathbf{u}(t)$  defined via  $\mathbf{x}(t) = \mathbf{x}^c + \mathbf{u}(t)$  follows the linearized dynamics

$$\dot{\mathbf{u}}(t) = \nabla \mathbf{f}(\mathbf{x})|_{\mathbf{x}=\mathbf{x}^c(t)} \mathbf{u}(t) =: \mathbf{L}(t)\mathbf{u}(t) , \quad (2.81)$$

see also *Section 2.2.5*. By rewriting (2.81) as  $\mathcal{L}\mathbf{u} = 0$  with the linear operator  $(\mathcal{L}\mathbf{y})(t) := \dot{\mathbf{y}}(t) - \mathbf{L}(t)\mathbf{y}(t)$ , it can be shown that the phase sensitivity function  $\mathbf{Z}$  is a solution of the adjoint problem

$$\mathcal{L}^*\mathbf{Z} = 0 , \quad \text{where} \quad (\mathcal{L}^*\mathbf{y})(t) := -\dot{\mathbf{y}}(t) - \mathbf{L}(t)^\top \mathbf{y}(t) ,$$

with initial condition  $\mathbf{Z}(0) \cdot \dot{\mathbf{x}} = \omega$ , which is (2.80). Importantly, solving the adjoint problem (2.79) & (2.80) for an oscillator in Hopf normal form reveals the same phase sensitivity function that has been reported in *Section 2.2.4* cf.<sup>86</sup>.

For arbitrary limit cycle oscillators, one can solve  $\mathcal{L}^*\mathbf{y} = 0$  numerically by integrating the equation  $\dot{\mathbf{y}} = -\mathbf{L}(t)^\top \mathbf{y}$  backward in time<sup>149</sup>. As long as the limit cycle is asymptotically stable, backward integration exactly retrieves the periodic solution of the adjoint equation and cancels possible higher harmonics out. In this way the adjoint method is efficiently automated in Ermentrout's software package XPPAUT<sup>150</sup>. As the numerical procedures do not rely on a critical distance to a bifurcation point, the adjoint method can provide a valuable reference to monitor accuracy, and, by this, the validity of analytic phase reduction techniques as a system gradually moves away from a supercritical Hopf point. We will exploit this capacity in the forthcoming *Sections 3.1* and *3.2*.

**XPPAUT and Matcont** The numerical exploration of the phase sensitivity function as the solution to the adjoint problem (2.79) & (2.80) may present a problem in itself. In fact, the solution  $Z_k(T) = Z(0)$  of (2.79) is periodic, so that we encounter a boundary value problem. While a direct integration is impossible, the XPPAUT package uses backward integration<sup>149</sup> after which the solution of (2.79) approaches the periodic solution corresponding to the phase sensitivity function. This algorithm, however, has to rely on a numerical interpolation of the Jacobian matrix being evaluated at the limit cycle solution. Another drawback of the procedure is the slow convergence of the adjoint solution towards the phase response curve when the limit cycle is only weakly stable. Govaerts and Sautois<sup>151</sup> proposed an alternative numerical approach to solve the adjoint problem. It does not suffer from the aforementioned shortcomings. Their algorithm solves the corresponding boundary value problem using an orthogonal collocation method with Gauss

collocation points. As a by-product, they obtain the phase sensitivity function. The method is fast, rendering it particularly useful when a large number of phase response curves are needed, e.g., for the evolution of limit cycles if one parameter of the system is changed. This method is implemented in the Matlab software package MatCont<sup>152</sup>.

### 2.3.1.2 Ermentrout & Kopell's reduction

An alternative method that relies on the gradient evaluated on the oscillator's limit cycle has been put forward by Ermentrout and Kopell<sup>146,147,153</sup>. They propose a coordinate transformation  $\mathbf{x}_k = \mathcal{T}_k(\theta_k, \boldsymbol{\rho}_k)$  resembling, at first sight, a phase-amplitude description; cf. *Section 3.3.7* for discussion. An isolated oscillator  $\dot{\mathbf{x}}_k = \mathbf{f}_k(\mathbf{x}_k)$ ,  $\mathbf{x}_k \in \mathbb{R}^n$ , has an asymptotically stable limit cycle solution  $\mathbf{x}_k^c(t)$  with period  $T_k$  and frequency  $\omega_k = 2\pi/T_k$ . Then, the transform  $\mathcal{T}_k$  maps  $\mathbf{x}_k$  to variables  $\theta_k \in \mathbb{S}^1$  and  $\boldsymbol{\rho}_k \in \mathbb{R}^{n-1}$ . The phase  $\theta_k$  parametrizes  $\mathbf{x}_k^c$  along the limit cycle  $\mathcal{C}$  and the amplitudes  $\boldsymbol{\rho}_k$  are normal coordinates in a neighborhood of  $\mathcal{C}$ , with  $\boldsymbol{\rho}_k = 0$  directly on it. One can choose the transform of the form

$$\mathbf{x}_k(t) = \mathcal{T}_k(\theta_k(t), \boldsymbol{\rho}_k(t)) = \mathbf{x}_k^c(\theta_k(t)) + \mathbf{M}_k(\theta_k(t)) \boldsymbol{\rho}_k(t) + \mathcal{O}^2(\boldsymbol{\rho}_k) , \quad (2.82)$$

where  $\mathbf{M}_k(\theta)$  is an  $n \times (n-1)$ -matrix and

$$\begin{aligned} \mathbf{M}_k(\theta)^\top \mathbf{M}_k(\theta) &= \mathbf{I}_{(n-1) \times (n-1)} \\ \mathbf{x}'_{0,k}(\theta)^\top \mathbf{M}_k(\theta) &= \mathbf{0}_{1 \times (n-1)} . \end{aligned} \quad (2.83)$$

The prime ' denotes the derivative with respect to  $\theta$ . Then for small  $\boldsymbol{\rho}_k$ , one can express the dynamics  $\dot{\mathbf{x}}_k = \mathbf{f}_k(\mathbf{x}_k)$  as

$$\dot{\theta}_k = \omega_k + \mathcal{O}(\boldsymbol{\rho}_k) , \quad \dot{\boldsymbol{\rho}}_k = \mathbf{a}_k(\theta_k) \boldsymbol{\rho}_k + o(\boldsymbol{\rho}_k) . \quad (2.84)$$

Coupling the oscillators according to  $\dot{\mathbf{x}}_k = \mathbf{f}_k(\mathbf{x}_k) + \mathbf{g}_k(\mathbf{x}_1, \dots, \mathbf{x}_N)$ , results in the dynamics

$$\dot{\theta}_k = \omega_k + h_k(\theta_1, \dots, \theta_N) + \mathcal{O}(|\{\boldsymbol{\rho}_1, \dots, \boldsymbol{\rho}_N\}|) , \quad (2.85a)$$

$$\dot{\boldsymbol{\rho}}_k = \mathbf{a}_k(\theta_k) \boldsymbol{\rho}_k + \mathbf{d}_k(\theta_1, \dots, \theta_N) + \mathcal{O}(|\{\boldsymbol{\rho}_1, \dots, \boldsymbol{\rho}_{k-1}, \boldsymbol{\rho}_{k+1}, \dots, \boldsymbol{\rho}_N\}|) + o(|\boldsymbol{\rho}_k|) . \quad (2.85b)$$

While the  $\mathbf{a}_k$  only depend on the  $\mathbf{f}_k$ 's, the  $h_k$  and  $\mathbf{d}_k$  also depend on the coupling terms  $\mathbf{g}_k$ ,  $k = 1, \dots, N$ . The precise form of the terms in the dynamics (2.85) as well as the corresponding proofs can be found in *Section S.7* of the *Supplementary Material*. In the limit of 'infinite attraction' to the limit cycle,  $\boldsymbol{\rho}_k \rightarrow 0$ , (2.85)

reduces to the  $\theta_k$  dynamics only. That is, the larger the strength of attraction of the limit cycle, the more accurate the phase model.

Ermentrout and Kopell showed that if the coupling functions  $\mathbf{g}_k$  have some specific form, the interaction terms in the reduced phase model display a *pulse-response coupling* like

$$\dot{\theta}_k = \omega_k + \alpha_0 \sum_{j=1}^N P_j(\theta_j) R(\theta_k) , \quad \alpha_0 \in \mathbb{R} . \quad (2.86)$$

The function  $P_j(\theta_j)$  represents a perturbation through oscillator  $j$  and  $R(\theta_k)$  can be understood as a phase response curve, see also<sup>153</sup> for explanatory comments on this relationship. From a historical point of view, Winfree was among the first who proposed reduced phase dynamics of the above form<sup>85</sup>. As to their derivation, we first assume that the coupling function  $\mathbf{g}_k : \mathbb{R}^{N \times n} \rightarrow \mathbb{R}^n$  can be expressed as the sum of pairwise interactions  $\mathbf{g}_k(\mathbf{x}_1, \dots, \mathbf{x}_N) = \sum_j \tilde{\mathbf{g}}_k(\mathbf{x}_j, \mathbf{x}_k)$ . Omitting the tildes, we suppose that the terms  $\mathbf{g}_k = (g_{k,1}, \dots, g_{k,n})^\top : \mathbb{R}^{2 \times n} \rightarrow \mathbb{R}^n$  are nonzero in only one variable, say  $g_{k,i}$ . We further assume that this component can be written as  $g_{k,i} = \alpha(\mathbf{x}_j)\beta(\mathbf{x}_k)$  for some functions  $\alpha, \beta : \mathbb{R}^n \rightarrow \mathbb{R}$ . Then, the functions  $h_k$  in (2.85a) decouple and we regain the dynamics (2.86).

This pulse-response type of phase models holds for oscillator dynamics with arbitrary large coupling strengths. However, if interactions are scattered along the period of the oscillators, the system can behave as though the coupling was averaged over a period<sup>147</sup>. In that case, the phase interaction function  $H(\theta_j - \theta_k) = (1/2\pi) \int_0^{2\pi} h_k(\phi + \theta_j - \theta_k, \phi) d\phi$  will only depend on the phase differences  $\psi_{kj} = \theta_k - \theta_j$ . When considering two coupled oscillators with pulse-response coupling in the reduced phase equations of the form  $h_k(\theta_k, \theta_j) = P(\theta_j)R(\theta_k)$  with a non-negative pulse function  $P(\theta) = 1 + \cos(\theta)$  and general response function  $R(\theta) = \sin(\theta)$ , the phase interaction function becomes purely sinusoidal,

$$H(\psi) = \frac{1}{2\pi} \int_0^{2\pi} h_k(\theta, \theta + \psi) d\theta = \frac{1}{2} \sin(\psi) .$$

Furthermore, if the rate of attraction to the limit cycle is finite, but the coupling is sufficiently weak, one can use invariant manifold theory<sup>154</sup> to establish an invariant torus. Single contributions through the coupling may not appear immediately. But cumulative coupling effects arise after one period and averaging is needed to constitute a phase interaction function  $H$ . For oscillators with only small frequency differences of order  $\mathcal{O}(\epsilon)$ , one can rewrite the isolated oscillator dynamics as  $\dot{\mathbf{x}}_k = \mathbf{f}_k(\mathbf{x}_k) = \mathbf{f}(\mathbf{x}_k) + \mathcal{O}(\epsilon)$  and subsume the  $\mathcal{O}(\epsilon)$  terms of frequency differences under the coupling terms  $\mathbf{g}_k$ . Then, formally we have identical oscillators with limit cycle

solutions  $\mathbf{x}^c(t)$  and frequencies  $\omega = 2\pi/T$ . Given small coupling strengths, one can also replace  $\mathbf{g}_k$  by  $\epsilon\mathbf{g}_k$ . By performing the coordinate transform (2.82) one finds that  $\boldsymbol{\rho}_k$  will be  $\epsilon$ -close to the invariant torus so that we can write  $\boldsymbol{\rho}_k = \epsilon\mathbf{s}_k$ . Following<sup>147</sup>, one eventually arrives at the phase interaction function  $H(\psi_{kj})$  for the differences  $\psi_{kj} = \phi_k - \phi_j$  of phase deviations  $\phi_k$  from the uncoupled limit cycle phases  $\theta_k = \omega_k t + \phi_k$ , which reads

$$H_k(\psi_{kj}) = \frac{1}{T} \int_0^T \mathbf{b}(t) \mathbf{s}_k(t) + \rho^{-1}(t) (\mathbf{x}^{c\prime}(t))^\top \mathbf{g}_k(\mathbf{x}^c(t), \mathbf{x}^c(t + \psi_{kj})) dt. \quad (2.87)$$

The exact form of  $\mathbf{b}(t)$  can be found in *Section S.7*. Simplifying the expression above, (2.87) can be recast as

$$H_k(\psi_{kj}) = \frac{1}{T} \int_0^T \mathbf{Z}(t) \cdot \mathbf{g}_k(\mathbf{x}^c(t), \mathbf{x}^c(t + \psi_{kj})) dt, \quad (2.88)$$

where  $\mathbf{Z}$  is the solution to the adjoint problem of the previous *Section 2.3.1*. In fact, Ermentrout and Kopell provided two different methods in the appendix of<sup>147</sup> to derive (2.88). While their second method overlaps to great extent with the adjoint method above, we recapitulate their other “geometric” method in *Section S.7*.<sup>[29]</sup> Both methods as well as the one presented in *Section 2.3.1* are equivalent and the difficulties remain to find exact solutions when evaluating the dynamics along the (analytically unknown) limit cycle trajectory. Nevertheless, these approaches have proven quite successful and serve for that reason as a valuable means to test and validate analytic results.

### 2.3.2 Direct method

Direct methods differ conceptually from adjoint methods in that they do not immediately solve for the phase sensitivity function  $\mathbf{Z}$ . Instead, direct methods aim at quantifying the phase response to an (arbitrarily small or large) stimulus  $\mathbf{p}$  of the limit cycle trajectory  $\mathbf{x}^c(t)$  at a particular phase  $\theta$ . We introduced this type of response as the phase response function  $G(\theta, \mathbf{p})$  in *Section 2.1* and presented an exact description how to determine  $G$ . This direct method can also be implemented experimentally, which dates back to the work by Glass, Mackey and co-workers<sup>155</sup> in the 1980s. Despite its simplicity, the experimental procedure is not very accurate when it comes to infinitesimal perturbations. That is why direct methods

---

<sup>[29]</sup> An alternative proof to establish phase equations for oscillatory neural networks is given in Theorem 9.1<sup>78</sup> by Hoppensteadt and Izhikevich. They focus on the phase dynamics of (2.85) and use normal form theory as presented in *Section 2.2.1* to describe perturbations  $P$  off the invariant manifold of (the product of) hyperbolic limit cycles. Ad-hoc they interpret their choice  $P \equiv 0$  as an ‘infinite attraction’ to the invariant manifold and thus link their result to Ermentrout and Kopell’s work.

have been avoided to compute the phase sensitivity function  $\mathbf{Z}$  via  $G(\theta, \mathbf{p})$  in the limit of infinitesimal perturbations  $\|\mathbf{p}\| \ll 1$ . Recently, however, Novičenko and Pyragas proposed an algorithm based on the same idea of the oscillator's response to short finite pulses at different phases of the limit cycle<sup>156</sup>. Their algorithm does not require any backward integration nor a numerical interpolation of the Jacobian. Moreover, it is faster than the algorithms implemented in XPPAUT, see *Section 2.3.1* above. This is especially true when the limit cycle is only weakly stable. The idea behind this algorithm builds on the (linearized) dynamics (2.81) of infinitesimal deviations  $\mathbf{u}$  from the limit cycle  $\mathcal{C} = \{\mathbf{x}^c(t) : 0 \leq t \leq T\}$  as the adjoint method,

$$\dot{\mathbf{u}}(t) = \nabla \mathbf{f}(\mathbf{x})|_{\mathbf{x}=\mathbf{x}^c(t)} \mathbf{u}(t) , \quad (2.89)$$

where  $\mathbf{x}^c(t)$  denotes the  $T$ -periodic limit cycle solution of  $\dot{\mathbf{x}} = \mathbf{f}(\mathbf{x})$  with initial condition  $\mathbf{x}(0) = \mathbf{x}^c(\theta)$  (initial phase  $\theta$ ). To obtain the  $j$ -th component  $Z_j$  of the phase sensitivity function  $\mathbf{Z}$ , we choose the initial condition  $\mathbf{u}(0) = (u_1(0), \dots, u_n(0))^\top$  with  $u_k(0) = \delta_{kj}$  where  $\delta_{kj}$  denotes the Kronecker- $\delta$ . Then, it can be found<sup>156</sup> that

$$Z_j(\theta) = \lim_{p \rightarrow \infty} \frac{\mathbf{f}(\mathbf{x}^c(\theta)) \cdot \mathbf{u}(pT)}{\mathbf{f}(\mathbf{x}^c(\theta)) \cdot \mathbf{f}(\mathbf{x}^c(\theta))} . \quad (2.90)$$

To improve this algorithm, the authors replaced the vector  $\mathbf{u}$  by the fundamental matrix  $\Phi$  and eventually extract the phase sensitivity function  $\mathbf{Z}$  from  $\Phi$ . For more details, we refer to their instructive work<sup>156</sup>, which includes numerical demonstrations of the algorithm and a comparison with the standard algorithm as implemented in XPPAUT.

For our purposes, we tested the standard algorithm, both using XPPAUT as well as our own adjoint solver implemented in Matlab (The Mathworks Inc., Natick, MA), against the one presented here. We found a very good agreement between all methods, such that we use either of them interchangeably as “the” numerical method unless stated otherwise.

# CHAPTER 3

## Collective behavior of coupled oscillators and their reduced phase models

*Having a battery of analytic and numerical phase reduction techniques introduced and explicated in the previous Chapter, we duly apply them to two classic examples. The first is a network of Brusselators, which is one of the most discussed chemical oscillators. The second example comprises a more elaborate interdisciplinary model of coupled Wilson-Cowan oscillators. Both of them illustrate the benefits and pitfalls of the different phase reduction techniques. A point-by-point application further allows for a thorough comparison between the techniques. The reduction of complex oscillatory systems is crucial for numerical analyses but more so for analytical estimates and model prediction. The most common reduction is towards phase oscillator networks that have proven successful in describing not only the transition between incoherence and global synchronization, but in predicting the existence of non-trivial network states. Many of these predictions have been confirmed in experiments. The phase dynamics, however, depends to large extent on the employed phase reduction technique.*

Adapted from: Pietras B., Daffertshofer A. (2018). *Network dynamics of coupled oscillators and phase reduction techniques, (Sections 5 – 7)*. Under review.

### 3.1 Networks of identical Brusselators

The Brusselator is a theoretical model of oscillating chemical reactions. It perfectly serves to illustrate our approaches to phase reduction introduced in *Chapter 2* since it exhibits a supercritical Hopf bifurcation. The system comprises four hypothetical chemical reactions and has been developed by the Brussels school around Ilya Prigogine and René Lefever<sup>157</sup> – hence the name. For a long time, reports on oscillating chemical reactions were facing harsh skepticism. Despite the strong interest in biological and biochemical oscillations in the 1950s and 60s, the discovery of oscillatory patterns in a closed chemical system by Belousov<sup>158</sup> in 1951 had to be meticulously reproduced and investigated for years by Zhabotinsky<sup>159</sup> until the nowadays so famous Belousov-Zhabotinsky reaction found its way into the scientific community<sup>160</sup>; for an overview of oscillating chemical reactions see also<sup>38,161,162</sup>. In a way, the Belousov-Zhabotinsky reaction was conceived as a manageable model of more complex systems, which simultaneously bore a close analogy to biology: Strogatz describes this analogy where “propagating waves of oxidation [...] annihilate upon collision just like waves of excitation in neural or cardiac tissue. [...] spiral waves are now an ubiquitous feature of chemical, biological, and physical excitable media”<sup>162</sup>. The original Belousov-Zhabotinsky reaction, which involves more than twenty elementary reaction steps, could effectively be rewritten in three differential equations. From a similar perspective, one can regard the Brusselator as a simplified chemical oscillator, which can be described in two differential equations. Despite its ability to exhibit oscillatory dynamics, as found in the Belousov-Zhabotinsky reaction, the Brusselator is a mere hypothetical model and is not based on a particular chemical reaction. Nonetheless, it serves as an exquisite example to apply the arsenal of phase reduction techniques presented in the previous section.<sup>[1]</sup>

---

<sup>[1]</sup> There exists also a natural extension of the Brusselator model into a two-component reaction-diffusion system, which allows for so-called chemical waves and other pattern formation, such as, e.g., traveling fronts or rotating spirals in an extended medium<sup>38</sup>. It is not only possible to define a phase for rhythmic patterns in extended media, but also to derive the corresponding phase dynamics from the underlying spatio-temporal dynamics, as has been successfully demonstrated by Nakao, Kawamura and co-workers<sup>87,163,164</sup>. This strategy can be used to determine a meaningful phase dynamics of periodic fluid flows<sup>165</sup>. It has been extended to reduce the phase dynamics of limit cycle solutions to general partial differential equations<sup>166</sup>. In the same way, the phase dynamics of collective oscillations of globally coupled noisy elements can be derived, given that these oscillations are solutions to a nonlinear Fokker-Planck equation<sup>167,168</sup>.

### 3.1.1 Single node dynamics

The chemical reactions of the Brusselator are described in terms of



which sum up to  $A + B \rightarrow C + D$ . Each of the reactions (3.1a–d) has a rate constant  $k_a$  to  $k_d$ . Under the assumption that the chemicals  $A$  and  $B$  are in vast excess, one can assume that their concentrations stay constant. On the other hand, the products  $C$  and  $D$  are constantly removed. The concentrations of  $X$  and  $Y$  will react sensitively to already weak perturbations and reach an oscillatory state when the overall reaction is far from an equilibrium solution. (3.1) can thus be considered a thermodynamically open system with the following rate equations for the (dimensionless) concentrations  $x = [X]$  and  $y = [Y]$

$$\begin{aligned} \dot{x} &= k_a[A] - k_b[B]x + k_c x^2 y - k_d x \\ \dot{y} &= k_b[B]x - k_c x^2 y \end{aligned} \quad (3.2)$$

with free parameters  $k_a[A]$ ,  $k_b[B]$ ,  $k_c$  and  $k_d$ . The rate equations (3.2) can be understood as follows: Reaction (3.1a) always leads to an increase of concentration  $x$ , which is proportional to the product of the rate  $k_a$  and the concentration  $[A]$  of chemical  $A$ . Likewise, reaction (3.1d) leads to a decrease of concentration  $x$  at rate  $k_d$ . Whenever the two chemicals  $B$  and  $X$  are involved in reaction (3.1b), this leads to an increase in concentration  $y$  that is proportional to the rate  $k_b$  times the concentrations of  $B$  and  $X$ , and a simultaneous decrease of the same amount of concentration  $x$ . Reaction (3.1c) can be understood in the same manner, only that this reaction leads to an increase in  $x$  and a (balanced) decrease in concentration  $y$ .

### 3.1.2 Coupled Brusselators

We consider a network of Brusselators by coupling multiple nodes  $\mathbf{x}_k = (x_k, y_k) \in \mathbb{R}^2$ ,  $k = 1, \dots, N$ . In the following, we will fix the rate constants  $k_c = k_d = 1$  and consider  $a = k_a[A]$ ,  $b = k_b[B] \in \mathbb{R}^+$  as possible bifurcation parameters. Our

*Brusselator network model* then reads

$$\begin{aligned}\dot{x}_k &= a - (b + 1)x_k + x_k^2 y_k + \kappa g_{k,x}(x_1, \dots, x_N, y_1, \dots, y_N) \\ \dot{y}_k &= b x_k - x_k^2 y_k + \kappa g_{k,y}(x_1, \dots, x_N, y_1, \dots, y_N)\end{aligned}\tag{3.3}$$

for some weak coupling strength  $0 \leq |\kappa| \ll 1$  and with coupling functions  $g_{k,x}, g_{k,y} : \mathbb{R}^{2N} \rightarrow \mathbb{R}$ . Without coupling,  $\kappa = 0$ , every node has a stable fixed point at  $(x_0, y_0) = (a, b/a)$ , which undergoes a supercritical Hopf bifurcation at  $b = 1 + a^2$ . Introducing the new variables  $\tilde{x}_k = x_k - x_0$  and  $\tilde{y}_k = y_k - y_0$ , we can shift the fixed point to the origin,  $(\tilde{x}_0, \tilde{y}_0) = (0, 0)$ . Moreover, we restrict the form of the coupling to be the sum of pairwise interactions between nodes  $\tilde{x}_k, \tilde{x}_j$ ,  $k \neq j$ , so that the dynamics (3.3) become

$$\begin{aligned}\dot{x}_k &= (b - 1)x_k + a^2 y_k + \frac{b}{a} x_k^2 + 2a x_k y_k + x_k^2 y_k + \frac{\kappa}{N} \sum_{j=1}^N C_{kj} g_x(\mathbf{x}_k, \mathbf{x}_j) \\ \dot{y}_k &= -b x_k - a^2 y_k - \frac{b}{a} x_k^2 - 2a x_k y_k - x_k^2 y_k + \frac{\kappa}{N} \sum_{j=1}^N C_{kj} g_y(\mathbf{x}_k, \mathbf{x}_j).\end{aligned}\tag{3.4}$$

Note that we omitted the tildes for the sake of readability. We also assumed the coupling terms  $\mathbf{g} = (g_x, g_y)$  to be identical across nodes. The adjacency matrix  $\mathbf{C} = \{C_{kj}\}$  specifies the connectivity between nodes  $\mathbf{x}_k$  and  $\mathbf{x}_j$ . We define the bifurcation parameter as

$$\mu = \frac{b}{1 + a^2} - 1\tag{3.5}$$

and aim at transforming the dynamics (3.4) into Jordan real form, that is, the linearized dynamics with Jacobian  $\mathbf{L}(\mu)$  around the fixed point  $(0, 0)$  is of the form

$$\begin{pmatrix} \dot{x}_k \\ \dot{y}_k \end{pmatrix} = \begin{pmatrix} \varrho(\mu) & -\omega(\mu) \\ \omega(\mu) & \varrho(\mu) \end{pmatrix} \begin{pmatrix} x_k \\ y_k \end{pmatrix},$$

To do so, we use the transformation matrix

$$\mathbf{T}(\mu) = \frac{1}{2(1+\mu)(1+a^2)} \begin{pmatrix} -(\mu + a^2(2 + \mu)) & \sqrt{4a^2 - \mu^2(1 + a^2)^2} \\ 2(1 + \mu)(1 + a^2) & 0 \end{pmatrix},\tag{3.6}$$

where  $\sqrt{4a^2 - \mu^2(1 + a^2)^2}/2 = \omega(\mu)$  is the emergent frequency of the oscillatory dynamics for  $\mu \geq 0$  and  $\omega_0 = \omega(0) = a$ .<sup>[2]</sup> The to-be-analyzed system then reads

$$\dot{\mathbf{x}}_k = \mathbf{L}(\mu)\mathbf{x}_k + \mathbf{T}^{-1}\mathbf{N}_1(\mathbf{T}\mathbf{x}_k; \mu) + \mathbf{T}^{-1}\mathbf{N}_2(\mathbf{T}\mathbf{x}_k; \mu) + \frac{\kappa}{N} \sum_{j=1}^N C_{kj} \mathbf{T}^{-1} \mathbf{g}(\mathbf{T}\mathbf{x}_k, \mathbf{T}\mathbf{x}_j) \quad (3.7)$$

with

$$\begin{aligned} \mathbf{L}(\mu) &= \frac{1}{2} \begin{pmatrix} \mu(1 + a^2) & -\sqrt{4a^2 - \mu^2(1 + a^2)^2} \\ \sqrt{4a^2 - \mu^2(1 + a^2)^2} & \mu(1 + a^2) \end{pmatrix} \\ \mathbf{N}_1(\mathbf{x}; \mu) &= \begin{pmatrix} (1 + \mu)(1 + a^2) & 2a & 0 \\ -(1 + \mu)(1 + a^2) & -2a & 0 \end{pmatrix} \begin{pmatrix} x^2 \\ xy \\ y^2 \end{pmatrix} \\ \mathbf{N}_2(\mathbf{x}; \mu) &= \begin{pmatrix} 0 & 1 & 0 & 0 \\ 0 & -1 & 0 & 0 \end{pmatrix} \begin{pmatrix} x^3 \\ x^2y \\ xy^2 \\ y^3 \end{pmatrix}. \end{aligned}$$

### 3.1.3 Identifying the Hopf normal form

To prepare the different reduction techniques, in particular Kuramoto's reductive perturbation and Poincaré's nonlinear transform approach, we first specify the parameters that are independent of the coupling.

**Kuramoto's reductive perturbation** Following *Section 2.2.2.1*, the normal form parameters  $\alpha, \beta$  in (2.41),

$$f(w, \bar{w}) = \alpha w - \beta |w|^2 w,$$

can be identified as

$$\alpha = \frac{1}{2}\mu(1 + a^2) + ia \quad \text{and} \quad \beta = \frac{1}{2} \left( 1 + \frac{2}{a^2} + i \frac{4 - 7a^2 + 4a^4}{3a^3} \right). \quad (3.8)$$

Note that  $\beta$  is independent of the bifurcation parameter  $\mu$ , whereas  $\alpha$  depends on  $\mu$ . Hence, varying  $\mu$  may strongly affect the normal form. The coupling parameters of order  $\mathcal{O}(\kappa)$  can be computed using the expressions above once the type of coupling has been established.

Considering one Brusselator as an integral element of a network of coupled

---

<sup>[2]</sup> Note that for  $a \geq 0$  and  $|\mu| \ll 1$ ,  $\mathbf{T}(\mu)$  can only become singular when  $\mu = a = 0$ . In this case,  $\det(\mathbf{T}(0)) = 0$ , and the Jacobian  $\mathbf{L}(0) = \mathbf{0}$  vanishes, too.

oscillators, each oscillator is now subject to ‘perturbations’ from the respective other nodes. The initial and indispensable step is to investigate how an individual Brusselator reacts to perturbations in general. For this, we determine the phase sensitivity function<sup>[3]</sup>  $\mathbf{Z}$  either analytically from the reduced Hopf normal form, or numerically as presented in *Sections 2.3 and 2.3.2*. The analytically derived phase sensitivity function is perfectly sinusoidal. It reads

$$\mathbf{Z}(\theta) = \frac{1}{R} \begin{pmatrix} -c_2 \cos \theta - \sin \theta \\ -c_2 \sin \theta + \cos \theta \end{pmatrix}, \quad \text{where } R^2 = \frac{\text{Re}(\alpha)}{\text{Re}(\beta)} \text{ and } c_2 = \frac{\text{Im}(\beta)}{\text{Re}(\beta)}, \quad (3.9)$$

$\alpha$  and  $\beta$  are determined by the analytic normal form reduction technique, e.g., by (3.8), see also *Section 2.2.5*. By contrast, the numerically computed phase sensitivity function may exhibit higher harmonics for growing distance from the Hopf bifurcation point as there is no preceding Hopf normal form reduction that imposes circular symmetry on the limit cycle.

**Poincaré’s reduction via nonlinear transforms** In a similar way, one can compute the (uncoupled part of the) normal form according to the *reduction approach via nonlinear transforms* from *Section 2.2.2.2*. There, no assumptions on the smallness of the bifurcation parameter  $\mu$  are imposed. On the one hand this improves the accuracy by making both  $\alpha, \beta$  depend on  $\mu$ . But on the other hand it yields equations that are too lengthy to report, given dynamics (3.7). As an alternative, we will compare the different reduced phase dynamics numerically and graphically.

### 3.1.4 Comparing analytic and numerical phase reductions

#### 3.1.4.1 Linear coupling

A comparison of the different phase sensitivity functions provides only limited insight about the network’s phase dynamics. Arguably more important is the shape of the entire phase interaction function  $H$ , which also accounts for the type of coupling. For our network of Brusselators, we first consider global, linear

---

<sup>[3]</sup> All phase reduction techniques discussed in *Sections 2.2 and 2.3* build on an explicit computation of the phase sensitivity function  $\mathbf{Z}$  except for the phase reduction approach based on  $S_N \times S^1$ -symmetry, *Section 2.2.6*. However, since this symmetry approach requires the underlying dynamics in Hopf normal form, one can readily extract  $\mathbf{Z}$  from the normal form parameters.

diffusive coupling between oscillators<sup>[4]</sup>

$$C_{kj}\mathbf{g}(\mathbf{x}_k, \mathbf{x}_j) = \begin{pmatrix} x_j - x_k \\ d(y_j - y_k) \end{pmatrix} \quad (3.10)$$

with some coupling constant  $d \in \mathbb{R}$  <sup>cf. 95</sup>;  $d \geq 0$  ‘weights’ the coupling between  $y_j$  and  $y_k$  relative to that between  $x_j$  and  $x_k$ .

In the following, we will investigate how collective dynamics of weakly and linearly coupled Brusselators can be predicted with the help of reduced phase models when varying the parameters  $a$ ,  $d$ , and  $\mu$ . We will focus on the boundaries between stability and instability of the fully synchronized state and of the (balanced) two cluster state. These boundaries are described in terms of the amplitudes  $a_n, b_n$  of the first and second harmonics of the phase interaction function (2.17),

$$H(\psi) = \sum_{n \geq 0} a_n \cos(n\psi) + b_n \sin(n\psi) .$$

i.e. for  $n = 1$  and  $n = 2$ , respectively.

**Analytic phase reductions** Recall that the sought-for dynamics (2.31) reads

$$\dot{w}_k = \alpha w_k - \beta |w_k|^2 w_k + \frac{\kappa}{N} \sum_{j=1}^N C_{kj} [\gamma w_j + \delta \bar{w}_k w_j^2] .$$

This means that the parameters  $\gamma$  and  $\delta$  remain to be specified. Along *Kuramoto’s reductive perturbation technique* we obtain for the Brusselator network with linear coupling (3.10)

$$\begin{aligned} \gamma &= \frac{1}{2} + \frac{d}{2} + i \frac{a}{2}(1+d) , \\ \delta &= -\frac{4 + a^2(2 - 10d) + d + a^4(-2 + 7d)}{9a^4} \\ &\quad - i \frac{4 + a^2(2 - 11d) + 2a^4(-1 + d) + 5d}{9a^3} . \end{aligned} \quad (3.11)$$

---

<sup>[4]</sup> Approximate linear coupling schemes have also been realized in experiments with electrochemical oscillators, see <sup>e.g., 95, 169</sup>, which underlines the relevance of this comparably simple type of coupling.

When combined with the parameters  $\alpha, \beta$  in (3.8), this leads to

$$\begin{aligned} c_1 &= \frac{\text{Im}(\gamma)}{\text{Re}(\gamma)} = \frac{-a(1-d)}{1+d}, \\ c_2 &= \frac{\text{Im}(\beta)}{\text{Re}(\beta)} = \frac{4-7a^2+4a^4}{6a+3a^3}, \\ c_3 &= \frac{\text{Im}(\delta)}{\text{Re}(\delta)} = \frac{a[4+a^2(2-11d)+2a^4(-1+d)+5d]}{4+a^2(2-10d)+d+a^4(-2+7d)}, \end{aligned} \quad (3.12)$$

and to the radius  $R = \mu \sqrt{\frac{a^2(1+a^2)}{2+a^2}}$ . From there we can derive the amplitudes  $a_1$ ,  $a_2$ ,  $b_1$ , and  $b_2$  of  $H$ , see *Section 2.2.3*.

Analogously, one can derive these amplitudes along *Poincaré's reduction via nonlinear transforms*. Although the parameters  $\alpha, \beta, \gamma, \delta$  are the main contributors to the reduced phase dynamics, the nonlinear transform approach allows to include corrective coupling terms  $g_{klmn}$  apart from  $\gamma = g_{0010}$  and  $\delta = g_{0120}$ , see *Section 2.2.2.2*. The resulting amplitudes  $a_1$ ,  $a_2$ ,  $b_1$ , and  $b_2$  of  $H$  using the nonlinear transform approach can thus be expected more accurate. Besides that corrective coupling terms are taken into account, the nonlinear transform approach also employs parameter-dependent transformations at every order. The reductive perturbation approach, in contrast, discards these parameter effects across all nonlinear terms.

As said, the explicit parameter-dependent expressions of  $a_1, a_2, b_1$ , and  $b_2$  are quite lengthy and, therefore, we compare the outcome of these two phase reduction techniques graphically. For this, we determined the stability boundaries of the synchronized state and of the balanced two cluster state in the  $a - d$  plane for a fixed radius of the limit cycle oscillations that emerged through the supercritical Hopf bifurcation. In particular, we investigated oscillations with radius  $R = 0.1$  and  $R = 0.4$ . These values correspond to the distance  $\mu > 0$  from the Hopf bifurcation point via  $\mu = R[(2+a^2)/(a^2(1+a^2))]^{1/2}$ . By increasing the parameter  $a$  between  $1 \leq a \leq 3$ ,  $\mu$  decreases from 0.49 to 0.14 for large-amplitude oscillations,  $R = 0.4$ , and from 0.12 to 0.035 for  $R = 0.1$ , respectively. Moreover,  $d$  is varied in the interval  $[0, 1]$ . The stability of the synchronized state can be directly assessed using the derivative  $H'(0)$  of the phase interaction function  $H$ , which we display in Fig. 3.1.

As  $H'(0)$  changes signs, the synchronized state switches from stable to unstable depending on the sign of the coupling  $\kappa$ . Note that the stability boundary of the synchronized state can be given by  $\{b_1 + 2b_2 = 0\}$  and the one of the two cluster state by  $\{b_2 = 0\}$  for the Hopf normal form network dynamics (2.31). The parameter regions where the fully synchronized and the two cluster states are stable are depicted in Fig. 3.2 for the reductive perturbation approach (panels a

and e) and the nonlinear transforms approach (b and f).

The differences between the two different analytic normal form reductions (together with a subsequent phase reduction) are hardly visible for small-amplitude oscillations, both in the  $H'(0)$ - and in the cluster plots. Increasing the radius of oscillation leads to a minor reduction in size of the synchronization region (depicted in red) for both reduction techniques. The boundary indicating the emergence of a stable (anti-phase) two cluster state (blue) is slightly bent following the reductive perturbation approach, but becomes a straight line in the nonlinear transform approach.

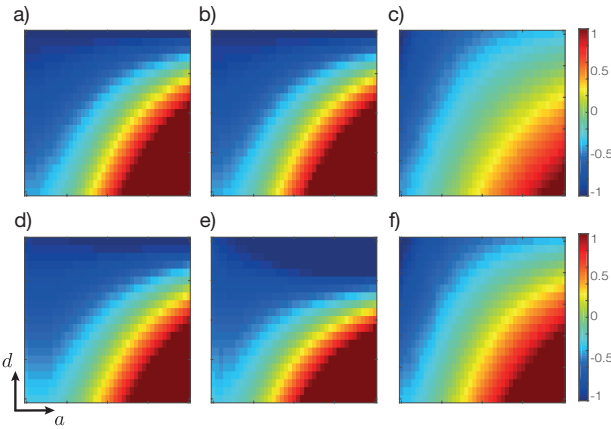


**Figure 3.1:** Stability of the globally synchronized state of the network of linearly coupled Brusselators is determined through the phase interaction function  $H$ . If  $\text{sgn}(\kappa)H'(0) > 0$ , the synchronized state is stable, otherwise unstable. In line with the subsequent analysis, we use  $\kappa < 0$  and show  $-H'(0)$  color coded in the  $a - d$  plane for (a-c) small-amplitude oscillations,  $R = 0.1$ , i.e. near the Hopf bifurcation point, and for (d-f) large-amplitude oscillations,  $R = 0.4$ , further away from the Hopf point. A change of stability occurs at  $H'(0) = 0$  (green), between positive (red) and negative (blue) areas. The phase interaction function is reduced via (a,d) Kuramoto's reductive perturbation approach, (b,e) Poincaré's nonlinear transform approach, and (c,f) the direct numerical method.

**Numerical phase reductions** We also determined the properties of the Brusselator's limit cycle and its phase sensitivity function  $H$  numerically using either of the reduction techniques presented in *Section 2.3*.<sup>[5]</sup> Extracting the amplitudes of the first and second harmonics of  $H$ , we again calculated the stability boundaries of the fully synchronized and two cluster states, respectively. The results are summarized in Fig. 3.1 (panels c, f) and Fig. 3.2 (panels c, g).

When comparing the network predictions to those based on the analytic techniques, we found that for small-amplitude oscillations the agreement appeared almost perfect and the stability boundaries are nearly identical. However, for large-amplitude oscillations, the different techniques diverged significantly. While

<sup>[5]</sup> In particular, we employed the direct numerical method presented Section 2.3.2.

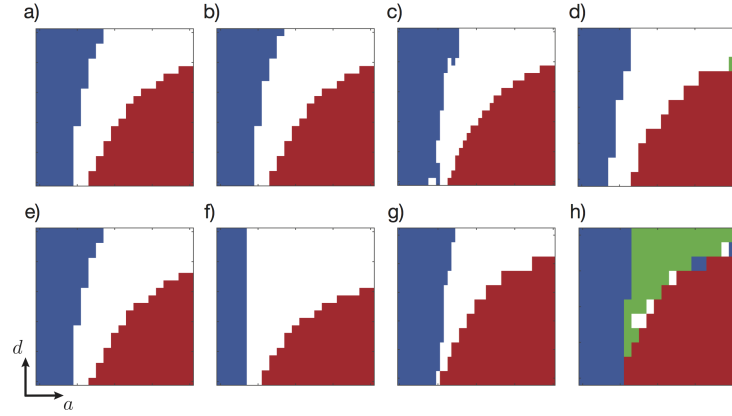


**Figure 3.2:** Stable globally synchronized states (red) and stable balanced two-cluster states (blue) of the network of linearly coupled Brusselators in the  $a - d$  plane for (a-d) small-amplitude, and for (e-h) large-amplitude oscillations with  $R = 0.1$  and  $R = 0.4$ , respectively. The (negative) coupling strength is set at  $\kappa = -0.001$ . Results are obtained via (a,e) Kuramoto's reductive perturbation approach, (b,f) Poincaré's nonlinear transform approach, and (c,g) the direct numerical method, and compared against (d,h) simulations of the full network of  $N = 30$  weakly coupled Brusselators. In the full network, also stable three-cluster states occurred (green).

the synchronization region shrank according to the analytic techniques, it enlarged following the numerical reduction. The boundary for the two cluster state slightly rectified, but it did not match either of the other two predicted lines.

**Network simulations** To test whether the predictions based on the reduced phase models actually recovered the original network dynamics, we simulated the dynamics of  $N = 30$  Brusselators coupled with some weak strength  $\kappa = -0.001$ . The results are shown in Fig. 3.2 (panels d, h). For both small- and large-amplitude oscillations, the analytic as well as the numeric phase reduction techniques performed sufficiently well. Yet, the numeric phase reduction outperformed the analytic ones for large-amplitude oscillations. This holds equally for the synchronization and the two-cluster regions. While both analytic techniques underestimated synchronization (smaller red area), the reductive perturbation approach slightly overestimated the two-cluster region and the nonlinear transform approach underestimated it. Finally, the network simulations revealed a large area where a three-cluster state is stable for large-amplitude oscillations, Fig. 3.2 (panel h). By construction, none of the phase reduction techniques was able to detect this. More details about the numeric implementations can be found in <sup>Appendix of 170</sup>.

### 3.1.4.2 Nonlinear coupling

The arguably more appealing problem is that of nonlinear coupling. To illustrate this we add to the diffusive linear coupling an additional coupling term  $\mathbf{g}_{\text{syn}}$  of the

form

$$\mathbf{g}_{\text{syn}}(\mathbf{x}_k, \mathbf{x}_j) = \hat{\mathbf{g}}(\mathbf{x}_k) \mathbf{S}(\mathbf{x}_j) \quad \text{for all } k \neq j = 1, \dots, N,$$

which may resemble a chemical synapse, see also *Section 3.3.5*. The function  $\mathbf{S} = (S_x, S_y)$  is usually of sigmoidal shape, which we simplify as a polynomial of some degree  $n \in \mathbb{N}$  – this can be thought of as, e.g., a truncated Taylor expansion of a sigmoidal function. As a particular example we choose the nonlinear coupling of the form<sup>[6]</sup>

$$\begin{aligned} \mathbf{g}(\mathbf{x}_k, \mathbf{x}_j) &= \mathbf{g}_{\text{diff}}(\mathbf{x}_k, \mathbf{x}_j) + \hat{\mathbf{g}}(\mathbf{x}_k) \mathbf{S}(\mathbf{x}_j) \\ &= \begin{pmatrix} x_j - x_k + g_1 x_j^2 + g_2 x_k x_j + g_3 x_k x_j^2 + g_4 x_k^2 x_j \\ d(y_j - y_k) \end{pmatrix} \end{aligned} \quad (3.13)$$

with coupling parameter  $d$  as in the linear case above, and with new nonlinear coupling terms scaled by  $g_j \in \mathbb{R}$ ,  $j = 1, \dots, 4$ . Here we already realize that in the reductive perturbation approach, the term  $g_4 x_k^2 x_j$  does not influence the resulting phase model as  $x_k^2 x_j$  is a resonant monomial.

**Analytic phase reductions** Equivalent to the case of linear coupling, we display the predictions about synchronization in Fig. 3.3 and about two cluster states in Fig. 3.4. The fixed coupling parameter values are

$$g_1 = 0.3, \quad g_2 = -0.2, \quad g_3 = 0.35, \quad g_4 = 0.3$$

while  $d$  is varied in the interval  $[0, 1]$  as before.

Again, the analytic predictions of network states for small-amplitude oscillations are roughly identical. However, for large-amplitude oscillations the differences between the two analytic techniques appear more drastic as compared to the linear coupling case. The synchronization region is enlarged following the nonlinear transform approach and by the same token the two cluster state region shrinks, consisting of an almost parallel stripe on the left and of a second, small triangular region in the top right corner of the  $a-d$  plane. On the other hand, the boundaries

<sup>[6]</sup> Expanding both  $\hat{\mathbf{g}} = (g_x, g_y)$  and  $\mathbf{S} = (S_x, S_y)$  as power series in  $\mathbf{x}_k = (x_k, y_k)$  and  $\mathbf{x}_j = (x_j, y_j)$ , respectively, we will consider in the following only non-zero  $x$ -components of the particular form

$$g_x(\mathbf{x}_k) = 1 + a_1 x_k + a_2 x_k^2 + \mathcal{O}^3(x_k) \quad \text{and} \quad S_x(\mathbf{x}_j) = b_1 x_j + b_2 x_j^2 + b_3 x_j^3 + \mathcal{O}^4(x_j).$$

In order to obtain (3.13), we choose the non-vanishing coefficients

$$a_1 = g_2/g_1, \quad a_2 = g_4/g_1, \quad b_1 = g_1, \quad b_2 = g_1 g_3/g_2.$$

predicted by the reductive perturbation method hardly vary when increasing the radius  $R$  of the limit cycle.

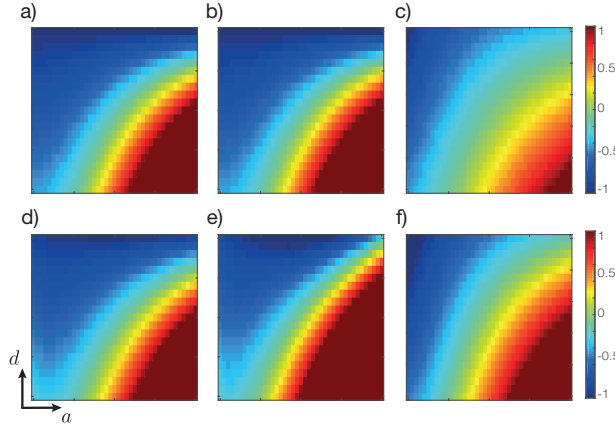


**Figure 3.3:** Stability of the globally synchronized state of the network of nonlinearly coupled Brusselators is determined through the phase interaction function  $H$ . If  $\text{sgn}(\kappa)H'(0) > 0$ , the synchronized state is stable, otherwise unstable. In line with the subsequent analysis, we use  $\kappa < 0$  and show  $-H'(0)$  color coded in the  $a - d$  plane for (a-c) small-amplitude oscillations,  $R = 0.1$ , i.e. near the Hopf bifurcation point, and for (d-f) large-amplitude oscillations,  $R = 0.4$ , further away from the Hopf point. A change of stability occurs at  $H'(0) = 0$  (green), between positive (red) and negative (blue) areas. The phase interaction function is reduced via (a,d) Kuramoto's reductive perturbation approach, (b,e) Poincaré's nonlinear transform approach, and (c,f) the direct numerical method.

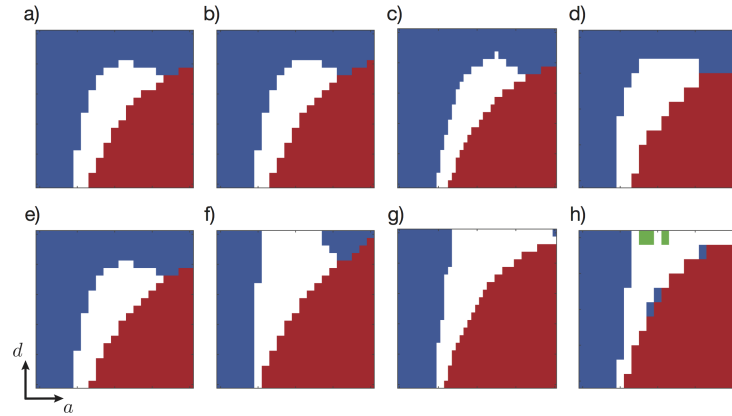


**Figure 3.4:** Stable globally synchronized states (red) and stable balanced two-cluster states (blue) of the network of nonlinearly coupled Brusselators in the  $a - d$  plane for (a-d) small-amplitude, and for (e-h) large-amplitude oscillations with  $R = 0.1$  and  $R = 0.4$ , respectively. The (negative) coupling strength is set at  $\kappa = -0.001$ . Results are obtained via (a,e) Kuramoto's reductive perturbation approach, (b,f) Poincaré's nonlinear transform approach, and (c,g) the direct numerical method, and compared against (d,h) simulations of the full network of  $N = 30$  weakly coupled Brusselators. In the full network, also stable three-cluster states occurred (green).

**Numerical phase reductions** As in the linear coupling case we used the numerical phase reduction technique to determine the stability boundaries of the synchronized and two cluster states. The results are depicted in Fig. 3.3 (panels c, f) and Fig. 3.4 (panels c, g). Remarkably, the predictions for small-amplitude oscillations and close to the Hopf bifurcation point agreed with those of the analytic reduction techniques. For the large-amplitude oscillations, the predictions of the numerically reduced phase model rather went in the direction as proposed by the nonlinear transform approach: The synchronization regions grows, the two cluster region shrinks. Strikingly, the triangular region in the top right corner has almost fully disappeared.

**Network simulations** As before, we simulated the dynamics of  $N = 30$  weakly coupled ( $\kappa = -0.001$ ) Brusselators but now employing the nonlinear coupling scheme. The results are depicted in Fig. 3.4 (panels d, h). We believe that they speak for themselves as the reading agrees with the results for the case of linear coupling. Again, we refer to the *Appendix*<sup>170</sup> for more details about the numerical implementation.

### 3.1.5 Other analytic phase reduction techniques

#### 3.1.5.1 Isochrons, Floquet eigenvectors, and $S_N \times S^1$ -symmetry

The first alternative analytic phase reduction techniques comprise of *Winfree's reduction via isochrons*, *Kuramoto's reduction via Floquet eigenvectors* and *Ashwin & Rodrigues' reduction via  $S_N \times S^1$ -symmetry*. As we explained in *Section 2.2.3* all these techniques will result in the same reduced phase model despite their different methodical background. Hence, there is no need to discuss this further.

#### 3.1.5.2 Haken's reduction via averaging

When introducing polar coordinates  $\mathbf{x}_k = (x_k, y_k) = (R_k \cos(\Omega t + \phi_k), R_k \sin(\Omega t + \phi_k))$  with  $\Omega = \text{Im}(\lambda_1(0))$ , one can realize that the right-hand side of (3.7) is of order  $\mathcal{O}(R_k)$ . Assuming that  $0 \leq \mu \ll 1$ , i.e. close to the Hopf bifurcation, the amplitude  $R_k \ll 1$  is small and we may consider to apply Haken's averaging to (3.7) as outlined in *Section 2.2.7*. For simplicity, we approximate all nonlinear terms in (3.7) by the corresponding expressions at the Hopf point,  $\mu = 0$ , that is, one can use  $\mathbf{T}(0), \mathbf{N}_1(\mathbf{x}; 0), \mathbf{N}_2(\mathbf{x}; 0)$ . In that case, averaging over one period

$T = 2\pi/\Omega$  will result in the approximate phase and amplitude dynamics

$$\begin{aligned}\dot{\phi}_k &= 1 + \frac{a}{8(1+a^2)} R_k^2 + \mathcal{O}(\kappa) \\ \dot{R}_k &= R_k \left[ -a + \mu - \frac{3a^2}{8(1+a^2)} R_k^2 \right] + \mathcal{O}(\kappa),\end{aligned}$$

where  $\mathcal{O}(\kappa)$  denotes the coupling terms. However, the uncoupled dynamics of the phase deviations  $\phi_k$  is too large for slight deviations from the offset frequency at the Hopf point. Moreover, the amplitude dynamics  $R_k$  does not exhibit a non-trivial fixed point solution unless  $0 < a \leq \mu \ll 1$  is very small, which stands in clear contrast to the well-established supercritical Hopf bifurcation character of the Brusselator. That is, in the current setting, this kind of averaging may yield spurious results and we will not proceed along these lines.

### 3.1.6 Summary & remarks

To summarize, we analyzed the collective dynamics of a network of weakly coupled Brusselators with respect to (stable) synchronized, incoherent, and balanced two-cluster states. Numerical reduction techniques are perfectly able to detect the correct dynamical regimes as revealed by full network simulations. Analytic reduction techniques, by contrast, capture the actual collective dynamics only in a close neighborhood to the Hopf bifurcation point. This holds across linear and nonlinear coupling schemes. For illustration, we fixed the parameter value  $a = 2.55$  and investigated numerically the resulting phase model in terms of the frequency term and the Fourier coefficients of first and second harmonics of the reduced phase interaction function  $H$ .

For linear coupling and close to the Hopf bifurcation point, the analytic reduction techniques do not only capture the correct collective dynamics, but they also provide the same order of amplitudes as obtained by numeric methods, see Table 3.1. Away from the Hopf point, the reduction techniques still perform considerably well, but slightly incorrect estimations of the first and second harmonics result in different predictions: according to the reductive perturbation approach a too strong second harmonic forces the phase dynamics into an incoherent state, whereas both the nonlinear transform approach and the numerical reduction correctly capture synchronization of the network, cf. Fig. 3.2 and Table 3.2.

Nonlinear coupling, by contrast, affects the performance more drastically. For small-amplitude oscillations, the differences in sign of the  $b_2$  values in Table 3.3 may be due to numerical artifacts, so that the (wrongly) predicted incoherent state by the nonlinear transform approach has to be taken with care in contrast to the correct prediction of a stable two-cluster state by the reductive perturbation

**Table 3.1:** Phase models derived with different reduction techniques for linear coupling and near the Hopf bifurcation,  $\mu = 0.0417$ . The oscillators' natural frequency is  $\omega$ , and  $a_n, b_n$  are the amplitudes of the Fourier components of the phase interaction function  $H$ . Symbols  $+/ -$  denote the sign of each amplitude. Their quantity corresponds to their influence on the dynamics, with  $+++$  representing dominant contributions of order  $\mathcal{O}(1)$ , while  $0^{+/-}$  corresponds to amplitudes  $\leq 10^{-3}$ . Parameters are  $(a, d) = (2.55, 0.65)$ . Exact numerical values can be found in the Appendix<sup>170</sup>.

Approach	$\omega$	$a_1$	$b_1$	$a_2$	$b_2$
Reductive perturbation	2.537	---	+	$0^+$	$0^-$
Nonlinear transform	2.524	---	+	+	-
Direct averaging	$\times$	$\times$	$\times$	$\times$	$\times$
Numerical/adjoint	2.474	++	+	$0^-$	$0^-$

**Table 3.2:** Phase models derived with different reduction techniques for linear coupling and away from the Hopf bifurcation,  $\mu = 0.1670$ . The notation is the same as in Table 3.1. Parameters are  $(a, d) = (2.55, 0.65)$ .

Approach	$\omega$	$a_1$	$b_1$	$a_2$	$b_2$
Reductive perturbation	2.348	---	+	++	--
Nonlinear transform	1.832	---	++	++	--
Direct averaging	$\times$	$\times$	$\times$	$\times$	$\times$
Numerical/adjoint	2.671	+++	++	-	-

approach and the numerical reduction. For large-amplitude oscillation, however, the phase reduction techniques diverge as shown in Fig. 3.4. Since the nonlinear transform approach respects the parameter-dependence in the normal form reduction, it outperforms the reductive perturbation approach and largely retrieves the results of the numeric reduction technique, see Table 3.4, where the amplitudes of first and second harmonics agree.

To conclude the example of coupled Brusselators, we can add that phase reduction techniques are, in general, capable of predicting the collective dynamics of weakly coupled networks by identifying the properties of the phase interaction function. We would like to point out, however, that nonlinear coupling terms strongly limit the applicability of analytic reduction techniques to a close vicinity of the Hopf bifurcation point. As nonlinear coupling can be an important and often non-negligible ingredient in realistic network models, we will focus more on this in the next section.

**Table 3.3:** Phase models derived with different reduction techniques for nonlinear coupling and near the Hopf bifurcation,  $\mu = 0.0417$ . The notation is the same as in Table 3.1 Parameters are  $(a, d) = (2.55, 0.75)$ .

Approach	$\omega$	$a_1$	$b_1$	$a_2$	$b_2$
Reductive perturbation	2.537	---	--	$0^+$	$0^+$
Nonlinear transform	2.524	---	--	+	$0^-$
Direct averaging	$\times$	$\times$	$\times$	$\times$	$\times$
Numerical/adjoint	2.474	++	-	$0^-$	$0^+$

**Table 3.4:** Phase models derived with different reduction techniques for nonlinear coupling and away from the Hopf bifurcation,  $\mu = 0.1670$ . The notation is the same as in Table 3.1 Parameters are  $(a, d) = (2.55, 0.75)$ .

Approach	$\omega$	$a_1$	$b_1$	$a_2$	$b_2$
Reductive perturbation	2.345	---	--	+	$0^+$
Nonlinear transform	1.832	---	++	++	-
Direct averaging	$\times$	$\times$	$\times$	$\times$	$\times$
Numerical/adjoint	2.671	+++	++	-	-

## 3.2 Networks of identical Wilson-Cowan neural masses

As a second example we use the seminal Wilson-Cowan neural mass model as a representative example for a smooth neural oscillator<sup>[7]</sup>. In their pioneering work<sup>69,70</sup> Wilson and Cowan derived a neural population model that comprises  $N_e$  excitatory and  $N_i$  inhibitory neurons. Denoting by  $e_n/i_n$  the firing rate of a single excitatory/inhibitory neuron, the respective mean firing rates can be given by the averages  $E = (1/N_e) \sum_{n=1}^{N_e} e_n$  and  $I = (1/N_i) \sum_{n=1}^{N_i} i_n$ . Every neuron receives inputs from all other neurons within the population and every excitatory neuron receives an external input  $p_n$ , whose average is given by  $P = (1/N_e) \sum_{n=1}^{N_e} p_n$ . Once the sum of all inputs exceeds a certain threshold  $\theta_n$ , a neuron elicits a spike. For a particular distribution of threshold values across the population, one can assign a sigmoidal activation function<sup>[8]</sup>  $\mathcal{S}$  to the population dynamics<sup>69</sup>. Alternatively, the introduction of  $\mathcal{S}$  can be motivated starting from a single neuron level and along an ergodicity argument, as the time average of individual, saturating firing rates equals the population average<sup>171</sup>. Without loss of generality, we choose  $\mathcal{S}[x] = 1/(1 + e^{-x})$  and denote the population-specific threshold values by  $\Theta_E$  and  $\Theta_I$  for the excitatory and inhibitory part, respectively. Then the coarse-grained dynamics of the mean firing rates of a neural population obeys the form

$$\begin{aligned} \mu_E \dot{E} &= -E(t) + [1 - r_E E] \mathcal{S}[a_E (c_{EE} E - c_{IE} I - \Theta_E + P)] , \\ \mu_I \dot{I} &= -I(t) + [1 - r_I I] \mathcal{S}[a_I (c_{EI} E(t) - c_{II} I - \Theta_I)] . \end{aligned} \quad (3.14)$$

The coupling parameters  $c_{kj}$  with  $k, j \in \{E, I\}$ , indicate the strength of interaction between the different parts within the population, and  $a_E, a_I$  define the slopes of the transfer function  $\mathcal{S}$ . The terms  $[1 - r_E E]$  and  $[1 - r_I I]$  represent the refractory dynamics of the excitatory and inhibitory subpopulations, respectively. They track the period of time during which the corresponding cells are incapable of being stimulated after an activation. In our considerations, we will neglect this term and set  $r_E = r_I = 0$ , thereby following Pinto and co-workers<sup>172</sup>, who showed that the terms effectively rescale the parameters of the nonlinear transfer function  $\mathcal{S}$ . For the sake of simplicity, we further consider the time scales  $\mu_E = \mu_I = 1$ . Depending on the choice of parameters, this model can exhibit rich dynamics such as self-sustained oscillations and multi-stability, see e.g.,<sup>69,78,79</sup>. Here, we restrict

<sup>[7]</sup> By smooth we refer to the smooth limit-cycle trajectory in the two-dimensional coordinate plane as in case of the Wilson-Cowan model. By contrast, integrate-and-fire models present an example for non-smooth neural oscillators, as the reset mechanism leads to discontinuities along the trajectory.

<sup>[8]</sup> Other names for the activation function  $\mathcal{S}$  are transfer function or gain function.

the parameter values to the dynamical regime in which every population  $(E, I)$  displays stable limit cycle oscillations.

To build a cortical network model, we connect  $N$  different populations of excitatory and inhibitory neurons  $(E_k, I_k)$ ,  $k = 1, \dots, N$ , via their excitatory parts<sup>41,42,67</sup>; see Fig. 3.5 for illustration.

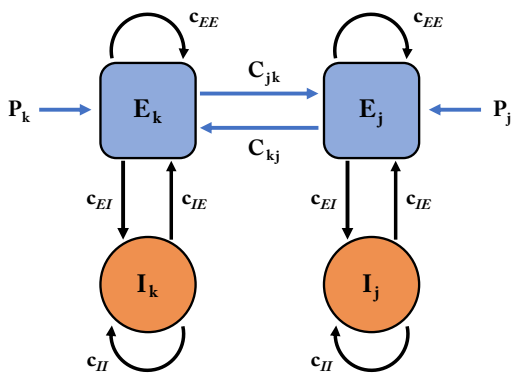


**Figure 3.5:** Network of two coupled Wilson-Cowan neural masses. Each neural population  $k$  contains excitatory and inhibitory units ( $E_k$  and  $I_k$ ), which are internally coupled with strengths  $c_{ij}$ ,  $i, j \in \{E, I\}$ . Moreover, the population receives an external input  $P_k$ . Interaction between two neural masses  $k, j$  occurs via their respective excitatory parts only, where  $C_{kj}$  denotes the connectivity whether node  $k$  receives input from node  $j$ .

Taken together the dynamics at node  $k$  becomes

$$\begin{aligned}\dot{E}_k &= -E_k + \mathcal{S} \left[ a_E \left( c_{EE} E_k - c_{IE} I_k - \Theta_E + P_k + \frac{\kappa}{N} \sum_{j=1}^N C_{kj} E_j \right) \right] \\ \dot{I}_k &= -I_k + \mathcal{S} [a_I (c_{EI} E_k - c_{II} I_k - \Theta_I)] .\end{aligned}\quad (3.15)$$

Here,  $0 \leq \kappa \ll 1$  denotes the overall coupling strength and  $C = \{C_{kj}\}_{k,j}$  is an adjacency matrix that indicates structural connectivity between two cortical regions  $k$  and  $j$ . The population specific average input  $P_k$  of the respective excitatory subpopulations may differ across the different cortical regions.

### 3.2.1 Single node dynamics

As for the Brusselator model, first we briefly discuss the dynamics of a single unit using dynamics (3.15) without coupling,  $\kappa = 0$ . Following<sup>41,42</sup>, we fix several parameters to physiologically motivated values

$$a_E = 1.2, a_I = 2, c_{EE} = c_{EI} = 10, c_{IE} = 6, c_{II} = 1, \Theta_E = 2.5, \Theta_I = 3.5 , \quad (3.16)$$

unless stated otherwise. Furthermore, we consider  $P_k$  to represent external inputs. Taking  $P_k$  as the bifurcation parameter results in the bifurcation diagram depicted in Fig. 3.6<sup>[9]</sup>.

<sup>[9]</sup> Despite the lack of symmetry, one can realize the resemblance with Hoppensteadt and Izhikevich's bifurcation diagram Fig. 2.12,<sup>78</sup> with  $\Theta_{E,I}$  as key parameters, as well as with the deriva-

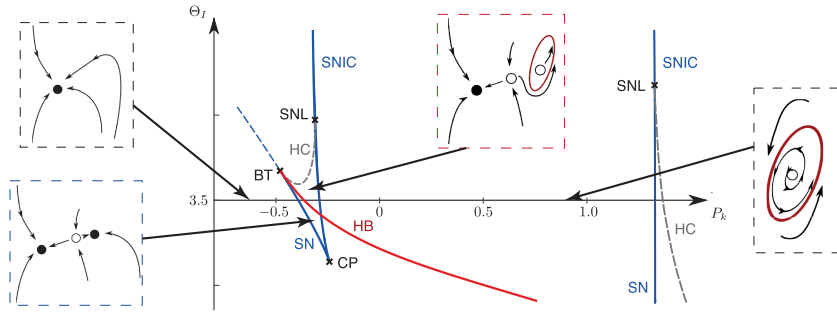


**Figure 3.6:** Bifurcation diagram of the uncoupled Wilson-Cowan model (3.15) with respect to the bifurcation parameter  $P_k$ . By increasing  $P_k$ , one can find four qualitatively different dynamical regimes possible; see inlets – filled/empty dots: stable/unstable fixed points, red: stable limit cycle. A saddle-node (SN) bifurcation at  $P_k \approx -0.3937$  initiates bistability of two stable fixed-points. The stable fixed point emerging from the SN bifurcation undergoes a supercritical Hopf bifurcation (HB) at  $P_k \approx -0.3663$ , while the saddle point coincides with the other stable fixed point and disappears in another SN bifurcation at  $P_k \approx -0.2914$ . Up to the SN bifurcation at  $P_k \approx 1.3272$  away from the stable limit-cycle. The latter is the unique attractor of the dynamics. The collision of the saddle point with the limit-cycle in a homoclinic bifurcation (HC) at  $P_k \approx 1.3648$  terminates the oscillatory regime. BT - Bogdanov-Takens point, CP - cusp point, SNL - saddle-node loop bifurcation, SNIC - saddle node on invariant cycle bifurcation.

### 3.2.2 Coupled Wilson-Cowan neural masses

We are interested in the dynamics of a network of coupled Wilson-Cowan neural masses of the form (3.15). The interplay between the excitatory and inhibitory parts of a single unit is governed by the coupling topology sketched in Fig. 3.5. By reason of appropriate rescaling, we couple distinct neural masses only via their excitatory parts, where the adjacency matrix  $C = C_{kj}$  defines structural links between the different neural masses. While the coupling term in (3.15) of interconnected neural masses appears natural when compared to the internal coupling structure of a single neural mass, it deserves some discussion.

In Wilson and Cowan's original work<sup>69</sup>, the sigmoid function was constructed in such a way that in the absence of external influences the baseline activity state  $(E_k, I_k) = (0, 0)$  is a fixed point. In our formulation, however, the sigmoid function takes on a slightly different form and a zero fixed point solution is no longer feasible. Hence, external perturbations through mutual interaction have a non-trivial impact: If we assume that all neural masses reside in a stationary state with mean (excitatory) firing rate  $E_k^0 > 0$  in the absence of coupling, then as soon as we increase the coupling strength,  $\kappa > 0$ , all neural masses will experience a sudden perturbation of strength  $\kappa \sum_j C_{kj} E_j > 0$  even if they are all identical. Not the presumably small relative distance  $E_j - E_j^0$  to the fixed point, but its

tion by Borisyuk and Kirillov<sup>79</sup>, who used  $P = P_k$  and  $c_3 = c_{EI}$  as key parameters.

absolute value  $E_j$  drives the network dynamics. For this reason, we propose a direct coupling in form of

$$\frac{\kappa}{N} \sum_{j=1}^N C_{kj} E_j \quad \mapsto \quad \frac{\kappa}{N} \sum_{j=1}^N C_{kj} (E_j - E_j^0) , \quad (3.17)$$

where  $E_j^0$  is the unstable fixed point solution of neural mass  $(E_j, I_j)$  in the absence of coupling. In general,  $E_j^0 = E_j^0(P_j)$  depends on the heterogeneous input  $P_j = P_H + \mu$ . Here,  $P_H$  denotes the value of external input at the supercritical Hopf bifurcation, cf. Fig. 3.6. When expanding  $E_j^0(P_H + \mu)$  around  $P_H$ , the coupling term (3.17) reduces to

$$\frac{\kappa}{N} \sum_{j=1}^N C_{kj} (E_j - E_j^0(P_H)) + \mathcal{O}(\kappa\mu) . \quad (3.18)$$

Consequently, the coupling term in the subsequently transformed dynamics (3.20) - (3.22) obtains the form

$$\frac{\kappa}{N} \sum_{j=1}^N C_{kj} (x_j + E_j^0) \quad \mapsto \quad \frac{\kappa}{N} \sum_{j=1}^N C_{kj} x_j . \quad (3.19)$$

### 3.2.3 Identifying the Hopf normal form

The type of bifurcation leading to limit-cycle oscillations usually manifests in the eigenspectrum of the linearized dynamics. In the case of a Hopf bifurcation, stable oscillations emerge around an unstable fixed point. We therefore expect that for an uncoupled  $(E_k, I_k)$ -node the Jacobian of the Wilson-Cowan dynamics (3.15) evaluated at the unstable fixed point  $(E_k^0, I_k^0)$  has a pair of complex conjugate eigenvalues with negative real part, which corresponds to the distance  $\mu := P_k - P_H$  to the Hopf bifurcation point. By changing the parameter  $P_k$ , both the position (and size and shape) of the limit cycle as well as the position of the fixed point change, that is,  $(E_k^0, I_k^0) = (E_k^0(\mu), I_k^0(\mu))$ .

It is advantageous to express the dynamics in terms of the deviations  $x_k = E_k - E_k^0 = E_k - E_k^0(\mu)$  and  $y_k = I_k - I_k^0 = I_k - I_k^0(\mu)$  around the unstable fixed points. Effectively, we shift the fixed point undergoing the Hopf bifurcation to the origin in phase and parameter space. The corresponding transformed system exhibits stable limit cycle behavior with identical phase and amplitude properties

as the original system. It reads

$$\begin{aligned}\dot{x}_k &= -\left(x_k + E_k^0(\mu)\right) \\ &+ \mathcal{S}\left[a_x\left(c_1\left(x_k + E_k^0(\mu)\right) - c_2\left(y_k + I_k^0(\mu)\right) - \Theta_x + \mu + \frac{\kappa}{N} \sum_{j=1}^N C_{jk} \left(x_j + E_j^0(\mu)\right)\right)\right] \\ \dot{y}_k &= -\left(y_k + I_k^0(\mu)\right) + \mathcal{S}\left[a_y\left(c_3\left(x_k + E_k^0(\mu)\right) - c_4\left(y_k + I_k^0(\mu)\right) - \Theta_y\right)\right],\end{aligned}\quad (3.20)$$

where we changed the notation of the parameters:

$$(a_E, a_I, c_{EE}, c_{IE}, c_{EI}, c_{II}, \Theta_E, \Theta_I) \mapsto (a_x, a_y, c_1, c_2, c_3, c_4, \Theta_x, \Theta_y).$$

Since  $(E_k^0(\mu), I_k^0(\mu))$  solves (3.20), one can simplify the transformed dynamics for weak coupling  $0 \leq \kappa \ll 1$  and sufficiently small  $\mu \ll 1$  by Taylor expanding the sigmoid function  $\mathcal{S}$  around the fixed point:

$$\begin{aligned}\dot{x}_k &= -x_k + \sum_{n=1}^{\infty} \frac{1}{n!} \mathcal{S}^{(n)} [\chi_{x,k}] \cdot a_x^n \left( c_1 x_k - c_2 y_k + \frac{\kappa}{N} \sum_{j=1}^N C_{jk} \left( x_j + E_j^0(\mu) \right) \right)^n \\ \dot{y}_k &= -y_k + \sum_{n=1}^{\infty} \frac{1}{n!} \mathcal{S}^{(n)} [\chi_{y,k}] \cdot a_y^n \left( c_3 x_k - c_4 y_k \right)^n.\end{aligned}\quad (3.21)$$

In (3.21) we abbreviated

$$\begin{aligned}\chi_{x,k} &= \chi_{x,k}(\mu) = a_x \left( c_1 E_k^0(\mu) - c_2 I_k^0(\mu) - \Theta_x + \mu \right) \\ \chi_{y,k} &= \chi_{y,k}(\mu) = a_y \left( c_3 E_k^0(\mu) - c_4 I_k^0(\mu) - \Theta_y \right).\end{aligned}$$

and  $\mathcal{S}^{(n)}$  refers to the  $n$ -th derivative of  $\mathcal{S}$ . Unfortunately, the sigmoidal shape of the original dynamics (3.15) does not allow for a simplified form of  $(E_k^0(\mu), I_k^0(\mu))$  in  $\mu$ , but one can find numerically a polynomial fit

$$\begin{aligned}E_k^0(\mu) &= E_k^0(P_H) + \mu \vartheta_E + \mathcal{O}^2(\mu) \\ I_k^0(\mu) &= I_k^0(P_H) + \mu \vartheta_I + \mathcal{O}^2(\mu),\end{aligned}$$

where  $(E_k^0(P_H), I_k^0(P_H))$  denotes the fixed point at the Hopf bifurcation. At this point, which corresponds to  $(x_k, y_k) = 0$ , the Jacobian of the dynamics (3.15) or (3.20) has purely complex eigenvalues  $\pm i\omega_0$ .

To simplify the dynamics, we discard higher-order terms in  $\mu$  and  $\kappa$  and write

$$\begin{aligned} \dot{x}_k &= -x_k + \sum_{n=1}^{\infty} \frac{1}{n!} \left( \mathcal{S}^{(n)} [\chi_x] + \mu \mathcal{S}^{(n+1)} [\chi_x] a_x (c_1 \vartheta_E - c_2 \vartheta_I + 1) \right) \cdot a_x^n (c_1 x_k - c_2 y_k)^n \\ &\quad + \kappa \sum_{m=0}^{\infty} \frac{1}{m!} \mathcal{S}^{(m+1)} [\chi_x] \cdot a_x^{m+1} (c_1 x_k - c_2 y_k)^m \cdot \sum_{j=1}^N \frac{C_{jk}}{N} (x_j + E_j(0)) \\ &\quad + \mathcal{O}^2(\mu) + \mathcal{O}^2(\kappa) + \mathcal{O}(\kappa\mu) \\ \dot{y}_k &= -y_k + \sum_{n=1}^{\infty} \frac{1}{n!} \left( \mathcal{S}^{(n)} [\chi_y] + \mu \mathcal{S}^{(n+1)} [\chi_y] a_y (c_3 \vartheta_E - c_4 \vartheta_I) \right) \cdot a_y^n (c_3 x_k - c_4 y_k)^n \\ &\quad + \mathcal{O}^2(\mu), \end{aligned} \tag{3.22}$$

where  $\chi_x = \chi_{x,k}(\mu = 0)$  and  $\chi_y = \chi_{y,k}(\mu = 0)$ .

Before continuing with simplifying the dynamics, we would like to add that in the limit of weak coupling, only monomials of the form  $x_k^a y_k^b x_j^c$  with  $c = 0$  or  $c = 1$  appear in the coupling term for the  $k$ -th neural mass. That is, the coupling effect from another neural mass  $j$  is at most linear and of order  $\mathcal{O}(x_j)$ . Still, the mixed terms  $x_k^a y_k^b x_j^c$  can lead to nonlinear coupling effects. One may ask: When do these nonlinear coupling effects invoke non-negligible phase-amplitude interactions? Or, put differently: What is the upper boundary for the weak coupling approximation? To the best of our knowledge, as of yet there is no general answer to this question. Stronger coupling, or strong perturbations, induce amplitude effects. But at which critical value of  $\kappa$  these amplitude modulations fail to admit a unique phase description of the single units, remains an open problem. Strikingly, the critical value is exceeded by far when oscillatory states lose stability and eventually cease to exist. Such a scenario has been coined amplitude death, which has attracted much attention in the literature. Analytic results about such coupling induced effects are limited to very small network sizes of a few coupled oscillators, see also *Appendix 3.3.5.1* for an illustration of oscillation death and its somehow connected counterpart, oscillation birth. For larger network sizes amplitude death states elude analytical tractability, but their occurrence in networks of coupled oscillators is reported in numerical studies<sup>173–177</sup>.

Considering from now on only weak coupling, we next incorporate the coupling form (3.18) in (3.22) and subsequently truncate the Taylor expansion after third order. Introducing the abbreviations

$$S_{xn} = \frac{1}{n!} S^{(n)} [\chi_{x,k}] a_x^n \quad \text{and} \quad S_{yn} = \frac{1}{n!} S^{(n)} [\chi_{y,k}] a_y^n,$$

we can write the dynamics (3.21) as

$$\begin{aligned}\dot{x}_k &= f_1(x_k, y_k) + \kappa g_k(\mathbf{X}) + \mathcal{O}^2(\kappa) , \\ \dot{y}_k &= f_2(x_k, y_k) ,\end{aligned}\tag{3.23}$$

where for  $\mathbf{X} = (\mathbf{x}_1, \dots, \mathbf{x}_N)$  and  $\mathbf{x}_k = (x_k, y_k)$  the functions  $\mathbf{f} = (f_1, f_2)$  and  $g_k$  are defined in the following way:

$$\begin{aligned}f_1(x, y) &= -x + S_{x1}(c_1x - c_2y) + S_{x2}(c_1^2x^2 - 2c_1c_2xy + c_2^2y^2) + S_{x3}(c_1x - c_2y)^3 , \\ f_2(x, y) &= -y + S_{y1}(c_3x - c_4y) + S_{y2}(c_3^2x^2 - 2c_3c_4xy + c_4^2y^2) + S_{y3}(c_3x - c_4y)^3 , \\ g_k(\mathbf{X}) &= S_{x1}\bar{x}_k + 2S_{x2}(c_1x_k - c_2y_k)\bar{x}_k + 3S_{x3}(c_1x_k - c_2y_k)^2\bar{x}_k .\end{aligned}\tag{3.24}$$

The bar  $\bar{\cdot}_k$  denotes the (weighted) average,  $\bar{x}_k = \frac{1}{N} \sum_{j=1}^N C_{jk}x_j$ . More concisely, we have for weak non-diffusive coupling between two Wilson-Cowan nodes  $\mathbf{x} = (x, y)$  and  $\tilde{\mathbf{x}} = (\tilde{x}, \tilde{y})$

$$\dot{\mathbf{x}} = \mathbf{J}\mathbf{x} + \mathbf{f}(\mathbf{x}; \mu) + \kappa \mathbf{g}(\mathbf{x}, \tilde{\mathbf{x}}) ,\tag{3.25}$$

with

$$\begin{aligned}\mathbf{f}(\mathbf{x}; \mu) &= \mathbf{N}_1 \begin{pmatrix} x^2 \\ xy \\ y^2 \end{pmatrix} + \mathbf{N}_2 \begin{pmatrix} x^3 \\ x^2y \\ xy^2 \\ y^3 \end{pmatrix} \quad \text{and} \\ \mathbf{g}(\mathbf{x}, \tilde{\mathbf{x}}; \mu) &= \left[ \mathbf{G}_1 + \mathbf{G}_2 \begin{pmatrix} x & 0 \\ y & 0 \end{pmatrix} + \mathbf{G}_3 \begin{pmatrix} x^2 & 0 \\ xy & 0 \\ y^2 & 0 \end{pmatrix} \right] \begin{pmatrix} \tilde{x} \\ \tilde{y} \end{pmatrix} .\end{aligned}$$

In these expression we abbreviated the matrices

$$\begin{aligned}\mathbf{J} &= \begin{pmatrix} -1 + S_{x1}c_1 & -S_{x1}c_2 \\ S_{y1}c_3 & -1 - S_{y1}c_4 \end{pmatrix} \quad \mathbf{N}_1 = \begin{pmatrix} S_{x2}c_1^2 & -2S_{x2}c_1c_2 & S_{x2}c_2^2 \\ S_{y2}c_3^2 & -2S_{y2}c_3c_4 & S_{y2}c_4^2 \end{pmatrix} \\ \mathbf{N}_2 &= \begin{pmatrix} S_{x3}c_1^3 & -3S_{x3}c_1^2c_2 & 3S_{x3}c_1c_2^2 & -S_{x3}c_2^3 \\ S_{y3}c_3^3 & -3S_{y3}c_3^2c_4 & 3S_{y3}c_3c_4^2 & -S_{y3}c_4^3 \end{pmatrix} \\ \mathbf{G}_1 &= S_{x1} \begin{pmatrix} 1 & 0 \\ 0 & 0 \end{pmatrix} \quad \mathbf{G}_2 = 2S_{x2} \begin{pmatrix} c_1 & -c_2 \\ 0 & 0 \end{pmatrix} \quad \mathbf{G}_3 = 3S_{x3} \begin{pmatrix} c_1^2 & -2c_1c_2 & c_2^2 \\ 0 & 0 & 0 \end{pmatrix} .\end{aligned}$$

Similiar to the Brusselator model, also here the Jacobian  $\mathbf{J} = \mathbf{J}(\mu)$  is not in Jordan real form. Using the eigenvectors corresponding to  $\mathbf{J}$ 's eigenvalues  $\lambda(\mu) =$

$\varrho(\mu) \pm i\omega(\mu)$  with  $\omega(0) = \omega_0$ , we can transform

$$\mathbf{L} = \mathbf{T}^{-1} \mathbf{J} \mathbf{T} = \begin{pmatrix} \varrho & -\omega \\ \omega & \varrho \end{pmatrix}. \quad (3.26)$$

Finally, we can rewrite (3.25) as

$$\dot{\mathbf{x}} = \mathbf{L}\mathbf{x} + \mathbf{T}^{-1}\mathbf{f}(\mathbf{T}\mathbf{x}; \mu) + \kappa\mathbf{T}^{-1}\mathbf{g}(\mathbf{T}\mathbf{x}, \mathbf{T}\tilde{\mathbf{x}}), \quad (3.27)$$

The dynamics (3.27) exhibits qualitatively the same behavior as (3.25), but due to the Jordan real form the circular symmetry of the limit cycle is now induced on the full dynamics.

**The connection between analytic phase reduction techniques** While *Kuramoto's reductive perturbation* does not require this last transformation and can be applied to (3.25), the dynamics in Jordan real form (3.27) are necessary for *Taken's reduction via Lie brackets*. For *Poincaré's reduction via nonlinear transforms* we have to reformulate the dynamics further, now in terms of a single complex variable  $z \in \mathbb{C}$  via the transformation

$$\mathbf{x} = z\mathbf{u}(\mu) + \bar{z}\bar{\mathbf{u}}(\mu), \quad (3.28)$$

with  $\mathbf{u}(\mu)$  being the right eigenvector of the Jacobian  $\mathbf{J}(\mu)$  corresponding to the eigenvalue  $\lambda(\mu)$ . (3.28) establishes a linear relation between  $\mathbf{x}$  and the real and imaginary part of  $z = z_R + iz_I$ . In particular,  $(z_R, z_I)$  are the coordinates of  $\mathbf{x}$  in the (real) eigenbasis of  $\mathbf{J}(\mu)$  composed by  $\{2\text{Re}(\mathbf{u}(\mu)), -2\text{Im}(\mathbf{u}(\mu))\}$ , that is, we recover the same transformation of  $\mathbf{J}(\mu)$  into its canonical Jordan real form as in (3.26).

### 3.2.4 Haken's reduction via averaging

In contrast to the Brusselator model discussed in *Section 3.1*, our version of the Wilson-Cowan dynamics (3.27) in Jordan real form allows a meaningful reduction along Haken's averaging approximation even without a transformation into Hopf normal form. Hence we discuss it first. We can insert the ansatz  $\mathbf{x}_k = (x_k, y_k) = (R_k \cos(\Omega t + \phi_k), R_k \sin(\Omega t + \phi_k))$  into (3.27), where  $R_k, \phi_k$  are amplitude and phase (deviations) of the oscillations at node  $k$ , which are slowly varying with respect to the (mean) frequency  $\Omega$  defined via the eigenvalues at the Hopf point,  $\Omega = \omega(0)$ . Near the onset of oscillations through a supercritical Hopf bifurcation,  $R_k \ll 1$  is small and, thus, the right-hand side of (3.27) is at least of order  $\mathcal{O}(R_k)$ . Given the slower time scales of  $R_k$  and  $\phi_k$ , one can average over one cycle  $T = 2\pi/\Omega$ . In line

with<sup>67</sup>, this direct averaging of the dynamics (3.27) yields the phase model

$$\dot{\phi}_k = \omega_k + \sum_{j=1}^N D_{kj} \sin(\phi_j - \phi_k + \Delta_{kj}) \quad (3.29)$$

with

$$D_{kj} = \frac{\kappa}{2N} S_{x1} \Lambda_k C_{kj} \frac{R_j}{R_k} \quad \text{and} \quad \Delta_{kj} = \arctan(\rho_k) - \Omega \tau_{kj}$$

where  $\Lambda_k^2 = 1 + \rho_k^2$  and  $\rho_k = \varpi_k^{-1} (S_{x1}c_1 + S_{y1}c_4)$ . Note that we here included time delays  $\tau_{kj}$  between nodes  $\mathbf{x}_k$  and  $\mathbf{x}_j$ , within the coupling function  $g_x$ , that is,  $g_x = g_x(\mathbf{x}_k, \mathbf{x}_j) = g_x(\mathbf{x}_k(t), \mathbf{x}_j(t - \tau_{kj}))$ , as discussed in more detail in *Appendix 3.3.4.2*. Note also that since  $S_{x1}, S_{y1}, c_1, c_4, \varpi_k \geq 0$ , we have  $\rho_k \geq 0$ . In the absence of delay, that is, for  $\boldsymbol{\tau} = (\tau_{k1}, \dots, \tau_{kN})$  and  $\tau_{kj} = \tau = 0$ , we have  $\Delta_{kj} \in (0, \pi/2)$ . On the other hand with delay we have  $\Delta_{kj} \in (-\pi/2, \pi/2)$  because  $\Omega \tau_{kj} \in (0, \pi/2)$ . In either case, (3.29) resembles the Kuramoto-Sakaguchi model with phase lag  $|\Delta_{kj}| \leq \pi/2$ , so that a transition to full synchronization occurs if the coupling strength  $\kappa$  exceeds a critical value  $\kappa_c = \kappa_c(\delta)$ , where  $\delta$  denotes the width of distribution of the natural frequency terms  $\omega_k$ . The natural frequency  $\omega_k$  can be determined as

$$\omega_k = -\Omega + \varpi_k \quad (3.30)$$

at least to first order in  $R_k$ ; here we used  $\varpi_k^2 = \det \mathbf{J} - (\text{tr } \mathbf{J})^2/4 = S_{x1}S_{y1}c_2c_3 - (S_{x1}c_1 + S_{y1}c_4)^2/4$ .  $\varpi_k$  is the imaginary part of the right eigenvalue of  $\mathbf{J}$ . Being near the Hopf bifurcation, we can safely assume that  $\varpi_k \approx \Omega$  and  $\omega_k \rightarrow 0$ . If the Wilson-Cowan dynamics is fully symmetric, that is, in particular  $c_1 = -c_4$ , then  $\rho_k \rightarrow 0$ , and we retrieve the actual Kuramoto model in the absence of any delay.

The here-presented averaging of the Wilson-Cowan network dynamics results in a phase dynamics (3.29), whose phase interaction function only consists of first harmonics. The absence of higher harmonics hampers, e.g., clustering effects. This is in remarkable contrast to the other phase models that have been derived from dynamics in Hopf normal form. The main reason is that the Hopf normal form reduction induces circular symmetry also on the coupling function  $g_x$ , that is, the coupling terms are transformed such that only resonant monomials survive. On the other hand, averaging considers the coupling terms as they are so that all nonlinear coupling terms eventually average out at zero because the coupling in (3.27) is only linear in  $\tilde{\mathbf{x}}$ . Irrespective of this remark, however, the direct averaging along Haken's method stands out for its simplicity and its potential to be applied in a straightforward way. Below, we will compare it against the other two analytic reduction techniques that build on the by now well-known reduction into Hopf

normal form prior to extracting the phase dynamics.

### 3.2.5 Comparing analytic and numerical phase reductions

The ultimate goal of any of the phase reduction techniques introduced above is to simplify the network dynamics of (weakly) coupled Wilson-Cowan neural masses in terms of a corresponding phase model (2.16),

$$\dot{\theta}_k = \omega + \frac{\kappa}{N} \sum_{j=1}^N C_{kj} H(\theta_k - \theta_j) .$$

For simplicity, we consider that all nodes are identical, in particular, they have the same natural frequency  $\omega_k = \omega$ , and that they are globally, or all-to-all, coupled with adjacency matrix  $C_{kj} = 1$  for all  $j \neq k$ . Note that the factor  $1/N$  is for convenience and ensures that the phase model is well-behaved in the limit  $N \rightarrow \infty$ . Recall that the phase interaction function  $H(\psi)$  admits a representation as a Fourier series (2.17),

$$\begin{aligned} H(\psi) &= \sum_{n \geq 0} a_n \cos(n\psi) + b_n \sin(n\psi) \\ &= a_0 + a_1 \cos(\psi) + b_1 \sin(\psi) + a_2 \cos(2\psi) + b_2 \sin(2\psi) + \dots . \end{aligned}$$

We illustrate the reduction to a phase model first close to the Hopf bifurcation, that is, for small distances  $\mu = P_k - P_H$ . After that, we will treat the case of larger distances, i.e. further away from the Hopf point. In both cases, we will compare the results of the analytic techniques *Kuramoto's reductive perturbation*, *Poincaré's reduction via nonlinear transforms* and *Haken's averaging* – the latter here denoted as *direct averaging*. We also include the results for numerical phase reduction techniques, where we complement the findings of the *adjoint method* using XPPAUT with those of the *direct method*. Both reduction techniques show consistent results, so that we will refer to them as one, here *numerical/adjoint*. The subsequent section will be devoted to direct numerical assessment without exploiting the Hopf normal form.

**Near the Hopf point** Applying the different reduction techniques in close vicinity of the Hopf bifurcation point, we find resulting Fourier coefficients of the phase interaction function  $H$  as summarized in Table 3.5. For typical parameter choices very near the Hopf bifurcation, the four different reduction techniques correctly recover the natural frequencies as well as the dominant first harmonics with a non-negligible and positive sinusoidal component.

**Table 3.5:** Phase models derived with different reduction techniques very close to the Hopf bifurcation ( $\mu = 0.0013$ ). The oscillators' natural frequency is  $\omega$ , and  $a_n, b_n$  are the amplitudes of the Fourier components of the phase interaction function  $H$ . Symbols  $+/ -$  denote the sign of each amplitude. Their quantity corresponds to their influence on the dynamics, with  $+++$  representing dominant contributions of order  $\mathcal{O}(1)$ , while  $0^{+/-}$  corresponds to amplitudes  $\leq 10^{-3}$ . Exact numerical values can be found in the Appendix<sup>170</sup>.

Approach	$\omega$	$a_1$	$b_1$	$a_2$	$b_2$
Reductive perturbation	0.701	---	+++	0 <sup>-</sup>	0 <sup>+</sup>
Nonlinear transform	0.701	---	+++	0 <sup>-</sup>	0 <sup>+</sup>
Direct averaging	0.701	---	++	0	0
Numerical/adjoint	0.701	--	+++	0 <sup>-</sup>	0 <sup>+</sup>

Using the numerical and normal form reductions, the amplitudes of the second harmonics turn out to be smaller of three orders of magnitude than the first harmonics. Therefore, we here consider the different phase models qualitatively identical. Moreover, the closer we choose the bifurcation parameter near the Hopf point, the more “accurate” becomes the numerical method: the phase interaction function resembles a pure sine curve, whereas the other analytic methods retain a dominant cosine component<sup>[10]</sup>, cf. the Appendix<sup>170</sup>.

In a next step, we vary the parameter  $P_k$  and slightly increase the distance  $\mu$  from the Hopf bifurcation point. Fig. 3.7 illustrates how sensitive a phase reduction to minute parameter changes is, note the smallness of  $\mu$ . The slope of the phase interaction function at the origin changes signs already close to the Hopf bifurcation point, which results in a different dynamics of the reduced phase model. It is thus crucial for a meaningful phase reduction to investigate the underlying model with respect to its bifurcation boundaries and to the corresponding governing dynamical regime. Only by this one can avoid false conclusions when linking the phase dynamics to the underlying model.

**Away from the Hopf point** There arises another highly intricate issue when choosing the parameter  $P_k$  such that the dynamics is further away from the Hopf bifurcation point: the different reduction techniques start to diverge from each other even more strongly, which is shown in Table 3.6.

<sup>[10]</sup> The Hopf normal forms obtained with the normal form reductions might be further transformed into the topological Hopf normal form, see<sup>122</sup>. In this case, the phase interaction function  $H$  becomes purely sinusoidal. However, this additionally requires a rescaling of time, after which a direct comparison with the other methods appears more difficult. We refer to<sup>122</sup> for more details of this laborious step.

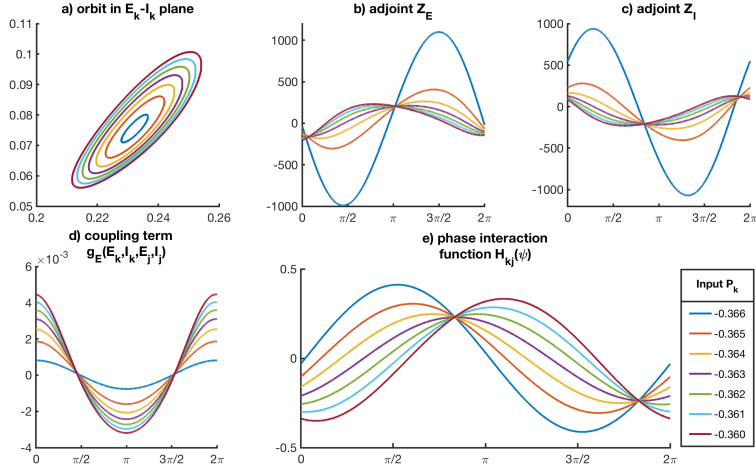


**Figure 3.7:** Phase interaction function: (a) Trajectory of the Wilson-Cowan dynamics in phase space, (b,c) numerically determined phase sensitivity function as solutions to the adjoint problem, (d) coupling term evaluated at the limit cycle, and (e) phase interaction function  $H$  for different input value parameters  $P_k \in (-0.366, -0.36)$ . As shown in (a), the limit cycle solution of the underlying (and uncoupled) Wilson-Cowan model changes its shape. Its amplitude grows monotonically. The shape of the phase sensitivity function  $\mathbf{Z}$  deviates from the initial shape, and higher harmonics seem to occur; see panels (b) and (c) – we refer to the two-component phase sensitivity function  $\mathbf{Z} = (Z_E, Z_I)$  as adjoints, underlying the here-applied numerical reduction technique. The phase interaction function  $H$  depends on both the phase sensitivity function and the coupling term and absorbs their variation (e). At a particular parameter value  $P_k$ , the derivative of  $H$  at the origin,  $H'(0)$ , changes signs. While a network of identical and globally coupled units will fully synchronize if  $H'(0) > 0$ , this state loses stability if  $H'(0)$  becomes negative. Hence, a small parameter change at about  $P_k = -0.364$  will cause qualitatively different network behavior – using XPPAUT, the change from  $H'(0) > 0$  to  $H'(0) < 0$  already appears at  $P_k = -0.3658$  and not at  $P_k = -0.364$ , which we can confirm using the adjoint solver implemented in Matlab.

**Table 3.6:** Phase models derived with different reduction techniques away from the Hopf bifurcation,  $\mu = 0.1663$ . The notation is the same as in Table 3.5.

Approach	$\omega$	$a_1$	$b_1$	$a_2$	$b_2$
Reductive perturbation	0.73	---	+++	--	++
Nonlinear transform	1.02	--	++	-	+
Direct averaging	1.33	--	++	0	0
Numerical/adjoint	0.94	--	--	-	-

Remarkably, only the numerical method captures the change of slope of the phase interaction function  $H$ , whose derivative at  $\psi = 0$  is dominated by  $b_1$  as has been illustrated in Fig. 3.7. In line with the findings for the Brusselator, Sec-

tion 3.1, we presume that the numerical method provides the best approximation of the phase dynamics. Then, only *Poincaré’s reduction via nonlinear transforms* recovers proper amplitudes of the first and second harmonics, at least in terms of orders of magnitude. While *Kuramoto’s reductive perturbation* overestimates the second harmonics, by construction *Haken’s averaging* does not contain any higher harmonics; see the Appendix<sup>170</sup> for exact numerical values. Strong first harmonics of the phase interaction function  $H$  amplify the coupling and thus result in faster (de-)synchronization, depending on the sign of the sinusoidal component. Second and higher harmonics, on the other hand, can play a crucial role for clustering. An over- or underestimation of the amplitudes of higher harmonics can hence lead to erroneous multiple- or one-cluster effects, respectively.

### 3.2.6 Numerical methods identify collective dynamics

The farther one moves away from the particular bifurcation boundary, the more the differently reduced phase models diverge. While the accuracy of analytic reduction techniques scales with distance to the bifurcation point, numerical reduction techniques may not suffer from this shortcoming and can capture the actual dynamics of the underlying high-dimensional oscillator networks to great accuracy. Hlinka and Coombes investigated in this way a network of identical Wilson-Cowan units with respect to its functional connectivity<sup>61</sup>. They showed that the predictions based on the derivative of the numerically reduced phase interaction function agreed almost perfectly with the synchronization properties of the original network, cf. their Figures 6 and 7. However, they reported small parameter regions in which their predictions did not match the actual dynamics. To recapitulate their results, we analyzed the Wilson-Cowan model with a different set of parameters as used in<sup>61</sup>, for more details see the Appendix<sup>170</sup>. In particular, we set  $\Theta_E + P_k \mapsto P_k$  and  $\Theta_I \mapsto Q_k$  and consider the inputs  $P_k$  and  $Q_k$  to the excitatory and inhibitory parts of neural mass  $k$  as bifurcation parameters. In Fig. 3.8, the colored region represents parameter values  $(P_k, Q_k)$  at which the Wilson-Cowan model exhibits self-sustained stable limit-cycle oscillations. This region falls perfectly within the analytically determined Hopf bifurcation boundaries, see e.g.,<sup>78</sup> for a more detailed bifurcation analysis.

According to the reduced phase model, the network will synchronize close to the Hopf bifurcation boundaries.<sup>[11]</sup> Hlinka and Coombes<sup>61</sup> assessed the synchronization properties of the original Wilson-Cowan model in terms of mean phase coherence and correlation. With this they confirmed that the network dynamics

---

<sup>[11]</sup> This can be anticipated from the topological normal form of the supercritical Hopf bifurcation: The corresponding phase sensitivity function  $H$  is purely sinusoidal with derivative  $H'(0) > 0$ . Thus, for positive coupling the network will synchronize.

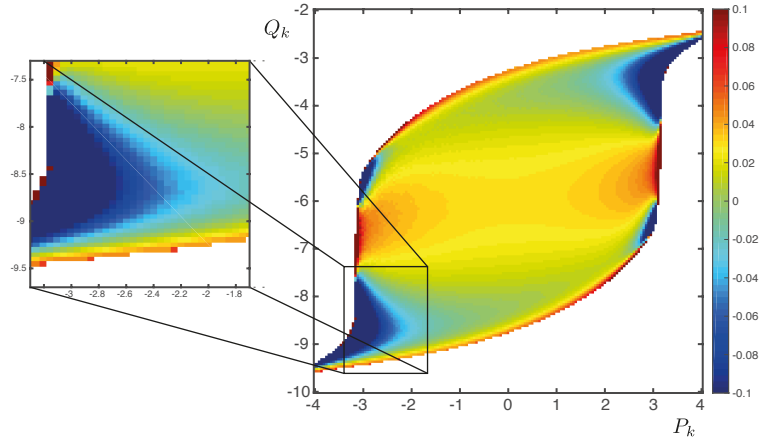


**Figure 3.8:** Oscillatory regime of the Wilson-Cowan neural mass model using the same parameters as in<sup>61</sup>. The color coding indicates the derivative of the phase interaction function  $H$  at  $\psi = 0$  determining the stability of the fully synchronized solution: if  $H'(0) > 0$  the fully synchronized solution is stable, and unstable otherwise. In view of the results in *Section 3.2.5*, we used the numerical/adjoint reduction method to generate this figure.

followed the predictions about global synchronization based on  $H'(0)$ . To show that higher harmonics of the phase interaction function  $H$  capture cases in which the fully synchronized solution is no longer stable, we zoomed in into the corresponding parameter region; see the inset in Fig. 3.8. The Hopf bifurcation occurs at the lower boundary between oscillatory and stationary behavior, where a positive value of  $H'(0)$  predicts synchronized oscillations, irrespective of the other (even) Fourier components. Moving upwards, i.e. increasing the parameter  $Q_k$ , leads to a change of signs,  $H'(0)$  becomes negative and the fully synchronized state is no longer stable.

Considering only first and second harmonics, Kori and co-workers summarized possible network states in<sup>95</sup> where they stated that for positive coupling strength (i) the fully synchronized solution (one-cluster state) is stable if  $b_1 > 0$  and  $b_1 \gg |b_2|$ , (ii) the incoherent solution (anti-cluster state) is stable if  $b_1 < 0$  and  $b_2 < 0$  with  $|b_1| \gg |b_2|$ , and (iii) the (balanced) two-cluster state is stable if  $b_1 < 0$  and  $b_2 > 0$ ; see also *Section 2.1.5.2*. Analyzing the numerically reduced phase interaction function with respect to the higher harmonics, we find that all of the three possible states above should be realizable. When fixing  $P_k = -3$  and using the *direct numerical method*, we find at  $Q_k = -9.3$  that  $b_1 > 0$ , at  $Q_k = -8.9$  that  $b_1 < 0$  and  $b_2 < 0$ , and at  $Q_k = -8.7$  that  $b_1 < 0$  and  $b_2 > 0$ ; for the exact numerical values we refer to the Appendix<sup>170</sup>.

To verify our predictions, we simulated a network of  $N = 30$  Wilson-Cowan models for these parameter values and with global coupling strength  $\kappa = 0.15$ . The simulations displayed the predicted fully synchronized solution, an anti-cluster

state, i.e. incoherence, and a stable two-cluster state, respectively; see Fig. 3.9. Interestingly, the other phase reduction techniques did not only fail to predict the existence of two-cluster states, but they also missed the change of stability of the fully synchronized solution; cf. Table 3.6.

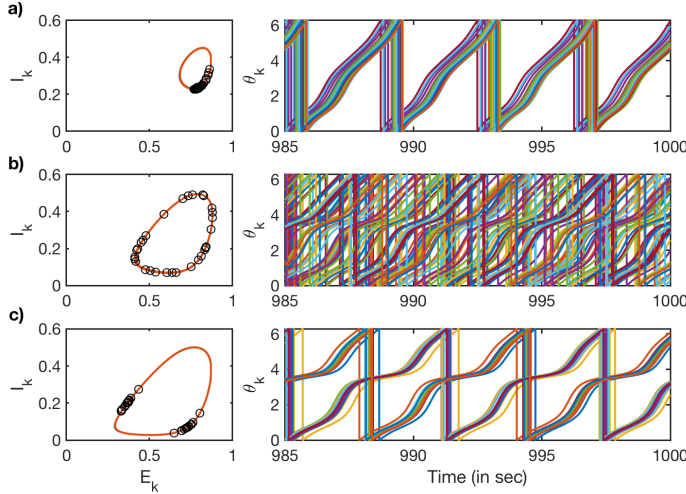


**Figure 3.9:** Non-trivial network dynamics of  $N = 30$  coupled Wilson-Cowan neural masses. The different network states (a) global synchronization, (b) incoherence, and (c) a balanced two-cluster state were predicted by the reduced phase model using the numerical/adjoint method. Displayed are final ( $T_{\text{end}} = 1000$  seconds) conditions ('o') on the uncoupled limit cycle (left column) and the extracted phases (right) for the last 15 seconds. We fixed the coupling strength at  $\kappa = 0.15$  and the simulations started from uniformly distributed initial conditions along the uncoupled limit cycle. Parameter values of  $(P_k, Q_k)$  are (a)  $(-3, -9.3)$ , (b)  $(-3, -8.9)$  and (c)  $(-3, -8.7)$ .

### 3.2.7 Summary & remarks

All the different analytic normal form reductions have the same background, cf. *Section 2.2.1*. Since all of them yield the same phase dynamics when starting from the same Hopf normal form one may expect a perfect agreement between the different reduction techniques. This is, however, only true when considering a normal form reduction accounting for the full dependence on the bifurcation parameter  $\mu$ . While Poincaré's reduction via nonlinear transforms respects the dependence on  $\mu$  throughout every reduction step, the other two methods neglect this accuracy by approximating nonlinear terms with the corresponding expressions evaluated at  $\mu = 0$ .

There are striking differences between the reduced phase models already at reasonably small distances  $\mu \ll 1$  from the Hopf bifurcation point. One may wonder whether reduced phase models indeed describe the phase dynamics of oscillator networks. Needless to say that not all techniques are appropriate to reduce the correct phase dynamics. Analytic techniques have shortcomings unless

parameters are considered in a direct vicinity of the Hopf bifurcation. On the other hand numerical reduction techniques bear the potential to accurately describe the respective phase dynamics so that predictions about the actual network dynamics can be drawn from the reduced phase model.

### 3.3 Discussion

The reduction of a network of interacting oscillatory systems into a network of coupled phase oscillators aims at simplifying the analysis of the collective, macroscopic network dynamics. General oscillatory networks usually have a high-dimensional, nonlinear dynamics. As explained, by looking at the phase dynamics one drastically reduces this dimensionality while keeping the option to infer (the stability of) collective network states. We will briefly discuss low-dimensional collective behavior and particular network states of coupled oscillators in *Sections 3.3.1* and *3.3.2*. Usefulness and strength of a model may be judged by its predictive power. Quantifying this can be a challenge. Models are built on assumptions, which restrict their applicability and range of use. Beyond this range, however, a model can lose its validity and the dynamics can significantly diverge from model predictions. All the listed phase reductions techniques dwell on several assumptions. A first assumptions requires a certain degree of homogeneity among the dynamics of the network's nodes, see *Sections 3.3.3*. Then, we considered only phase reductions for deterministic systems and without delay. In principle, reduction methods can be generalized to cope with noise and delay to some extent, see *Section 3.3.4*. Another crucial assumptions is that most, if not all, of the phase reductions rely on the theory of weakly coupled oscillators<sup>78</sup>: Every node of the original network has to exhibit stable limit cycle oscillations without any coupling to other nodes. And, the coupling strength has to be sufficiently weak so that amplitude effects can largely be neglected, that is, each node's dynamics remains close to the respective unperturbed limit cycle solution while (and despite) interacting with other nodes. How the form and structure of coupling between nodes can influence the collective behavior will be addressed in *Section 3.3.5*. The collective dynamics do not only depend on the coupling between nodes, but also on the oscillatory nature of the nodal dynamics. Reducing a meaningful phase model can thus become intricate for nonlinear, or even non-smooth oscillators (*Section 3.3.6*). More recently, several phase reduction techniques have been refined and extended so that the assumptions inherent to the theory of weakly coupled oscillators might be loosened, at least to a certain degree. This also brings up the topic of phase-amplitude reductions, see *Section 3.3.7*. Although we only touch on this important subject, needless to say that also here a compromise between analytic and numerical reduction methods

has to be found, as we conclude in *Section 3.3.8*.

### 3.3.1 Low-dimensional description of network behavior

A major advantage of coupled phase oscillator models is that they typically give rise to only a few macroscopic variables, which in addition often allow for an intuitive interpretation<sup>178</sup>, as, e.g., the Kuramoto order parameter. Following the Watanabe-Strogatz theory<sup>80</sup>, it is possible to derive the exact time evolution of three collective variables for a network of at least three identical and globally coupled phase oscillators. In a similar spirit, one can describe the time-asymptotic dynamics of a complex order parameter of a network (of infinitely many phase oscillators on a low-dimensional) on the so-called Ott-Antonsen manifold<sup>81,82</sup>. In both cases, the main restriction is that the phase interaction function must only contain first harmonics, but no higher harmonics. Both approaches are indeed strongly related<sup>178</sup>. Given its simplicity, the Ott-Antonsen theory is more popular and widely applied. The dimensionality of the resulting order parameter dynamics is the lowest possible to create a proper picture of the network behavior<sup>179</sup>. However, to apply the Ott-Antonsen theory comes at a price. First, the number of oscillators has to tend to the continuum limit. Second, the natural frequency terms have to follow an analytic distribution function with finite width, such as Gaussian or Lorentzian distributions. That is, the oscillators must not be identical. Although there are approaches to identify correction terms to the Ott-Antonsen manifold in case of finite-sized networks, at least for the subcritical (asynchronous) regime<sup>180–184</sup>, our own preliminary simulations show clear divergences from the manifold when decreasing the network size below  $N = 200$  coupled nodes. The assumption on the frequency terms, however, can somehow be loosened in the limit of “nearly identical” oscillators, and when initial conditions are selected properly<sup>179</sup>. For particular connectivity structures, this opens the possibility for chimera states to emerge; see the recent and extensive review<sup>185</sup> for more details.

### 3.3.2 Cluster states

Closely linked to chimera states is the emergence of stable cluster states. While network synchronization of coupled oscillators is commonly referred to as single-cluster states, i.e. the stationary probability distribution function of the oscillators’ properties is unimodal, in general also (multi-)cluster states, or states of generalized synchrony, can exist and become attractors of the macroscopic dynamics, see for an overview e.g.,<sup>186</sup>. Two main ingredients for cluster states are particular connectivity structures and/or higher harmonics in the phase interaction func-

tion. As to the latter see *Section 2.1.5.2* and we also refer to the comprehensive Fig. 14 in<sup>89</sup>. Clustering in neural networks irrespective of a particular underlying clustered connectivity has been investigated in different neural population models, ranging from all-to-all coupled Hodgkin-Huxley-like microscopic dynamics<sup>187</sup> to more macroscopic, biological networks<sup>188</sup>. Another important ingredient to generate cluster states appears to be delay-coupling in neural networks<sup>189</sup> or neural masses<sup>44</sup>. As such it is not surprising that the same clustering effect through delay has also been found for networks of pulse-coupled oscillators<sup>190–192</sup>. For the Wilson-Cowan model we will discuss the (clustering) effects of time delays in more detail in *Section 3.3.4.2*. Clustering has been rigorously manifested and numerically explored in globally coupled phase oscillator models, see e.g.,<sup>89,93,94,193–195</sup>, where often symmetry aspects determine stability of cluster states. The theory of weakly coupled oscillators allows for translating appropriate conditions for cluster states into the framework of nonlinearly coupled Stuart-Landau oscillators<sup>141</sup>.

A thorough analysis of clustering behavior in globally coupled heterogeneous Stuart-Landau oscillators can be found in<sup>196</sup>. Stuart-Landau oscillators have the advantage that the dynamics is generic for coupled dynamical systems near a Hopf bifurcation, such that the actual dimension of the dynamics can drastically be reduced and theoretical results can readily be applied in order to predict cluster states<sup>95</sup>: it is due to higher harmonics in the phase interaction function  $H$  that clustering behavior occurs. It is noteworthy that cluster states can naturally appear and are attracting if the coupling is either non-pairwise, i.e. the interaction is between more than two oscillators<sup>141</sup>, and/or is nonlinear, which automatically yields higher harmonics in the phase interaction function<sup>95,141</sup>. Interestingly, cluster states can become macroscopic attractors already for linear coupling<sup>196</sup>. However, a reasonably large shift between frequency parameters is required here, so that the network of Stuart-Landau oscillators must be sufficiently heterogeneous. That, in turn, prohibits an immediate application of the theory of weakly coupled oscillators, where the frequency mismatch of the oscillators has to tend to zero.

### 3.3.3 Identical versus heterogeneous oscillators

As our main focus lies on an accurate phase description of networks of interacting oscillators, it appears legitimate to oversimplifyingly assume that the coupled nonlinear oscillators are (almost) identical. This simplification has two advantages: First, it facilitates the derivation of the phase model insofar as it is sufficient to consider the phase dynamics of only two coupled neural oscillators. Second, it allows to predict the network behavior of the reduced phase model based solely on the phase interaction function. The assumption of identical nodes is, however,

inaccurate. This is in particular the case when modeling realistic networks of bio-physiological, chemical, or neuronal oscillators. Given for instance the immense number of neurons in the human brain together with the fact that no two neurons are identical, modeling two neural oscillators as nearly identical is far from realistic. Nonetheless, different brain regions may share similar properties concerning their collective dynamics, so that a network of (more or less) identical neural masses still appears an acceptable candidate for a brain network model.

Approaches to determine the stability of synchronized network or cluster states along the master stability function formalism or via symmetry arguments rely on coupled identical oscillators, cf. *Section 2.1.5*. To some extent, though, some extensions of the methods above have been proposed in order to deal with (small) heterogeneity among oscillators, see, e.g., an extended master stability function approach for nearly identical systems<sup>197–199</sup>. It is also true that the theory on phase reductions, as presented in *Sections 2.2 – 2.3*, holds for heterogeneous oscillators as long as their frequencies are  $\epsilon$ -close such that small heterogeneities can be subsumed under the coupling terms, see e.g.,<sup>89</sup>. Practical application, nevertheless, becomes more cumbersome, in particular for the numerical reduction methods, when the phase dynamics has to be retrieved for each oscillator individually. Still, another option could be that the heterogeneity only affects the natural frequency terms, but leaves the phase interaction terms identical. This scenario, although again it is hardly plausible, allows to treat the resulting phase oscillator network in terms of heterogeneous Kuramoto-like coupled oscillators. Under a certain form of heterogeneity, that is, given some analytic distribution of the natural frequencies, and in the limit of infinitely many oscillators, the theories mentioned in *Section 3.3.1* allow to describe the macroscopic behavior of the network on a low-dimensional manifold.

### 3.3.4 Extended analytic phase reduction techniques

Throughout the outline of the different phase reduction techniques, we skipped an intricate feature of realistic oscillatory networks: the self-sustained limit cycle dynamics can also be subject to noisy and time-dependent perturbations, or to time-delayed coupling with other oscillators. How will such inputs change the oscillators dynamics, their phase description and eventually the network behavior?

#### 3.3.4.1 Stochastic and time-varying systems

Exemplarily, we reconsider the Wilson-Cowan neural mass model (3.15) with population-specific input  $P_k$  that combines both a stochastic term and a deter-

ministic time-varying term,

$$P_k = \xi_k(t) + P_0 ((1 + A_k \sin(\omega_{p,k} t + \phi_{0,k})) . \quad (3.31)$$

The deterministic term oscillates sinusoidally with amplitude  $A_k$ , frequency  $\omega_{p,k}$  and phase shift  $\phi_{0,k}$ .  $\xi_k(t)$  is an arbitrary noise term. When restricting it to white Gaussian noise, the noise characteristics are given by  $\langle \xi_k(t) \rangle = 0$  and  $\langle \xi_k(t) \xi_l(s) \rangle = 2D^2 \delta(k-l) \delta(t-s)$ , where  $\langle \cdot \rangle$  denotes averaging over the realizations of  $\xi_k$ , and  $D \geq 0$  scales the noise intensity. In either case, noise and time-variability can lead to more complex dynamics and may complicate the phase reduction to great extent.

Periodic forcing without noise, i.e.  $A_k > 0$  and  $D = 0$ , can, in general, already lead to quasi-periodic oscillations of the single neural masses. Quasi-periodic oscillations can also be caused by the time-delay structure, see *Section 3.3.4.2*, or by unidirectional coupling<sup>200</sup>. Phase reduction techniques for weakly connected quasi-periodic Wilson-Cowan oscillators have been proposed by Izhikevich<sup>201</sup>, and further extended by Demirt and co-workers<sup>202</sup>. The application to networks of weakly coupled Wilson-Cowan neural masses where time-periodic input is inducing quasi-periodic oscillations at the single node level, however, is still missing and requires further investigation. Likewise, non-autonomous input functions may generate chaotic oscillations. While a phase can be defined for chaotic oscillators<sup>203</sup>, to the best of our knowledge no phase reduction approach has been attempted for weakly coupled chaotic oscillators.

Recently, several studies have extended the deterministic Wilson-Cowan model by a noisy component<sup>204–209</sup>. The origin of an additional noise term can be motivated in various ways: intrinsic fluctuations in neural activity, microscopic randomness in neural connectivity, or stochastic perturbations due to finite-size effects; see<sup>210,211</sup> and the references therein. Moreover, there is still an ongoing discussion about stochastic descriptions of meso-scale neural populations, see, e.g., the recently proposed model by Schwalger and co-workers<sup>212</sup>. We here aim at revising briefly how one can rigorously describe a network model of stochastic Wilson-Cowan neural masses in terms of their phase dynamics. To do so, we consider noisy external input  $P_k(t) = P_{0,k} + \varepsilon \xi_k(t)$  to the external part of the  $k$ th Wilson-Cowan population and omit further state-dependencies, i.e. the dynamics of interest read

$$\dot{E}_k = -E_k + S \left[ a_E \left( c_{EE}E_k - c_{IE}I_k - \Theta_E + P_{0,k} + \frac{\kappa}{N} \sum_{l=1}^N C_{kl}E_l \right) + \varepsilon \xi_k(t) \right] \quad (3.32a)$$

$$\dot{I}_k = -I_k + S [a_I (c_{EI}E_k - c_{II}I_k - \Theta_I)] . \quad (3.32b)$$

We assume that the noise is weak, i.e.  $\varepsilon \ll 1$  is sufficiently small, and, as before, we consider the parameter regime exhibiting self-sustained oscillations when  $\kappa = 0 = \varepsilon$ . The perturbations by noise will affect the limit cycle oscillations in the same manner as is done by the other weakly coupled Wilson-Cowan populations. In particular, the effects of noisy perturbations crucially depend on the phase sensitivity function  $\mathbf{Z}$  of the Wilson-Cowan neural mass, and a reduced dynamics is favorable. Therefore, it appears legitimate to linearize about the noise term such that we arrive at the dynamics (3.32a) of the excitatory part now given by

$$\dot{E}_k = -E_k + S \left[ a_E \left( c_{EE}E_k - c_{IE}I_k - \Theta_E + P_{0,k} + \frac{\kappa}{N} \sum_{l=1}^N C_{kl}E_l(t) \right) \right] + \varepsilon \sigma_k \xi_k(t) + \mathcal{O}(\kappa \varepsilon, \varepsilon^2) , \quad (3.33)$$

$$\sigma_k = \sigma_k(E_k, I_k) = S [a_E (c_{EE}E_k - c_{IE}I_k - \Theta_E + P_{0,k})] + \mathcal{O}(\kappa) .$$

Note that the multiplicative character of the noise becomes evident as  $\xi_k(t)$  appears in the sigmoidal transfer function  $S[\cdot]$  in (3.32). Again, the aim is to deduce the phase dynamics of the network of coupled Wilson-Cowan neural masses with noisy input. In general, noise can lead to strongly irregular oscillations, such that an extended phase description for stochastic oscillators is needed as has been suggested alternatively by Schwabedal and Pikovsky<sup>213</sup> and Thomas and Lindner<sup>214</sup>. In the case of weak noise these strong irregularities may not arise, and we can rely on phase reduction methods for stochastic limit-cycle oscillators with both additive and multiplicative noise<sup>215-218</sup>. The main focus in these references lies on the synchronization of a network by common (white and colored) noise, but not necessarily on a phase description where coupling and noise terms affect the oscillators' phase dynamics. Nonetheless, the work provides important insight into the subtleties of phase reduction that arise due to (distinct) characteristic time scales of both the noise and the deterministic dynamics<sup>87</sup>.

To be more precise, let  $\tau_\xi$  and  $\tau_\rho$  denote the characteristic correlation time of the noise and the relaxation time of the amplitude of the limit cycle, respectively. For simplicity, we assume  $\tau_\rho$  to be independent of the phase  $\theta$ . In the case of white noise, we can consider the limit  $\tau_\xi \rightarrow 0$ . Moreover, when the dynamics converges

towards the limit cycle solution instantaneously, we can assume the ‘phase limit’  $\tau_\rho \rightarrow 0$ . In general, however, both  $\tau_\xi$  and  $\tau_\rho$  are finite. If we ignore the coupling for a moment, then the general form of the phase dynamics associated to (3.32) reads<sup>217</sup>

$$\dot{\theta}_k = \left[ \omega_k + \frac{\varepsilon^2}{1 + (\tau_\xi/\tau_\rho)} Y(\theta_k) \right] + \varepsilon Z(\theta_k) \xi_k(t) \quad (3.34)$$

in the Stratonovich interpretation<sup>219</sup>. Note that in (3.34) the natural frequency  $\omega_k$  of the oscillator may vary when driven by white noise. Although this variation is of order  $\mathcal{O}(\varepsilon^2)$ , it is of the same intensity as effects due to additional forcing, or coupling, and might therefore not be neglected<sup>87</sup>. In order to derive the the actual expressions of  $Z(\theta_k) = Z_k(\theta_k)$  and  $Y(\theta_k) = Y_k(\theta_k)$ , we first have to define the phase and amplitude coordinates  $\theta_k, \rho_k$  similarly as in *Section 2.3.1.2*. These definitions hold in a vicinity  $U$  of the limit cycle solution  $(E_k^c(t), I_k^c(t)) = (E_k^c(\theta_k), I_k^c(\theta_k))$  of the unperturbed system whose period is  $T_k = 2\pi/\omega_k$ . Then, we find

$$Z_k(\theta_k) = \mathbf{Z}_k \cdot \begin{pmatrix} \sigma_k(E_k, I_k) \\ 0 \end{pmatrix} \Big|_{(E_k, I_k) = (E_k^c, I_k^c)},$$

where  $\mathbf{Z}_k$  is the phase sensitivity function of the (deterministic and uncoupled) neural mass  $k$ . The expression  $Y_k(\theta_k)$  is more complicated and crucially depends on the amplitude dynamics  $\rho_k$  evaluated on the limit cycle. For the general forms of  $Z_k(\theta_k)$  and  $Y_k(\theta_k)$ , we refer to<sup>216,217</sup>. Note, however, that in the limit of weak coupling,  $0 < \kappa \ll 1$ , we arrive at

$$\dot{\theta}_k = \omega_k + \frac{\varepsilon^2}{1 + (\tau_\xi/\tau_\rho)} Y_k(\theta_k) + \frac{\kappa}{N} \sum_{j=1}^N H_{kj}(\theta_j - \theta_k) + \varepsilon Z_k(\theta_k) \xi_k(t) \quad (3.35)$$

with  $H_{kj}$  the usual phase interaction function introduced earlier; for the underlying theory see<sup>38,168,220–223</sup>. For the practical application of an analytic reduction it is again advantageous to first cast the dynamics (3.32) into Hopf normal form, determine the phase sensitivity function  $\mathbf{Z}$  and the amplitude dynamics  $\rho_k$ , and subsequently apply a phase reduction resulting into (3.35). We would like to remark that when the amplitude dynamics towards the limit cycle is much faster than the correlation time  $\tau_\xi$  of the noise, or when the limit cycle is sufficiently robust against amplitude perturbations, then the ratio  $\tau_\xi/\tau_\rho$  can be assumed to tend to infinity and the term with  $Y_k(\theta)$  will vanish. In this case, the phase reduction to  $\dot{\theta}_k = \omega_k + \varepsilon Z_k(\theta_k) \xi_k(t)$  is of the same (non-stochastic) nature as the ‘standard’ phase reduction method<sup>217</sup>.

In the end, the phase reduction of the stochastic Wilson-Cowan neural mass network is based on strong assumptions on the weakness of perturbations through coupling and noise. Although there are recent extensions to strongly perturbed

limit cycle oscillators<sup>224</sup>, the method dwells on the separation of a slow but large-amplitude component and weak fluctuations of the perturbation. In this sense, the approach seems rather adequate to model weakly coupled oscillators with changing background activity<sup>225</sup>. Although not explicitly mentioned, the incorporation of noise appears to be straightforward. External input functions, both deterministic and stochastic, can lead to complex collective behavior, such as the onset of collective oscillations<sup>167</sup> or stochastic, i.e. noise-induced, synchronization<sup>215,218</sup>. However, a comprehensive theory for the reduction of dimensionality in terms of phase (and amplitude) dynamics is still being sought for and remains in the focus of current research.

### 3.3.4.2 Systems with delay

Another important feature of a realistic network topology is the incorporation of a transmission rate, that is, the time needed for the signal of oscillator  $k$  to perturb or affect oscillator  $j$ . Up to now, we only considered infinitely fast, or instantaneous, interactions between oscillators. However, in general one ought to take also the (transient) dynamics of signal propagation into account, which is mainly, and sufficiently well, approximated by an additional delay structure.

In the following, we briefly revisit the phase reduction theory for delay-coupled systems. As in the previous sub-section, we focus on the Wilson-Cowan mass model. Delays can occur both within a single neural mass and between distinct neural masses. Usually, the (internal) interactions are assumed to be considerably fast compared to the typical transmission speed across cortical regions. Therefore, delays within each neural mass can be neglected so that only delays in the coupling between different neural masses generate a global (cortical) delay structure. Such delay structure can be neurobiologically motivated when, e.g., inferred from diffusion spectrum imaging. Once axonal pathways have been identified, the Euclidean distances between connected brain regions and physiologically realistic conduction velocities then provide an estimate on the delays  $\tau_{kl}$  between nodes  $k, l$ . The network dynamics with time-delay read

$$\dot{E}_k = -E_k + S \left[ a_E \left( c_{EE}E_k - c_{IE}I_k - \Theta_E + P_k + \frac{\kappa}{N} \sum_{l=1}^N C_{kl}E_l(t - \tau_{kl}) \right) \right] \quad (3.36a)$$

$$\dot{I}_k = -I_k + S [a_I (c_{EI}E_k - c_{II}I_k - \Theta_I)] . \quad (3.36b)$$

Assuming that the time delays  $\tau_{kl}$  are of the same order of magnitude as the period  $T_k$  of oscillation of each of the neural masses, they will manifest themselves as model-dependent phase shifts  $\Delta_{kl} = (2\pi/T_k)\tau_{kl}$  in the coupling function of the

reduced phase dynamics:

$$\dot{\theta}_k = \omega_k + \kappa \sum_{l=1}^N H(\theta_l - \theta_k - \Delta_{kl}) ; \quad (3.37)$$

for the derivation see e.g.,<sup>42,44,48</sup>. Intuitively, this phase shift can be explained within the theory of weakly coupled oscillators: Given that  $\kappa \ll 1$  is small, the time-delayed coupling term corresponds to a phase-shifted point on the (uncoupled) limit cycle. When expanding the phase interaction function  $H$  in Fourier space, the phase shifts  $\Delta_{kl}$  will effectively shape the amplitudes of the odd and even harmonics, i.e. of the sine and cosine components, respectively, which may affect the collective dynamics of the network. In fact, prior studies that respected transmission delays in phase oscillator networks have reported elaborate synchronization dynamics<sup>226–230</sup>.

In the case of time delays where a phase shift-approximation as above is not adequate, e.g., when  $\tau$  represents the time of propagation of the signal from one neuron to another, the dynamics become more complex. Indeed, delayed dynamical systems are infinite-dimensional, and thus present a serious mathematical challenge. Numerical tools have been developed such as DDE-BiFTOOL<sup>231,232</sup>, which can be used to investigate the dynamical properties of coupled systems with delay. Coombes and Laing<sup>233</sup> applied the methods to a single Wilson-Cowan population with multiple time delays. In particular, time delays influence the creation of oscillations as well as the form of the limit-cycle. Even quasi-periodic orbits can emerge, as has been shown for a slightly different version of a Wilson-Cowan population with delays<sup>234</sup>. How coupling, with and without delays, to other Wilson-Cowan populations further shapes the oscillatory properties of the single neural masses has not been answered yet.

Similar to coupling-induced oscillations, which will be the focus in the following *Section 3.3.5.1*, also the incorporation of time delays may lead to oscillations. It is noteworthy that phase reduction techniques have been extended to tackle these delay-induced oscillations<sup>87,235,236</sup>. The theoretical framework developed there has yet to be generalized to analyze weakly coupled delay-induced limit-cycle oscillators. Likewise, another open and crucial question is whether reduction techniques can be applied to deduce a phase model when oscillations are not necessarily delay-induced but strongly affected by the delay: delays leading to too strong amplitude effects prohibit phase reductions without a loss of (too much) information so that alternative ways have to be found.

### 3.3.5 Coupling functions

The coupling dynamics of interacting nonlinear oscillators is a research theme already in itself, and we do not dare to even intend to treat this subject thoroughly. The interaction between two units can take too many forms, is too diverse and may feature too distinct dynamics, so that most of the times realistic coupling scenarios are approximated by simpler terms to render a network analysis feasible. When confronted with interacting systems, it is important to identify the correct type of coupling function between them, especially given the role of coupling dynamics in shaping non-trivial network behavior. Therefore, we will briefly comment on general aspects of coupling terms, on the modeling approximations of realistic coupling as well as on the effects of coupling matrices reflecting realistic structural connectivity. All of them can, and usually do, influence the reduction of a phase model.

As we briefly noted in our Brusselator example, *Section 3.1*, for systems with dynamics  $\dot{x} = f(x) + g(x, y)$  the character of the coupling can be *direct*,  $g(x, y) = g(y)$ , *diffusive*,  $g(x, y) = g(y - x)$ , *reactive*,  $g(x, y) = (\epsilon + i\beta)g(x - y)$ , *conjugate*,  $g(x, y) = g(x - Py)$ , as a *chemical synapse*,  $g(x, y) = g(x)S(y)$  with  $S(\cdot)$  of sigmoidal shape, or *environmental*,  $g(x, y) = \epsilon \int_0^t e^{-\kappa(t-s)}(x(s) + y(s))ds$ ; see the recent review<sup>237</sup> and the references therein. One may further distinguish between *linear* and *nonlinear* coupling, depending on the order of  $g(x, y)$ . While the original dynamics of interacting systems exhibit one or more coupling functions of the types above, their counterpart in the corresponding and reduced phase model often boils down to either a diffusive phase coupling term  $\tilde{g}(\theta_x, \theta_y) = \tilde{g}(\theta_x - \theta_y)$  or to a pulse-response coupling of the form  $\tilde{g}(\theta_x, \theta_y) = P(\theta_y)R(\theta_x)$ . How coupling terms of the original dynamics translate into the particular phase coupling functions, depends both on the characteristics of the underlying dynamical system as well as on the strength of interaction. The pulse-response coupling, as was established by Winfree in his original work<sup>85</sup>, appears to be the more general form of phase interactions where the coupling term is the product of the external perturbation  $P(\theta_y)$  through the other oscillator with the response  $R(\theta_x)$  of the perturbed oscillator, the latter commonly referred to as the phase response function. Averaging procedures, however, can be applied if the perturbations and/or coupling strength are sufficiently weak, in which case a diffusive phase coupling term can be recovered again. Moreover, there are other exceptions where an averaging procedure is also possible, such as when multiple strong pulses are dispersed around the cycle, cf. 147.

We are also fully aware that models of interconnected nonlinear oscillators, in particular neural oscillators, often feature rather complex coupling terms with in-

dividual dynamics<sup>153,238,239</sup>. Keyword here is ‘event driven’ coupling. For instance, let two neurons be connected via a chemical synapse. When the presynaptic neuron elicits a spike, an action potential travels along the axon and provokes the release of neurotransmitters at the synapse. This in turn leads to a temporary change of the membrane potential of the postsynaptic neuron with characteristic finite rise and fall times. Taken together, event driven coupling can be defined as the time-resolved interaction between nodes (e.g., neurons) that is triggered through a particular event (e.g., the spiking of the presynaptic neuron). This transient dynamical process can be described mathematically with a linear differential operator that has a given response (or Green’s function). When allowing for this kind of complex coupling, the corresponding network model becomes more detailed and high-dimensional. Still, the theory outlined in *Chapter 2* above applies also in this case and a proper phase model can be reduced. The coupling functions in the reduced phase model, however, are now time-dependent and can become arbitrarily difficult. Sometimes, these reduced coupling functions can be approximated and continue to provide an accurate model of the underlying system, see e.g.,<sup>240</sup>. We discourage, however, from ad hoc approximations without a sensitive assessment of both the full dynamics and the reduced, or simplified, phase dynamics. Here, we first analyzed the parameter range in which the nonlinear, sigmoidal coupling function in the Wilson-Cowan neural mass model can be adequately approximated by polynomial terms, and then we employed the analytic reduction techniques for these parameters, cf. *Section 3.2*. Incorporating delays between cortical regions or spatial kernels leads to far more intricate coupling dynamics, see e.g.,<sup>241</sup>, and *Section 3.3.4.2*. Friston popularized Volterra series to model inherent nonlinear interactions when also taking neuronal transients into account, i.e. the recent history of neural activity of connected neuronal populations<sup>242</sup>. Phase reduction strategies have been extended recently to cope with time-varying external perturbations<sup>224,225,243</sup>, which hints at ways how to tackle dynamically more intricate coupling terms. However, a thorough analysis of complex coupling functions and their translation into phase models is beyond the scope of this review. Yet, we trust that our results can help to construct particular phase coupling terms, which especially becomes important for the modeling of neural cross-frequency interactions<sup>244,245</sup>.

### 3.3.5.1 Coupling-induced behavior

The reduction of phase dynamics from a network of coupled oscillators retains its mathematical justification as long as the theory of weakly coupled oscillators applies. However, no rigorous definition of weak coupling exists, nor a concrete limit of the coupling strength at which the character of interaction switches from

weak to strong. Usually, phase reduction is achieved with the tacit understanding that each isolated system already displays stable limit cycle oscillations, which is a necessary condition for the theory of weakly coupled oscillators. However, in some cases it is the coupling between systems that induces oscillations. Smale was among the first to investigate the emergence of oscillations via a Hopf bifurcation due to diffusive coupling<sup>246</sup>. On the other hand, coupling between systems can also make oscillations cease. Ermentrout and Kopell reported this kind of oscillation death for a chain of Wilson-Cowan neural masses<sup>153</sup>, see also the work by Daffertshofer and van Wijk on a (heterogeneous) network of Wilson-Cowan neural masses<sup>42</sup>.

Those effects only occur for reasonably large coupling strengths, and a straightforward identification of the phase dynamics as within the theory of weak coupling is not possible. While sufficiently weak coupling ensures that the shape and the frequency of the limit-cycle orbits remain almost unchanged, strong coupling leads to non-negligible amplitude effects. These can destabilize synchronized states, cause (amplitude and thus) oscillation death or collective chaos, and a phase reduction has only been proposed for quite restrictive assumptions; see<sup>224</sup> and the references therein. Hence, phase-amplitude reductions<sup>247–249</sup> have to be employed that also take interactions between phase and amplitude dynamics into account. The theory of weakly coupled oscillators additionally requires that the actual trajectories of the oscillators are always close to the isolated limit-cycle solution. Recently, Wilson and Ermentrout proposed a method that allows for a phase reduction farther away from the underlying periodic orbit<sup>250</sup>, thereby admitting also stronger perturbations and coupling strengths, see also *Section 3.3.7*. For the sake of conciseness, we omitted the difficulties mentioned above, knowing well the intricacies tied to a more careful investigation of other urgent questions beyond the realm of the weak coupling limit. Yet, we would like to briefly discuss the emergence of oscillations through coupling, as well as their cessation.

**Oscillation birth and clustering** From an analytic point of view, it appears illustrative to start with two coupled identical oscillators, which rest in a stationary state when uncoupled. As can be seen in the corresponding bifurcation diagram in Fig. 3.10, oscillations can be induced through coupling via a Hopf bifurcation (red dot). The critical coupling strength can be determined analytically, see also<sup>173</sup>. In our example, it is considerably small with  $\kappa = 0.0531$  (note that we did not rescale the coupling by a factor  $1/N$ ). Interestingly, already for two coupled oscillators the initial conditions have a major impact on the resulting dynamics: while for coupling strengths  $\kappa < 0.6$  (see green dot), all initial conditions run either into the same two limit cycles or into the low activity resting state (blue solid curve), for larger coupling strengths only identical initial conditions result into the same

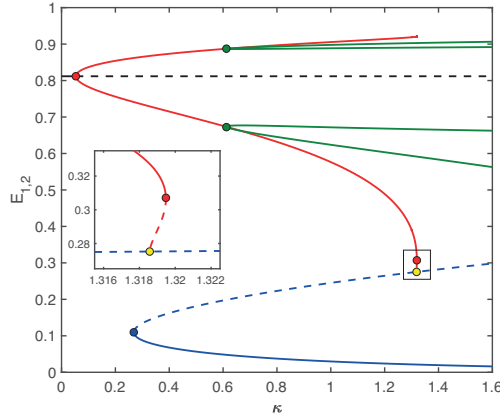


**Figure 3.10:** Bifurcation diagram of two coupled identical Wilson-Cowan neural masses with parameters  $P = -3$  and  $Q = -9.4$ . At low coupling strengths  $\kappa < 0.05$ , the two units are at rest (black solid curve). Oscillations emerge at the Hopf bifurcation (red dot), where the resting state becomes unstable (black dashed). The limit cycles of the two oscillators (red curves display upper and lower limit) are identical up to the green dot. Beyond this point, identical initial conditions of the neural masses result in the two identical limit cycles with upper and lower limits as shown in red. Finally, oscillations cease through a fold bifurcation of limit cycles for higher coupling strengths (second red dot). The yellow dot represents a homoclinic bifurcation, induced through the unstable counterpart (blue dashed) of the pair of fixed points that emerged through a saddle-node bifurcation (blue dot). For non-identical initial conditions of the neural masses, the attracting limit cycles are distinct for coupling strengths higher than at the green dot. Stable oscillations (with limits on either the outer or inner branches of the green curves) are then also possible beyond those coupling strengths for which identical initial conditions evolve into a low-activity resting state (blue solid).

(red) limit cycles. Different initial conditions for the two coupled neural masses may still lead to stable oscillations, but the respective limit cycles can differ in amplitude and shape (green curves). Moreover, oscillations starting from distinct initial conditions are stable for even larger coupling strengths, where those from identical initial conditions have ceased through a fold bifurcation of limit cycles (see the inset).

Based on our brief analytic insights concerning only two coupled oscillators, we anticipate that coupling-induced effects will increase the dynamic intricacy of larger networks of strongly coupled oscillators. To illustrate this, we simulated a fully connected network of 30 identical Wilson-Cowan neural masses starting from random initial conditions. Fig. 3.11 displays the network behavior for different coupling strengths. Without coupling, the network remains at rest (top row). For weak coupling, there is perfect synchronization between coupling-induced oscillations. Moreover, all oscillators describe the same limit cycle (middle row). For stronger coupling, the coupling-induced oscillations become more complex. Different oscillators form clusters, which furthermore evolve on distinct limit cycles (bottom row).

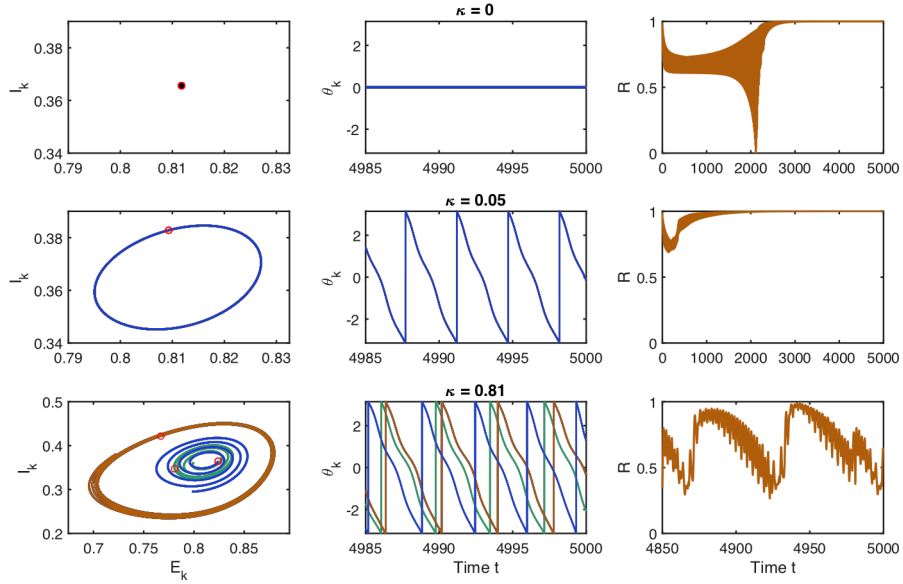


**Figure 3.11:** Coupling induced behavior of  $N = 30$  globally coupled identical Wilson-Cowan neural masses with parameters  $P = -3$  and  $Q = -9.4$ . Without coupling (top row), only the resting state is stable. At low coupling strength  $\kappa = 0.05$  (middle row), all neural masses synchronize on the same limit cycle. At very high coupling strength  $\kappa = 0.81$  (bottom row), the neural masses form three clusters on distinct limit cycles and show intermittent synchronization. Left: dynamics of all neural masses in the  $E_k - I_k$  plane for the lase  $t = 15$  seconds. Middle: extracted phases of all neural masses. Right: real Kuramoto order parameter displaying phase synchronization of the network.

**Oscillation death and quasiperiodic dynamics** To investigate the phenomenon of oscillation death, we chose parameters such that a single, unperturbed Wilson-Cowan neural mass exhibited stable limit-cycle oscillations. Starting again with two coupled identical oscillators, we display the corresponding bifurcation diagram with respect to the coupling strength in Fig. 3.12. For identical initial conditions, the red curves represent the upper and lower limit of the amplitude of the (identical) limit cycles. Note that oscillation death occurs via a homoclinic bifurcation (yellow dot). For distinct initial conditions, we find again two different oscillatory regimes: at low coupling strengths, both limit cycles coincide. However, for larger coupling strengths beyond  $\kappa \approx 0.45$  (red dot) each neural mass exhibits quasiperiodic behavior, as depicted in Fig. 3.12b.

Similar to before, we also simulated the network dynamics and confirmed the analytic predictions extrapolated from two coupled oscillators to a larger network. Results are shown in Fig. 3.13. Note that the parameters  $P, Q$  are chosen such that the reduced phase model predicts asynchronous network dynamics for low coupling strengths, as is demonstrated by the simulations (top row). Stronger coupling leads first to a general increase in network synchronization as indicated by the (mean value of the) Kuramoto order parameter, and to quasiperiodic dynamics (middle row). Eventually, for even stronger coupling oscillations cease and the dynamics

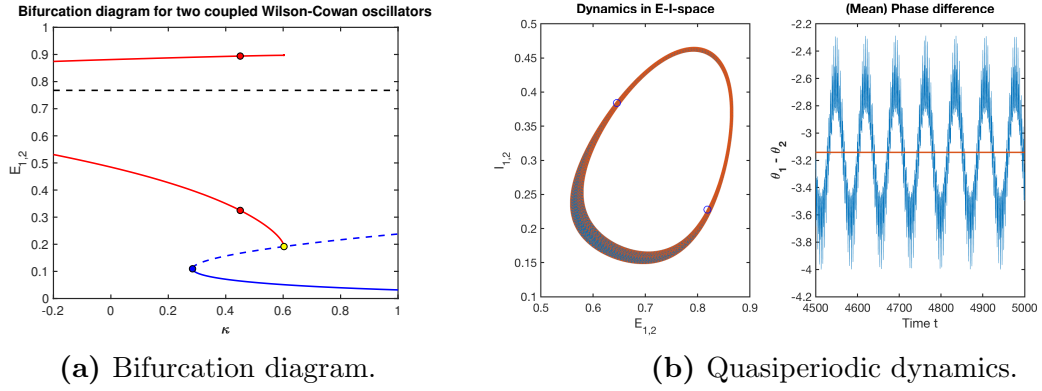


**Figure 3.12:** Oscillation death: bifurcation diagram similar to Fig. 3.10, now starting with stable limit cycle oscillations without coupling. Oscillation death occurs via a homoclinic bifurcation (yellow dot) for identical initial conditions. The red dots denote the emergence of quasiperiodic behavior for distinct initial conditions. In (b) quasiperiodic behavior is depicted for coupling strength  $\kappa = 0.475$

collapse into a low activity state (bottom row).

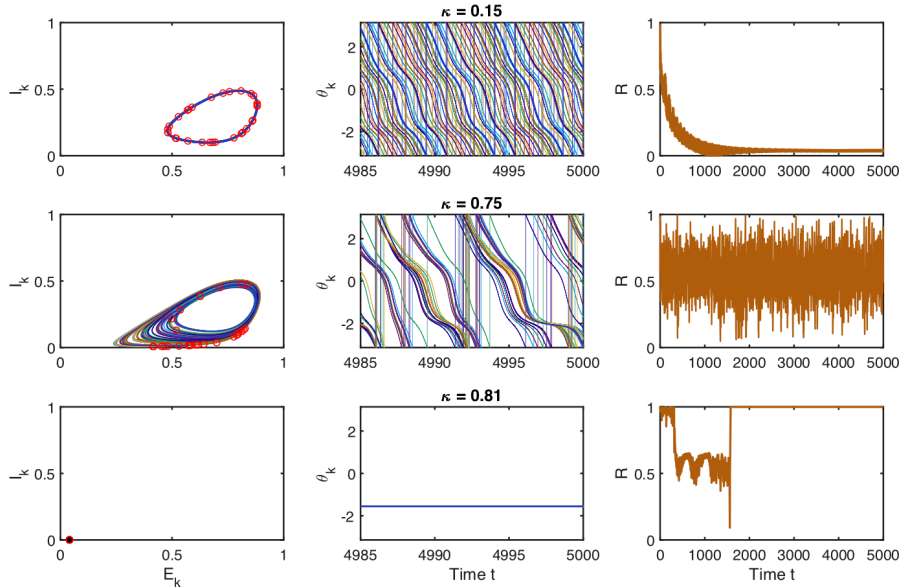


**Figure 3.13:** Coupling induced behavior of  $N = 30$  globally coupled identical Wilson-Cowan neural masses with parameters  $P = -3$  and  $Q = -9$ . At low coupling strength  $\kappa = 0.15$  (top row), all neural masses desynchronize on the same limit cycle as predicted by the phase model. At intermediate coupling strength  $\kappa = 0.75$  (middle row), oscillators move along quasiperiodic trajectories and tend to synchronize. At very high coupling strength  $\kappa = 0.81$  (bottom row), oscillation death occurs and the neural masses run into a low activity resting state. Left: dynamics of all neural masses in the  $E_k - I_k$  plane for the last  $t = 15$  seconds. Middle: extracted phases of all neural masses. Right: real Kuramato order parameter displaying phase synchronization of the network.

### 3.3.5.2 Effects of structural connectivity

The analytic insight with respect to the bifurcation diagram of two coupled oscillators, helped us in *Section 3.3.5.1* to draw conclusions about possible network states of  $N \gg 2$  globally coupled oscillators. As mentioned before, pairwise interaction between the oscillators in a network allows us to generalize the findings about two oscillators to larger networks. In principle, however, the coupling terms can combine the simultaneous effects from more than one oscillator, which results in a multivariate coupling function with more than two input variables. Multivariate interaction has recently attracted increased attention; an overview can be found in Section II.C.3<sup>237</sup> and see various references therein. As long as the coupling is sufficiently weak, phase reduction techniques can cope also with multivariate coupling terms, see, e.g., Malkin's Theorem in *Section 2.3.1*. Moreover, reduced phase models may feature phase interaction functions with up to four interacting phases, see the reduction via  $S_N \times S^1$ -symmetry in *Section 2.2.6*. Still, already in the case where the phase interaction function only depends on pairwise phase differences, the network can exhibit rich and non-trivial dynamics as seen before.

Another important factor that can shape the network dynamics is the structural connectivity between nodes. The underlying network topology plays a significant role for the observed network behavior. In particular, many results about expected network behavior based on (higher harmonics of) the reduced phase interaction function are no longer valid when the connectivity structure deviates from global, all-to-all coupling, as we will illustrate below. Yet, on a first level, the derivative of the reduced phase interaction function can still provide important information about (remote) synchronization properties of a realistically connected network, see e.g.,<sup>58</sup>.

As before, we assume that possibly multivariate coupling terms  $\mathbf{g}_k(\mathbf{x}_1, \dots, \mathbf{x}_N)$  of the underlying oscillator model of  $N$  interacting nonlinear oscillators can safely be approximated by the sum over pairwise coupling terms

$$\mathbf{g}_k(\mathbf{x}_1, \dots, \mathbf{x}_N) \approx \sum_{j=1} C_{kj} \mathbf{g}(\mathbf{x}_k, \mathbf{x}_j).$$

If such a decomposition is not possible for all units of the network, an exit strategy may be the following: first, the network is parceled into interacting subnetworks, and subsequently each oscillating subnetwork is characterized in terms of its macroscopic rhythm, employing collective phase description methods as devised by Kawamura, Nakao, Kuramoto and co-workers<sup>167,168,221,222</sup>.

As usual our goal is to establish a phase model of the form (2.16),

$$\dot{\theta}_k = \omega + \frac{\kappa}{N} \sum_{j=1}^N C_{kj} H(\theta_k - \theta_j) , \quad (3.38)$$

where  $C_{kj}$  denote the entries of the *adjacency* or *connectivity matrix*, which represents the structural connectivity between oscillators. In the simplest case, all oscillators are coupled to all the others, that is the case of global coupling with  $C_{kj} = 1$  for all  $k \neq j$ . More realistic network topologies, on the other hand, can be translated into adjacency matrices that respect graph-theoretical properties of, e.g., the structural brain connectivity as derived from diffusion tensor imaging. The effects of the network topology on the macroscopic behavior are to great extent still unclear. Indeed, particular features in the network topology, such as, e.g., small-worldness, which is believed to resemble the connectivity of the human brain, elude analytic treatment completely, but at the same time bear rich non-trivial network behavior<sup>251–254</sup>.

To give a slight insight into the additional complexity, we compared the simulated phase dynamics with the phases extracted from the original Wilson-Cowan neural mass model (3.15) and considered three different coupling topologies: a fully connected homogeneous network, an anatomical network reported by Hagmann and co-workers<sup>255</sup>, and a network with small-world topology generated by the Watts-Strogatz model<sup>256</sup>; see Fig. 3.14 for the corresponding adjacency matrices.

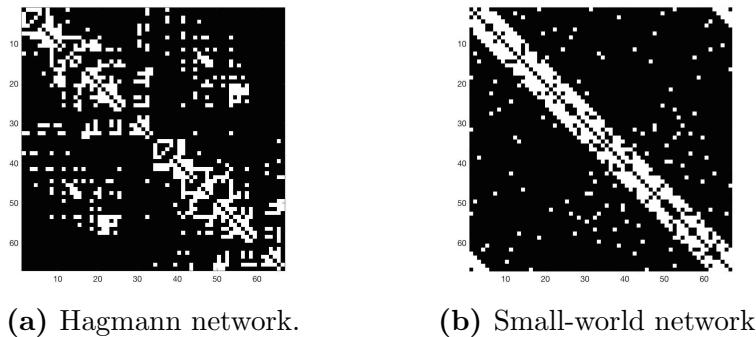


**Figure 3.14:** Connectivity matrices for the Hagmann dataset and the generated small-world topology using an average degree of 10 and a rewiring probability of 0.2.

Following *Section 3.2.5*, we simulated the network in the parameter regions where we expect synchronization, incoherence and cluster states, and changed the connectivity matrix subsequently. As displayed in Fig. 3.15, the particular connectivity structures led to macroscopic dynamics that became indistinguishable from one another, the red and blue graphs correspond to small-world and Hagmann network connectivity, respectively. Only in case of a fully connected homogeneous

network, see the black graphs, the actual dynamics matched the predictions of the numerically reduced phase model.

Moreover, we simulated the different phase models as retrieved by the four reduction techniques. The numerically reduced phase dynamics (black graphs) correctly captured the original Wilson-Cowan dynamics for full connectivity, see the left column in Fig. 3.16. For non-trivial connectivity structures, however, none of the phase models can follow the predictions based on the (global) phase interaction function  $H$ . While for the small-world network (middle column) the simulations hint slightly at the synchronous, asynchronous and two-cluster regimes, respectively from top to bottom, the observed dynamics on the Hagmann network appear arbitrary. Note that the direct averaging technique (green graphs) leads to synchronized macroscopic behavior for almost all parameter settings and connectivity structures. The two analytic techniques feature rather distinct behavior for full connectivity: the reductive perturbation approach (red) leads to full synchronization, whereas the nonlinear transform approach (blue) results in a two cluster state. On the other hand, for the small-world and Hagmann networks, the two techniques converge to the same network behavior. For more details about the connectivity structures as well about the simulations, we refer to the Appendix<sup>170</sup>.

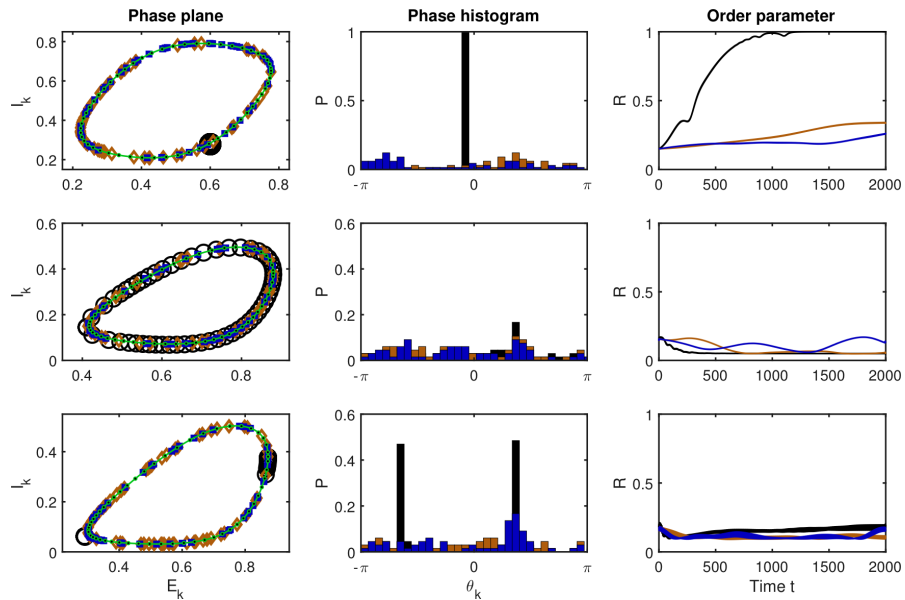


**Figure 3.15:** Simulation of the Wilson-Cowan dynamics at coupling strength  $\kappa = 0.15$  for regimes as predicted by the reduced phase model: synchronization (top row), asynchrony (middle) and two-cluster state (bottom). Left: final ( $T = 2000$ ) position of all 66 connected Wilson-Cowan oscillators on the unperturbed limit cycle (green) with random initial conditions (black dots). Middle: phase histogram of final Wilson-Cowan oscillators. Right: phase synchronization of the network measured with the real Kuramoto order parameter with a moving average over 20 seconds. Colors correspond to full connectivity (black, circles), small world (blue, diamonds), and Hagmann (red, squares).

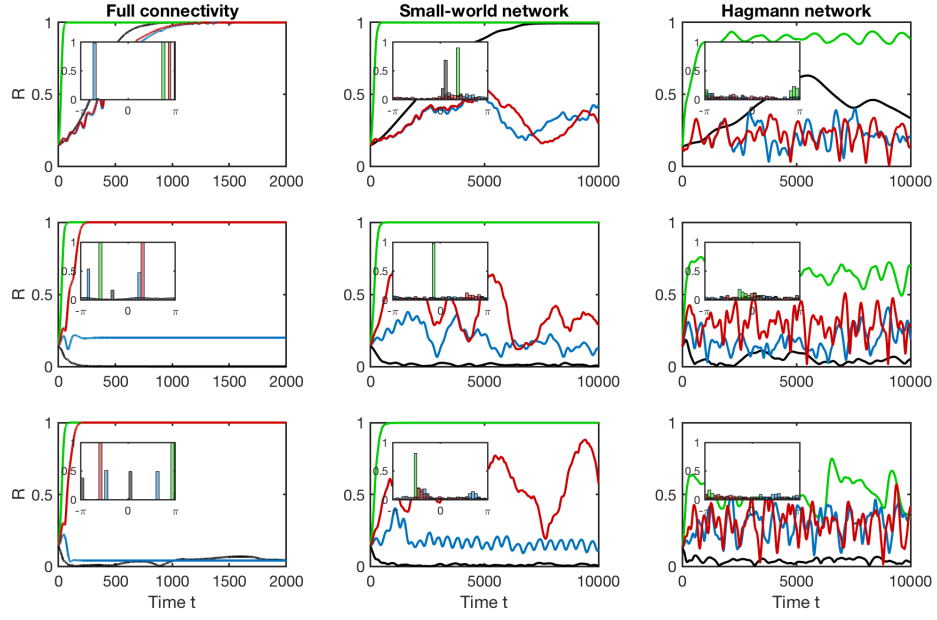


**Figure 3.16:** Simulation of the reduced phase models at coupling strength  $\kappa = 0.25$  with full (left column), small-world (middle) and Hagmann network connectivity (right). Insets show histogram of the final ( $T = 2000$  for full connectivity, and  $T = 10000$  otherwise) phase distribution for  $N = 200$  oscillators ( $N = 66$  for Hagmann network). Colors correspond to numerical reduction (black), direct averaging (green), reductive perturbation (red), and nonlinear transform approach (blue).

In a nutshell, we can conclude that topology effects overcome otherwise precise predictions of the phase model such that even the least accurate direct averaging method does not perform worse than the other techniques.

### 3.3.6 Phase versus other oscillators

#### 3.3.6.1 Nonlinear oscillators

The limitations as presented in *Section 3.3.5* culminate in the natural question how well phase models are actually able to approximate and predict the behavior of the network model of coupled, often high-dimensional nonlinear oscillators. As shown in *Sections 3.1* and *3.2*, a properly tailored phase reduction can lead to a phase model that not only describes synchronization transitions of the underlying model accurately, but also captures non-trivial network behavior such as cluster states. It can, however, also be the case that complex emergent phenomena, e.g., cluster states (and chimera states as a special case of clustering), self-organized quasiperiodic synchrony, or amplitude death, are due to amplitude effects in the oscillator network. Then, the validity of a reduced (and averaged) phase model is highly questionable. To give an example, Rosenblum and Pikovsky considered a system of identical Stuart-Landau oscillators with global nonlinear coupling<sup>90–92</sup>.

In deriving the corresponding phase dynamics, they found<sup>90</sup> a dynamic dependence of the coupling strength as well as of the amplitudes of the first harmonics on the network's order parameter. It is true that the resulting phase model is integrable within the Watanabe-Strogatz theory. However, the additional dynamics pose an irreconcilable obstacle for the varying phase interaction function to be retrieved: The numerical phase reduction techniques only provide a static picture. But also the normal form reduction methods, which usually transform the original dynamics near a supercritical Hopf bifurcation into the form of Stuart-Landau oscillators, fail to respect the higher order dependence on the order parameter, even in case of constant global coupling<sup>91,92</sup>. The reason is that the particular nonlinear coupling term considered by Rosenblum and Pikovsky will be culled as it merely provides higher order corrections to the first dominant harmonics, see *Section 2.2.1.2*. Interestingly, nonlinear coupling is not necessary to induce non-trivial network behavior. Sethia and Sen considered it surprising that chimera states in a network of Stuart-Landau oscillator already exist for linear coupling<sup>257</sup>. However, the results by Kori and co-workers, who detected cluster states as well as slow switching behavior for a network of diffusively coupled Brusselators based on their reduced phase model<sup>95</sup>, and also our findings, suggest that complex and rich network behavior can be predicted by adequately derived phase models.

### 3.3.6.2 Non-smooth oscillators

The way the  $T$ -periodic limit cycle  $\mathcal{C}$  has been introduced above, suggests that the trajectory  $\phi(t; \mathbf{x}^c)$  is a smooth curve in phase space for  $0 \leq t \leq kT$  with  $k \rightarrow \infty$ . However, the definition of  $\mathcal{C}$  also holds for non-smooth trajectories, e.g., for a piece-wise smooth trajectory that features sudden jumps. In this manner it is possible to define a phase also for so-called integrate-and-fire neuron models: every time the voltage variable exceeds a particular threshold value, a spike is elicited and the voltage is reset to a lower reset value. For the time between two spikes, the voltage can then be parametrized in terms of a phase value. Consequently, it is possible to determine the phase dynamics of an integrate-and-fire model<sup>102</sup>. Politi and Rosenblum recently demonstrated the equivalence between phase-oscillator and integrate-and-fire models in the weak-coupling limit for a fully connected network of identical units<sup>258</sup>. Moreover, models of electric circuits with discontinuous switching or gait models with sudden collisions with the ground feature non-smoothness of the state variables. The dynamical systems describing these models are usually called hybrid dynamical systems. If they exhibit limit-cycles, then one refers to those oscillations as hybrid limit-cycle oscillations. The recent work<sup>259</sup> by Shirasaka, Kurebayashi and Nakao provides a detailed mathematical account of the phase reduction of such hybrid limit-cycle oscillators.

### 3.3.7 Phase-amplitude models

A more general approach to the definition of phases and amplitudes is the transformation into a so-called phase-amplitude model. Typically, one introduces a moving orthonormal coordinate system around the limit cycle and fixes one axis pointing in the direction of the tangent vector along the periodic orbit. The coordinate corresponding to this tangential axis indicates the phase whereas all other coordinates are associated with the distance from the limit cycle, previously defined as amplitudes. Phase-amplitude descriptions allow for tracking dynamical phenomena that are not visible within the isochronal (phase) description. Examples are shear-induced chaos or oscillation death. The recent review by Ashwin, Coombes, and Nicks<sup>89</sup> and the references therein provide more details. Despite the greater accuracy of phase-amplitude models, however, isochronal phase models are often in favor for their simplicity and are generally valid as long as perturbations are weak, or considerably moderate. For larger perturbations, discarding the amplitude dynamics may be improper. It seems promising to introduce a simplified coordinate system via so-called isostable coordinates, which correctly describes the phase dynamics away from the limit-cycle<sup>250</sup>. This approach does not rely on the weak coupling assumption. Likewise promising are recent approaches that allow, e.g., for large external perturbation that oscillate at sufficiently slow<sup>224,225</sup> or fast frequencies<sup>243</sup>. In *Section 2.3.1.2*, we briefly sketched a phase reduction approach that crucially relies on the fast relaxation rate of the oscillator towards its limit cycle. There, the introduced phase-amplitude coordinate system reduces by means of a separation of time scales to a phase description only.

As a final note we would like to add that *Koopman operators* provide a very useful framework to accurately describe transient dynamics of systems with stable limit cycles in reduced phase and amplitude coordinates. Similar to the notion of isochrons as level sets of the same asymptotic phase value, it is possible to define the above-mentioned *isostables* as a set of initial conditions that have the same relaxation rate towards the attracting limit cycle<sup>260</sup>. An isostable represents an amplitude degree of freedom, which in addition is independent of the phase and of other amplitude degrees of freedom. Both isochrons and isostables can be understood from a unified perspective via the spectral properties of the Koopman (composition) operator<sup>247,260,261</sup>. This operator has proven to be of invaluable use for dynamic mode decomposition, a data-driven approach to complex nonlinear systems. Wilson and Moehlis further extended the theory to systems with limit cycle attractors<sup>262</sup>. A rigorous extension to phase-amplitude dynamics, also away from the limit cycle, has recently been proposed by Shirasaka, Kurebayashi and Nakao<sup>247</sup>; see also<sup>263</sup> including an alternative numerical approach to compute the

phase and amplitude responses via a forward-integration method. The Koopman operator framework further allows to reduce phase and amplitude dynamics in a consistent way and can be implemented numerically. As we mainly focused on weak perturbations off the limit cycle, such that amplitude effects become negligible, we refrain from further elaboration on the Koopman operator theory and refer the interested reader to the literature, see<sup>247</sup> and numerous references therein.

### 3.3.8 Analytic approaches versus numerics – a final word

The ‘competition’ between analytic phase reduction techniques and numeric reduction techniques boils down to seeking a compromise between qualitative insights and quantitative accuracy of the resulting phase model. Either, one can gain analytic insights into how parameters of the underlying oscillatory dynamics translate into the phase model, which may come at the cost of losing accuracy as soon as the dynamics are away from a bifurcation point. Or, we derive the phase dynamics numerically and with high accuracy, but may forego explicit analytic expressions that can provide an intuition about which parameters of the underlying model influence the phase dynamics to what extent and in which direction. We therefore advise to combine both analytic and numerical reduction techniques. In this way, numerical techniques can, e.g., be used to verify the validity of analytic reduction techniques so that analytic insights can be gained in an optimally extended neighborhood around a bifurcation point.

---

# CHAPTER 4

## Interactions between networks of heterogeneous phase oscillators

*Populations of oscillators can display a variety of synchronization patterns depending on the populations' intrinsic coupling and the coupling between them. We consider two coupled, symmetric (sub)populations with unimodal frequency distributions. If internal and external coupling strengths are identical, a change of variables transforms the system into a single population of oscillators whose natural frequencies are bimodally distributed. Otherwise an additional bifurcation parameter  $\kappa$  enters the dynamics. By using the Ott-Antonsen ansatz, we rigorously prove that  $\kappa$  does not lead to new bifurcations, but that a symmetric two-coupled-population-network and a network with a symmetric bimodal frequency distribution are topologically equivalent. Seeking for generalizations, we further analyze a symmetric trimodal network vis-à-vis three coupled symmetric unimodal populations. Here, however, the equivalence with respect to stability, dynamics and bifurcations of the two systems does no longer hold.*

Adapted from: Pietras B., Deschle N., Daffertshofer A. (2016). *Equivalence of coupled networks and networks with multimodal frequency distributions: conditions for the bimodal and trimodal case*. Phys. Rev. E **94**, 052211.  
doi: 10.1103/PhysRevE.94.052211.

## 4.1 ‘Multimodal networks’ or ‘networks of networks’?

The Kuramoto model is seminal for describing synchronization patterns in networks of phase oscillators. It has been investigated to great detail in numerous studies using different approaches; for reviews see e.g.,<sup>39,264</sup>. The analytical treatment typically relies on the formation of a common variable, the so-called order parameter, and seeks to pinpoint its dynamics. The more recently suggested ansatz by Ott and Antonsen<sup>81</sup> proved particularly fruitful for analyzing this dynamics. It applies to the thermodynamic limit, i.e. to infinitely large populations, and it contains major simplifications including the ‘parametrization’ of the phase distribution’s Fourier transform. Abrams and co-workers<sup>265</sup> were the first to describe the dynamics of two coupled populations using the Ott-Antonsen ansatz, confirming earlier results based on perturbation techniques<sup>266–268</sup>; see also Laing’s extension including heterogeneity and phase lags<sup>269</sup>. Similarly, Kawamura and co-workers<sup>270</sup> derived a collective phase sensitivity function to describe synchronization across subpopulations, but they assumed only very weak coupling between them. A detailed bifurcation analysis of these dynamics without such restrictions, however, is still missing.

We discuss a network of two populations of Kuramoto oscillators with unimodally distributed natural frequencies. The dynamics will be compared with that of a single population of oscillators with bimodally distributed frequencies. The latter case has been extensively studied by Martens and co-workers<sup>271</sup>. In Fig. 4.1 we sketch the contrasting network configurations. Here we prove that a symmetric two-population network does fully resemble the case of one network with bimodally distributed frequencies. Assuming that the internal coupling strength (identical for both networks) can be distinct from the bidirectional external coupling strength, we introduce another degree of freedom in the dynamics, and by that go beyond a simple change of variables, which may transform the bimodal description into two populations. As we will show, this additional parameter does not lead to qualitatively different dynamics. Instead we prove the topological equivalence of the two systems.

A natural question is whether this equivalence can be generalized. For this we couple more than two populations and compare their dynamics to a network with a multimodal frequency distribution. We show that for a symmetric trimodal network vis-à-vis three subpopulations with identical internal coupling and identical (though distinct to the internal coupling strength) bidirectional external coupling, the dynamics already differ qualitatively from each other. Therefore, in the sym-

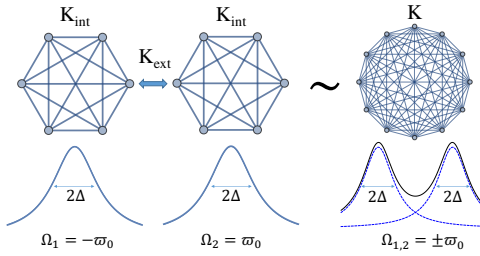


**Figure 4.1:** Two all-to-all coupled networks (left) with unimodal frequency distributions each; a single all-to-all coupled network (right) with a symmetric bimodal frequency distribution function.

metric case considered here, the topological equivalence between coupled networks and networks with multimodal frequency distributions appears limited to two coupled networks vs. one bimodal network, and fails when considering more than two subpopulations.

## 4.2 Revisiting the existing theory on interacting populations of Kuramoto phase oscillators

The Kuramoto model displays the long-term dynamics of a system of  $N \in \mathbb{N}$  weakly-coupled limit-cycle oscillators, where each oscillator  $k$  is fully described by its phase  $\theta_k$ . The latter evolves in time by following the dynamics

$$\dot{\theta}_k = \omega_k + \frac{K}{N} \sum_{j=1}^N \sin(\theta_j - \theta_k) . \quad (4.1)$$

Here, the natural frequencies  $\omega_k$  are drawn from a distribution function  $g(\omega)$ , and  $K$  denotes the strength of the all-to-all-coupling between the oscillators. In his original work<sup>38</sup> Kuramoto assumed  $g$  to be symmetric and centered around the origin thanks to the rotational invariance of the model. Introducing the notion of a complex-valued order parameter

$$z = \frac{1}{N} \sum_{j=1}^N e^{i\theta_j} , \quad (4.2)$$

allows for measuring the degree of synchronization in the system. For the thermodynamic limit of infinitely many oscillators,  $N \rightarrow \infty$ , Kuramoto derived a critical coupling strength  $K_c$  at which the incoherent solution, i.e.  $z = 0$ , becomes unstable and a partially synchronized state,  $z = \text{const} \in (0, 1]$ , emerges<sup>38, see also 272</sup>. In the case of a unimodal Lorentzian frequency distribution of width  $\Delta$  and centered

at  $\omega_0 = 0$ , this critical coupling is given by

$$K_c = \frac{2}{\pi g(0)} = 2\Delta . \quad (4.3)$$

In particular, the onset, and in the following also the extent of synchronized behavior depends crucially on both coupling strength  $K$  and distribution width  $\Delta$ .

Of particular interest for our work is the coupling of two such Kuramoto networks. There we define two order parameters: A global one covers the entire network. Equivalently, we can decompose the global order parameter into local ones, each describing the dynamics of a single subpopulation. The interplay of these local order parameters has already been investigated in the literature. In 1991 Okuda and Kuramoto investigated the mutual entrainment of two oscillatory populations under the influence of noise<sup>273</sup>. All oscillators were assumed to have identical natural frequencies in their respective population and the resulting dynamics differed depending on coupling strength  $K$ , noise strength  $D$ , and the distance between the population-specific frequencies  $\Delta\omega_0$ . Next to a global incoherent and partially synchronized solution, they did not only find the existence of an oscillatory steady state, which was later referred to as “standing wave” solution by Crawford<sup>274</sup>, but numerical results revealed regimes of multistability, i.e. the coexistence of (at least) two stable solutions. Montbrió and co-workers<sup>266</sup> extended and generalized these findings by changing the setting slightly: Instead of letting the system be driven by noise, they assumed inhomogeneous natural frequencies drawn from unimodal distributions (per population). In the case of Lorentzians, they derived stability boundaries and illustrated their results for two coupled populations with numerical performance, and were among the first to discover “chimera states” states, a notion that later that year had been introduced by Abrams and Strogatz<sup>275</sup> to denote regions of synchronization in an unsynchronized surrounding.

We would like to briefly comment on these two seemingly identical approaches: the first, in which the phase dynamics of identical oscillators is subject to noise, and the second, in which one considers heterogeneous oscillators without noise. As to the former, Okuda and Kuramoto assumed that the oscillators in each population have identical natural frequencies, i.e.  $\omega_{\sigma,k} = \omega_\sigma$  for all  $k = 1, \dots, N_\sigma$ , and, in general,  $\omega_1 \neq \omega_2$ . Let us rearrange their governing equation as follows (cf. Eq.(2.1)

in<sup>273</sup> with  $\Gamma(\phi) = \sin(\phi)$  and  $K^{(1)} = K^{(2)} = K$ :

$$\dot{\theta}_{\sigma,k} = \omega_\sigma + \frac{K}{N} \sum_{\sigma'=1}^2 \sum_{j=1}^N \sin(\theta_{\sigma',j} - \theta_{\sigma,k}) + \xi_{\sigma,k}(t) \quad (4.4a)$$

$$= \tilde{\omega}_{\sigma,k} + \frac{K}{N} \sum_{\sigma'=1}^2 \sum_{j=1}^N \sin(\theta_{\sigma,j} - \theta_{\sigma,k}) , \quad (4.4b)$$

where  $\tilde{\omega}_{\sigma,k}(t) := (\omega_\sigma + \xi_{\sigma,k}(t))$ , and  $\xi_{\sigma,k}(t) = \xi_k(t)$  denote independent Gaussian noise processes with statistics  $\langle \xi_k(t) \rangle = 0$  and  $\langle \xi_k(t) \xi_j(t') \rangle = 2D\delta_{k,j}\delta(t - t')$ . As Sakaguchi argued<sup>276</sup>, in the thermodynamic limit the dynamics of the Langevin equations (4.4a) can be described by a Fokker-Planck equation, whose diffusion coefficient coincides with the noise strength  $D$ . Given that the  $\xi_{\sigma,k}(t)$  are Gaussian noise terms, one can consider the population dynamics (4.4a) as an Ornstein-Uhlenbeck (OU) process. Then, the results by Okuda and Kuramoto<sup>273</sup> appear in a different light. OU processes possess a Lorentzian shaped power spectrum. That is, assuming complex-valued relaxation rates  $H_\sigma = -\Delta - i\omega_\sigma$ , the power spectra of the corresponding OU processes read

$$S_\sigma(\omega) = \frac{\Delta}{(\omega - \omega_\sigma)^2 + \Delta^2} ,$$

see Eq.(1.8.38) in<sup>277</sup>. In due course, this noise-driven approach dwelling on the Fokker-Planck equation is equivalent to the case of coupled phase oscillators with natural frequencies drawn from Lorentzian distributions. This equivalence becomes evident in the continuum limit of oscillators, a necessary assumption for deriving mean-field dynamics by both a Fokker-Planck formalism <sup>see, e.g., 38,273,278</sup>, and by the Ott-Antonsen ansatz<sup>81,82,271</sup>. Hence, the following section can be understood as an analytic confirmation (and extension) of the numerical results by Okuda and Kuramoto<sup>273</sup>, who assumed two symmetric  $\delta$ -peaks as their bimodal frequency distribution and allowed Gaussian noise processes to drive the system as in (4.4a). Note that this equivalence mentioned is only valid for the linearized dynamics. Indeed, this linearization is sufficient for characterizing fixed points and bifurcation boundaries. When, however, considering the fully nonlinear system with noise, the Ott-Antonsen ansatz, which the following analysis will heavily dwell on, does no longer exhibit the exact dynamics <sup>see, e.g., 279</sup>.

Before 2008, the general idea to analytically reveal the dynamical behavior of these systems was to investigate small perturbations of (the distribution function) of the incoherent state. Major simplifications for characterizing oscillatory systems arose with Ott and Antonsen's breaking idea to simplify the Fourier series of the oscillators' distribution functions<sup>81</sup>; see *Section 4.3*. Their proof that the manifold

of such a class of distribution functions does indeed capture the long-term dynamics of Kuramoto (and more general) models<sup>82,83</sup> paved the way for the success of the Ott-Antonsen ansatz, see also *Chapter 5*. Martens and co-workers<sup>271</sup> were the first to tackle a bimodal Kuramoto network with the new theory and revealed a thorough bifurcation diagram including stability properties of the corresponding solutions. Although the disguise of two coupled unimodal Kuramoto networks as a single network with natural frequencies following a bimodal distribution has often been claimed, above all in the Appendix of<sup>271</sup>, a rigorous proof has never been provided yet.

### 4.3 Two-population dynamics along the Ott-Antonsen ansatz

We consider two symmetric populations of  $N$  phase oscillators  $\theta_{\sigma,k}$  each, with  $\sigma = 1, 2$  and  $k = 1, \dots, N$ . The oscillators have natural frequencies  $\omega_{\sigma,k}$  distributed according to Lorentzians  $g_\sigma$  of width  $\Lambda_1 = \Lambda_2 = \Lambda$  that are centered around  $+\varpi_0$  and  $-\varpi_0$ , respectively. We assume all-to-all coupling within each population with strength  $K_{\text{int}}$ , and also all-to-all coupling across populations with strength  $K_{\text{ext}}$ . The corresponding dynamics obeys the form

$$\dot{\theta}_{\sigma,k} = \omega_{\sigma,k} + \frac{K_{\text{int}}}{N} \sum_{j=1}^N \sin(\theta_{\sigma,j} - \theta_{\sigma,k}) + \frac{K_{\text{ext}}}{N} \sum_{j=1}^N \sin(\theta_{\sigma',j} - \theta_{\sigma,k}) \quad (4.5)$$

with  $(\sigma, \sigma') = (1, 2)$  or  $(2, 1)$ . Set  $K_{\text{int}} = K_{\text{ext}} = K$ , and let  $\theta_k = \theta_{1,k}$  and  $\theta_{N+k} = \theta_{2,k}$ . Then, (4.5) reads

$$\dot{\theta}_k = \omega_k + \frac{K}{2N} \sum_{j=1}^{2N} \sin(\theta_j - \theta_k) , \quad k = 1, \dots, 2N , \quad (4.6)$$

with  $\omega_k$  drawn from a bimodal distribution  $g = (g_1 + g_2)/2$  with  $g_{1,2}$  as defined earlier. This change of variables unveils the equivalence of both descriptions. Here, a crucial point is the assumption that the intrinsic coupling strength equals the external one. In the next section we will prove that both systems are topologically equivalent even if  $\kappa = K_{\text{ext}}/K_{\text{int}} \neq 1$ .

To avoid confusion with the bimodal approach of Martens et al., we discriminate between internal and external coupling strengths  $K_{\text{int}} \neq K_{\text{ext}}$ . We consider the limit  $N \rightarrow \infty$  and introduce continuous, time-dependent distribution functions  $f_\sigma$  of the subpopulations' oscillators. The integral of  $f_\sigma$  over phase and frequency

defines the (local) order parameters

$$z_\sigma = \int_{\mathbb{R}} \int_0^{2\pi} f_\sigma(\omega, \theta, t) e^{i\theta} d\theta d\omega ,$$

i.e. a (circular) ‘mean value’ for each population  $\sigma$ . The Ott-Antonsen ansatz<sup>81</sup> incorporates the  $2\pi$ -periodicity of  $f_\sigma$  and further simplifies its Fourier series to a single Fourier component  $\alpha_\sigma(\omega, t)$ , i.e.

$$f_\sigma(\omega, \theta, t) = \frac{g_\sigma(\omega)}{2\pi} \left\{ 1 + \left[ \sum_{n=1}^{\infty} \alpha_\sigma(\omega, t)^n e^{in\theta} + \text{c.c.} \right] \right\} .$$

With the normalization

$$\int_0^{2\pi} f_\sigma(\omega, \theta, t) d\theta = g_\sigma(\omega) := \frac{\Lambda}{\pi} \frac{1}{(\omega - \omega_\sigma)^2 + \Lambda^2} ,$$

where  $\omega_{1/2} = \pm\varpi_0$ , the dynamics of the order parameters  $z_\sigma$  reduce to

$$\dot{z}_\sigma = -(\Lambda \mp i\varpi_0) z_\sigma + \frac{K_{\text{int}}}{2} z_\sigma (1 - |z_\sigma|^2) + \frac{K_{\text{ext}}}{2} (z_{\sigma'} - z_\sigma^2 z_{\sigma'}^*) . \quad (4.7)$$

Since  $g_\sigma(\omega)$  are continuous, non-constant frequency distributions, the Ott-Antonsen manifold comprises the entire dynamics<sup>82</sup>. Next, we rewrite the order parameters as  $z_\sigma = \rho_\sigma e^{i\phi_\sigma}$  such that with the assumed symmetry  $\rho := \rho_1 = \rho_2$  the system (4.7) transforms into

$$\begin{aligned} \dot{\rho} &= -\Lambda\rho + \frac{\rho}{2}(1 - \rho^2) [K_{\text{int}} + K_{\text{ext}} \cos \psi] \\ \dot{\psi} &= 2\varpi_0 - K_{\text{ext}}(1 + \rho^2) \sin \psi ; \end{aligned} \quad (4.8)$$

here we introduced the mean relative phase between the subpopulations as  $\psi = \phi_2 - \phi_1$ . Finally, we rescale the parameters by means of  $\tau = K_{\text{int}} \cdot t$ ,  $\kappa = K_{\text{ext}}/K_{\text{int}}$ ,  $\Delta = 2\Lambda/K_{\text{int}}$  and  $\omega_0 = 2\varpi_0/K_{\text{int}}$ , substitute  $q = \rho^2$ , and transform  $q(t) \rightarrow q(\tau)$  as well as  $\psi(t) \rightarrow \psi(\tau)$  if not stated otherwise<sup>[1]</sup>. Then, we find for  $0 < \rho \leq 1$

$$\begin{aligned} \dot{q} &= q [1 - \Delta - q + \kappa(1 - q) \cos \psi] \\ \dot{\psi} &= \omega_0 - \kappa(1 + q) \sin \psi ; \end{aligned} \quad (4.9)$$

from hereon the dot notation refers to the derivative with respect to  $\tau$ . The system (4.9) resembles Eqs. (25 & 26) in<sup>271</sup> with the additional parameter  $\kappa$ . For  $\kappa = 1$  both systems agree entirely<sup>[2]</sup>. As we will show, the additional parameter  $\kappa$

<sup>[1]</sup> We consider  $K_{\text{int}} \neq 0$  and note that the scaling does not affect the quality of bifurcations, i.e. the original and scaled systems are topologically equivalent.

<sup>[2]</sup> Our unscaled system (4.8) is an exact representation of Eqs. (22 & 23) for  $\tilde{K} = K/2$  in the

does not alter the qualitative bifurcation scheme of our network. Hence, we can understand the bimodal formulation as an equivalent representation of the network consisting of two symmetric subpopulations.

## Incoherent state

Before discussing (4.9) in more detail, we briefly analyze the stability of the fully incoherent state  $q = 0$ . Following Martens et al.<sup>271</sup>, we linearize (4.7) around  $z_1 = z_2 = 0$  and find two pairs of degenerated eigenvalues

$$\lambda_{1/3} = \lambda_{2/4} = 1 - \Delta \mp \sqrt{\kappa^2 - \omega_0^2} \quad (4.10)$$

expressed in the aforementioned, rescaled parameters. Given the rotational invariance of the incoherent state, we expected this degeneracy. The incoherent state is linearly stable if and only if the real parts of these eigenvalues are less than or equal to zero. Using  $\kappa \geq 0$  and  $\omega_0 \geq 0$  we find the stability boundary as

$$\Delta = 1 + \begin{cases} \sqrt{\kappa^2 - \omega_0^2} & \text{for } \kappa \geq \omega_0 \\ 0 & \text{otherwise} \end{cases}, \quad (4.11)$$

which can be confirmed by perturbing the uniform distribution  $f(\omega, \theta, t) = (2\pi)^{-1}$ ; see Montbrió and co-workers<sup>266</sup> or Okuda and Kuramoto<sup>273</sup>. Crossing this boundary for  $\kappa \geq \omega_0$  corresponds to a degenerated transcritical bifurcation, while crossing the half line  $\Delta = 1$  resembles a degenerated supercritical Hopf bifurcation; see Fig. 4.2, where the red plane displays the Hopf bifurcation and the orange cone the transcritical one.

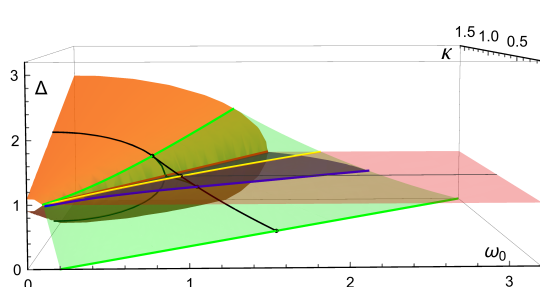


**Figure 4.2:** Bifurcation boundaries. Red plane: Hopf, orange cone: transcritical, green plane (within green lines): saddle node, blue: homoclinic bifurcation. Blue line: Saddle-node loop curve, yellow: intersection of Hopf and SN, black lines: cross-section at  $\kappa = 0.8$ , see also Fig. 4.4.

notation of<sup>271</sup>.

## Bifurcation analysis of the coherent state

Coming back to the system (4.9) we realize that its fixed points satisfy  $1 - \Delta - q = \kappa(1 - q) \cos \psi$  and  $\omega_0 = \kappa(1 + q) \sin \psi$ . Combining these using  $\cos^2 \psi + \sin^2 \psi = 1$  yields  $\kappa^2 = ((1 - \Delta - q)/(1 - q))^2 + (\omega_0/(1 + q))^2$ , or, equivalently,

$$\omega_0 = \pm \frac{1 + q}{1 - q} \sqrt{\Delta(2 - 2q - \Delta) - (1 - \kappa^2)(1 - q)^2} \quad (4.12)$$

as the implicit form of a hyperplane of fixed points  $q_s = q_s(\omega_0, \Delta, \kappa)$ . After inserting  $\partial\omega_0/\partial q = 0$  in (4.12), the solution  $\omega_0 = \omega_0(\Delta, \kappa)$  forms a surface (green in Fig. 4.2) across which a saddle-node bifurcation appears. If both subpopulations contain oscillators with identical natural frequencies  $\omega_\sigma$ , i.e. if  $\Delta = 0$ , then the saddle-node curve emerges from  $\kappa = \omega_0/2$ . We stress this because in the literature the saddle-node curve has only been approximated numerically, while here we find that the Ott-Antonsen ansatz allows for deriving an analytical solution in a straightforward manner. The saddle-node plane starts at  $(\omega_0, \Delta) = (2\kappa, 0)$  and approaches tangentially the transcritical bifurcation plane at  $(\omega_0, \Delta) = 1/4(\sqrt{8\kappa^2 - 2 + 2\sqrt{1 + 8\kappa^2}}, 3 + \sqrt{1 + 8\kappa^2})$ . This solution is consistent with the intersection point  $(\omega_0, \Delta)_{\kappa=1} = (\sqrt{3}/2, 3/2)$  reported in<sup>271</sup>.

## Can a change in $\kappa$ lead to new bifurcation behavior?

To show that the parameter  $\kappa$  does not lead to qualitatively new macroscopic behavior, we let  $G_1(q, \psi; \Delta, \omega_0, \kappa)$  denote the right-hand side of (4.9) and define  $G_2(q, \psi; \Delta, \omega_0, \kappa) = \det\{\partial_{(q, \psi)} G_1(q, \psi; \Delta, \omega_0, \kappa)\}$ . For  $\kappa = 1$  it follows that

$$\mathbf{G}(q, \psi; \Delta, \omega_0, \kappa) := \begin{pmatrix} G_1(q, \psi; \Delta, \omega_0, \kappa) \\ G_2(q, \psi; \Delta, \omega_0, \kappa) \end{pmatrix} = 0 \quad (4.13)$$

along the saddle-node curve; cf. Eq. (33) in<sup>271</sup>. According to the implicit function theorem, there is no qualitative change in the  $(\Delta, \omega_0)$ -bifurcation diagram if

$$\partial_\kappa \mathbf{G}(q, \psi; \Delta, \omega_0, \kappa) \neq 0 \quad (4.14)$$

for any neutrally stable fixed point  $(q, \psi; \Delta, \omega_0, \kappa) =: \mathbf{x}$ . Here, however, we have to extend this to a family of fixed points  $\mathbf{x}_s = \mathbf{x}(\Delta)$  along the saddle-node curve parametrized by  $\Delta$ . Therefore, if (4.14) holds for a fixed point  $\mathbf{x}_1$ , i.e. if  $\partial_\kappa \mathbf{G}(\mathbf{x}_1) \neq 0$ , then we still may end up at another point  $\mathbf{x}_2$  on that curve. We circumvent this case by also requiring for any arbitrary  $a \in \mathbb{R}$

$$\partial_\kappa G_1(q, \psi; \Delta, \omega_0, \kappa) \neq a \cdot \partial_\Delta G_1(q, \psi; \Delta, \omega_0, \kappa) \quad (4.15)$$

at every point along the saddle-node curve. Fig. 4.3 shows that the inequality (4.14) holds for all  $\mathbf{x}_s$ . We note that, because  $\dot{\psi}$  is independent of  $\Delta$ , it suffices to consider only the second equation of  $\partial_\kappa G_1$ , which is non-zero for  $0 \leq \Delta < 4$ . That is, the bifurcation diagram is persistent against (small) perturbations around  $\kappa=1$  and there are no bifurcations of co-dimension larger than 2.

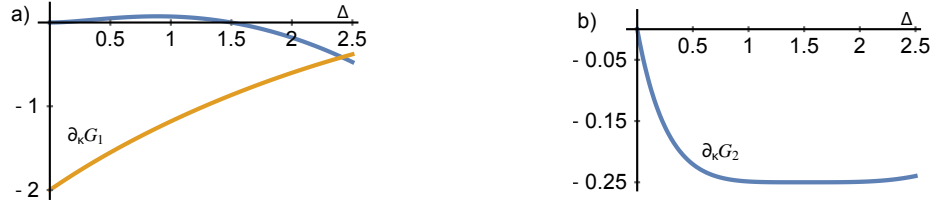


**Figure 4.3:** Partial derivatives of  $\partial_\kappa G$  along the saddle-node-plane at  $\kappa = 1$ ; (a) first (blue) and second (orange) component of  $\partial_\kappa G_1(\Delta)$ , (b)  $\partial_\kappa G_2(\Delta)$ .

## Multistability and oscillatory regimes

As to co-dimension 2 bifurcations, Martens and co-workers suggested the existence of saddle-node loop bifurcation points on the saddle-node plane below the Hopf bifurcation that can be identified numerically. In fact, the reduced dynamics (4.9) has a Jacobian along the saddle-node plane that is (conjugate to) a diagonal matrix with only one zero eigenvalue in the parameter range under study. This underlines the saddle-node character of that plane, but more importantly, it shows that these equations cannot be exploited for bifurcation points of co-dimension 2.

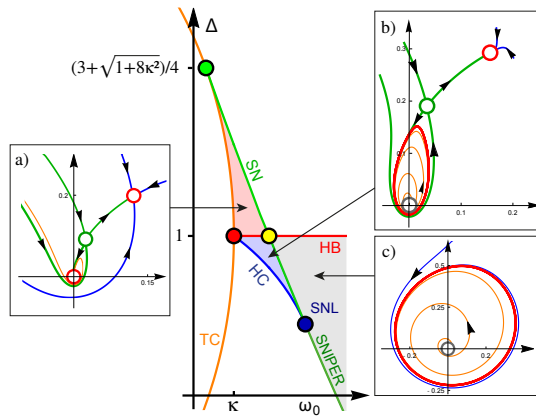


**Figure 4.4:** Bifurcation boundaries: cross-section of Fig. 4.2 at  $\kappa < 1$ ; red: Hopf, orange: transcritical, green: saddle node, blue: homoclinic, blue point: saddle-node loop bifurcation. Insets:  $(q, \psi)$ -phase portraits (in polar coordinates) in their specific parameter regions, red circle: stable fixed point, gray: unstable fixed point, green: saddle point. The bistability region (red/blue) overlaps with the oscillatory regime (blue/gray). (a) Coexistence of two stable fixed points, (b) a stable fixed point outside a stable limit cycle, (c) the more regular, stable limit cycle away from the SN curve.

Numerical simulations demonstrate the existence of a multistability region; cf.

Fig. 4.4 and Martens et al.'s Figs. 5 & 7a. Multistability has been reported independently in<sup>266,269,271,273</sup>. The red parameter region, bounded by the transcritical cone (orange curve), the Hopf plane (red) and the saddle-node plane (green), reveals the coexistence of another stable, but non-trivial fixed point next to the stable incoherent solution (separated by a saddle point). In the blue parameter region left to the saddle-node plane and below the red Hopf plane, the incoherent solution has undergone a supercritical Hopf bifurcation such that a stable limit cycle coexists with the pair of stable fixed and saddle points. For the transverse stability properties of our solutions, i.e. stability against perturbations off the symmetry  $\rho_1 = \rho_2$ , we refer to Section IV. in<sup>271</sup>. Due to the equivalence of both the bimodal and the two subpopulation system, the stability results there can be readily adopted. Note that the equivalence also holds when introducing small time delays; see the Appendix of<sup>280</sup>.

Particularly interesting for future applications are the limit cycle oscillations in the plane spanned by  $q \cos \psi$  and  $q \sin \psi$ , shown in Figs. 4.4(b) and (c). There, both  $q(t + T) = q(t)$  and  $\psi(t + T) = \psi(t) \bmod 2\pi$  hold for all  $t \in \mathbb{R}$  given a fixed period length  $T = T(\Delta, \omega_0, \kappa)$ . We study these oscillations in more detail by introducing the global complex-valued order parameter  $z = (z_1 + z_2)/2$ , whose magnitude  $|z| = R$  reads<sup>[3]</sup>

$$R = \frac{\rho}{\sqrt{2}} \sqrt{1 + \cos \psi} \quad (4.16)$$

with  $\rho = \sqrt{q}$ . If  $\dot{\psi}(t) \neq 0$ , then  $R(t)$  will oscillate. We would like to note that in this case oscillations in  $R$  would be even observable without  $q$  being periodic. However, for all parameter values outside the oscillatory regime, the dynamics contains stable fixed points at which obviously  $\dot{\psi} = 0$ , i.e.  $R \rightarrow \text{const}$ . As can be seen in Fig. 4.4(b), the limit cycle is deformed: it is neither circular nor symmetric about the origin. Then, also  $q$  oscillates, i.e. not only the global order parameter  $R$  oscillates, but so do the local ones  $\rho = \rho_1 = \rho_2$ . For larger  $\omega_0$  the limit cycle gains symmetry, but does not become a perfect circle. Hence oscillations contain higher harmonics; see Fig. 4.4(c). Future studies will address more details of the parameter dependency on the frequency and amplitude of the  $\rho$  and  $R$  oscillations as well as on their relative phase shift.

## Summary of the bifurcation scheme

Figs. 4.5 and 4.6 provide a comprehensive overview of the bifurcation scheme of system (4.9). The red plane displays the supercritical Hopf bifurcation while the

<sup>[3]</sup> The absolute value of the global order parameter  $z$  reads in general:  $R = |z| =$

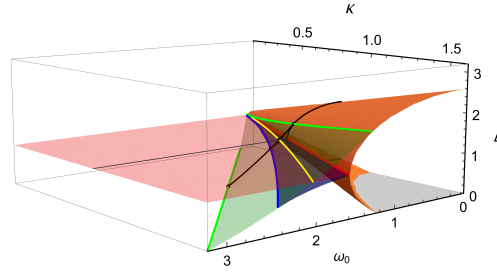


**Figure 4.5:** Bifurcation boundaries – back view of Fig. 4.2. Red plane: Hopf, orange cone: transcritical, green plane (within green lines): saddle node, blue: homoclinic bifurcation. Blue line: Saddle-node loop curve, yellow: intersection of Hopf and SN, black lines: cross-section at  $\kappa = 0.8$ , see also Fig. 4.6.

orange cone represents the transcritical bifurcation. Between the green curves we find the saddle-node plane, which denotes the parameter values, for which a pair of a stable fixed point and a saddle point emerges as a neutral fixed point. Along the saddle-node plane, however, we have to distinguish two cases of this bifurcation. For all points on the plane with  $\Delta$  bigger than some critical value  $\Delta_c$ , the neutral fixed point emerges away from the stable limit cycle (for  $\Delta \leq 1$ ), or away from the stable incoherent solution ( $\Delta \geq 1$ ). For  $\Delta \leq \Delta_c < 1$  the creation of that fixed point takes place directly on the limit cycle, where  $\Delta_c$  denotes the value for the co-dimension 2 bifurcation points (blue) on the green plane in Fig. 4.5 — for  $\kappa = 1$  this critical parameter is  $\Delta = \Delta_c \approx 0.7384$ . In particular, the emergent fixed point is about to split into a pair of a stable fixed point and a saddle point, therefore it destroys the limit cycle by forcing the period to infinity. This is a saddle-node infinite-period bifurcation (SNIPER or SNIC). The (blue) critical

$$\frac{1}{2} |\rho_1 e^{i\phi_1} + \rho_2 e^{i\phi_2}| = \frac{1}{2} \sqrt{\rho_1^2 + \rho_2^2 + 2\rho_1\rho_2 \cos(\phi_2 - \phi_1)}.$$

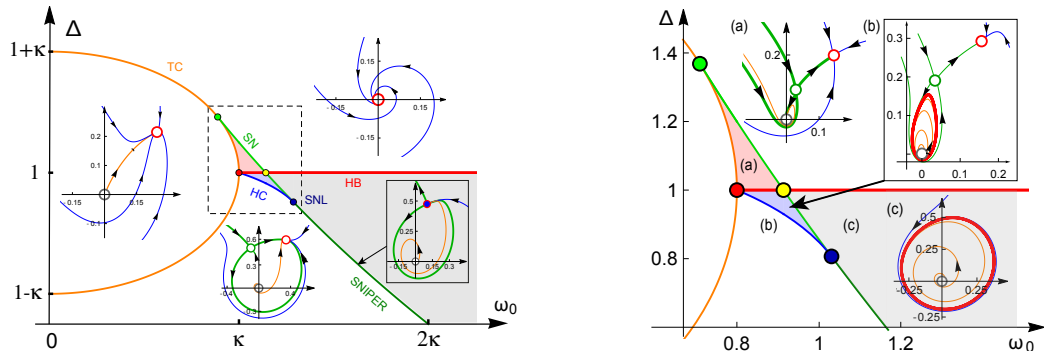


**Figure 4.6:** Bifurcation boundaries (left) and bistability region (dashed / right): cross-section of Fig. 4.5 at  $\kappa < 1$ . Red: Hopf, orange: transcritical, green: saddle node, blue: homoclinic, blue point: saddle-node loop bifurcation. Insets:  $(q, \psi)$ -phase portraits (in polar coordinates) in their specific parameter regions, red circle: stable, gray: unstable fixed point, green: saddle point. The right figure is a detailed view of the dashed box in the left figure.

curve  $\Delta_c = \Delta_c(\omega_0, \kappa)$ , which separates the two types of saddle-node bifurcations, consists of saddle-node loop bifurcation points, which are also bifurcation points of co-dimension 2.

Furthermore, numerics reveals a plane connecting the (blue) saddle-node loop curve with the (red) curve  $\{\Delta = 1, \kappa = \omega_0 \mid \kappa, \omega_0 \geq 0\}$ . The latter curve comprises the parameter values for which the saddle point (emerging from the saddle-node bifurcation) collapses with the stable incoherent solution, which then becomes unstable. Along the blue plane in Fig. 4.5, a homoclinic bifurcation takes place. Here, the saddle point approaches the limit cycle, which is therefore destroyed in the end. Fig. 4.6 displays the cross-section at  $\kappa = 0.8$  of the three-dimensional bifurcation boundaries, and elucidates the generic dynamical behavior within the corresponding parameter regions. As we have proven above, this cross-section is representative for all  $\kappa > 0$ . Unfortunately, analytic formulas for the homoclinic and saddle-node loop bifurcations are still missing both in the bimodal case as well as in the subpopulation approach, and we have to rely on the numerics.

## 4.4 Extension to three interacting populations

Given that two coupled networks and networks with bimodal frequency distributions are equivalent, it appears obvious to search for generalizations. Can we derive a similar equivalence, as before, between multiple coupled unimodal networks and networks with symmetric multimodal frequency distributions? Anderson and co-workers studied communities of oscillators in systems with multiple subpopulations<sup>281</sup>. They included mixes of attractive and repulsive couplings (in our notation  $K_{\text{int}}$  and  $K_{\text{ext}}$  should differ in sign) rendering the dynamics too diverse for analytical treatment. Closer to our approach, however, is the work by Komarov and Pikovsky<sup>282</sup> who showed a variety of synchronization characteristics as well as the emergence of chaotic states in the case of three positively coupled subpopulations. Thereby, they extended the numerical results for a trimodal network driven by noise<sup>283</sup>; see also our comment above about noise driven networks with  $\delta$ -functions as frequency distributions.

We sketch the case of three subpopulations with a unimodal Lorentzian frequency distribution each:  $g_\sigma(\omega) = (\Lambda/\pi)/((\omega - (-\varpi_0, 0, +\varpi_0))^2 + \Lambda^2)$  with peaks at  $(-\varpi_0, 0, +\varpi_0)$ <sup>[4]</sup>. This is compared with oscillators with a symmetric trimodal frequency distribution:  $g(\omega) = \beta \cdot g_1(\omega) + \alpha \cdot g_2(\omega) + \beta \cdot g_3(\omega)$  with  $\alpha = (4\varpi_0^2 - 2\Lambda^2)/(12\varpi_0^2)$ ,

---

<sup>[4]</sup>  $\varpi_0$  is assumed to be sufficiently large to guarantee isolated peaks and all distributions have width  $\Lambda$ .

and  $\beta = (4\varpi_0^2 + \Lambda^2)/(12\varpi_0^2)$  [5]. The two systems read

$$\dot{\theta}_k = \omega_k + \frac{K}{3N} \sum_{j=1}^{3N} \sin(\theta_j - \theta_k) \quad (4.17a)$$

$$\dot{\theta}_{\sigma,k} = \omega_{\sigma,k} + \sum_{\tau=1}^3 \frac{K_{\sigma,\tau}}{N} \sum_{j=1}^N \sin(\theta_{\tau,j} - \theta_{\sigma,k}), \quad (4.17b)$$

where  $K_{\sigma,\tau} = K_{|\sigma-\tau|}$  with  $K_0$  denoting the internal coupling strength  $K_{\text{int}}$  within each population,  $K_1$  the coupling strength between adjacent populations, and  $K_2$  that between distant populations, see Fig. 4.7. In (4.17a) we have  $k = 1, \dots, 3N$ ,

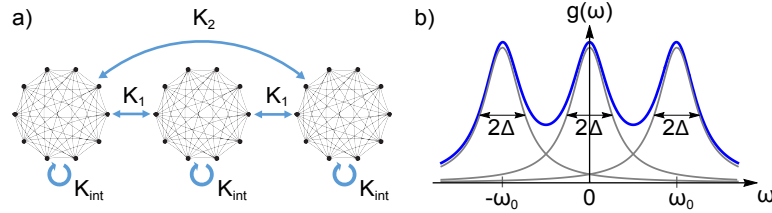


**Figure 4.7:** (a) Three all-to-all coupled networks; (b) symmetric trimodal frequency distribution function.

while in (4.17b)  $k = 1, \dots, N$  and  $\sigma = 1-3$ . When considering the thermodynamic limit, however, both systems consist of a continuum of oscillators. As before, we introduce (local) order parameters  $z_\sigma = \rho_\sigma e^{i\phi_\sigma}$ . Since the two outer populations are considered symmetric, we use  $\rho_{13} \equiv \rho_1 = \rho_3$  and  $\phi_2 - \phi_1 = \phi_2 - \phi_3 := \psi$ . By this we find the dynamics of (4.17a) after rescaling  $\tau = (K/2) \cdot t$  and  $\omega_0 = 2\varpi_0/K$  and  $\Delta = 2\Lambda/K$  and  $\kappa_\alpha = \alpha$  and  $\kappa_\beta = \beta$  as

$$\begin{aligned} \dot{\rho}_{13} &= \rho_{13} \left[ -\Delta + (1 - \rho_{13}^2) \left( \kappa_\alpha \frac{\rho_2}{\rho_{13}} \cos \psi + \kappa_\beta (1 + \cos 2\psi) \right) \right] \\ \dot{\rho}_2 &= \rho_2 \left[ -\Delta + (1 - \rho_2^2) \left( \kappa_\alpha + 2\kappa_\beta \frac{\rho_{13}}{\rho_2} \cos \psi \right) \right] \\ \dot{\psi} &= \omega_0 - (1 + \rho_{13}^2) \left( \kappa_\alpha \frac{\rho_2}{\rho_{13}} \sin \psi + \kappa_\beta \sin 2\psi \right). \end{aligned} \quad (4.18)$$

Accordingly, we rescale system (4.17b) using  $K = K_{\text{int}} + K_1 + K_2$  and  $\tau = (K/2) \cdot t$ ,

[5] The symmetric trimodal distribution features three peaks of the distribution function that have the same height. Our notion is not to be mistaken with the case where three symmetric unimodal distributions, i.e. identical widths and centers symmetrically arranged, sum equally up to form the trimodal distribution. Then, the middle peak is dominant, which we prevent by weighting the central distribution less than the outer two.

$\Delta = 2\Lambda/K$ ,  $\omega_0 = 2\varpi_0/K$  and abbreviate  $\kappa_{\alpha,\beta} = 2K_{1,2}/K$ , which yields

$$\begin{aligned}\dot{\rho}_{13} &= \rho_{13} \left[ -\Delta + (1 - \rho_{13}^2) \left( \kappa_0 + \kappa_\alpha \frac{\rho_2}{\rho_{13}} \cos \psi + \kappa_\beta \cos 2\psi \right) \right] \\ \dot{\rho}_2 &= \rho_2 \left[ -\Delta + (1 - \rho_2^2) \left( \kappa_0 + 2\kappa_\alpha \frac{\rho_{13}}{\rho_2} \cos \psi \right) \right] \\ \dot{\psi} &= \omega_0 - (1 + \rho_{13}^2) \left[ \kappa_\alpha \frac{\rho_2}{\rho_{13}} \sin \psi + \kappa_\beta \sin 2\psi \right],\end{aligned}\quad (4.19)$$

where  $\kappa_0 = 1 - \kappa_\alpha - \kappa_\beta$ . Both systems can display a richer dynamical behavior than the dynamics (4.9) since they, e.g., contain coupling terms of first and second harmonics, which may result in 2 : 1-phase synchronization. When it comes to linking the two, we realize that they are only identical for the special case

$$\kappa_\alpha = \kappa_\beta = \frac{1}{3} \Rightarrow \alpha = \beta.$$

As  $\alpha$  and  $\beta$  only differ by  $\Lambda^2/(4\varpi_0)$ , this implies  $\Lambda \rightarrow 0$ , hence the distribution function will consist of three  $\delta$ -peaks and the inhomogeneity is strongly reduced. As a consequence, the Ott-Antonsen manifold may not exhibit the whole dynamics of our system<sup>82</sup> and our description may remain incomplete, as has been found by Martens for even stronger symmetry assumptions in a network of three populations, though including phase lags<sup>284</sup>. This is an arguably heuristic way of saying. In the following, we would therefore like to show that for our symmetric setup the dynamics of the two systems indeed differ qualitatively from each other.

Both systems can be described by the governing equations for  $\rho_{13}, \rho_2$  and  $\psi$ . This enabled us to reduce the originally six-dimensional dynamics with  $z_j \in \mathbb{C}$  to three dimensions. Furthermore, the control parameters are  $\Delta$  and  $\omega_0$ , and the coupling parameters are  $\kappa_\alpha$  and  $\kappa_\beta$ . In the symmetric trimodal case, the latter two are already fully described by the corresponding control parameters, i.e.  $\kappa_{\alpha,\beta} = \kappa_{\alpha,\beta}(\Delta, \omega_0)$ . Thus, the bifurcation diagram is two-dimensional. In contrast, in the three-network case we are free to choose  $\kappa_\alpha, \kappa_\beta$  as long as they fulfill  $0 \leq \kappa_{\alpha,\beta} < 1$  and  $0 \leq \kappa_\alpha + \kappa_\beta < 1$ . This implies that the bifurcation diagram becomes four-dimensional and we may be confronted with bifurcations of co-dimension higher than 2.

#### 4.4.1 Symmetric trimodal network

We first analyze the trimodal system with respect to fixed points and their stability, which leads us to the bifurcation diagram presented in Fig.4.8a. We consider  $(\rho_{13}, \rho_2, \psi)$  as cylindrical coordinates with  $\rho_{13,2} \in [0, 1]$  and  $\psi \in [0, 2\pi)$ ;  $\rho_2$  represents the height of the cylinder. For our symmetry assumptions, these variables

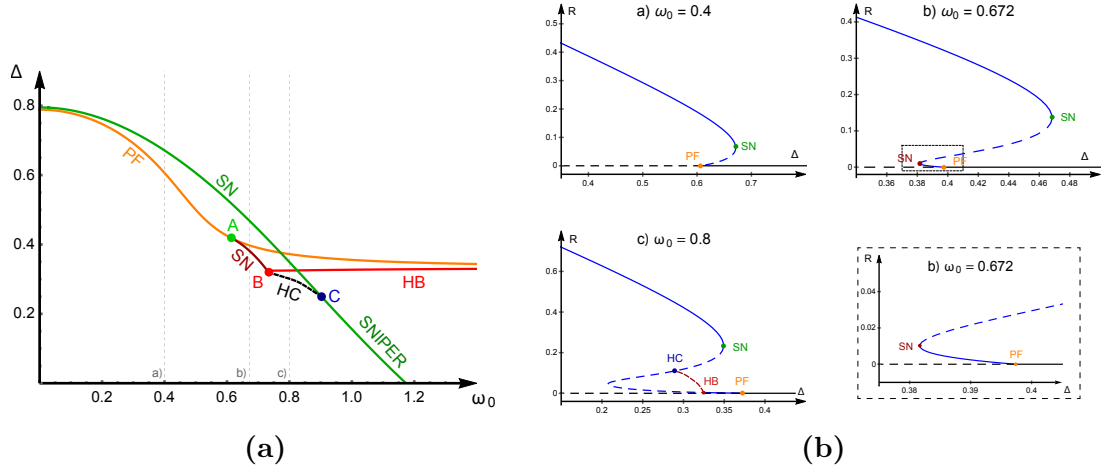


**Figure 4.8:** (a) Bifurcation boundaries of the symmetric trimodal network. Curves display a pitchfork (PF, orange), Hopf (HB, red), saddle-node (SN, green and dark red), SNIPER (green) and homoclinic (HC, black) bifurcation. Points denote codimension 2-bifurcations: Cusp (A), Bogdanov-Takens (B) and Saddle Node Loop (C). (b) Order parameter  $R$  versus  $\Delta$  for fixed  $\omega_0$  according to the dashed lines a),b),c) in Fig.4.8a. Solid lines denote stable, dashed lines unstable fixed points. The dark red line in c) denotes maximum amplitude of the (stable) limit cycle around the unstable fixed point. When the upper unstable fixed point coalesces with the limit cycle, oscillations cease in an homoclinic (HC) bifurcation.

fully represent the order parameter dynamics of the system (4.17a) away from the incoherent solution

$$z = \frac{1}{3} (z_1 + z_2 + z_3) \equiv 0 , \quad (4.20)$$

since for  $z_j = 0$  the phases  $\phi_j$ , and hence  $\psi$  are not defined. Nevertheless, the cylindrical dynamics (4.18) still indicate the origin  $\rho_{13} = 0 = \rho_2$  as a fixed point, so that the dynamical picture remains valid for  $\rho_{13,2} \geq \epsilon > 0$  with  $\epsilon$  arbitrary small. The system exhibits the symmetry  $(\rho_{13}, \rho_2, \psi) \mapsto (-\rho_{13}, -\rho_2, \psi)$ , such that the cylinder defined above can be point mirrored about the origin to  $\rho_2 \in [-1, 0]$ . In due course, bifurcation points as well as bifurcating branches off the incoherent solution will always appear in pairs  $(\pm \rho_{13}^*, \pm \rho_2^*, \psi^*)$ .

Having this said, we can focus on the bifurcation diagram Fig.4.8a. The orange curve denotes a pitchfork (PF) bifurcation of the incoherent solution  $z = 0$ , at which it loses stability for  $\Delta < \Delta_{PF}(\omega_0)$ . Point  $A = (\omega_A, \Delta_A) \approx (0.614, 0.418)$  (green) on the curve denotes the point where the PF bifurcation changes from subcritical ( $\omega_0 < \omega_A$ ) to supercritical ( $\omega_0 > \omega_A$ ). Let us first consider the parameter region where the PF bifurcation is subcritical, see, e.g., the dashed gray vertical line a). At the PF point there are two unstable solution branches bifurcating off the incoherent solution ( $\Delta > \Delta_{PF}$ ), which gain stability via a saddle-node (SN) bifurcation (green curve). Between the SN and the PF curves we find bistability of the stable incoherent solution together with a non-trivial fixed point – the

branch with  $\rho_2 < 0$  is not a physical solution as here the global order parameter has negative absolute value,  $|z| < 0$ .

Beyond point  $A$  the incoherent solution undergoes a supercritical PF bifurcation ( $\omega_0 > \omega_A$ ). The stable branches can then either lose stability via a SN bifurcation (dark red,  $\omega_0 < \omega_B$ ), which will be regained via a second SN bifurcation at the green curve, or the branches undergo a Hopf bifurcation (HB), see the red curve, beyond which we have oscillations of the order parameter. The point  $B$  (red), which distinguishes the two cases, is a Bogdanov-Takens point (co-dimension 2). Interestingly, oscillations can also cease. One possibility for this is that the unstable branch of the (green) SN bifurcation coalesces with the limit cycle, leading to a homoclinic (HC) bifurcation (black/dashed). The other possibility is that the SN bifurcation takes place directly on the limit cycle, leading to a SNIPER (saddle-node infinite period, or SNIC) bifurcation (green). The point  $C$  (dark blue), where the SN, HC, and SNIPER curves meet, is referred to as a saddle-node loop bifurcation; see also the discussion above for two coupled networks, *Section 4.3*.

Alternatively, we can characterize solutions via the behavior of the (global) order parameter  $z(t)$ , which evolves in the complex unit disc. To compare our results with<sup>283</sup>, we focus on the absolute value  $R(t) = |z(t)| \in \mathbb{R}$  that reads in the cylindrical variables

$$R(t) = \frac{1}{3} \sqrt{2\rho_{13}^2 + \rho_2^2 + 4\rho_{13}\rho_2 \cos \psi} . \quad (4.21)$$

Fig. 4.8b displays the typical behavior of  $R$  along the dashed gray vertical lines a), b), c) in Fig. 4.8a. Since we are only interested in physical solutions, we concentrate on  $R(t) \in [0, 1]$ . For small values of  $\omega_0 < \omega_A \approx 0.614$  – in scenario a) in Fig. 4.8 we used  $\omega_0 = 0.4$  –, there is a subcritical pitchfork bifurcation (orange dot), where  $R \equiv 0$  loses stability. The off-branching solution is first unstable and gains stability at the saddle-node point (SN, green). For  $\Delta_{PF} \leq \Delta_{SN}$  we find multistability of two fixed points. In scenario b) in Fig. 4.8 we consider  $\omega_0 = 0.672 > \omega_A$ . Here, the PF bifurcation of  $R \equiv 0$  is supercritical. The non-trivial stable solution loses stability at the first SN point (dark red), before it regains stability at the second SN point (green). During this snaking behavior, we find multistability of the incoherent solution with a non-trivial solution for  $\Delta_{PF} \leq \Delta \leq \Delta_{SN,green}$ , and of two non-trivial solutions for  $\Delta_{SN,red} \leq \Delta \leq \Delta_{PF}$ . This is typical near cusp bifurcations, because of which point  $A$  in Fig. 4.8a can be considered a (degenerate) cusp point. For even larger  $\omega_0$ , e.g.,  $\omega_0 = 0.8$  as in scenario c) in Fig. 4.8, the incoherent solution loses stability at  $\Delta_{PF}$  and then the stable branch undergoes a Hopf bifurcation (HB, red dot). In between, a SN bifurcation appeared at  $\Delta_{SN}$ , where the stable branch is monotonic increasing and

the unstable branch decreases until it touches the limit cycle at  $\Delta_{HC}$ . At this point the oscillations, whose upper bound is depicted as a red dashed curve, cease in a homoclinic bifurcation.

We would like to remark that our findings confirm earlier results by Acebrón and co-workers<sup>283</sup>. Furthermore, we extend the theory for a symmetric trimodal Kuramoto model with a qualitative bifurcation analysis of all the fixed points. In particular, all bifurcation boundaries found in Fig. 4.8a could be derived analytically (except for a numerical approximation of the HC curve), which again manifests the capacity of the OA ansatz.

#### 4.4.2 Three coupled symmetric networks

With a proper bifurcation diagram of the symmetric trimodal network at hand, we now focus on the network consisting of three all-to-all coupled symmetric populations each with a unimodal frequency distributions, see schematic in Fig. 4.7a). The external coupling strengths  $K_{1,2}$  for near and distant interactions across sub-population boundaries, respectively, led to two additional bifurcation parameters  $\kappa_{\alpha,\beta}$  in the order parameter dynamics. Using the symmetry assumptions as presented above, we are able to describe this dynamics as a 3-dimensional system of coupled ODEs with in total four bifurcation parameters. A description of the full bifurcation scheme is beyond the scope of the paper. However, in order to disprove the claim that three coupled networks and the trimodal network are topologically equivalent, at least in the symmetric case considered here, it suffices to present a single counter example.

We consider again the cylindrical coordinates  $(\rho_{13}, \rho_2, \psi)$ , whose dynamics are given by (4.19). Transforming them into Euclidean coordinates  $(x, y, z)$  in the cylinder

$$Z = \{(x, y, z) \in \mathbb{R}^3 \mid 0 \leq x^2 + y^2 \leq 1 \text{ and } 0 \leq z \leq 1\}$$

with  $x = \rho_{13} \cos \psi$ ,  $y = \rho_{13} \sin \psi$  and  $z = \rho_2$ , the dynamics in Euclidean space read

$$\begin{aligned} \dot{x} &= -\Delta x - \omega_0 y + (1 - \kappa_\alpha - 2\kappa_\beta)(1 - x^2 - y^2) + (1 - x^2 + y^2)(\kappa_\alpha z + 2\kappa_\beta x) , \\ \dot{y} &= -\Delta y + \omega_0 x + (1 - \kappa_\alpha - 2\kappa_\beta)(1 - x^2 - y^2) - 2\kappa_\alpha x y z - 4\kappa_\beta x^2 y , \\ \dot{z} &= -\Delta z + (1 - z^2) [(1 - \kappa_\alpha - \kappa_\beta)z + 2\kappa_\alpha x] . \end{aligned} \tag{4.22}$$

For  $\kappa_\alpha + 2\kappa_\beta \neq 1$  the origin  $(0, 0, 0)$  is no longer a fixed point of the transformed system (4.22). This shows that the introduction of polar coordinates  $z_j = \rho_j e^{i\phi_j}$  is only valid away from the incoherent solution  $z_j = 0 = \rho_j$  for all  $j = 1, 2, 3$ . Note that for the full six-dimensional dynamics, the incoherent solution  $z = (z_1 + z_2 +$

$z_3)/3 \equiv 0$  is always a solution. However, the subsequent transformations into polar, cylindrical and Euclidean coordinates show that the reflection symmetry as in the trimodal case breaks down in three population approach when we choose coupling parameters off the line  $\{\kappa_\alpha + 2\kappa_\beta = 1\}$ . Hence, we expect already here qualitative changes of the bifurcation boundaries from those obtained in the trimodal case.

Moreover, we can detect a qualitative difference for more similar settings, i.e. when reflection symmetry is maintained. Therefore, we assume in the following that  $\kappa_\alpha + 2\kappa_\beta = 1$ . In fact, the  $\kappa_{\alpha,\beta}$  of the trimodal network do fulfill this property. A bifurcation analysis of system (4.22) with respect to fixed points and their stability equivalent to Section 4.4.1 reveals the following bifurcation diagram Fig. 4.9. Note that here we fixed the coupling parameters to  $\kappa_\alpha = 0.4$  and  $\kappa_\beta = 0.3$ .

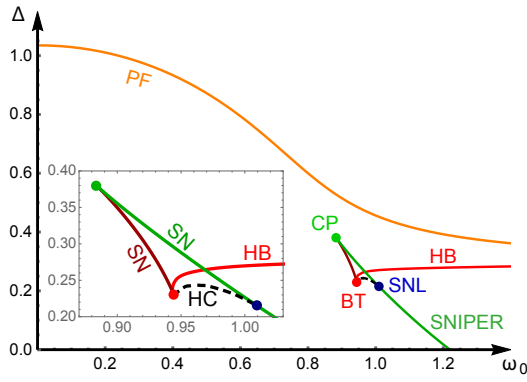


**Figure 4.9:** Bifurcation boundaries of three coupled symmetric networks with coupling parameters  $\kappa_\alpha = 0.4$  and  $\kappa_\beta = 0.3$ . Colors and abbreviations correspond to those in Fig. 4.8a.

Nonetheless, we consider this example representative. We achieved similar bifurcation diagrams for a broad variety of parameter choices, even if we allowed  $\kappa_{\alpha,\beta}$  to depend on  $\Delta$  and  $\omega_0$  as in the trimodal case. Comparing Figs. 4.8a and 4.9, one recognizes similar bifurcations, such as a pitchfork (PF, orange), a Hopf (HB, red), two saddle-node (SN, green and dark red), a SNIPER (green), and a homoclinic (HC, black/dashed) bifurcation curve. The major difference, however, is that the PF bifurcation of the incoherent solution is supercritical for all parameter values  $\Delta \geq 0, \omega_0 \geq 0$ . Moreover, the point  $A$  moves down in the parameter space away from the PF curve. There, it becomes a cusp point (CP), from which both SN curves (green and dark red) emerge. It is true that we still find a multistability region bounded by the SN and the HC curves, see also the inset in Fig. 4.9. Above the HB curve, there are two stable non-trivial fixed points, while below the HB curve a stable fixed point and a stable limit cycle coexist. However, we do not find stable solutions coexisting with the incoherent solution while being stable. Therefore it is safe to argue that the symmetric trimodal network and the network of three coupled symmetric populations are not topologically equivalent.

## 4.5 Discussion and conclusion

The Ott-Antonsen ansatz strongly boosted the analysis of Kuramoto models. Networks are assumed to consist of a continuum of oscillators, whose long-term dynamical behavior can be derived in the thermodynamic limit. Of particular interest for this paper is the extension to multiple coupled networks. A simple change of variables may transform two symmetrically coupled networks (with oscillators whose natural frequencies follow a unimodal distribution each) into one global network where the natural frequencies are drawn from a symmetric bimodal distribution. When assuming that internal and external coupling strengths in the two-population case differ, this transformation breaks down, and one is left with an additional degree of freedom. As we have proven in this paper, the additional parameter does not lead to new bifurcations but leaves both systems topologically equivalent. Stability, dynamics, and bifurcations of a symmetric two population system of phase oscillators are equivalent to a single population with a bimodal frequency distribution. This topological equivalence can also be shown when introducing small symmetric time-delays that allows for a phase-lag parameter reduction.

In the second part we aimed for generalizing the equivalence between multimodal and multiple coupled networks. However, already for the case of three subpopulations, where we adapted the same symmetry assumptions as in the two-population/bimodal case, this equivalence does no longer hold. Our symmetry assumptions are admittedly restrictive. Above all they only represent a slice of possible network configurations. That is, we cannot claim that the dynamics discussed here should be considered generic or not. However, our example clearly shows that the symmetric bidirectional coupling topology (cf.  $K_{1,2}$  in Fig. 4.7) does not admit its dynamics to be described by a single network of oscillators whose natural frequencies follow a symmetric trimodal distribution. A detailed analysis in the presence of asymmetries in both the two-population/bimodal approach and the multiple populations/multimodal networks is beyond the scope of the present paper but will be published elsewhere<sup>285</sup>.

Throughout the paper we based our work on the original Kuramoto model, a network of phase oscillators that are all-to-all coupled through the sine of the pairwise phase differences. Coupling two of such networks leads to new long-term behavior such as partially-synchronized states, so-called chimeras in the case of identical oscillators <sup>see, e.g., 286</sup>. Also, multistable regimes and oscillatory solutions are possible. For sure, non-local coupling, the introduction of phase-lag parameters as in<sup>265,266,284</sup>, or of more general time-delays <sup>see, e.g., 287</sup>, would have further enriched the dynamics. Recently, Martens, Bick and Panaggio investigated how the intro-

duction of heterogeneous phase-lags in our two-population-scenario of *Section 4.3* shapes the dynamics. The additional control parameters were internal versus external phase-lag parameters next to (internal and external) coupling strengths and the intrinsic frequency  $\omega$ . Assuming only homogeneous oscillators in both populations renders the OA ansatz not applicable in a rigorous way. However, it has been argued that in the limit of zero width of the frequency distribution,  $\Delta \rightarrow 0$ , the assumption of “nearly identical” oscillators enabled the authors to analyze the system analytically<sup>288</sup>. Interestingly, they found chaotic attractors and resonance effects, which shows again the variety of dynamics of a mere two-population system, and highlights the importance to really understand their behavior.

In our two-population/bimodal scenarios the governing dynamics could be reduced to be effectively two-dimensional. Hence, they cannot exhibit chaos. On the other hand, in the three-population/trimodal network chaotic trajectories should be possible. Though our focus mainly lay on (disproving) the equivalence between the different approaches, a full picture should also take chaos in both systems into account by assessing maximal Lyapunov exponents<sup>289</sup> see also 284,288.

Away from the symmetry assumptions considered throughout this work, but also when dealing with non-local coupling, phase-lag parameters, general time-delay or even finite-sized networks, i.e. in particular when the OA ansatz can no longer be applied, topological equivalences, or even (weaker) correspondences between multimodal and multiple coupled networks have to be demonstrated in order to show that coupled networks and networks with multimodal frequency distributions are equivalent, indeed. The analytic tractability of the Ott-Antonsen ansatz helped us to rigorously prove first results about similarities and differences between these two approaches. We believe that, despite the limited range of application of such models, our findings can be assumed seminal for a broader variety of models, and therefore will further enlighten the view on an accurate interchangeability of the notions of multimodal networks and coupled unimodal networks, which in the end will increase the flexibility to derive and specify models in diverse fields of applications.

# CHAPTER 5

## Parameter-dependent oscillatory systems

The Ott-Antonsen (OA) ansatz [*Chaos* 18, 037113 (2008), *Chaos* 19, 023117 (2009)] has been widely used to describe large systems of coupled phase oscillators. If the coupling is sinusoidal and if the phase dynamics does not depend on the specific oscillator, then the macroscopic behavior of the systems can be fully described by a low-dimensional dynamics. Does the corresponding manifold remain attractive when introducing an intrinsic dependence between an oscillator's phase and its dynamics by additional, oscillator specific parameters? To answer this we extended the OA ansatz and proved that parameter-dependent oscillatory systems converge to the OA manifold given certain conditions. Our proof confirms recent numerical findings that already hinted at this convergence. Furthermore we offer a thorough mathematical underpinning for networks of so-called theta neurons, where the OA ansatz has just been applied. In a final step we extend our proof by allowing for time-dependent and multi-dimensional parameters as well as for network topologies other than global coupling. This renders the OA ansatz an excellent starting point for the analysis of a broad class of realistic settings.

Adapted from: Pietras B., Daffertshofer A. (2016). *Ott-Antonsen attractiveness for parameter-dependent oscillatory networks*. *Chaos* **26**, 103101.  
doi: 10.1063/1.4963371.

## 5.1 Collective dynamics and parameter dependence

Coupled phase oscillators are being widely used to describe synchronization phenomena. The study of their collective dynamics has experienced a major breakthrough by the results by Ott and Antonsen<sup>81–83</sup>. The asymptotic behavior of the mean field of infinitely many coupled oscillators can be cast into a reduced, low-dimensional system of ordinary differential equations. The evolution is hence captured by the so-called Ott-Antonsen (OA) manifold.

Very recently, the OA ansatz has been applied to networks of theta neurons see, e.g.,<sup>290–296</sup>. A particular property of coupled, inhomogeneous theta neurons is that both the phase of a single neuron as well as its dynamics depend on a parameter, which establishes an intrinsic relation between them. While numerical results suggest the attractiveness of the OA manifold in the presence of such a parameter dependence, it has as to yet not been proven whether the dynamics really converges to it. For a certain class of parameter dependencies we here extend the existing theory of the OA ansatz and show that the OA manifold continues to asymptotically attract the mean field dynamics.

Parameter-dependent systems and their description through the OA ansatz have been considered by, e.g., Strogatz and co-workers<sup>297</sup>, Wagemaker and co-workers<sup>298</sup>, and So and Barreto<sup>299</sup>. There, parameters seemingly did not yield a correlation between an oscillator’s phase and its dynamics but a rigorous proof for this is still missing. We explicitly address this last point. In particular, we prove a conjecture later formulated by Montbrió and co-workers<sup>293</sup> on the attractiveness of the OA manifold for parameter-dependent systems. The case of parameters serving as mere auxiliary variables readily follows from our result – we will refer to this as “weak” parameter dependence<sup>[1]</sup>. By showing that a network of theta neurons can be treated as a parameter-dependent oscillatory system, our result establishes an immediate link to networks of quadratic integrate-and-fire (QIF) neurons: That is, the so-called Lorentzian ansatz as an equivalent approach to the OA ansatz is analytically substantiated. By this we may exert an important impact in mathematical neuroscience.

Finally, we extend the parameter dependence for more general classes of networks. First, we address non-autonomous systems and show that our proof can be applied to time-varying parameters. An important example here is a biologically

---

<sup>[1]</sup> Parameter-dependent systems comprise a wide class of systems, from which we here only choose a single family. This family represents a rather weak parameter-dependent system. However, we refrain from this notion since weak parameter dependence would imply that parameter changes have little to no considerable effect. Here, the original proof by Ott and Antonsen has to be changed, such that the parameter effect can be strong. We use the attribute “weak” to highlight that a specific oscillator does not depend on the additional parameter but its mean field dynamics only.

realistic approach to oscillatory systems proposed by Winfree<sup>85</sup>. Second, we include multiple distributed parameters illustrated by coupled limit-cycle oscillators with shear. Third, we apply our proof to networks with different coupling topologies including non-local coupling by using an heterogeneous mean field approach.

## 5.2 Extending the Ott-Antonsen ansatz for parameter-dependent systems

The Kuramoto model can be considered the most seminal description of globally coupled networks of phase oscillators. It has been investigated in great detail but its various extensions still make it *the* model-to-work-with when it comes to the study of network dynamics<sup>39,264</sup>. We adopt the notion of Montbrió, Pazó, and Roxin<sup>293</sup> and write the Kuramoto-like model as

$$\dot{\theta}_j = \omega_j + \text{Im} [H e^{-i\theta_j}] , \quad (5.1)$$

where the phase dynamics of the  $j$ -th oscillator ( $j = 1, \dots, N$ ) depends on its natural frequency  $\omega_j$  and a driving complex-valued field  $H$ . The latter can depend on time  $t$ , on the mean field  $z(t) = \sum_{j=1}^N e^{i\theta_j(t)}$ , and on other auxiliary variables, but not on the (index of) oscillator, i.e. it remains identical for all oscillators  $j = 1, \dots, N$ . Given the right-hand side of (5.1), the oscillators are *sinusoidally coupled*.

In the thermodynamic limit ( $N \rightarrow \infty$ ) the OA ansatz yields solutions for the dynamical evolution of the corresponding distribution function (of all the oscillators), which are attracted towards a reduced manifold of states<sup>81,82</sup>. Central to this is the description of the system via its distribution density  $\rho(\theta, \omega, t)$ . The quantity  $\rho(\theta, \omega, t) d\theta d\omega$  is the fraction of oscillators whose phases are in the range  $[\theta, \theta + d\theta]$  and have natural frequencies in  $[\omega, \omega + d\omega]$  at time  $t$ . The distribution function  $\rho$  obeys the continuity equation

$$\partial_t \rho + \partial_\theta (\rho \nu) = 0 \quad (5.2)$$

with velocity field

$$\nu(\theta, \omega, t) = \omega + \text{Im} [H(t) e^{-i\theta}] . \quad (5.3)$$

The latter can equivalently be written as<sup>297,298</sup>

$$\nu(\theta, \omega, t) = f e^{i\theta} + h + f^* e^{-i\theta} . \quad (5.4)$$

In agreement with the assumptions on  $H$  we require that the functions  $f$  and  $h$

may explicitly depend on time  $t$ , on the (now continuum form of the) mean field  $z(t) = \int_{-\infty}^{\infty} \int_0^{2\pi} \rho e^{i\theta} d\theta d\omega$ , and on other auxiliary variables, but not on the phase  $\theta$  itself.

Asymptotic attractiveness of the OA manifold, given by distribution functions of the form

$$\rho(\theta, \omega, t) = \frac{g(\omega)}{2\pi} \left\{ 1 + \left[ \sum_{n=1}^{\infty} \alpha(\omega, t)^n e^{in\theta} + \text{c.c.} \right] \right\} \quad (5.5)$$

that satisfy the normalization condition

$$\int_{-\infty}^{\infty} \int_0^{2\pi} \rho(\theta, \omega, t) d\theta d\omega = 1 , \quad (5.6)$$

has been proven for continuous frequency distribution functions  $g(\omega)$  of non-zero width and for  $H$  being independent of  $\theta$ ; c.c. stands for complex conjugate. Other requirements include  $|\alpha(\omega, t)| \leq 1$ , and some analytic continuity conditions.<sup>81,82</sup>

In what follows we extend this approach by rigorously proving the asymptotic attractiveness of the OA manifold in the case of  $H$  and  $\omega$  depending on an additional parameter  $\eta$  that may also influence  $\theta$ . Equivalently, we include a time- and  $\eta$ -dependence of  $f$  and  $h$  in (5.4). By this, we allow for an intrinsic relation between  $\theta, H$ , and  $\omega$ , or  $\theta, f$ , and  $h$ , respectively. As of today, the attractiveness of the OA manifold in the (time- and) parameter-dependent case has only been hypothesized<sup>178,297</sup> but not proven.

### 5.2.1 Parameter-dependent systems

When including additional parameters at the oscillator level, the dynamics (5.1) becomes

$$\dot{\theta}_j = \Omega(\omega_j, \eta_j) + \text{Im} [H(\eta_j, t) e^{-i\theta_j}] . \quad (5.7)$$

The natural frequency  $\Omega$  of oscillator  $j$  may therefore deviate from  $\omega_j$ , which promotes further heterogeneity among oscillators. Moreover the driving field  $H$  may depend on  $\eta_j$ . The right-hand side of (5.7) expresses a certain dependence on the (index of the)  $j$ -th oscillator. Hence, such a dependence is no longer exclusive to the sinusoidal coupling, but also affects the natural frequency  $\Omega(\omega_j, \eta_j)$  and the driving field  $H(\eta_j, t)$ .

When considering  $\eta$  a random variable, we may regard  $\eta_j$  to be drawn from a distribution function  $g(\eta)$ . Likewise  $\omega_j$  may be drawn from a (different) distribution function. The oscillator-specific parameter  $\eta_j$  may change this distribution function in the oscillator's favor. Therefore, we here incorporate a joint distribution  $g(\omega, \eta)$  in the normalization condition (5.6). In general,  $\omega$  and  $\eta$  are not independent and the joint distribution consists of two nested distributions. We

hence replace  $\Omega(\omega_j, \eta_j)$  by  $\omega(\eta_j)$ . Then, in the continuum limit (5.7) reads:

$$\partial_t \theta(\eta, t) = \omega(\eta, t) + \text{Im} [H(\eta, t) e^{-i\theta}] . \quad (5.8)$$

The relation through  $\eta$  becomes now even more evident as the temporal derivative of  $\theta$  has become partial.

Again, one can introduce a distribution function  $\rho(\theta, \omega, \eta, t)$ , which now additionally depends on  $\eta$ . And again, this distribution function satisfies the continuity equation (5.2) with velocity field (5.8). In line with the parameter-independent case, in which the distribution function  $g(\omega)$  of the natural frequencies  $\omega$  had non-zero width<sup>81,82</sup>, we assume that the distribution function  $g(\eta)$  of the parameter  $\eta$  also has non-zero width. The frequency  $\omega$ , thus, cannot be constant but depends on  $\eta$ . Likewise, the driving field  $H$  depends on  $\eta$ . Importantly, these two terms exhibit so an implicit dependence on  $\theta$ , such that the proof for the attractiveness of the OA manifold as has been derived in<sup>82</sup> may no longer hold. However, there is strong numerical incentive that the OA manifold fully covers the long-term behavior of the dynamics of the population of parameter-dependent phase oscillators, see e.g., 178,290–296,300–304.

In the following we demonstrate the proof of this conjecture for a particular class of parameter-dependent systems. We consider  $\eta$  to follow a Lorentzian distribution and assume that  $\omega$  depends linearly on  $\eta$ , i.e.  $\omega(\eta, t) = a \cdot \eta + c$ , where, without loss of generality, we set  $a = 1$  and consider  $c = c(t) \in L_{1,\text{loc}}(\mathbb{R})$  a locally integrable, and in particular piecewise smooth, function. Our line of argument follows closely that of Ott and Antonsen<sup>82</sup> but we extend their results whenever necessary. We would like to note that our findings remain valid for a larger class of distribution functions as has been depicted in detail in<sup>83</sup>. We will comment on this and consider more general  $\eta$ -dependencies of  $\omega$  in *Sections 5.2.2 and 5.4*.

Let  $g(\eta)$  be a Lorentzian centered around  $\eta = \eta_0$  with width  $\Delta$ , i.e.  $g(\eta) \sim L(\eta_0, \Delta)$ . For the aforementioned linear dependency  $\omega(\eta, t) = a \cdot \eta + c$ , we have  $\tilde{g}(\omega) = \hat{g}(\eta) \sim L(\eta_0 + c, \Delta)$  with frequency  $\omega = \omega(\eta)$  that, in general, will depend on  $\eta$ . In this case  $\omega$  is fully described by (the distribution of)  $\eta$  and the distribution density reduces to  $\rho(\theta, \omega, \eta, t) = \rho(\theta, \eta, t)$ .<sup>[2]</sup> This can be expanded as a Fourier series in  $\theta$  similar to Eqs.(5&6) in<sup>82</sup>, where it is further decomposed into  $\rho(\theta, \eta, t) = \hat{g}(\eta)/(2\pi) \cdot [1 + \rho_+(\theta, \eta, t) + \rho_-(\theta, \eta, t)]$ . Next to the assumption that the analytic continuation of  $\rho_+$  ( $\rho_-$ ) into  $\text{Im}(\theta) > 0$  ( $\text{Im}(\theta) < 0$ ) has no singularities and decays to zero as  $\text{Im}(\theta) \rightarrow +\infty$  ( $\text{Im}(\theta) \rightarrow -\infty$ ), we exploit the symmetry of the Fourier expansion and focus on  $\rho_+$ . In particular, we expect  $\rho_+$  to fulfill these conditions

<sup>[2]</sup> Alternatively, the dependence  $\omega(\eta)$  may be constituted by considering  $\rho$  as a conditional probability density  $\rho(\theta, \omega, t|\eta) = \rho(\theta, \omega|\eta, t)$  in line with<sup>293</sup>.

initially, i.e.  $\rho_+(\theta, \eta, 0)$  can be continued into the complex  $\eta$ -plane, is analytic in  $\text{Im}(\eta) < 0$  and decays to zero for  $\text{Im}(\eta) \rightarrow -\infty$ . These conditions will then be satisfied for all  $t > 0$ .<sup>81</sup>

We can further decompose  $\rho_+$  into two parts,  $\rho_+ = \hat{\rho}_+ + \hat{\rho}'_+$ , where the inhomogeneous solution  $\hat{\rho}'_+$  lies on the OA manifold and follows the dynamics given by Eq.(9) in<sup>82</sup>. For the sake of completeness, this dynamics prescribes the evolution of the Fourier coefficients  $\hat{\rho}'_+$  to the form  $\hat{\rho}'_+(\eta, t) = [\alpha(\eta, t)]^n$ , and reads

$$\partial_t \alpha + i\eta \alpha + \frac{1}{2} (H\alpha^2 - H^*) = 0 . \quad (5.9)$$

The quantity  $\hat{\rho}_+$ , on the other hand, is the (homogeneous) solution of

$$\partial_t \hat{\rho}_+ + \partial_\theta \left\{ \left[ \omega + \frac{1}{2i} (H e^{-i\theta} - H^* e^{i\theta}) \right] \hat{\rho}_+ \right\} = 0 . \quad (5.10)$$

Both the frequency  $\omega$  and the field  $H$  may depend explicitly on  $\eta$ . To guarantee that the dynamics (5.7), whose state at time  $t$  can be represented by the afore-defined order parameter  $z(t)$  in its continuous form,

$$z(t) = \int_{-\infty}^{\infty} \int_0^{2\pi} \rho(\theta, \eta, t) e^{i\theta} d\theta d\eta , \quad (5.11)$$

is asymptotically attracted by the OA manifold, it suffices to show that

$$\lim_{t \rightarrow +\infty} \int_{-\infty}^{+\infty} \hat{\rho}_+(\theta, \eta, t) \hat{g}(\eta) d\eta = 0 \quad (5.12)$$

holds.<sup>82</sup> Before showing this, however, we would first like to remark that, without loss of generality, the center of the Lorentzian frequency distribution  $\hat{g}(\eta) \sim L(\eta_0 + c, \Delta)$  can be considered zero since we may introduce a change of variables,  $\tilde{\theta} = \theta - (\eta_0 t + C(t))$ , where  $C(t)$  is an antiderivative of  $c(t)$ . Furthermore, we can adjust (5.12) by substituting  $\hat{g}$  by  $g$ .

If  $\hat{\rho}_+$  is analytic in the lower half  $\eta$ -plane and decays to zero as  $\text{Im}(\eta) \rightarrow -\infty$  as assumed above, one can multiply (5.10) by  $g(\eta) d\eta$  and integrate the result by employing the residue theorem. Hence, the integrals can be evaluated at the residue of the enclosed pole of  $g(\eta)$  at  $\eta = -i\Delta$ . We find

$$\begin{aligned} & \partial_t \hat{\rho}_+(\theta, -i\Delta, t) + \partial_\theta \left\{ -i\Delta \cdot \hat{\rho}_+(\theta, -i\Delta, t) + \right. \\ & \left. \frac{1}{2i} \left[ \int_{-\infty}^{+\infty} H(\eta, t) \hat{\rho}_+(\theta, \eta, t) g(\eta) d\eta e^{-i\theta} - \int_{-\infty}^{+\infty} H^*(\eta, t) \hat{\rho}_+(\theta, \eta, t) g(\eta) d\eta e^{i\theta} \right] \right\} = 0 . \end{aligned}$$

The two remaining integrals can be determined provided that  $H$  and  $H^*$  have no singularities in the lower half  $\eta$ -plane and do not increase “too” fast for  $\text{Im}(\eta) \rightarrow -\infty$ . Since  $g$  is a Schwartz function, that is, a smooth, rapidly decreasing function, we only need  $H$  to diverge at most sub-exponentially. For common choices of  $H$ , as listed in<sup>82</sup>, these requirements are met indeed, which yields

$$\partial_t f_+(\theta, t) + \partial_\theta [v(\theta, t) f_+(\theta, t)] = 0 , \quad (5.13)$$

$$v(\theta, t) = -i \left[ \Delta + \frac{1}{2} (e^{-i\theta} H(t) - e^{i\theta} H^*(t)) \right] . \quad (5.14)$$

Here we substituted  $f_+(\theta, t) = \hat{\rho}_+(\theta, -i\Delta, t)$  and  $H(t) = H(-i\Delta, t)$ . These equations agree exactly with Eqs.(17 & 18) in<sup>82</sup>. Hence, following the same reasoning around Eqs.(19-31) in<sup>82</sup> one can conclude that (5.12) is fulfilled. To underscore the line of argument, we would like to give a short sketch of the proof. First, by introducing a conformal transformation of the upper half complex  $\theta$ -plane into the unit disc via  $w = e^{i\theta}$ , one can rewrite (5.13 & 5.14) as

$$\frac{d}{dt} \tilde{f}_+(w, t) + \tilde{f}_+(w, t) \partial_w \tilde{v}(w, t) = 0 , \quad (5.15)$$

where  $\tilde{f}_+$  and  $\tilde{v}$  are the transformed functions from (5.13 & 5.14), and  $d/dt = \partial/\partial t + \tilde{v}\partial/\partial w$ . (5.15) can be integrated using the method of characteristics for linear and homogeneous partial differential equations<sup>305</sup>. Here we require  $\tilde{f}_+ \in C^2(\mathbb{R})$  but  $\tilde{v}$  does not need to be continuous. This yields

$$\tilde{f}_+(w, t) = \tilde{f}_+(W(w, 0), 0) \exp [-\mu(w, t)] , \quad (5.16)$$

as solution with

$$\mu(w, t) = \int_0^t \partial_{w'} \tilde{v}(w', t')|_{w'=W(w, t')} dt' , \quad (5.17)$$

and the characteristics are given by

$$\partial_{t'} W(w, t') = \tilde{v}(W(w, t'), t') , \quad (5.18)$$

with final condition  $W(w, t) = w$ . Finally, in order to show that  $\tilde{f}_+(w, t) \rightarrow 0$  for  $t \rightarrow \infty$ , which, by (5.16), we prove that

$$\lim_{t \rightarrow \infty} \text{Re} [\mu(w, t)] = +\infty . \quad (5.19)$$

The details for the rather lengthy computation can be found in<sup>82</sup>. We here we would only like to mention that the integral in (5.17) is split into three distinct parts, each of which is evaluated and while two of them remain bounded, the third

diverges at the rate  $\Delta t$ , presuming  $\Delta > 0$ . This eventually completes the proof and underlines the importance that the distribution function  $g(\eta)$  must have non-zero width  $\Delta$ . We would also like to note that in the final step of the proof the continuity of  $v$  is required, i.e.  $H$  in (5.14) must be continuous. If one includes, e.g., square functions in the time-dependent parts of the frequency term and/or driving field, one is confronted with jump discontinuities, which become present in the right-hand side of (5.14) either directly or indirectly via the order parameter  $z(t)$ . A closer look at<sup>82</sup>, however, confirms that for small jumps the reasoning can be guaranteed and for proper choices of a time constant  $T$  their Eq.(31) holds. Thus, we can argue that OA attractiveness will be maintained even in the case of discontinuities, which also confirms our rather long assumption for  $c(t)$  to be in  $L_{1,\text{loc}}(\mathbb{R})$  in the linear dependence of  $\omega(\eta) = a\eta + c$ .

So far we only considered a Lorentzian distribution and some linear dependence of  $\omega$  on  $\eta$ . However, our result can be extended to a much broader class of distribution functions  $g(\eta)$ , non-linear dependencies  $\omega(\eta)$ , or even joint distributions  $g(\omega, \eta)$  in the case of  $\Omega(\omega, \eta)$ ; see *Section 5.2.2* below. Hence, it is proper to say that the asymptotic attractiveness of the OA manifold for parameter-dependent systems of coupled phase oscillators is generic. Note that the proof remains identical if  $\theta = \theta(t)$  does not depend on the parameter  $\eta$ , that is, when there is no correlation between specific oscillators and their dynamics. We call this case “weak” parameter dependence, which has been considered in several earlier studies e.g.,<sup>178,297–299</sup>, where parameters were introduced as auxiliary variables. Our result therefore confirms the attractiveness of the OA manifold also in this case, as has simplifyingly been taken for granted in the afore-cited studies.

## 5.2.2 General parameter distributions

As already mentioned in *Section 5.2.1*, the assumptions of a linear relation between  $\omega$  and  $\eta$  and of  $\eta$  being drawn from a Lorentzian can be loosened in many respects. We first consider  $g(\eta)$  to still be a Lorentzian centered around  $\eta = \eta_0$  with width  $\Delta$ , i.e.  $g(\eta) \sim L(\eta_0, \Delta)$ . The linear dependency  $\omega(\eta, t) = a \cdot \eta + c$  may be generalized by considering both  $a = a(t)$  and  $c = c(t)$  time-dependent. Then, by the common transformation properties for Lorentzian (Cauchy) distributions,  $\omega$  follows a Lorentzian of the form  $g(\omega) \sim L(a\eta_0 + c, \Delta|a|)$ . Let  $a \neq 0$  be constant. Then a similar change of variables,  $\tilde{\theta} = \theta - (a\eta_0 t + C(t))$ , with  $C(t)$  being the antiderivative of  $c(t)$ , keeps the distribution function centered around 0. Without loss of generality we set  $a = 1$ ; even if  $a = a(t)$  and  $a(t) > 0$  or  $a(t) < 0$  for all  $t > 0$ , the rescaling of  $\theta$  retrieves that we can stick to our assumption  $a = 1$ . If, however,  $a$  changes sign at, e.g.,  $t = t_0$ , then the scale parameter  $\Delta|a|$  tends to

zero for  $t \rightarrow t_0$ . Due to (5.5) also  $\rho(\theta, \omega, t)$  will exhibit a  $\delta$ -peak at  $t = t_0$ . In this case our results are not readily applicable<sup>83</sup>. However, if  $\dot{a}(t_0) \neq 0$ , then we can shift the initial time to zero,  $t_0 \mapsto 0$ . Whenever  $\rho_+(\theta, \omega, t_0)$  satisfies the necessary initial conditions, the OA manifold will remain attracting for all  $t > t_0$ , given that  $t_0 = \max\{t \in \mathbb{R} \mid a(t) = 0\}$ .

We proceed with more general cases of frequency and parameter distributions. In<sup>83</sup> the authors elegantly extend the original proof, which considers only Lorentzian frequency distributions: Instead of demanding analytic continuity of both the frequency distribution  $g(\omega)$  and the initial condition into the whole lower half of the complex  $\omega$ -plane, it suffices that  $g$  and the initial condition have analytic continuations into a strip  $S$  defined by  $0 \geq \text{Im}(\omega) > -\sigma$  and  $-\infty \leq \text{Im}(\omega) \leq +\infty$  with  $\sigma > 0$ , where neither of them has singularities and both approach zero as  $|\omega| \rightarrow \infty$ . Thereby the class of applicable distribution functions includes Gaussians, sech-distributions, and many more, and even multimodal distributions can be incorporated as long as these functions have finite non-zero widths <sup>see references in</sup><sup>83</sup>. This approach can be adopted and used in our  $\eta$ -parameter-dependent case. For this let us assume again individual oscillators given by (5.7). As mentioned in *Section 5.2.1*, we might be confronted with a nesting of the distributions  $\tilde{g}(\omega)$  and  $g(\eta)$  for  $\omega$  and  $\eta$ . In particular, the latter may determine the first in an oscillator-specific way. That is the reason why the resulting distribution function  $\hat{g}(\eta)$  can become arbitrarily complicated. However, as long as the analytic continuations of  $\tilde{g}$  and  $g$  into the strip  $S$  (for some  $\sigma > 0$  as defined above) do not have singularities, and neither  $\tilde{g}$  nor  $g$  features a  $\delta$ -peak in their time evolutions, also  $\hat{g}$  will behave as required. An additional requirement is that the product  $H(\eta, t)\hat{g}(\eta)$  satisfies these conditions, too. This means that we have to find a strip  $S' \subset S$ , defined by  $0 < \sigma' \leq \sigma$ , in which  $H\hat{g}$  has an analytic continuation, does not have singularities, its time evolution does not feature  $\delta$ -peaks (if necessary we have to reset the initial time point after such a peak), and that we require  $|H(\eta_r + i\eta_i, t)\hat{g}(\eta_r + i\eta_i)| \rightarrow 0$  for  $|\eta_r| \rightarrow \infty$  and  $0 > \eta_i > -\sigma'$ . In particular,  $H$  must not grow faster than  $\hat{g}$  decays, such that the OA manifold continues to capture the long-term dynamics of the system.

We would like to remark that initial conditions on the oscillator distribution function,  $\rho(\theta, \eta, 0)$ , play an important role. If they fail to be satisfied, this may hinder the OA manifold to attract the dynamics. For an example we would like to refer to Appendix C of<sup>306</sup>, in which the specific time point has to be determined appropriately in order to set up promising initial conditions.

In summary, we have proved that the OA ansatz captures the time-asymptotic

dynamics of parameter-dependent systems of coupled oscillators of the form

$$\partial_t \theta(\eta, t) = \Omega(\omega, \eta, t) + \text{Im}[H(\eta, t)e^{-i\theta}]$$

if next to the basic assumptions<sup>82</sup> the following additional requirements are fulfilled:

- The complex-valued driving field  $H(\cdot, t)$  admits an analytic continuation into a strip  $S \subset \mathbb{C}^-$  and does not diverge too fast for  $\text{Re}(\sigma) \rightarrow \pm\infty$  with  $\sigma \in S$ .<sup>[3]</sup>
- Both  $\Omega(\omega, \eta, \cdot)$  and  $H(\eta, \cdot)$  are locally integrable in time:  $\Omega(\omega, \eta, \cdot), H(\eta, \cdot) \in L_{1,\text{loc}}(\mathbb{R})$ .
- The joint distribution  $g(\omega, \eta)$  admits an analytic continuation into the strip  $S$  and is such that  $\Omega(\omega, \eta, t)$  follows a distribution of non-zero width in at least one parameter (and for at most a finite number of instants  $t_k$  in time).

### 5.3 Networks of quadratic integrate-and-fire neurons

As mentioned above, there is a variety of recent papers that showed numerically how the dynamics of networks of theta neurons is time asymptotically attracted by the OA manifold<sup>290–292</sup>. Recently, Montbrió and co-workers studied how the macroscopic dynamics of a network of quadratic integrate-and-fire (QIF) neurons is described by a low-dimensional system by using a so-called Lorentzian ansatz<sup>293</sup>. By transforming the QIF neurons into a network of theta neurons, their Lorentzian ansatz does resemble the OA ansatz with parameter-dependent frequency and driving field, as considered in *Section 5.2.1*.

To be more precise, the dynamics of the membrane potential  $V_j$  of a QIF neuron may be described by

$$\dot{V}_j = V_j^2 + I_j, \quad \text{if } V_j \geq V_p, \text{ then } V_j \leftarrow V_r, \quad (5.20)$$

for  $j = 1, \dots, N$ . Here,  $I_j$  denotes an input current,  $V_p$  a peak value, and  $V_r$  a reset value. Once the membrane potential  $V_j$  reaches  $V_p$ , the neuron emits a spike, and  $V_j$  will be reset to  $V_r$ . Commonly, the limit  $V_p = -V_r \rightarrow \infty$  is considered. The input current  $I_j$  consists of a neuron-specific quenched component  $\eta_j$ , a common time-dependent input  $I(t)$  and a coupling term  $Js(t)$ , combining the synaptic weight  $J$  and a smooth mean synaptic activation  $s(t)$ , resulting in

$$I_j = \eta_j + Js(t) + I(t). \quad (5.21)$$

---

<sup>[3]</sup>  $H$  can be regarded as a “tempered distribution”.

The latter two time-dependent components are identical for all neurons in the network. In order to describe the macroscopic behavior of the network, Montbri  and co-workers used the Lorentzian ansatz

$$\rho(V|\eta, t) = \frac{1}{\pi} \frac{x(\eta, t)}{[V - y(\eta, t)]^2 - x(\eta, t)^2} , \quad (5.22)$$

with center  $y(\eta, t)$  and time-dependent half-width  $x(\eta, t)$ , which turns out to exhibit the long-term solution for the distribution of the membrane potentials. The properties  $x(\eta, t)$  and  $y(\eta, t)$  that define the distribution function (5.22) are also closely linked to the firing rate of the neuronal population and to the mean membrane potential, respectively. While the Lorentzian ansatz applies to the (membrane voltage) dynamics of QIF neurons, we are here primarily interested in the phase dynamics. Using  $V_j = \tan(\theta_j/2)$  one can transform (5.20 & 5.21) into theta neurons<sup>307</sup>,

$$\dot{\theta}_j = (1 - \cos \theta_j) + (1 + \cos \theta_j) [\eta_j + J \cdot s(t) + I(t)] . \quad (5.23)$$

In (5.23) the time-independent injected current  $\eta_j$  is drawn from a distribution function  $g(\eta)$ . For the sake of legibility we abbreviate the non-autonomous part of (5.23) as

$$J \cdot s(t) + I(t) = c(t) - 1 .$$

Rearranging terms and considering the thermodynamic limit, one can rewrite (5.23) as

$$\partial_t \theta(\eta, t) = \nu(\theta, \eta, t) = \Omega(\eta, t) + \text{Im} [H(\eta, t) e^{-i\theta}] \quad (5.24)$$

with  $H(\eta, t) = i(-1 + \eta + Js + I) = i(\eta + c - 2)$  and  $\Omega(\eta, t) = \eta + c$  cf.<sup>293</sup>.

To apply our result from above, one has to show that  $H$  does not diverge exponentially when  $\text{Im}(\eta) \rightarrow -\infty$ , and that  $c(t)$  possesses an antiderivative. On the one hand, for the components of  $c(t)$  with  $s(t)$  being smooth and  $I(t)$  piecewise smooth and (locally) integrable, there will always exist an antiderivative of  $c(t)$ . On the other hand, we have  $H(\eta) = i\eta + \text{const}$ , such that  $H$  grows only linearly for  $\text{Im}(\eta) \rightarrow -\infty$ .

To be more precise and in view of Section 5.2.2, we have  $H(\eta) = i(\eta + c - 2)$  and  $\hat{g}(\eta) \sim L(\eta_0 + c, \Delta)$ , so that  $\hat{g}$  decays exponentially for  $|\eta_r| \rightarrow \infty$  and hence  $H$  must not increase at an exponential rate. In fact,  $H$  does not have any singularities in the whole complex  $\eta$ -plane (except for  $|\eta| \rightarrow \infty$ ), and  $H(\eta_r + i\eta_i) = -\eta_i + i\eta_r + \text{const} = \mathcal{O}(\eta_r)$  for  $|\eta_r| \rightarrow \infty$ . Consequently, for large  $|\eta_r|$ , the product  $H\hat{g}$  will be dominated by  $\hat{g}$  such that all assumptions are fulfilled. Thus, we can confirm again the asymptotic attractiveness of the OA manifold.<sup>[4]</sup> What is more, due to the

<sup>[4]</sup> To give a brief idea of the proof, it is important to note that, next to the assumption that in  $S'$  the product  $H\hat{g}$  decays to zero for  $|w| \rightarrow \infty$ , the crucial point for proving the attractiveness of

existence of a conformal mapping between the quantity  $w(\eta, t) = x(\eta, t) + iy(\eta, t)$  and the function  $\alpha(\eta, t)$  defining the OA manifold (5.5)<sup>[5]</sup>, see also Eq.(15) in<sup>293</sup>, we have also proven the attractiveness of the Lorentzian ansatz (5.22) for a network of QIF neurons.

## 5.4 Further applications

So far, we only considered non-independent frequency and parameter distributions,  $\tilde{g}(\omega)$  and  $g(\eta)$ , respectively. In general, however, one cannot take this “simple” dependence for granted. The additional parameter might be multi-dimensional, i.e.  $\eta \in \mathbb{R}^n$  with  $n > 1$ . When considering the thermodynamic limit of infinitely many coupled oscillators, the dynamics (5.7) may obey

$$\partial_t \theta(\eta, t) = \Omega(\omega, \eta, t) + \text{Im} [H(\eta, t) e^{-i\theta}] . \quad (5.25)$$

Employing the OA ansatz for this system one has to encounter distribution functions given by

$$\begin{aligned} \rho(\theta, \omega, \eta, t) &= \frac{g(\omega, \eta)}{2\pi} \left\{ 1 + \left[ \sum_{k=1}^{\infty} \alpha(\omega, \eta, t)^k e^{ik\theta} + \text{c.c.} \right] \right\} \\ &\int_{\mathbb{R}^n} \int_{-\infty}^{\infty} \int_0^{2\pi} \rho(\theta, \omega, t) d\theta d\omega d\eta = 1 ; \end{aligned} \quad (5.26)$$

the joint distribution  $g(\omega, \eta)$  is a major modification to the setting considered before. Does the OA manifold remain attracting? (5.25) suggests the phase  $\theta = \theta(\eta, t)$  to depend on the parameter  $\eta$  in line with our notion of parameter-dependent systems. But it is unclear whether the OA manifold is attracting even without this particular correlation between phase, natural frequency, and driving field. If, however, the OA attractiveness can be proven for systems with generalized natural frequency  $\Omega$  and driving field  $H$  as in (5.25), this will allow for a further and even broader extension of the existing theory. In the following we first list a few examples for which numerical simulations have been reported and that give strong incentive that the OA ansatz may indeed be valid. We will show how our proof can be adopted, thereby confirm the OA attractiveness, and set the numerical results on solid ground. Last, we provide some general properties of  $\Omega$  and  $H$  for which

---

the OA manifold is that  $\sigma' > 0$ . To be more precise, given the integral expression (equivalent to) (5.12), the idea is to shift the path of integration from the real  $\eta$ -axis to the line  $\eta_r + i\eta_i$  with  $0 > \eta_i > -\sigma'$ ,  $-\infty \leq \eta_r \leq \infty$ , for details see<sup>83</sup>. This leads directly to (5.13 & 5.14) from where one can complete the proof along the known formalism outlined in *Section 5.2.1*.

<sup>[5]</sup> We substituted  $\omega$  by  $\eta$  in line with our arguments in *Section 5.2.1*. However, we do assume an implicit dependence  $\omega = \omega(\eta)$ .

the OA ansatz holds.

We start with the Winfree model<sup>85</sup> which is an early mathematical description of synchronization phenomena in large populations of biological oscillators. Rewritten in terms of (5.25) this model takes the form

$$\begin{aligned}\partial_t \theta &= \Omega(\omega, \eta, t) + \text{Im} [H(\eta, t)e^{-i\theta}] \\ \Omega(\omega, \eta, t) &= \omega + \sigma\eta(t), \quad H(\eta, t) = e^{-i\beta}\eta(t), \quad \text{and} \quad \eta(t) = \varepsilon h(t),\end{aligned}\tag{5.27}$$

where  $h(t)$  is a smooth function depending only on the mean field  $z(t)$  but not on the phase itself<sup>286</sup>. In particular, this model contains time-dependent parameters see also 308.

Next, we consider reaction-diffusion systems with heterogeneous, self-oscillating elements. In particular, we study the mean-field version of the complex Ginzburg-Landau equation, whose equation describes a population of globally coupled limit-cycle oscillators. Hence, we can rewrite the dynamics in form of (5.25). By introducing a shear (or nonisochronicity) parameter  $\eta$  as an additional random variable and transforming the system through a phase reduction, the governing equations in the continuum limit read<sup>300–302</sup>.

$$\begin{aligned}\partial_t \theta &= \Omega(\omega, \eta, t) + \text{Im} [H(\eta, t)e^{-i\theta}] \\ \Omega(\omega, \eta, t) &= \omega + K\eta \quad \text{and} \quad H(\eta, t) = Kz(1 - i\eta),\end{aligned}\tag{5.28}$$

where  $K$  denotes the coupling strength and  $z = z(t)$  is the order parameter. The frequency  $\omega$  and the shear  $\eta$  are drawn from a joint distribution  $g(\omega, \eta)$ . In contrast to *Section 5.2.1*, we explicitly allow the additional parameter  $\eta$  to be drawn from another frequency distribution. For the joint distribution one has to address two scenarios. Either, the random variables are independent, such that the joint distribution can be split into  $g(\omega, \eta) = g_1(\omega)g_2(\eta)$ , or they are not. Iatsenko and co-workers, who independently investigated the Kuramoto model with both distributed natural frequencies  $\omega$  and distributed coupling strengths  $\eta$ , coined the term *uncorrelated* joint distributions when the two random variables  $\omega$  and  $\eta$  are independent, as opposed to *correlated* joint distributions see<sup>303,304,309</sup>. Furthermore, frequency-weighted coupling<sup>310,311</sup>, i.e. the driving field additionally depends on  $\omega$ ,  $H = H(\omega, \eta, t)$ , can be approached with the formalism introduced above.

As a third point, we will deal with systems that are not all-to-all coupled but exhibit some particular (and sparse) network topology. Therefore, these networks can barely be studied analytically. Although it was conjectured and numerically illustrated by Barlev, Antonsen, and Ott<sup>312</sup> in 2011 that the OA ansatz can be extended for uniform in-degree, Erdős-Rényi, and scale-free networks, a thorough proof has as yet not been delivered. However, the upcoming branch of hetero-

geneous mean fields<sup>313</sup> presents a promising loophole to overcome this obstacle of intricate network topologies. We will prove that heterogeneous mean field models indeed fall in a category whose mean field dynamics can be described along the OA ansatz. Given a network with a particular degree distribution, it is possible to introduce so-called degree-block variables, whose dynamics govern the evolution of all nodes which have the same degree  $k$ . This approach reveals the same equations as the annealed networks approximation<sup>39,314</sup>, which can hence be considered equivalent. Recent studies considered the heterogeneous mean fields of the Kuramoto model, e.g., on scale-free<sup>315–317</sup> and random Erdős-Rényi networks<sup>315</sup>. The starting point is a specifically coupled Kuramoto network with coupling strength  $K$  and adjacency matrix  $A = (a_{ij})$  with  $i, j = 1, \dots, N$ ,

$$\dot{\theta}_j = \omega_j + K \sum_{k=1}^N a_{jk} \sin(\theta_k - \theta_j) . \quad (5.29)$$

We can cluster various node dynamics by replacing the adjacency term with an expectation value for their node degree  $\eta_j$ . Ideally, the underlying topology exhibits some well-defined degree distribution  $P(\eta)$ . In the continuum limit  $N \rightarrow \infty$ , these node degrees are substituted in the phase dynamics as weighted, distributed coupling strengths, so that the governing dynamics read

$$\begin{aligned} \partial_t \theta(\eta, t) &= \Omega(\omega, \eta, t) + \text{Im} [H(\eta, t) e^{-i\theta}] \\ \Omega(\omega, \eta, t) &= \omega \quad \text{and} \quad H(\eta, t) = K\eta z(t) , \end{aligned} \quad (5.30)$$

where  $\omega$  and  $\eta$  are drawn from a joint distribution  $g(\omega, \eta) = P(\eta)g_1(\omega)$ . This setup is amenable to, e.g., random fields, as has been presented in<sup>317</sup> where oscillators are enforced through local fields, which find their way into the specific forms for  $\Omega$  and  $H$ .

In all these different classes of parameter-dependent networks, we will show how the OA attractiveness can be regained.

### 5.4.1 Winfree model

As said, the Winfree model describes macroscopic synchronization phenomena of large oscillator systems whose individual nodes are naturally pulse-coupled with one another. The introduction of phase response curves (PRC) allows for quantifying how the phase of an oscillator responds to the pulse-like perturbations from the other oscillators. The general form of the model reads at the single node level

$$\dot{\theta}_j = \omega_j + Q(\theta_j) \frac{\varepsilon}{N} \sum_{k=1}^N P(\theta_k) , \quad (5.31)$$

where  $\varepsilon$  denotes the coupling strength,  $Q$  is the PRC and  $P$  is a pulse-like signal. Following the notation of Pazó and Montrbrió<sup>286</sup>, we consider PRCs with sinusoidal shape,

$$Q(\theta) = \sigma - \sin(\theta + \beta) , \quad (5.32)$$

with an offset parameter  $\sigma$ , and a phase-lag  $\beta$ . Moreover, we assume the pulse-like signal to be smooth,

$$P(\theta) = P_n(\theta) = a_n(1 + \cos \theta)^n , \quad (5.33)$$

with  $n \in \mathbb{N}_{\geq 1}$  controlling the width of the pulses, and  $a_n$  is a normalizing constant. In the thermodynamic limit, we regain (5.27) as

$$\partial_t \theta = \omega + \varepsilon \sigma h(t) + \text{Im} [\varepsilon e^{-i\beta} h(t) e^{-i\theta}] , \quad (5.34)$$

where the coupling function incorporates the smooth mean field

$$h(t) = h_n(t) = \int_0^{2\pi} P_n(\theta) d\theta = 1 + 2(n!)^2 \sum_{k=1}^n \frac{\text{Re}(z^k)}{(n+k)!(n-k)!} \quad (5.35)$$

with  $z$  the common (Kuramoto) order parameter (5.11). The frequency  $\Omega(\omega, t) = \omega + c(t)$  with  $c(t) = \varepsilon \sigma h(t)$  has a form identical to *Section 5.2.1*, where  $\omega$  follows a Lorentzian frequency distribution  $g(\omega)$ . Since the order parameter  $z(t)$  is bounded with  $|z| \leq 1$ , we have  $h(t) \geq 0$  for all  $t \geq 0$ . Furthermore, the driving field does not depend on additional parameters, so that our proof can be directly applied, confirming that the OA ansatz holds and the OA manifold indeed captures the long-term dynamics of the Winfree model.

An alternative proof for the case of time-dependent frequency and driving field can be found in<sup>308</sup>. However, as we have depicted in *Section 5.2.2*, our proof generalizes their findings and extends them to a broader class of frequency distribution functions  $g(\omega)$ . Of particular interest in the non-autonomous extension is also the matter of discontinuities. Recall that in *Section 5.3* we introduced a time-dependent input current  $I(t)$ , see (5.21), which can, e.g., take the form of a square function with jump-discontinuities. Our proof applies to this specific feature and confirms existing numerical results<sup>293</sup>.

### 5.4.2 Limit-cycle oscillations with shear

Investigating collective synchronization usually addresses networks of coupled elementary oscillatory units. The dynamics of these units may be described in normal form

$$\dot{\varrho} = \varrho(1 - \varrho^2) , \quad \dot{\theta} = \omega + \eta(1 - \varrho^2) , \quad (5.36)$$

where  $\varrho$  denotes the radius and  $\omega$  determines the frequency of rotation on the stable limit cycle with  $\varrho(t) \equiv 1$ . The parameter  $\eta$  quantifies the shear, or non-isochronicity, of the flow, i.e. how strongly perturbations away from the limit cycle modify the phase dynamics. When we consider an all-to-all coupled population of  $N \gg 1$  of these oscillatory units, we arrive at the mean-field version of the complex Ginzburg-Landau equation with dissipative coupling

$$\dot{z}_j = z_j \left[ 1 + i(\omega_j + \eta_j) - (1 + i\eta_j) |z_j|^2 \right] + \frac{K}{N} \sum_{k=1}^N (z_k - z_j) ; \quad (5.37)$$

$z_j = \varrho_j e^{i\theta_j}$ . Heterogeneity among the population is promoted by having the frequency  $\omega_j$  and shear parameters  $\eta_j$  drawn from a distribution function  $g(\omega, \eta)$ . In the weakly coupled case, i.e. the coupling strength  $|K|$  is small, a phase reduction allows us to describe the dynamics of the system by their phases only. In the continuum limit  $N \rightarrow \infty$ , we can introduce the phase distribution function  $\rho(\theta, \omega, \eta, t)$ . Note that  $\omega$  and  $\eta$  are independent, so that neither of them is redundant. Accordingly, the order parameter  $z$  takes now the form

$$z(t) = \int_{-\infty}^{\infty} \int_{-\infty}^{\infty} \int_0^{2\pi} \rho(\theta, \omega, \eta, t) e^{i\theta} d\theta d\omega d\eta . \quad (5.38)$$

Thus, the phase dynamics reads

$$\partial_t \theta = \omega + K\eta + \text{Im} [Kz(t)(1 - i\eta)e^{-i\theta}] , \quad (5.39)$$

and the phase distribution function satisfies the continuity equation

$$\partial_t \rho + \partial_\theta (v\rho) = 0 , \quad (5.40)$$

with  $v$  the right-hand side of (5.39) see also 300,302. Using the notion of (5.25), the frequency and the driving field are both time-varying and depend on the additional shear parameter  $\eta$ :

$$\Omega(\omega, \eta, t) = \omega + K\eta , \quad H(\eta, t) = Kz(t)(1 - i\eta) . \quad (5.41)$$

To assure that the OA manifold indeed exhibits the mean field dynamics of this system with shear, we have to adapt our proof from Section 5.2.2 for the joint distribution  $g(\omega, \eta)$ .

The general idea is again to decompose the distribution function  $\rho$  in Fourier

space into

$$\rho(\theta, \omega, \eta, t) = \frac{g(\omega, \eta)}{2\pi} [1 + \rho_+(\theta, \omega, \eta, t) + \rho_-(\theta, \omega, \eta, t)] \quad (5.42)$$

and use symmetry assumptions to focus on  $\rho_+$ , which again will be decomposed into  $\rho_+ = \hat{\rho}_+ + \hat{\rho}'_+$ . While  $\hat{\rho}'_+$  lies on the OA manifold and has Fourier coefficients  $\hat{\rho}'_{+,n} = [\alpha(\omega, \eta, t)]^n$ ,  $\hat{\rho}_+$  solves

$$\partial_t \hat{\rho}_+ + \partial_\theta \left\{ \left[ \Omega(\omega, \eta, t) + \frac{1}{2i} (H(\eta, t)e^{-i\theta} - H(\eta, t)^*e^{i\theta}) \right] \hat{\rho}_+ \right\} = 0. \quad (5.43)$$

The assumptions on the analytic continuation properties of *Section 5.2.2* hold – in particular we need analytic continuations with respect to both  $\omega$  and  $\eta$  into strips  $S_\omega$  and  $S_\eta$ . Hence we have to show that

$$\lim_{t \rightarrow \infty} \int_{-\infty}^{\infty} \int_{-\infty}^{\infty} \hat{\rho}_+(\theta, \omega, \eta, t) g(\omega, \eta) d\omega d\eta = 0. \quad (5.44)$$

Discussing general solutions of (5.44) given an arbitrary joint distribution function are beyond the scope of this paper. However, for particular  $g(\omega, \eta)$  we can affirm the attractiveness of the OA manifold for these parameter-dependent systems. To begin with, we use the assumption of Montbri  and Paz  that the joint distribution can be written as the product of two Lorentzians<sup>300</sup>,

$$g(\omega, \eta) = g_1(\omega)g_2(\eta) = \frac{\delta/\pi}{(\omega - \omega_0)^2 + \delta^2} \frac{\gamma/\pi}{(\eta - \eta_0)^2 + \gamma^2}. \quad (5.45)$$

Multiplying (5.43) with  $g(\omega, \eta)$  and integrating over  $(\omega, \eta)$ , we can use Fubini's theorem (on the assumption of integrability of  $\Omega g \hat{\rho}_+$  and  $H g \hat{\rho}_+$ ) and compute the double integral by changing the order of integration. First, we can evaluate the integral over  $\omega$  by applying the residue theorem as in *Section 5.2.1* and then move on to the second integral, which reads

$$\begin{aligned} \partial_t \hat{\rho}_+(\theta, \omega_0 - i\delta, -i\gamma, t) = \\ - \int_{-\infty}^{\infty} \partial_\theta \left\{ \left[ \Omega(\omega_0 - i\delta, \eta, t) + \frac{1}{2i} (H(\eta, t)e^{-i\theta} - H(\eta, t)^*e^{i\theta}) \right] g_2(\eta) \hat{\rho}_+(\theta, \omega_0 - i\delta, \eta, t) \right\} d\eta. \end{aligned}$$

While the term  $\int \Omega g_2 \hat{\rho}_+$  can be evaluated at the pole  $\eta = \eta_0 \pm i\gamma$  ( $\pm$  depending on the contour of integration, which again depends on the coupling  $K$ , see also<sup>300</sup>), we have to assure that the product  $H(\eta, t)g_2(\eta)$  vanishes for  $\text{Im}(\eta) \rightarrow \pm\infty$ . Indeed, the linear growth of  $H$  in  $\eta$ , see (5.41), will be dominated by the exponential decay of  $g_2$ , such that the residue theorem can be applied here, too, which results finally in (5.13)&(5.14), from which the claim follows as presented in *Section 5.2.1*.

As has been shown in *Section 5.2.2*, the restrictions to unimodal Lorentzians can be dropped and the OA attractiveness is sustained. Here we can even handle  $\delta$ -functions as long as one of the partial distribution functions has finite width: due to the special form of  $\Omega(\omega, \eta, t)$ , the OA ansatz holds for homogeneous frequencies  $\omega_j = \omega$  while the shear is heterogeneous and the coupling  $K > 0$  does not vanish.

The case in which the joint distribution  $g(\omega, \eta)$  is no longer uncorrelated, i.e. if the first equality in (5.45) fails, demands a more careful investigation in order to estimate the long-time evolution of  $\hat{\rho}_+$ . Although the ultimate goal is to categorize adequate joint distributions that allow for the OA ansatz, there might appear a variety of uncertainties for a general proof. For instance, to the best of our knowledge it is an open problem whether and how singularities can appear in joint distributions given smooth marginal distributions. This issue becomes even more intricate in the case for multi-dimensional parameters  $\eta \in \mathbb{R}^n$ ,  $n \in \mathbb{N}$ . However, there are certain approaches using the OA ansatz for parameter-dependent systems with correlated joint distributions, which we would like to briefly revise.

The introduction of shear into the oscillator system shows how an additional parameter can be treated as a random variable and thereby changing the natural frequency and driving field of the original Kuramoto model. A more fundamental approach has been presented by Petkoski and co-workers<sup>303,304,308,309</sup>: Given the Kuramoto model with heterogeneous natural frequencies, they assume the coupling strengths to be drawn from a distribution function. That is, their model reads

$$\dot{\theta}_j = \omega_j + \frac{K_j}{N} \sum_{k=1}^N \sin(\theta_k - \theta_j) \quad (5.46)$$

with  $(\omega, K)$  following a joint distribution  $g(\omega, K)$ . Given the strong resemblance between their numerical simulations and the predictions via the OA ansatz, the authors realized that the latter “formulas were derived on the assumption of at least asymptotic validity of the OA ansatz.”<sup>303</sup> They also investigated necessary initial conditions with respect to their analytic continuation and applicability to the OA ansatz. Unfortunately, they did not prove that their system dynamics (5.46) does not belong to the class of systems considered in the proofs by Ott and Antonsen<sup>81–83</sup>. We would like to remind that a general characterization of correlated joint distributions  $g(\omega, K) \neq g_1(\omega)g_2(K)$  which are applicable for the extended OA ansatz is hardly feasible. However, for three examples used in literature we can prove that the OA manifold defines the asymptotic evolution of the whole system.

First, let  $g(\omega, K) \sim \delta(K - k) \left[ \omega^2 + e^{-\omega^2} \right]^{-1}$ , see Fig. 1 in<sup>304</sup>. The specific form with the  $\delta$ -function in  $K$  reduces system (5.46) to the common Kuramoto model

with heterogeneous frequencies  $\omega \propto g_1(\omega) = [\omega^2 + e^{-\omega^2}]^{-1}$ , which can be dealt with along the proof of the original OA ansatz.

The other two examples are more elaborate in that the joint distribution functions are given by<sup>303</sup>

$$g(\omega, K) = (1-p)\delta(K - K_1)L(\omega; \omega_0, \gamma_1) + p\delta(K - K_2)L(\omega; -\omega_0, \gamma_2), \quad (5.47)$$

with  $p \in (0, 1]$ , and

$$g(\omega, K) = \Gamma(K) \sum_{n=1}^{N_q} q_n L(\omega; \omega_n, \gamma_n) \quad \text{with} \quad \sum_{n=1}^{N_q} q_n(K) = 1. \quad (5.48)$$

Here,  $L(\omega; \omega_n, \gamma_n)$  denotes a Lorentzian with width  $\gamma_n > 0$  and centered around  $\omega = \omega_n$ , and  $\Gamma(K)$  is a multimodal- $\delta$ -function. For properly chosen  $q_{1,2}$  the distributions (5.48) can be regarded a generalization of (5.47) so that it suffices to consider the former. For simplicity, let  $N_q = 2$ , i.e.  $g(\omega, K)$  be a bimodal joint distribution. Inserting  $g(\omega, K)$  in the definition of the order parameter (5.38), we can decompose the latter into  $z(t) = q_1 z_1(t) + q_2 z_2(t)$  with  $q_1 + q_2 = 1$ . Put differently, we can view our system as two all-to-all coupled populations with population-specific coupling strengths  $K_{1,2}$ . Given that the frequency distributions are Lorentzians of finite width  $\gamma_{1,2}$ , the results for two-population/bimodal Kuramoto models<sup>271,280,318</sup> can be readily applied, which confirms the attractiveness of the OA manifold for this kind of joint distributions. Note that we do not require  $q_n \in [0, 1]$  but may choose, e.g.,  $q_1 = \delta/(\delta - \xi) > 1$  and  $q_2 = -\xi/(\delta - \xi) < 0$ . Then, the bimodal distribution results from one Lorentzian being subtracted from the other one, which, in principle allows the central minimum between the two peaks to converge to zero<sup>318</sup>. The case of multiple Kuramoto populations with specific coupling strengths can be approached by transforming the system into one global system whose oscillators' frequencies follow a multimodal distribution consisting of weighted inhomogeneous unimodal distributions, which can mirror the underlying coupling topology across populations<sup>285</sup>.

Admittedly, the aforementioned examples are not exhaustive, let alone complete. They represent a concise set of a broad variety of joint distribution functions. Nevertheless, we believe that our results may be a major breakthrough for the applicability of the OA ansatz for systems with more intricate distribution functions. First extensions concentrated on a multiple-population-approach and have been presented in<sup>299,319,320</sup>. Skardal and Restrepo<sup>319</sup> focused on hierarchical synchrony effects in modular networks and investigated how local and global synchrony evolve differently by allowing for different subpopulation sizes, heterogeneous intra- and

inter-population coupling strengths as well as population-specific frequency distributions. Reformulating their approach results in (5.48). This rigorously establishes the agreement of the predictions by the OA ansatz and their numerical results. So and co-workers, on the other hand, aimed for synchronization criteria in a network of two coupled populations with static and time-varying coupling topologies<sup>267,320</sup>. Their governing equations can be cast into (5.47) when additionally considering  $K = K(t)$  to be time-dependent. Also, they numerically determined macroscopic chaos by assuming a single network with bimodally distributed natural frequencies<sup>299</sup>. Combining our results from this section together with the preceding part where we incorporated non-autonomicity, we again corroborate the numerous numerical findings by providing the ingredients to prove the implicit assumption that the OA ansatz holds for these kinds of parameter-dependent and non-autonomous systems.

### 5.4.3 Heterogeneous mean field models

While the general case of uncorrelated joint distributions has already been covered in the preceding *Section 5.4.2*, we would like to concentrate on the specific derivation of the heterogeneous mean field model. Recall the standard Kuramoto model on a given network,

$$\dot{\theta}_j = \omega_j + K \sum_{k=1}^N a_{jk} \sin(\theta_k - \theta_j) , \quad (5.49)$$

where  $K$  is the coupling strength and the adjacency matrix is given by  $A = (a_{ij})_{i,j=1,\dots,N}$ . We substitute the adjacency values  $a_{jk} \in \{0, 1\}$  by their expectation values  $\langle a_{jk} \rangle \in [0, 1]$ , which are given by

$$\langle a_{jk} \rangle = \frac{\eta_j \eta_k}{N \langle \eta \rangle} . \quad (5.50)$$

Introducing the complex order parameter as

$$z = \frac{1}{N \langle \eta \rangle} \sum_{k=1}^N \eta_k e^{i\theta_k} ,$$

the dynamics for all nodes with the same degree  $\eta_k$  read

$$\dot{\theta}_k = \omega_k + K \eta_k \text{Im}(z e^{-\theta_k}) .$$

In this special form, in which the single nodes are replaced by block-degree variables, we returned to the all-to-all coupling. For a given degree distribution  $P(\eta)$

property (5.50) also holds in the continuum limit  $N \rightarrow \infty$  where the governing dynamics read

$$\partial_t \theta(\eta, t) = \omega + \text{Im} [K\eta z(t)e^{-i\theta}] , \quad (5.51)$$

with  $\omega$  and  $\eta$  being drawn from a joint distribution  $g(\omega, \eta) = P(\eta)g_1(\omega)$ . As above we can introduce a phase distribution function  $\rho(\theta, \omega, \eta, t)$ , which fulfills the continuity equation  $\partial_t \rho + \partial_\theta(v\rho) = 0$  with  $v$  the right-hand side of (5.51). Note, however, that depending on the underlying network topology and its degree distribution  $P(\eta)$ , one has to choose the domain of  $\eta$  properly. In the case of a scale-free network, the degree distribution follows  $P(\eta) \propto \eta^{-\gamma}$  with  $\gamma > 1$ . Hence the normalization conditions for the distribution function  $\rho$  obey

$$\int_1^\infty \int_0^{2\pi} \rho(\theta, \omega, \eta, t) d\theta d\eta = g_1(\omega) \quad \text{and} \quad \int_{-\infty}^\infty \int_0^{2\pi} \rho(\theta, \omega, \eta, t) d\theta d\omega = P(\eta) .$$

We can apply the OA ansatz as above. By the same reasoning as in *Section 5.4.2*, we can prove the OA attractiveness for heterogeneous mean field models, rendering also non-globally coupled oscillator networks applicable for the OA theory, which guarantees that their mean field dynamics evolve on a low-dimensional manifold.

Before elaborating more on coupling schemes other than global coupling, we briefly discuss further topological network effects such as nodal correlations between in and out degrees, correlations between nodal frequencies and degrees, and degree as well as so-called frequency assortativity in the formation of links. Recent numerical findings by Restrepo, Ott, and Skardal<sup>321,322</sup> exploited assortative networks and gave strong incentive to believe that their dimensionality reduction techniques along the OA ansatz do capture the dynamics of the full network. An assortativity function  $a_{\mu' \rightarrow \mu}$  represents the probability that a link exists from an oscillator with target property  $\mu'$  to one with property  $\mu$ . Using this one can indicate an exact instruction on how to construct a network model of the form (5.49). The nodal properties  $\mu$  are chosen in such a way that the network displays, e.g., a particular degree<sup>321</sup> ( $\mu = k$ ), frequency<sup>322</sup> ( $\mu = \omega_0$ ), or even a combined ( $\mu = \{k, \omega_0\}$ ) assortativity. Key ingredient for relating this to the OA ansatz is the reformulation of the order parameter. We first define

$$z(\mu, t) = \sum_{\mu'} P_{\mu'} a_{\mu' \rightarrow \mu} \iint \rho_{\mu'}(\theta, \omega, t) e^{i\theta} d\theta d\omega , \quad (5.52)$$

where  $\rho_{\mu'}(\theta, \omega, t) = \rho(\theta, \omega, \mu', t)$  is the common phase distribution function with target property  $\mu'$ , see (5.26),  $P_{\mu'} = P_p(\mu')$  is a normalized target property distribution, and  $a_{\mu' \rightarrow \mu} = a(\mu' \rightarrow \mu)$  the assortativity function; for details see<sup>321,322</sup>. Then, we can integrate over all possible properties  $\mu$  – note that we write the sum

over the target properties  $\mu'$  also in integral form – and we arrive at the order parameter

$$z(t) = \frac{1}{\langle \eta \rangle} \iint P_p(\mu) P_p(\mu') a(\mu' \rightarrow \mu) \iint \rho(\theta, \omega, \mu', t) e^{i\theta} d\theta d\omega d\mu' d\mu, \quad (5.53)$$

with  $\langle \eta \rangle$  the average degree. Given a specific degree distribution  $P(\eta)$  one finally ends up with (5.51), from which we can follow the lines of argument as presented above to complete the proof. The addition of assortativity in the network topology enriches the existing theory further. It discloses many new qualitative effects on the dynamics such as transitions between steady state, periodic, quasiperiodic attractors, and even macroscopic chaos may emerge without external driving or time-varying parameters.

#### 5.4.4 Non-local coupling

Two months before Ott and Antonsen published their ansatz, Ko and Ermentrout investigated the creation of partially locked states in a network of identical all-to-all coupled oscillators due to inhomogeneous coupling<sup>323</sup>. Instead of heterogeneity of the oscillators' frequencies, it was the coupling heterogeneity that led to partial synchronization. Carlo Laing analytically investigated this network of globally coupled oscillators with coupling strengths drawn from a power-law distribution<sup>324</sup> along the line of the OA ansatz – recall the resemblance to the heterogeneous mean field approach for scale-free networks. Assuming “nearly” identical oscillators, i.e. the frequencies  $\omega$  were drawn from a Lorentzian with width  $0 < \Delta \ll 1$ , he could verify the earlier results that were derived via a self-consistency argument<sup>323</sup>, and extend them by including a thorough bifurcation analysis. Our findings in Section 5.4.2 put these results on a solid mathematical ground.

Of particular interest is Laing's work on a ring of oscillators<sup>269,324</sup>. For a given ring topology, the typical coupling scheme is neither local neighbor-to-neighbor, nor global coupling. Instead, the oscillators are non-locally coupled via a coupling kernel  $G$ . We assume that each oscillator  $j = 1, \dots, N$  has some fixed spatial position  $x_j \in [-\pi, \pi]$ , a natural frequency  $\omega_j$  drawn from a continuous distribution function  $g(\omega)$  with non-zero width, and interacts with the others depending on the distance between their sites modulo periodic boundary conditions. The governing dynamics read

$$\dot{\theta}_j = \omega_j + \frac{2\pi}{N} \sum_{j=1}^N G(x_k - x_j) \sin(\theta_k - \theta_j + \alpha), \quad (5.54)$$

where  $\alpha$  is a phase-lag parameter and  $G: \mathbb{R} \rightarrow \mathbb{R}$  a continuous even and  $2\pi$ -periodic

coupling function<sup>325</sup>. We retrieve global coupling, if  $G \neq 0$  is constant. Commonly used coupling functions  $G$  are of exponential form  $G(x) \sim e^{-\kappa|x|}$  with  $\kappa > 0$ , or of trigonometric form  $G(x) = 1/2\pi(1 + A \cos x + B \sin x)$  with  $A > 0, B \geq 0$ . The reflection symmetry of  $G$  is lost for  $B \neq 0$ . In the continuum limit, the velocity field (5.8) becomes

$$\begin{aligned} \partial_t \theta &= \omega + \text{Im} [H(x, t)e^{-i\theta}] , \\ H(x, t)e^{i\alpha} &= \int_{-\pi}^{\pi} G(x - y) \int_{-\infty}^{\infty} \int_0^{2\pi} \rho(\theta, y, \omega, t)e^{i\theta} d\theta d\omega dy . \end{aligned} \quad (5.55)$$

While the inner two integrals have the form of a local complex order parameter  $z(y, t)$ , measuring the synchronization degree of oscillators around  $y$ , we can interpret the last integral as a convolution of the local order parameter with the (spatial coupling) kernel  $G$ . In particular, we can regard the dynamics  $\partial_t \theta(x, t)$  of an oscillator at position  $x$  as being controlled by the local mean field  $H(x, t)$ . Unlike the case of global coupling, the order parameter has become space-dependent and thus the driving field. However, a similar “physical picture” as for global coupling is valid: practically we deal with an assembly of independent oscillators under the control of a common forcing field<sup>325,326</sup>. We now go a step further and interpret the space variable  $x$  as a subpopulation index<sup>327</sup>. Equivalent to the block-degree variables in the heterogeneous mean field approach, we consider the subpopulation index as a parameter that follows a particular, in this case a uniform, distribution function. Hence, (5.55) represents the governing dynamics of a parameter-dependent system, for which we proved the OA attractiveness in the preceding sections.

#### 5.4.5 External forcing and time delay

Already in their original work, Ott and Antonsen proposed that their ansatz extends to external forcing and the incorporation of time delays. However, recent results that leaned against the OA ansatz for tackling more intricate issues of external forcing and/or time delays went beyond the reach of the original proof. Therefore, we first revisit the existing theory and revise the proof appropriately with the concepts introduced above.

Ott and Antonsen considered the forced Kuramoto model<sup>81</sup>,

$$\dot{\theta}_j = \omega_j + \frac{K}{N} \sum_{k=1}^N \sin(\theta_k - \theta_j) + \eta \sin(\varpi t - \theta_j) . \quad (5.56)$$

Rearranging terms, moving in a rotating frame,  $\theta \rightarrow \theta + \varpi t$ , and considering the

thermodynamic limit, the velocity field reads

$$\begin{aligned}\partial_t \theta &= \Omega(\omega, \varpi) + \text{Im} [H(\omega, K, \eta, t) e^{-i\theta}] , \\ \Omega(\omega, \varpi) &= \omega - \varpi , \quad H(\omega, K, \eta, t) = Kz(t) + \eta ,\end{aligned}\tag{5.57}$$

with  $z(t)$  the common Kuramoto order parameter. While Ott and Antonsen provided a proof for systems with constants  $K, \varpi$ , and  $\eta$ , conjoining thereby the numerical findings and the extensive analysis by Childs and Strogatz<sup>328</sup>, we generalized their proof extensively in *Section 5.2.1*. By this, the additional parameters  $\varpi$  and  $\eta$  that characterize the forcing can be both random and time-dependent variables. This adaptation renders a more detailed analysis of, for instance, the circadian rhythm problem possible. One extension has been published very recently addressing the east-west asymmetry of jet-lag<sup>329</sup>, where a discontinuous phase quantity  $p$  is added to model the travel across time-zones. The adapted model reads

$$\dot{\theta}_j = \omega_j + \frac{K}{N} \sum_{k=1}^N \sin(\theta_k - \theta_j) + \eta \sin(\varpi t - \theta_j + p(t)) ,\tag{5.58}$$

where  $p$  jumps from one constant value to another depending on the corresponding time-zone. In particular,  $p(t)$  is locally integrable, which allows for a thorough analytic description of how the human organism may adapt after several cross-time-zone travels. This extends the existing work where the authors solely focused on the recovery dynamics of circadian rhythms after a single travel “shock”.

To address the presence of time delays, let us first concentrate on time-delayed coupling, i.e. the response of oscillator  $j$  at time  $t$  depends on the state of another oscillator  $k$  at time  $t - \tau_{kj}$ . Here,  $\tau_{kj}$  is some specific delay time for the interaction. In general, the single oscillator dynamics may be given by

$$\dot{\theta}_j(t) = \omega_j + \frac{K}{N} \sum_{k=1}^N \sin(\theta_k(t - \tau_{kj}) - \theta_j(t)) .\tag{5.59}$$

There already exists a plethora of studies<sup>287,324,330</sup> considering the case in which  $\tau_{kj}$  follows some given distribution function  $h(\tau)$ . That the OA ansatz also holds in this case, has been proven by Ott and Antonsen<sup>82</sup>, where they generalized their original idea of identical time delays<sup>81</sup>,  $\tau_{kj} = \tau'$  for all  $j, k = 1, \dots, N$ , i.e.  $h(\tau) = \delta(\tau - \tau')$ . The driving field  $H$  of the original velocity field (5.3) is replaced by

$$H = K \int_{\Omega} h(\tau) z(t - \tau) d\tau ,$$

where  $\Omega \subset \mathbb{R}$  is the domain of the time delay distribution  $h$  and  $z(t)$  the common Kuramoto order parameter. Slightly more elaborate and not covered by Ott and Antonsen's original proof is the extension to so-called coupling adaptation<sup>331</sup>. The coupling strength is no longer constant but slowly adapts depending on the current coupling strength and the delayed order parameter. As long as the function that models the adaptation process is locally integrable, our extended proof guarantees the OA attractiveness for such time-varying parameter-dependent systems. For this reason we believe that the mainly numerical work by Skardal and co-workers<sup>331</sup> can also be analytically substantiated. This will not only contribute to exploring the underlying phenomena of explosive synchronization<sup>332,333</sup>, but also enhance the modeling of information processing and memory effects, for which network adaptation is crucial<sup>334–336</sup>.

## 5.5 Relaxation dynamics towards the Ott-Antonsen manifold

As discussed, we allow time-varying parameters to affect the oscillator dynamics. The change of parameters comes with its time scale(s). The change can be periodic. This periodicity may also influence the evolution of the mean field and thereby the OA manifold. Therefore, the relation between this periodicity and the characteristic time of the system to approach the manifold needs to be investigated. If the relaxation dynamics onto the manifold is way slower than the characteristic time scale of the time-varying manifold itself, then our findings will remain true for the limit  $t \rightarrow \infty$ . They are, however, of minor interest for describing the transient behavior of the mean field. Several numerical results<sup>293,303,304,308</sup> suggest that the relaxation to the OA manifold is reasonably fast, in some cases even instantaneous. To address this analytically, we briefly recall the proof for the attractiveness from *Section 5.2.1*. After having Fourier expanded the phase distribution function  $\rho(\theta, \eta, t)$ , and then decomposed the positive Fourier modes into a part that already lies on the manifold,  $\hat{\rho}'_+$ , and a residual part  $\hat{\rho}_+$ , we showed how the latter converged to zero in a weak sense, cf. (5.12). We can extract the relaxation time to the OA manifold from out of the proof: From (5.13 & 5.14) we obtain a solution  $f_+(\theta, t) = \hat{\rho}'_+(\theta, -i\sigma, t)$ , with  $\sigma' > \sigma > 0$  where  $\hat{\rho}'_+(\theta, \eta, t)$  admits an analytic continuation into the strip  $S = \{\eta \in \mathbb{C} \mid -\infty \leq \text{Re}(\eta) \leq \infty, 0 \geq \text{Im}(\eta) \geq -\sigma'\}$ ; the solution (5.16) obeys

$$\tilde{f}_+(w, t) = \tilde{f}_+(W(w, 0), 0) \exp[-\mu(w, t)] ,$$

hence the relaxation time  $\tau$  is by definition

$$const \cdot \exp(-t/\tau) = \exp[-\mu(w, t)] \Rightarrow \tau = \frac{t}{\text{Re}[\mu(w, t)]}. \quad (5.60)$$

Put differently,  $\text{Re}[\mu(w, t)]$  scales with  $\sigma t$ , such that  $\tau = 1/\sigma$ . The wider the frequency distribution becomes, the larger  $\sigma$  can be chosen. Thus, one may argue that the characteristic time scale decreases with increasing heterogeneity among the single oscillators. This relation has already been noted for a particular example of a Lorentzian frequency distribution by Ott and Antonsen<sup>81</sup>. It has been investigated in more detail by Petkoski and Stefanovska for the non-autonomous Kuramoto model<sup>308</sup>. Interestingly, there is an intrinsic relation between the frequency inhomogeneity and the coupling strength. Therefore, at critical coupling strengths, which distinguish different dynamical regimes, the relaxation times tend to infinity, which has been reported independently by Petkoski et al.<sup>308</sup> and Yoon et al.<sup>316</sup> for the full Kuramoto network, its non-autonomous version and the heterogeneous mean field model.

For the non-autonomous case we would like to mention that the proof presented in *Section 5.2.1* entirely holds for continuous time-varying parameters. Introducing discontinuities in either the frequency  $\Omega$  and/or the driving field  $H$ , however, will eventually lead to a non-continuous right-hand side of (5.14) – due to  $H$  itself, or via the order parameter  $z$ , which absorbs the time-varying part of  $\Omega$  and influences  $H$  directly or indirectly. While employing the method of characteristics still can be performed, estimating the integral in (5.17) cannot exploit the continuity assumption and a proper evaluation has to be circumvented. In spite of this sinister outlook, numerical results remain promising; for instance, the simulations in<sup>293</sup> with a square input function (Fig.2a,c,e,g therein). A possible way to overcome this obstacle might be to approximate the jumps by smooth sigmoid functions, which might be valid as long as the height of the jumps is lower than their length. Another more rigorous approach might be to find weak solutions for (5.13 & 5.14) and estimate their long-time behavior. There, a starting point could be the very recent results by Dietert, Fernandez and co-workers, who investigated stability properties of different dynamical regimes of the Kuramoto model in a mathematically rigorous way, confirming the exponential decay to the manifold<sup>337–339</sup>. More details are way beyond the scope of our paper.

Interestingly, the approach by Dietert and others is based on the idea of “Landau damping” in plasma physics. Strogatz, Mirollo and Matthews were the first who incorporated this concept in order to understand relaxation dynamics of the Kuramoto model<sup>272,340</sup>. They showed that for frequency distributions  $g(\omega)$  supported on the whole real axis, the decay towards the incoherent state is exponentially fast

for coupling strengths below the critical threshold,  $K < K_c$ . If  $g(\omega)$  has compact support, i.e.  $g$  is non-zero only on a compact interval  $[-\gamma, \gamma] \subset \mathbb{R}$ ,  $0 < \gamma < \infty$ , the rate may be considerably slower, even polynomial. In the example they used to illustrate their result, the authors assumed the frequencies  $\omega$  to be distributed uniformly on  $\mathcal{I} = [-\gamma, \gamma]$ , i.e.  $g(\omega) = 1/2\gamma$  if  $\omega \in \mathcal{I}$ , and 0 otherwise. The jump discontinuities of  $g$  on  $\partial\mathcal{I}$ , however, prohibited an analytic continuation of  $g$  into a strip  $S$  in the lower complex  $\omega$ -plane, contradicting the required conditions for applying the OA ansatz<sup>83</sup>. That is why the proofs above cannot be applied here, and our argumentation about the relaxation times remains unaffected.

Last but not least, we would like to add that decay times typically depend on initial conditions. Pikovsky and Rosenblum pointed out that for identical macroscopic, i.e. mean field, initial conditions the microscopic initial states can lead to very different transient dynamics towards the OA manifold, see Section 3.2 in<sup>178</sup>. A more thorough investigation about this specific topic has not been undergone, yet, but might shed light on the underlying dynamics of the microscopic variables of large oscillatory systems in contrast to its mean field behavior.

## 5.6 Discussion and conclusion

The OA ansatz has proven considerably fruitful for investigating the macroscopic behavior of systems of coupled phase oscillators in terms of a low-dimensional system. Although parameter dependence has already been mentioned in Ott and Antonsen's original work, parameters were merely considered auxiliary variables and the velocity field was required to incorporate the phase only through a sinusoidal coupling term.

Our main result was to prove that the  $\eta$ -dependence sustains the time-asymptotic attractiveness of the OA manifold for systems of coupled oscillators. For this we required that the driving field  $H$  does not have singularities in the complex  $\eta$ -plane and that it diverges at most sub-exponentially for  $\text{Im}(\eta) \rightarrow -\infty$ , next to the conditions in the original Ott and Antonsen formulation<sup>81,82</sup>. Furthermore, we assumed the frequency  $\omega(\eta, t)$  to be linear in  $\eta$ . We were able to depict the proof step by step. Subsequently we loosened the restrictive assumptions and showed that our results remain valid for a much broader class of distribution functions  $g(\eta)$  as well as more complex dependencies of the driving field  $H(\eta)$  and the natural frequencies  $\omega(\eta)$  on the parameter  $\eta$ .

Although the main idea of introducing a common parameter  $\eta$  was to correlate the driving field and the natural frequency with their specific oscillator, our proof is identical for the case when  $\eta$  does only influence the mean field dynamics. By this, we have proved the claim in<sup>83</sup> that the OA manifold remains attractive in the

“weak” parameter-dependent case when  $H$  depends on “other non-phase-oscillator variables obeying auxiliary dynamical systems.”

Common choices of  $H$  and  $\omega$  usually fulfill the aforementioned assumptions as stated in *Section 5.2.1*. That is, our result can be immediately applied in a variety of circumstances. Here, we highlighted an application in mathematical neuroscience. By this, our findings strengthen the theory of coupled theta neurons: The many recent numerical findings in<sup>293</sup> and the references therein are finally set in a solid mathematical framework. Moreover, the link between QIF neurons and theta neurons has been underscored by proving the attractiveness of the Lorentzian ansatz.

We generalized and extended existing proofs for non-autonomous systems. In particular we addressed the Winfree model, which is biologically more realistic than the Kuramoto model and therefore closer to applications. We also addressed coupled oscillatory systems with an additional shear parameter, another important tool to render the Kuramoto model more realistic. The major novelty was our rigorous proof of the OA attractiveness for systems with uncorrelated joint distribution functions when more parameters than only the natural frequencies are treated as a random variable. This finding opened the way for networks with specific underlying coupling topologies other than the restrictive global coupling. Using the heterogeneous mean field approach, we showed how these networks can be treated along the OA ansatz. First steps were also taken in the direction of correlated joint distributions.

All in all, we consider the explicit dependence on an additional parameter  $\eta$  of both the oscillator’s phase and the (non-sinusoidal) components an important extension introducing an intrinsic relation between phase, frequency, and driving field of an oscillator. The latter two are correlated with the phase so that the  $\eta$ -dependence does not allow for applying the original theory.

Still, there are several open problems concerning the mean field dynamics of an oscillatory system and its description by a low-dimensional system. A first urgent one is the case of  $\delta$ -peaked frequency distributions. Numerical simulations<sup>341</sup> and heuristic arguments hint at convergence of the OA manifold, where a proper mathematical derivation is omitted under the pretence of “nearly identical oscillators”<sup>269,288,342</sup>. A thorough proof would render the OA ansatz rigorously applicable to “chimera states”, a topic that is particularly en vogue; see, e.g., the recent review paper by Panaggio and Abrams<sup>185</sup>. Importantly, such a proof has to circumvent the main argument of Ott and Antonsen’s original proof, where the width  $\Delta > 0$  of the distribution  $g(\omega)$  allowed for a consequent evaluation of the mean field dynamics. On the other hand, Pikovsky and Rosenblum<sup>343</sup> already showed that more complicated dynamics can emerge from the OA manifold when

describing the system along the Watanabe-Strogatz ansatz<sup>80</sup>. Deviations from the OA ansatz appear only if the Watanabe-Strogatz constants of motion are not uniformly distributed over the whole domain, but only over a compact subset. Given (a) the direct correspondence between the constants of motion and the initial conditions of phases in the OA ansatz<sup>80,178</sup>, and (b) the necessary requirements on (analytic continuation properties of) the initial conditions, it may be worth investigating the influence of nonuniform distributions of the constants of motion and whether this may hinder the initial conditions of phases to satisfy the requirements of the OA ansatz.

Another intriguing open problem is whether the mean field dynamics is attracted by a low-dimensional manifold when the parameter dependence of the frequency and driving field is extended by an explicit dependence on the individual phases. A recent example is given by Laing<sup>344</sup>, who considered the driving field  $H$  to follow a dynamics that explicitly depends on the phase  $\theta$ . This system exhibits partial synchronization patterns, which are also covered by the OA ansatz, but any attempt to apply the OA ansatz has been avoided “due to the dynamics of the extra variables.”<sup>344</sup>

When the coupling term incorporates higher harmonics see, e.g., 345,346, no low-dimensional analytic solution for the mean field evolution has been found. This is another open question whether further generalizations of the work of Ott and Antonsen<sup>81</sup> can be rigorously manifested. We believe that our current proof for parameter-dependent networks is a good starting point for tackling these important issues.

---

# CHAPTER 6

## Criticality in neural mass phase oscillator models

*Modeling and interpreting (partial) synchronous neural activity can be a challenge. We illustrate this by deriving the phase dynamics of two seminal neural mass models: the Wilson-Cowan firing rate model and the voltage-based Freeman model. We established that the phase dynamics of these models differed qualitatively due to an attractive coupling in the first and a repulsive coupling in the latter. Using empirical structural connectivity matrices, we determined that the two dynamics cover the functional connectivity observed in resting state activity. We further searched for two pivotal dynamical features that have been reported in many experimental studies: (1) a partial phase synchrony with a possibility of a transition towards either a desynchronized or a (fully) synchronized state; (2) long-term autocorrelations indicative of a scale-free temporal dynamics of phase synchronization. Only the Freeman phase model exhibited scale-free behavior. Its repulsive coupling, however, let the individual phases disperse and does not allow for a transition into a synchronized state. The Wilson-Cowan phase model, by contrast, could switch into a (partially) synchronized state, but it did not generate long-term correlations although being located close to the onset of synchronization, i.e. in its critical regime. That is, the phase-reduced models can display one of the two dynamical features, but not both.*

Adapted from: Daffertshofer A., Ton R., Pietras B., Kringsbach M.L., Deco G. (2018). *Scale-freeness or partial synchronization in neural mass phase oscillator networks: pick one of two?* NeuroImage **180** 428–441.  
doi: 10.1016/j.neuroimage.2018.03.070.

## 6.1 Scale-freeness and partial synchronization

Characterizing the underlying dynamical structure of macroscopic brain activity is a challenge. Models capturing this large-scale activity can become very complex, incorporating multidimensional neural dynamics and complicated connectivity structures<sup>347,348</sup>. Neural mass models, or networks thereof, that cover the dynamics of neural populations offer a lower-dimensional and therefore appealing alternative<sup>11,349,350</sup>. To further enhance analytical tractability one may consider the (relative) phase dynamics between neural masses. We previously showed under which circumstances certain neural mass models can be reduced to mere phase oscillators<sup>42,44</sup> – see also<sup>41,48,61</sup> – and thus established a direct link between these two types of models. A minimal model describing phase dynamics is the Kuramoto network<sup>38,351</sup>, which in its original form consists of globally coupled phase oscillators. Generalizations of this model by adding delays and complex coupling structures result in a wide variety of complex dynamics<sup>40,264</sup>. Even in its original form, however, the Kuramoto model is capable of showing non-trivial collective dynamics. A mere change of the (global) coupling strength can yield a spontaneous transition from a desynchronized to a synchronized state, i.e. the dynamics can pass through a critical regime.

Synchronization of neural activity plays a crucial role in neural functioning<sup>352</sup>. In the human brain, synchronized activity can be found at different levels. At the microscopic level temporal alignment in neuronal firing is a prerequisite for measurable cortical oscillations<sup>353</sup>. However, it also manifests itself at the macroscopic level in the form of global resting state networks<sup>354,355</sup>. Synchronization properties are modulated under the influence of task conditions in, e.g., motor performance<sup>356</sup>, visual perception<sup>19</sup>, cognition<sup>357</sup> and information processing<sup>358–360</sup>. Epilepsy, schizophrenia, dementia and Parkinson’s disease come with pathological synchronization structures<sup>5,361</sup>. When aiming for a concise but encompassing description of brain dynamics, a macroscopic network model should capture this wide range of synchronization phenomena.

According to the so-called criticality hypothesis<sup>362</sup>, the human brain is a dynamical system in the vicinity of a critical regime. Its dynamics is located at the cusp of dynamic instability reminiscent of a non-equilibrium phase transition in thermodynamic systems<sup>363,364</sup>. The conceptual appeal of the critical brain lies in the fact that networks operating in this regime show optimal performance in several characteristics relevant to cortical functioning<sup>365</sup>. Critical dynamics often display power laws in multiple variables<sup>366</sup> and have been observed in, e.g., size and duration distributions of neuronal avalanches<sup>367</sup> and EEG cascades<sup>368</sup>. Power-laws are also manifested as scale-free autocorrelation structures of the amplitude envelopes

of encephalographic activity<sup>369,370</sup>. Very recently, long-range temporal correlations have been reported in fluctuations of the phase (synchronization) dynamics in neural activity<sup>371,372</sup>. The nature of these power-law forms in the correlation structure can be quantified by the Hurst exponent  $H$ <sup>373</sup>. Its value characterizes the correlations between successive increments of the signal, with  $H > 0.5$  marking persistent behavior in the time series, i.e. positive, long-range correlations, and  $H < 0.5$  anti-persistent behavior, i.e. a negative auto-correlation.

In this study we considered the phase descriptions of two classical neural mass networks: the Wilson-Cowan firing rate and Freeman voltage model, both equipped with neurobiologically motivated coupling and delay structures. Coupling and delay structures were obtained from DTI data and the Euclidean distances between nodes, respectively. To anticipate, the two models lead to two qualitatively different phase synchronization dynamics.

## 6.2 Phase description of neural mass models

Phase reduction techniques, as have been introduced in *Chapter 2* together with some exemplary applications in *Chapter 3*, are key to describe the Wilson-Cowan and Freeman neural mass models in terms of their phase dynamics. To facilitate the comparison between the network models and the experimental MEG data, we assumed each network to consist of  $N = 90$  coupled nodes whose oscillatory dynamics were described by the respective neural mass model. The resulting phase dynamics of each node  $k = 1, \dots, N$  were found to obey the form

$$\dot{\phi}_k = \omega_k + \frac{1}{N} \sum_{l=1}^N D_{kl} \sin(\phi_l - \phi_k + \Delta_{kl}) \quad (6.1)$$

with  $\omega_k$  denoting the natural frequency of the oscillator at node  $k$ .  $D_{kl}$  is the phase coupling matrix, which incorporated the particular dynamics of the underlying neural mass model and the structural connectivity of the network. The coupling between neural masses was scaled by a strength factor  $K$ . Moreover, we assumed that time delays  $\tau_{kl}$  between nodes  $k$  and  $l$  were of the same order of magnitude as the period of oscillation, such that they could be captured by phase shifts  $\Delta_{kl}$  in the phase dynamics. The model-dependent terms  $\omega_k$ ,  $D_{kl}$  and  $\Delta_{kl}$  will be explicated in the subsequent presentations of the neural mass models.

### 6.2.1 Wilson-Cowan model

The first neural mass model we studied is the Wilson-Cowan model that describes the dynamics of firing rates of neuronal populations<sup>69</sup>. We always considered

properly balanced pairs of excitatory and inhibitory populations,  $E_k = E_k(t)$  and  $I_k = I_k(t)$ , respectively. We placed such pairs at every node of a network. Nodes were coupled to other nodes through the connections between excitatory populations given by a DTI-derived coupling matrix  $S_{kl}$  forming a network of  $k = 1, \dots, 90$  nodes. We illustrate the basic structure of this network in Fig. 6.1 and the coupling matrix in Fig. 6.2, left panel. The dynamics per node  $k$  was cast in the form

$$\begin{aligned} \mu_k \dot{E}_k &= -E_k + \mathcal{Q} \left[ a_E \left( c_{EE} E_k - c_{EI} I_k - \theta_E + q_k + K \sum_{l=1}^N S_{kl} E_l(t - \tau_{kl}) \right) \right] \\ \mu_k \dot{I}_k &= -I_k + \mathcal{Q} \left[ a_I (c_{IE} E_k - c_{II} I_k - \theta_I) \right], \end{aligned} \quad (6.2)$$

where the coupling constants  $c_{EI}$ ,  $c_{IE}$ ,  $c_{EE}$ ,  $c_{II}$  quantify the coupling strength within each ( $E/I$ ) pair. The function  $\mathcal{Q}[x] = (1 + e^{-x})^{-1}$  is a sigmoid function<sup>[1]</sup> that introduces the thresholds  $\theta_E$  and  $\theta_I$  that need to be exceeded by the total input into neural mass  $k$  to elicit firing; the parameters  $a_E$  and  $a_I$  describe the slopes of the sigmoids. The delays  $\tau_{kl}$  were determined by conduction velocity and the Euclidean distance between nodes  $k, l$ . In the following, delay values are given in milliseconds. Appropriate choices of the time constants  $\mu_k$  and external inputs  $q_k$  guaranteed self-sustained oscillations in the alpha band (8-13 Hz). By randomizing the constant external inputs  $q_k, \mu_k$  across  $k$  we introduced heterogeneity in oscillation frequencies.

The phase dynamics could be derived along Haken's reduction via averaging, see *Section 2.2.7* for details. We transformed the system to its corresponding polar coordinates around an unstable focus, and described its dynamics in terms of the periodic function  $A_k \cos(\Omega t + \phi_k)$ , with  $A_k$  denoting the amplitude,  $\phi_k$  the relative phase, and  $\Omega$  the central frequency of the oscillation. We averaged the dynamics over one period  $2\pi/\Omega$  under the assumption that the characteristic time scale of the  $A_k$  and  $\phi_k$  dynamics significantly exceeded this period, i.e.  $|\dot{A}_k/A_k|, |\dot{\phi}_k| \ll |\Omega|$ . That is, the variables  $\phi_k$ ,  $A_k$  evolved slowly enough to be considered constant within one period. In consequence, we obtained the Wilson-Cowan phase model (6.1) with expressions (superscript WC)

$$\begin{aligned} \omega_k^{\text{WC}} &= -\Omega + \frac{\varpi_k}{\mu_k} \\ D_{kl}^{\text{WC}} &= \frac{K}{2\mu_k} \mathcal{Q}' \left[ \chi_{E,k}^{(0)} \right] a_E \left[ 1 + \Lambda_k^2 \right]^{\frac{1}{2}} S_{kl} \frac{R_l}{R_k} \\ \Delta_{kl}^{\text{WC}} &= \arctan(\Lambda_k) - \Omega \tau_{kl} \end{aligned} \quad (6.3)$$

<sup>[1]</sup> Note the slight change of notation compared with *Section 3.2*.

where  $\mathcal{Q}'$  denotes the derivative of  $\mathcal{Q}$  resulting from a Taylor approximation around the points  $\chi_{E,k}^{(0)}, \chi_{I,k}^{(0)}$ ; the detailed expressions of the aforementioned unstable focus as well as the definition of the parameters  $\Lambda_k$  and  $\varpi_k$  are given in *Section 3.2.4*; see also *Appendix B.1* of<sup>67</sup>. By virtue of the definition of  $\mathcal{Q}$ , one has  $\mathcal{Q}' \geq 0$ .

### 6.2.2 Freeman model

The Freeman model<sup>75</sup> describes the mean membrane potentials  $E_k, I_k$  of neural populations. In analogy to (6.2) its dynamics per node can be given by

$$\begin{aligned}\ddot{E}_k &= -(\alpha_k + \beta_k) \dot{E}_k - \alpha_k \beta_k E_k + \alpha_k \beta_k q_k + \\ &+ \alpha_k \beta_k \gamma K \sum_{l=1}^N S_{kl} \mathcal{Q} \left[ \frac{E_l(t - \tau_{kl}) - \theta}{\sigma} \right] - \alpha_k \beta_k c_{EI} \gamma \mathcal{Q} \left[ \frac{I_k - \theta}{\sigma} \right] \\ \ddot{I}_k &= -(\alpha_k + \beta_k) \dot{I}_k - \alpha_k \beta_k I_k + \alpha_k \beta_k c_{IE} \gamma \mathcal{Q} \left[ \frac{E_k - \theta}{\sigma} \right],\end{aligned}\quad (6.4)$$

where  $k = 1, \dots, N$  with  $N$  being the number of excitatory populations – the corresponding schematic is again given in Fig. 6.1. The sigmoid function  $\mathcal{Q}[x]$  here covers the effects of pulse coupled neurons in the populations adjusted by the scaling parameter<sup>374</sup>  $\gamma$ . The parameters  $\alpha_k, \beta_k$  represent mean rise and decay times of the neural responses in population  $k$ , which we here varied to introduce frequency heterogeneity in the system. Analogous to (6.2) appropriate parameter values guaranteed self-sustained oscillations in the alpha frequency band.

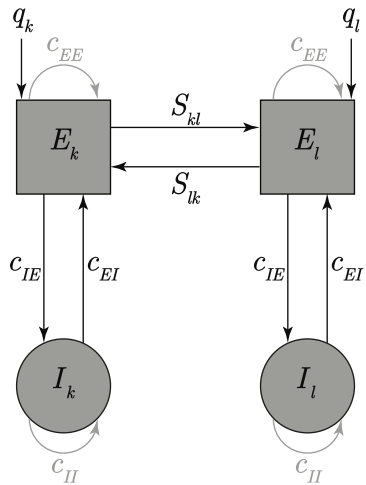


**Figure 6.1:** Coupling structure of both neural mass networks. A proper balance between excitatory ( $E_k$ ) and inhibitory ( $I_k$ ) populations leads to self-sustained oscillations in the network. Self-coupling ( $c_{EE}, c_{II}$ ) is only present in the Wilson-Cowan network and, hence, plotted in gray. External inputs are indicated by  $q_k$ . The coupling matrix  $S_{kl}$  connecting the excitatory populations was based on structural DTI data.

In (6.4) we separated the excitatory and inhibitory nodes to stress the similarity between both networks. For the sake of simplicity, however, we rather combine both equations in (6.4) into a single one. To this end we introduce the variable  $V = [E, I]^T$  and incorporate the terms  $c_{EI}, c_{IE}$ , and the scaled structural coupling matrix  $K \cdot S$  into an ‘overall’ coupling matrix  $C^F = \begin{bmatrix} K \cdot S & -c_{EI} \mathbf{1} \\ c_{IE} \mathbf{1} & \mathbf{0} \end{bmatrix}$  with  $\mathbf{1}$  and  $\mathbf{0}$

denoting the identity and the zero matrix, respectively; see Fig. 6.2, right panel. This abbreviation yields the form

$$\ddot{V}_k = -(\alpha_k + \beta_k) \dot{V}_k - \alpha_k \beta_k V_k + \alpha_k \beta_k q + \alpha_k \beta_k \gamma \sum_{l=1}^{2N} C_{kl}^F \mathcal{Q} \left[ \frac{V_l(t - \tau_{kl}) - \theta}{\sigma} \right], \quad (6.5)$$

with  $k, l = 1, \dots, 2N$ . In (6.5), the delays  $\tau_{kl}$  between excitatory nodes are equal to delays  $\tau_{kl}$  in (6.4). Note that we assumed delays between the local pairs of excitatory and inhibitory nodes ( $[k \ l] = [1, \dots, N; k+N]$  and  $[k \ l] = [l+N; 1, \dots, N]$ ) to be negligible.

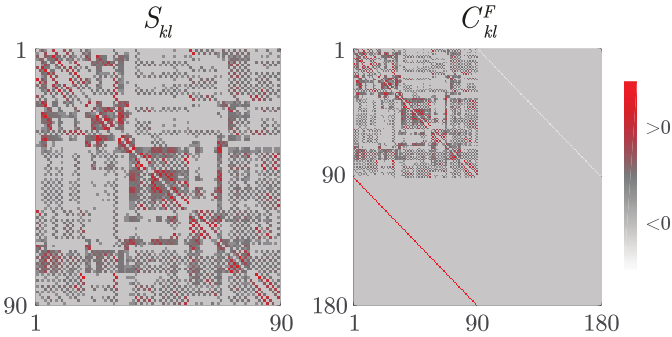


**Figure 6.2:** Illustration of the DTI-derived structural connectivity matrix  $S_{kl}$  and the matrix  $C_{kl}^F$  in (6.6). In the latter we incorporated the inter-pair coupling  $c_{EI}$  and  $c_{IE}$  together with the scaled structural connectivity  $K \cdot S_{kl}$ . The upper left block of  $C_{kl}^F$  has the same structure as  $S_{kl}$ . The two diagonals represent the coupling strengths  $c_{EI}$  and  $c_{IE}$ .

Following the same phase reduction method as above, we eventually obtained the Freeman phase model (6.1) where the expressions (superscript F) for  $\omega_k$ ,  $D_{kl}$  and  $\Delta_{kl}$  read

$$\begin{aligned} \omega_k^F &= \frac{\alpha_k \beta_k - \Omega^2}{2\Omega} \\ D_{kl}^F &= -\alpha_k \beta_k \frac{\gamma}{2\Omega} \frac{A_l}{A_k} \mathcal{Q}' \left[ V_l^{(0)} \right] C_{kl}^F \\ \Delta_{kl}^F &= \frac{\pi}{2} - \Omega \tau_{kl}; \end{aligned} \quad (6.6)$$

here  $V_l^{(0)}$  refers to the unstable focus – we refer to <sup>Appendix B.2 of 67</sup> and <sup>44</sup> for details.

## Remarks on the phase description

**The phase reduction method** The inherent complexity of the underlying network model of neural masses, including the heterogeneity among nodes, their structural connectivity and the occurrent time delays, confines the applicability of most

phase reduction techniques presented in *Chapter 2*. Nevertheless, Haken's reduction method appears a valid compromise as long as the oscillatory dynamics of each node remain close to the Hopf bifurcation boundary, see also *Section 3.2*.

**The reduced phase models** It is important to realize that due to the inhibitory coupling  $c_{EI}$ , the coupling matrix  $C_{kl}^F$  and hence  $D_{kl}^F$  have both positive and negative entries. In contrast, for  $S_{kl}$  and hence for  $D_{kl}^{WC}$  we have  $S_{kl}, D_{kl}^{WC} \geq 0$ . This change in sign can have major consequences. For instance, the Wilson-Cowan phase model (6.3) resembles the Kuramoto-Sakaguchi model with phase lag  $\Delta_{kl}$ ; for  $\tau_{kl} = \tau = 0$  we have  $\Delta_{kl} \in (0, \pi/2)$ , and otherwise  $\Delta_{kl} \in (-\pi/2, \pi/2)$  since  $\Omega\tau_{kl} \in (0, \pi/2)$  and because of our particular choice of parameters which yields  $\Lambda_k \geq 0$ . That is, a transition to full synchronization can occur if the coupling strength  $K$  exceeds a critical value  $K_c$ . However, from (6.6) it follows that the left upper block of  $D_{kl}^F$  contains negative entries. Together with the  $\pi/2$  phase shift, the Freeman phase dynamics is therefore more closely related to the repulsive cosine-variant of the Kuramoto network<sup>375,376</sup>. As will be shown below, this qualitative difference in dynamics led to profound contrasts in model behavior.

**Numeric simulations** Phase time series  $\phi_k(t)$  were obtained by integrating the system (6.1) using either (6.3) or (6.6). We first determined the fixed points  $E_k^{(0)}, I_k^{(0)}$  (Wilson-Cowan) or  $V_k^{(0)}$  (Freeman) around which we observed stable oscillations. For these oscillations we also determined the characteristic (central) frequency  $\Omega$  and amplitudes  $A_k$ . We followed the same numerical procedure as a previous publication of the group<sup>44</sup>. In brief, these initial estimates were achieved by a five second simulation of the systems (6.2)/(6.5) until they reached a steady state and using an Euler scheme with time step  $\Delta t = 1$  ms. To compute the central frequency  $\Omega$ , we determined the power spectral density per node and considered  $\Omega$  as the lowest frequency with a coinciding peak for all nodes. The choice for the Euler method was motivated by the implementation of delays in the coupling terms. Testing a more elaborated predictor/corrector algorithm<sup>377</sup> revealed little to no difference but required far more numerical resources.

The control parameters in this study were conduction velocity  $v$  and global coupling strength  $K$ . Conduction velocity  $v$  determined delay values  $\tau_{kl}$ , by assuming  $\tau_{kl}$  to be proportional to the Euclidean distance  $\mathcal{D}_{kl}$  between nodes  $k, l$ , i.e.  $\tau_{kl} = \mathcal{D}_{kl}/v$ . The range of coupling strengths amounted to  $K = [0, 0.1, \dots, 0.7, 0.8]$ . Conduction velocities were  $v = [1, 2, \dots, 10, 12, 15, 30, 60, \infty]$  ms<sup>-1</sup> leading to average delay values  $\langle \tau_{kl} \rangle = [75, 39, 25, 19, 15, 13, 11, 9.4, 8.4, 7.5, 6.3, 5.0, 2.5, 1.3, 0]$  ms. We performed simulations of the phase dynamics (6.1) only for parameter values that resulted in oscillations in the underlying neural mass dynamics

(6.2)/(6.4) because only in this case a phase reduction can be considered valid (in consequence the range of  $K$  values displayed in Fig. 6.4 varies).

Integration of the phase systems (6.1) was performed by means of an adaptive Runge-Kutta (4,5) algorithm with variable step size. Simulation time  $T = 302$  seconds matched the length of the available empirical time series, where we discarded the first two seconds of simulation to avoid transient effects due to the first random initial condition. To exclude effects of a specific natural frequency distribution of  $\omega_k^{(\cdot)}$ ,  $T$  was split into twenty bins with random duration  $T_n > 14$  s. The initial condition of bin  $n$  was matched to the last sample of bin  $n - 1$ . For each  $n$  a new set of parameter values  $q_k, \mu_k$  (Wilson-Cowan) or  $\alpha_k, \beta_k$  (Freeman) was chosen at random, under the constraint that the characteristic frequency  $\Omega$  fell within the alpha band in all cases. The parameters  $\mu_k, q_k, \alpha_k, \beta_k$ , and  $T_n$  were drawn at random but the corresponding sets were kept equal across all simulation conditions, i.e. for all combinations of  $K$  and  $\langle \tau_{kl} \rangle$ . We thus obtained twenty sets  $\{\omega_k^{(\cdot)}, D_{kl}^{(\cdot)}\}$ . For all parameter values we generated ten realizations by choosing different initial conditions and permutations of the set  $\{\omega_k^{(\cdot)}, D_{kl}^{(\cdot)}\}$  for each run. Results were averaged over these realizations for each combination of parameter values.

Further parameter values were chosen in such a way that the neural mass networks (6.2) and (6.4) displayed self-sustained alpha band oscillations. For the Wilson-Cowan model the parameters amounted to  $a_E = 1$ ,  $a_I = 1$ ,  $c_{II} = -2$ ,  $c_{IE} = c_{EE} = c_{EI} = 10$ ,  $\theta_E = 2$ ,  $\theta_I = 4.5$ ,  $q_k \in [-0.15, 0.15]$  and  $\mu_k \in [0.125, 0.175]$  where the latter two were randomly chosen to introduce heterogeneity in oscillation frequencies throughout the network. For the Freeman model we chose  $c_{EI} = c_{IE} = 1$ ,  $c_{EE} = c_{II} = 0$ ,  $q_k = 20$ ,  $\theta = 15$ ,  $\gamma = 250$ ,  $\alpha_k \in [60, 80]$  and  $\beta_k \in [165, 185]$ . The parameters  $\alpha_k, \beta_k$  were chosen randomly to introduce heterogeneity in the oscillation frequency in the network.

## 6.3 Comparing model behavior with experimental MEG data

### 6.3.1 Power-law behavior

We measured the amount of synchronization via the phase coherence, i.e. the modulus of the Kuramoto order parameter given as

$$R(t) = \frac{1}{N} \left| \sum_{k=1}^N e^{i\phi_k(t)} \right|, \quad (6.7)$$

where  $\phi_k(t)$  followed the dynamics (6.1).

Next, we assessed the autocorrelation structure of  $R(t)$  by means of a detrended fluctuation analysis (DFA)<sup>378</sup>. In DFA the cumulative sum of a time series  $y(k)$ , i.e.  $Y(t) = \sum_{k=1}^t y(k)$ , is divided into non-overlapping segments  $Y_i(t)$  of length  $T_{\text{seg}}$ . Upon removing the linear trend  $Y_i^{\text{trend}}(t)$  in segment  $i$ , the fluctuations  $F_i(T_{\text{seg}})$  corresponding to window length  $T_{\text{seg}}$  are given by

$$F_i(T_{\text{seg}}) = \sqrt{\frac{1}{T_{\text{seg}}} \int_0^{T_{\text{seg}}} (Y_i(t) - Y_i^{\text{trend}}(t))^2}. \quad (6.8)$$

When these fluctuations scale as a power law, i.e.  $F_i(T_{\text{seg}}) \sim (T_{\text{seg}})^\alpha$ , the fluctuations, and hence the associated autocorrelations, can be considered scale-free. The corresponding scaling exponent  $\alpha$  resembles the Hurst exponent<sup>373</sup>  $H$  and characterizes the correlation structure (the resemblance is proper if  $y(t)$  stems from a fractional Gaussian noise process). We assessed the presence of a power law in  $F_i$  in a likelihood framework by testing this model against a set of alternatives<sup>379</sup>. By applying the Bayesian information criterion (BIC) we could determine the model that constituted the optimal compromise between goodness-of-fit and parsimony<sup>380</sup>. More details of the DFA and model comparison are given in *Appendix 6.7.1*.

To determine the significance of the model results, we constructed surrogate data sets by generating 90 phase times series  $\phi_k^{(\text{surr})}(t)$ , which equalled the number of excitatory nodes. The surrogate phase time-series consisted of random fluctuations around linear trends sampled from the  $\omega_k^F$  distribution using the same  $T_n$  partitions as in the model simulation conditions. We used a Wilcoxon rank-sum test to test the results from surrogate time series against simulated time series in a non-parametric way. For evaluation of the scaling exponents, we only incorporated those conditions that showed power-law scaling as assessed by the BIC.

### 6.3.2 Functional connectivity

We compared spatial correlation structures in terms of the functional connectivity matrices generated by both models with an empirically observed functional connectivity. For the latter we incorporated a previously published data set<sup>45,372</sup>. We refer to<sup>45</sup> for details concerning data acquisition and preprocessing of both the MEG and the DTI derived anatomical coupling matrix  $S$  that was used in the coupling matrices  $D_{kl}^{(\cdot)}$  given in (6.3&6.6). In brief, MEG of ten subjects was recorded in resting state conditions (eyes closed) for approximately five minutes. These MEG signals were beamformed onto a 90 node brain parcellation<sup>381</sup>, such that 90 time-series  $y_k(t)$  were obtained with a sampling frequency of 250 Hz. The

signals  $y_k(t)$  were bandpass filtered in the frequency range 8-12 Hz and subjected to a Hilbert transform to obtain the analytical signal, from which the Hilbert phase could be extracted.

Using the phase time series from both MEG data,  $\phi_k^{(\text{MEG})}(t)$ , and phase time series generated by (6.1),  $\phi_k^{(\text{sim})}(t)$ , we calculated the pair-wise functional connectivity  $P^{(\cdot)}$  via the pair-wise phase synchronization in the form of the phase locking value (PLV)<sup>29</sup>. In its continuous form its matrix elements are defined as

$$P_{kl}^{(\cdot)} = \left| \frac{1}{T} \int_0^T e^{i(\phi_l^{(\cdot)}(t) - \phi_k^{(\cdot)}(t))} dt \right|. \quad (6.9)$$

Note that for  $P^{(\text{MEG})}$  we removed all individual samples that displayed relative phases in intervals  $I$  around 0 or  $\pm\pi$ , as for these samples true interaction and effects of volume conduction could not be disentangled<sup>382</sup>. The intervals  $I$  were defined as  $I = \pm I_w/2$ ,  $I_w = \Omega_c \cdot F_s$  where  $\Omega_c$  is the center frequency (in this case 10 Hz) and  $F_s$  the sampling frequency. In the simulations we calculated the PLV matrix according to (6.9) for each partition  $T_n$  and afterwards averaged the thus obtained twenty PLV matrices.

### 6.3.3 Synchronization

Although both  $R(t)$  and  $P_{kl}^{(\cdot)}$  are synchronization measures, they measure two qualitatively different forms of synchronization, which is the reason why they offer resolution in either the temporal or the spatial domain, respectively. Functional connectivity  $P_{kl}^{(\cdot)}$  measures temporal alignment of two phase time series  $\phi_k^{(\cdot)}(t)$ ,  $\phi_l^{(\cdot)}(t)$  by means of an averaging over time in (6.9), such that  $P_{kl}^{(\cdot)}$  provides resolution in the spatial domain, as indicated by the subscript  $kl$ . In contrast, from (6.7) it follows that calculating  $R(t)$  involves an average over  $k$ , i.e. over spatial coordinates, for each time instant  $t$ . This measure therefore provides resolution in time. That is,  $P_{kl}^{(\cdot)}$  measures temporal synchronization and offers spatial resolution, whereas for  $R(t)$  the opposite holds.

To gain more insight into the mechanisms responsible for the differential effects on synchronization behavior in the two models, we further considered the measures

$$\langle R(t) \rangle = \frac{1}{T} \int_0^T R(t) dt \quad \text{and} \quad \langle P^{(\cdot)} \rangle = \frac{1}{2N(N-1)} \sum_{k=1}^N \sum_{l=1}^{k-1} P_{kl}^{(\cdot)}, \quad (6.10)$$

that is,  $\langle R(t) \rangle$  is the temporal average<sup>[2]</sup> of the order parameter and  $\langle P^{(\cdot)} \rangle$  corresponds to the average magnitude of pair-wise phase synchronization over the

<sup>[2]</sup> In a strict sense, the time dependence of the temporal average  $\langle R(t) \rangle$  is redundant. Still, we keep this notation to demarcate this average from a spatial averaging over the network.

network.

**Statistics** Model performance in terms of replicating spatial correlation structure was measured by calculating the Pearson correlation coefficient  $\rho$  between the lower triangular entries of  $P^{(\text{sim})}$  and  $P^{(\text{MEG})}$ , where we excluded the main diagonal to omit spurious correlations. Since the sampling distribution of the  $P^{(\cdot)}$  entries are not normally distributed, we applied a Fisher z-transform before calculating the correlations. Restricting ourselves to the lower-diagonal entries was sufficient due to the symmetry in the phase coherence measure. We also excluded the diagonal entries to avoid spurious correlations resulting from the trivial value  $P_{kk}^{(\cdot)} = 1$ .

## 6.4 Results

### 6.4.1 Power-law behavior

Only the Freeman phase dynamics generated power laws and thus long-range temporal correlations in the evolution of phase synchronization for a broad range of parameter values. In Fig. 6.3a we display the results as function of coupling strength  $K$  and mean delay  $\tau_{kl}$ . Since for none of the parameter values the Wilson-Cowan phase model yielded power laws, we do not show the corresponding results for this model. The average value ( $\pm$  SD) of the scaling exponents was  $\alpha = 0.56 \pm 0.02$  for the Freeman model, which is significantly different from the surrogate results  $\alpha = 0.501 \pm 0.012$  ( $p < 10^{-4}$ ). In this average we only considered those realizations that were classified as power laws. This result qualitatively agreed with the observed value in MEG data ( $\alpha = 0.62$ ,<sup>372</sup>), as both indicate persistent behavior and thus long-range temporal correlations.

Fig. 6.3b provides examples of the log-log fluctuation plots for a single realization ( $K = 0.7$ ,  $\langle \tau \rangle = 9.4$ ) for both the Freeman and the Wilson-Cowan based model (upper and lower panel, respectively). The latter clearly deviated from linearity indicating that it did not scale as a power law. There the model selection procedure assigned a piece-wise linear function (dashed gray in Fig. 6.3b) to the  $F_i$  results confirming the deviation from linearity. Other parameter values yielded similar results for this model. The Freeman phase model yielded a power law with scaling exponent  $\alpha = 0.56$ ; Fig. 6.3b, upper panel.

### 6.4.2 Functional connectivity & synchronization

As said, we quantified functional connectivity as pair-wise phase synchronization of the phase variables  $\phi_k^{(\cdot)}$  following either the dynamics (6.1) indicated by the su-

perscript (sim) or (surr) or the instantaneous Hilbert phase extracted from source-reconstructed MEG data, superscript (MEG). Model performance was quantified by means of the Pearson correlation coefficient  $\rho$  between the  $P^{(\text{sim})}$  and  $P^{(\text{MEG})}$  matrices. Maximal  $P^{(\text{MEG})}$ - $P^{(\text{sim})}$  correlations were  $\rho = 0.56$  in both models for parameter values ( $K = 0.8, \langle \tau_{kl} \rangle = 9.4$ ) for the Freeman and ( $K = 0.7, \langle \tau_{kl} \rangle = 9.4$ ) for the Wilson-Cowan phase model (Fig. 6.4). This value is comparable to values reported in previous simulation studies<sup>45,383,384</sup>, but in contrast to the latter two studies no critical coupling strength was found at which model-data correlations collapse. The Freeman phase model appeared less sensitive to overall coupling strength than the Wilson-Cowan phase dynamics.

We mentioned above that  $R(t)$  and  $P_{kl}^{(\cdot)}$  measure two qualitatively different forms of synchronization. That  $P_{kl}^{(\cdot)}$  and  $R(t)$  indeed constitute two different aspects of synchronization is reflected in the results. Whereas the qualitative difference in the phase coupling matrices  $D_{kl}^{\text{WC}}$  and  $D_{kl}^{\text{F}}$  did affect the autocorrelation structure in  $R(t)$  (Fig. 6.3b), i.e. the Wilson-Cowan model did not resemble power-law behavior while the Freeman model did, it had only a minor influence on func-

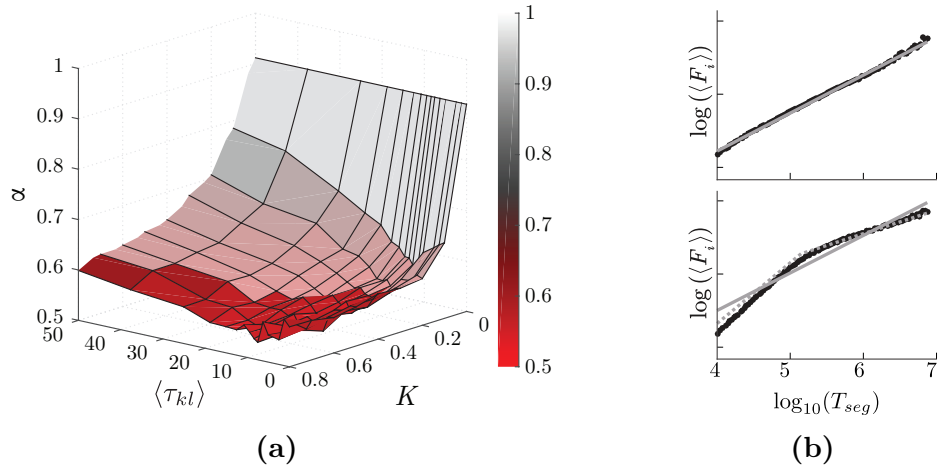


**Figure 6.3:** (a) DFA results for the  $R(t)$  autocorrelations generated by the Freeman phase model as a function of coupling strength  $K$  and mean delay  $\langle \tau_{kl} \rangle$  (in milliseconds). Colors code the values of the scaling exponents  $\alpha$  and are indicated by the colorbar. In all cases we observed persistent behavior in line with our empirical findings. (b) Examples of the fluctuation plots for the Freeman phase and Wilson-Cowan phase model (upper and lower panel, respectively) for  $K = 0.7; \langle \tau \rangle = 9.4$  together with the linear fits (gray) and the assigned model (dashed gray;  $f_\theta^{10}$  in (6.13)). The values on the x-axis are in milliseconds on a logarithmic scale (based on segment sizes of  $10^4$  to about  $10^{6.8}$  ms). On the vertical axis the expectation value of  $F_i$  is shown that was determined via the corresponding probability densities  $\tilde{p}_n$ ; see also Appendix 6.7.1. The Wilson-Cowan phase model did not result in scale-free correlations for any of the parameter values, with typical results for the log-log fluctuation plots similar to (b, lower panel). The DFA result for the Freeman phase model (b, upper panel) was classified as a power law with  $\alpha = 0.56$  – this was significantly different from mere random noise when tested against surrogates.

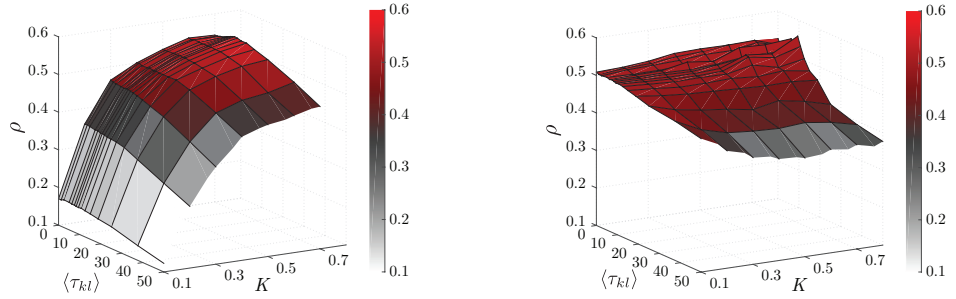


**Figure 6.4:** Pearson correlation values between the Fisher-z transformed  $P^S$  and  $P^{(\text{MEG})}$  functional connectivity matrices for the Wilson-Cowan phase model (left) and the Freeman phase model (right) as function of coupling  $K$  and mean delay  $\langle \tau_{kl} \rangle$  (milliseconds). The colored shading codes the correlation values and correspond to the colorbar on the right-hand side. The non-shaded area corresponds to the case in which the correlation was not significant. To respect weak coupling, the maximum coupling strength was set to  $K = 0.7$ . Results were averaged over ten realizations for every parameter combination.

tional connectivity in that in both cases a similar maximum correlation with the empirical functional connectivity could be achieved (Fig. 6.4).

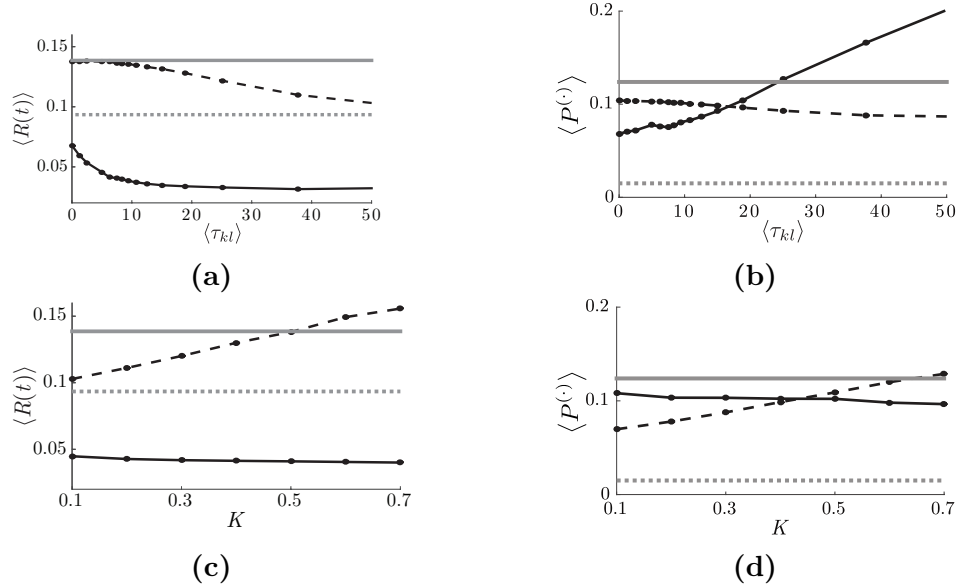


**Figure 6.5:** Mean values  $\langle R(t) \rangle$  as function of delay  $\langle \tau_{kl} \rangle$  in milliseconds (a) and coupling strength (c). Black solid lines correspond to the Freeman phase model results, dashed black lines to those for the Wilson-Cowan phase model. Empirical values are indicated by the solid gray lines, surrogate values by dashed gray lines. (b) and (d) show averaged functional connectivity  $\langle P^{(\cdot)} \rangle$  as function of delay (in milliseconds) and coupling strength respectively. Values are averaged over coupling values  $K = 0.1, \dots, 0.7$  when displayed as function of delay and over  $\langle \tau_{kl} \rangle = 0, \dots, 75$  as function over coupling strength.

The averaged measures  $\langle R(t) \rangle$  and  $\langle P^{(\cdot)} \rangle$  served to quantify differential effects on synchronization behavior in the two models. In Fig. 6.5 we display the results as function of both delay and coupling together with the surrogate and MEG data values. As expected from the repulsive coupling in the Freeman phase model, phases

were dispersed with  $\langle R(t) \rangle$  values significantly below surrogate values ( $p < 10^{-4}$ ). In contrast, the Wilson-Cowan model resulted in a partially synchronized state, which better corresponded to empirical findings (gray solid lines). In accordance with the results on  $P^{(\text{sim})}$ - $P^{(\text{MEG})}$  correlations, the qualitative difference between models in  $\langle R(t) \rangle$  did not transfer to pair-wise synchronization magnitude  $\langle P^{(\cdot)} \rangle$ . That is, both models yielded significantly larger  $\langle P^{(\cdot)} \rangle$  values than obtained for the surrogate data set ( $p < 10^{-4}$ ). This was the case despite the spatial desynchronization of the network of Freeman models.

This striking result led us to further assess the dynamics of both phase models by supplementary simulations with considerably larger coupling strengths. These coupling values were beyond the weak coupling assumption, rendering the validity of the phase dynamics for these parameter values questionable; see also Appendix of<sup>67</sup>. It did, however, provide additional insight into the dynamical properties of the phase model (6.1), especially with respect to the synchronizability of these networks. As shown in Fig. 6.6, the Freeman phase model did not allow for a (partially) synchronized state even for large coupling strength. In contrast, for sufficiently small delays the Wilson-Cowan phase model entered a fully synchronized state. This is consistent with the coupling structure of both models given by (6.6) and (6.3), respectively.

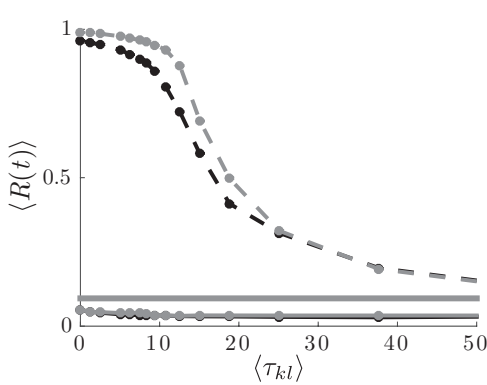


**Figure 6.6:** Mean values  $\langle R(t) \rangle$  for large coupling values equivalent to  $K = 5$  (black) and  $K = 10$  (gray) for the Freeman (solid) and Wilson-Cowan (dashed) phase models. The gray solid line denotes the surrogate  $\langle R \rangle$  value. While, consistent with the standard Kuramoto model strong coupling induced a synchronized state in the Wilson-Cowan phase dynamics, this was not the case for the Freeman phase model. The delay values  $\langle \tau_{kl} \rangle$  are in milliseconds.

Although the degree of phase synchronization of the Freeman phase model was consistent with a repulsively coupled phase oscillator network, the inhibitory connections in  $C_{kl}^F$  made a direct comparison with the repulsive cosine variant of the Kuramoto network non-trivial. Nevertheless we expected these models to show similar behavior, since the inhibitory connections were rather sparse compared to excitatory ones (Fig. 6.2). To test this, we also considered an alternative: a Freeman model that only comprised the excitatory part  $D_{kl}^F$ , i.e. the left upper block of this matrix. Results are summarized in Appendix of<sup>67</sup>. In a nutshell, these results indicate that the scale-free correlation structure displayed by the Freeman phase

model is caused by (the nature of) the coupling between the excitatory units. Its dynamics can thus be understood by considering the phase dynamics (6.1)/(6.6) as a repulsively coupled Kuramoto network.

## 6.5 Discussion

We contrasted the phase dynamics derived from two seminal neural mass models, representing the integrated contribution of large numbers of neurons within populations. Neural mass models have been used for modelling a wide range of neural phenomena, ranging from the origin of alpha band oscillations and evoked potentials<sup>71,74</sup> to the onset of pathological brain activity patterns such as epileptic seizures<sup>385,386</sup>. The phase reduction yielded phase oscillator networks that differed qualitatively in their coupling structure. Nevertheless, both models performed comparably well in the spatial domain as assessed by the  $P^{(\text{sim})}$ - $P^{(\text{MEG})}$  correlations, i.e. they resulted in similar pair-wise synchronization characteristics as featured by the experimentally observed data. A related finding has been reported by Messé and coworkers<sup>387</sup> who showed that model performance in terms of  $P$  correlations was relatively independent of nodal dynamics. Here it is important to realize that structural connectivity has a high predictive value for (empirical) functional connectivity<sup>44,61,388</sup>, which here could also be confirmed by correlating  $P_{kl}^{(\text{sim})}$  and  $S_{kl}$  (see Fig. 6.7). That is, both models generated functional connectivity structures that were highly correlated with  $S_{kl}$ . This same notion forms the basis for the general finding in RSN modelling studies that optimal model performance occurs near the critical point<sup>355</sup>. The critical slowing down around the bifurcation point allows for a maximal reflection of  $S_{kl}$  into functional connectivity<sup>383</sup>. We showed that the reflection of structural into functional connectivity may occur in two models generating qualitatively different dynamics. This indicates that an inference about the dynamical regime, in particular regarding criticality, on basis of the  $P$  correlations alone is non-trivial – at least for the phase oscillator models considered here; see also<sup>389</sup> for a related conclusion. Whether this extends to more complex networks consisting of detailed neuronal models is beyond the scope of the current study.

In contrast to the pair-wise phase synchronization (PLV), the models differed qualitatively regarding the phase synchronization quantified by the phase coherence  $R(t)$ . In particular, only the Freeman phase model displayed scale-free autocorrelation structures observed in data, revealing complex characteristics in its dynamics. The values of the scaling exponents ( $\alpha > 0.5$ ) revealed the presence of long-range temporal correlations, which qualitatively agrees with the correlation structures reported in brain activity<sup>369–372</sup>.

In the Kuramoto model<sup>351</sup>, critical coupling strength is the value of the coupling parameter  $K$  for which the desynchronized state loses stability and the system enters a (partially) synchronized regime<sup>272</sup>. Here, synchronization is quantified by  $R(t)$ , and hence measures spatial synchronization in the network. Functional connectivity, however, is determined by the temporal alignment of, in the present study, phase signals  $\phi_l(t)$ ,  $\phi_k(t)$  and thus reflects a fundamentally different form of synchronization. We showed that these forms of synchronization were affected differently by the generating dynamics: pair-wise synchronization largely agreed between models, whereas  $R(t)$  did not. The average value and the autocorrelation structure of  $R(t)$  were affected by the qualitative difference in coupling structure between models.

The Wilson-Cowan phase model displayed a transition into a fully synchronized state for sufficiently large coupling; see Fig. 6.6. Combined with the partial synchronization displayed in Figs. 6.5c and 6.5a, this indicates that the Wilson-Cowan model for  $K = [0.1, 0.7]$  is located at the onset of synchronization, i.e. in its critical regime. Although associated with critical dynamics<sup>366</sup>, we did not observe power-law correlation structures in this model. Similar findings have been reported<sup>390</sup> for phase difference time series  $\Phi_{kl}(t) = \phi_l(t) - \phi_k(t)$ , not only in case of the standard uniformly coupled Kuramoto network, but also for a more biologically plausible model incorporating a DTI derived coupling matrix and distance-related delays *see also*<sup>43</sup>. However, long-range temporal correlations were observed in  $\Phi_{kl}(t)$  as well as  $R(t)$  in resting state brain activity in<sup>371</sup> and<sup>372</sup>, respectively. This suggests that the critical regime in Kuramoto-type networks has different properties compared to the dynamical regime of the resting brain, be the latter critical or not.

The desynchronized state for the repulsive coupling in the Freeman phase model (6.6) was consistent with various analytical results<sup>91,375,376,391</sup>; cf. Fig. 6.6. A desynchronized network, however, does not exclude complex dynamics as reflected in the presence of scale-free autocorrelations in the Freeman model. The topology of this model may be regarded as related to phase oscillator networks consisting of so-called conformists and contrarians studied in<sup>376,392</sup>. The latter showed that, even for small networks, a variety of complex dynamics including chaos may occur. A similar finding has recently been reported by Sadilek and Thurner<sup>48</sup>, who studied a two-layered Kuramoto network derived from the same Wilson-Cowan dynamics as considered here. They identified a chaotic region with the largest Lyapunov exponents arising at the boundary of synchronization, i.e. in the critical regime. By changing the value of the delay parameter range, this model could switch between a synchronized and desynchronized state through a bifurcation.

Despite the fact that the model in<sup>48</sup> and the Wilson-Cowan phase model in the

current study were derived from the same dynamics (6.2), both networks are quite different in their topology and in their delay structure. The model in<sup>48</sup> contained an excitatory and inhibitory layer, whereas this was not the case in (6.1)/(6.3). The reason for this discrepancy is that Sadilek and Thurner described the oscillatory trajectory solely by the phase variable, whereas we also took amplitude into account <sup>see also</sup><sup>41,42</sup>. As a consequence the reduction in dimensionality in the Wilson-Cowan phase description that we found when deriving (6.1)/(6.3) from (6.2), did not occur in<sup>48</sup>. As a consequence, the inhibitory connections in the neural mass dynamics were retained in the phase model in that study. A second distinction between both models is the delay structure. In both models (6.2) and (6.4) we regarded the delays between excitatory and inhibitory units to be negligible compared to those between excitatory units, as these connections represented long-range connections subject to finite conduction delays. In contrast, the delay parameter in<sup>48</sup> quantified the delay between excitatory and inhibitory units and excitatory-excitatory delays were assumed to be zero.

With the two models considered here we could explain two profound phenomena observed in brain activity. The Freeman phase model generated the type of auto-correlation structures observed in brain activity, but its coupling structure resulted in a desynchronized network, i.e. low  $R(t)$  values, that did not agree with MEG recordings (see Fig. 6.5). Additionally it could not account for a transition into partially synchronized states, let alone the (pathological) fully synchronized one. In contrast, the Wilson-Cowan phase model could cover these synchronization phenomena, but it did not show the complex dynamics associated with (resting state) brain activity. The fundamental difference in coupling structure, combined with the analytical results discussed above, suggests that these dynamical properties are mutually exclusive for the models considered here.

We are left with the question, whether one of these models could be modified in such a way that it can exhibit both phenomena. First we have to admit that our DTI-based construction of anatomy and delays is a clear simplification of the ‘real’ structural connectivity. Adjusting this may have major consequences for the resulting phase dynamics. The aforementioned study by Sadilek and Thurner<sup>48</sup> gives an indication for this, since they showed that a connectivity structure allowing for comparatively dense inhibitory connectivity yielded complex dynamics in the form of chaos. Interestingly, in other types of models inhibitory connections have been shown to be determinants in generating critical states<sup>393–395</sup> and for information transfer<sup>365,396</sup>. However, these results reflected the dynamics within a neural population rather than the dynamics in the global cortical network considered here. Neurophysiological findings indicate that the long-range connections between areas are excitatory with inhibitory connections only providing local in-

hibitory feedback<sup>349,397,398</sup>. From such a neurophysiological perspective we regard our coupling structure to be more realistic in the context of global cortical networks than the one in<sup>48</sup>. Thus, although incorporating inhibitory connections could potentially merge the dynamical properties of the Wilson-Cowan and Freeman phase descriptions, such a coupling structure would violate its neurophysiological plausibility and thus the appeal of deriving these networks from a neural mass dynamics. This is not to say that the network in<sup>48</sup> is unrealistic from a neurophysiological point-of-view, but both the connectivity and the delay structure may be more representative of local interactions within a cortical region than of global large-scale brain networks considered here.

As an alternative one may extend the models to the stochastic regime, e.g., by adding noise to the firing rate or membrane dynamics. Dynamic noise is known for its capacity to alter the correlation structure of global outcome variables like the order parameter  $R(t)$ . Dynamic noise can also influence synchronization patterns and that not only by causing phase diffusion or shifting the critical point at which synchronization may emerge; in the case of common noise, it may even induce synchronization. A more detailed discussion of network dynamics under impact of random fluctuations, however, is far beyond the scope of the current study.

Delays in networks can lead to very complex dynamics. Since we considered the dynamics of the relative phases that were assumed to evolve slowly with respect to the oscillation frequency  $\Omega$ , the delays between neural masses mapped to mere phase shifts in (6.1). Therefore a comparison of the networks in which delays explicitly influence the phase interactions, such as in<sup>43</sup> and the analytical results by<sup>399–401</sup>, cannot be readily made. In the case of delayed phase interactions, however, scale-free correlations could not be observed in a phase oscillator network incorporating a similar coupling scheme to the one employed here<sup>43,390</sup>. Taken together, our findings suggest that phase oscillator networks without dense inhibitory coupling throughout the whole network, are not capable of showing the entire dynamic spectrum of resting state brain activity. Whether this limitation is posed by the phase oscillator network itself or the consequence of collapsing population dynamics onto a low-dimensional description in the form of a neural mass model remains to be seen.

## 6.6 Conclusion

We illustrated some challenges when deriving and interpreting the phase dynamics of neural mass models. As an example we employed networks of Wilson-Cowan firing rate models and networks of voltage-based Freeman models. The phase dynamics of these models differed qualitatively by means of an attractive coupling

in the first and a repulsive coupling in the latter. While both phase dynamics did cover the functional connectivity observed in resting state activity, they failed to describe two pivotal dynamical features that have been reported in many experimental studies: (1) a partial phase synchrony with a possibility of a transition towards either a desynchronized or a (fully) synchronized state; (2) long-term autocorrelations indicative of a scale-free temporal dynamics of phase synchronization. The phase dynamics of the Freeman model exhibited scale-free behavior and the Wilson-Cowan phase model could switch into a (partially) synchronized state. However, none of the phase models allowed for describing both dynamical features in unison.

There is a range of possibilities to modify these models, e.g., by misbalancing excitatory and inhibitory units or by introducing delays that are biologically less plausible than the ones we chose. Alternatively, one may consider the phase dynamics further away from the onset of oscillations (Hopf-bifurcation) that limits analytic approaches. By either of these adjustments one may lose the direct link to the structural connectivity structure. In our example, neither of the phase dynamics can capture the full dynamical spectrum observed in cortical activity. We have to conclude that modeling phase synchronization and, in particular, inferring characteristics of its underlying neural mass dynamics require great care.

**Acknowledgments** We would like to thank Mark Woolrich for his contribution to data acquisition and analysis and the fruitful discussion about interpretation of our findings.

## 6.7 Appendix

### 6.7.1 Detrended fluctuation analysis with model comparison

To assess the temporal character of  $\phi_k^{(\cdot)}$ , we determined the Kuramoto order parameter

$$R(t) = \frac{1}{N} \left| \sum_{k=1}^N e^{i\phi_k^{(\cdot)}(t)} \right| .$$

That is, we only used the excitatory phases to calculate  $R(t)$ . In analogy with the procedure for empirical data discussed in<sup>372</sup>, we z-scored the  $R(t)$  time series, such that differences in scaling behavior could not be attributed to differences in the stationary statistics of the  $R(t)$  time series. We resampled  $R(t)$  to 250 Hz to match the sampling frequency of the data as well as to obtain an equally spaced time axis necessary for the detrended fluctuation analysis (DFA)<sup>378</sup> used

to characterize the  $R(t)$  autocorrelation structure. To assess the presence of scale-free autocorrelations in  $R(t)$ , we used a modified version of the conventional DFA procedure. We shortly summarize this below; for a detailed explanation we refer to<sup>379</sup>.

In line with the outline around (6.8), consider (the cumulative sum of) a time series  $Y(t)$ ,  $t = 1, \dots, N$  that is divided into  $\lfloor N/n \rfloor$  non-overlapping segments  $Y_i(t)$  of length  $n$  with  $t = 1, \dots, n$ . Upon removing the linear trend  $Y_i^{\text{trend}}(t)$  in segment  $i$ , the fluctuations  $F_i(n)$  corresponding to window length  $n$  are given by

$$F_i(n) = \sqrt{\frac{1}{n} \sum_{t=1}^n (Y_i(t) - Y_i^{\text{trend}}(t))^2}$$

In the conventional DFA procedure one calculates the average fluctuation magnitudes

$$\bar{F}_i(n) = \sqrt{\frac{1}{\lfloor N/n \rfloor} \sum_{i=1}^{\lfloor N/n \rfloor} F_i^2(n)}.$$

We regarded  $\{F_i\}$  as a set of  $\lfloor N/n \rfloor$  realizations of the ‘stochastic’ variable  $F_i$  and determined its probability density  $p_n(F_i)$ . When these fluctuations scale as a power law, i.e.  $F_i(n \cdot c) = n^\alpha F_i(c)$ , we find that  $\log(F_i(n \cdot c)) = \alpha \log(n) + \log(F_i(c))$ . Hence, under a transformation to logarithmic coordinates  $\tilde{n} = \log(n)$ ,  $\tilde{F}_i = \log(F_i)$ , a power law appears as a linear relationship. To identify whether power-law scaling was present we fitted a set of candidate models  $f_\theta(\tilde{n})$  parametrized by the set  $\theta$ . The linear model corresponding to power-law scaling was contained in this set, such that we could compare it against alternatives. For this comparison we defined the log-likelihood function as

$$\ln(\mathcal{L}(\theta|f_\theta)) = \ln \left( \prod_n \tilde{p}_n(f_\theta) \right) = \sum_n \ln \left( \tilde{p}_n(f_\theta) \right). \quad (6.11)$$

where  $\tilde{p}_n$  denotes the probability density  $p_n$  transformed to the double logarithmic coordinate system. In (6.11) one evaluates for each  $n$  the probability density  $\tilde{p}$  at model value  $f_\theta(\tilde{n})$  and defines the likelihood function as its product. The purpose of calculating  $\mathcal{L}$  was to be able to use of the Bayesian Information criterion (BIC) defined as

$$\text{BIC} = -2 \ln(\mathcal{L}_{\max}) + k \ln(M) \quad (6.12)$$

to compare different models  $f_\theta$ . In (6.12)  $M$  denotes the number of different interval sizes  $n$ ,  $k$  the number of parameters in the model (the size of the set  $\theta$ )

and  $\mathcal{L}_{\max}$  the maximized likelihood with respect to a particular model  $f_{\theta}^{(\cdot)}$ . The model resulting in a minimal value of the BIC compared to alternative models was considered to be the optimal model; providing the optimal compromise between goodness-of-fit and parsimony<sup>380</sup>. The set of candidate models was given by a combination of polynomial forms including the sought-for linear model. We further included an alternative exponential model fit as well as the form resulting from an Ornstein-Uhlenbeck process and, last but not least, a piece-wise linear model:

$$\begin{aligned}
 f_{\theta}^1(x) &= \theta_1 + \theta_2 x & f_{\theta}^2(x) &= \theta_1 + \theta_2 x^2 \\
 f_{\theta}^3(x) &= \theta_1 + \theta_2 x + \theta_3 x^2 & f_{\theta}^4(x) &= \theta_1 + \theta_2 x^3 \\
 f_{\theta}^5(x) &= \theta_1 + \theta_2 x + \theta_3 x^3 & f_{\theta}^6(x) &= \theta_1 + \theta_2 x^2 + \theta_3 x^3 \\
 f_{\theta}^7(x) &= \theta_1 + \theta_2 x + \theta_3 x^2 + \theta_4 x^3 & f_{\theta}^8(x) &= \theta_1 + \theta_2 e^{\theta_3 x} \\
 f_{\theta}^9(x) &= \theta_1 + \frac{1}{\ln(10)} \ln \left( \theta_1 \left( 1 - e^{-\theta_2 e^{\ln(10)x}} \right) \right) \\
 f_{\theta}^{10}(x) &= \begin{cases} \theta_1 + \theta_2 x & x \leq \theta_4 \\ C + \theta_3 x & x > \theta_4 \end{cases} \quad \text{with } C = \theta_1 + (\theta_2 - \theta_3)\theta_4 .
 \end{aligned} \tag{6.13}$$

The scaling exponent  $\alpha$  was determined as the slope of the linear relationship  $f_{\theta}$ , i.e.  $\alpha = \theta_2$  in  $f_{\theta}^1(x)$ . When reporting mean  $\alpha$  values, we only use those  $\alpha$  values obtained in realizations for which the BIC indicated power-law scaling. We also calculated the finite-size corrected Akaike information criterion  $AIC_c = -2 \ln \mathcal{L}_{\max} + 2k + \frac{2k(k+1)}{M-k-1}$  which led to similar results (not shown). We determined  $F_i$  for the range of interval sizes  $n = [10, N/10]$ , where  $N$  denotes the length of the time series, here amounting to  $300 \cdot 250 = 7.5 \cdot 10^4$  samples.

### 6.7.2 Correlating functional and structural connectivity

We computed the correlation between  $P_{kl}^{(\text{sim})}$  and  $S_{kl}$  to show that both models generated functional connectivity structures that were highly correlated with  $S_{kl}$ ; see Fig. 6.7.

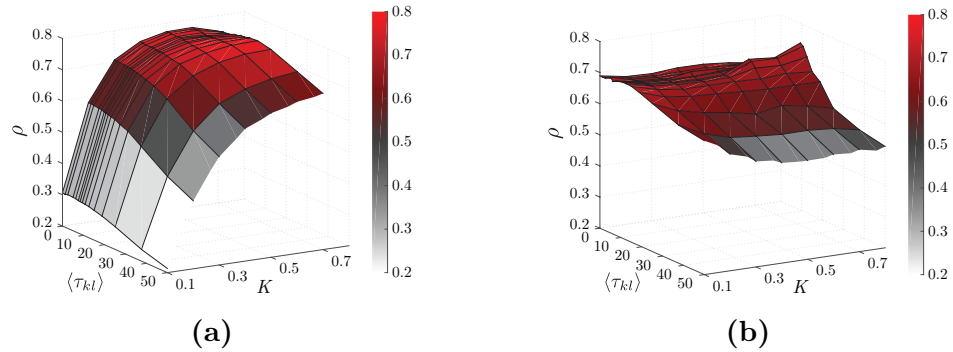


**Figure 6.7:** Pearson correlation values between the  $P^S$  and  $S_{kl}$  matrices for (a) the Wilson-Cowan phase model and (b) the Freeman phase model as function of coupling strength  $K$  and mean delay  $\langle \tau_{kl} \rangle$  (in milliseconds). The colors code the correlation values and correspond to the colorbar at the right. Correlation values were averaged over ten realizations for each parameter combination. Note the similarity of this figure with Fig. 6.4 suggesting that the reflection of  $S_{kl}$  is an important determinant in high functional connectivity correlations <sup>cf. 402</sup>.

# CHAPTER 7

## Epilogue

*Synchronous, coherent interaction is key –*

Phase synchronization is a fundamental concept to assess and quantify coherent network activity. This dissertation aimed at a thorough introduction to analyzing the phase dynamics of oscillatory networks. The human brain represents an important example of a complex oscillatory network. It therefore provides an ideal playground for mathematical and computational neuroscientists where we can apply ideas and tools from nonlinear dynamics and complex systems theories to model the experimentally observed, collective dynamics that emerge from the interplay of a multitude of neurons. In particular, I focused on populations of neurons that exhibit rhythmic macroscopic behavior and investigated the mutual interaction of these oscillatory neural populations, typically represented as coupled neural masses.

In *Chapter 1* I introduced the concept of synchronization in the realm of neural dynamics, and addressed the notion of phase synchronization as a powerful means to describe the interplay of neuronal oscillations and coherent brain network activity. *Chapter 2* presents an extensive overview of phase reduction techniques. I explicated both numerical and analytical techniques to derive the phase dynamics of oscillator networks. Moreover, I complemented the overview with an outline of normal form reductions, which form an integral part of analytical phase reduction techniques. In *Chapter 3* I subsequently illustrated the different phase reductions along two seminal examples of oscillator networks. The first part dealt with a network of identical Brusselators, which is an exemplary chemical oscillator. The Brusselator model displays a broad spectrum of complex dynamics and is at the same time mathematically tractable. It was therefore perfectly suited for testing how phase reduction techniques differ when allowing for more realistic, complex and nonlinear coupling schemes. The second part focused on the phase reduction of a network of identical Wilson-Cowan neural masses, which can be considered a raw model for introducing biophysical realism in macroscopic neural dynamics. I concluded that analytic phase reduction techniques provide a parametrization of the phase dynamics in terms of the underlying model parameters. Close to bifurcation boundaries, the analytically reduced phase models perform equally well as those derived numerically. Further away from bifurcation boundaries, numerical reduction techniques outperform analytic approaches, however at the price for computationally expensive scanning of the parameter regions in order to gain intuition about the influence of particular parameters on the collective phase dynamics.

In *Chapters 4* and *5* I briefly left a rigorous phase reduction aside and concentrated on the collective dynamics of coupled phase oscillators. In *Chapter 4* I elucidated the effects of network-network and cross-frequency interactions. I found that the phase synchronization properties of two coupled symmetric populations of

phase oscillators coincide with those of a single population whose oscillators follow a bimodal frequency distribution. Following the Ott-Antonsen theory, I was able to exactly describe the low-dimensional collective dynamics of the networks. In *Chapter 5* I extended the existing Ott-Antonsen theory to parameter-dependent oscillatory systems. An important example of this class of oscillators is the theta neuron, which corresponds to the quadratic integrate-and-fire model, resembling a spiking neuron. I illustrated the proof along a network of quadratic integrate-and-fire neurons and thus put a broader applicability of the Ott-Antonsen theory on mathematically firm ground.

Eventually, I returned to reduced phase models in *Chapter 6* and investigated the phase dynamics of Wilson-Cowan and Freeman neural mass models. Given experimental MEG data displaying large-scale brain activity at the edge of criticality, the aim was to model two corresponding but distinct dynamical features, namely partial phase synchronization and scale-free temporal dynamics. The Freeman phase model exhibited scale-free behavior, whereas the Wilson-Cowan phase model showed a transition to partial synchrony. However, neither of the reduced phase models could capture the full dynamical spectrum of cortical oscillatory activity.

We are left to discuss the implications of the foregoing studies, including their implicated results as well as their relevance for neuroscience. In the following *Section 7.1* I will briefly revisit the research questions initially stated in *Section 1.3*. I will address general aspects of phase reductions in *Section 7.2*, shed light on the predictive power of phase models in *Section 7.3*, and place the previously addressed neural mass models in context of other frequently used neural oscillators in *Section 7.4*, before I conclude with a brief outlook.

## 7.1 Revisiting the research questions

The first part of the dissertation arguably sought for an answer to the question,

- *What is the best way to distill the phase dynamics of a complex oscillatory network?*

There exist a short and a long answer. The long one follows the reasoning of *Chapter 2*. The mathematical theory of different phase reduction techniques and their comparison have been illustrated in various applications in *Chapter 3*. The short answer to the research question is: there is no easy solution. Determining an accurate phase model that captures the (phase) dynamics of a complex oscillatory network is a challenge. Although sophisticated mathematical theory and numerical analysis techniques exist, the main problem is that there is no ground truth

of exact phase dynamics of complex oscillatory networks. Despite the seemingly philosophical touch, the statement builds on the fact that phase (and amplitude) variables are essentially relativistic observables and no absolute properties of (complex) oscillatory behavior. Yet, within the realm of weakly coupled limit-cycle oscillators the phase description becomes instrumental in characterizing the state of each oscillator. From this perspective, phase reduction techniques as outlined in *Chapter 2* are crucial in that they enable us to properly derive a phase model that corresponds to the actual phase dynamics. While both analytical and numerical phase reduction techniques have their respective pros and cons, I suggest the following: The interplay between analytics and numerics is key to validate the phase model. Analytic intuition should be combined with numerical accuracy and the phase dynamics can be accurately distilled from the underlying network model.

- *Under which circumstances can a low-dimensional description capture the collective dynamics of complex phase oscillator networks?*

Here, I refer to *Chapters 4* and *5* for all mathematical details. Network-inherent properties, such as an underlying connectivity structure or distributed parameters across the nodes, specify the complexity of a network, and thus shape the collective dynamics. The Ott-Antonsen ansatz had been successfully introduced to capture the exact low-dimensional macroscopic dynamics of phase oscillator networks, whose major complexity was confined to a smooth distribution of natural frequencies<sup>81</sup>. A first more complex situation arose by allowing for multiple peaks in the frequency distribution function<sup>271</sup>. The low-dimensional description of the corresponding collective dynamics capitalized on introducing local (Kuramoto) order parameters around the peaks of the distribution. These local quantities suggested to disentangle the full network into interacting but separate populations of phase oscillators. In *Chapters 4* I rigorously proved that this view can indeed be justified, at least for a particularly symmetric case. Seen from another perspective, my proof points at a way how network-network interactions can be summarized within a single (bigger) network that allows for casting the collective dynamics onto the low-dimensional Ott-Antonsen manifold.

Further examples of complex phase oscillator networks whose collective dynamics are low-dimensional and that can be retrieved along the Ott-Antonsen ansatz, were addressed in *Chapter 5*. Buzzword here is “parameter-dependent oscillatory systems”. Upon a reformulation into a particular phase model whose phase interaction function is dominated by first harmonics only, I simplified the nodal dynamics of the network by introducing appropriate parameter distributions or by identifying additional dynamics as time-varying parameters. In this way, I could set the applicability of the Ott-Antonsen theory on firm ground and use low-dimensional

systems of differential equations to describe the exact collective dynamics of networks of quadratic integrate-and-fire (aka theta) neurons, of pulse-coupled Winfree oscillators, of limit-cycle oscillators with shear, as well as of networks with particular connectivity structures, external forcing, and time delay.

- *Do phase oscillator networks cover seminal characteristics of experimental data from the cortex?*

In order to find a satisfying and comprehensive answer, the utility of phase models has to be judged critically and for their predictive power, which will be addressed in more detail in *Section 7.3*. *Chapter 6* provided a suitable scenario to test whether neurophysiologically sophisticated phase models can capture the complex dynamical notions of experimental data. In short, the phase time series of resting state MEG data under investigation featured a dynamical spectrum that could not be reflected in phase models reduced from seminal neural mass descriptions. The reasons for the apparent gap between the recorded data and the simulated phase dynamics can only be hypothesized. Considering the nature of the available data, one possible reason comprises frequency and amplitude modulations that are inherent in the experimental data but ignored in the phase model. Allowing for time variability in the phase model can be a first step to bridge the gap to data.

## 7.2 Networks of complex neural oscillators and phase reductions

Phase reduction is a powerful method to simplify the analysis of a network of interacting oscillatory systems. While the systems' dynamics are governed by nonlinear and often high-dimensional differential equations, a phase reduction generally allows for a dynamical description of the network's nodes in terms of one-dimensional phase variables only. Unfortunately, a unique phase reduction does not exist and there is no straightforward recipe, either, along which *the* phase dynamics should be reduced. Instead, one has to choose from a variety of different phase reduction techniques, all of which have their advantages and disadvantages. This renders the notion of phase dynamics somewhat ambiguous. As has been shown in *Section 2*, for any chosen technique, the reduced phase dynamics have to be considered with care. With the present inventory of phase reduction techniques we pointed out similarities and differences between techniques. A common basis that all techniques share is the theory of weakly coupled oscillators. The system has to exhibit stable limit-cycle oscillations without the (external) influence or perturbation through coupling or noise. And, the coupling strength has to be sufficiently weak so that

the full dynamics remain close to the unperturbed limit cycles, and amplitude effects can be neglected. Under these assumptions, a comparison between reduction techniques is possible, which can generally be grouped in analytic, and numerical approaches.

While numerical approaches can be used to reduce phase dynamics for almost every kind of oscillatory dynamics, analytic approaches heavily rely on emerging oscillations via a supercritical Hopf bifurcation. In this case the analytic phase reduction splits into a two-step reduction: a normal form reduction brings the original dynamics in Hopf normal form and, subsequently, phase reduction extracts the corresponding phase dynamics. Once a system has been brought into Hopf normal form, all phase reduction techniques, including numerical approaches, result in the same reduced phase model, at least, in leading order. Differences between analytic approaches do occur, though, due to different normal form reductions. Their accuracy depends on the distance to the Hopf bifurcation point. Very close to this point, the reduced phase models coincide almost perfectly for different analytic and numerical reduction techniques.

Analytic techniques have the advantage that they allow for a parametrization of the reduced phase model in terms of the original model parameters. Numerical reduction techniques, by contrast, remain “black boxes”, at least to some degree, and the link between phase model parameters and original parameters may remain opaque. For larger distances from the bifurcation point, however, numerical techniques clearly outperform the analytic ones. A combination of both analytic and numerical reduction techniques hence appears unavoidable when looking for a thorough picture of the emerging collective dynamics of interacting oscillators.

A brief comment is at place about the Haken approach, also coined ad-hoc averaging in *Chapter 3*, and upon which the phase descriptions in *Chapter 6* dwell. This method clearly stands out for its pragmatic applicability. In a straightforward way, it allows to express the phase model parameters in terms of the original dynamics. Moreover, it avoids the assumptions of the theory for weakly coupled oscillators. As long as small-amplitude oscillatory dynamics are of (or can be transformed into) circular shape, it is possible to (semi-) analytically reduce the corresponding phase dynamics – no matter whether these oscillations have emerged through a supercritical Hopf, any other or no bifurcation at all, whether they are induced by coupling strength or coupling direction, or induced by noise or delay. This approach may lack mathematical rigor, and the reduced phase dynamics have to be compared to the actual evolution of the phases. However, it can hint at the role of particular model parameters on the network dynamics, which numerical techniques can only achieve by a computationally expensive scanning of the parameter space.

Last but not least, a thorough comparison between different methodological approaches usually implies a quantitative account to what extent these techniques generate qualitatively equivalent results, which, in our case, are the resulting phase models. It would be desirable to present particular error estimates for each technique. When based on the original model parameters, it might be possible to set upper bounds beyond which a reduction technique can no longer be applied to determine the corresponding phase dynamics at a given (small) error. Such estimates are, however, few and far between. We hope that our inventory in *Chapter 3* will serve to establish this long-needed error estimation.

## 7.3 The predictive power and limitations of (reduced) phase models

The reduction of a network of interacting oscillatory systems into a network of coupled phase oscillators serves to facilitate the analysis of the collective, network dynamics. In general, the oscillatory dynamics per node can be quite complex and their evolution may be governed by a high-dimensional system of coupled nonlinear differential equations. Phase reduction techniques allow to express the state of each node in terms of a single, one-dimensional phase variable. The resulting phase model thus reduces the dimensionality of the network dynamics to great extent. But, how powerful is such a phase model? Obviously, this question is connected to the first research question above. Yet, a satisfying answer must also address the predictive power of phase models in general, and of reduced phase models in particular. Whether a comprehensive observable of the collective dynamics can be expressed in terms of the phase dynamics will be challenged in *sub-section 7.3.1*. And whether phase models can be used to describe experimental data is in the focus of *sub-section 7.3.2*.

**Is a phase model a good model?** A phase model, like any other model, is neither good nor bad. A model cannot be good, or bad. It is either descriptive, or it is not. A model can be more descriptive, or less. That is, it is more or less accurate in a particular parameter region. And, it may uphold this accuracy over a larger or smaller parameter region. Phase models capture the phase dynamics of oscillatory systems. Not more, and not less. They gain their predictive power by allowing for an accurate description of the phase dynamics of the underlying system, and thus by predicting possible collective behavior of coupled oscillators based on the dynamics of the phase relationships between them.

**Predictive power of phase models** Usefulness and strength of a model is, in general, judged by its predictive power. In view of this dissertation, the question arises whether a simplified phase model can still provide an accurate description of the oscillatory system under investigation. Quantifying the accuracy, and thus the predictive power, of a phase model can be a challenge. It becomes particularly difficult if such an assessment is supposed to be both quantitative and qualitative. Qualitatively, an accurate phase model has to correctly describe the different dynamical regimes of the underlying model as well as the transitions from one regime to another. Quantitatively, an accurate phase model reflects the various qualitative features of the underlying model, and, at the same time, numerical differences between the respective observables of the original and the approximate models converge to zero. A qualitative and quantitative assessment of the phase model is especially important to determine a certain (parameter) range of validity and applicability. Within this range, the model can be applied and is accurate up to some error bounds. Beyond this range, however, it may lose its validity in a strict sense and the actual dynamics diverge from predictions by the reduced or simplified model.

As an example, I consider the case of a finite network of slightly heterogeneous, nonlinear but smooth oscillators that are coupled with respect to an adjacency matrix  $C$ . If these oscillations emerged through a supercritical Hopf bifurcation, then for parameter values close to the Hopf point it seems reasonable to approximate the network by coupled Kuramoto phase oscillators as long as the coupling is sufficiently weak. There are, however, three main concerns that have to be considered in order to predict network behavior by relying on the extensive literature about the Kuramoto model.

1) How important is *structural connectivity*? If the adjacency matrix  $C$  is sufficiently dense, one may approximate it with an all-to-all coupling scheme without losing too much accuracy. Obviously, *sufficiently* and *too much* are always relative and can only be quantified from case to case. The matrix  $C$ , however, can also entail more complex connectivity structures, such as network modularity or small-worldness. In the former case, it may be possible to extract modular structures and define interacting subpopulations that have similar internal properties. We investigated a special, symmetric case of interacting subpopulations in *Chapter 4*. For small-world and more realistic brain connectivity structures, simplifying assumptions have to be made with care. The underlying network topology may obscure other properties of the phase model and lead to false conclusions, see also the Discussion of *Chapter 3*. In either case, the qualitative predictions of the phase model may diverge from the actual network dynamics.

2) How important is *heterogeneity*? As has been briefly addressed in *Section 3.3*,

there exist powerful techniques that allow for an exact low-dimensional description of the collective dynamics of a network, such as the Watanabe-Strogatz theory<sup>80</sup> or the Ott-Antonsen theory<sup>81</sup>, see also<sup>178</sup>. Both theories rely on a particular distribution of the heterogeneity (up to the limit of identical oscillators). The heterogeneity is usually expressed in the natural frequency terms of the coupled oscillators, but can also emerge through other parameters, see *Chapter 5*. If the heterogeneity can be approximated by a distribution function admissible to either of the theories, then explicit equations for the evolution of the network's observables can be derived. This makes not only a qualitative prediction of the network behavior possible, but also a quantitative comparison to the actual dynamics. Let me remark that also multimodal distributions are admissible. Given the results on the interchangeability of a bimodal network formulation vis-à-vis a network-network formulation from *Chapter 4*, the theories above apply also to interacting populations of oscillators.

3) How important is *network size*? Next to the assumptions on network heterogeneity, a rigorous application of the Ott-Antonsen theory dwells on a fairly large network. In fact, the theory is valid in the continuum limit when the network size tends to infinity. This assumption is far from realistic for any biological network, and even though the number of neurons in the human brain is reasonably large, it still is finite. The literature suggest various approaches to determine so-called finite size fluctuations around the exact macroscopic dynamics whose evolution is governed by a few differential equations that are, strictly speaking, only valid for infinitely many oscillators<sup>180–184</sup>. These fluctuations introduce a seemingly stochastic character into the phase dynamics, which may clash with the deterministic nature of the actual network dynamics. A way out can be to apply some temporal averaging. But then averages may remove important transient behavior. In consequence, a compromise between a quantitative and a qualitative fit of the macroscopic dynamics has to be found.

In summary, phase models provide the opportunity to express the collective network dynamics in a low-dimensional system of differential equations. Some basic assumptions on the structural connectivity and the heterogeneity of the underlying oscillatory network model have to be fulfilled, however, to allow for an approximation of the network by such a phase model. The predictions of the phase models can then be tested against the actual network dynamics and the dynamics of the respective observables can be compared both qualitatively and quantitatively. In this way, an assessment of the phase model's predictive power becomes feasible.

**Predictive power of reduced phase models** The reduction of a meaningful phase model along the reduction techniques presented in *Chapter 2* builds on a

handful of assumptions. As mentioned above, most reduction techniques rely on the theory of weakly coupled oscillators<sup>78</sup>. Recently, phase reduction techniques have been refined and extended so that the assumptions inherent to the theory of weakly coupled oscillators can be loosened to a certain degree, see *Section 3.3*. Still, the closeness (in parameter space) to a particular bifurcation boundary is a key ingredient for an accurate analytic phase reduction. In fact, bifurcation boundaries explicitly delimit the range of applicability of a mathematically sound phase reduction. Analytic phase reductions also provide the possibility to quantify the accuracy of the phase dynamics at each node. This allows for a more detailed assessment of macroscopic observables, and it becomes possible to trace back whether particular parameters of the underlying network model are responsible for a possible discrepancy between macroscopic observables.

### 7.3.1 Observables

Closely linked to the question of predictive power of a phase model is that of the kind of predictions a (reduced) phase model is capable of. There are some observables of the network that can be quantified with the phase model, but for other observables the full network dynamics have to be exploited. In most cases, reduced phase dynamics are used to infer (the stability of) stationary collective network states. As we have seen in *Chapter 3*, phase reductions provide a useful means to predict whether one-, two-, or  $m$ -cluster states of the network are stable. These predictions are based on the form of the reduced phase interaction function. In principle, also complex and non-stationary network states can be foreseen through the phase reduction, e.g., self-consistent partial synchrony or slow switching behavior, see *Section 2.1.5.2*. However, the transient and time-varying behavior of non-stationary solutions requires rather a qualitative than a quantitative analysis of the observable.

Throughout the dissertation I considered the degree of phase synchronization as the main observable, which we measured in terms of the Kuramoto order parameter. For each point in time, the Kuramoto order parameter quantifies to what extent the phases of the oscillators are mutually synchronized. Again one may ask whether this order parameter is a good observable? And again, the answer has to be that an observable is neither good nor bad. An observable has to be chosen such that it can describe the aspects under investigation. Or rather the other way round, the available observables define which aspects can be investigated. Considering the (network's average) degree of synchronization, a simple value between 0 (full asynchrony) and 1 (full synchrony) may hint at some coherent behavior. But it does not reveal any implicit structure of the oscillators, such as phase cluster-

ing. In *Section 3.1*, I resorted to a phase clustering algorithm that determined the number of clusters at a particular point in time. Unfortunately, such a snapshot does not indicate whether these clusters persist over a longer period of time, that is, whether the cluster states are stable. To investigate their stability, we labeled the oscillators with respect to their (initial) cluster membership, and traced the Kuramoto order parameter of only those oscillators within the same initial cluster. If the Kuramoto order parameter stayed above some threshold value over some time and its variance was negligible, we concluded that the corresponding cluster was indeed stable. This example already shows the intricacy of observables: while a qualitative inspection by eye, say, of the oscillators' evolution in phase space, immediately shows that, e.g., two clusters are stable and remain at a constant (phase) difference from each other, the quantitative validation requires several subsequent analysis steps.

As has been addressed in *Chapter 6* in detail, the Kuramoto order parameter provides a time-resolved spatial measure of phase synchronization, but it does not indicate any temporal alignment of the phase time series of two oscillators. For the latter, a temporal average of pair-wise phase synchronization in the form of the phase locking value may hint at functional connectivity structures within a network.

There are further important observables that help to quantify collective behavior. To name but another two, valuable information about the collective dynamics of finite-sized networks of coupled (phase) oscillators can be extracted, for instance, from the generalized (Daido) order parameters<sup>169,403</sup>. Another important concept may be that of susceptibility<sup>404,405</sup> when investigating the effect of external (stochastic) perturbations on oscillatory networks.

At the end of the day, the predictive power of (reduced) phase models is intricately linked with quantifiable observables. For this reason, it is important to clearly state the object of investigation and how this can be observed and quantified with macroscopic variables. Predicting the behavior of these observables by using the (reduced) phase model can cut an extensive analysis of the full underlying system short. In this way, the collective dynamics can be described correctly as long as the parameter region falls within the previously determined range of use of the phase model.

### 7.3.2 Modeling experimental data

Revisiting the results of *Chapter 6*, the reduced phase models of Wilson-Cowan and Freeman neural masses were not able to simultaneously describe two important features of the experimental resting state data. Despite realistic connectivity

and time-delay structures, the neural mass phase models either described (spatial) partial phase synchrony or detected (temporal) scale-freeness, but none of the phase models captured both features of the experimental phase time series that were extracted from recorded MEG data after beamforming onto a 90-node brain parcellation, filtering in the alpha band (8-12 Hz), and constructing the analytic signal using the Hilbert transform. One may speculate about the origin why the phase models cannot capture both dynamical features of the phase dynamics of resting state networks. Points of departure comprise both data analysis and model reduction. Stepping over the model-inherent assumptions of the seminal Wilson-Cowan and Freeman neural mass models dating back to Wilson and Cowan<sup>69</sup> and Freeman<sup>75</sup>, as well as over our assumptions on the subsequent phase reductions, see *Section 6.2*, I would like to focus on the nature of the filtered data. Although the data is confined to a 4 Hz-narrow frequency range, the oscillatory dynamics exhibit both frequency and amplitude modulations, which cannot be disentangled easily<sup>see, e.g., Fig. 1 in 372</sup>. It goes without saying that explanations for these modulations (and emerging brain rhythms, in general) are vague and still being sought for. Nonetheless, the structural connectivity of the brain as obtained from DTI data together with parcellation schemes, either in the form of functional neuroimaging<sup>406</sup> or neuroanatomical and cytoarchitectonic approaches<sup>407</sup>, allows for a coarse-grained description of interconnected areas in terms of neural masses or neuronal populations. As demonstrated in *Chapter 6*, it is apparently not sufficient to approximate the oscillatory dynamics in each such brain area by a reduced neural mass phase oscillator in order to retain the full picture of critical brain dynamics expressed in terms of phase synchronization measures. Formulated in a more positive way, our results still reveal that neural mass phase models were, in fact, able to describe at least one aspect of criticality, which supports the use of phase models for large-scale brain networks – as long as these neural mass phase models were properly derived and applied within reasonable model-specific boundaries.

More accurate models should take frequency and amplitude modulations into account. These modulations may or may not be due to strong coupling effects through other brain areas. If so, unfortunately, a mathematically rigorous phase reduction, as outlined in *Chapter 2*, would not be feasible. A different starting point for a more adequate neural mass description requires time-varying parameters in the neural mass models, and/or may introduce additional dynamics. Again, a subsequent phase reduction is beyond the realm of mathematically thorough reduction techniques. An exit strategy can involve phase-amplitude models. The recent developments within the Koopman operator framework<sup>260,261</sup> appear promising for a meaningful and simplified phase-amplitude description of neural mass models.

Whether the dynamical notions of criticality manifest in those models is, however, beyond the scope of this dissertation.

## 7.4 Coupled neural masses and other neural oscillator models

The main neuronal population model that has recurrently been used in this dissertation is the Wilson-Cowan neural mass model. Its rich dynamic behavior and the various bifurcations it may undergo renders the dynamics representative for neural oscillator models. Naturally, the representativeness of the model is not alone justified in the correct types of bifurcation through which oscillations emerge, as, e.g., the FitzHugh-Nagumo<sup>408</sup> or Morris-Lecar<sup>409</sup> models are generic neural oscillators close to Hopf and homoclinic (and SNIC) bifurcations, respectively. But the dynamics of the Wilson-Cowan model also resembles the qualitative behavior of the other neural oscillator models away from the bifurcation boundaries. At the bifurcation points, the respective normal forms enforce a particular dynamic behavior and a reduced network model of coupled oscillators can be established. Further away from the bifurcation, however, the shape of the particular limit cycle changes. This has an immediate effect on the coupling term, on the phase sensitivity function  $Z$  and thus on the phase interaction function  $H$  of the corresponding phase model. In *Section 7.4.1*, I briefly comment on how higher harmonics in the phase interaction function emerge, which are crucial for non-trivial collective behavior, and we show that the underlying mechanisms are similar across neural oscillator models. As we refer again to normal forms, the quadratic integrate-and-fire neuron deserves a closer inspection, too. It is the canonical model for a SNIC bifurcation, which defines together with the Hopf bifurcation the most prominent transitions to oscillatory behavior. I will comment further on the emergence of collective dynamics of coupled spiking neurons, as is the integrate-and-fire model, in *Section 7.4.2*.

### 7.4.1 Emergence of higher harmonics in the phase interaction function

The phase sensitivity function  $Z$  and the coupling term evaluated on the respective limit cycles, are the main contributors to the phase interaction function  $H$  of the reduced phase model, and thus influence the (predictions on the) collective network dynamics. A biophysically realistic description of the coupling dynamics between oscillators plays a pivotal role in the corresponding phase dynamics and can lead

to higher harmonics in the phase interaction function  $H$ . This is in particular true when the underlying dynamics has to be transformed in Hopf normal form in an intermediate step. In fact for Hopf normal forms, the shape of the phase sensitivity function  $\mathbf{Z}$  remains always sinusoidal, even for normal forms of higher order, see *Section 2.2.5*. Therefore, it is crucial to compute the transformed and nonlinear coupling terms in normal form so that higher harmonics in  $H$  and non-trivial (phase) network behavior can occur.

In view of numerical phase reduction methods, the intermediate normal form reduction, including a careful transformation of the nonlinear coupling terms, becomes obsolete. Still, higher harmonics may emerge for rather simple yet nonlinear coupling between neural oscillators. In this case, it is of paramount importance to accurately assess the properties of the limit cycle dynamics, which become evident in the phase sensitivity function  $\mathbf{Z}$ . I would like to remark that the correct determination of higher harmonics in the latter has a twofold influence: not only may it lead to higher harmonics in the reduced phase model, but it also gives crucial information about a (numerical) phase extraction from the neural dynamics in terms of time-series analysis. If higher harmonics become dominant and in the extreme case, the limit cycle trajectory exhibits self-crossings in the phase plane, a straightforward phase extraction using the Hilbert transform will not be sufficient to define a meaningful phase. For this reason, I investigated the emergence of higher harmonics in the phase sensitivity function when moving through parameter space.

To anticipate my main finding, in very close vicinity to the Hopf and SNIC bifurcation boundaries, the phase sensitivity function is well described by the analytically predicted form, that is, it consists of first harmonics only. However, moving away from the bifurcation point but still staying in close proximity, higher harmonics in the phase sensitivity function become dominant. This phenomenon is not a peculiar feature of the Wilson-Cowan neural mass model, but appears generic across neural oscillator models see, e.g., also Figure 4 in <sup>102</sup>. I numerically determined the adjoint solution for the phase sensitivity function of the Wilson-Cowan dynamics and investigated how its shape changed along the parameter space. Extending the analysis in Fig. 3.7, I further increased the input parameter  $P_k$  up to the point where limit-cycle oscillations ceased via another bifurcation, see Fig. 7.1. Although the first harmonic is the dominant one throughout the parameter space, the analysis is quite insightful. When considering the fixed parameter values from *Section 3.2.1*, oscillations emerge via a Hopf and cease through a homoclinic bifurcation. Directly on the Hopf bifurcation at  $P_k \approx -0.3663$ , the first harmonics is not only dominant, but also exclusive: the amplitudes of the second and higher harmonics converge to zero faster than exponentially. This is perfectly in line with

the analytically predicted purely sinusoidal shape of the phase sensitivity function. On the other side, the nature of the homoclinic bifurcation becomes also apparent. All harmonics tend to a non-vanishing constant amplitude, giving rise to the exponential character of the bifurcation, see also<sup>102</sup> for theoretical arguments. Between these oscillation boundaries, higher harmonics have a non-negligible effect on the phase sensitivity function and must not be discarded. This becomes even more striking when investigating the phase sensitivity function near SNIC bifurcations. While higher harmonics vanish directly on the bifurcation points and thereby allow the phase sensitivity function to take the known (co-)sinusoidal shape  $1 - \cos(\theta)$ , off these bifurcation points but in their immediate vicinity the amplitudes of the higher harmonics contribute to the shape beyond merely higher-order corrections. This sensitivity of the phase sensitivity function to even small parameter changes

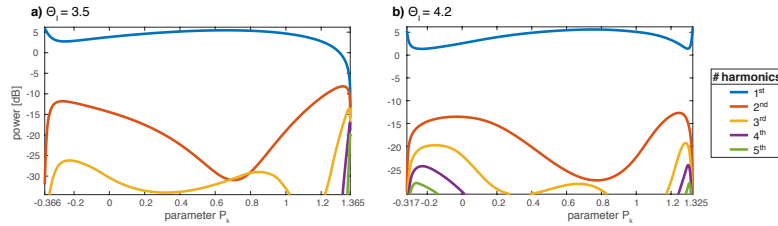


**Figure 7.1:** Higher harmonics in the phase sensitivity function of the Wilson-Cowan neural mass model for varying input  $P_k$ .

is not a model-specific phenomenon, but it is inherent in most generic oscillator models. Brown and co-workers<sup>102</sup> already reported changing phase sensitivity functions, but did not explicitly point to this sensitivity. More rigorously, I compared the numerically computed phase sensitivity function as the solutions to the adjoint problem near and away the typical bifurcation boundaries. The generic bifurcations (Hopf, homoclinic and SNIC) appear for different parameter values in the Wilson-Cowan model. On the other hand, the FitzHugh-Nagumo model displays oscillatory behavior near a Hopf bifurcation, and the Morris-Lecar model can be tuned such that its dynamics are either close to a homoclinic or a SNIC bifurcation. In Fig. 7.2 I illustrate how quickly the shape of the phase sensitivity function changes and higher harmonics occur for increasing distances  $d$  from the respective bifurcation points in parameter space from  $d = 1/10000$  to  $d = 1/10$ . It thus becomes crucial to properly define the parameters in all neural oscillator models in order to not be ‘surprised’ by emerging nonlinear and complex coupling effects. Consequently, an ad-hoc approximation of bio-physiologically accurate nonlinear oscillator models, realistic coupling dynamics included, with a simpler generic oscillator model, or even with its normal form, has to be regarded with greatest care, and moreover may only be sound in an embryonically small parameter region around the respective bifurcation boundary. Emerging higher harmonics

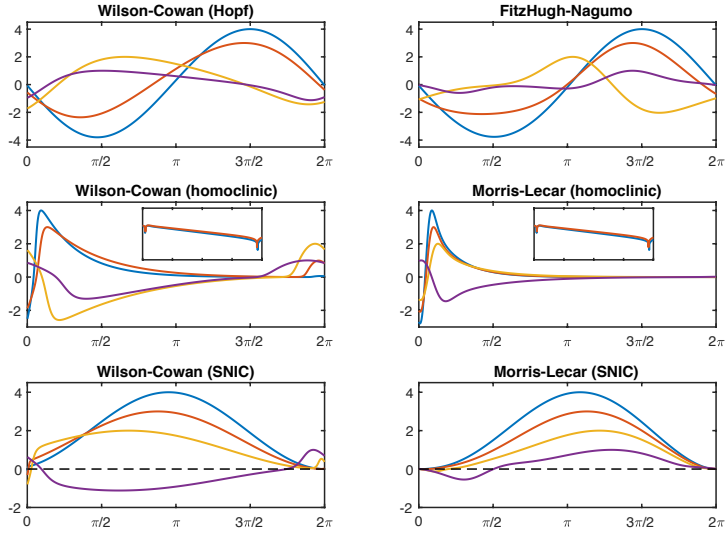


**Figure 7.2:** Phase sensitivity functions (numerically computed via the adjoint method) quickly diverge from the analytically predicted shape in the Wilson-Cowan neural mass model (left) and in generic neural oscillator models (right) close to Hopf (FitzHugh-Nagumo model) as well as to homoclinic and SNIC bifurcations (Morris-Lecar model for different parameter values). The normal forms predict sinusoidal (Hopf), exponential (homoclinic) and cosinusoidal/non-negative (SNIC) adjoint solutions near the respective bifurcation points. Non-negligible higher harmonics emerge for increasing distance  $d$  from the bifurcations. Colors represent this distance in parameter space:  $d = 1/10000$  (blue),  $d = 1/1000$  (red),  $d = 1/100$  (yellow),  $d = 1/10$  (violet). Insets for the homoclinic bifurcations show the first two graphs in log-scale and display exponential decay. Phase sensitivity functions are normalized in amplitude.

of the phase sensitivity function away from bifurcation boundaries and nonlinear coupling terms will mutually interact and catalyze, thus generate rich and highly non-trivial network effects. A careful investigation of particular parameter regions and the corresponding dynamical regimes as well as their respective bifurcation boundaries has to precede the appropriate choice of reduction technique, such that meaningful and representative phase dynamics can be extracted.

### 7.4.2 A note on integrate-and-fire neurons

The normal form for the SNIC (saddle-node on a limit cycle, also SNIPER) bifurcation is given by the quadratic integrate-and-fire (QIF) neuron model, which was introduced in more detail in *Section 5.3*. If a model exhibits dynamics close to a SNIC bifurcation, it can be reduced to the QIF model in a straightforward way<sup>307,410,411</sup>. The QIF model, like any other integrate-and-fire model, is strictly speaking a pure phase model due to the absence of amplitude effects<sup>412</sup>. It can be readily transformed into the theta neuron model<sup>307</sup>, which underlines the QIF

neuron's 'phase' character. The reduction of high(er)-dimensional neural oscillator models into integrate-and-fire models has thus to be considered with care. In general, the oscillatory dynamics of higher-dimensional neural oscillators close to a SNIC bifurcation describe a smooth closed limit cycle in phase space. Along this limit cycle, the dynamics can be well described to be of integrate-and-fire type. This description holds approximately also in the immediate vicinity of the limit cycle. If, however, perturbations kick the dynamics off the limit cycle, amplitude dynamics towards the limit cycle have to be taken into account. The amplitude effects, even if the rate towards the limit cycle is sufficiently high, are crucial to analytically determine the phase response to the (finite) perturbation. Weak coupling allows to approximate the phase response linearly and by using the phase sensitivity function, which directly follows from the normal form. However, the so-obtained phase model is only valid on the limit cycle and lacks a rigorous justification for stronger coupling strengths. Moreover, this approach does not allow to establish the (often informative) isochrons, much less a meaningful phase-amplitude model. The global character of the SNIC bifurcation, opposed to the local Hopf bifurcation, presents an insurmountable obstacle for a mathematically thorough, step-by-step reduction of the original dynamics. For this reason, I chose to focus solely on dynamics close to a Hopf bifurcation in *Chapters* 2 and 3. This choice was not meant to undermine the importance of other bifurcations, but served perfectly our purposes to present an inventory of different reduction techniques.

**Network dynamics of spiking neurons** The SNIC bifurcation, and the QIF neuron model itself, proved to be of fundamental importance for extending the Ott-Antonsen theory to parameter-dependent systems in *Chapter* 5. The transformation into a theta neuron revealed a phase dynamics that depended on an additional parameter, thus requiring a more sophisticated treatment than available in the literature. The corresponding proof that networks of QIF neurons fall in the category of phase models applicable to the Ott-Antonsen theory, automatically captured further extensions, one of which addressed so-called heterogeneous mean field models, see *Section* 5.4.3. This in particular allowed for applying the Ott-Antonsen theory to coupled phase oscillators given a specific connectivity structure. Recently, the group around Ott and Antonsen treated in the same manner QIF networks with non-trivial connectivity<sup>413</sup>. This extension opens the way to further expand the range of applicability of spiking and pulse-coupled neurons, as is the QIF model, to more realistic neural network topologies.

## 7.5 Concluding remarks and outlook

Not only interaction but synchronized and coherent interaction is key for the functioning of the brain. This dissertation addressed how phase synchronization phenomena emerge and can be measured in coupled neuronal population models. Even though phase synchronization is but one measure of neural synchrony and coherent brain activity, the underlying concept is fundamental and captivates with its simplicity and tractability. Investigating the collective dynamics of complex systems by means of phase synchronization, however, bears some intricacies when applied in a mathematically rigorous way. The first part of this dissertation provides an inventory of phase reduction techniques and highlights some sensitive issues in the reduction. Taking them in mind, allows to set the modeling of phase synchronization on a firm ground. The second part of the dissertation dealt with applications of (reduced) phase models, and pointed at possible extensions of mathematically sound approaches to simplify the collective network dynamics. In the end, phase synchronization can be used in many oscillatory networks as a well-descriptive observable to quantify collective behavior.

Looking both back- and forward, there remain many questions that have developed during my PhD research project “Frequency-doubling bifurcations in neuronal networks – a means of cross-frequency interactions”, and that await answers. The nature of such questions concerns both mathematical as well as neuroscientific aspects. Importantly, satisfactory answers will require a healthy balance between these two disciplines, and analytic insights have to be combined with experimental evidence and intuition. The emergence and function of brain rhythms still needs to be elucidated, and how the interplay between distinct cortical and subcortical rhythms shapes collective brain dynamics, thus leading to coherent behavior and cognition, is widely unclear. We believe that changes on the micro-scale affect the macroscopic dynamics. For this reason we investigated how tuning the parameters of coupled (neural) oscillators induced different (brain) network behavior, and thus generated macroscopic rhythms.

**Asymmetry and time variability** A straightforward example for cross-frequency interactions between neuronal populations presented a network of two coupled, symmetric populations of Kuramoto oscillators, as analyzed in *Chapter 4*. The oscillators’ natural frequencies of either population were distributed around a mean, which was different for each population. Thereby I modeled the interplay of different frequency bands in neural networks. Depending on the width of the frequency distributions, on the distance between their respective means and on the overall coupling strength, the collective dynamics indeed showed macroscopic oscillations

and even a frequency-doubling bifurcation occurred (which is typically masked as a Hopf bifurcation in the rotating frame formulation). While I considered a highly symmetric setup, it can be interesting to include more realistic asymmetries: Neural populations featuring cortical low-frequency rhythms (delta, theta, or alpha) usually show a frequency distribution in a fairly narrow frequency band, whereas higher-frequency rhythms (beta, or gamma) cover wider frequency bands. Moreover, the lower the frequency of cortical oscillations, the higher their amplitude. ‘Translated’ into a mathematical phase oscillator model, these amplitude effects can be expressed in a coupling strength asymmetry. Whether these asymmetries allow for a similar topological equivalence between coupled and multimodal networks as in *Chapter 4*, will be shown in future studies.

As mentioned above, experimental data suggest (beamformed) cortical dynamics that have a certain frequency variability. This can be modeled in terms of time-varying natural frequency terms, see also the pioneering work by Petkoski and Stefanovska<sup>308</sup> on a Kuramoto model with time-varying parameters. The interaction of such parameter-dependent oscillatory systems and their collective dynamics was the central issue in *Chapter 5*. Whether and how the adaptation of phase models to include variable frequencies indeed results into exhibiting all dynamical features of criticality as addressed in *Chapter 6*, remains another open problem.

**Collective dynamics of spiking neurons and cortical models** Emergent rhythmic behavior of networks of spiking neurons is an important topic in the field. The mathematical proof in *Chapter 5* captures the dynamics of spiking, quadratic integrate-and-fire neurons due to their transformation into parameter-dependent phase oscillators, aka theta neurons (this nomenclature is not to be confused with the cortical theta rhythms). A rigorous application of the theory requires global coupling of all neurons. The coupling between neurons can, in general, occur through chemical or electrical synapses. Coupling effects at chemical synapses are induced through the firing rates of the adjacent neurons. The global coupling assumption, however, lets each neuron ‘see’ only the mean firing rate of the population, which in turn facilitates the network analysis in terms of the macroscopic observables – mean firing rate and mean membrane potential. In the quadratic integrate-and-fire model, chemical coupling alone does not lead to rhythmic macroscopic behavior<sup>[1]</sup>, which would manifest in oscillatory firing rates and membrane potential fluctuations. Following the discussion about oscillations

---

<sup>[1]</sup> We here refer to instantaneous chemical coupling as in<sup>293</sup>. If, however, we incorporate synaptic dynamics as in<sup>414</sup>, or change the form of synaptic activation<sup>290,291,415,416</sup>, macroscopic oscillations do emerge.

and synchronization in the *Introduction*, this may indicate that chemical synapses are not sufficient to synchronize a network. One way to induce oscillations is to couple two populations of spiking neurons representing the excitatory (E) part and inhibitory (I) part of a neural network, very similar to the assumptions of the Wilson-Cowan model. Dumont and co-workers considered such a spiking E-I network model<sup>417</sup> and determined the stability and robustness of collective oscillations in terms of the (macroscopic) phase sensitivity function. Not only does this work combine the different aspects of the dissertation at hand, it also points at a possible way to underpin the oscillatory nature of phenomenological neural mass models, such as the Wilson-Cowan model. Similar in nature, Rodrigues and co-workers proposed mappings between a leaky integrate-and-fire model and the Freeman model<sup>418</sup>. A rigorous derivation of (low-dimensional) cortical models of spiking neurons certainly presents a possibly critical endeavor to overcome the frequent criticism of heuristic neural mass model. To provide a neuroscientifically satisfactory cortical model, neural plasticity should be incorporated. But including the corresponding concepts into mathematical tractable model equations requires a great deal of effort. Although synaptic and homeostatic plasticity are conceptually well-understood, low-dimensional descriptions of network behavior that respect plasticity rules at the microscopic level are long being sought for.

# SUPPLEMENTARY MATERIAL

<i>S.1</i>	<i>Kuramoto's reductive perturbation</i>	216
<i>S.2</i>	<i>Higher-order corrections and nonlinear coupling</i>	221
<i>S.3</i>	<i>Poincaré's reduction via nonlinear transforms</i>	226
<i>S.4</i>	<i>Takens' reduction via Lie brackets</i>	237
<i>S.5</i>	<i>Ashwin &amp; Rodrigues' reduction via <math>S_N \times S^1</math>-symmetry</i>	242
<i>S.6</i>	<i>Malkin's adjoint method</i>	248
<i>S.7</i>	<i>Limit of infinite attraction method</i>	249

# LIST OF SYMBOLS

Throughout *Chapter 2* and the *Supplementary Material* we use:

$\mathbf{x}, x, y$	Real-valued state variable (non bold-face = scalar)
$z$	Complex-valued state variable
$\mathcal{X} \subset \mathbb{R}^n$	State space
$n \in \mathbb{N}$	Dimension of state space
$\mathcal{F}$	Vector field
$\phi$	Flow
$\mathbf{f}, f$	Nonlinear function prescribing the internal dynamics (non bold-face = scalar)
$\mathbf{g}, g$	Nonlinear coupling function (non bold-face = scalar)
$\mathbf{L}$	Jacobian matrix
$\mathbf{J}$	Diagonalized Jacobian
$\lambda = \varrho + i\omega$	Eigenvalues of the Jacobian
$\mu$	Bifurcation parameter
$\kappa$	Coupling strength
$\mathbf{p}$	Perturbation
$t$	Time
$\tau$	Slow time
$\mathcal{C}$	Limit cycle
$\mathbf{x}^c, x^c, y^c$	State variable on the limit cycle
$\theta^c$	Phase on the limit cycle
$R_k$	Amplitude of oscillation (radius of the limit cycle)
$\rho_k, r_k$	Amplitude (distance to the limit cycle)
$\mathcal{B}$	Basin of attraction
$\mathcal{I}$	Isochron
$\Theta: \mathcal{X} \rightarrow \mathbb{S}^1$	(Asymptotic) phase map

$\theta$	Phase
$\psi$	Phase difference
$\omega$	Natural frequency
$g(\omega)$	Natural frequency distribution
$T$	Period
$Q: \mathbb{S}^1 \rightarrow \mathbb{R}$	Infinitesimal phase response curve
$G: \mathbb{S}^1 \times \mathbb{R}^n \rightarrow \mathbb{R}$	Phase response function
$\mathbf{Z}: \mathbb{S}^1 \rightarrow \mathbb{R}^n$	Phase sensitivity function in $n$ real dimensions
$Z: \mathbb{S}^1 \rightarrow \mathbb{C}$	Phase sensitivity function in one complex dimension
$H$	Phase interaction function
$a_n, b_n$	Amplitudes of phase interaction function
$\mathbf{C} = \{C_{jk}\}_{j,k}$	Adjacency matrix, where $j, k = 1, \dots, N$
$N \in \mathbb{N}$	Network size
$\tau_{jk}$	Time delay between nodes $j$ and $k$
$R$	Kuramoto order parameter (real-valued)
$\Psi$	Mean phase
$w \in \mathbb{C}$	Normal form variable
$M \in \mathbb{N}$	Order of normal form
$\sigma_m = u_m + iv_m$	Coefficients of Hopf normal form
$\alpha, \beta, \gamma, \delta \in \mathbb{C}$	Coefficients of the Hopf normal form of an oscillator network
$\lambda^{\text{intra}}$	Eigenvalue associated with intracluster perturbations
$\lambda^{\text{inter}}$	Eigenvalue associated with intercluster perturbations
$\mathbf{I}, \mathbf{I}_n$	Identity matrix in $\mathbb{R}^{n \times n}$
$\bar{\cdot}$	Complex conjugation
$\langle \cdot \rangle$	Temporal average (over one period)
$\langle \cdot, \cdot \rangle$	Inner product on $\mathbb{R}^n$ , also used in dot-notation
$[\cdot, \cdot]$	Lie bracket
$S^1$	Rotation group on $\mathbb{C}^N$
$S_N$	Permutation group on $\mathbb{C}^N$
$\mathcal{L}$	Linear operator

## S.1 Kuramoto's reductive perturbation

Let us consider two coupled systems  $\mathbf{x}, \mathbf{x}' \in \mathbb{R}^n$ , whose dynamics are described by

$$\dot{\mathbf{x}} = \mathbf{f}(\mathbf{x}, t; \mu) + \kappa \mathbf{g}(\mathbf{x}, \mathbf{x}', t; \mu) \quad (\text{S.1})$$

and an equivalent expression for  $\mathbf{x}'$ , with  $\mathbf{f}: \mathbb{R}^n \rightarrow \mathbb{R}^n$ , the coupling function  $\mathbf{g}: \mathbb{R}^n \times \mathbb{R}^n \rightarrow \mathbb{R}^n$  with coupling strength  $\kappa \in \mathbb{R}$  and a bifurcation parameter  $\mu \in \mathbb{R}$ . We assume  $\mathbf{x}_0(\mu)$  a steady solution for  $\kappa = 0$ , i.e.,  $\mathbf{f}(\mathbf{x}_0(\mu); \mu) = 0$  for all  $\mu$ . We set

$$\tilde{\mathbf{x}} = \mathbf{x} - \mathbf{x}_0 \quad \text{and} \quad \tilde{\mathbf{x}}' = \mathbf{x}' - \mathbf{x}_0 ,$$

and expand  $\mathbf{f}$  around  $\mathbf{x} = \mathbf{x}_0$ , or around  $\tilde{\mathbf{x}} = 0$ , respectively. By omitting the tilde, we have

$$\mathbf{f}(\mathbf{x}; \mu) = \mathbf{n}_1(\mathbf{x}; \mu) + \mathbf{n}_2(\mathbf{x}, \mathbf{x}; \mu) + \mathbf{n}_3(\mathbf{x}, \mathbf{x}, \mathbf{x}; \mu) + \mathcal{O}(|\mathbf{x}|^4) ,$$

where the  $\mathbf{n}_k$ 's are given by

$$\mathbf{n}_k(\mathbf{u}^{(1)}, \mathbf{u}^{(2)}, \dots, \mathbf{u}^{(k)}; \mu) = \sum_{i_1, \dots, i_k=1}^n \frac{1}{k!} \left( \frac{\partial^k F(\mathbf{x}; \mu)}{\partial x_{i_1} \partial x_{i_2} \dots \partial x_{i_k}} \right)_{\mathbf{x}=\mathbf{0}} u_{i_1}^{(1)} u_{i_2}^{(2)} \dots u_{i_k}^{(k)} \quad (\text{S.2})$$

with  $\mathbf{u}^{(j)} = (u_1^{(j)}, \dots, u_n^{(j)}) \in \mathbb{R}^n$ . Note that the  $\mathbf{n}_k$  are symmetric in their arguments  $\mathbf{u}^{(1)}, \dots, \mathbf{u}^{(k)}$ . We further expand  $\mathbf{n}_k$  with respect to  $\mu$ , e.g.,  $\mathbf{n}_1(\mathbf{x}; \mu) = \hat{\mathbf{L}}_0 \mathbf{x} + \mu \hat{\mathbf{L}}_1 \mathbf{x} + \dots$ , and obtain

$$\mathbf{f}(\mathbf{x}; \varepsilon^2) = \hat{\mathbf{L}}_0 \mathbf{x} + \mu \hat{\mathbf{L}}_1 \mathbf{x} + M_0 \mathbf{x} \mathbf{x} + N_0 \mathbf{x} \mathbf{x} \mathbf{x} + \mathcal{O}(|\mathbf{x}|^4) , \quad (\text{S.3})$$

where  $M_0 \mathbf{u} \mathbf{v} = \mathbf{n}_2(\mathbf{u}, \mathbf{v}; \mu = 0)$  and  $N_0 \mathbf{u} \mathbf{v} \mathbf{w} = \mathbf{n}_3(\mathbf{u}, \mathbf{v}, \mathbf{w}; \mu = 0)$ . We thus discarded all  $\mathcal{O}(\mu)$  terms in  $\mathbf{n}_2$  and  $\mathbf{n}_3$  in (S.3). Furthermore, we Taylor-expand  $\mathbf{g}$  as

$$\mathbf{g}(\mathbf{x}, \mathbf{x}') = G_0 + G_{10} \mathbf{x} + G_{01} \mathbf{x}' + G_{20} \mathbf{x}^2 + G_{11} \mathbf{x} \mathbf{x}' + G_{02} \mathbf{x}'^2 + \dots . \quad (\text{S.4})$$

The underlying assumption of the derivation is that the system undergoes a supercritical Hopf bifurcation at  $\mu = 0$  (and  $\kappa = 0$ ). Then, the operator  $\hat{\mathbf{L}}_0$  has a set of eigenvalues  $\sigma(\hat{\mathbf{L}}_0) = \{\lambda^\alpha \mid \alpha = 1, \dots, n\}$ , each of which can be expanded as  $\lambda^\alpha = \lambda_0^\alpha + \mu \lambda_1^\alpha + \dots$ . The Hopf bifurcation condition requires that  $\lambda_0^1 = -\lambda_0^2 = i\omega_0$  are purely imaginary and that  $\text{Re}(\lambda_0^\alpha) > 0$  for all  $\alpha > 2$ . For convenience, we set  $\mathbf{u} = \mathbf{u}_1$  as the right eigenvector of  $\hat{\mathbf{L}}_0$  corresponding to the eigenvalue  $\lambda_0^1 = \lambda_0$ , that is

$$\hat{\mathbf{L}}_0 \mathbf{u} = \lambda_0 \mathbf{u} \quad \text{and} \quad \hat{\mathbf{L}}_0 \bar{\mathbf{u}} = \bar{\lambda}_0 \bar{\mathbf{u}}$$

where  $\lambda_0^2 = \bar{\lambda}_0$ . Likewise, we denote by  $\mathbf{v} = \mathbf{v}_1$  the left eigenvector of  $\hat{\mathbf{L}}_0$  corresponding to the eigenvalue  $\lambda_0^1 = \lambda_0$ :  $\mathbf{v} \hat{\mathbf{L}}_0 = \lambda_0 \mathbf{v}$ . The left and right eigenvectors fulfill  $\mathbf{v} \bar{\mathbf{u}} = \bar{\mathbf{v}} \mathbf{u} = 0$ . Besides, we normalize them such that  $\mathbf{v} \mathbf{u} = \bar{\mathbf{v}} \bar{\mathbf{u}} = 1$ . In particular, we have

$$\begin{aligned} \lambda_0 &= \sigma_0 + i\omega_0 = \mathbf{v} \hat{\mathbf{L}}_0 \mathbf{u} \\ \lambda_1 &= \sigma_1 + i\omega_1 = \mathbf{v} \hat{\mathbf{L}}_1 \mathbf{u} . \end{aligned}$$

From this, we see that the solution to the linearized unperturbed system,  $\dot{\mathbf{x}} = \hat{\mathbf{L}}_0 \mathbf{x}$ , is given by

$$\mathbf{x}_0(t) = w e^{i\omega_0 t} \mathbf{u} + \bar{w} e^{-i\omega_0 t} \bar{\mathbf{u}} , \quad (\text{S.5})$$

where  $w$  is an arbitrary complex number, which we will refer to as the complex amplitude. Taking the full dynamics (S.1) including the perturbations into account,  $\mathbf{x}(t)$  generally deviates from  $\mathbf{x}_0(t)$ . In order to describe the asymptotic evolution of  $\mathbf{x}(t)$ , we consider the complex amplitude  $w$  to be time dependent. In the following, we will derive the

dynamics of  $w$  in the form

$$\dot{w} = g(w, \bar{w}) + \varepsilon^2 \kappa g(w, \bar{w}, w', \bar{w}') , \quad (\text{S.6})$$

where the prime ' indicates the coupled oscillator.

To begin with, we define  $\varepsilon = \sqrt{|\mu|}$  and  $\chi = \text{sgn } \mu$ . We can consider  $\mathbf{x} = \mathbf{x}_1 + \mathbf{x}_2 + \dots$  where  $\mathbf{x}_l = \mathcal{O}(\varepsilon^l)$  and abbreviating  $\mathbf{n}_1(\mathbf{x}) = \mathbf{Lx}$ , we have  $\mathbf{L} = \hat{\mathbf{L}}_0 + \chi \varepsilon^2 \hat{\mathbf{L}}_1 + \mathcal{O}(\varepsilon^4)$ . We further introduce a scaled time  $\tau = \varepsilon^2 t$  such that  $\mathbf{x} = \mathbf{x}(t, \tau)$  depends both on  $t$  and  $\tau$ , which should be treated as mutually independent. Then, the time derivative becomes

$$\frac{d}{dt} \rightarrow \frac{\partial}{\partial t} + \varepsilon^2 \frac{\partial}{\partial \tau} .$$

Taken together, (S.3) reads

$$\begin{aligned} \left( \frac{\partial}{\partial t} + \varepsilon^2 \frac{\partial}{\partial \tau} - \hat{\mathbf{L}}_0 - \varepsilon^2 \chi \hat{\mathbf{L}}_1 - \dots \right) (\mathbf{x}_1 + \mathbf{x}_2 + \dots) = \\ M_0 \mathbf{x}_1 \mathbf{x}_1 + (2M_0 \mathbf{x}_1 \mathbf{x}_2 + N_0 \mathbf{x}_1 \mathbf{x}_1 \mathbf{x}_1) + \mathcal{O}(\varepsilon^4) \\ + \kappa [G_0 + \varepsilon (G_{10} \mathbf{x}_1 + G_{01} \mathbf{x}'_1) + \varepsilon^2 (G_{20} \mathbf{x}_1 \mathbf{x}_1 + G_{11} \mathbf{x}_1 \mathbf{x}'_1 + G_{02} \mathbf{x}'_1 \mathbf{x}'_1) + \mathcal{O}(\varepsilon^3)] . \end{aligned} \quad (\text{S.7})$$

As we consider merely weak coupling, that is,  $0 < \kappa \ll \mu \ll 1$ , it is appropriate to assume  $\kappa \mapsto \varepsilon^2 \kappa$ . The right-hand side of (S.7) becomes

$$(M_0 \mathbf{x}_1 \mathbf{x}_1 + \kappa G_0) + (2M_0 \mathbf{x}_1 \mathbf{x}_2 + N_0 \mathbf{x}_1 \mathbf{x}_1 \mathbf{x}_1 + \varepsilon^2 \kappa [G_{10} \mathbf{x}_1 + G_{01} \mathbf{x}'_1]) + \mathcal{O}(\varepsilon^4) . \quad (\text{S.8})$$

The term in the first parentheses is of order  $\mathcal{O}(\varepsilon^2)$  and the term in the second of order  $\mathcal{O}(\varepsilon^3)$ . Note further that for this particular choice of coupling parameter  $\eta = \varepsilon^2 \kappa$ , the coupling function reduces to at most linear coupling terms. If, e.g.,  $\eta = \mathcal{O}(\varepsilon)$ , then also quadratic terms have to be taken into account. Here, however, we constrain ourselves to mere linear coupling.

Equating the coefficients of different powers of  $\varepsilon$  in (S.7), we get a set of equations of the form

$$\left( \frac{\partial}{\partial t} - \hat{\mathbf{L}}_0 \right) \mathbf{x}_\nu = \mathbf{B}_\nu , \quad \nu = 1, 2, \dots , \quad (\text{S.9})$$

where  $\mathbf{B}_\nu = \mathcal{O}(\varepsilon^\nu)$  and the first  $\mathbf{B}_\nu$ 's are given by

$$\begin{aligned} \mathbf{B}_1 &= 0 , \\ \mathbf{B}_2 &= M_0 \mathbf{x}_1 \mathbf{x}_1 + \varepsilon^2 \kappa G_0 , \\ \mathbf{B}_3 &= - \left( \varepsilon^2 \frac{\partial}{\partial \tau} - \varepsilon^2 \chi \hat{\mathbf{L}}_1 \right) \mathbf{x}_1 + 2M_0 \mathbf{x}_1 \mathbf{x}_2 + N_0 \mathbf{x}_1 \mathbf{x}_1 \mathbf{x}_1 + \varepsilon^2 \kappa [G_{10} \mathbf{x}_1 + G_{01} \mathbf{x}'_1] . \end{aligned} \quad (\text{S.10})$$

Note that, in general, the  $\mathbf{B}_\nu$ 's are depending on  $\mathbf{x}_{\nu'}$  with  $\nu' < \nu$ . Therefore, we can solve the system (S.9) of linear inhomogeneous differential equations subsequently. In order to ease the computation, we can make use of the following *solvability condition*.

**Lemma S.1.** *The solvability condition for system (S.9) reads*

$$\mathbf{v} \mathbf{B}_\nu^{(1)}(\tau) = 0 , \quad (\text{S.11})$$

where  $\mathbf{B}_\nu^{(1)}$  is the first Fourier coefficient of the expansion

$$\mathbf{B}_\nu(t, \tau) = \sum_{l=-\infty}^{\infty} \mathbf{B}_\nu^{(l)}(\tau) e^{il\omega_0 t} . \quad (\text{S.12})$$

*Proof.* First of all, we use the fact that

$$\int_0^{2\pi/\omega_0} \mathbf{v} \mathbf{B}_\nu e^{-i\omega_0 t} dt = \int_0^{2\pi/\omega_0} \mathbf{v}^\top \cdot \mathbf{B}_\nu e^{-i\omega_0 t} dt = 0 , \quad (\text{S.13})$$

which we prove via

$$\begin{aligned} \int_0^{2\pi/\omega_0} \mathbf{v}^\top \cdot \mathbf{B}_\nu e^{-i\omega_0 t} dt &\stackrel{(\text{S.9})}{=} \int_0^{2\pi/\omega_0} \left[ \mathbf{v}^\top \cdot \left( \frac{\partial}{\partial t} - \hat{\mathbf{L}}_0 \right) \mathbf{x}_\nu \right] e^{-i\omega_0 t} dt \quad (\text{note that } \lambda_0 = i\omega_0) \\ &= \int_0^{2\pi/\omega_0} \left[ \mathbf{v}(\lambda_0 \mathbf{x}_\nu) - (\mathbf{v} \hat{\mathbf{L}}_0) \mathbf{x}_\nu \right] e^{-i\omega_0 t} dt = 0 , \end{aligned}$$

where the second equality is due to partial integration and the last due to  $\mathbf{v}$  being the left eigenvector of  $\hat{\mathbf{L}}_0$  corresponding to the eigenvalue  $\lambda_0$ .

Having a closer look at system (S.9), the homogeneous part suggests that the  $\mathbf{x}_\nu$ 's are  $2\pi$ -periodic functions of  $\omega_0 t$ . Hence, also  $\mathbf{B}_\nu = \mathbf{B}_\nu(t, \tau)$  has to be  $2\pi$ -periodic, which admits the Fourier expansion (S.12). Substituting the latter into (S.13), we have

$$\int_0^{2\pi/\omega_0} \mathbf{v} \mathbf{B}_\nu e^{-i\omega_0 t} dt = \sum_{l=-\infty}^{\infty} \int_0^{2\pi/\omega_0} \mathbf{v} \mathbf{B}_\nu^{(l)}(\tau) e^{i(l-1)\omega_0 t} dt = 0 .$$

Evaluating all the integrals on the right-hand side, we see that all but the one where  $l = 1$  vanish, which leaves the solvability condition (S.11).  $\square$

Now, one can solve system (S.9) iteratively. For  $\nu = 1$ , we have

$$\left( \frac{\partial}{\partial t} - \hat{\mathbf{L}}_0 \right) \mathbf{x}_1 = 0 ,$$

which provides the “neutral solution”

$$\mathbf{x}_1(t, \tau) = w(\tau) \mathbf{u} e^{i\omega_0 t} + c.c. \quad (\text{S.14})$$

where  $w(\tau)$  is the complex amplitude and *c.c.* stands for the complex conjugate of the foregoing part. In particular, we have  $|w(\tau)| = \mathcal{O}(\varepsilon)$ . As to  $\nu = 2$ , we would like to mention first that since  $\mathbf{x}_1 \propto e^{i\omega_0 t}$ , the term  $M_0 \mathbf{x}_1 \mathbf{x}_1 \propto e^{2i\omega_0 t}$ . Due to the solvability condition (S.13), we know that (i)  $\mathbf{B}_2$  has to be periodic and that (ii) the constant coupling term  $G_0$  has to vanish as it will be averaged out. In the case that the coupling

function  $\mathbf{g}$  in (S.1) is explicitly time-dependent, in particular, all terms  $G_{jk}$  in (S.4) have to be time-dependent, we can likewise Fourier expand  $G_0$  and see that the first two coefficients  $G_0^{(0)} = G_0^{(1)} = 0$  have to vanish. Moreover, we can argue in the same manner that all even Fourier coefficients  $G_{jk}^{(2n)}, n = 0, 1, 2, \dots$ , of any coupling term  $G_{jk}, j, k \in \mathbb{N}$ , must be zero. In any case,  $\mathbf{B}_2$  only contains zeroth and  $\geq 2$ nd harmonics, and the same holds for  $\mathbf{x}_2(t, \tau)$ . Therefore, we can write

$$\mathbf{x}_2(t, \tau) = \mathbf{V}_+ w(\tau)^2 e^{2i\omega_0 t} + \mathbf{V}_- \bar{w}(\tau)^2 e^{-2i\omega_0 t} + \mathbf{V}_0 |w(\tau)|^2 + h.h. \quad (\text{S.15})$$

where *h.h.* stands for higher harmonics that will not be further defined. Substituting  $\mathbf{x}_2$  into (S.9) and equating coefficients of different harmonics, we can solve the equation for the constants  $\mathbf{V}_{\pm,0}$  and find

$$\mathbf{V}_+ = \overline{\mathbf{V}_-} = -\left(\hat{\mathbf{L}}_0 - 2i\omega_0\right)^{-1} M_0 \mathbf{u} \mathbf{u} \quad \text{and} \quad \mathbf{V}_0 = -2\hat{\mathbf{L}}_0^{-1} M_0 \mathbf{u} \bar{\mathbf{u}}. \quad (\text{S.16})$$

For  $\nu = 3$ , we first substitute in  $\mathbf{x}_1$  and  $\mathbf{x}_2$  into  $\mathbf{B}_3$  as given in (S.10), and subsequently solve for the first Fourier coefficient

$$\begin{aligned} \mathbf{B}_3^{(1)}(\tau) = & -\left(\varepsilon^2 \frac{\partial}{\partial \tau} - \varepsilon^2 \chi \hat{\mathbf{L}}_1\right) w(\tau) \mathbf{u} + \left(2M_0 \mathbf{u} \mathbf{V}_0 + 2M_0 \bar{\mathbf{u}} \mathbf{V}_+ + 3N_0 \mathbf{u} \mathbf{u} \bar{\mathbf{u}}\right) |w(\tau)|^2 w(\tau) \\ & + \varepsilon^2 \kappa \left(G_{10} \mathbf{u} w(\tau) + G_{01} \mathbf{u} w'(\tau)\right), \end{aligned} \quad (\text{S.17})$$

where we assumed no explicit dependence of  $\mathbf{g}$  on time. Using the solvability condition (S.11), i.e.,  $\mathbf{v} \mathbf{B}_3^{(1)} = 0$ , and that  $\mathbf{v} \mathbf{w} \mathbf{u} = w$ , we finally arrive at the amplitude equation

$$\dot{w} = \alpha w - \beta |w|^2 w + \varepsilon^2 \kappa (\gamma_1 w + \gamma_2 w') \quad (\text{S.18})$$

with complex constants

$$\begin{aligned} \alpha &= \mathbf{v} \varepsilon^2 \chi \hat{\mathbf{L}}_1 \mathbf{u}, \\ \beta &= -(2\mathbf{v} M_0 \mathbf{u} \mathbf{V}_0 + 2\mathbf{v} M_0 \bar{\mathbf{u}} \mathbf{V}_+ + 3\mathbf{v} N_0 \mathbf{u} \mathbf{u} \bar{\mathbf{u}}), \\ \gamma_1 &= \mathbf{v} G_{10} \mathbf{u}, \\ \gamma_2 &= \mathbf{v} G_{01} \mathbf{u}. \end{aligned} \quad (\text{S.19})$$

Going back to the original notation with the  $\mathbf{n}_k$ 's and noting that the latter are linear in each of their arguments, we find

$$\beta = -2\mathbf{v} \mathbf{n}_3(\mathbf{u}, \mathbf{u}, \bar{\mathbf{u}}) + 4\mathbf{v} \mathbf{n}_2(\bar{\mathbf{u}}, \hat{\mathbf{L}}_0^{-1} \mathbf{n}_2(\mathbf{u}, \bar{\mathbf{u}})) + 2\mathbf{v} \mathbf{n}_2(\mathbf{u}, (\hat{\mathbf{L}}_0 - 2i\omega_0)^{-1} \mathbf{n}_2(\mathbf{u}, \mathbf{u})). \quad (\text{S.20})$$

As a final remark about the dot-notation in the amplitude equation (S.18), we replaced  $\varepsilon^2 \partial/\partial \tau$  by  $\partial/\partial t$ , such that the derivative is now taken with respect to the original time  $t$ , although  $w = w(\varepsilon^2 t)$  changes only slowly.

Coming back to the initial dynamics (S.1), we seek for the phase dynamics of the

perturbed solution  $\mathbf{x}(t)$  from the linearized solution  $\mathbf{x}_0(t)$ . We can write  $\mathbf{x}(t)$  as

$$\mathbf{x}(t) = w(t)e^{i\omega_0 t} \mathbf{u} + \bar{w}(t)e^{-i\omega_0 t} \bar{\mathbf{u}} + h.h. \quad (\text{S.21})$$

Differentiating with respect to time  $t$  and inserting (S.18) gives  $\dot{\mathbf{x}}(t) = W e^{i\omega_0 t} \mathbf{u} + c.c. + h.h.$ , where  $W = \dot{w} + i\omega_0 w$  describes the full amplitude dynamics

$$\dot{w} = (\alpha + i\omega_0)w - \beta|w|^2w + \varepsilon^2\kappa(\gamma_1 w + \gamma_2 w') \quad (\text{S.22})$$

on the slower time scale, where the natural frequency  $\omega_0$  is added to the dynamics of mere amplitude deviations (S.18).

Following the theory of weakly coupled oscillators, the crucial assumption for the coupling constant is that

$$\eta = \varepsilon^2\kappa \quad \text{with } 0 < \kappa < \varepsilon \ll 1. \quad (\text{S.23})$$

This allows the linear coupling term to be correct of order  $\mathcal{O}(\varepsilon)$ . Higher-order corrections of the coupling term up to order  $\mathcal{O}(\varepsilon^3)$  have been presented by Kori and co-workers<sup>95</sup> and we will elaborate on them further in *Section S.2*. If we drop the assumption (S.23), we may consider nonlinear coupling terms in the phase-space dynamics (S.1). Furthermore, the inhomogeneities  $\mathbf{B}_\nu$  in the reduced system (S.9) take more intricate forms and the derivation leading to the amplitude equation (S.18) has to be revised accordingly.

**Remark.** *The here presented Reductive Perturbation Method as one possible phase reduction technique has been established by Kuramoto<sup>38</sup>. Another technique closely linked is the so-called Renormalization Group Method of Goldenfeld, Oono and co-workers<sup>419,420</sup>. Kunihiro demonstrates the intricate link between the two methods<sup>421</sup>: Kuramoto's solvability condition (S.11) is circumvented by introducing an appropriately chosen constant  $\delta$  such that unwanted secular terms vanish.*

## S.2 Higher-order corrections and nonlinear coupling

We here follow the theory established in the preceding section. Not only do we want to establish higher-order corrections of the coupling term up to order  $\mathcal{O}(\varepsilon^3)$  as presented by Kori and co-workers<sup>95</sup>, but also we refrain from the direct, linear coupling. Note that the results (S.19) for the parameters  $\alpha, \beta, \gamma_{1,2}$  remain the same for nonlinear coupling. Yet, if we allow for higher-order corrections in the amplitude equation (S.18), that is, in

$$\dot{w} = \alpha w - \beta|w|^2w + \varepsilon^2\kappa(\gamma w' + \delta\bar{w}w'^2), \quad (\text{S.24})$$

the additional parameter  $\delta$  will incorporate the nonlinear effects of the underlying coupling nonlinearity in the original dynamics.

Therefore, let us consider in the notation of the preceding section, the coupling func-

tion

$$\begin{aligned} \mathbf{g}(\mathbf{x}, \mathbf{x}') &= G_{10}\mathbf{x} + G_{01}\mathbf{x}' + G_{20}(\mathbf{x}) + G_{11}(\mathbf{x}, \mathbf{x}') + G_{02}(\mathbf{x}') \\ &\quad + G_{30}(\mathbf{x}) + G_{21}(\mathbf{x}, \mathbf{x}') + G_{12}(\mathbf{x}, \mathbf{x}') + G_{03}(\mathbf{x}') + \dots, \end{aligned} \quad (\text{S.25})$$

where the functions

$$G_{jk}(\mathbf{x}, \mathbf{x}') = G_{jk}(\underbrace{\mathbf{x}, \dots, \mathbf{x}}_{j \text{ times}}, \underbrace{\mathbf{x}', \dots, \mathbf{x}'}_{k \text{ times}}) \quad (\text{S.26})$$

are of order for  $G_{jk} = \mathcal{O}(\varepsilon^{j+k})$  for  $\mathbf{x}, \mathbf{x}' = \mathcal{O}(\varepsilon)$ . For instance, we are interested in the effect of nonlinear coupling terms  $xx', yx', x^2x', xyx', y^2x'$  when  $\mathbf{x} = (x, y), \mathbf{x}' = (x', y')$  are two-dimensional. Possible examples for  $G_{jk}$  are  $G_{11}(\mathbf{x}, \mathbf{x}') = a \cdot xx' + b \cdot yx'$  or  $G_{21}(\mathbf{x}, \mathbf{x}') = c \cdot x^2x' + d \cdot xyx' + e \cdot y^2x'$  with parameters  $a, \dots, e$ . More general, if we write all possible products of  $(x, y), (x', y')$  of order  $j+k$  as a vector

$$(x, y)^j * (x', y')^k := \begin{pmatrix} x^j x'^k, x^{j-1} y x'^k, \dots, y^j x'^k, x^j x'^{k-1} y', \dots, \dots, y^j y'^k \\ x^j x'^k, x^{j-1} y x'^k, \dots, y^j x'^k, x^j x'^{k-1} y', \dots, \dots, y^j y'^k \end{pmatrix}^\top,$$

we can rewrite the coupling terms  $G_{jk}$  as

$$G_{jk}((x, y), (x', y')) = \mathbf{G}_{jk} \left[ (x, y)^j * (x', y')^k \right] \quad (\text{S.27})$$

with  $\mathbf{G}_{jk}$  a  $2 \times (j+1)(k+1)$ -matrix. In particular,  $\mathbf{G}_{10}$  and  $\mathbf{G}_{01}$  are quadratic,  $2 \times 2$ -matrices.

As before, we denote by  $\mathbf{x}_0(t)$  the solution to the linearized unperturbed system  $\dot{\mathbf{x}} = \hat{\mathbf{L}}_0 \mathbf{x}$ . The general solution, though, will be of the form

$$\mathbf{x} = \mathbf{x}_0(w, \bar{w}, \theta) + \boldsymbol{\rho}(w, \bar{w}, w', \bar{w}', \theta) \in \mathbb{R}^n, \quad (\text{S.28})$$

with  $w \in \mathbb{C}$  following the dynamics (S.6). For convenience, we rewrite the dynamics as

$$\dot{\mathbf{x}} = \hat{\mathbf{L}}_0 \mathbf{x} + \varepsilon^2 \hat{\mathbf{L}}_1 \mathbf{x} + \mathbf{n}_2(\mathbf{x}, \mathbf{x}) + \mathbf{n}_3(\mathbf{x}, \mathbf{x}, \mathbf{x}) + \varepsilon^2 \kappa \mathbf{g}(\mathbf{x}, \mathbf{x}'), \quad (\text{S.29})$$

$$\dot{w} = \mathcal{W}(w, \bar{w}, w', \bar{w}'). \quad (\text{S.30})$$

The functions  $\mathcal{W}$  and  $\boldsymbol{\rho}$  have to be determined perturbatively, as outlined in the preceding section. Note also that  $\mathcal{W}$  is free from  $\theta = \theta(t)$ . If we insert the ansatz (S.28) into (S.29) and use (S.30), we find

$$\mathcal{L}_0 \boldsymbol{\rho} = \mathcal{W} \exp(i\theta) \mathbf{u} + \bar{\mathcal{W}} \exp(-i\theta) \bar{\mathbf{u}} + \mathbf{b}(w, \bar{w}, w', \bar{w}', \theta), \quad (\text{S.31})$$

with the operator  $\mathcal{L}_0 = \left( \hat{\mathbf{L}}_0 - \omega_0 \frac{\partial}{\partial \theta} \right)$ , the right eigenvector  $\mathbf{u}$  of  $\hat{\mathbf{L}}_0$  corresponding to the eigenvalue  $i\omega_0$ , and where

$$\begin{aligned} \mathbf{b} &= -\varepsilon^2 \hat{\mathbf{L}}_1 \mathbf{x} - \mathbf{n}_2(\mathbf{x}, \mathbf{x}) - \mathbf{n}_3(\mathbf{x}, \mathbf{x}, \mathbf{x}) \\ &\quad - \varepsilon^2 \kappa \mathbf{G}(\mathbf{x}, \mathbf{x}') + \mathcal{W} \frac{\partial \boldsymbol{\rho}}{\partial w} + \bar{\mathcal{W}} \frac{\partial \boldsymbol{\rho}}{\partial \bar{w}} + \mathcal{W}' \frac{\partial \boldsymbol{\rho}}{\partial w'} + \bar{\mathcal{W}}' \frac{\partial \boldsymbol{\rho}}{\partial \bar{w}'}. \end{aligned} \quad (\text{S.32})$$

Regarding (S.31) formally as an inhomogeneous linear differential equation for  $\rho(\theta)$  where the right-hand side is the inhomogeneous part, we solve it by first expanding  $\rho(\theta)$  and  $\mathbf{b}(\theta)$  as

$$\rho(\theta) = \sum_{l=-\infty}^{\infty} \rho^{(l)} \exp(il\theta) , \quad \mathbf{b}(\theta) = \sum_{l=-\infty}^{\infty} \mathbf{b}^{(l)} \exp(il\theta) . \quad (\text{S.33})$$

Then, we use that  $\exp(i\theta)\mathbf{u}$  and its complex conjugate are by construction the zero eigenvectors of the operator  $\mathcal{L}_0$ , i.e.  $\mathcal{L}_0(\exp(i\theta)\mathbf{u}) = \mathcal{L}_0(\exp(-i\theta)\bar{\mathbf{u}}) = 0$ . Since the left-hand side of (S.31) does not contain any of these zero-eigenvector components due to the action of  $\mathcal{L}_0$ , we require that these components are canceled also in the right-hand side – this is the solvability condition corresponding to (S.11) in the preceding section. Inserting the expansions (S.33) into (S.31) and comparing the first coefficients in the basis  $\{\exp(il\theta) \mid l \in \mathbb{Z}\}$ , the solvability condition reads

$$\mathcal{W} = -\mathbf{v}\mathbf{b}^{(1)} , \quad (\text{S.34})$$

where  $\mathbf{v}$  is the left eigenvector of  $\hat{\mathbf{L}}_0$  corresponding to the eigenvector  $i\omega_0$ . For completeness, we find for the other coefficients

$$\rho^{(l)} = \left( \hat{\mathbf{L}}_0 - il\omega_0 \right)^{-1} \mathbf{b}^{(l)} , \quad (l \neq \pm 1) , \quad (\text{S.35})$$

$$\rho^{(1)} = \left( \hat{\mathbf{L}}_0 - i\omega_0 \right)^{-1} \left( \mathbf{b}^{(1)} + \mathcal{W}\mathbf{u} \right) , \quad (\text{S.36})$$

$$\rho^{(-1)} = \left( \hat{\mathbf{L}}_0 + i\omega_0 \right)^{-1} \left( \mathbf{b}^{(-1)} + \bar{\mathcal{W}}\bar{\mathbf{u}} \right) . \quad (\text{S.37})$$

Furthermore, we expand  $\rho^{(l)}$  and  $\mathbf{b}^{(l)}$  in powers of  $\varepsilon$ :

$$\rho^{(l)} = \sum_{\nu=2}^{\infty} \varepsilon^{\nu} \tilde{\rho}_{\nu}^{(l)} = \sum_{\nu=2}^{\infty} \rho_{\nu}^{(l)} , \quad \mathbf{b}^{(l)} = \sum_{\nu=2}^{\infty} \varepsilon^{\nu} \tilde{\mathbf{b}}_{\nu}^{(l)} = \sum_{\nu=2}^{\infty} \mathbf{b}_{\nu}^{(l)} , \quad (\text{S.38})$$

or, correspondingly, we have

$$\rho = \sum_{\nu=2}^{\infty} \varepsilon^{\nu} \tilde{\rho}_{\nu} = \sum_{\nu=2}^{\infty} \rho_{\nu} , \quad \mathbf{b} = \sum_{\nu=2}^{\infty} \varepsilon^{\nu} \tilde{\mathbf{b}}_{\nu} = \sum_{\nu=2}^{\infty} \mathbf{b}_{\nu} . \quad (\text{S.39})$$

Likewise, we want to expand  $\mathcal{W}$ . As we are close to a Hopf bifurcation, the only resonant terms in  $w, \bar{w}$  are of the form  $|w|^n w$  with  $n = 0, 1, 2, \dots$ ; see main text *Section 2.2.2.1* and<sup>112,122</sup>. Since  $w, w' = \mathcal{O}(\varepsilon)$  and based on our previous reasoning, the only mixed terms with non-negligible effect on the amplitude dynamics (S.6) are of odd powers in  $\varepsilon$ . This justifies an expansion of the form

$$\mathcal{W} = \sum_{\nu=1}^{\infty} \varepsilon^{2\nu+1} \tilde{\mathcal{W}}_{2\nu+1} = \sum_{\nu=1}^{\infty} \mathcal{W}_{2\nu+1} . \quad (\text{S.40})$$

In total, we have  $\mathcal{W}_{\nu} = \mathcal{O}(\varepsilon^{\nu}) (\nu \geq 3)$ ,  $\mathbf{b}_{\nu}, \rho_{\nu} = \mathcal{O}(\varepsilon^{\nu}) (\nu \geq 2)$ , and  $\mathbf{x}_0 = \mathcal{O}(\varepsilon)$ . In order

to calculate  $\mathcal{W}_\nu$ , we need expressions for  $\mathbf{b}_\mu$  with  $1 \leq \mu \leq \nu$ . After substituting all the expansions above into (S.32), we compare terms of same order in  $\varepsilon$ . Respecting the symmetry of the  $\mathbf{n}_k$ 's in their arguments, we find

$$\mathbf{b}_2 = -\mathbf{n}_2(\mathbf{x}_0, \mathbf{x}_0) , \quad (\text{S.41})$$

$$\mathbf{b}_3 = -\varepsilon^2 \hat{\mathbf{L}}_1 \mathbf{x}_0 - 2\mathbf{n}_2(\mathbf{x}_0, \boldsymbol{\rho}_2) - \mathbf{n}_3(\mathbf{x}_0, \mathbf{x}_0, \mathbf{x}_0) - \kappa \varepsilon^2 (G_{10} \mathbf{x}_0 + G_{01} \mathbf{x}'_0) , \quad (\text{S.42})$$

$$\begin{aligned} \mathbf{b}_4 &= -\varepsilon^2 \hat{\mathbf{L}}_1 \boldsymbol{\rho}_2 - 2\mathbf{n}_2(\mathbf{x}_0, \boldsymbol{\rho}_3) - \mathbf{n}_2(\boldsymbol{\rho}_2, \boldsymbol{\rho}_2) - 3\mathbf{n}_3(\mathbf{x}_0, \mathbf{x}_0, \boldsymbol{\rho}_2) \\ &\quad - \kappa \varepsilon^2 \left[ G_{10} \boldsymbol{\rho}_2 + G_{01} \boldsymbol{\rho}'_2 + G_{20}(\mathbf{x}_0, \mathbf{x}_0) + G_{11}(\mathbf{x}_0, \mathbf{x}'_0) + G_{02}(\mathbf{x}'_0, \mathbf{x}'_0) \right] , \end{aligned} \quad (\text{S.43})$$

$$\begin{aligned} \mathbf{b}_5 &= -\varepsilon^2 \hat{\mathbf{L}}_1 \boldsymbol{\rho}_3 - 2\mathbf{n}_2(\mathbf{x}_0, \boldsymbol{\rho}_4) - 2\mathbf{n}_2(\boldsymbol{\rho}_2, \boldsymbol{\rho}_3) - 3\mathbf{n}_3(\mathbf{x}_0, \mathbf{x}_0, \boldsymbol{\rho}_3) - 3\mathbf{n}_3(\mathbf{x}_0, \boldsymbol{\rho}_2, \boldsymbol{\rho}_2) \\ &\quad + \mathcal{W}_3 \frac{\partial \boldsymbol{\rho}_2}{\partial w} + \bar{\mathcal{W}}_3 \frac{\partial \boldsymbol{\rho}_2}{\partial \bar{w}} + \mathcal{W}'_3 \frac{\partial \boldsymbol{\rho}_2}{\partial w'} + \bar{\mathcal{W}}'_3 \frac{\partial \boldsymbol{\rho}_2}{\partial \bar{w}'} \\ &\quad - \kappa \varepsilon^2 \left[ G_{10} \boldsymbol{\rho}_3 + G_{01} \boldsymbol{\rho}'_3 + 2G_{20}(\mathbf{x}_0, \boldsymbol{\rho}_2) + G_{11}(\mathbf{x}_0, \boldsymbol{\rho}'_2) + G_{11}(\boldsymbol{\rho}_2, \mathbf{x}'_0) + 2G_{02}(\mathbf{x}'_0, \boldsymbol{\rho}'_2) \right] \\ &\quad - \kappa \varepsilon^2 \left[ G_{30}(\mathbf{x}_0, \mathbf{x}_0, \mathbf{x}_0) + G_{21}(\mathbf{x}_0, \mathbf{x}_0, \mathbf{x}'_0) + G_{12}(\mathbf{x}_0, \mathbf{x}'_0, \mathbf{x}'_0) + G_{03}(\mathbf{x}'_0, \mathbf{x}'_0, \mathbf{x}'_0) \right] . \end{aligned} \quad (\text{S.44})$$

Using the solvability condition (S.34), we can calculate  $\mathcal{W}_3 = -\mathbf{v} \mathbf{b}_3^{(1)}$  via

$$\begin{aligned} \mathbf{b}_3^{(1)} &= -\varepsilon^2 \hat{\mathbf{L}}_1 \mathbf{x}_0^{(1)} - 2\mathbf{n}_2(\mathbf{x}_0, \boldsymbol{\rho}_2)^{(1)} - \mathbf{n}_3(\mathbf{x}_0, \mathbf{x}_0, \mathbf{x}_0)^{(1)} - \kappa \varepsilon^2 (G_{10} \mathbf{x}_0^{(1)} + G_{01} \mathbf{x}'_0^{(1)}) \\ &= -\varepsilon^2 \hat{\mathbf{L}}_1 \mathbf{x}_0^{(1)} - 2\mathbf{n}_2(\mathbf{x}_0^{(1)}, \boldsymbol{\rho}_2^{(0)}) - 2\mathbf{n}_2(\mathbf{x}_0^{(-1)}, \boldsymbol{\rho}_2^{(2)}) \\ &\quad - \mathbf{n}_3(\mathbf{x}_0^{(1)}, \mathbf{x}_0^{(1)}, \mathbf{x}_0^{(-1)}) - \kappa \varepsilon^2 (G_{10} \mathbf{x}_0^{(1)} + G_{01} \mathbf{x}'_0^{(1)}) . \end{aligned} \quad (\text{S.45})$$

Combining (S.35) and (S.41), we have

$$\boldsymbol{\rho}_2^{(0)} = \hat{\mathbf{L}}_0^{-1} \mathbf{b}_2^{(0)} = -2\hat{\mathbf{L}}_0^{-1} \mathbf{n}_2(\mathbf{x}_0^{(1)}, \mathbf{x}_0^{(-1)}) , \quad (\text{S.46})$$

$$\boldsymbol{\rho}_2^{(2)} = (\hat{\mathbf{L}}_0 - 2i\omega_0)^{-1} \mathbf{b}_2^{(2)} = (\hat{\mathbf{L}}_0 - 2i\omega_0)^{-1} \mathbf{n}_2(\mathbf{x}_0^{(1)}, \mathbf{x}_0^{(1)}) . \quad (\text{S.47})$$

Finally, noting that  $\mathbf{x}_0^{(1)} = w\mathbf{u}$  and  $\mathbf{x}_0^{(-1)} = w\bar{\mathbf{u}}$ , we retrieve from (S.46)

$$\mathcal{W}_3 = \varepsilon^2 \alpha - \beta |w|^2 w + \varepsilon^2 \kappa [\gamma_{10} w + \gamma_{01} w'] , \quad (\text{S.48})$$

with

$$\alpha = \mathbf{v} \hat{\mathbf{L}}_1 \mathbf{u} , \quad (\text{S.49})$$

$$\beta = -3\mathbf{v} \mathbf{n}_3(\mathbf{u}, \mathbf{u}, \bar{\mathbf{u}}) + 4\mathbf{v} \mathbf{n} \left( \mathbf{u}, \hat{\mathbf{L}}_0^{-1} \mathbf{n}_2(\mathbf{u}, \bar{\mathbf{u}}) \right) + 2\mathbf{v} \mathbf{n}_2 \left( \bar{\mathbf{u}}, (\hat{\mathbf{L}}_0 - 2i\omega_0)^{-1} \mathbf{n}_2(\mathbf{u}, \mathbf{u}) \right) , \quad (\text{S.50})$$

$$\gamma_{10} = \mathbf{v} G_{10} \mathbf{u} , \quad \gamma_{01} = \mathbf{v} G_{01} \mathbf{u} . \quad (\text{S.51})$$

Analogously, we calculate  $\mathcal{W}_5 = -\mathbf{v}\mathbf{b}_5^{(1)}$ :

$$\begin{aligned}
\mathbf{b}_5^{(1)} = & -\varepsilon^2 \hat{\mathbf{L}}_1 \boldsymbol{\rho}_3^{(1)} - 2\mathbf{n}_2(\mathbf{x}_0, \boldsymbol{\rho}_4)^{(1)} - 2\mathbf{n}_2(\boldsymbol{\rho}_2, \boldsymbol{\rho}_3)^{(1)} \\
& - 3\mathbf{n}_3(\mathbf{x}_0, \mathbf{x}_0, \boldsymbol{\rho}_3)^{(1)} - 3\mathbf{n}_3(\mathbf{x}_0, \boldsymbol{\rho}_2, \boldsymbol{\rho}_2)^{(1)} \\
& + \mathcal{W}_3 \frac{\partial \boldsymbol{\rho}_2^{(1)}}{\partial w} + \bar{\mathcal{W}}_3 \frac{\partial \boldsymbol{\rho}_2^{(1)}}{\partial \bar{w}} + \mathcal{W}'_3 \frac{\partial \boldsymbol{\rho}_2^{(1)}}{\partial w'} + \bar{\mathcal{W}}'_3 \frac{\partial \boldsymbol{\rho}_2^{(1)}}{\partial \bar{w}'} - \kappa \varepsilon^2 \left[ G_{10} \boldsymbol{\rho}_3^{(1)} + G_{01} \boldsymbol{\rho}'_3^{(1)} \right] \\
& - \kappa \varepsilon^2 \left[ 2G_{20}(\mathbf{x}_0, \boldsymbol{\rho}_2)^{(1)} + G_{11}(\mathbf{x}_0, \boldsymbol{\rho}'_2)^{(1)} + G_{11}(\boldsymbol{\rho}_2, \mathbf{x}'_0)^{(1)} + 2G_{02}(\mathbf{x}'_0, \boldsymbol{\rho}'_2)^{(1)} \right] \\
& - \kappa \varepsilon^2 \left[ G_{30}(\mathbf{x}_0, \mathbf{x}_0, \mathbf{x}_0)^{(1)} + G_{21}(\mathbf{x}_0, \mathbf{x}_0, \mathbf{x}'_0)^{(1)} \right. \\
& \quad \left. + G_{12}(\mathbf{x}_0, \mathbf{x}'_0, \mathbf{x}'_0)^{(1)} + G_{03}(\mathbf{x}'_0, \mathbf{x}'_0, \mathbf{x}'_0)^{(1)} \right] \tag{S.52}
\end{aligned}$$

Again, we have to expand the terms as before, which we show here for only the first line of (S.52), the other terms follow equivalently,

$$\begin{aligned}
\mathbf{n}_2(\mathbf{x}_0, \boldsymbol{\rho}_4)^{(1)} &= \mathbf{n}_2(\mathbf{x}_0^{(1)}, \boldsymbol{\rho}_4^{(0)}) + \mathbf{n}_2(\mathbf{x}_0^{(-1)}, \boldsymbol{\rho}_4^{(2)}) , \\
\mathbf{n}_2(\boldsymbol{\rho}_2, \boldsymbol{\rho}_3)^{(1)} &= \mathbf{n}_2(\boldsymbol{\rho}_2^{(2)}, \boldsymbol{\rho}_3^{(-1)}) + \mathbf{n}_2(\boldsymbol{\rho}_2^{(1)}, \boldsymbol{\rho}_3^{(0)}) + \mathbf{n}_2(\boldsymbol{\rho}_2^{(0)}, \boldsymbol{\rho}_3^{(1)}) \\
& \quad + \mathbf{n}_2(\boldsymbol{\rho}_2^{(-1)}, \boldsymbol{\rho}_3^{(2)}) + \mathbf{n}_2(\boldsymbol{\rho}_2^{(-2)}, \boldsymbol{\rho}_3^{(3)}) , \\
\mathbf{n}_3(\mathbf{x}_0, \mathbf{x}_0, \boldsymbol{\rho}_3)^{(1)} &= \mathbf{n}_3(\mathbf{x}_0^{(1)}, \mathbf{x}_0^{(1)}, \boldsymbol{\rho}_3^{(-1)}) + 2\mathbf{n}_3(\mathbf{x}_0^{(1)}, \mathbf{x}_0^{(-1)}, \boldsymbol{\rho}_3^{(1)}) + \mathbf{n}_3(\mathbf{x}_0^{(-1)}, \mathbf{x}_0^{(-1)}, \boldsymbol{\rho}_3^{(3)}) , \\
\mathbf{n}_3(\mathbf{x}_0, \boldsymbol{\rho}_2, \boldsymbol{\rho}_2)^{(1)} &= 2\mathbf{n}_3(\mathbf{x}_0^{(1)}, \boldsymbol{\rho}_2^{(2)}, \boldsymbol{\rho}_2^{(-2)}) + 2\mathbf{n}_3(\mathbf{x}_0^{(1)}, \boldsymbol{\rho}_2^{(1)}, \boldsymbol{\rho}_2^{(-1)}) + 2\mathbf{n}_3(\mathbf{x}_0^{(1)}, \boldsymbol{\rho}_2^{(0)}, \boldsymbol{\rho}_2^{(0)}) \\
& \quad + 2\mathbf{n}_3(\mathbf{x}_0^{(-1)}, \boldsymbol{\rho}_2^{(2)}, \boldsymbol{\rho}_2^{(0)}) + \mathbf{n}_3(\mathbf{x}_0^{(-1)}, \boldsymbol{\rho}_2^{(1)}, \boldsymbol{\rho}_2^{(1)}) .
\end{aligned}$$

We aim for those terms that contribute to  $\kappa \varepsilon^2 \bar{w} w'^2$ . Following Kori et al.<sup>95</sup>, we can exclude all terms that (a) include  $\boldsymbol{\rho}_2$ , (b) include  $\mathbf{x}_0^{(1)}$ , and (c) include  $\mathbf{x}_0^{(-1)}$  twice. We find the remaining terms

$$\begin{aligned}
& -\varepsilon^2 \hat{\mathbf{L}}_1 \boldsymbol{\rho}_3^{(1)} - 2\mathbf{n}_2 \left( \mathbf{x}_0^{(-1)}, \boldsymbol{\rho}_4^{(2)} \right) \\
& - \kappa \varepsilon^2 \left[ G_{10} \boldsymbol{\rho}_3^{(1)} + G_{01} \boldsymbol{\rho}'_3^{(1)} + G_{11} \left( \mathbf{x}_0^{(-1)}, \boldsymbol{\rho}'_2^{(2)} \right) + G_{12} \left( \mathbf{x}_0^{(-1)}, \mathbf{x}'_0^{(1)}, \mathbf{x}'_0^{(1)} \right) \right] . \tag{S.53}
\end{aligned}$$

The first term can be dropped because the coupling term included there is linear. Furthermore, the first two terms in brackets can be dropped, too, as each yields exclusively either  $w, \bar{w}$  or  $w', \bar{w}'$ . Hence, the only relevant terms in  $\mathbf{b}_5^{(1)}$  are the two last terms in brackets and the  $\kappa$ -dependent term in

$$- \mathbf{n}_2 \left( \mathbf{x}_0^{(-1)}, \boldsymbol{\rho}_4^{(2)} \right) . \tag{S.54}$$

As to the latter, according to (S.35) and (S.43) the  $\kappa$ -dependent terms in  $\boldsymbol{\rho}_4^{(2)}$  are

$$\begin{aligned}
& \left( \hat{\mathbf{L}}_0 - 2i\omega_0 \right)^{-1} \left( -\kappa \varepsilon^2 \left[ G_{10} \boldsymbol{\rho}_2^{(2)} + G_{01} \boldsymbol{\rho}'_2^{(2)} \right. \right. \\
& \quad \left. \left. + G_{20}(\mathbf{x}_0^{(1)}, \mathbf{x}_0^{(1)}) + G_{11}(\mathbf{x}_0^{(1)}, \mathbf{x}'_0^{(1)}) + G_{02}(\mathbf{x}'_0^{(1)}, \mathbf{x}'_0^{(1)}) \right] \right) .
\end{aligned}$$

For the same reasons as above, all but the second and the last term in brackets can be

dropped. Using (S.41), we have

$$\rho'_2^{(2)} = \left( \hat{\mathbf{L}}_0 - 2i\omega_0 \right)^{-1} \left( -\mathbf{n}_2 \left( \mathbf{x}'_0^{(1)}, \mathbf{x}'_0^{(1)} \right) \right) = -w'^2 \left( \hat{\mathbf{L}}_0 - 2i\omega_0 \right)^{-1} \mathbf{n}_2(\mathbf{u}, \mathbf{u}) . \quad (\text{S.55})$$

Hence, (S.54) reduces to the  $\kappa$ -dependent terms

$$-2\kappa\varepsilon^2\bar{w}w'^2\mathbf{n}_2\left(\bar{\mathbf{u}}, \left(\hat{\mathbf{L}}_0 - 2i\omega_0\right)^{-1} \left[ G_{01} \left( \hat{\mathbf{L}}_0 - 2i\omega_0 \right)^{-1} \mathbf{n}_2(\mathbf{u}, \mathbf{u}) - G_{02}(\mathbf{u}, \mathbf{u}) \right] \right) . \quad (\text{S.56})$$

In addition to this term, we find additionally

$$+ \kappa\varepsilon^2\bar{w}w'^2 \left[ G_{11} \left( \bar{\mathbf{u}}, \left( \hat{\mathbf{L}}_0 - 2i\omega_0 \right)^{-1} \mathbf{n}_2(\mathbf{u}, \mathbf{u}) \right) - G_{12}(\bar{\mathbf{u}}, \mathbf{u}, \mathbf{u}) \right] . \quad (\text{S.57})$$

Taken (S.56) and (S.57) together, we find the following expression for  $\delta$  in (S.24):

$$\begin{aligned} \delta = 2\mathbf{v}\mathbf{n}_2\left(\bar{\mathbf{u}}, \left( \hat{\mathbf{L}}_0 - 2i\omega_0 \right)^{-1} \left[ G_{01} \left( \hat{\mathbf{L}}_0 - 2i\omega_0 \right)^{-1} \mathbf{n}_2(\mathbf{u}, \mathbf{u}) - G_{02}(\mathbf{u}, \mathbf{u}) \right] \right) \\ - \mathbf{v}G_{11} \left( \bar{\mathbf{u}}, \left( \hat{\mathbf{L}}_0 - 2i\omega_0 \right)^{-1} \mathbf{n}_2(\mathbf{u}, \mathbf{u}) \right) + \mathbf{v}G_{12}(\bar{\mathbf{u}}, \mathbf{u}, \mathbf{u}) . \end{aligned} \quad (\text{S.58})$$

Note that in the case of linear coupling, all  $G_{jk}$  vanish but  $G_{01}$ , in which case we confirm the results by Kori et al.<sup>95</sup>.

### S.3 Poincaré's reduction via nonlinear transforms

We consider two weakly coupled two-dimensional oscillators  $\mathbf{x} = (x, y)$ ,  $\mathbf{x}' = (x', y') \in \mathbb{R}^2$  near a supercritical Hopf bifurcation, whose general dynamics is given by

$$\dot{\mathbf{x}} = \mathbf{f}(\mathbf{x}, t; \mu) + \kappa \mathbf{g}(\mathbf{x}, \mathbf{x}', t; \mu) \quad (\text{S.59})$$

and which we seek to transform into a generic normal form

$$\dot{w} = \alpha w - \beta|w|^2 w + \kappa h(w, w') , \quad (\text{S.60})$$

where the complex parameters  $\alpha = \alpha(\mu)$ ,  $\beta = \beta(\mu)$  and the coupling function<sup>[2]</sup>  $h$  have to be determined subsequently. For the sake of legibility, we drop the explicit time-dependence of  $\mathbf{f}$  and  $\mathbf{g}$ , and note that the theory also holds when allowing for time variations.

By definition and without loss of generality, the dynamics of an uncoupled unit

$$\dot{\mathbf{x}} = \mathbf{f}(\mathbf{x}; \mu) \quad (\text{S.61})$$

---

<sup>[2]</sup> In this section we denote the coupling function of the resulting Hopf normal form by  $h$  and thereby deviate from the general notation  $g$ .

has for all sufficiently small  $|\mu| \ll 1$  the equilibrium  $(0, 0)$  with eigenvalues

$$\lambda_{1,2}(\mu) = \varrho(\mu) \pm i\omega(\mu) , \quad (\text{S.62})$$

where  $\varrho(0) = 0$  and  $\omega(0) = \omega_0 > 0$ . The first Lyapunov coefficient  $l_1(0) = -\text{Re } \beta(0)/\omega(0)$ , which depends on the properties of the function  $\mathbf{f}$ , does not vanish and  $\varrho'(0) \neq 0$ . In particular, we can rewrite (S.61) as

$$\frac{d}{dt} \begin{pmatrix} x \\ y \end{pmatrix} = \mathbf{L}(\mu) \begin{pmatrix} x \\ y \end{pmatrix} + \mathbf{F} \left( \begin{pmatrix} x \\ y \end{pmatrix}; \mu \right) \quad \text{with} \quad \mathbf{L}(\mu) = \begin{pmatrix} a_{11}(\mu) & a_{12}(\mu) \\ a_{21}(\mu) & a_{22}(\mu) \end{pmatrix} , \quad (\text{S.63})$$

where we further set  $\sigma(\mu) = \text{tr } \mathbf{L}(\mu)$  and  $\Delta(\mu) = \det \mathbf{L}(\mu)$ , such that

$$\lambda_{1,2}(\mu) = \frac{1}{2} \left[ \sigma(\mu) \pm \sqrt{\sigma(\mu)^2 - 4\Delta(\mu)} \right] . \quad (\text{S.64})$$

The Hopf bifurcation assumption translates into  $\sigma(0) = 0$  and  $\Delta(0) = \omega_0^2 > 0$ . For small  $|\mu|$ , we can introduce

$$\varrho(\mu) = \frac{1}{2}\sigma(\mu), \quad \omega(\mu) = \frac{1}{2}\sqrt{4\Delta(\mu) - \sigma(\mu)^2} \quad (\text{S.65})$$

and set  $\lambda_1 = \lambda$ ,  $\lambda_2 = \bar{\lambda}$ . As can already be anticipated, the parameter  $\alpha$  in (S.60) is exactly the eigenvalue  $\lambda$ .

Let us now couple this unit,  $\mathbf{x} = (x, y)$ , to another identical unit,  $\mathbf{x}' = (x', y')$ , that is,  $\mathbf{f} = \mathbf{f}'$ , via the coupling function  $\mathbf{g}(\mathbf{x}, \mathbf{x}')$  and with coupling strength  $\kappa \in \mathbb{R}$ . In general,  $\mathbf{g}$  depends on both the control parameter  $\mu$  and the coupling  $\kappa$ . Since  $|\kappa| \ll 1$  is sufficiently small, we will assume that the coupling function depends on  $\kappa$  only up to first order, so that the system of interest reads

$$\dot{\mathbf{x}} = \mathbf{f}(\mathbf{x}; \mu) + \kappa \tilde{\mathbf{g}}(\mathbf{x}, \mathbf{x}'; \mu) + \mathcal{O}(\kappa^2) , \quad (\text{S.66})$$

where  $\tilde{\mathbf{g}} = \mathbf{g} + \mathcal{O}(\kappa)$ . In the following we omit the tilde. While common normal form transforms merely consider single units, the following lemmata along the line of Chapter 3, Lemmata 3.3 – 3.6, in<sup>122</sup> are adapted to take the full, coupled system (S.66) into account. By subsequently applying the theory outlined in this section, we can derive the transformed equations in Hopf normal form and thereby allow for a reduction of the dynamics onto the center manifold where we provide also the exact transformations of the nonlinear terms in the coupling function  $\mathbf{g}$ . To start with, we first rewrite the dynamics in complex form.

**Lemma S.2.** *By introducing a complex variable  $z \in \mathbb{C}$ , system (S.66) can be written for sufficiently small  $|\mu|$  as a single equation:*

$$\dot{z} = \lambda(\mu)z + \tilde{f}(z, \bar{z}; \mu) + \kappa \tilde{g}(z, \bar{z}, z', \bar{z}'; \mu) + \mathcal{O}(\kappa^2) , \quad (\text{S.67})$$

where  $\tilde{f}, \tilde{g} = \mathcal{O}(|z|^2)$  are smooth functions of  $(z, \bar{z}; \mu)$ , and  $(z, \bar{z}, z', \bar{z}'; \mu)$ , respectively.

Note that  $z$  refers to unit  $\mathbf{x}$  and  $z'$  represents  $\mathbf{x}'$ .

*Proof.* As we assume  $\mathbf{x}$  and  $\mathbf{x}'$  being identical in the uncoupled case,  $\kappa = 0$ , the following reasoning applies to both  $\mathbf{x}$  and  $\mathbf{x}'$ . Let  $\mathbf{u}(\mu) = (u_1(\mu), u_2(\mu))^\top \in \mathbb{C}^2$  be a right eigenvector of  $\mathbf{L}(\mu)$  corresponding to the eigenvalue  $\lambda(\mu)$ :  $\mathbf{L}(\mu)\mathbf{u}(\mu) = \lambda(\mu)\mathbf{u}(\mu)$ , and let  $\mathbf{v}(\mu) = (v_1(\mu), v_2(\mu)) \in \mathbb{C}^{1 \times 2}$  be the corresponding left eigenvector:  $\mathbf{v}(\mu)\mathbf{L}(\mu) = \lambda(\mu)\mathbf{v}(\mu)$ . We assume  $\mathbf{u}, \mathbf{v}$  are normalized such that  $\mathbf{v}(\mu)\mathbf{u}(\mu) = v_1(\mu)u_1(\mu) + v_2(\mu)u_2(\mu) = 1$ . Every vector  $\mathbf{x} \in \mathbb{R}^2$  can be uniquely represented for any small  $|\mu|$  as

$$\mathbf{x} = z\mathbf{u}(\mu) + \bar{z}\bar{\mathbf{u}}(\mu) \quad (\text{S.68})$$

for some complex  $z$  and provided the eigenvectors are specified. Then,  $z = v(\mu)\mathbf{x}$ . A rigorous justification can be found in Lemma 3.3,<sup>122</sup>. By vector calculus we find that

$$\begin{aligned} \dot{z} &= \mathbf{v}(\mu)\dot{\mathbf{x}} = \mathbf{v}(\mu) [\mathbf{L}(\mu)\mathbf{x} + \mathbf{F}(\mathbf{x}; \mu) + \kappa\mathbf{g}(\mathbf{x}, \mathbf{x}'; \mu) + \mathcal{O}(\kappa^2)] \\ &= \mathbf{v}(\mu)\mathbf{L}(\mu)\mathbf{x} + \mathbf{v}(\mu)\mathbf{F}(z\mathbf{u}(\mu) + \bar{z}\bar{\mathbf{u}}(\mu); \mu) \\ &\quad + \kappa\mathbf{v}(\mu)g(z\mathbf{u}(\mu) + \bar{z}\bar{\mathbf{u}}(\mu), z'\mathbf{u}(\mu) + \bar{z}'\bar{\mathbf{u}}(\mu); \mu) + \mathcal{O}(\kappa^2) \\ &= \lambda(\mu)z + \tilde{f}(z, \bar{z}; \mu) + \kappa\tilde{g}(z, \bar{z}, z', \bar{z}'; \mu) + \mathcal{O}(\kappa^2), \end{aligned} \quad (\text{S.69})$$

where  $\mathbf{F}$  denotes the nonlinear part of the function  $\mathbf{f}(\mathbf{x}; \mu) = \mathbf{L}(\mu)\mathbf{x} + \mathbf{F}(\mathbf{x}; \mu)$ .  $\square$

It is favorable to write  $\tilde{f}$  as a formal Taylor series in the two complex variables  $z$  and  $\bar{z}$ :

$$\tilde{f}(z, \bar{z}; \mu) = \sum_{k+l \geq 2} \frac{1}{k!l!} f_{kl}(\mu) z^k \bar{z}^l, \quad (\text{S.70})$$

where

$$f_{kl}(\mu) = \left. \frac{\partial^{k+l}}{(\partial z)^k (\partial \bar{z})^l} \mathbf{v}(\mu) \mathbf{f}(z\mathbf{u}(\mu) + \bar{z}\bar{\mathbf{u}}(\mu); \mu) \right|_{z=0}$$

for  $k + l \geq 2$ ,  $k, l = 0, 1, \dots$ .

**Remark.** Suppose at  $\mu = 0$  the function  $\mathbf{f}(\mathbf{x}, 0)$  in (S.66) is represented as

$$\mathbf{f}(\mathbf{x}, 0) = \frac{1}{2}\mathbf{B}(\mathbf{x}, \mathbf{x}) + \frac{1}{6}\mathbf{C}(\mathbf{x}, \mathbf{x}, \mathbf{x}) + \mathcal{O}(\|\mathbf{x}\|^4),$$

where  $\mathbf{B}(\mathbf{p}, \mathbf{q})$  and  $\mathbf{C}(\mathbf{p}, \mathbf{q}, \mathbf{r})$  are symmetric multilinear vector functions of  $\mathbf{p}, \mathbf{q}, \mathbf{r} \in \mathbb{R}^2$ . In coordinates, we have

$$\mathbf{B}_i(\mathbf{p}, \mathbf{q}) = \sum_{j,k=1}^2 \left. \frac{\partial^2 f_i(\boldsymbol{\xi}, 0)}{\partial \xi_j \partial \xi_k} \right|_{\boldsymbol{\xi}=0} p_j q_k, \quad i = 1, 2,$$

and

$$\mathbf{C}_i(\mathbf{p}, \mathbf{q}, \mathbf{r}) = \sum_{j,k,l=1}^2 \left. \frac{\partial^3 f_i(\boldsymbol{\xi}, 0)}{\partial \xi_j \partial \xi_k \partial \xi_l} \right|_{\boldsymbol{\xi}=0} p_j q_k r_l, \quad i = 1, 2.$$

Then,

$$\mathbf{B}(z\mathbf{u} + \bar{z}\bar{\mathbf{u}}, z\mathbf{u} + \bar{z}\bar{\mathbf{u}}) = z^2\mathbf{B}(\mathbf{u}, \mathbf{u}) + 2z\bar{z}\mathbf{B}(\mathbf{u}, \bar{\mathbf{u}}) + \bar{z}^2\mathbf{B}(\bar{\mathbf{u}}, \bar{\mathbf{u}}) , \quad (\text{S.71})$$

where  $\mathbf{u} = \mathbf{u}(0), \mathbf{v} = \mathbf{v}(0)$ . Hence, the Taylor coefficients  $f_{kl}$  of the quadratic terms in  $\tilde{f}(z, \bar{z}, 0)$ , i.e.  $k + l = 2$ , can be expressed by

$$f_{20} = \mathbf{v}\mathbf{B}(\mathbf{u}, \mathbf{u}), \quad f_{11} = \mathbf{v}\mathbf{B}(\mathbf{u}, \bar{\mathbf{u}}), \quad f_{02} = \mathbf{v}\mathbf{B}(\bar{\mathbf{u}}, \bar{\mathbf{u}}) . \quad (\text{S.72})$$

Similar calculations with  $\mathbf{C}$  give

$$f_{21} = \mathbf{v}\mathbf{C}(\mathbf{u}, \mathbf{u}, \bar{\mathbf{u}}) . \quad (\text{S.73})$$

The following two lemmata are the key to transform system (S.66) into Hopf normal form. In fact, both are polynomial coordinate transformations whose coefficients depend smoothly on  $\mu$ . The proofs of the respective lemma use their inverse transformations, which are again smoothly dependent on  $\mu$  but not necessarily polynomial. However, we will not provide the proofs here but refer to Chapter 3.5 in<sup>122</sup>. It is worth mentioning that in some neighborhood of the origin  $\mathbf{x} = (0, 0)$ , these transformations are *near-identical* due to their linear parts.

The first lemma transforms the equation into one without any quadratic terms:

**Lemma S.3** (Lemma 3.4<sup>122</sup>). *The equation*

$$\dot{z} = \lambda z + \frac{f_{20}}{2}z^2 + f_{11}z\bar{z} + \frac{f_{02}}{2}\bar{z}^2 + \mathcal{O}(|z|^3) , \quad (\text{S.74})$$

where  $\lambda = \lambda(\mu) = \varrho(\mu) + i\omega(\mu)$ ,  $\varrho(0) = 0, \omega(0) = \omega_0 > 0$ , and  $f_{kl} = f_{kl}(\mu)$ , can be transformed by an invertible parameter-dependent change of complex coordinate

$$z = w + \frac{h_{20}}{2}w^2 + h_{11}w\bar{w} + \frac{h_{02}}{2}\bar{w}^2$$

for all sufficiently small  $|\mu|$ , into an equation without quadratic terms:

$$\dot{w} = \lambda w + \mathcal{O}(|w|^3).$$

The second lemma transforms the quadratic-free equation into an equation with only one cubic term left:

**Lemma S.4** (Lemma 3.5<sup>122</sup>). *The equation*

$$\dot{z} = \lambda z + \frac{f_{30}}{6}z^3 + \frac{f_{21}}{2}z^2\bar{z} + \frac{f_{12}}{2}z\bar{z}^2 + \frac{f_{03}}{6}\bar{z}^3 + \mathcal{O}(|z|^4) , \quad (\text{S.75})$$

where  $\lambda = \lambda(\mu) = \varrho(\mu) + i\omega(\mu)$ ,  $\varrho(0) = 0, \omega(0) = \omega_0 > 0$ , and  $f_{kl} = f_{kl}(\mu)$ , can be transformed by an invertible parameter-dependent change of complex coordinate

$$z = w + \frac{h_{30}}{6}w^3 + \frac{h_{21}}{2}w^2\bar{w} + \frac{h_{12}}{2}w\bar{w}^2 + \frac{h_{03}}{6}\bar{w}^3$$

for all sufficiently small  $|\mu|$ , into an equation with only one cubic term:

$$\dot{w} = \lambda w + c_1 w^2 \bar{w} + \mathcal{O}(|w|^4),$$

where  $c_1 = c_1(\mu) = f_{21}/2$ .

Combining the previous two lemmata, we can achieve the *Poincaré normal form for the Hopf bifurcation* cf. also Lemma 3.6 in 122.

**Lemma S.5.** *The equation*

$$\dot{z} = \lambda z + \sum_{2 \leq k+l \leq 3} \frac{1}{k!l!} f_{kl} z^k \bar{z}^l + \kappa \tilde{g}(z, \bar{z}, z', \bar{z}'; \mu) + \mathcal{O}(|Z|^4, \kappa^2), \quad (\text{S.76})$$

with  $Z = (z, z')$ , and where  $\lambda = \lambda(\mu) = \varrho(\mu) + i\omega(\mu)$ ,  $\varrho(0) = 0$ ,  $\omega(0) = \omega_0 > 0$ , and  $f_{kl} = f_{kl}(\mu)$ , and where  $\tilde{g}$  denotes  $\tilde{g}$  truncated after cubic terms, can be transformed by an invertible parameter-dependent change of complex coordinate, smoothly depending on the parameter,

$$z = \psi(w) = w + \frac{h_{20}}{2} w^2 + h_{11} w \bar{w} + \frac{h_{02}}{2} \bar{w}^2 + \frac{h_{30}}{6} w^3 + \frac{h_{12}}{2} w \bar{w}^2 + \frac{h_{03}}{6} \bar{w}^3, \quad (\text{S.77})$$

for all sufficiently small  $|\mu|$ , into an equation with only one cubic term:

$$\dot{w} = \lambda w - \beta w^2 \bar{w} + \kappa h(w, \bar{w}, w', \bar{w}') + \mathcal{O}(|W|^4, \kappa^2), \quad (\text{S.78})$$

with  $W = (w, w')$ , and where  $\beta = \beta(\mu) = -c_1(\mu)$  is given by

$$c_1 = \frac{f_{20}f_{11}(2\lambda + \bar{\lambda})}{2|\lambda|^2} + \frac{|f_{11}|^2}{\lambda} + \frac{|f_{02}|^2}{2(2\lambda - \bar{\lambda})} + \frac{f_{21}}{2}, \quad (\text{S.79})$$

and  $h$  has only polynomial components of degree lower or equal than 3, i.e.  $h$  is of the form

$$h(w, \bar{w}, w', \bar{w}') = \sum_{0 \leq k+l+m+n \leq 3} h_{klmn} w^k \bar{w}^l w'^m \bar{w}'^n, \quad (\text{S.80})$$

where for  $k + l + m + n = 0$  we have  $h_{klmn} = \tilde{g}_{klmn}$  with the latter being the Taylor coefficients of  $\tilde{g}$ , and if  $\tilde{g}$  has no constant term, i.e.  $\tilde{g}_{0000} = 0$ , then  $h_{klmn} = \tilde{g}_{klmn}$  holds also for  $k + l + m + n = 1$ .

*Proof.* The first part of the proof is a combination of the previous two lemmata. We apply the first lemma to (S.76) in order to get rid of the quadratic terms. Then, we can apply the second lemma and arrive at the amplitude equation as wanted. Note that by the first transformation the coefficients of the cubic and higher order terms may have changed. Therefore, the coefficients of the inverse transforms as given in the proofs for the two lemmata as in 122 are no longer valid in our scenario. Once the two subsequent near-identity transforms have been established, we can also apply them to the coupling term. Indeed, the near-identity character leaves the linear terms unchanged such that  $h_{klmn} = g_{klmn}$  at order  $\mathcal{O}(|Z|, |W|)$ .

Practically, the idea of finding the coefficients in (S.78) breaks down to identifying the coefficients  $a_{jk}$  of a local inverse transform up to order  $\mathcal{O}(|w|^4)$ :

$$w = \psi^{-1}(z) = z + a_{20}z^2 + a_{11}z\bar{z} + z_{02}\bar{z}^2 + a_{30}z^3 + a_{21}z^2\bar{z} + a_{12}z\bar{z}^2 + a_{03}\bar{z}^3 + \dots . \quad (\text{S.81})$$

Inserting the forward transform (S.77) into (S.81) and evaluating the right- and left-hand sides coefficient-wise, provides the inverse coefficients  $a_{jk}$ :

$$\begin{aligned} a_{20} &= -\frac{h_{20}}{2}, \quad a_{11} = -h_{11}, \quad a_{02} = -\frac{h_{02}}{2}, \\ a_{30} &= -\frac{h_{30}}{6} + \frac{h_{20}^2}{2} + \frac{h_{11}\bar{h}_{02}}{2}, \\ a_{21} &= \frac{3h_{20}h_{11}}{2} + |h_{11}|^2 + \frac{|h_{02}|^2}{2}, \\ a_{12} &= -\frac{h_{12}}{2} + \frac{h_{20}h_{02}}{2} + h_{11}^2 + \frac{h_{11}\bar{h}_{20}}{2} + \frac{\bar{h}_{11}h_{02}}{2}, \\ a_{03} &= -\frac{h_{03}}{6} + \frac{h_{11}h_{02}}{2} + \frac{\bar{h}_{20}h_{20}}{2}. \end{aligned}$$

By differentiating the inverse transform (S.81) with respect to  $t$  and by using the abbreviations  $f(z) = \sum_{k,l} 1/(k!l!) f_{kl} z^k \bar{z}^l$ ,  $g(z, z') = \tilde{g}(z, \bar{z}, z', \bar{z}')$ , and  $f(w) = f(\psi(w))$ ,  $g(w, w') = g(\psi(w), \psi(w'))$ , we have

$$\begin{aligned} \dot{w} &= \frac{d}{dt} \psi^{-1}(z) = \dot{z} + 2a_{20}z\dot{z} + a_{11}\dot{z}\bar{z} + a_{11}z\dot{\bar{z}} + \dots \\ &= \lambda z + f(z) + \kappa g(z, z') + 2a_{20} [\lambda z^2 + f(z)z + \kappa g(z, z')z] \\ &\quad + a_{11} [(\lambda + \bar{\lambda})z\bar{z} + \overline{f(z)}z + f(z)\bar{z} + \kappa(\overline{g(z, z')})z + g(z, z')\bar{z}] + \dots \\ &= \lambda\psi(w) + f(w) + 2a_{20} [\lambda\psi(w)^2 + f(w)\psi(w)] \\ &\quad + a_{11} [(\lambda + \bar{\lambda})\psi(w)\psi(\bar{w}) + \overline{f(w)}\psi(w) + f(w)\psi(\bar{w})] + \dots \\ &\quad + \kappa [g(w, w') + 2a_{20}g(w, w')\psi(w) + a_{11} (\overline{g(w, w')}\psi(w) + g(w, w')\psi(\bar{w})) + \dots] \\ &\stackrel{!}{=} \lambda w - \beta w^2 \bar{w} + \kappa h(w, \bar{w}, w', \bar{w}') + \mathcal{O}(|w|^4), \end{aligned}$$

where we inserted the dynamics (S.76) in the second equality and used the forward transform (S.77) in the third equality. Note that we assumed that  $z$  and  $z'$  coincide in the uncoupled case  $\kappa = 0$ . That is why the coordinate transforms  $z = \psi(w)$  and  $z' = \psi'(w')$  take the same form, that is,  $\psi = \psi'$ . Now, by collecting terms of the same order and requiring that all quadratic and cubic terms except for the  $w\bar{w}^2$ -coefficient  $\beta$  are zero, we can solve the last equality and find  $\beta = -c_1$  as (S.79) and the resulting coefficients  $h_{jk}$  of the forward transform (S.77) as

$$h_{20} = \frac{f_{20}}{\lambda}, \quad h_{11} = \frac{f_{11}}{\bar{\lambda}}, \quad h_{02} = \frac{f_{02}}{2\bar{\lambda} - \lambda},$$

and

$$\begin{aligned} h_{30} &= \frac{f_{30}}{2\bar{\lambda}} + \frac{3f_{20}^2}{2\lambda^2} + \frac{3f_{11}\bar{f}_{02}}{2|\lambda|^2} \frac{\bar{\lambda} - \lambda}{2\lambda - \bar{\lambda}}, \\ h_{21} &= \frac{f_{21}}{2\bar{\lambda}} + \frac{f_{20}f_{02}}{2\bar{\lambda}(2\bar{\lambda} - \lambda)} + \frac{f_{11}^2}{\bar{\lambda}^2} + \frac{f_{11}\bar{f}_{20}}{2\bar{\lambda}^3} (3\bar{\lambda} - 2\lambda) + \frac{\bar{f}_{11}f_{02}}{2|\lambda|^2} \frac{2\bar{\lambda} - 3\lambda}{2\bar{\lambda} - \lambda}, \\ h_{03} &= \frac{f_{03}}{3\bar{\lambda} - \lambda} + \frac{3\bar{f}_{20}f_{02}}{\bar{\lambda}(3\bar{\lambda} - \lambda)} + \frac{3f_{11}f_{02}}{(3\bar{\lambda} - \lambda)(2\bar{\lambda} - \lambda)}. \end{aligned}$$

The next step is to evaluate all terms of order  $\kappa$ , that is, to find the  $h_{klmn}$ 's from

$$h(w, \bar{w}, w', \bar{w}') = g(w, w') + 2a_{20}g(w, w')\psi(w) + a_{11} \left( \overline{g(w, w')} \psi(w) + g(w, w')\psi(\bar{w}) \right) + \dots \quad (\text{S.82})$$

Since  $\psi(w) = \mathcal{O}(w)$ , we have that  $h(w, \bar{w}, w', \bar{w}') = g(w, w')$  at order  $\mathcal{O}(1)$ . Moreover, if  $g(0, 0) = 0$ , i.e.  $g$  has no constant term, then  $h(w, \bar{w}, w', \bar{w}') = g(w, w')$  holds up to order  $\mathcal{O}(w, w')$ . We expand  $\tilde{g}$  into a formal Taylor series as has been done before for  $\tilde{f}$ ,

$$\tilde{g}(z, \bar{z}, z', \bar{z}'; \mu) = \sum_{0 \leq k+l+m+n} \frac{1}{k!l!m!n!} \tilde{g}_{klmn}(\mu) z^k \bar{z}^l z'^m \bar{z}'^n. \quad (\text{S.83})$$

Then,  $g(w, w') = \tilde{g}(\psi(w), \psi(\bar{w}), \psi(w'), \psi(\bar{w}'); \mu)$  and since  $\psi(w) = w + \mathcal{O}(|w|^2)$ , we have that  $h_{0000} = \tilde{g}_{0000}$ , and if  $\tilde{g}_{0000} = 0$ , then

$$h_{klmn} = \tilde{g}_{klmn} \quad \text{for } k + l + m + n = 1, \quad k, l, m, n \geq 0.$$

□

**Remark.** The coefficient  $\beta$  reduces at the bifurcation parameter value  $\mu = 0$  to

$$\beta(0) = \frac{-i}{2\omega_0} \left( f_{20}f_{11} - 2|f_{11}|^2 - \frac{1}{3}|f_{02}|^2 \right) - \frac{f_{21}}{2}. \quad (\text{S.84})$$

Note that, together with the foregoing remark, the normal form resembles to great extent the formula derived in the reductive perturbation method, see the main text's Section 2.2.2.1, although the latter pursues an alternative way to arrive at the amplitude equation.

In the following, we will briefly state the relationship between the original coupling function  $\mathbf{g}(\mathbf{x}, \mathbf{x}'; \mu)$  in (S.66) and the coupling coefficients  $h_{klmn}$  of the dynamics in Hopf normal form as in Lemma S.5. Recall from Lemma S.2 that we can write  $\mathbf{g}(\mathbf{x}, \mathbf{x}'; \mu)$  in complex form as

$$\tilde{g}(z, \bar{z}, z', \bar{z}'; \mu) = \mathbf{v}(\mu) \mathbf{g}(z\mathbf{v}(\mu) + \bar{z}\bar{\mathbf{v}}(\mu), z'\mathbf{v}(\mu) + \bar{z}'\bar{\mathbf{v}}(\mu); \mu). \quad (\text{S.85})$$

Given a Taylor expansion of  $\mathbf{g} = (g_1, g_2)^\top$  with  $\mathbf{x} = (x, y)^\top, \mathbf{x}' = (x', y')^\top$ ,

$$g_i(\mathbf{x}, \mathbf{x}', a) = \sum_{0 \leq k+l+m+n} \frac{1}{k!l!m!n!} g_{klmn}^{(i)}(a) x^k y^l x'^m y'^n, \quad \text{for } i = 1, 2, \quad (\text{S.86})$$

there exists a mapping

$$\left\{ \left( g_{klmn}^{(1)}, g_{klmn}^{(2)} \right) \right\} \mapsto \{ \tilde{g}_{klmn} \}$$

from the coupling coefficients  $g_{klmn}^{(i)}$  of the original dynamics (S.66) to those of the complex-valued coupling function (S.83). To be precise, substituting  $\mathbf{x} = (zu_1(\mu) + \bar{z}\bar{u}_1(\mu), zu_2(\mu) + \bar{z}\bar{u}_2(\mu))^T$  and an equivalent expression for  $\mathbf{x}'$  into (S.86), we have

$$\begin{aligned} \tilde{g}(z, z', \bar{z}, \bar{z}'; \mu) &= \sum_{i=1}^2 v_i(\mu) g_i(zu(\mu) + \bar{z}\bar{u}(\mu), z'u(\mu) + \bar{z}'\bar{u}(\mu); \mu) \\ &= \sum_{i=1}^2 \sum_{0 \leq k+l+m+n} \frac{1}{k!l!m!n!} v_i(\mu) g_{klmn}^{(i)}(\mu) \left\{ [zu_1(\mu) + \bar{z}\bar{u}_1(\mu)]^k [zu_2(\mu) + \bar{z}\bar{u}_2(\mu)]^l \right. \\ &\quad \left. \cdot [z'u_1(\mu) + \bar{z}'\bar{u}_1(\mu)]^m [z'u_2(\mu) + \bar{z}'\bar{u}_2(\mu)]^n \right\} \end{aligned}$$

Using the binomial theorem,  $(a+b)^n = \sum_{k=0}^n \binom{n}{k} a^k b^{n-k}$ , we can simplify the equation to

$$\begin{aligned} \tilde{g}(z, z', \bar{z}, \bar{z}'; \mu) &= \\ &\sum_{0 \leq k+l+m+n} \left\{ \frac{1}{k!l!m!n!} \left( \sum_{i=1}^2 v_i(\mu) g_{klmn}^{(i)}(\mu) \right) \cdot \left[ \sum_{a=0}^k \sum_{b=0}^l \sum_{c=0}^m \sum_{d=0}^n \binom{k}{a} \binom{l}{b} \binom{m}{c} \binom{n}{d} \right. \right. \\ &\quad \left. \cdot \left( u_1^{a+c} \bar{u}_1^{k+m-a-c} u_2^{b+d} \bar{u}_2^{l+n-b-d} \right) z^{a+b} \bar{z}^{k+l-a-b} z'^c \bar{z}'^{m+n-c-d} \right] \right\} \\ &\stackrel{!}{=} \sum_{0 \leq k+l+m+n} \frac{1}{k!l!m!n!} \tilde{g}_{klmn}(\mu) z^k \bar{z}^l z'^m \bar{z}'^n. \end{aligned}$$

Note that  $\mathbf{u} = \mathbf{u}(\mu)$  still depends on the parameter  $\mu$ , which we omitted for the sake of simplicity. Equating the sums in the first equation and collecting coefficients of the same order leads directly to the correct expressions for  $\tilde{g}_{klmn}$  of the second equation.

Once we have the coefficients  $\tilde{g}_{klmn}$ , we can apply the forward transform (S.77) to the coupling function (S.83) as has been done at the end of Lemma S.5, and express  $\tilde{g}$  in terms of  $w, w'$  as the formal power series

$$\begin{aligned} g(w, w') &= \tilde{g}(\psi(w), \psi(\bar{w}), \psi(w'), \psi(\bar{w}')) \\ &= \sum_{k+l+m+n \geq 0} \frac{1}{k!l!m!n!} \tilde{g}_{klmn} \psi(w)^k \psi(\bar{w})^l \psi(w')^m \psi(\bar{w}')^n \\ &=: \sum_{k+l+m+n \geq 0} g_{klmn} w^k \bar{w}^l w'^m \bar{w}'^n. \end{aligned} \tag{S.87}$$

Due to the near-identity character of the transform  $\psi(w)$ , the terms  $\tilde{g}_{klmn}$  and  $g_{klmn}$

coincide for  $k + l + m + n \in \{0, 1\}$ . Yet, for higher-order terms we have

$$\begin{aligned} g_{2000} &= \frac{1}{2}\tilde{g}_{2000} + \frac{h_{20}}{2}\tilde{g}_{1000} + \frac{\bar{h}_{02}}{2}\tilde{g}_{0100}, & g_{1010} &= \tilde{g}_{1010}, \quad g_{1001} = \tilde{g}_{1001}, \\ g_{0200} &= \frac{1}{2}\tilde{g}_{0200} + \frac{h_{02}}{2}\tilde{g}_{1000} + \frac{\bar{h}_{20}}{2}\tilde{g}_{0100}, & g_{0110} &= \tilde{g}_{0110}, \quad g_{0101} = \tilde{g}_{0101}, \\ g_{0020} &= \frac{1}{2}\tilde{g}_{0020} + \frac{h_{20}}{2}\tilde{g}_{0010} + \frac{\bar{h}_{02}}{2}\tilde{g}_{0001}, & g_{1100} &= \tilde{g}_{1100} + h_{11}\tilde{g}_{1000} + \bar{h}_{11}\tilde{g}_{0100}, \\ g_{0002} &= \frac{1}{2}\tilde{g}_{0002} + \frac{h_{02}}{2}\tilde{g}_{0010} + \frac{\bar{h}_{20}}{2}\tilde{g}_{0001}, & g_{0011} &= \tilde{g}_{0011} + h_{11}\tilde{g}_{0010} + \bar{h}_{11}\tilde{g}_{0001}, \end{aligned}$$

and some particular terms of third order

$$\begin{aligned} g_{2100} &= \frac{1}{2}\tilde{g}_{2100} + \left( \frac{h_{20}}{2} + \bar{h}_{11} \right) \tilde{g}_{1100} + \frac{\bar{h}_{12}}{2}\tilde{g}_{0100} \\ g_{2001} &= \frac{1}{2}\tilde{g}_{2001} + \frac{h_{20}}{2}\tilde{g}_{1001} + \frac{\bar{h}_{02}}{2}\tilde{g}_{0101} \\ g_{0120} &= \frac{1}{2}\tilde{g}_{0120} + \frac{h_{20}}{2}\tilde{g}_{0110} + \frac{\bar{h}_{02}}{2}\tilde{g}_{0101} \\ g_{0021} &= \frac{1}{2}\tilde{g}_{0021} + \left( \frac{h_{20}}{2} + \bar{h}_{11} \right) \tilde{g}_{0011} + \frac{\bar{h}_{12}}{2}\tilde{g}_{0001} \\ g_{1110} &= \tilde{g}_{1110} + h_{11}\tilde{g}_{1010} + \bar{h}_{11}\tilde{g}_{0110} \\ g_{1011} &= \tilde{g}_{1011} + h_{11}\tilde{g}_{1010} + \bar{h}_{11}\tilde{g}_{0101}. \end{aligned}$$

We can insert (S.87) into (S.82)

$$\begin{aligned} h(w, \bar{w}, w', \bar{w}') &= \sum_{k+l+m+n \geq 0} h_{klmn} w^k \bar{w}^l w'^m \bar{w}'^n \\ &= \left( \sum_{k+l+m+n \geq 0} g_{klmn} w^k \bar{w}^l w'^m \bar{w}'^n \right) \\ &\quad + 2a_{20} \left( \sum_{k+l+m+n \geq 0} g_{klmn} w^k \bar{w}^l w'^m \bar{w}'^n \right) \cdot \psi(w) + \dots, \end{aligned} \tag{S.88}$$

and solve for the  $h_{klmn}$ 's. As has been shown in the main text's *Section 2.2.1.2\**, we only need a particular choice of coupling coefficients, which are

$$\begin{aligned} h_{0000} &= g_{0000}, \\ h_{0010} &= g_{0010} + 2a_{20}g_{0000} + a_{11}\bar{g}_{0000}, \\ h_{0001} &= g_{0001} + a_{11}g_{0000} + 2a_{02}\bar{g}_{0000}, \end{aligned}$$

$$\begin{aligned}
h_{2100} &= g_{2100} + a_{20} [2g_{1100} + h_{20}g_{0100} + 2h_{11}g_{1000}] \\
&\quad + a_{02} [2\bar{g}_{0200} + 2\bar{h}_{11}\bar{g}_{0100} + \bar{h}_{02}\bar{g}_{1000} + \bar{h}_{12}\bar{g}_{0000}] \\
&\quad + a_{11} \left[ g_{2000} + \bar{g}_{1100} + \bar{h}_{11}g_{1000} + \frac{\bar{h}_{02}}{2}g_{0100} + \frac{h_{20}}{2}\bar{g}_{1000} + h_{11}\bar{g}_{0100} + \frac{\bar{h}_{12}}{2}g_{0000} \right] \\
&\quad + 3a_{30} [g_{0100} + 2h_{11}g_{0000}] + a_{21} [2g_{1000} + \bar{g}_{1000} + (h_{20} + 2\bar{h}_{11})g_{0000} + 2h_{11}\bar{g}_{0000}] \\
&\quad + a_{12} [2\bar{g}_{0100} + \bar{h}_{02}g_{0000} + (h_{20} + 2\bar{h}_{11})\bar{g}_{0000}] + 3a_{03}\bar{h}_{02}\bar{g}_{0000}, \\
h_{2001} &= g_{2001} + 2a_{20} \left[ g_{1001} + \frac{h_{20}}{2}g_{0001} \right] + a_{11} \left[ \frac{\bar{h}_{02}}{2}g_{0001} + \bar{g}_{0110} + \frac{h_{20}}{2}\bar{g}_{0010} \right] \\
&\quad + 2a_{02} \frac{\bar{h}_{02}}{2}\bar{g}_{0010} + 3a_{30}g_{0001} + a_{21}\bar{g}_{0010}, \\
h_{0120} &= g_{0120} + a_{11}g_{0020} + 2a_{02}\bar{g}_{0002}, \\
h_{0021} &= g_{0021}, \\
h_{1110} &= g_{1110} + 2a_{20} [g_{0110} + h_{11}g_{0010}] + a_{11} [g_{1010} + \bar{h}_{11}g_{0010} + \bar{g}_{1001} + h_{11}\bar{g}_{0001}] \\
&\quad + 2a_{02} [\bar{g}_{0101} + \bar{h}_{11}\bar{g}_{0001}] + 2a_{21}g_{0010} + 2a_{12}\bar{g}_{0001}, \\
h_{1011} &= g_{1011} + 2a_{20}g_{0011} + a_{11}\bar{g}_{0011} .
\end{aligned}$$

In comparison with the reductive perturbation approach presented in the main text's *Section 2.2.2.1*, we thus find the coefficients

$$h_{0010} = g_{0010} = \tilde{g}_{0010} = v_1(\mu)g_{0010}^{(1)}u_1(\mu) + v_2(\mu)g_{0010}^{(2)}u_2(\mu) , \quad (\text{S.89})$$

$$\begin{aligned}
h_{0120} &= g_{0120} - h_{11}g_{0020} - h_{02}\bar{g}_{0002} \\
&= \frac{1}{2} \left( \tilde{g}_{0120} - h_{11}\tilde{g}_{0020} - h_{02}\bar{\tilde{g}}_{0002} + h_{20}\tilde{g}_{0110} + \bar{h}_{02}\tilde{g}_{0101} \right. \\
&\quad \left. - h_{11}h_{20}\tilde{g}_{0010} - h_{11}\bar{h}_{02}\tilde{g}_{0001} - |h_{02}|^2\bar{\tilde{g}}_{0010} - h_{20}h_{02}\bar{\tilde{g}}_{0001} \right) .
\end{aligned} \quad (\text{S.90})$$

Note that the first term in parentheses,  $\tilde{g}_{0120}$ , can be ascribed to the coupling function  $G_{12}$ , the second and third to  $G_{02}$ , the fourth and fifth to  $G_{11}$ , and the latter four to  $G_{01}$ , as they are used in *Section S.1*. In particular, in case of linear coupling in the original dynamics, only the terms corresponding to  $G_{01}$  survive and (S.90) reduces to

$$h_{0120} = -\frac{1}{2} \left( h_{11}h_{20}\tilde{g}_{0010} + h_{11}\bar{h}_{02}\tilde{g}_{0001} + |h_{02}|^2\bar{\tilde{g}}_{0010} + h_{20}h_{02}\bar{\tilde{g}}_{0001} \right) . \quad (\text{S.91})$$

Last but not least, we consider a network of  $N > 2$  coupled oscillators  $\mathbf{x}_k = (x_k, y_k) \in \mathbb{R}^2$ ,  $k = 1, \dots, N$ , following the equivalent dynamics to (S.66),

$$\dot{\mathbf{x}}_k = \mathbf{f}(\mathbf{x}_k; \mu) + \kappa \mathbf{g}_k(\mathbf{x}_1, \dots, \mathbf{x}_N; \mu) + \mathcal{O}(\kappa^2) . \quad (\text{S.92})$$

In principle, the reasoning above naturally extends to the full system dynamics (S.92). Especially the type of coupling between oscillators fully translates into the corresponding coupling function  $h_k$  in the reduced normal form dynamics  $\dot{w}_k = \alpha w_k - \beta w_k^2 \bar{w}_k +$

$\kappa h_k(w_1, \dots, w_N)$ . In fact, we can prove the following

**Lemma S.6.** *As before, we consider system (S.92), where each uncoupled unit  $\mathbf{x}_k$  is close to a supercritical Hopf bifurcation with  $|\mu| \ll 1$  and that the coupling between units is sufficiently weak,  $0 < \kappa \ll |\mu| \ll 1$ . If the coupling function*

$$\mathbf{g}_k(\mathbf{x}_1, \dots, \mathbf{x}_N; \mu) = \hat{\mathbf{g}}_k(\mathbf{x}_1, \dots, \mathbf{x}_N) := \sum_{j=1}^N \mathbf{g}_{kj}(\mathbf{x}_j, \mathbf{x}_k)$$

*can be decomposed into the sum of pairwise coupling functions  $\mathbf{g}_{kj}$ , then also the coupling function  $h_k$  in the reduced Hopf normal form decomposes into pairwise interactions,*

$$h_k(w_1, \dots, w_N) = \sum_{j=1}^N h_{kj}(w_j, w_k) .$$

*Proof.* The demonstration of the lemma is constructive and follows closely the proof of Lemma S.5. The main assumption lies within the theory of weak coupling can be justified in following way, see also the reasoning and proof around Theorem 5.8.<sup>78</sup>: A mathematically rigorous normal form reduction of the full network may consider coordinate transforms of the form  $Z = \Psi(W)$  where  $Z = (z_1, \dots, z_N)$ ,  $W = (w_1, \dots, w_N)$  and  $\Psi = (\psi_1, \dots, \psi_N)$  with  $\psi_j = \psi_j(w_1, \dots, w_N)$ . This general transformation can presumably lead to mixed coupling terms in the normal form beyond pairwise interactions; see Section S.5 for the full Hopf normal form of a network with  $S_N \times S^1$ -equivariance. For weak coupling, however, we may consider  $\psi_j(w_1, \dots, w_N) \approx \psi_j^0(w_j) + \kappa \psi_j^1(w_1, \dots, w_N)$  and for  $\kappa \rightarrow 0$  we have  $\psi_j(w_1, \dots, w_N) = \psi_j^0(w_j)$ . Given that the uncoupled systems are all identical, the local coordinate transforms  $\psi_j^0 = \psi$  coincide with (S.77), which results in  $\Psi(W) \approx (\psi(w_1), \dots, \psi(w_N))$ . Then, the proof of the Lemma follows immediately.

For the sake of completeness, we here provide the details of the proof: Recall that we identified both the normal form and coupling parameters  $\beta, h_{klmn}$  by inserting the local coordinate transform  $\psi(w)$ , see (S.77), into the derivative of the local inverse transform (S.81) and by a subsequent comparison of coefficients. Focusing on the terms of order  $\mathcal{O}(\kappa)$ , we have

$$\begin{aligned} \dot{w}_k &= f(w_k) + \kappa \left[ g_k(w_1, \dots, w_N) + 2a_{20}g_k(w_1, \dots, w_N)\psi(w_k) \right. \\ &\quad \left. + a_{11}(\overline{g_k(w_1, \dots, w_N)}\psi(w_k) + g_k(w_1, \dots, w_N)\psi(\bar{w}_k)) + \dots \right] \end{aligned} \quad (\text{S.93})$$

with  $f(w)$  consisting of terms that eventually become  $\alpha w - \beta w^2 \bar{w} + \mathcal{O}(|w|^4)$ . Recall also that the coupling function  $g_k(w_1, \dots, w_N)$  is determined from the original coupling  $\hat{\mathbf{g}}_k$  via the transformations

$$\hat{\mathbf{g}}_k(\mathbf{x}_1, \dots, \mathbf{x}_N) \longmapsto \tilde{g}_k(z_1, \dots, z_N) \longmapsto g_k(w_1, \dots, w_N) .$$

Each of these transformations respects the form of coupling. In particular, for

$$\hat{\mathbf{g}}_k(\mathbf{x}_1, \dots, \mathbf{x}_N) = \sum_j g_{kj}(\mathbf{x}_j, \mathbf{x}_k),$$

then  $\tilde{g}_k$  and eventually also  $g_k$  can be decomposed exactly into

$$g_k(w_1, \dots, w_N) = \sum_j g_{kj}(w_j, w_k).$$

Inserting this into (S.93) and given that  $\psi(w_k)$  is a polynomial only in  $w_k$ , the right-hand side of (S.93) can be written in the form  $f(w_k) + \kappa \sum_j h_{kj}(w_j, w_k)$  with

$$\begin{aligned} h_{kj}(w_j, w_k) := & g_{kj}(w_j, w_k) + 2a_{20}g_{kj}(w_j, w_k)\psi(w_k) \\ & + a_{11} \left( \overline{g_{kj}(w_j, w_k)}\psi(w_k) + g_{kj}(w_j, w_k)\psi(\bar{w}_k) \right) + \dots + \mathcal{O}(|w|^4). \end{aligned}$$

□

## S.4 Takens' reduction via Lie brackets

We consider a two-dimensional system  $\mathbf{x} = (x, y) \in \mathbb{R}^2$  near a Hopf bifurcation. For a small perturbation parameter  $\mu > 0$  and an equilibrium solution with eigenvalues  $\pm i\omega_0 \neq 0$  at  $\mu = 0$ , we can shift the origin appropriately such that  $\mathbf{x} = 0$  is the equilibrium solution undergoing a supercritical Hopf bifurcation. Furthermore, we can bring the system into Jordan real form so that the dynamics expanded as a Taylor series around  $\mathbf{x} = 0$  reads

$$\dot{\mathbf{x}} = \mathbf{L}\mathbf{x} + \mathbf{F}_2(\mathbf{x}) + \mathbf{F}_3(\mathbf{x}) + \dots + \mathbf{F}_r(\mathbf{x}) + \mathcal{O}(|z|^{r+1}), \quad (\text{S.94})$$

with

$$\begin{aligned} \mathbf{L} &= \mathbf{L}_0 + \mu \mathbf{L}_1 + \mathcal{O}(\mu^2) = \begin{pmatrix} 0 & -\omega_0 \\ \omega_0 & 0 \end{pmatrix} + \mu \begin{pmatrix} \beta & -\alpha \\ \alpha & \beta \end{pmatrix} + \mathcal{O}(\mu^2), \\ \mathbf{F}_2(\mathbf{x}) &= \begin{pmatrix} F_{21}(\mathbf{x}) \\ F_{22}(\mathbf{x}) \end{pmatrix} = \begin{pmatrix} a_{20} & a_{11} & a_{02} \\ b_{20} & b_{11} & b_{02} \end{pmatrix} \begin{pmatrix} x^2 \\ xy \\ y^2 \end{pmatrix}. \end{aligned}$$

Note that for  $\mu > 0$  we can introduce  $\mu = \varepsilon^2$  with  $0 < \varepsilon \ll 1$  and that the common asymptotic scaling  $\mathcal{O}(z_i) = \varepsilon$  is used in (S.94) and all subsequent series approximations. Note further that we can also extend the ( $n = 2$ )-dimensional system  $\dot{\mathbf{x}} = \mathbf{f}(\mathbf{x}; \mu)$  to the larger,  $n + 1$ -dimensional system

$$\begin{aligned} \dot{\mathbf{x}} &= \mathbf{f}(\mathbf{x}; \mu), \\ \dot{\mu} &= 0. \end{aligned} \quad (\text{S.95})$$

We can perform the normal form calculations in a likewise manner, requiring the coordinate transforms  $\underline{\mathbf{P}}(\mathbf{x}; \mu)$  to be of the form  $\underline{\mathbf{P}}(\mathbf{x}; \mu) = (\mathbf{P}(\mathbf{x}; \mu); \mu)$ . Apparently, they will leave the equation  $\dot{\mu} = 0$  invariant, but transform  $\dot{\mathbf{x}} = \mathbf{f}(\mathbf{x}; \mu)$  in a  $\mu$ -dependent way. Practically, the normal form calculations remain the same, yet the  $n$ -dimensional normal form system remains in normal form as  $\mu$  is varied to drive the system through the bifurcation. While the normal form transformation following Poincaré in the main text's *Section 2.2.2.2* takes the parameter dependence into account, the reductive perturbation approach in the main text's *Section 2.2.2.1* does not consider the extended system. As the deviations between these two approaches are hardly noticeable, we will stick to the non-extended system also in this section – given that the higher order normal form is meant for illustration purposes only.<sup>[3]</sup>

Now, for  $\mathbf{w} = (w_1, w_2)^\top$  and  $\mathcal{P}_k$  denoting the set of homogeneous polynomials of order  $k$ , we find the Lie bracket for system (S.94) with  $L = \mathbf{L}_0 \mathbf{x}$  and  $\mathbf{p}_k = (p_{k1}, p_{k2})^\top \in \mathcal{P}_k$  as

$$\text{ad } L(\mathbf{p}_k)(\mathbf{w}) = \begin{pmatrix} 0 & -\omega_0 \\ \omega_0 & 0 \end{pmatrix} \begin{pmatrix} p_{k1}(\mathbf{w}) \\ p_{k2}(\mathbf{w}) \end{pmatrix} - \begin{pmatrix} \partial p_{k1}/\partial x & \partial p_{k1}/\partial y \\ \partial p_{k2}/\partial x & \partial p_{k2}/\partial y \end{pmatrix} \begin{pmatrix} 0 & -\omega_0 \\ \omega_0 & 0 \end{pmatrix} \begin{pmatrix} w_1 \\ w_2 \end{pmatrix}. \quad (\text{S.96})$$

For second-order normal forms, we are looking for a transformation  $\mathbf{p}_2$  of the form  $\mathbf{x} = \mathbf{w} + \mathbf{p}_2(\mathbf{w})$ , where

$$\mathbf{p}_2(\mathbf{w}) = \begin{pmatrix} p_{21}(\mathbf{w}) \\ p_{22}(\mathbf{w}) \end{pmatrix} = \begin{pmatrix} \sum_{j=0}^2 c_{ij} w_1^i w_2^j \\ \sum_{j=0}^2 d_{ij} w_1^i w_2^j \end{pmatrix}, \quad i = 2 - j. \quad (\text{S.97})$$

We shall perform the Lie bracket operation (S.96) on each basis element of  $\mathcal{P}_2$ , which is given by

$$\mathcal{P}_2 = \text{span} \left\{ \begin{pmatrix} w_1^2 \\ 0 \end{pmatrix}, \begin{pmatrix} w_1 w_2 \\ 0 \end{pmatrix}, \begin{pmatrix} w_2^2 \\ 0 \end{pmatrix}, \begin{pmatrix} 0 \\ w_1^2 \end{pmatrix}, \begin{pmatrix} 0 \\ w_1 w_2 \end{pmatrix}, \begin{pmatrix} 0 \\ w_2^2 \end{pmatrix} \right\}. \quad (\text{S.98})$$

We find

$$\text{ad } L(\mathcal{P}_2) = \text{span} \left\{ \begin{pmatrix} w_1^2 & w_1 w_2 & w_2^2 & 0 & 0 & 0 \\ 0 & 0 & 0 & w_1^2 & w_1 w_2 & w_2^2 \end{pmatrix} \cdot \mathbf{A}_L^2 \right\} = \mathcal{P}_2 \cdot \mathbf{A}_L^2, \quad (\text{S.99})$$

with

$$\mathbf{A}_L^2 = \omega_0 \begin{pmatrix} 0 & -1 & 0 & -1 & 0 & 0 \\ 2 & 0 & -2 & 0 & -1 & 0 \\ 0 & 1 & 0 & 0 & 0 & -1 \\ 1 & 0 & 0 & 0 & -1 & 0 \\ 0 & 1 & 0 & 2 & 0 & -2 \\ 0 & 0 & 1 & 0 & 1 & 0 \end{pmatrix}.$$

<sup>[3]</sup> In this particular section the order of the normal form is indicated by the index  $k$  of the subsequent transformations  $\mathbf{p}_k$ . Compared to the notation in all other parts of the thesis,  $k = 3$  corresponds to second-order normal forms,  $k = 5$  to third-order, etc.

We can compute  $\det(\mathbf{A}_L^2) = 8\omega_0 > 0$  for  $\omega_0 > 0$ , that is,  $\mathbf{A}_L^2$  is non-singular and has full rank. This implies that the image of  $\mathcal{P}_2$  under  $\text{ad } L$  is the whole subspace  $\mathcal{P}_2$ , and therefore all second order terms can be removed by a suitable change of variables. Indeed, substituting (S.97) into (2.53) of the main text and using that

$$(D\mathbf{p}(\mathbf{w}))^{-1} = (\mathbf{I} + D\mathbf{p}_k(\mathbf{w}))^{-1} = \mathbf{I} - D\mathbf{p}_k(\mathbf{w}) + \mathcal{O}(|w|^2) , \quad (\text{S.100})$$

we have

$$\dot{\mathbf{w}} = \sum_{N=0}^{\infty} (-1)^N [D\mathbf{p}_2(\mathbf{w})]^N \left\{ \mathbf{Lw} + \mathbf{Lp}_2(\mathbf{w}) + \sum_{n=2}^{\infty} \sum_{m=0}^n \frac{D^m \mathbf{F}_n(\mathbf{w})}{m!} [\mathbf{p}_2(\mathbf{w})]^m \right\} \quad (\text{S.101})$$

$$= \mathbf{Lw} + \sum_{n=2}^{\tilde{N}} \mathbf{F}_n^{(1)}(\mathbf{w}) \quad (\text{S.102})$$

where we truncated the Taylor series at order  $\tilde{N}$  and with

$$\mathbf{F}_n^{(1)}(\mathbf{w}) = \begin{pmatrix} F_{n1}^{(1)}(\mathbf{w}) \\ F_{n2}^{(1)}(\mathbf{w}) \end{pmatrix} = \begin{pmatrix} \sum_{j=0}^2 a_{ij}^{(1)} w_1^i w_2^j \\ \sum_{j=0}^2 b_{ij}^{(1)} w_1^i w_2^j \end{pmatrix} , \quad n = 2, \dots, \tilde{N}, \quad i = 2 - j ; \quad (\text{S.103})$$

the number in the superscript parentheses refers to the index of coordinate transformations. Since the complement  $\mathcal{H}_2$  of  $\text{im}(\text{ad } L(\mathcal{P}_2))$  in  $\mathcal{P}_2$  is  $\mathcal{H}_2 = \{0\}$ , we have

$$\mathbf{F}_2^{(1)}(\mathbf{w}) = \mathbf{F}_2(\mathbf{w}) + L\mathbf{p}_2(\mathbf{w}) - D\mathbf{p}_2(\mathbf{w}) \cdot L(\mathbf{w}) = 0 , \quad (\text{S.104})$$

that is,  $a_{ij}^{(1)} = b_{ij}^{(1)} = 0$  for all  $i + j = 2$ . Note that in order to derive  $\mathbf{F}_2^{(1)}$  at order  $\mathcal{O}(\varepsilon^2)$ , we again used that  $\mu = \varepsilon^2$  and that  $\mathbf{F}_n^{(l)} = \mathcal{O}(\varepsilon^n)$  in the series representation (S.103). Solving now the linear algebraic equation (S.104) for  $\mathbf{p}_2$  in the space  $\mathcal{P}_2$ , we find the coefficients  $c_{ij}, d_{ij}$  in (S.97) as

$$\begin{pmatrix} c_{20} \\ c_{11} \\ c_{02} \\ d_{20} \\ d_{11} \\ d_{02} \end{pmatrix} = -(\mathbf{A}_L^2)^{-1} \begin{pmatrix} a_{20} \\ a_{11} \\ a_{02} \\ b_{20} \\ b_{11} \\ b_{02} \end{pmatrix} = \frac{-1}{3\omega_0} \begin{pmatrix} b_{20} + a_{11} + 2b_{02} \\ -2a_{20} - b_{11} + 2a_{02} \\ 2b_{20} - a_{11} + b_{02} \\ a_{20} + b_{11} - 2a_{02} \\ -2b_{20} + a_{11} + 2b_{02} \\ -2a_{20} - b_{11} - a_{02} \end{pmatrix} . \quad (\text{S.105})$$

As said, the higher order normal form computations build upon each other iteratively. Hence, for the third-order normal form we are looking for a transformation  $\mathbf{x} = \mathbf{w} + \mathbf{p}_3(\mathbf{w})$  with

$$\mathbf{p}_3(\mathbf{w}) = \begin{pmatrix} P_{31}(\mathbf{w}) \\ P_{32}(\mathbf{w}) \end{pmatrix} = \begin{pmatrix} \sum_{j=0}^3 c_{ij} w_1^i w_2^j \\ \sum_{j=0}^3 d_{ij} w_1^i w_2^j \end{pmatrix} , \quad i = 3 - j . \quad (\text{S.106})$$

$\mathcal{P}_3$  is eight-dimensional and given by

$$\mathcal{P}_3 = \text{span} \left\{ \begin{pmatrix} w_1^3 \\ 0 \end{pmatrix}, \begin{pmatrix} w_1^2 w_2 \\ 0 \end{pmatrix}, \begin{pmatrix} w_1 w_2^2 \\ 0 \end{pmatrix}, \begin{pmatrix} w_2^3 \\ 0 \end{pmatrix}, \begin{pmatrix} 0 \\ w_1^3 \end{pmatrix}, \begin{pmatrix} 0 \\ w_1^2 w_2 \end{pmatrix}, \begin{pmatrix} 0 \\ w_1 w_2^2 \end{pmatrix}, \begin{pmatrix} 0 \\ w_2^3 \end{pmatrix} \right\}. \quad (\text{S.107})$$

Similar to (S.99), we find now

$$\text{ad } L(\mathcal{P}_3) = \mathcal{P}_3 \cdot \mathbf{A}_L^3 \quad (\text{S.108})$$

with

$$\mathbf{A}_L^3 = \omega_0 \begin{pmatrix} 0 & -1 & 0 & 0 & -1 & 0 & 0 & 0 \\ 3 & 0 & -2 & 0 & 0 & -1 & 0 & 0 \\ 0 & 2 & 0 & -3 & 0 & 0 & -1 & 0 \\ 0 & 0 & 1 & 0 & 0 & 0 & 0 & -1 \\ 1 & 0 & 0 & 0 & 0 & -1 & 0 & 0 \\ 0 & 1 & 0 & 0 & 3 & 0 & -2 & 0 \\ 0 & 0 & 1 & 0 & 0 & 2 & 0 & -3 \\ 0 & 0 & 0 & 1 & 0 & 0 & 1 & 0 \end{pmatrix}.$$

We can calculate that the vectors

$$\begin{aligned} \mathbf{e}_1 &= (1, 0, 1, 0, 0, 1, 0, 1)^\top \\ \mathbf{e}_2 &= (0, -1, 0, -1, 1, 0, 1, 0)^\top \end{aligned}$$

are two eigenvectors corresponding to the zero eigenvalue of  $\mathbf{A}_L^3$ . Therefore,  $\mathbf{A}_L^3$  induces a non-vanishing complementary space  $\mathcal{H}_3$  given by

$$\mathcal{H}_3 = \mathcal{P}_3 \cdot (\mathbf{e}_1 \ \mathbf{e}_2) = \text{span} \left\{ \begin{pmatrix} w_1(w_1^2 + w_2^2) \\ w_2(w_1^2 + w_2^2) \end{pmatrix}, \begin{pmatrix} -w_2(w_1^2 + w_2^2) \\ w_1(w_1^2 + w_2^2) \end{pmatrix} \right\}. \quad (\text{S.109})$$

The resulting third-order normal form takes the following form

$$\begin{aligned} \dot{w}_1 &= \beta\mu w_1 - (\alpha\mu + \omega_0)w_2 + a_1 w_1(w_1^2 + w_2^2) - b_1 w_2(w_1^2 + w_2^2) + \mathcal{O}(|w_1|^5, |w_2|^5), \\ \dot{w}_2 &= (\alpha\mu - \omega_0)w_1 + \beta\mu w_2 + a_1 w_2(w_1^2 + w_2^2) + b_1 w_1(w_1^2 + w_2^2) + \mathcal{O}(|w_1|^5, |w_2|^5), \end{aligned} \quad (\text{S.110})$$

where  $a_1, b_1$  are to be determined. In the same manner as before, we have

$$\begin{aligned} \dot{w} &= \sum_{N=0}^{\tilde{N}} (-1)^N [D\mathbf{p}_3(\mathbf{w})]^N \left\{ \mathbf{L}\mathbf{w} + \mathbf{L}\mathbf{p}_3(\mathbf{w}) + \sum_{n=2}^{\tilde{N}} \sum_{m=0}^n \frac{D^m \mathbf{F}_n(\mathbf{w})}{m!} [\mathbf{p}_3(\mathbf{w})]^m \right\} \\ &= \mathbf{L}\mathbf{w} + \mathbf{F}_2^{(1)}(\mathbf{w}) + \sum_{n=3}^{\tilde{N}} \mathbf{F}_n^{(2)}(\mathbf{w}) \end{aligned} \quad (\text{S.111})$$

where

$$\mathbf{F}_n^{(2)}(\mathbf{w}) = \begin{pmatrix} F_{n1}^{(2)}(\mathbf{w}) \\ F_{n2}^{(2)}(\mathbf{w}) \end{pmatrix} = \begin{pmatrix} \sum_{j=0}^2 a_{ij}^{(2)} w_1^i w_2^j \\ \sum_{j=0}^2 b_{ij}^{(2)} w_1^i w_2^j \end{pmatrix}, \quad n = 3, \dots, \tilde{N}, \quad i = 3 - j. \quad (\text{S.112})$$

Thus, we have to solve

$$\mathbf{F}_3^{(2)}(\mathbf{w}) = \mathbf{F}_3^{(1)}(\mathbf{w}) + L\mathbf{p}_3(\mathbf{w}) - D\mathbf{p}_3(\mathbf{w}) \cdot L(\mathbf{w}) = \mathcal{H}_3(\mathbf{w}) \quad (\text{S.113})$$

for  $\mathbf{p}_3$ , which we can rewrite in terms of the basis functions of  $\mathcal{P}_3$  as

$$\mathbf{A}_L^3 \cdot \boldsymbol{\xi} = \mathbf{F}_3^{(1)} - \mathcal{H}_3 =: \boldsymbol{\kappa} \quad (\text{S.114})$$

where we used (S.109) to get

$$\begin{aligned} \boldsymbol{\xi} &= \{c_{30}, c_{21}, c_{12}, c_{03}, d_{30}, d_{21}, d_{12}, d_{03}\}^\top, \\ \boldsymbol{\kappa} &= \{a_{30}^{(1)} - a_1, a_{21}^{(1)} + b_1, a_{12}^{(1)} - a_1, a_{03}^{(1)} + b_1, b_{30}^{(1)} - b_1, b_{21}^{(1)} - a_1, b_{12}^{(1)} - b_1, b_{03}^{(1)} - a_1\}^\top. \end{aligned}$$

Following the procedure outlined in<sup>138,139</sup>, we find the resulting coefficients as

$$\begin{aligned} \begin{pmatrix} a_1 \\ b_1 \end{pmatrix} &= \frac{1}{8} \begin{pmatrix} a_{12}^{(1)} + 3a_{03}^{(1)} + b_{21}^{(1)} + 3b_{03}^{(1)} \\ -a_{21}^{(1)} - 3a_{03}^{(1)} + b_{12}^{(1)} + 3b_{30}^{(1)} \end{pmatrix}, \\ \begin{pmatrix} c_{30} \\ c_{21} \\ c_{12} \\ c_{03} \end{pmatrix} &= \frac{1}{8\omega_0} \begin{pmatrix} 0 \\ 3a_{30}^{(1)} - 3a_{12}^{(1)} + b_{21}^{(1)} - b_{03}^{(1)} \\ 3a_{21}^{(1)} - 3a_{03}^{(1)} + b_{30}^{(1)} + b_{12}^{(1)} \\ 0 \end{pmatrix}, \\ \begin{pmatrix} d_{30} \\ d_{21} \\ d_{12} \\ d_{03} \end{pmatrix} &= \frac{1}{4\omega_0} \begin{pmatrix} a_{30}^{(1)} + a_{12}^{(1)} - b_{21}^{(1)} - b_{03}^{(1)} \\ a_{21}^{(1)} + 3a_{03}^{(1)} + 5b_{30}^{(1)} - b_{12}^{(1)} \\ 3a_{30}^{(1)} + a_{12}^{(1)} + b_{21}^{(1)} + 5b_{03}^{(1)} \\ a_{21}^{(1)} + a_{03}^{(1)} + b_{30}^{(1)} + b_{12}^{(1)} \end{pmatrix}. \end{aligned} \quad (\text{S.115})$$

Applying the same procedure, we can continue these calculations and derive the coefficients of the normal forms of order 5 and higher. Generalizing system (S.110), the normal form of order  $(2M - 1)$  can be written as

$$\begin{aligned} \frac{d}{dt} \begin{pmatrix} w_1 \\ w_2 \end{pmatrix} &= \begin{pmatrix} \beta\mu & -(\alpha\mu + \omega_0) \\ (\alpha\mu + \omega_0) & \beta\mu \end{pmatrix} \begin{pmatrix} w_1 \\ w_2 \end{pmatrix} \\ &+ \sum_{j=1}^{M-1} (w_1^2 + w_2^2)^j \begin{pmatrix} a_j & -b_j \\ b_j & a_j \end{pmatrix} \begin{pmatrix} w_1 \\ w_2 \end{pmatrix} + \mathcal{O}(|w|^{2M+3}), \end{aligned} \quad (\text{S.116})$$

or in complex form for  $w \in \mathbb{C}$  as

$$\dot{w} = [(\beta + i\alpha)\mu + i\omega_0]w + \sum_{j=1}^{M-1} (a_j + ib_j)|w|^{2j}w + \mathcal{O}(|w|^{2M+3}). \quad (\text{S.117})$$

For fifth order, the next coefficients can be found as

$$\begin{pmatrix} a_2 \\ b_2 \end{pmatrix} = \frac{1}{16} \begin{pmatrix} 5a_{50}^{(3)} + a_{32}^{(3)} + a_{14}^{(3)} + b_{41}^{(3)} + b_{23}^{(3)} + 5b_{05}^{(3)} \\ -a_{41}^{(3)} - a_{23}^{(3)} - a_{14}^{(3)} - a_{05}^{(3)} + 5b_{50}^{(3)} + b_{32}^{(3)} + b_{14}^{(3)} \end{pmatrix}. \quad (\text{S.118})$$

The corresponding coefficients  $c_{ij}, d_{ij}$  with  $i + j = 5$  for the transform  $\mathbf{p}_5(w)$  are listed in<sup>138</sup>. The complexity of computing the coefficients for higher order normal forms increases rapidly – determining  $a_{ij}^{(3)}, b_{ij}^{(3)}$  builds recursively on  $a_{ij}^{(2)}, b_{ij}^{(2)}$  and the lower order near-identity transformations  $\mathbf{p}_k, k \leq 4$ . It becomes necessary to implement efficient algorithms in symbolic computation software without running in danger of overflow errors due to memory storage. An arithmetic algorithm including the computation of normal forms up to order 11 has been presented in<sup>139</sup>.

Once higher-order normal forms and their corresponding series of transformations  $\mathbf{p}_k$  have been established, the latter can be applied to the coupling term  $\kappa \mathbf{g}(\mathbf{x}, \mathbf{x}')$  of (2.51). For our purposes, however, it is sufficient to consider the transformed coupling up to third order. As we have illustrated the derivation of the coupling term using nonlinear transforms in great detail in the main text's *Section 2.2.2.1*, we refrain here from further cumbersome calculations.

## S.5 Ashwin & Rodrigues' reduction via $S_N \times S^1$ -symmetry

Ashwin and Rodrigues consider in<sup>141</sup> coupled oscillators  $w_k \in \mathbb{C}, k = 1, \dots, N > 4$ , which follow the dynamics

$$\dot{w}_k = f(w_k; \mu) + \kappa g(w_k, w_1, \dots, w_{k-1}, w_{k+1}, \dots, w_N; \mu) + \mathcal{O}(\kappa^2), \quad (\text{S.119})$$

and where the whole network respects full permutation symmetry  $S_N$  and rotational invariance  $S^1$ . Using equivariant theory, they prove their main result in terms of the following phase reduction.

**Theorem S.7** (Theorem 3.2.<sup>141</sup>). *Consider system (S.119) with  $S_N$ -symmetry (for fixed  $N > 4$ ) such that the  $N$  uncoupled systems ( $\kappa = 0$ ) undergo a generic supercritical Hopf bifurcation on  $\mu$  passing through  $\mu = 0$ . There exists  $\mu_0 > 0$  and  $\kappa_0 = \kappa_0(\mu)$  such that for any  $\mu \in (0; \mu_0)$  and  $|\kappa| < \kappa_0(\mu)$  the system (S.119) has an attracting  $C^r$ -smooth invariant  $N$ -dimensional torus for arbitrarily large  $r$ . On this invariant torus, the phases*

$\theta_k$  of the flow can be expressed as a coupled oscillator system

$$\dot{\theta}_k = \tilde{\Omega}(\theta, \kappa) + \kappa \left( H_k^{(2)}(\theta) + H_k^{(3)}(\theta) + H_k^{(4)}(\theta) \right) \quad (\text{S.120})$$

$$\begin{aligned} H_k^{(2)}(\theta) &= \frac{1}{N} \sum_{j=1}^N g_2(\theta_j - \theta_k) \\ H_k^{(3)}(\theta) &= \frac{1}{N^2} \sum_{j,l=1}^N g_3(\theta_j + \theta_l - 2\theta_k) + \frac{1}{N^2} \sum_{j,l=1}^N g_4(2\theta_j - \theta_l - \theta_k) \\ H_k^{(4)}(\theta) &= \frac{1}{N^3} \sum_{j,l,m=1}^N g_5(\theta_j + \theta_l - \theta_m - \theta_k) \end{aligned} \quad (\text{S.121})$$

for fixed  $0 < \mu < \mu_0$  in the limit  $\kappa \rightarrow 0$ , where  $\tilde{\Omega}(\theta, \kappa)$  is independent of  $k$  and

$$\begin{aligned} g_2(\varphi) &= \xi_1^0 \cos(\varphi + \chi_1^0) + \mu \xi_1^1 \cos(\varphi + \chi_1^1) + \mu \xi_2^1 \cos(2\varphi + \chi_2^1) \\ g_3(\varphi) &= \mu \xi_3^1 \cos(\varphi + \chi_3^1) \\ g_4(\varphi) &= \mu \xi_4^1 \cos(\varphi + \chi_4^1) \\ g_5(\varphi) &= \mu \xi_5^1 \cos(\varphi + \chi_5^1) . \end{aligned} \quad (\text{S.122})$$

The constants  $\xi_i^j$  and  $\chi_i^j$  are generically non-zero. The natural frequency  $\tilde{\Omega}$  of each oscillator in the reduced phase dynamics (S.120) is given by

$$\tilde{\Omega}(\theta, \kappa) = \Omega + \kappa \mu \left[ \frac{-\vartheta_4}{\beta_R} \cos(\psi_4) - \frac{\vartheta_5}{\beta_R N^2} \sum_{j,k=1}^N \cos(\psi_5 + \theta_j - \theta_k) \right] \quad (\text{S.123})$$

with  $\Omega = \alpha_I - \mu(\beta_I/\beta_R) + \mathcal{O}(\mu^2)$ . The error term truncated in (S.120) satisfies  $\tilde{g} = \mathcal{O}(\mu^2)$  uniformly in the phases  $\theta_k$ . This truncation by removing  $\tilde{g}$  and  $\mathcal{O}(\kappa^2)$  terms is valid over time intervals  $0 < t < \tilde{t}$  where  $\tilde{t} = \mathcal{O}(\kappa^{-1}\mu^{-2})$  in the limit  $0 < \kappa \ll \mu \ll 1$ . In particular, for any  $N$ , this approximation involves up to four interacting phases.

Before we go into detail of the proof, we first state an immediate corollary for large oscillator systems of the form (S.119) with  $S_N \times S^1$ -equivariance, where each uncoupled system is close to a supercritical Hopf bifurcation.

**Corollary S.8.** *In the limit of weak coupling  $0 < \kappa \ll 1$  and for a reasonably large network size  $N \gg 4$ , the coupled oscillator system (S.120) reduces to*

$$\dot{\theta}_k = \Omega + \hat{\kappa} \varepsilon^2 \left( \frac{1}{N} \sum_{j=1}^N \left[ \xi_1^0 \cos(\theta_j - \theta_k + \chi_1^0) + \varepsilon^2 \xi_2^1 \cos(2(\theta_j - \theta_k) + \chi_2^1) \right] + \mathcal{O}(\varepsilon^3) \right) \quad (\text{S.124})$$

with  $\Omega = \alpha_I - \varepsilon^2(\beta_I/\beta_R) + \mathcal{O}(\varepsilon^4)$  and  $\varepsilon^2 = \mu$  as well as  $\hat{\kappa} = \kappa \varepsilon^2$  with  $\varepsilon > 0$ . In particular, the phase interaction function of (S.124) consists of first and second harmonics with merely pairwise interactions.

*Proof.* For large  $N \gg 4$ , we can assume that  $1/N = \mathcal{O}(\varepsilon)$  where  $\varepsilon > 0$  is such that

$\varepsilon^2 = \mu$ . In the weak coupling limit, we set  $\hat{\kappa} = \kappa\varepsilon^2$ . The natural frequency  $\Omega$  coincides with  $\tilde{\Omega}$  at order  $\mathcal{O}(\varepsilon^4, \hat{\kappa}\varepsilon^4)$ , see also (S.123). The terms  $H_k^{(3)}(\theta), H_k^{(4)}(\theta)$  in *Theorem S.7* are of order  $\mathcal{O}(\hat{\kappa}\varepsilon^5)$ . Moreover, the term  $\mu\xi_1^1 \cos(\varphi + \chi_1^1)$  in  $g_2(\theta)$  is only some higher-order correction to the first harmonics, and can thus be discarded. The remaining terms finally constitute (S.124).  $\square$

The proof of *Theorem S.7* can be found in<sup>141</sup> where the authors use Theorem 3.1, which is proven in Theorem 4.2,<sup>422</sup>. It is noteworthy that this Theorem 3.1 provides a thorough decomposition of the coupling function  $g(w_1, \dots, w_N; \mu)$  when given as a polynomial of degree lower or equal than 3. In fact, any polynomial function  $h: \mathbb{C}^N \rightarrow \mathbb{C}^N$  of degree lower or equal than 3 with  $N \geq 4$  and which respects the  $S_N \times S^1$ -equivariance can be written as  $h = (h_1, \dots, h_N)$  where

$$\begin{aligned} h_1(w_1, w_2, \dots, w_N) &= \sum_{i=-1}^{11} a_i \hat{h}_i(w_1, w_2, \dots, w_N) \\ h_2(w_1, w_2, \dots, w_N) &= h_1(w_2, w_1, \dots, w_N) \\ &\vdots \\ h_N(w_1, w_2, \dots, w_N) &= h_1(w_N, w_2, \dots, w_1) \end{aligned} \tag{S.125}$$

and  $\hat{h}_0(w) = w_1$ ,  $\hat{h}_1(w) = |w_1|^2 w_1$ , as well as

$$\begin{aligned} \hat{h}_{-1}(w) &= \frac{1}{N} \sum_{j=1}^N w_j, & \hat{h}_2(w) &= w_1^2 \frac{1}{N} \sum_{j=1}^N \bar{w}_j, & \hat{h}_3(w) &= |w_1|^2 \frac{1}{N} \sum_{j=1}^N w_j, \\ \hat{h}_4(w) &= w_1 \frac{1}{N} \sum_{j=1}^N |w_j|^2, & \hat{h}_5(w) &= w_1 \frac{1}{N^2} \sum_{j,k=1}^N w_j \bar{w}_k, & \hat{h}_6(w) &= \bar{w}_1 \frac{1}{N} \sum_{j=1}^N w_j^2, \\ \hat{h}_7(w) &= \bar{w}_1 \frac{1}{N^2} \sum_{j,k=1}^N w_j w_k, & \hat{h}_8(w) &= \frac{1}{N} \sum_{j=1}^N |w_j|^2 w_j, & \hat{h}_9(w) &= \frac{1}{N^2} \sum_{j,k=1}^N w_j^2 \bar{w}_k, \\ \hat{h}_{10}(w) &= \frac{1}{N^2} \sum_{j,k=1}^N w_j |w_k|^2, & \hat{h}_{11}(w) &= \frac{1}{N^3} \sum_{j,k,l=1}^N w_j w_k \bar{w}_l, \end{aligned} \tag{S.126}$$

for constants  $a_i \in \mathbb{C}, i = -1, \dots, 11$ . Note that in order to respect the rotational invariance, no constant terms can appear. Moreover, the symmetries make all polynomial terms of degree two vanish. Now, assuming that the linear term  $a_0 w_1$  and the first cubic term  $a_1 |w_1|^2 w_1$  are contained in  $f(w_1) = \alpha w_1 - \beta |w_1|^2 w_1$  as in (2.23) in the main text, we are left with in total 11 coupling terms  $a_i \hat{h}_i$  that will determine the phase interaction function of the reduced phase dynamics (S.120). Writing the complex constants as

$$a_j = \rho_j e^{i\phi_j},$$

Ashwin and Rodrigues<sup>141</sup> indicate instructions how to derive the desired constants  $\xi_i^j$

and  $\chi_i^j$  in (S.122). First one determines  $\vartheta_j$  and  $\psi_j$ ,  $j = -1, 1, \dots, 11$ , by

$$\vartheta_j \cos(\psi_j + \phi) := \rho_j \sin(\phi_j + \phi) - \frac{\beta_I}{\beta_R} \rho_j \cos(\phi_j + \phi) ,$$

where  $\beta_I/\beta_R = C(0)/A(0)$  with  $C(0) = -2\beta_I/\beta_R$  and  $A(0) = -2$  with  $\beta = \beta_R + i\beta_I$ . Using Eq.(4.30) of<sup>141</sup> and abbreviating

$$\delta = \frac{C'(0)A(0) - C(0)A'(0)}{A(0)^2} = \lim_{\lambda \rightarrow 0} \frac{d}{d\lambda} \frac{C(\lambda)}{A(\lambda)} , \quad (\text{S.127})$$

one can deduce

$$\begin{aligned} \xi_1^0 &= \vartheta_{-1}, & \chi_1^0 &= \psi_{-1}, \\ \xi_1^1 &= -\frac{1}{\beta_R} \sqrt{[\vartheta_2 \cos(\psi_2) + \vartheta_3 \cos(\psi_3) + \vartheta_8 \cos(\psi_8) + \vartheta_{10} \cos(\psi_{10}) + \delta \beta_R \rho_{-1} \cos(\phi_{-1})]^2 +} \\ &\quad + [-\vartheta_2 \sin(\psi_2) + \vartheta_3 \sin(\psi_3) + \vartheta_8 \sin(\psi_8) + \vartheta_{10} \sin(\psi_{10}) + \delta \beta_R \rho_{-1} \sin(\phi_{-1})]^2 + \mathcal{O}(\mu), \\ \chi_1^1 &= \arctan \left( \frac{-\vartheta_2 \sin(\psi_2) + \vartheta_3 \sin(\psi_3) + \vartheta_8 \sin(\psi_8) + \vartheta_{10} \sin(\psi_{10}) + \delta \beta_R \rho_{-1} \sin(\phi_{-1})}{\vartheta_2 \cos(\psi_2) + \vartheta_3 \cos(\psi_3) + \vartheta_8 \cos(\psi_8) + \vartheta_{10} \cos(\psi_{10}) + \delta \beta_R \rho_{-1} \cos(\phi_{-1})} \right), \\ \xi_2^1 &= -\vartheta_6/\beta_R + \mathcal{O}(\mu), & \chi_2^1 &= \psi_6, \\ \xi_3^1 &= -\vartheta_7/\beta_R + \mathcal{O}(\mu), & \chi_3^1 &= \psi_7, \\ \xi_4^1 &= -\vartheta_9/\beta_R + \mathcal{O}(\mu), & \chi_4^1 &= \psi_9, \\ \xi_5^1 &= -\vartheta_{11}/\beta_R + \mathcal{O}(\mu), & \chi_5^1 &= \psi_{11} . \end{aligned} \quad (\text{S.128})$$

In particular, we can determine an explicit value for  $\delta$  as presented in the following lemma.

**Lemma S.9.** *For the dynamics*

$$\dot{z} = \alpha z - \beta |z|^2 z + \tau(z), \quad \text{where } \tau(z) = \varkappa z^4 + \mathcal{O}(z^5),$$

*we get an explicit value for  $\delta$  as defined in (S.127), which reads*

$$\delta = -2 \frac{\varkappa_I}{\alpha_R^2} + \frac{5}{2} \frac{\varkappa_R \alpha_I}{\alpha_R^3} .$$

*Moreover, if  $\varkappa = 0$ , then also  $\delta = 0$ .*

*Proof.* In the following, we will use that  $\lambda \in \mathbb{R}$  and that we can write  $\tau(z) = \tau_R(z) + i\tau_I(z)$  with  $\tau_{R/I}$  real-valued functions. For  $x \in \mathbb{R}$ , we have

$$\tau_R(x) = \varkappa_R x^4 + \mathcal{O}(x^5) \quad \text{and} \quad \tau_I(x) = \varkappa_I x^4 + \mathcal{O}(x^5) .$$

As has been defined in<sup>141</sup>,  $A(\lambda)$  and  $C(\lambda)$  are given by

$$\begin{aligned} A(\lambda) &= \frac{U'_R(R_*)}{\lambda} \quad \text{with} \quad U'_R(z) = \lambda + 3\alpha z^2 + \tau'_R(z)z + \tau_R(z) \\ C(\lambda) &= \frac{R_*(\lambda)B(\lambda)}{\sqrt{\lambda}} \quad \text{with} \quad B(\lambda) = \frac{2\alpha_I R_* + \tau'_I(R_*)}{\sqrt{\lambda}} \end{aligned}$$

and  $R_* = R_*(\lambda)$  is the solution of

$$0 = \lambda + \alpha_R R_*^2 + \tau_R(R_*^2) \implies R_*^2(\lambda) = \frac{\lambda}{-\alpha_R} + \mathcal{O}(\lambda) .$$

That is,

$$\frac{C(\lambda)}{A(\lambda)} = \frac{2\alpha_I R_*^2 + \tau'_I(R_*)R_*}{\lambda + 3\alpha_R R_*^2 + \tau'_R(R_*) + \tau_R(R_*)} .$$

Dividing by  $R_*^2$  and substituting in the leading order of  $R_*^2$ , we find

$$\frac{C(\lambda)}{A(\lambda)} = \frac{2\alpha_I - \frac{4\kappa_I}{\alpha_R}\lambda + \mathcal{O}(\lambda^2)}{2\alpha_R - \frac{5\kappa_R}{\alpha_R}\lambda + \mathcal{O}(\lambda^2)} .$$

Hence, it follows

$$\delta = \left. \frac{d}{d\lambda} \right|_{\lambda=0} \frac{C(\lambda)}{A(\lambda)} = \frac{-8\kappa_I + 10\kappa_R \frac{\alpha_I}{\alpha_R}}{4\alpha_R^2} ,$$

which gives the desired result. Additionally, if  $\tau(z) = \mathcal{O}(z^5)$ , or even  $\tau \equiv 0$ , we have  $\kappa = 0$ , and therefore also  $\delta = 0$ .  $\square$

We close this section of the *Supplementary material* with a few brief comments on the coupling functions  $g_k$  in the (Hopf) normal form description (S.119) of the full network of coupled identical systems close to a supercritical Hopf bifurcation.

**Remark.** *If the coupling function  $g_k$  in the Hopf normal form description can be fully decomposed into the sum of pairwise interactions between oscillators, the following coupling parameters as introduced in (S.125) all vanish,*

$$a_5 = a_7 = a_9 = a_{10} = a_{11} = 0 .$$

*The only non-vanishing coefficients of the Hopf normal form description are*

$$a_{-1} = h_{0010}, \quad a_2 = h_{2001}, \quad a_3 = h_{1110}, \quad a_4 = h_{1011}, \quad a_6 = h_{0120}, \quad a_8 = h_{0021} .$$

*This means that the constants*

$$\xi_1^0, \xi_1^1, \xi_2^1 \quad \text{and} \quad \chi_1^0, \chi_1^1, \chi_2^1$$

are non-zero, which leads to the reduced phase dynamics

$$\begin{aligned}\dot{\theta}_k &= \Omega + \kappa \varepsilon^2 \frac{-\vartheta_4}{\beta_R} \cos(\psi_4) \\ &+ \frac{\kappa}{N} \sum_{j=1}^N [\xi_1^0 \cos(\theta_j - \theta_k + \chi_1^0) + \varepsilon^2 (\xi_1^1 \cos(\theta_j - \theta_k + \chi_1^1) + \xi_2^1 \cos(2(\theta_j - \theta_k) + \chi_2^1))].\end{aligned}\quad (\text{S.129})$$

Note that the coupling term in (S.129) consists again of the first two harmonics only: the terms  $\xi_1^0 \cos(\varphi + \chi_1^0) + \varepsilon \xi_1^1 \cos(\varphi + \chi_1^1)$  can be comprised by trigonometric identities to  $\xi_1 \cos(\varphi + \chi_1)$ . Yet, the contribution of the second term to the (collected) first harmonic is only minor due to the magnitude being of order  $\mathcal{O}(\varepsilon^2)$ , and hence can be neglected. Moreover, the amplitude of the second harmonic  $\cos(2\varphi + \chi_2^1)$  is  $\mathcal{O}(\varepsilon^2)$ , that is, of one order higher than the first harmonic. In total, the only constants that represent major contributions to the phase dynamics are  $\xi_1^0$  and  $\xi_2^1$ , which correspond by (S.128) to  $a_{-1} = h_{0010}$  and  $a_6 = h_{0120}$ , respectively – these are also the main contributors to the phase dynamics considered in Section S.2. Besides, disregarding the minor corrections of order  $\mathcal{O}(\varepsilon^2)$ , the natural frequency term  $\Omega = \alpha_I - \alpha_R \beta_I / \beta_R$  (note that  $\alpha_R = \varepsilon^2 = \mu$ ) coincides with the one derived in the main text's Section 2.2.2.

In general, the coupling functions  $g_k$  in the Hopf normal form description of the full network are not restricted to pairwise interactions, but they are linear combinations of the 11 terms given in (S.126). Deducing the respective factors in this linear combination from the underlying dynamics  $\dot{\mathbf{x}}_k = \mathbf{f}(\mathbf{x}_k) + \kappa \mathbf{g}_k(\mathbf{x}_1, \dots, \mathbf{x}_N)$  with  $N \geq 4$  in a general way is beyond the scope of this dissertation. Such a general normal form reduction would probably distort the ostensive link between the original coupling functions  $\mathbf{g}_k$  and the normal form coupling functions  $g_k$ : The structure of pairwise interactions in the underlying dynamics,  $\mathbf{g}_k(\mathbf{x}_1, \dots, \mathbf{x}_N) = \sum_j \mathbf{g}_{kj}(\mathbf{x}_k, \mathbf{x}_j)$ , may not be respected in the reduced Hopf normal form description  $g_k(w_1, \dots, w_N) \neq \sum_j g_{kj}(w_k, w_j)$ .

Still, given our goal to provide a phase reduction of the underlying dynamics, it appears sufficient to concentrate on those coupling terms in the Hopf normal form that have significant contributions to the reduced phase dynamics. The independent considerations and derivations in Section 2.2.1.2 and Corollary S.8 suggest that for large networks in the limit of weak coupling the dominant coupling terms are indeed those stated in the previous *remark*. As a consequence, we only need to find these coupling parameters. While a mathematically thorough normal form reduction for large  $N$  becomes rather lengthy and hence unpractical, the approaches in the main text's Section 2.2.2 seem to provide decent approximations for the sought-for coupling parameters, as demonstrated by the numerical simulations throughout *Chapter 3*. Nonetheless, both are approximations for the following distinct reasons: Following *Kuramoto's reductive perturbation approach*, in particular cf. Section S.2, the derivation is based on mere pairwise interactions of the underlying dynamics and the subsequent reduction steps only respect the bifurcation parameter-dependence up to first order. On the other hand, following *Poincaré's nonlinear transform approach* the parameter-dependence is preserved throughout the

reduction but the transformation steps are solely targeted at the Hopf normal form of a single oscillator but not at the Hopf normal form of the full network, see *Section S.3*. This latter assumption may be justified in the limit of weak coupling <sup>see also</sup><sup>78</sup>, but a rigorous proof, or an error estimate, respectively, are missing.

## S.6 Malkin's adjoint method

The phase sensitivity function, or infinitesimal phase response function, is defined as  $\mathbf{Z}(\theta) = \nabla \Theta(\mathbf{x})|_{\mathbf{x}=\mathbf{x}^c(\theta)}$ , which is the gradient of the (asymptotic) phase map  $\Theta(\mathbf{x})$  evaluated on the limit cycle  $\mathcal{C} = \{\mathbf{x}^c(t) : t \in \mathbb{R}\}$ . In general, it is not easy to find analytic expressions for the phase map so that it becomes cumbersome to compute  $\mathbf{Z}$  and  $\mathbf{g}$  in the direct way. However, as it turns out, the function  $\mathbf{Z}(\theta)$  is the solution to the adjoint problem associated with the dynamics

$$\dot{\mathbf{x}}_k = \mathbf{f}(\mathbf{x}_k) + \kappa \mathbf{g}_k(\mathbf{x}_1, \dots, \mathbf{x}_N), \quad \mathbf{x}_k \in \mathbb{R}^n, \quad k = 1, \dots, N, \quad (\text{S.130})$$

when linearized about the uncoupled limit-cycle. Indeed, and thereby following the theory of weakly coupled oscillators, in the uncoupled case ( $\kappa = 0$ ), the equation  $\dot{\mathbf{x}} = \mathbf{f}(\mathbf{x})$  has a  $T$ -periodic asymptotically stable limit cycle  $\mathcal{C}$ .  $\mathbf{x}^c(t)$  denotes such a  $T$ -periodic limit cycle solution, whose frequency is  $\omega = 2\pi/T$ . After an infinitesimal perturbation  $\mathbf{p}$  the perturbed trajectory  $\mathbf{x}(t) = \mathbf{x}^c(t) + \mathbf{u}(t)$  can be considered arbitrarily close to the limit cycle, such that the dynamics of  $\mathbf{u}(t)$  can be assumed linear. By linearizing  $\dot{\mathbf{x}} = \mathbf{f}(\mathbf{x})$  around the limit cycle, we define the matrix  $\mathbf{L}(t) \in \mathbb{R}^{n \times n}$  as

$$\mathbf{L}(t) = \nabla \mathbf{f}(\mathbf{x})|_{\mathbf{x}=\mathbf{x}^c(t)} . \quad (\text{S.131})$$

Solutions to the linearized equation satisfy

$$\left( \frac{d}{dt} - \mathbf{L}(t) \right) \mathbf{y}(t) =: (\mathcal{L}\mathbf{y})(t) = 0 , \quad (\text{S.132})$$

where  $\mathcal{L}$  is a linear operator on the space of  $\mathbb{R}^n$ -valued  $T$ -periodic functions. We define the standard inner product  $\langle \cdot, \cdot \rangle$  on  $T$ -periodic functions in  $\mathbb{R}^n$  as

$$\langle \mathbf{u}(t), \mathbf{v}(t) \rangle = \int_0^T \mathbf{u}(t) \cdot \mathbf{v}(t) dt . \quad (\text{S.133})$$

Then, the adjoint linear operator  $\mathcal{L}^*$  satisfies  $\langle \mathbf{u}, \mathcal{L}\mathbf{v} \rangle = \langle \mathcal{L}^*\mathbf{u}, \mathbf{v} \rangle$ . In particular, we find that

$$(\mathcal{L}^*\mathbf{y}(t))(t) = -\dot{\mathbf{y}}(t) - \mathbf{L}(t)^\top \mathbf{y}(t) . \quad (\text{S.134})$$

When determining the phase shift between the asymptotic phase  $\theta_p = \Theta(\mathbf{x}^c + \mathbf{p})$  after an infinitesimal perturbation  $\mathbf{p} = \mathbf{u}(t)$  at time  $t_0$  and the unperturbed phase  $\theta^c = \Theta(\mathbf{x}^c)$ ,

we note that for the phase shift  $\Delta\theta = \theta_p - \theta^c$  we have

$$\Delta\theta = \left\langle \mathbf{Z}(t), \mathbf{x}^c(t) + \mathbf{u}(t) - \mathbf{x}^c(t) \right\rangle + \mathcal{O}(|\mathbf{u}|^2). \quad (\text{S.135})$$

Moreover, the phase shift  $\Delta\theta$  is independent of time after the perturbation at  $t = t_0$ . Hence,

$$\begin{aligned} 0 &= \frac{d}{dt} \left\langle \mathbf{Z}(t), \mathbf{u}(t) \right\rangle = \left\langle \frac{d\mathbf{Z}(t)}{dt}, \mathbf{u}(t) \right\rangle + \left\langle \mathbf{Z}(t), \frac{d\mathbf{u}(t)}{dt} \right\rangle \\ &= \left\langle \frac{d\mathbf{Z}(t)}{dt}, \mathbf{u}(t) \right\rangle + \left\langle \mathbf{Z}(t), \mathbf{L}(t)\mathbf{u}(t) \right\rangle = \left\langle \frac{d\mathbf{Z}(t)}{dt}, \mathbf{u}(t) \right\rangle + \left\langle \mathbf{L}(t)^\top \mathbf{Z}(t), \mathbf{u}(t) \right\rangle \\ &= \left\langle \frac{d\mathbf{Z}(t)}{dt} + \mathbf{L}(t)^\top \mathbf{Z}(t), \mathbf{u}(t) \right\rangle = \left\langle -(\mathcal{L}^* \mathbf{Z})(t), \mathbf{u}(t) \right\rangle. \end{aligned}$$

As the perturbation  $\mathbf{u}(t)$  was assumed arbitrary, it follows that

$$\mathcal{L}^* \mathbf{Z}(t) = 0. \quad (\text{S.136})$$

Furthermore, by definition we have  $\Theta(\mathbf{x}^c(\theta)) = \theta$ . Differentiating both sides with respect to  $t$ , we find with  $\dot{\theta} = \omega$  that

$$\dot{\Theta}(\mathbf{x}^c(\theta)) = \mathbf{Z}(t) \cdot \frac{d\mathbf{x}^c(\theta)}{dt} = \omega. \quad (\text{S.137})$$

This normalization uniquely defines  $\mathbf{Z}(t)$  as the solution of  $\mathcal{L}^* \mathbf{Z} = 0$  and  $\mathbf{Z} \cdot d\mathbf{x}^c/dt = \omega$ .

## S.7 Limit of infinite attraction method

We derive the phase interaction function  $H$  for two coupled oscillators  $k \neq j$  with strongly attracting limit cycles, as has been considered by Ermentrout and Kopell<sup>147</sup>. The dynamics, where possible inhomogeneities among the oscillators have been subsumed in the respective coupling terms, are given by

$$\dot{\mathbf{x}}_k = \mathbf{f}(\mathbf{x}_k) + \kappa \mathbf{g}_k(\mathbf{x}_k, \mathbf{x}_j), \quad \mathbf{x}_k \in \mathbb{R}^n. \quad (\text{S.138})$$

We search for solutions of the form

$$\mathbf{x}_k(t) = \mathbf{x}_0(t) + \varepsilon \mathbf{u}_k(t), \quad (\text{S.139})$$

where  $\mathbf{x}_0(t)$  denotes a  $T$ -period limit cycle solution of  $\dot{\mathbf{x}} = \mathbf{f}(\mathbf{x})$  with frequency  $\omega = 2\pi/T$ , and  $\mathbf{u}_k$  is such that it converges to zero for solutions on the limit cycle  $\mathbf{x}(t) = \mathbf{x}^c(t)$ .

Note that we can parametrize the limit cycle solution via the phase  $\theta_k = \theta_k(t) \in \mathbb{S}^1$ , such that effectively we search for a transformation  $T_k = T_k(\theta_k(t), \boldsymbol{\rho}_k)$  with  $\boldsymbol{\rho}_k \in \mathbb{R}^{n-1}$  that maps a solution  $\mathbf{x}_k \in \mathbb{R}^n$  of (S.138) in an equivalent form to (S.139), given as

$$\mathbf{x}_k(t) = \mathbf{x}_0(\theta_k(t)) + \mathbf{M}(\theta_k(t)) \boldsymbol{\rho}_k(t) + \mathcal{O}(|\boldsymbol{\rho}_k|^2) \quad (\text{S.140})$$

with the  $n \times (n - 1)$ -matrix  $\mathbf{M}$  that satisfies

$$\mathbf{M}(\theta)^\top \mathbf{M}(\theta) = \mathbf{I}_{(n-1) \times (n-1)} \quad \text{and} \quad \mathbf{x}'_0(\theta)^\top \mathbf{M}(\theta) = 0$$

for all  $\theta \in \mathbb{S}^1$ ; the prime ' denotes the derivative with respect to  $\theta$ . The corresponding dynamics of the normal coordinates phase  $\theta_k$  and  $\rho_k$  can be derived<sup>153</sup> as

$$\begin{aligned} \dot{\theta}_k &= \omega + h_k(\theta_k, \theta_j) + \mathcal{O}(|\rho_k, \rho_j|) , \\ \dot{\rho}_k &= \mathbf{a}(\theta_k)\rho_k + \mathbf{d}_k(\theta_k, \theta_j) + \mathcal{O}(|\rho_j|) + o(|\rho_k|) . \end{aligned} \quad (\text{S.141})$$

Introducing the Jacobian  $\mathbf{L}(\theta) = \nabla \mathbf{f}(\mathbf{x})|_{\mathbf{x}=\mathbf{x}_0(\theta)}$  of  $\mathbf{f}$  evaluated at the limit cycle  $\mathbf{x}_0$ , and denoting  $\rho = |\mathbf{x}'_0|^2$ , the functions  $h_k$ ,  $\mathbf{a}$  and  $\mathbf{d}_k$  can be found as

$$\begin{aligned} h_k(\theta_k, \theta_j) &= \omega \frac{\mathbf{x}'_0(\theta_k)^\top}{\rho(\theta_k)} [(\mathbf{L}(\theta_k) + \mathbf{L}(\theta_k)^\top) \mathbf{M}(\theta_k) \rho_k + \kappa \mathbf{g}_k(\mathbf{x}_0(\theta_k), \mathbf{x}_0(\theta_j))] \\ \mathbf{a}(\theta_k) &= \omega [\mathbf{M}(\theta_k)^\top \mathbf{L}(\theta_k) \mathbf{M}(\theta_k) + \mathbf{M}'(\theta_k)^\top \mathbf{M}(\theta_k)] \\ \mathbf{d}_k(\theta_k, \theta_j) &= \omega \kappa \mathbf{M}(\theta_k)^\top \mathbf{g}_k(\mathbf{x}_0(\theta_k), \mathbf{x}_0(\theta_j)) . \end{aligned} \quad (\text{S.142})$$

For a two-dimensional system  $\mathbf{x}_k \in \mathbb{R}^2$  with the limit cycle solution  $\mathbf{x}_0(t) = (u_0(t), v_0(t))$ , we have  $\rho = |\mathbf{x}'_0(t)|^2 = u'_0(t)^2 + v'_0(t)^2$  and can set  $\mathbf{M}(t) = (v'_0(t), -u'_0(t)) / \sqrt{\rho(t)}$ , which fulfills the required conditions above.

Note furthermore that the equations (S.141) with (S.142) are general and hold for any coupling strength  $\kappa \in \mathbb{R}$ . In the case of weak coupling,  $0 \leq \kappa \ll 1$ , and in the limit of strong attraction,  $\rho_k \rightarrow 0$ , we can average  $h_k$  over one period and find the phase interaction function

$$H_k(\theta_k - \theta_j) = \frac{1}{2\pi} \int_0^{2\pi} \omega \rho(t + \theta_k)^{-1} \mathbf{x}'_0(t + \theta_k)^\top \mathbf{g}_k(\mathbf{x}_0(t + \theta_k), \mathbf{x}_0(t + \theta_j)) dt . \quad (\text{S.143})$$

In a more rigorous way, we now allow finite attraction to the limit cycle, but furthermore assume weak coupling  $0 \leq \kappa = \varepsilon \ll 1$  and that the normal coordinate  $\rho_k$  is  $\varepsilon$ -close to the limit cycle. We can thus introduce  $\rho_k = \varepsilon s_k$ , and (S.141) becomes

$$\begin{aligned} \dot{\theta}_k &= \omega + \varepsilon [\mathbf{b}(\theta_k) s_k + \rho(\theta_k)^{-1} \mathbf{x}'_0(\theta_k)^\top \mathbf{g}_k(\mathbf{x}_0(\theta_k), \mathbf{x}_0(\theta_j))] + \mathcal{O}(\varepsilon^2) , \\ \dot{s}_k &= \mathbf{a}(\theta_k) s_k + \mathbf{M}(\theta_k)^\top \mathbf{g}_k(\mathbf{x}_0(\theta_k), \mathbf{x}_0(\theta_j)) + \mathcal{O}(\varepsilon) , \end{aligned} \quad (\text{S.144})$$

with  $\mathbf{b}(\theta_k) = \omega \rho(\theta_k)^{-1} \mathbf{x}'_0(\theta_k)^\top [\mathbf{L}(\theta_k) + \mathbf{L}(\theta_k)^\top] \mathbf{M}(\theta_k)$ . Additionally, we set  $\omega = 1$  without loss of generality. In order to determine the phase interaction function  $H_k$  for finite  $\rho_k$ , we have to take the additional term  $\mathbf{b}(\theta_k) s_k$  into account when applying averaging as in (S.143).

Before deriving the averaged solution, we first recall that we are looking for solutions of the form (S.139), in which  $\mathbf{u}_k$  now additionally evolves on a slower time scale  $\tau = \varepsilon t$ , that is, we seek for solutions

$$\mathbf{x}_k(t) = \mathbf{x}_0(t + \theta_k(\tau)) + \varepsilon \mathbf{u}_k(t, \tau, \varepsilon) . \quad (\text{S.145})$$

We substitute this ansatz in (S.138) and find at first order in  $\varepsilon$

$$\begin{aligned}\mathcal{L}(t + \theta_k) \mathbf{u}_k(t, \tau, 0) &\equiv \left[ \frac{d}{dt} - \mathbf{L}(t + \theta_k) \right] \mathbf{u}_k(t, \tau, 0) \\ &= -\mathbf{x}'_0(t + \theta_k) \frac{\partial \theta_k}{\partial \tau} + \mathbf{g}_k(\mathbf{x}_0(t + \theta_k), \mathbf{x}_0(t + \theta_j)).\end{aligned}\quad (\text{S.146})$$

To solve (S.146) for periodic solutions  $\mathbf{u}_k$ , we rely on the Fredholm alternative<sup>see, e.g., 423</sup> according to which

$$\mathcal{L}(t) \boldsymbol{\xi}(t) = \mathbf{g}(t) \quad (\text{S.147})$$

has a  $2\pi$ -periodic solution  $\boldsymbol{\xi}(t)$  if and only if

$$\int_0^{2\pi} \boldsymbol{\chi}(t) \mathbf{g}(t) = 0, \quad (\text{S.148})$$

where  $\boldsymbol{\chi}(t)$  solves the corresponding homogeneous adjoint problem

$$\mathcal{L}^*(t) \boldsymbol{\chi}(t) \equiv \left[ \frac{d}{dt} - \mathbf{L}(t)^\top \right] \boldsymbol{\chi}(t) = 0. \quad (\text{S.149})$$

We achieve uniqueness of the solution by requiring the normalization condition

$$\frac{1}{2\pi} \int_0^{2\pi} \boldsymbol{\chi}(t) \mathbf{x}'_0(t) = 1. \quad (\text{S.150})$$

Hence, in order to find a solution of (S.146), we combine (S.148) and (S.150) to obtain

$$\frac{\partial \theta_k}{\partial \tau} = \tilde{H}_k(\theta_k - \theta_j) \equiv \frac{1}{2\pi} \int_0^{2\pi} \boldsymbol{\chi}(t) \mathbf{g}_k(\mathbf{x}_0(t), \mathbf{x}_0(t + \theta_k - \theta_j)) dt. \quad (\text{S.151})$$

The function  $\boldsymbol{\chi}(t)$  turns out to be

$$\boldsymbol{\chi}(t) = [\rho(t)^{-1} \mathbf{x}'_0(t) \boldsymbol{\varrho}(t)]^\top \quad (\text{S.152})$$

with

$$\boldsymbol{\varrho}(t)^\top = \left[ Q(2\pi) [\mathbf{I}_{(n-1) \times (n-1)} - \mathbf{E}(2\pi)]^{-1} - Q(t) \right] \mathbf{E}(t)^{-1} \mathbf{M}(t)^\top,$$

where  $\mathbf{E}(t)$  is the solution to  $d\mathbf{E}/dt = \mathbf{a}(t)\mathbf{E}$  with initial condition  $\mathbf{E}(0) = \mathbf{I}_{(n-1) \times (n-1)}$  and  $Q(t)$  satisfies  $Q(t) = \int_0^t \mathbf{b}(s)\mathbf{E}(s)ds$ . Indeed, inserting the ansatz

$$\boldsymbol{\chi}(t) = \mathbf{x}'_0(t) \boldsymbol{\xi}(t) + \mathbf{M}(t) \mathbf{z}(t) \quad (\text{S.153})$$

into the adjoint problem (S.149) with normalization (S.150), we find that  $\boldsymbol{\xi}(t) = \rho(t)^{-1}$  and  $\mathbf{z}$  satisfies  $\mathbf{z}' = -\mathbf{a}(t)^\top \mathbf{z} - \mathbf{b}(t)^\top$ , which eventually leads to the unique solution (S.152). For more mathematical details, we refer to<sup>147</sup>.

## REFERENCES

- [1] Varela, F., Lachaux, J.-P., Rodriguez, E. & Martinerie, J. The brainweb: phase synchronization and large-scale integration. *Nat. Rev. Neurosci.* **2**, 229–239 (2001).
- [2] Steriade, M. Cellular substrates of brain rhythms. In Niedermeyer, E. & Lopes Da Silva, F. (eds.) *Electroencephalography basic principles, clinical applications, and related fields*, 31–84 (Lippincott Williams & Wilkins, 2005).
- [3] Buzsáki, G. & Draguhn, A. Neuronal oscillations in cortical networks. *Science* **304**, 1926–1929 (2004).
- [4] Buzsáki, G. *Rhythms of the Brain* (Oxford University Press, 2006).
- [5] Schnitzler, A. & Gross, J. Normal and pathological oscillatory communication in the brain. *Nat. Rev. Neurosci.* **6**, 285–296 (2005).
- [6] Uhlhaas, P. J. & Singer, W. Neural synchrony in brain disorders: relevance for cognitive dysfunctions and pathophysiology. *Neuron* **52**, 155–168 (2006).
- [7] Bressler, S. L. & Kelso, J. S. Coordination dynamics in cognitive neuroscience. *Frontiers in Neuroscience* **10** (2016).
- [8] Bressler, S. L. & Menon, V. Large-scale brain networks in cognition: emerging methods and principles. *Trends in Cognitive Sciences* **14**, 277–290 (2010).
- [9] Engel, A. K., Fries, P. & Singer, W. Dynamic predictions: oscillations and synchrony in top-down processing. *Nat. Rev. Neurosci.* **2**, 704–716 (2001).
- [10] Fries, P. A mechanism for cognitive dynamics: neuronal communication through neuronal coherence. *Trends in Cognitive Sciences* **9**, 474–480 (2005).
- [11] Deco, G., Jirsa, V. K., Robinson, P. A., Breakspear, M. & Friston, K. The dynamic brain: from spiking neurons to neural masses and cortical fields. *PLoS Comput. Biol.* **4**, e1000092 (2008).
- [12] Jirsa, V. K. & Haken, H. A derivation of a macroscopic field theory of the brain from the quasi-microscopic neural dynamics. *Physica D* **99**, 503–526 (1997).
- [13] Coombes, S. Large-scale neural dynamics: simple and complex. *NeuroImage* **52**, 731–739 (2010).
- [14] Siettos, C. & Starke, J. Multiscale modeling of brain dynamics: from single neurons and networks to mathematical tools. *Wiley Interdisciplinary Reviews: Systems Biology and Medicine* **8**, 438–458 (2016).
- [15] Breakspear, M. Dynamic models of large-scale brain activity. *Nature Neuroscience* **20**, 340–352 (2017).
- [16] Singer, W. Binding by synchrony. *Scholarpedia* **2**, 1657 (2007). Revision #124403.
- [17] Nunez, P. L. Toward a quantitative description of large-scale neocortical dynamic function and EEG. *Behavioral and Brain Sciences* **23**, 371–398 (2000).
- [18] Singer, W. Synchronization of cortical activity and its putative role in information processing and learning. *Annual Review of Physiology* **55**, 349–74 (1993).
- [19] Singer, W. & Gray, C. M. Visual feature integration and the temporal correlation hypothesis. *Annual Review of Neuroscience* **18**, 555–586 (1995).

- [20] Singer, W. Neuronal synchrony: a versatile code for the definition of relations? *Neuron* **24**, 49–65 (1999).
- [21] Buzsáki, G., Logothetis, N. & Singer, W. Scaling brain size, keeping timing: evolutionary preservation of brain rhythms. *Neuron* **80**, 751–764 (2013).
- [22] Womelsdorf, T., Valiante, T. A., Sahin, N. T., Miller, K. J. & Tiesinga, P. Dynamic circuit motifs underlying rhythmic gain control, gating and integration. *Nature Neuroscience* **17**, 1031 (2014).
- [23] Brunel, N. & Hakim, V. Fast global oscillations in networks of integrate-and-fire neurons with low firing rates. *Neural Computation* **11**, 1621–1671 (1999).
- [24] Pazó, D. & Montbrió, E. From quasiperiodic partial synchronization to collective chaos in populations of inhibitory neurons with delay. *Phys. Rev. Lett.* **116**, 238101 (2016).
- [25] Renart, A. *et al.* The asynchronous state in cortical circuits. *Science* **327**, 587–590 (2010).
- [26] Wang, X.-J. Neurophysiological and computational principles of cortical rhythms in cognition. *Physiological Reviews* **90**, 1195–1268 (2010).
- [27] Dauwels, J., Vialatte, F., Musha, T. & Cichocki, A. A comparative study of synchrony measures for the early diagnosis of Alzheimer’s disease based on EEG. *NeuroImage* **49**, 668 – 693 (2010).
- [28] Golomb, D. Neuronal synchrony measures. *Scholarpedia* **2**, 1347 (2007). Revision #123400.
- [29] Lachaux, J.-P., Rodriguez, E., Martinerie, J. & Varela, F. J. Measuring phase synchrony in brain signals. *Human Brain Mapping* **8**, 194–208 (1999).
- [30] Gray, C. M. Synchronous oscillations in neuronal systems: mechanisms and functions. *J. Comput. Neurosci.* **1**, 11–38 (1994).
- [31] MacKay, W. A. Synchronized neuronal oscillations and their role in motor processes. *Trends in Cognitive Sciences* **1**, 176–183 (1997).
- [32] Palva, J. M., Palva, S. & Kaila, K. Phase synchrony among neuronal oscillations in the human cortex. *J. Neurosci.* **25**, 3962–3972 (2005).
- [33] Schack, B. & Weiss, S. Quantification of phase synchronization phenomena and their importance for verbal memory processes. *Biological Cybernetics* **92**, 275–287 (2005).
- [34] Sauseng, P. & Klimesch, W. What does phase information of oscillatory brain activity tell us about cognitive processes? *Neuroscience & Biobehavioral Reviews* **32**, 1001–1013 (2008).
- [35] Thut, G., Miniussi, C. & Gross, J. The functional importance of rhythmic activity in the brain. *Current Biology* **22**, R658 – R663 (2012).
- [36] Honey, C. J., Kötter, R., Breakspear, M. & Sporns, O. Network structure of cerebral cortex shapes functional connectivity on multiple time scales. *PNAS* **104**, 10240–10245 (2007).
- [37] Ghosh, A., Rho, Y., McIntosh, A. R., Kötter, R. & Jirsa, V. K. Noise during rest enables the exploration of the brain’s dynamic repertoire. *PLoS Comput. Biol.* **4**, e1000196 (2008).
- [38] Kuramoto, Y. *Chemical oscillations, turbulence and waves* (Springer, 1984).
- [39] Rodrigues, F. A., Peron, T. K. D., Ji, P. & Kurths, J. The Kuramoto model in complex networks. *Physics Reports* **610**, 1 – 98 (2016).
- [40] Breakspear, M., Heitmann, S. & Daffertshofer, A. Generative models of cortical oscillations: neurobiological implications of the Kuramoto model. *Frontiers in Human Neuroscience* **4** (2010).
- [41] Schuster, H. & Wagner, P. A model for neuronal oscillations in the visual cortex. *Biological Cybernetics* **64**, 77–82 (1990).

[42] Daffertshofer, A. & van Wijk, B. On the influence of amplitude on the connectivity between phases. *Frontiers in Neuroinformatics* **5**, 6 (2011).

[43] Cabral, J., Hugues, E., Sporns, O. & Deco, G. Role of local network oscillations in resting-state functional connectivity. *NeuroImage* **57**, 130 – 139 (2011).

[44] Ton, R., Deco, G. & Daffertshofer, A. Structure-function discrepancy: inhomogeneity and delays in synchronized neural networks. *PLoS Comput. Biol.* **10**, e1003736 (2014).

[45] Cabral, J., Kringelbach, M. L. & Deco, G. Exploring the network dynamics underlying brain activity during rest. *Progress in Neurobiology* **114**, 102 – 131 (2014).

[46] Cabral, J. *et al.* Exploring mechanisms of spontaneous functional connectivity in MEG: How delayed network interactions lead to structured amplitude envelopes of band-pass filtered oscillations. *NeuroImage* **90**, 423 – 435 (2014).

[47] Tasseff, R. *et al.* Mouse hair cycle expression dynamics modeled as coupled mesenchymal and epithelial oscillators. *PLoS Comput. Biol.* **10**, 1–21 (2014).

[48] Sadilek, M. & Thurner, S. Physiologically motivated multiplex Kuramoto model describes phase diagram of cortical activity. *Scientific Reports* **5** (2015).

[49] Schmidt, R., LaFleur, K. J. R., de Reus, M. A., van den Berg, L. H. & van den Heuvel, M. P. Kuramoto model simulation of neural hubs and dynamic synchrony in the human cerebral connectome. *BMC Neuroscience* **16**, 54 (2015).

[50] Dumas, G., Chavez, M., Nadel, J. & Martinerie, J. Anatomical connectivity influences both intra- and inter-brain synchronizations. *PLoS One* **7**, 1–11 (2012).

[51] Yan, B. & Li, P. The emergence of abnormal hypersynchronization in the anatomical structural network of human brain. *NeuroImage* **65**, 34 – 51 (2013).

[52] Watanabe, T. Rich-club network topology to minimize synchronization cost due to phase difference among frequency-synchronized oscillators. *Physica A* **392**, 1246 – 1255 (2013).

[53] Ponce-Alvarez, A. *et al.* Resting-state temporal synchronization networks emerge from connectivity topology and heterogeneity. *PLoS Comput. Biol.* **11**, 1–23 (2015).

[54] Moon, J.-Y., Lee, U., Blain-Moraes, S. & Mashour, G. A. General relationship of global topology, local dynamics, and directionality in large-scale brain networks. *PLoS Comput. Biol.* **11**, 1–21 (2015).

[55] Moon, J.-Y. *et al.* Structure shapes dynamics and directionality in diverse brain networks: Mathematical principles and empirical confirmation in three species. *Scientific Reports* **7**, 46606 EP – (2017).

[56] Schmidt, H., Petkov, G., Richardson, M. P. & Terry, J. R. Dynamics on networks: The role of local dynamics and global networks on the emergence of hypersynchronous neural activity. *PLoS Comput. Biol.* **10**, 1–16 (2014).

[57] Gómez-Gardeñes, J., Zamora-López, G., Moreno, Y. & Arenas, A. From modular to centralized organization of synchronization in functional areas of the cat cerebral cortex. *PLoS One* **5**, e12313 (2010).

[58] Nicosia, V., Valencia, M., Chavez, M., Díaz-Guilera, A. & Latora, V. Remote synchronization reveals network symmetries and functional modules. *Phys. Rev. Lett.* **110**, 174102 (2013).

[59] Vuksanović, V. & Hövel, P. Functional connectivity of distant cortical regions: role of remote synchronization and symmetry in interactions. *NeuroImage* **97**, 1–8 (2014).

[60] Tauro, C. B., Tamarit, F. A., Gleiser, P. M. *et al.* Modeling spatial patterns in the visual cortex. *Phys. Rev. E* **90**, 042818 (2014).

[61] Hlinka, J. & Coombes, S. Using computational models to relate structural and functional brain connectivity. *European Journal of Neuroscience* **36**, 2137–2145 (2012).

[62] Honey, C. J. & Sporns, O. Dynamical consequences of lesions in cortical networks. *Human Brain Mapping* **29**, 802–809 (2008).

[63] Vásá, F. *et al.* Effects of lesions on synchrony and metastability in cortical networks. *NeuroImage* **118**, 456 – 467 (2015).

[64] Kitzbichler, M. G., Smith, M. L., Christensen, S. R. & Bullmore, E. Broadband criticality of human brain network synchronization. *PLoS Comput. Biol.* **5**, 1–13 (2009).

[65] Botcharova, M., Farmer, S. F. & Berthouze, L. Markers of criticality in phase synchronization. *Frontiers in Systems Neuroscience* **8** (2014).

[66] Botcharova, M., Berthouze, L., Brookes, M. J., Barnes, G. R. & Farmer, S. F. Resting state MEG oscillations show long-range temporal correlations of phase synchrony that break down during finger movement. *Frontiers in Physiology* **6** (2015).

[67] Daffertshofer, A., Ton, R., Pietras, B., Kringselbach, M. L. & Deco, G. Scale-freeness or partial synchronization in neural mass phase oscillator networks: Pick one of two? *NeuroImage* **180**, 428 – 441 (2018).

[68] Lee, W. H., Bullmore, E. & Frangou, S. Quantitative evaluation of simulated functional brain networks in graph theoretical analysis. *NeuroImage* **146**, 724–733 (2017).

[69] Wilson, H. R. & Cowan, J. D. Excitatory and inhibitory interactions in localized populations of model neurons. *Biophysical Journal* **12**, 1–24 (1972).

[70] Wilson, H. R. & Cowan, J. D. A mathematical theory of the functional dynamics of cortical and thalamic nervous tissue. *Kybernetik* **13**, 55–80 (1973).

[71] Lopes da Silva, F., Hoeks, A., Smits, H. & Zetterberg, L. Model of brain rhythmic activity. *Biological Cybernetics* **15**, 27–37 (1974).

[72] Lopes da Silva, F., Van Rotterdam, A., Barts, P., Van Heusden, E. & Burr, W. Models of neuronal populations: the basic mechanisms of rhythmicity. *Progress in Brain Research* **45**, 281–308 (1976).

[73] Lopes da Silva, F. Neural mechanisms underlying brain waves: from neural membranes to networks. *Electroencephalography and Clinical Neurophysiology* **79**, 81–93 (1991).

[74] Jansen, B. H. & Rit, V. G. Electroencephalogram and visual evoked potential generation in a mathematical model of coupled cortical columns. *Biological Cybernetics* **73**, 357–366 (1995).

[75] Freeman, W. J. Mass action in the nervous system (1975).

[76] Amari, S. Dynamics of pattern formation in lateral-inhibition type neural fields. *Biological Cybernetics* **27**, 77–87 (1977).

[77] Kilpatrick, Z. P. Wilson-Cowan Model. In Jaeger, D. & Jung, R. (eds.) *Encyclopedia of Computational Neuroscience*, 3159–3163 (Springer, 2015).

[78] Hoppensteadt, F. C. & Izhikevich, E. M. *Weakly Connected Neural Networks* (Springer, 1997).

[79] Borisyuk, R. M. & Kirillov, A. B. Bifurcation analysis of a neural network model. *Biological Cybernetics* **66**, 319–325 (1992).

[80] Watanabe, S. & Strogatz, S. H. Constants of motion for superconducting Josephson arrays. *Physica D* **74**, 197–253 (1994).

[81] Ott, E. & Antonsen, T. M. Low dimensional behavior of large systems of globally coupled oscillators. *Chaos* **18** (2008).

[82] Ott, E. & Antonsen, T. M. Long time evolution of phase oscillator systems. *Chaos* **19** (2009).

[83] Ott, E., Hunt, B. R. & Antonsen, T. M. Comment on ‘Long time evolution of phase oscillator systems’ [Chaos 19, 023117 (2009)]. *Chaos* **21**, 025112 (2011).

[84] Mardia, K. V. & Jupp, P. E. *Directional statistics* (John Wiley & Sons, 2009).

[85] Winfree, A. T. Biological rhythms and the behavior of populations of coupled oscillators. *J. Theoret. Biol.* **16**, 15–42 (1967).

[86] Ermentrout, G. B. & Terman, D. H. *Mathematical foundations of neuroscience* (Springer, 2010).

[87] Nakao, H. Phase reduction approach to synchronisation of nonlinear oscillators. *Contemporary Physics* **57**, 188–214 (2016).

[88] Pecora, L. M. & Carroll, T. L. Master stability functions for synchronized coupled systems. *Phys. Rev. Lett.* **80**, 2109 (1998).

[89] Ashwin, P., Coombes, S. & Nicks, R. Mathematical frameworks for oscillatory network dynamics in neuroscience. *The Journal of Mathematical Neuroscience* **6**, 2 (2016).

[90] Rosenblum, M. & Pikovsky, A. Self-organized quasiperiodicity in oscillator ensembles with global nonlinear coupling. *Phys. Rev. Lett.* **98**, 064101 (2007).

[91] Pikovsky, A. & Rosenblum, M. Self-organized partially synchronous dynamics in populations of nonlinearly coupled oscillators. *Physica D* **238**, 27 – 37 (2009).

[92] Rosenblum, M. & Pikovsky, A. Two types of quasiperiodic partial synchrony in oscillator ensembles. *Phys. Rev. E* **92**, 012919 (2015).

[93] Okuda, K. Variety and generality of clustering in globally coupled oscillators. *Physica D* **63**, 424–436 (1993).

[94] Hansel, D., Mato, G. & Meunier, C. Clustering and slow switching in globally coupled phase oscillators. *Phys. Rev. E* **48**, 3470 (1993).

[95] Kori, H., Kuramoto, Y., Jain, S., Kiss, I. Z. & Hudson, J. L. Clustering in globally coupled oscillators near a Hopf bifurcation: theory and experiments. *Phys. Rev. E* **89**, 062906 (2014).

[96] Kori, H. & Kuramoto, Y. Slow switching in globally coupled oscillators: robustness and occurrence through delayed coupling. *Phys. Rev. E* **63**, 046214 (2001).

[97] Kori, H. Slow switching in a population of delayed pulse-coupled oscillators. *Phys. Rev. E* **68**, 021919 (2003).

[98] Clusella, P., Politi, A. & Rosenblum, M. A minimal model of self-consistent partial synchrony. *New Journal of Physics* **18**, 093037 (2016).

[99] Komarov, M. & Pikovsky, A. Multiplicity of singular synchronous states in the Kuramoto model of coupled oscillators. *Phys. Rev. Lett.* **111**, 204101 (2013).

[100] Komarov, M. & Pikovsky, A. The Kuramoto model of coupled oscillators with a bi-harmonic coupling function. *Physica D* **289**, 18–31 (2014).

[101] Bick, C., Timme, M., Paulikat, D., Rathlev, D. & Ashwin, P. Chaos in symmetric phase oscillator networks. *Phys. Rev. Lett.* **107**, 244101 (2011).

[102] Brown, E., Moehlis, J. & Holmes, P. On the phase reduction and response dynamics of neural oscillator populations. *Neural Computation* **16**, 673–715 (2004).

[103] Hesse, J., Schleimer, J.-H. & Schreiber, S. Qualitative changes in phase-response curve and synchronization at the saddle-node-loop bifurcation. *Phys. Rev. E* **95**, 052203 (2017).

[104] Murdock, J. *Normal forms and unfoldings for local dynamical systems* (Springer, 2006).

[105] Haken, H. *Synergetics: Introduction and advanced topics* (Springer, 2013).

[106] Tass, P. *Phase Resetting in Medicine and Biology: Stochastic Modelling and Data Analysis* (Springer, 2007).

[107] Chow, S.-N., Li, C. & Wang, D. *Normal forms and bifurcation of planar vector fields* (Cambridge University Press, 1994).

[108] Aburn, M. J. *Critical fluctuations and coupling of stochastic neural mass models*. Ph.D. thesis, University of Queensland (2016).

[109] Poincaré, H. & Magini, R. Les méthodes nouvelles de la mécanique céleste. *Il Nuovo Cimento (1895-1900)* **10**, 128–130 (1899).

[110] Takens, F. Normal forms for certain singularities of vector fields. *Ann. Inst. Fourier* **23**, 163–195 (1973).

[111] Takens, F. Singularities of vector fields. *Publications Mathématiques de l'IHÉS* **43**, 47–100 (1974).

[112] Guckenheimer, J. & Holmes, P. J. *Nonlinear oscillations, dynamical systems, and bifurcations of vector fields* (Springer, 2013).

[113] Nayfeh, A. H. *The method of normal forms* (John Wiley & Sons, 2011).

[114] Yu, P. Computation of normal forms via a perturbation technique. *Journal of Sound and Vibration* **211**, 19–38 (1998).

[115] Nayfeh, A. H. & Mook, D. T. *Nonlinear oscillations* (John Wiley & Sons, 2008).

[116] Huseyin, K. *Multiple Parameter Stability Theory and Its Applications: Bifurcations, Catastrophes, Instabilities ...* (Clarendon Press, 1986).

[117] Sanders, J. A., Verhulst, F. & Murdock, J. A. *Averaging methods in nonlinear dynamical systems*, vol. 59 (Springer, 2007).

[118] Chow, S.-N. & Hale, J. K. *Methods of bifurcation theory*, vol. 251 (Springer, 2012).

[119] LIU, Y.-R. & LI, J.-B. Theory of values of singular point in complex autonomous differential systems. *Science in China Series A-Mathematics, Physics, Astronomy & Technological Science* **33**, 10–23 (1990).

[120] Chen, H. & Liu, Y. Linear recursion formulas of quantities of singular point and applications. *Applied mathematics and computation* **148**, 163–171 (2004).

[121] Han, M. & Yu, P. *Normal forms, Melnikov functions and bifurcations of limit cycles*, vol. 181 (Springer Science & Business Media, 2012).

[122] Kuznetsov, Y. A. *Elements of applied bifurcation theory* (Springer, 1998).

[123] Van der Beek, C. Normal forms and periodic solutions in the theory of non-linear oscillations. existence and asymptotic theory. *International journal of non-linear mechanics* **24**, 263–279 (1989).

[124] Leung, A. & Zhang, Q. Higher order normal form and period averaging. *Journal of sound and vibration* **217**, 795–806 (1998).

[125] Leung, A. Y. & Zhang, Q. Normal form computation without central manifold reduction. *Journal of Sound and Vibration* **266**, 261–279 (2003).

[126] Coullet, P. & Spiegel, E. A. Amplitude equations for systems with competing instabilities. *SIAM Journal on Applied Mathematics* **43**, 776–821 (1983).

[127] Bruno, A. *Local Methods in Nonlinear Differential Equations* (Springer, 1989).

[128] Kahn, P. B. & Zarmi, Y. *Nonlinear dynamics: exploration through normal forms* (Courier Corporation, 2014).

[129] Elphick, C., Tirapegui, E., Brachet, M., Coullet, P. & Iooss, G. A simple global characterization for normal forms of singular vector fields. *Physica D* **29**, 95–127 (1987).

[130] Cushman, R. & Sanders, J. A. *Nilpotent Normal Forms and Representation Theory of  $sl(2, \mathbb{R})$*  (Vrije Universiteit Amsterdam, Subfaculteit Wiskunde en Informatica, 1985).

[131] Murdock, J. Hypernormal form theory: foundations and algorithms. *Journal of Differential Equations* **205**, 424–465 (2004).

[132] Belitskii, G. R. Invariant normal forms of formal series. *Functional Analysis and Its Applications* **13**, 46–47 (1979).

[133] Baider, A. Unique normal forms for vector fields and hamiltonians. *Journal of Differential Equations* **78**, 33–52 (1989).

[134] Baider, A. & Churchill, R. Unique normal forms for planar vector fields. *Mathematische Zeitschrift* **199**, 303–310 (1988).

[135] Sattinger, D. *Topics in Stability and Bifurcation Theory* (Springer, 1973).

[136] Haken, H. Higher order corrections to generalized Ginzburg-Landau equations of non-equilibrium systems. *Zeitschrift für Physik B Condensed Matter* **22**, 69–72 (1975).

[137] Haken, H. *Synergetics: a workshop : proceedings of the International Workshop on Synergetics at Schloss Elmau, Bavaria, May 2-7, 1977* (Springer, 1977).

[138] Leung, A., Qichang, Z. & Yushu, C. Normal form analysis of Hopf bifurcation exemplified by Duffing’s equation. *Shock and Vibration* **1**, 233–240 (1994).

[139] Leung, A. & Ge, T. An algorithm for higher order Hopf normal forms. *Shock and Vibration* **2**, 307–319 (1995).

[140] Cesari, L. *Asymptotic behavior and stability problems in ordinary differential equations*, vol. 16 (Springer Berlin Heidelberg, 1971).

[141] Ashwin, P. & Rodrigues, A. Hopf normal form with  $S_N$  symmetry and reduction to systems of nonlinearly coupled phase oscillators. *Physica D* **325**, 14–24 (2016).

[142] Bick, C., Ashwin, P. & Rodrigues, A. Chaos in generically coupled phase oscillator networks with nonpairwise interactions. *Chaos* **26**, 094814 (2016).

[143] Bogoliubov, N. N., Mitropol’skii, I. A. & Mitropolsky, Y. A. *Asymptotic methods in the theory of non-linear oscillations* (CRC Press, 1961).

[144] Haken, H. *Advanced Synergetics: Instability Hierarchies of Self-organizing Systems and Devices* (Springer, 1983).

[145] Jordan, D. W. & Smith, P. *Nonlinear ordinary differential equations: an introduction to dynamical systems* (Oxford University Press, 1999).

[146] Ermentrout, G. B. & Kopell, N. Frequency plateaus in a chain of weakly coupled oscillators, I. *SIAM Journal on Mathematical Analysis* **15**, 215–237 (1984).

[147] Ermentrout, G. B. & Kopell, N. Multiple pulse interactions and averaging in systems of coupled neural oscillators. *Journal of Mathematical Biology* **29**, 195–217 (1991).

[148] Malkin, I. Methods of Poincaré and Liapunov in theory of non-linear oscillations. *Gostexizdat* (1949).

[149] Williams, T. L. & Bowtell, G. The calculation of frequency-shift functions for chains of coupled oscillators, with application to a network model of the lamprey locomotor pattern generator. *J. Comput. Neurosci.* **4**, 47–55 (1997).

[150] Ermentrout, B. *Simulating, analyzing, and animating dynamical systems: a guide to XPPAUT for researchers and students* (SIAM, 2002).

[151] Govaerts, W. & Sautois, B. Computation of the phase response curve: A direct numerical approach. *Neural Computation* **18**, 817–847 (2006).

[152] Dhooge, A., Govaerts, W., Kuznetsov, Y. A., Meijer, H. G. & Sautois, B. New features of the software matcont for bifurcation analysis of dynamical systems. *Mathematical and Computer Modelling of Dynamical Systems* **14**, 147–175 (2008).

[153] Ermentrout, G. & Kopell, N. Oscillator death in systems of coupled neural oscillators. *SIAM Journal on Applied Mathematics* **50**, 125–146 (1990).

[154] Fenichel, N. & Moser, J. Persistence and smoothness of invariant manifolds for flows. *Indiana University Mathematics Journal* **21**, 193–226 (1971).

[155] Guevara, M. R., Glass, L., Mackey, M. C. & Shrier, A. Chaos in neurobiology. *IEEE Transactions on Systems, Man, and Cybernetics* **13**, 790–798 (1983).

[156] Novičenko, V. & Pyragas, K. Computation of phase response curves via a direct method adapted to infinitesimal perturbations. *Nonlinear Dynamics* **67**, 517–526 (2012).

[157] Glansdorff, P. & Prigogine, I. *Thermodynamic Theory of Structure, Stability and Fluctuations* (Wiley, 1971).

[158] Belousov, B. P. Oscillations reaction and its mechanism (in Russian). *Sbornik Referatov po Radiacioni Medicine* 145 (1959).

[159] Zhabotinsky, A. M. Periodical oxidation of malonic acid in solution (a study of the Belousov reaction kinetics). *Biofizika* **9**, 306–311 (1964).

[160] Field, R. J. & Burger, M. *Oscillations and traveling waves in chemical systems* (Wiley, 1985).

[161] Epstein, I. R., Kustin, K., De Kepper, P. & Orbán, M. Oscillating chemical reactions. *Scientific American* **248**, 112–123 (1983).

[162] Strogatz, S. H. *Nonlinear dynamics and chaos: with applications to physics, biology, chemistry, and engineering* (CRC Press, 2018).

[163] Nakao, H., Yanagita, T. & Kawamura, Y. Phase-reduction approach to synchronization of spatiotemporal rhythms in reaction-diffusion systems. *Phys. Rev. X* **4**, 021032 (2014).

[164] Kawamura, Y. & Nakao, H. Collective phase description of oscillatory convection. *Chaos* **23**, 043129 (2013).

[165] Taira, K. & Nakao, H. Phase-response analysis of synchronization for periodic flows. *Journal of Fluid Mechanics* **846**, R2 (2018).

[166] Kawamura, Y. & Tsubaki, R. Phase reduction approach to elastohydrodynamic synchronization of beating flagella. *Phys. Rev. E* **97**, 022212 (2018).

[167] Kawamura, Y., Nakao, H. & Kuramoto, Y. Collective phase description of globally coupled excitable elements. *Phys. Rev. E* **84**, 046211 (2011).

[168] Kawamura, Y. Collective phase reduction of globally coupled noisy dynamical elements. *Phys. Rev. E* **95**, 032225 (2017).

[169] Zhai, Y., Kiss, I. Z., Daido, H. & Hudson, J. L. Extracting order parameters from global measurements with application to coupled electrochemical oscillators. *Physica D* **205**, 57 – 69 (2005).

[170] Pietras, B. & Daffertshofer, A. Network dynamics of coupled oscillators and phase reduction techniques. *Submitted for publication* (2018).

[171] Marreiros, A. C., Daunizeau, J., Kiebel, S. J. & Friston, K. J. Population dynamics: variance and the sigmoid activation function. *NeuroImage* **42**, 147–157 (2008).

[172] Pinto, D. J., Brumberg, J. C., Simons, D. J., Ermentrout, G. B. & Traub, R. A quantitative population model of whisker barrels: re-examining the Wilson-Cowan equations. *J. Comput. Neurosci.* **3**, 247–264 (1996).

[173] Aronson, D. G., Ermentrout, G. B. & Kopell, N. Amplitude response of coupled oscillators. *Physica D* **41**, 403–449 (1990).

[174] Mirolo, R. E. & Strogatz, S. H. Amplitude death in an array of limit-cycle oscillators. *J. Stat. Phys.* **60**, 245–262 (1990).

[175] Sen, A., Dodla, R., Johnston, G. L. & Sethia, G. C. Amplitude death, synchrony, and chimera states in delay coupled limit cycle oscillators. In Atay, F. M. (ed.) *Complex Time-Delay Systems: Theory and Applications*, 1–43 (Springer, 2010).

[176] Saxena, G., Prasad, A. & Ramaswamy, R. Amplitude death: The emergence of stationarity in coupled nonlinear systems. *Physics Reports* **521**, 205 – 228 (2012).

[177] Koseska, A., Volkov, E. & Kurths, J. Oscillation quenching mechanisms: Amplitude vs. oscillation death. *Physics Reports* **531**, 173–199 (2013).

[178] Pikovsky, A. & Rosenblum, M. Dynamics of heterogeneous oscillator ensembles in terms of collective variables. *Physica D* **240**, 872–881 (2011).

[179] Pietras, B. & Daffertshofer, A. Ott-Antonsen attractiveness for parameter-dependent oscillatory systems. *Chaos* **26**, 103101 (2016).

[180] Daido, H. Discrete-time population dynamics of interacting self-oscillators. *Progr. Theoret. Phys.* **75**, 1460–1463 (1986).

[181] Daido, H. Intrinsic fluctuations and a phase transition in a class of large populations of interacting oscillators. *J. Stat. Phys.* **60**, 753–800 (1990).

[182] Hildebrand, E. J., Buice, M. A. & Chow, C. C. Kinetic theory of coupled oscillators. *Phys. Rev. Lett.* **98**, 054101 (2007).

[183] Buice, M. A. & Chow, C. C. Correlations, fluctuations, and stability of a finite-size network of coupled oscillators. *Phys. Rev. E* **76**, 031118 (2007).

[184] Hong, H., Chaté, H., Tang, L.-H. & Park, H. Finite-size scaling, dynamic fluctuations, and hyperscaling relation in the Kuramoto model. *Phys. Rev. E* **92**, 022122 (2015).

[185] Panaggio, M. J. & Abrams, D. M. Chimera states: coexistence of coherence and incoherence in networks of coupled oscillators. *Nonlinearity* **28**, R67 (2015).

[186] Arenas, A., Díaz-Guilera, A., Kurths, J., Moreno, Y. & Zhou, C. Synchronization in complex networks. *Physics Reports* **469**, 93–153 (2008).

[187] Golomb, D., Wang, X.-J. & Rinzel, J. Synchronization properties of spindle oscillations in a thalamic reticular nucleus model. *Journal of Neurophysiology* **72**, 1109–1126 (1994).

[188] Kaneko, K. Relevance of dynamic clustering to biological networks. *Physica D* **75**, 55–73 (1994).

[189] Cao, J. & Li, L. Cluster synchronization in an array of hybrid coupled neural networks with delay. *Neural Networks* **22**, 335–342 (2009).

[190] Ernst, U., Pawelzik, K. & Geisel, T. Synchronization induced by temporal delays in pulse-coupled oscillators. *Phys. Rev. Lett.* **74**, 1570 (1995).

[191] Ernst, U., Pawelzik, K. & Geisel, T. Delay-induced multistable synchronization of biological oscillators. *Phys. Rev. E* **57**, 2150 (1998).

[192] Timme, M., Wolf, F. & Geisel, T. Unstable attractors induce perpetual synchronization and desynchronization. *Chaos* **13**, 377–387 (2003).

[193] Ashwin, P. & Swift, J. W. The dynamics of  $n$  weakly coupled identical oscillators. *Journal of Nonlinear Science* **2**, 69–108 (1992).

[194] Brown, E., Holmes, P. & Moehlis, J. Globally coupled oscillator networks. *Perspectives and problems in nonlinear science: A celebratory volume in honor of Larry Sirovich* 183–215 (2003).

[195] Orosz, G., Moehlis, J. & Ashwin, P. Designing the dynamics of globally coupled oscillators. *Progr. Theoret. Phys.* **122**, 611–630 (2009).

[196] Shing Lee, W., Ott, E. & Antonsen Jr, T. M. Phase and amplitude dynamics in large systems of coupled oscillators: Growth heterogeneity, nonlinear frequency shifts, and cluster states. *Chaos* **23**, 033116 (2013).

[197] Sun, J., Bollt, E. M. & Nishikawa, T. Master stability functions for coupled nearly identical dynamical systems. *EPL* **85**, 60011 (2009).

[198] Sorrentino, F. & Porfiri, M. Analysis of parameter mismatches in the master stability function for network synchronization. *EPL* **93**, 50002 (2011).

[199] Zhang, Y. & Motter, A. E. Identical synchronization of nonidentical oscillators: when only birds of different feathers flock together. *Nonlinearity* **31**, R1 (2018).

[200] Maruyama, Y., Kakimoto, Y. & Araki, O. Analysis of chaotic oscillations induced in two coupled Wilson–Cowan models. *Biological Cybernetics* **108**, 355–363 (2014).

[201] Izhikevich, E. M. Weakly connected quasi-periodic oscillators, FM interactions, and multiplexing in the brain. *SIAM Journal on Applied Mathematics* **59**, 2193–2223 (1999).

[202] Demirt, A., Gu, C. & Roychowdhury, J. Phase equations for quasi-periodic oscillators. In *2010 IEEE/ACM International Conference on Computer-Aided Design (ICCAD)*, 292–297 (IEEE, 2010).

[203] Schwabedal, J. T. C., Pikovsky, A., Kralemann, B. & Rosenblum, M. Optimal phase description of chaotic oscillators. *Phys. Rev. E* **85**, 026216 (2012).

[204] Benayoun, M., Cowan, J. D., van Drongelen, W. & Wallace, E. Avalanches in a stochastic model of spiking neurons. *PLoS Comput. Biol.* **6**, e1000846 (2010).

[205] Wallace, E., Benayoun, M., Van Drongelen, W. & Cowan, J. D. Emergent oscillations in networks of stochastic spiking neurons. *PLoS One* **6**, e14804 (2011).

[206] Gigante, G., Deco, G., Marom, S. & Del Giudice, P. Network events on multiple space and time scales in cultured neural networks and in a stochastic rate model. *PLoS Comput. Biol.* **11**, 1–23 (2015).

[207] Goychuk, I. & Goychuk, A. Stochastic wilson–Cowan models of neuronal network dynamics with memory and delay. *New Journal of Physics* **17**, 045029 (2015).

[208] Cowan, J. D., Neuman, J. & van Drongelen, W. Wilson–Cowan equations for neocortical dynamics. *The Journal of Mathematical Neuroscience* **6**, 1 (2016).

[209] Zankoc, C., Biancalani, T., Fanelli, D. & Livi, R. Diffusion approximation of the stochastic Cowan-Wilson model. *Chaos, Solitons & Fractals* **103**, 504 – 512 (2017).

[210] Bressloff, P. C. Spatiotemporal dynamics of continuum neural fields. *J. Phys. A* **45**, 033001 (2011).

[211] Kuehn, C. & Riedler, M. G. Large deviations for nonlocal stochastic neural fields. *The Journal of Mathematical Neuroscience* **4**, 1 (2014).

[212] Schwalger, T., Deger, M. & Gerstner, W. Towards a theory of cortical columns: From spiking neurons to interacting neural populations of finite size. *PLoS Comput. Biol.* **13**, 1–63 (2017).

[213] Schwabedal, J. T. C. & Pikovsky, A. Phase description of stochastic oscillations. *Phys. Rev. Lett.* **110**, 204102 (2013).

[214] Thomas, P. J. & Lindner, B. Asymptotic phase for stochastic oscillators. *Phys. Rev. Lett.* **113**, 254101 (2014).

[215] Teramae, J. & Tanaka, D. Robustness of the noise-induced phase synchronization in a general class of limit cycle oscillators. *Phys. Rev. Lett.* **93**, 204103 (2004).

[216] Yoshimura, K. & Arai, K. Phase reduction of stochastic limit cycle oscillators. *Phys. Rev. Lett.* **101**, 154101 (2008).

[217] Teramae, J., Nakao, H. & Ermentrout, G. B. Stochastic phase reduction for a general class of noisy limit cycle oscillators. *Phys. Rev. Lett.* **102**, 194102 (2009).

[218] Bressloff, P. C. Stochastic Fokker-Planck equation in random environments. *Phys. Rev. E* **94**, 042129 (2016).

[219] Gardiner, C. *Stochastic Methods: A Handbook for the Natural and Social Sciences* (Springer, 2009).

[220] Kawamura, Y., Nakao, H. & Kuramoto, Y. Noise-induced turbulence in nonlocally coupled oscillators. *Phys. Rev. E* **75**, 036209 (2007).

[221] Kawamura, Y., Nakao, H., Arai, K., Kori, H. & Kuramoto, Y. Collective phase sensitivity. *Phys. Rev. Lett.* **101**, 024101 (2008).

[222] Kori, H., Kawamura, Y., Nakao, H., Arai, K. & Kuramoto, Y. Collective-phase description of coupled oscillators with general network structure. *Phys. Rev. E* **80**, 036207 (2009).

[223] Kawamura, Y. Collective phase dynamics of globally coupled oscillators: Noise-induced anti-phase synchronization. *Physica D* **270**, 20–29 (2014).

[224] Kurebayashi, W., Shirasaka, S. & Nakao, H. Phase reduction method for strongly perturbed limit cycle oscillators. *Phys. Rev. Lett.* **111**, 214101 (2013).

[225] Park, Y. & Ermentrout, B. Weakly coupled oscillators in a slowly varying world. *J. Comput. Neurosci.* **40**, 269–281 (2016).

[226] Zanette, D. H. Propagating structures in globally coupled systems with time delays. *Phys. Rev. E* **62**, 3167 (2000).

[227] Jeong, S.-O., Ko, T.-W. & Moon, H.-T. Time-delayed spatial patterns in a two-dimensional array of coupled oscillators. *Phys. Rev. Lett.* **89**, 154104 (2002).

[228] Ko, T.-W. & Ermentrout, G. B. Effects of axonal time delay on synchronization and wave formation in sparsely coupled neuronal oscillators. *Phys. Rev. E* **76**, 056206 (2007).

[229] Ermentrout, B. & Ko, T.-W. Delays and weakly coupled neuronal oscillators. *Philos. Trans. Royal Soc. A* **367**, 1097–1115 (2009).

[230] Petkoski, S. *et al.* Heterogeneity of time delays determines synchronization of coupled oscillators. *Phys. Rev. E* **94**, 012209 (2016).

[231] Engelborghs, K., Luzyanina, T. & Roose, D. Numerical bifurcation analysis of delay differential equations using DDE-BIFTOOL. *ACM Transactions on Mathematical Software (TOMS)* **28**, 1–21 (2002).

[232] Sieber, J., Engelborghs, K., Luzyanina, T., Samaey, G. & Roose, D. DDE-BIFTOOL manual-bifurcation analysis of delay differential equations. *arXiv preprint arXiv:1406.7144* (2014).

[233] Coombes, S. & Laing, C. Delays in activity-based neural networks. *Philos. Trans. Royal Soc. A* **367**, 1117–1129 (2009).

[234] Song, Z.-G. & Xu, J. Stability switches and double Hopf bifurcation in a two-neural network system with multiple delays. *Cognitive Neurodynamics* **7**, 505–521 (2013).

[235] Novičenko, V. & Pyragas, K. Phase reduction of weakly perturbed limit cycle oscillations in time-delay systems. *Physica D* **241**, 1090–1098 (2012).

[236] Kotani, K. *et al.* Adjoint method provides phase response functions for delay-induced oscillations. *Phys. Rev. Lett.* **109**, 044101 (2012).

[237] Stankovski, T., Pereira, T., McClintock, P. V. E. & Stefanovska, A. Coupling functions: Universal insights into dynamical interaction mechanisms. *Rev. Mod. Phys.* **89**, 045001 (2017).

[238] Traub, R. D. & Wong, R. Synchronized burst discharge in disinhibited hippocampal slice. I. Initiation in CA2-CA3 region. *Journal of Neurophysiology* **49**, 442–458 (1983).

[239] Hansel, D., Mato, G. & Meunier, C. Phase dynamics for weakly coupled Hodgkin-Huxley neurons. *EPL* **23**, 367 (1993).

[240] Brown, E. *et al.* The influence of spike rate and stimulus duration on noradrenergic neurons. *J. Comput. Neurosci.* **17**, 13–29 (2004).

[241] Jirsa, V. K. Neural field dynamics with local and global connectivity and time delay. *Philos. Trans. Royal Soc. A* **367**, 1131–1143 (2009).

[242] Friston, K. J. The labile brain. I. Neuronal transients and nonlinear coupling. *Philos. Trans. Royal Soc. B* **355**, 215–236 (2000).

[243] Pyragas, K. & Novičenko, V. Phase reduction of a limit cycle oscillator perturbed by a strong amplitude-modulated high-frequency force. *Phys. Rev. E* **92**, 012910 (2015).

[244] Jirsa, V. & Müller, V. Cross-frequency coupling in real and virtual brain networks. *Frontiers in Computational Neuroscience* **7** (2013).

[245] Stankovski, T., Ticcinelli, V., McClintock, P. V. & Stefanovska, A. Neural cross-frequency coupling functions. *Frontiers in Systems Neuroscience* **11** (2017).

[246] Smale, S. A mathematical model of two cells via Turing's equation. In *The Hopf Bifurcation and Its Applications*, 354–367 (Springer, 1976).

[247] Shirasaka, S., Kurebayashi, W. & Nakao, H. Phase-amplitude reduction of transient dynamics far from attractors for limit-cycling systems. *Chaos* **27**, 023119 (2017).

[248] Wedgwood, K. C., Lin, K. K., Thul, R. & Coombes, S. Phase-amplitude descriptions of neural oscillator models. *The Journal of Mathematical Neuroscience* **3**, 2 (2013).

[249] Castejón, O., Guillamon, A. & Huguet, G. Phase-amplitude response functions for transient-state stimuli. *The Journal of Mathematical Neuroscience* **3**, 13 (2013).

[250] Wilson, D. & Ermentrout, B. Greater accuracy and broadened applicability of phase reduction using isostable coordinates. *Journal of Mathematical Biology* (2017).

[251] Rothkegel, A. & Lehnertz, K. Recurrent events of synchrony in complex networks of pulse-coupled oscillators. *EPL* **95**, 38001 (2011).

[252] Ansmann, G., Karnatak, R., Lehnertz, K. & Feudel, U. Extreme events in excitable systems and mechanisms of their generation. *Phys. Rev. E* **88**, 052911 (2013).

[253] Rothkegel, A. & Lehnertz, K. Irregular macroscopic dynamics due to chimera states in small-world networks of pulse-coupled oscillators. *New Journal of Physics* **16**, 055006 (2014).

[254] Ansmann, G., Lehnertz, K. & Feudel, U. Self-induced switchings between multiple space-time patterns on complex networks of excitable units. *Phys. Rev. X* **6**, 011030 (2016).

[255] Hagmann, P. *et al.* Mapping the structural core of human cerebral cortex. *PLoS Biology* **6**, e159 (2008).

[256] Watts, D. J. & Strogatz, S. H. Collective dynamics of 'small-world' networks. *Nature* **393**, 440–442 (1998).

[257] Sethia, G. C. & Sen, A. Chimera states: The existence criteria revisited. *Phys. Rev. Lett.* **112**, 144101 (2014).

[258] Politi, A. & Rosenblum, M. Equivalence of phase-oscillator and integrate-and-fire models. *Phys. Rev. E* **91**, 042916 (2015).

[259] Shirasaka, S., Kurebayashi, W. & Nakao, H. Phase reduction theory for hybrid nonlinear oscillators. *Phys. Rev. E* **95**, 012212 (2017).

[260] Mauroy, A., Mezić, I. & Moehlis, J. Isostables, isochrons, and koopman spectrum for the action-angle representation of stable fixed point dynamics. *Physica D* **261**, 19–30 (2013).

[261] Budišić, M., Mohr, R. & Mezić, I. Applied Koopmanism. *Chaos* **22**, 047510 (2012).

[262] Wilson, D. & Moehlis, J. Isostable reduction of periodic orbits. *Phys. Rev. E* **94**, 052213 (2016).

[263] Mauroy, A. & Mezić, I. Global computation of phase-amplitude reduction for limit-cycle dynamics. *Chaos* **28**, 073108 (2018).

[264] Acebrón, J. A., Bonilla, L. L., Pérez Vicente, C. J., Ritort, F. & Spigler, R. The Kuramoto model: A simple paradigm for synchronization phenomena. *Review Modern Physics* **77**, 137–185 (2005).

[265] Abrams, D. M., Mirolo, R., Strogatz, S. H. & Wiley, D. A. Solvable model for chimera states of coupled oscillators. *Phys. Rev. Lett.* **101**, 084103 (2008).

[266] Montbrió, E., Kurths, J. & Blasius, B. Synchronization of two interacting populations of oscillators. *Phys. Rev. E* **70**, 056125 (2004).

[267] Barreto, E., Hunt, B., Ott, E. & So, P. Synchronization in networks of networks: The onset of coherent collective behavior in systems of interacting populations of heterogeneous oscillators. *Phys. Rev. E* **77**, 036107 (2008).

[268] So, P., Cotton, B. C. & Barreto, E. Synchronization in interacting populations of heterogeneous oscillators with time-varying coupling. *Chaos* **18** (2008).

[269] Laing, C. R. Chimera states in heterogeneous networks. *Chaos* **19**, 013113 (2009).

[270] Kawamura, Y., Nakao, H., Arai, K., Kori, H. & Kuramoto, Y. Phase synchronization between collective rhythms of globally coupled oscillator groups: Noiseless nonidentical case. *Chaos* **20** (2010).

[271] Martens, E. A. *et al.* Exact results for the Kuramoto model with a bimodal frequency distribution. *Phys. Rev. E* **79**, 026204 (2009).

[272] Strogatz, S. H. From Kuramoto to Crawford: exploring the onset of synchronization in populations of coupled oscillators. *Physica D* **143**, 1–20 (2000).

[273] Okuda, K. & Kuramoto, Y. Mutual entrainment between populations of coupled oscillators. *Progr. Theoret. Phys.* **86**, 1159–1176 (1991).

[274] Crawford, J. D. Amplitude expansions for instabilities in populations of globally-coupled oscillators. *J. Statist. Phys.* **74**, 1047–1084 (1994).

[275] Abrams, D. M. & Strogatz, S. H. Chimera states for coupled oscillators. *Phys. Rev. Lett.* **93**, 174102 (2004).

[276] Sakaguchi, H. Cooperative phenomena in coupled oscillator systems under external fields. *Progr. Theoret. Phys.* **79**, 39–46 (1988).

[277] Keizer, J. *Statistical Thermodynamics of Nonequilibrium Processes* (Springer, 1987).

[278] Strogatz, S. H. & Mirollo, R. E. Stability of incoherence in a population of coupled oscillators. *J. Stat. Phys.* **63**, 613–635 (1991).

[279] Sonnenschein, B. & Schimansky-Geier, L. Approximate solution to the stochastic Kuramoto model. *Phys. Rev. E* **88**, 052111 (2013).

[280] Pietras, B., Deschle, N. & Daffertshofer, A. Equivalence of coupled networks and networks with multimodal frequency distributions: Conditions for the bimodal and trimodal case. *Phys. Rev. E* **94**, 052211 (2016).

[281] Anderson, D. *et al.* Multiscale dynamics in communities of phase oscillators. *Chaos* **22** (2012).

[282] Komarov, M. & Pikovsky, A. Effects of nonresonant interaction in ensembles of phase oscillators. *Phys. Rev. E* **84**, 016210 (2011).

[283] Acebrón, J. A., Perales, A. & Spigler, R. Bifurcations and global stability of synchronized stationary states in the Kuramoto model for oscillator populations. *Phys. Rev. E* **64**, 016218 (2001).

[284] Martens, E. A. Bistable chimera attractors on a triangular network of oscillator populations. *Phys. Rev. E* **82**, 016216 (2010).

[285] Pietras, B., Deschle, N. & Daffertshofer, A. On the equivalence of coupled and multimodal networks. *unpublished*.

[286] Pazó, D. & Montbrió, E. Low-dimensional dynamics of populations of pulse-coupled oscillators. *Phys. Rev. X* **4**, 011009 (2014).

[287] Lee, W. S., Ott, E. & Antonsen, T. M. Large coupled oscillator systems with heterogeneous interaction delays. *Phys. Rev. Lett.* **103**, 044101 (2009).

[288] Martens, E. A., Bick, C. & Panaggio, M. J. Chimera states in two populations with heterogeneous phase-lag. *Chaos* **26**, 094819 (2016).

[289] Pikovsky, A. & Politi, A. *Lyapunov Exponents: A Tool to Explore Complex Dynamics* (Cambridge University Press, 2016).

[290] Luke, T. B., Barreto, E. & So, P. Complete classification of the macroscopic behavior of a heterogeneous network of theta neurons. *Neural Computation* **25**, 3207–3234 (2013).

[291] So, P., Luke, T. B. & Barreto, E. Networks of theta neurons with time-varying excitability: Macroscopic chaos, multistability, and final-state uncertainty. *Physica D* **267**, 16–26 (2014).

[292] Laing, C. R. Derivation of a neural field model from a network of theta neurons. *Phys. Rev. E* **90**, 010901 (2014).

[293] Montbrió, E., Pazó, D. & Roxin, A. Macroscopic description for networks of spiking neurons. *Phys. Rev. X* **5**, 021028 (2015).

[294] Laing, C. R. Phase oscillator network models of brain dynamics. *Computational Models of Brain and Behavior*. Wiley-Blackwell (2016).

[295] Byrne, Á., Brookes, M. J. & Coombes, S. A mean field model for movement induced changes in the beta rhythm. *J. Comput. Neurosci.* **43**, 143–158 (2017).

[296] Coombes, S. & Byrne, Á. Next generation neural mass models. In Corinto, F. & Torcini, A. (eds.) *Nonlinear Dynamics in Computational Neuroscience*, 1–16 (Springer, 2019).

[297] Marvel, S. A., Mirollo, R. E. & Strogatz, S. H. Identical phase oscillators with global sinusoidal coupling evolve by Möbius group action. *Chaos* **19**, 043104 (2009).

[298] Wagemakers, A., Barreto, E., Sanjuán, M. A. F. & So, P. Control of collective network chaos. *Chaos* **24**, 023127 (2014).

[299] So, P. & Barreto, E. Generating macroscopic chaos in a network of globally coupled phase oscillators. *Chaos* **21** (2011).

[300] Montbrió, E. & Pazó, D. Shear diversity prevents collective synchronization. *Phys. Rev. Lett.* **106**, 254101 (2011).

[301] Pazó, D. & Montbrió, E. The Kuramoto model with distributed shear. *EPL* **95**, 60007 (2011).

[302] Montbrió, E. & Pazó, D. Collective synchronization in the presence of reactive coupling and shear diversity. *Phys. Rev. E* **84**, 046206 (2011).

[303] Iatsenko, D., Petkoski, S., McClintock, P. V. E. & Stefanovska, A. Stationary and traveling wave states of the Kuramoto model with an arbitrary distribution of frequencies and coupling strengths. *Phys. Rev. Lett.* **110**, 064101 (2013).

[304] Iatsenko, D., McClintock, P. V. E. & Stefanovska, A. Glassy states and super-relaxation in populations of coupled phase oscillators. *Nature Comm.* **5**, 4118 (2014).

[305] Evans, L. C. *Partial differential equations* (American Mathematical Soc., 1998).

[306] Ott, E., Platig, J. H., Antonsen, T. M. & Girvan, M. Echo phenomena in large systems of coupled oscillators. *Chaos* **18** (2008).

[307] Ermentrout, G. B. & Kopell, N. Parabolic bursting in an excitable system coupled with a slow oscillation. *SIAM Journal on Applied Mathematics* **46**, 233–253 (1986).

[308] Petkoski, S. & Stefanovska, A. Kuramoto model with time-varying parameters. *Phys. Rev. E* **86**, 046212 (2012).

[309] Petkoski, S., Iatsenko, D., Basnarkov, L. & Stefanovska, A. Mean-field and mean-ensemble frequencies of a system of coupled oscillators. *Phys. Rev. E* **87**, 032908 (2013).

[310] Wang, H. & Li, X. Synchronization and chimera states of frequency-weighted Kuramoto-oscillator networks. *Phys. Rev. E* **83**, 066214 (2011).

[311] Xu, C. *et al.* Synchronization of phase oscillators with frequency-weighted coupling. *Scientific Reports* **6** (2016).

[312] Barlev, G., Antonsen, T. M. & Ott, E. The dynamics of network coupled phase oscillators: An ensemble approach. *Chaos* **21** (2011).

[313] Vespignani, A. Modelling dynamical processes in complex socio-technical systems. *Nature Physics* **8**, 32–39 (2012).

[314] Dorogovtsev, S., Goltsev, A. & Mendes, J. Critical phenomena in complex networks. *Review Modern Physics* **80**, 1275–1335 (2008).

[315] Coutinho, B., Goltsev, A., Dorogovtsev, S. & Mendes, J. Kuramoto model with frequency-degree correlations on complex networks. *Phys. Rev. E* **87**, 032106 (2013).

[316] Yoon, S., Sindaci, M. S., Goltsev, A. & Mendes, J. Critical behavior of the relaxation rate, the susceptibility, and a pair correlation function in the Kuramoto model on scale-free networks. *Phys. Rev. E* **91**, 032814 (2015).

[317] Lopes, M., Lopes, E., Yoon, S., Mendes, J. & Goltsev, A. Synchronization in the random-field Kuramoto model on complex networks. *Phys. Rev. E* **94**, 012308 (2016).

[318] Pazó, D. & Montbrió, E. Existence of hysteresis in the Kuramoto model with bimodal frequency distributions. *Phys. Rev. E* **80**, 046215 (2009).

[319] Skardal, P. S. & Restrepo, J. G. Hierarchical synchrony of phase oscillators in modular networks. *Phys. Rev. E* **85**, 016208 (2012).

[320] So, P., Cotton, B. C. & Barreto, E. Synchronization in interacting populations of heterogeneous oscillators with time-varying coupling. *Chaos* **18** (2008).

[321] Restrepo, J. G. & Ott, E. Mean-field theory of assortative networks of phase oscillators. *EPL* **107**, 60006 (2014).

[322] Skardal, P. S., Restrepo, J. G. & Ott, E. Frequency assortativity can induce chaos in oscillator networks. *Phys. Rev. E* **91**, 060902 (2015).

[323] Ko, T.-W. & Ermentrout, G. B. Partially locked states in coupled oscillators due to inhomogeneous coupling. *Phys. Rev. E* **78**, 016203 (2008).

[324] Laing, C. R. The dynamics of chimera states in heterogeneous Kuramoto networks. *Physica D* **238**, 1569–1588 (2009).

[325] Omel’chenko, O. E. Coherence–incoherence patterns in a ring of non-locally coupled phase oscillators. *Nonlinearity* **26**, 2469 (2013).

[326] Kuramoto, Y. & Battogtokh, D. Coexistence of coherence and incoherence in nonlocally coupled phase oscillators. *Nonlinear Phenom. Complex Syst.* **5**, 380–5 (2002).

[327] Wolfrum, M., Omel’chenko, O. E., Yanchuk, S. & Maistrenko, Y. L. Spectral properties of chimera states. *Chaos* **21**, 013112 (2011).

[328] Childs, L. M. & Strogatz, S. H. Stability diagram for the forced Kuramoto model. *Chaos* **18**, 043128 (2008).

[329] Lu, Z. *et al.* Resynchronization of circadian oscillators and the east-west asymmetry of jet-lag. *Chaos* **26** (2016).

[330] Petkoski, S. *et al.* Heterogeneity of time delays determines synchronization of coupled oscillators. *Phys. Rev. E* **94**, 012209 (2016).

[331] Skardal, P. S., Taylor, D. & Restrepo, J. G. Complex macroscopic behavior in systems of phase oscillators with adaptive coupling. *Physica D* **267**, 27 – 35 (2014).

[332] Gómez-Gardenes, J., Gómez, S., Arenas, A. & Moreno, Y. Explosive synchronization transitions in scale-free networks. *Phys. Rev. Lett.* **106**, 128701 (2011).

[333] Danziger, M. M. *et al.* Explosive synchronization coexists with classical synchronization in the Kuramoto model. *Chaos* **26** (2016).

[334] Lellis, P. D., Bernardo, M. D., Sorrentino, F. & Tierno, A. Adaptive synchronization of complex networks. *Int. J. Comput. Math.* **85**, 1189–1218 (2008).

[335] Aoki, T. & Aoyagi, T. Co-evolution of phases and connection strengths in a network of phase oscillators. *Phys. Rev. Lett.* **102**, 034101 (2009).

[336] Eom, Y.-H., Boccaletti, S. & Caldarelli, G. Concurrent enhancement of percolation and synchronization in adaptive networks. *Scientific Reports* **6**, 27111 (2016).

[337] Dietert, H. Stability and bifurcation for the Kuramoto model. *Journal de Mathématiques Pures et Appliquées* **105**, 451–489 (2016).

[338] Fernandez, B., Gérard-Varet, D. & Giacomin, G. Landau damping in the Kuramoto model. In *Annales Henri Poincaré*, 1–31 (Springer, 2015).

[339] Dietert, H., Fernandez, B. & Gérard-Varet, D. Landau damping to partially locked states in the Kuramoto model. *Communications on Pure and Applied Mathematics* **71**, 953–993 (2018).

[340] Strogatz, S. H., Mirollo, R. E. & Matthews, P. C. Coupled nonlinear oscillators below the synchronization threshold: relaxation by generalized Landau damping. *Phys. Rev. Lett.* **68**, 2730 (1992).

[341] Omel’chenko, O. E., Wolfrum, M. & Laing, C. R. Partially coherent twisted states in arrays of coupled phase oscillators. *Chaos* **24**, 023102 (2014).

[342] Laing, C. R. Disorder-induced dynamics in a pair of coupled heterogeneous phase oscillator networks. *Chaos* **22**, 043104 (2012).

[343] Pikovsky, A. & Rosenblum, M. Partially integrable dynamics of hierarchical populations of coupled oscillators. *Phys. Rev. Lett.* **101**, 264103 (2008).

[344] Laing, C. R. Chimeras in networks with purely local coupling. *Phys. Rev. E* **92**, 050904 (2015).

[345] Skardal, P. S., Ott, E. & Restrepo, J. G. Cluster synchrony in systems of coupled phase oscillators with higher-order coupling. *Phys. Rev. E* **84**, 036208 (2011).

[346] Terada, Y. & Aoyagi, T. Dynamics of two populations of phase oscillators with different frequency distributions. *Phys. Rev. E* **94**, 012213 (2016).

[347] Izhikevich, E. M. & Edelman, G. M. Large-scale model of mammalian thalamocortical systems. *PNAS* **105**, 3593–3598 (2008).

[348] Deco, G. & Jirsa, V. Ongoing cortical activity at rest: Criticality, multistability, and ghost attractors. *J. Neurosci.* **32**, 3366–3375 (2012).

[349] Sotero, R. C., Trujillo-Barreto, N. J., Iturria-Medina, Y., Carbonell, F. & Jimenez, J. C. Realistically coupled neural mass models can generate EEG rhythms. *Neural Computation* **19**, 478–512 (2007).

[350] Ponten, S., Daffertshofer, A., Hillebrand, A. & Stam, C. J. The relationship between structural and functional connectivity: graph theoretical analysis of an EEG neural mass model. *NeuroImage* **52**, 985–994 (2010).

[351] Kuramoto, Y. Self-entrainment of a population of coupled non-linear oscillators. In *International symposium on mathematical problems in theoretical physics*, 420–422 (Springer, 1975).

[352] Fries, P. Neuronal gamma-band synchronization as a fundamental process in cortical computation. *Annual Review of Neuroscience* **32**, 209–224 (2009).

[353] Pfurtscheller, G. & Da Silva, F. L. Event-related EEG/MEG synchronization and desynchronization: basic principles. *Clinical Neurophysiology* **110**, 1842–1857 (1999).

[354] Biswal, B., Zerrin Yetkin, F., Haughton, V. & Hyde, J. Functional connectivity in the motor cortex of resting human brain using echo-planar MRI. *Magnetics Resonance in Medicine* **34**, 537–541 (1995).

[355] Deco, G., Jirsa, V. & McIntosh, A. Emerging concepts for the dynamical organization of resting-state activity in the brain. *Nature Reviews Neuroscience* **12**, 43–56 (2011).

[356] van Wijk, B. C., Beek, P. J. & Daffertshofer, A. Neural synchrony within the motor system: what have we learned so far? *Frontiers in Human Neuroscience* **6** (2012).

[357] Fell, J. & Axmacher, N. The role of phase synchronization in memory processes. *Nature Reviews Neuroscience* **12**, 105–118 (2011).

[358] Fries, P., Nikolić, D. & Singer, W. The gamma cycle. *Trends in Neurosciences* **30**, 309–316 (2007).

[359] Singh, K. D. Which ‘neural activity’ do you mean? fMRI, MEG, oscillations and neurotransmitters. *NeuroImage* **62**, 1121–1130 (2012).

[360] Voytek, B. & Knight, R. T. Dynamic network communication as a unifying neural basis for cognition, development, aging, and disease. *Biological Psychiatry* **77**, 1089–1097 (2015).

[361] Broyd, S. J. *et al.* Default-mode brain dysfunction in mental disorders: a systematic review. *Neuroscience & Biobehavioral Reviews* **33**, 279–296 (2009).

[362] Beggs, J. M. The criticality hypothesis: how local cortical networks might optimize information processing. *Philos. Trans. Royal Soc. A* **366**, 329–343 (2008).

[363] Chialvo, D. Emergent complex neural dynamics. *Nature Physics* **6**, 744–750 (2010).

[364] Beggs, J. & Timme, N. Being critical of criticality in the brain. *Frontiers in Physiology* **3** (2012).

[365] Shew, W. & Plenz, D. The functional benefits of criticality in the cortex. *The Neuroscientist* **19**, 88–100 (2013).

[366] Stanley, H. *Introduction to phase transitions and critical phenomena* (Oxford University Press, 1971).

[367] Beggs, J. & Plenz, D. Neuronal avalanches in neocortical circuits. *J. Neurosci.* **23**, 11167–11177 (2003).

[368] Fagerholm, E. D. *et al.* Cascades and cognitive state: focused attention incurs subcritical dynamics. *J. Neurosci.* **35**, 4626–4634 (2015).

[369] Linkenkaer-Hansen, K., Nikouline, V., Palva, J. M. & Ilmoniemi, R. J. Long-range temporal correlations and scaling behavior in human brain oscillations. *J. Neurosci.* **21**, 1370–1377 (2001).

[370] Palva, J. M. *et al.* Neuronal long-range temporal correlations and avalanche dynamics are correlated with behavioral scaling laws. *PNAS* **110**, 3585–3590 (2013).

[371] Botcharova, M., Berthouze, L., Brookes, M. J., Barnes, G. & Farmer, S. F. Resting state MEG oscillations show long-range temporal correlations of phase synchrony that break down during finger movement. *Frontiers in Physiology* **6** (2015).

[372] Daffertshofer, A., Ton, R., Kringselbach, M. L., Woolrich, M. & Deco, G. Distinct criticality of phase and amplitude dynamics in the resting brain. *NeuroImage* (2018).

[373] Hurst, H. Long-term storage capacity of reservoirs. *Transactions of the American Society of Civil Engineering* **116**, 770–808 (1951).

[374] Marreiros, A., Daunizeau, J., Kiebel, S. & Friston, K. Population dynamics: Variance and the sigmoid activation function. *NeuroImage* **42**, 147–157 (2008).

[375] Van Mieghem, P. A complex variant of the Kuramoto model. Tech. Rep. 20090811, Delft University of Technology (2009).

[376] Burylko, O., Kazanovich, Y. & Borisyuk, R. Bifurcation study of phase oscillator systems with attractive and repulsive interaction. *Phys. Rev. E* **90**, 022911 (2014).

[377] Shampine, L. F. & Thompson, S. Solving DDEs in Matlab. *Applied Numerical Mathematics* **37**, 441–458 (2001).

[378] Peng, C.-K. *et al.* Mosaic organization of DNA nucleotides. *Phys. Rev. E* **49**, 1685 (1994).

[379] Ton, R. & Daffertshofer, A. Model selection for identifying power-law scaling. *NeuroImage* **136**, 215 – 226 (2016).

[380] Burnham, K. P. & Anderson, D. R. *Model selection and multimodel inference: a practical information-theoretic approach* (Springer, 2002).

[381] Tzourio-Mazoyer, N. *et al.* Automated anatomical labeling of activations in spm using a macroscopic anatomical parcellation of the MNI MRI single-subject brain. *NeuroImage* **15**, 273–289 (2002).

[382] Nolte, G. *et al.* Identifying true brain interaction from EEG data using the imaginary part of coherency. *Clinical Neurophysiology* **115**, 2292–2307 (2004).

[383] Deco, G. *et al.* Resting-state functional connectivity emerges from structurally and dynamically shaped slow linear fluctuations. *J. Neurosci.* **33**, 11239–11252 (2013).

[384] Deco, G. *et al.* How local excitation–inhibition ratio impacts the whole brain dynamics. *J. Neurosci.* **34**, 7886–7898 (2014).

[385] Breakspear, M. *et al.* A unifying explanation of primary generalized seizures through nonlinear brain modeling and bifurcation analysis. *Cerebral Cortex* **16**, 1296–1313 (2006).

[386] Rodrigues, S. *et al.* Transitions to spike-wave oscillations and epileptic dynamics in a human cortico-thalamic mean-field model. *J. Comput. Neurosci.* **27**, 507–526 (2009).

[387] Messé, A., Rudrauf, D., Benali, H. & Marrelec, G. Relating structure and function in the human brain: relative contributions of anatomy, stationary dynamics, and non-stationarities. *PLoS Comput. Biol.* **10**, e1003530 (2014).

[388] Bullmore, E. & Sporns, O. Complex brain networks: graph theoretical analysis of structural and functional systems. *Nature Reviews Neuroscience* **10**, 186–198 (2009).

[389] Hansen, E. C., Battaglia, D., Spiegler, A., Deco, G. & Jirsa, V. K. Functional connectivity dynamics: Modeling the switching behavior of the resting state. *NeuroImage* **105**, 525 – 535 (2015).

[390] Botcharova, M., Farmer, S. F. & Berthouze, L. Markers of criticality in phase synchronization. *Frontiers in Systems Neuroscience* **8** (2014).

[391] Pikovsky, A. & Rosenblum, M. Dynamics of globally coupled oscillators: Progress and perspectives. *Chaos* **25** (2015).

[392] Hong, H. & Strogatz, S. H. Conformists and contrarians in a Kuramoto model with identical natural frequencies. *Phys. Rev. E* **84**, 046202 (2011).

[393] Mazzoni, A. *et al.* On the dynamics of the spontaneous activity in neuronal networks. *PLoS One* **2**, e439 (2007).

[394] Tetzlaff, C. *et al.* Self-organized criticality in developing neuronal networks. *PLoS Comput. Biol.* **6**, e1001013 (2010).

[395] Shew, W., Yang, H., Yu, S., Roy, R. & Plenz, D. Information capacity and transmission are maximized in balanced cortical networks with neuronal avalanches. *J. Neurosci.* **31**, 55–63 (2011).

[396] Deco, G. & Hugues, E. Balanced input allows optimal encoding in a stochastic binary neural network model: an analytical study. *PLoS One* **7**, e30723 (2012).

[397] Kandel, E. R., Schwartz, J. H., Jessell, T. M. *et al.* *Principles of Neural Science* (McGraw-Hill, 2013).

[398] Douglas, R. J. & Martin, K. A. Neuronal circuits of the neocortex. *Annual Reviews in Neuroscience* **27**, 419–451 (2004).

[399] Kim, S., Park, S. H. & Ryu, C. S. Multistability in coupled oscillator systems with time delay. *Phys. Rev. Lett.* **79**, 2911–2914 (1997).

[400] Yeung, M. K. S. & Strogatz, S. H. Time delay in the Kuramoto model of coupled oscillators. *Phys. Rev. Lett.* **82**, 648–651 (1999).

[401] Choi, M. Y., Kim, H. J., Kim, D. & Hong, H. Synchronization in a system of globally coupled oscillators with time delay. *Phys. Rev. E* **61**, 371–381 (2000).

[402] Robinson, P. A. Interrelating anatomical, effective, and functional brain connectivity using propagators and neural field theory. *Phys. Rev. E* **85**, 011912 (2012).

[403] Daido, H. Order function and macroscopic mutual entrainment in uniformly coupled limit-cycle oscillators. *Progr. Theoret. Phys.* **88**, 1213–1218 (1992).

[404] Daido, H. Population dynamics of randomly interacting self-oscillators. I: Tractable models without frustration. *Progr. Theoret. Phys.* **77**, 622–634 (1987).

[405] Daido, H. Susceptibility of large populations of coupled oscillators. *Phys. Rev. E* **91**, 012925 (2015).

[406] Arslan, S. *et al.* Human brain mapping: A systematic comparison of parcellation methods for the human cerebral cortex. *NeuroImage* **170**, 5 – 30 (2018).

[407] Zilles, K. & Amunts, K. Centenary of Brodmann’s map – conception and fate. *Nat. Rev. Neurosci.* **11**, 139 EP – (2010).

[408] FitzHugh, R. Impulses and physiological states in theoretical models of nerve membrane. *Biophysical Journal* **1**, 445 – 466 (1961).

[409] Morris, C. & Lecar, H. Voltage oscillations in the barnacle giant muscle fiber. *Biophysical Journal* **35**, 193–213 (1981).

[410] Ermentrout, B. Type I membranes, phase resetting curves, and synchrony. *Neural Computation* **8**, 979–1001 (1996).

[411] Hansel, D. & Mato, G. Asynchronous states and the emergence of synchrony in large networks of interacting excitatory and inhibitory neurons. *Neural Computation* **15**, 1–56 (2003).

[412] Hansel, D., Mato, G. & Meunier, C. Synchrony in excitatory neural networks. *Neural Computation* **7**, 307–337 (1995).

[413] Chandra, S. *et al.* Modeling the network dynamics of pulse-coupled neurons. *Chaos* **27**, 033102 (2017).

[414] Devalle, F., Roxin, A. & Montbrió, E. Firing rate equations require a spike synchrony mechanism to correctly describe fast oscillations in inhibitory networks. *PLoS Comput. Biol.* **13**, 1–21 (2017).

[415] Ratas, I. & Pyragas, K. Macroscopic self-oscillations and aging transition in a network of synaptically coupled quadratic integrate-and-fire neurons. *Phys. Rev. E* **94**, 032215 (2016).

[416] Ratas, I. & Pyragas, K. Symmetry breaking in two interacting populations of quadratic integrate-and-fire neurons. *Phys. Rev. E* **96**, 042212 (2017).

[417] Dumont, G., Ermentrout, G. B. & Gutkin, B. Macroscopic phase-resetting curves for spiking neural networks. *Phys. Rev. E* **96**, 042311 (2017).

[418] Rodrigues, S., Chizhov, A. V., Marten, F. & Terry, J. R. Mappings between a macroscopic neural-mass model and a reduced conductance-based model. *Biological Cybernetics* **102**, 361–371 (2010).

[419] Goldenfeld, N., Martin, O. & Oono, Y. Intermediate asymptotics and renormalization group theory. *Journal of Scientific Computing* **4**, 355–372 (1989).

[420] Goldenfeld, N., Martin, O., Oono, Y. & Liu, F. Anomalous dimensions and the renormalization group in a nonlinear diffusion process. *Phys. Rev. Lett.* **64**, 1361 (1990).

[421] Kunihiro, T. The renormalization-group method applied to asymptotic analysis of vector fields. *Progr. Theoret. Phys.* **97**, 179–200 (1997).

- [422] Rodrigues, A. *Bifurcations of Dynamical Systems with Symmetry*. Ph.D. thesis, University of Porto (2007).
- [423] Hale, J. *Ordinary differential equations* (Wiley, 1969).

# MAIN CONTRIBUTIONS

- An extensive review of various phase reduction and Hopf normal form reduction techniques of networks of linearly coupled oscillators.  
(Chapter 2)
- An extension of current reduction techniques in order to cope with nonlinear coupling terms, including novel mathematical proofs.  
(Chapter 2, Supplementary Material)
- An analytic and numerical exploration of two classic examples of coupled oscillators, a network of Brusselators and a network of Wilson-Cowan neural masses.  
(Chapter 3)
- A detailed discussion of the limitations and possible further extensions of phase reduction techniques.  
(Chapter 3)
- A proof of the topological equivalence between a two-population setup of phase oscillators with unimodal frequency distributions and a single population network with a bimodal frequency distribution.  
(Chapter 4)
- A proof of the validity of the Ott-Antonsen ansatz to reduce parameter-dependent oscillatory systems, including non-autonomous systems.  
(Chapter 5)
- An extensive review of networks of spiking neurons and of coupled phase oscillators that fall within the class of parameter-dependent oscillatory systems.  
(Chapter 5)
- A comparison of the phase dynamics of networks built on distinct neural mass models for their capacity to describe two pivotal dynamical features of criticality in MEG signals.  
(Chapter 6)

## ACKNOWLEDGEMENTS

It is my pleasant duty to put on record my thanks and gratitude to all of those who made this dissertation possible. I want to thank especially:

- First and foremost, Andreas. Since our first get-together at Café de Jaren in spring 2015, I was sure that in Amsterdam I would get all the guidance, support and supervision I needed for my upcoming PhD project. Always ready to offer help and advice, you introduced the younger me to a new environment around human movement scientists and accompanied me as I took my first steps as the exotic mathematician in the Coordination Dynamics Group. During the last three years, you helped me to learn a lot about many different facets both in science and in life. You let me explore the scientific world on numerous occasions in and outside of the Netherlands, and I am very grateful for the freedom to also shape the PhD project, “my baby”, to my preferences!
- Aneta. Thank you very much for your kind hospitality in Lancaster, which I was allowed to call home for a year. You gave me room to think, to delve further into mathematical details, but also to see physics through different eyes and, in particular, from a perspective of time series analysis. The trips to the Lakes together with Peter and the Nonlinear and Biomedical Physics groups were always a welcoming opportunity to enrich one’s views and to recharge.
- Peter. I appreciate your wise words, the constant willingness to help, and your administrative support in Lancaster. Thank you very much.
- The members of my examination committees in Lancaster and Amsterdam, Stephen Coombes, Ernest Montbrió, Arkady Pikovsky, Bob Rink, Jeroen Smeets, Robin Tucker. Thank you for your time and effort in assessing the manuscript. I appreciated all your comments and suggestions, which helped to increase the quality of my thesis.
- Nicolás and my fellow musketeers, Federico and Maxime. Do I have to express my thanks or my apologies for innumerable hours where I used and

abused you as sparring partners, to listen to, but also to discuss and scrutinize my thoughts and ideas? In any case, life without you wouldn't have been half as much fun!

- The whole COSMOS family. Throughout the various meetings at so many different places I had the privilege to encounter many great scientists and even greater human beings. I am glad to have been part of COSMOS and happy about all the new friendships that developed in this time. Special thanks go to our steering committee, Arkady Pikovsky, Michael Rosenblum and Antonio Politi, and to our project manager, Caroline Reid. The wonderful time we had together wandering around Europe and science would certainly have not been possible without their efforts. Not only did the consortium provide the grounds for our scientific growth. But they also trusted us, the 15 PhD candidates, with the organization of the AMCOS conference in Barcelona in March 2018. The success of this event was stupendous and a personal highlight of my PhD project. It was an honor to pull the strings alongside all of you. We definitely ran the show!
- A number of people who ignited my interest in neuroscience, who helped me gain a closer understanding of scientific concepts in mathematics, physics and beyond, and who challenged my mathematical skills, Klaus Lehnertz, Ulrike Feudel, Stephen Coombes, Ernest Montbrió, Hiroya Nakao, Oleh Omel'chenko, Christian Bick. I enjoyed and I am thankful for many fruitful and inspiring discussions with you.
- The coordination dynamics group, our late lunch group (including Nico, Jacob, Yajie, Cristina, Eva, Marija, Clara, Eero, Rok, Alice and Vera), and all the other colleagues and PhDs at the Vrije Universiteit Amsterdam, who substantially improved my work-life balance over lunch and coffee, during PhD weekends and pub crawls, on morning swims or afternoon runs, en tijdens borrels en andere feestjes. Dank jullie wel allemaal. Het was erg gezellig!
- The Lancaster group (including Fede, Max, Ola, Ticci, Will, Miroslav, Vamsi and Gemma) for providing a lighthearted atmosphere in and outside the office. All the curry and table football nights at Grad Bar, the morning strolls around Saturday's market with Leo's piadina and Buccelli's coffee, the barbecue parties at Primrose Street, the escapes to Manchester and Liverpool, the climbing and squash nights and throwing frisbees across the campus fields – thanks to all who made this such a unique experience.

- The sprint team Phast. A huge thanks to all of you with whom I could share my passion in sports and pushing the limits. Het was een bijzondere ervaring met jullie mee te trainen – een ongelofelijke, indrukwekkende, fanatieke maar ook geestige en plezante manier om samen te sporten, borrelen en grapjes te maken, opdat ik weer met een frisse blik naar mijn onderzoek kan kijken. Ik heb er erg van genoten!
- Last but not least, my parents. Ohne Eure grenzenlose Unterstützung und Euren unermüdlichen Rückhalt würde ich hier jetzt nicht stehen. Danke!

“I do not consider myself less ignorant than most people.  
I have been and still am a seeker,  
but I have ceased to question stars and books;  
I have begun to listen to the teaching my blood whispers to me.”

Hermann Hesse – *Demian* (1919)